

School of Doctoral Studies in Biological Sciences

University of South Bohemia in České Budějovice

Faculty of Science

**The role of macrophages in the regulation of systemic
metabolism in *Drosophila***

Ph.D. Thesis

Mgr. Gabriela Krejčová

Supervisor:

Mgr. et Mgr. Adam Bajgar, Ph.D.

Faculty of Science, University of South Bohemia in České Budějovice

České Budějovice 2023

This thesis should be cited as:

Krejčová, G. (2023): The role of macrophages in the regulation of systemic metabolism in *Drosophila*. Ph.D. Thesis, in English – 364 pp. Faculty of Science, University of South Bohemia, České Budějovice, Czech Republic.

Annotation

Macrophages are immensely versatile cells in the mammalian body, fulfilling roles ranging from protection against pathogenic intruders and engulfing apoptotic cells to morphogenesis and maintenance of tissue homeostasis. This impressive functional versatility may be achieved due to plasticity of macrophage cellular metabolism called metabolic polarization. The adoption of different polarization phenotypes by macrophages determines their function and is essential for the health of the organism. Nonetheless, if the cells lose their metabolic plasticity or polarize inadequately to a particular situation, it can lead to the development of chronic pathological states such as metabolic syndrome. Metabolic polarization of immune cells is thus a key factor in determining whether macrophage function within the organism will be adaptive or pathological.

Despite *Drosophila melanogaster* represents a major model organism for immunological studies, the metabolic setup of activated immune cells has not been addressed up to now. The results of this thesis document that *Drosophila* immune cells undergo metabolic polarization toward aerobic glycolysis when challenged by extracellular bacteria. Mammals alike, this cellular metabolic switch is regulated by the transcription factor HIF1 α , thus documenting the conservation of this process between insects and vertebrates. Furthermore, we show that the adoption of aerobic glycolysis is directly linked to the production of the signaling factor IMPL2, which induces the mobilization of lipid stores from the fat body *via* the silencing of insulin signaling. By this mechanism, immune cells secure sufficient nutrients for successful elimination of the pathogen. Moreover, the mammalian *Impl2* homolog *IGFBP7* appears to act analogously in the mammalian liver not only during severe infectious states but also in the liver of obese individuals. While such macrophage activity in regulating systemic metabolism is beneficial to the host during bacterial infection, it becomes maladaptive when chronically activated.

Further evidence for a metabolism-regulatory role of immune cells has been found during insect metamorphosis and early post-metamorphic development. This thesis documents that during this period, macrophages infiltrate and engulf the histolyzing larval fat body and convert nutrients into storage peptides and lipoproteins. Subsequently, these nutrients are exploited by the maturing adult structures.

Declaration

[In Czech]

Prohlašuji, že jsem autorem této kvalifikační práce a že jsem ji vypracovala pouze s použitím pramenů a literatury uvedených v seznamu použitých zdrojů.

[In English]

I hereby declare that I am the author of this thesis and that I have used only those sources and literature detailed in the list of references.

České Budějovice, 27.11.2023

Mgr. Gabriela Krejčová

Financial support

This work was supported by the Czech Science Foundation grants (projects 23-06133S and 20-14030S) awarded to Adam Bajgar, PhD. Gabriela Krejčová was the recipient of two individual project grants (026/2021/P and 050/2019/P) funded by the Grant Agency of the University of South Bohemia.

Acknowledgements

As the path to obtaining a PhD is bumpy and sometimes really long, both subjectively and objectively, for us and for our loved ones, we meet many people along the way. Therefore, the following paragraphs are by no means exhaustive or complete.

First and foremost, none of my achievements would have been accomplished without Adam. Thank you for openly sharing all your knowledge, ideas, wisdom and skills you have. Your spirit has been inspiring me at times when I felt like staying “Comfortably Numb”. Thank you for being willing to discuss in situations when I was “Dazed and Confused” from our work and from scientific career. Thank you for always being here, even “In My Time of Dying”, when “Time Stand Still” because the reviewers gave us “No Quarter” again and we had no choice but to be true “Brothers in Arms”. I am not ceasing to have “High Hopes” that we will be able to “Ramble On” our scientific journey “Over the Hills and Far Away”. As evident, I will always cherish the years of dissections while listening to music coming out of those old raspy speakers.

I want to thank my fellow “PhD friends from the corridor”, former and present, particularly Pája, Becky, and Martina, with whom we shared the highs and lows. My gratitude also goes to the past and present lab members and people from the neighboring laboratories, especially those who welcomed us when we needed shelter. I appreciate everyone who attempted to create a kind and joyful atmosphere. I am grateful to Lucka for her conscientious care of our fly stocks and all her help in maintaining the lab. On that note, I must also thank Marcela who was always very kind and helpful despite my complete ignorance of bureaucratic paperwork and administrative procedures.

I would like to acknowledge the Laboratory of Microscopy and Histology of the Biology Centre CAS for the access to the confocal microscope, which helped me tremendously to unravel the astonishing beauty of macrophages and where I experienced many hours of joy. My PhD studies would not have been so colorful if it weren't for this equipment. Similarly, I thank to the Laboratory of Electron Microscopy of the Biology Centre CAS for the access to the electron microscopes. Those grayscale images allowed us to look deeper and provided us with another layer of observations. I am also indebted to the Department of Medical Biology where we were sorting the cells.

I thank to every fly researcher who provided us with their fly stocks, to all our collaborators, without whom our discoveries would not have happened, and to the funders for allowing us to answer our scientific questions. I also value all the researchers and brilliant minds who have contributed to the development of genetic tools in fruit flies and thus helped establish this model as we know it today.

V neposlední řadě si zaslouží nezměrné poděkování moje rodina a to především za zázemí, které mi celý život poskytovali, za jejich lásku, podporu a snahu porozumět všem těm mým řečem a nářkům o buňkách, grantech a publikování. Děkuju.

Děkuji také ještě jedné rodině, a to té taneční, rodině Daima Dancers. Díky, že tolerujete, že mouchy vítězí nad tréninky.

List of papers and manuscripts, and author's contribution

The thesis is based on the following manuscripts (listed chronologically):

Morgantini, C., Jager, J., Li, X., Levi, L., Azzimato, V., Sulen, A., Barreby, E., Xu, C., Tencerova, M., Näslund, E.,**Krejčová, G.**, Bajgar, A., and Aouadi, M. (2019). Liver macrophages regulate systemic metabolism through non-inflammatory factors. *Nature Metabolism*. 1, 445–459. 10.1038/s42255-019-0044-9.

(IF = 19.89, citations = 75)

G.K. was involved in conducting the Drosophila experiments. She participated in preparation of the flies, confocal microscopy imaging and tissue sampling. She reviewed and validated the manuscript.

Dolezal, T., **Krejčova, G.**, Bajgar, A., Nedbalova, P., and Strasser, P. (2019). Molecular regulations of metabolism during immune response in insects. *Insect Biochemistry and Molecular Biology* 109, 31–42. 10.1016/j.ibmb.2019.04.005.

(IF = 4.42, citations = 102)

G.K. participated in literature research concerning the section about the metabolic setup of activated immune cells, design and preparation of the schemes. She reviewed and validated the manuscript.

Bajgar, A., Saloň, I., **Krejčová, G.**, Doležal, T., Jindra, M., and Štěpánek, F. (2019). Yeast glucan particles enable intracellular protein delivery in *Drosophila* without compromising the immune system. *Biomaterials Science* 7, 4708–4719. 10.1039/C9BM00539K.

(IF = 7.59, citations = 10)

G.K. was involved in confocal microscopy imaging, data analysis and conducting the experiments during the revisions. She reviewed and validated the submitted manuscript.

Krejčová, G., Danielová, A., Nedbalová, P., Kazek, M., Strych, L., Chawla, G., Tennessen, J.M., Lieskovská, J., Jindra, M., Doležal, T., et al. (2019). *Drosophila* macrophages switch to aerobic glycolysis to mount effective antibacterial defense. *Elife* 8. 10.7554/eLife.50414.

(IF = 8.71, citations = 64)

G.K. participated in design of the experiments, preparation of the fly crosses, tissue sampling, data curation and analysis, and writing the manuscript. She contributed to figure preparation. G.K. conducted the experiments and analyzed the data required during the revision process.

Bajgar, A., **Krejčová, G.**, and Doležal, T. (2021). Polarization of Macrophages in Insects: Opening Gates for Immuno-Metabolic Research. *Frontiers in Cell and Developmental Biology* 9. 10.3389/fcell.2021.629238.

(IF = 6.08, citations = 8)

G.K. participated in conceptualization, literature research of the topic, graphic design, as well as revision of the manuscript. She prepared the confocal and electron microscopy images and schematic illustrations. She approved the submitted manuscript.

Bajgar, A., and **Krejčová, G.** (2023). On the origin of the functional versatility of macrophages. *Frontiers in Physiology* 14. 10.3389/fphys.2023.1128984.

(IF = 4.75, citations = 3)

G.K. contributed to conceptualization of the manuscript, literature research of the related publications, writing, graphic design, and revision of the article.

Krejčová, G., Morgantini, C., Zemanová, H., Lauschke, V., Kovářová, J., Kubásek, J., Nedbalová, P., Kamps-Hughes, N., Moos M., Aouadi, M., Doležal, T., Bajgar, A. (2023). Macrophage-derived insulin antagonist *ImpL2* induces lipoprotein mobilization upon bacterial infection. *The EMBO Journal*. 10.15252/emj.2023114086.

(IF = 13.78, citations = 0)

*G.K. was involved significantly in conceptualization of the manuscript and experimental design. She participated in sampling of *Drosophila* tissues, fruit fly data acquisition and analysis, figure preparation and writing of the manuscript. She measured and analyzed the data from 3D liver spheroids. She was responsible for writing the figure legends. G.K. contributed to data curation and analysis required during the revisions. She reviewed the submitted version.*

Krejčová, G., Saloň, I., Klimša, V., Ulbrich, P., Ayse, A., Bajgar, A., Štěpánek, F. (2023). Magnetic yeast glucan particles for antibody-free separation of viable macrophages from *Drosophila melanogaster*. Accepted in *ACS Biomaterials Science & Engineering*. 10.1021/acsbmaterials.3c01199

*G.K. participated in conceptualization of the manuscript, experimental design, tissue sampling, acquisition of the *Drosophila* data and their analysis. She prepared the figures and schemes concerning the *Drosophila* part of the manuscript. She was involved in conceiving the *Drosophila* experiments and data analysis required during the revision of the manuscript. She reviewed and validated the submitted version.*

Krejčová, G., Danielová, A., Sehadová, H., Dyčka, F., Kubásek, J., Moos, M., Bajgar, A. (2023). Macrophages play a nutritive role in post-metamorphic maturation in *Drosophila*.

Under review in *Development*.

G.K. participated significantly in conceptualization of the manuscript and design of the experiments. She was involved in preparation of the flies, sampling of the tissues, data acquisition and analysis, and writing the manuscript. She was responsible for preparation of the figures, writing the figure legends

and the supplementary file. She performed the experiments and analyzed the data during the revision process. She reviewed and validated the submitted version.

Bajgar, A., **Krejčová, G.**, Ruphuy, G., Sonntag, E., Štěpánek, F. (2023). Macrophage-specific delivery of atorvastatin by yeast glucan particles intervenes bactericidal function in *Drosophila*.

Under review in *Insect Molecular Biology*

G.K. participated in conceptualization of the manuscript and experimental design. She was involved in tissue sampling, acquisition and analysis of the Drosophila data, and writing the manuscript. She contributed to conceiving the experiments required during the manuscript revisions. She reviewed and validated the submitted manuscript.

Co-author agreement

Mgr. Adam Bajgar, Ph.D., the supervisor of this Ph.D. thesis and co-author of the above papers fully acknowledges the stated contribution of Mgr. Gabriela Krejčová to these publications and unpublished manuscripts.

Mgr. Adam Bajgar, Ph.D.

TABLE OF CONTENTS

Bibliographic description.....	ii
Declaration.....	iii
Financial support.....	iv
Acknowledgements.....	v
List of papers and manuscripts and author’s contribution.....	vi
PROLOGUE.....	1
1 INTRODUCTION.....	5
1.1 INTRODUCTION OVERVIEW.....	5
1.2 DISCOVERY OF MACROPHAGES.....	6
1.3 FUNCTIONAL VERSATILITY OF MACROPHAGES.....	7
1.3.1 SPECIAL FEATURES OF MACROPHAGES.....	7
1.3.2 ROLES IN FIGHTING THE PATHOGEN.....	9
1.3.3 NON-CANONICAL ROLES.....	12
1.3.3.1 RESOLUTION OF INFECTION AND WOUND HEALING.....	13
1.3.3.2 CLEARANCE OF SENESCENT AND APOPTOTIC CELLS.....	14
1.3.3.3 REBUILDING OF BODY PLAN.....	15
1.3.3.4 ERYTHROPHAGOCYTOSIS, ERYTHROPOIESIS AND IRON RECYCLING.....	16
1.3.3.5 STIMULATION OF THERMOGENESIS.....	17
1.3.3.6 CHOLESTEROL RECYCLING.....	18
1.3.3.7 DESTRUCTION OF TUMORS.....	19
1.3.3.8 MORPHOGENESIS AND ORGANOGENESIS.....	20
1.3.3.9 SURFACTANT HOMEOSTASIS.....	22
1.4 METABOLIC PLASTICITY OF MACROPHAGES.....	22
1.4.1 M1 METABOLIC POLARIZATION.....	22
1.4.2 M2 METABOLIC POLARIZATION.....	27
1.4.3 OTHER POLARIZATION STATES.....	28
1.5 INADEQUATE POLARIZATION UNDERLIES MANY DISEASES.....	29
1.6 MACROPHAGE PLASTICITY AS A LEGACY OF THEIR ORIGIN.....	32
1.7 <i>DROSOPHILA MELANOGASTER</i> FOR RESEARCH OF MACROPHAGE FUNCTIONS.....	34
1.7.1 IMMUNE SYSTEM OF <i>DROSOPHILA</i>	35
1.7.1.1 VARIOUS FUNCTIONS OF <i>DROSOPHILA</i> MACROPHAGES.....	39
1.7.1.1.1 ROLES IN FIGHTING THE PATHOGEN.....	39
1.7.1.1.2 WOUND HEALING AND REGENERATION IN <i>DROSOPHILA</i>	40

1.7.1.1.3 CLEARANCE OF <i>DROSOPHILA</i> APOPTOTIC CELLS AND REBUILDING OF BODY PLAN.....	42
1.7.1.1.4 ADJUSTMENT OF <i>DROSOPHILA</i> SYSTEMIC METABOLISM.....	44
1.7.1.1.5 DESTRUCTION OF <i>DROSOPHILA</i> TUMORS.....	46
1.7.1.1.6 MORPHOGENESIS AND ORGANOGENESIS IN <i>DROSOPHILA</i>	47
1.7.2 METABOLIC SETUP OF <i>DROSOPHILA</i> MACROPHAGES.....	48
2 AIMS OF THE THESIS.....	50
3 OUTLINE OF RESEARCH.....	51
4 PUBLISHED PAPERS.....	57
Chapter I	
<i>Drosophila</i> macrophages switch to aerobic glycolysis to mount effective antibacterial defense.....	57
Chapter II	
Molecular regulations of metabolism during immune response in insects.....	83
Chapter III	
Macrophage-derived insulin antagonist <i>ImpL2</i> induces lipoprotein mobilization.....	96
Chapter IV	
Liver macrophages regulate systemic metabolism through non-inflammatory factors.....	153
Chapter V	
Polarization of macrophages in insects: Opening gates for immuno-metabolic research.....	169
Chapter VI	
On the origin of the functional versatility of macrophages.....	190
Chapter VII	
Yeast glucan particles enable intracellular protein delivery in <i>Drosophila</i>	210
5 UNPUBLISHED PAPERS	
Chapter VIII	
Macrophages play a nutritive role in post-metamorphic maturation in <i>Drosophila</i>	228
Chapter XI	
Macrophage-specific delivery of atorvastatin by yeast glucan particles intervenes bactericidal function in <i>Drosophila</i>	273
Chapter X	
Magnetic yeast glucan particles for antibody-free separation of viable macrophages from <i>Drosophila melanogaster</i>	299
6 DISCUSSION & PERSPECTIVES.....	322
7 REFERENCES.....	329
8 CURRICULUM VITAE.....	360

“Disease is not the prerogative of man and the domestic animals, so it was quite natural to see if the lower animals, with very simple organizations, showed pathological phenomena, and if so, infection, cure and immunity could be observed among them.”

Elie Metchnikoff

In the past decades, macrophages have been perceived primarily as the guardians of our bodies against invading pathogens, and the majority of researchers have predominately studied their “canonical” functions connected with the elimination of invading pathogen, such as recognition of microbes, their phagocytosis and elimination, as well as the orchestration of the adaptive immune response by antigen presentation and cytokine production. However, in recent years it has become obvious that the functional versatility of macrophages goes far beyond their classical protective roles. It was already Elie Metchnikoff himself, the father of immunology, discoverer of macrophages and founder of the phagocytic theory, who studied these amoeba-like cells in the mesoglea of starfish larvae primarily for their nutritive functions in this primitive organism. Since their discovery in 1882, macrophages have been shown to play a surprisingly rich repertoire of functions that can be hardly found in other cells in the body. Thus, macrophages play a major role in the clearance of senescent and apoptotic cells, destruction of tumors and foreign materials, wound healing, reverse cholesterol transport, iron handling, morphogenesis, tissue regeneration, angiogenesis, regulation of tissue homeostasis and systemic metabolism. In addition, specialized subsets of macrophages reside in various tissues in which they perform highly specialized roles, such as catabolism of pulmonary surfactants in the lung, regulation of gut microbiota in the intestine or regulation of insulin sensitivity in adipose tissue.

The astonishing functional versatility of these cells is enabled by the plasticity of their cellular metabolism. Indeed, macrophages performing distinct functions differ from each other in the pathways preferentially utilized for energy production, or in metabolism of lipids and amino acids. By fine-tuning their metabolism, they are able to take up sufficient energy or synthesize the building blocks and various metabolic precursors essential for a given task. Although primarily adaptive, the metabolic polarization of macrophages in the wrong context or its dysregulation underlies the development of many pathological states. Indeed, pathological macrophage polarization has been connected with the development of atherosclerosis, type II diabetes, asthma, or rheumatoid arthritis.

Although the undoubtable importance of macrophages in the body of multicellular animals, knowledge of their function and role is mostly limited to mice and humans. The fruit fly, *Drosophila melanogaster*, has been extensively used as a model organism to study the functions of the innate immune system. Despite it has been instrumental in one of the greatest immunological discoveries, the discovery of *toll* in 1996, not much has been done on the “non-canonical” roles of macrophages in

insects. Surprisingly, a key aspect of macrophage polarization, the cellular metabolic plasticity, has not been properly investigated either, thus limiting the use of this model organism for research on macrophage functions, diseases connected to improper macrophage polarization, and immunometabolism in general. This apparent gap led us to investigate the metabolic program of activated macrophages. We have shown that bacteria-activated *Drosophila* macrophages undergo a metabolic switch toward aerobic glycolysis and that this adjustment is orchestrated by the transcription factor HIF1 α as in mammals (Krejčová *et al.*, 2019). Such metabolic reprogramming stems from suddenly increased demands for energy and metabolic precursors required to eliminate the pathogen. To meet the sudden nutritional demands, the cells secrete signaling factors that affect the metabolism of other organs and tissues in the body to either reduce nutrient consumption by non-immune tissues or induce nutrient mobilization from stores. In this way, the immune system secures privileged access to resources, and thus behaves selfishly in terms of inter-organ communication, as summarized in our review (Doležal *et al.*, 2019).

The high energy demands of activated phagocytes are indeed connected with changes in systemic metabolism. During sepsis, individuals experience a loss of metabolic stores, an increase in plasma glucose and lipoproteins, and a reduction in energy-intensive processes such as cognition, motility, growth, and reproduction. Since we consider activated macrophages as superior cells to many other tissues, we searched for potential macrophage-derived factors that would adjust systemic energy handling to supplement activated macrophages. We identified *Imaginal morphogenesis protein Late-2 (ImpL2)* to be produced by activated macrophages in response to HIF1 α activation, resulting in mobilization of lipoproteins in the fat body *via* silencing of insulin signaling in this tissue. The mobilized lipoproteins are engulfed by macrophages and exploited as a source of nutrients to effectively combat the pathogen. The circle closes. Thus, we have found a factor that translates the enhanced metabolic needs of activated macrophages to ensure nutrient redistribution upon infection *via* intervention of insulin signaling in the central metabolic organ. Our observations thus indicate that silencing of insulin signaling, perceived by most as a pathological state associated with obesity and diabetes, is originally an adaptive strategy to overcome the infection. In this work, we have also attempted to show that *Drosophila* research can still bring new paradigms and answers relevant to human health, despite the general public shakes their heads in wonder when they hear that one does research using some peculiar flies. Indeed, we have documented that the mechanism of energy redistribution during infection appears to be conserved between *Drosophila* and mammals as liver macrophages produce the mammalian IMPL2 homolog IGFBP7, which has the potential to induce mobilization of lipoproteins in hepatocytes (Krejčová *et al.*, 2023). We hope that this discovery will open the gates to immunometabolic studies in insects with relevance to mammalian models and humans, as summarized in our review paper (Bajgar, Krejčová and Doležal, 2021).

However, over the past years of my studies, I have learned that macrophages are not only our guardian angels, but their initially protective role can easily twist into an inferno (in my case, they

become my nightmare due to the three-year publishing process of the abovementioned *Impl2* paper). Macrophage behavior still remains enigmatic under certain circumstances. For reasons not fully understood, exposure of macrophages to excessive amounts of lipids also leads to their polarization. In a collaborative study, we discovered that secretion of IMPL2 by macrophages is not exclusively associated with bacterial infection. Interestingly, IGFBP7/IMPL2 is produced by mammalian liver macrophages/*Drosophila* macrophages in obese individuals and is responsible for chronic imbalances in lipid metabolism (Morgantini *et al.*, 2019).

This has led us to believe that many diseases associated with inadequate adjustment of macrophage metabolism should be tackled with targeted macrophage-specific treatments for their repolarization. To this end, a macrophage-specific delivery system is required. In an effort to develop such, we exploited glucan particles (GPs) derived from baker's yeast, which represent an attractive bait for the phagocytes. GPs can be loaded with various cargoes and modified with fluorescent tags on their surface (Bajgar *et al.*, 2019). *Via* these, small-molecule inhibitors of various metabolic pathways can also be delivered. Using this tool, we revealed that macrophage-specific delivery of atorvastatin, the most commonly prescribed statin, abrogates the mevalonate pathway in these cells, resulting in reduced survival of bacterial infection. These results thus imply the importance of the mevalonate pathway in pro-inflammatory macrophages and consequently serve as proof of concept that intervention of macrophage metabolic polarization can be used as a therapeutic approach in disease (Krejčová *et al.*, unpublished). Since GPs are exclusively engulfed by macrophages as the only professional phagocytes in *Drosophila*, we hypothesized that this specificity could be exploited to isolate a pure macrophage population from adult flies. For this purpose, we prepared GPs loaded with magnetic nanoparticles. Indeed, after systemic administration of these composites, a pure population of viable macrophages can be separated from other cells by a magnetic column (Krejčová *et al.*, accepted). Since this tool is based on the ancient mechanism of phagocytosis, it may represent a potent strategy for obtaining, influencing, or labeling macrophages even in non-model insect species, opening up possibilities not only for their research but also for boosting their immune system and thus improving resistance to various pathogens.

Besides their pro-inflammatory function, macrophages can also be tolerogenic, play a major role in tissue homeostasis, resolution of inflammation, clearance of cellular debris, healing and shaping various tissues and structures, and thus represent a potent morphogenic power. During *Drosophila* metamorphosis, adult structures are built *de novo* from islands of progenitor cells called imaginal discs, while many larval tissues undergo histolysis. An example of such an organ is the larval fat body. We have noticed that macrophages infiltrate and engulf the dying cells of the larval fat body in freshly emerged virgins and exhibit features of adipose tissue macrophages in obese individuals. Interestingly, they exhibit enhanced energy derivation, cellular respiration and nutrient processing, and produce lipoproteins and storage peptides that serve to support the development of newly formed adult structures. In this respect, their function is reminiscent of nutritional phagocytosis indicating that macrophages can adopt an unexpected role in lower animals. These results thus raise the question whether an analogous

macrophage role can also be observed during metamorphosis or embryogenesis of vertebrates, as well as during daily cell turnover and regeneration (Krejčová *et al.*, unpublished).

All these observations led us to wonder about their immense roles and about their origin. After years of macrophage research, we realized that nothing in biology makes sense except in the light of evolution, exactly as Theodosius Dobzhansky postulated. Therefore, we tried to trace the origin of their pro-inflammatory and anti-inflammatory roles in evolution in a Hypothesis and Theory article (Bajgar and Krejčová, 2023).

From the very first encounter, I fell for these spreading green glowing cells (thanks to the endogenously produced GFP label) of so many various shapes, sometimes reminiscent of a sunny side up egg, sometimes with a ballerina-like skirt, other times with spiky protrusions, crawling on trachea or infiltrating various tissues, building a “snowman” in starved flies, containing an astonishing number of phagolysosomes when offered bacterial fragments, looking completely foamy when exposed to lipids, and sometimes also multinucleated (despite the prevailing opinion in the field that they do not divide in adults) (Fig. 1). Hours and hours of staring at these cells and imaging have brought me much sheer joy, and I hope to be lucky enough to witness even stranger things done by these remarkable cells in the future, and perhaps in other insect organisms as well.

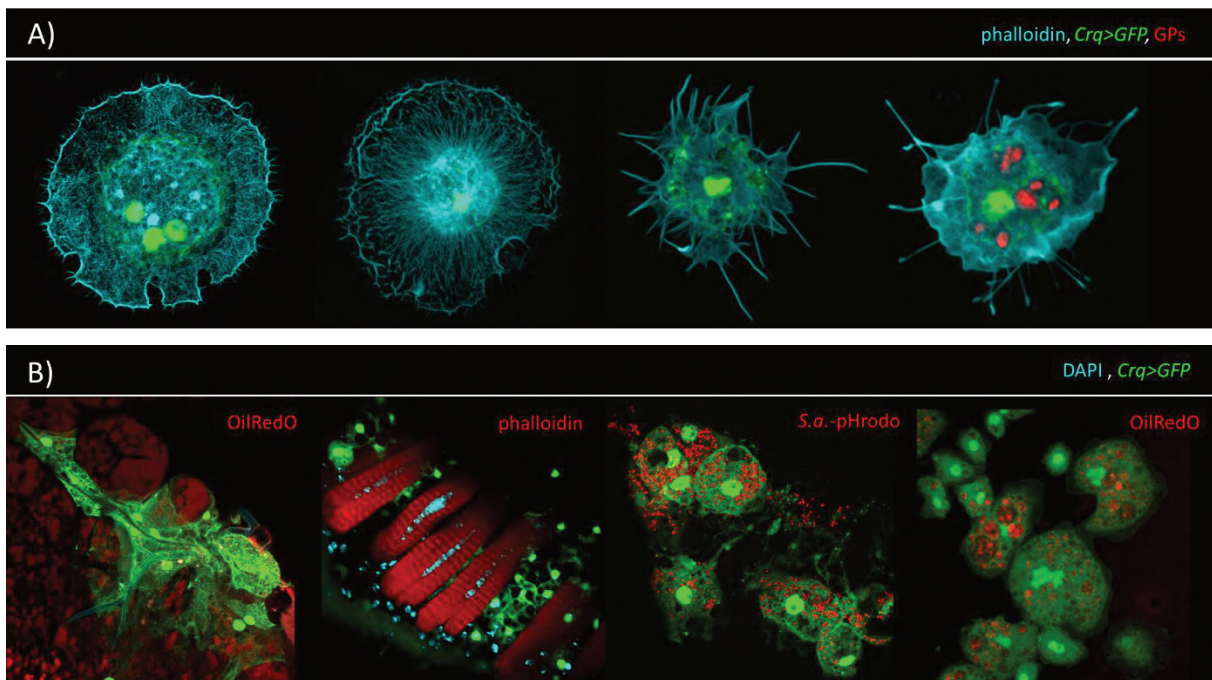


Figure 1: **Macrophages are immensely photogenic cells.** (A) Representative confocal images documenting various shapes of macrophages and (B) their ability to crawl along the trachea toward the fat body in adults, being intercalated between muscles in starved flies, their capability to perform many phagocytic events, and their foamy phenotype with multiple nuclei upon nutrient restriction (from left to right). *The images were captured by FluoView3000 Olympus Confocal Microscope at the Biology Centre CAS.*

1. INTRODUCTION

1.1 INTRODUCTION OVERVIEW

Macrophage-like cells exist in organisms from echinoderms to man, and it is often argued that macrophages represent the most versatile cells in the human body (Wood and Martin, 2017). Their functions range from protecting the host from invading pathogens to maintaining tissue homeostasis or regulating systemic metabolism. Although their function is primarily protective and thus beneficial to the host, dysregulation of macrophage polarization or polarization in an inappropriate context has been connected with the progression of many diseases such as diabetes, autoimmune diseases, rheumatoid arthritis or atherosclerosis (Wood and Martin, 2017). Macrophages thus represent a potential target for therapeutic intervention in these illnesses (Li *et al.*, 2023). However, understanding their adaptive behavior and comprehending the mechanisms behind the adoption of polarization states must precede the design of a therapeutic approach to their pathological functioning.

The objective of this thesis is to investigate the metabolic setup and the role of insect macrophages in the modulation of systemic metabolism in individuals under diverse physiological and pathological conditions utilizing the model organism *Drosophila melanogaster*.

The subsequent paragraphs present and summarize knowledge covering the unique features and characteristics of these cells that enable the broad palette of macrophage versatile roles (1.3. FUNCTIONAL VERSATILITY OF MAROPHAGES). As macrophage function is closely intertwined with cellular metabolism, the next chapters delve into the metabolic adjustments of pro- and anti-inflammatory vertebrate macrophages (1.4 METABOLIC PLASTICITY OF MACROPHAGES). Emphasizing the importance of understanding macrophage metabolic polarization, the following paragraphs are dedicated to the dysregulation of macrophage metabolic polarization as a basis for the development of many maladies and briefly touch on the need to develop macrophage-specific delivery tools to combat these diseases (1.5 INADEQUATE POLARIZATION UNDERLIES MANY DISEASES). The evolutionary origins of the diverse roles of macrophages are discussed in an effort to comprehend the counterintuitive pathological behavior of macrophages in chronic diseases and the triggers of dysregulated macrophage polarization (1.6 MACROPHAGE PLASTICITY AS A LEGACY OF THEIR ORIGIN). To provide the necessary background information for the interpretation of the results of this thesis, the subsequent chapters describe the immune system of *Drosophila melanogaster* (1.7.1 IMMUNE SYSTEM OF *DROSOPHILA*) and provide insights into the various macrophage roles described in *Drosophila* so far (1.7.1.1 VARIOUS FUNCTIONS OF *DROSOPHILA* MACROPHAGES). The final chapter of the introduction addresses the limited information on the energy handling and cellular metabolic pathways of activated *Drosophila* macrophages that enable them to perform their diverse roles, and highlights the need to investigate the metabolic adjustments of activated insect macrophages (1.7.2 METABOLIC SETUP OF *DROSOPHILA* MACROPHAGES).

1.2 DISCOVERY OF MACROPHAGES

Whilst most of the cells in human body are dedicated to quite specific roles, macrophages are capable of a plethora of distinct functions, exhibiting thus remarkable functional versatility. As a key component of innate immunity, macrophages serve as the front line of the immune system, actively patrolling the organism to defend against invading pathogens and other harmful entities. They are responsible for the recognition, phagocytosis and elimination of the threat and subsequent activation of the adaptive immune system via secretion of cytokines. While much effort has been invested in understanding their “canonical” roles, less attention has been dedicated to comprehend their “non-canonical” functions such as maintenance of tissue homeostasis or regulation of the systemic metabolism despite it was the discoverer of macrophages himself, who extensively studied these cells as a harmonizing force of multicellular organisms.

Elie Metchnikoff believed that multicellular organisms are intrinsically disharmonious entities as different cell lineages struggle and compete between each other for nutrients (Sengoopta, 1993). Therefore, he was asking himself a question of what is the harmonizing force that preserves integrity of an organism. While studying embryological development of simple animals without gut, he came to conviction that the wandering cells originated from mesoderm engulf other cells and digest it *via* intracellular digestion (Teti, Biondo and Beninati, 2016). By this means, these cells not only nourish themselves but also transport these nutrients to other cells and harmonize the organism by removing the extracellular debris both during embryogenesis and during senescence (Tauber, 2003). Since that time, he began to image that similar cells may have a protective role in the organism against foreign invaders (Fig. 2).

Elie Metchnikoff conducted his famous experiment in Messina in December 1882, when he introduced a rose thorn to the body of transparent starfish larva and left it there overnight. Early the next morning he came back and witnessed with immense joy that the thorn has been surrounded by specialized cells, phagocytes. Thus, he formed the theory of phagocytosis and discovered the innate immune defense (Teti, Biondo and Beninati, 2016). In 1908, he was awarded Nobel Prize in Physiology or Medicine “in recognition of their work on immunity” together with Paul Ehrlich, the discoverer of humoral immune response.

Although Metchnikoff was the one to fully appreciate the potential of these cells, many naturalists



Figure 2: Metchnikoff’s drawing of macrophages reacting to injury in a Triton embryo. Retrieved from *Molecular Cell Biology* (Tauber, 2003).

before him have witnessed that some cells of an organism contain internalized substances. In 1847, Albert von Kölliker observed cells in spleen that contained particles and later, Preyer noticed the engulfment of erythrocytes by cells in spleen (Yona and Gordon, 2015). However, it did not occur to them that this phenomenon may be underlying the engulfment of senescent cells in an organism and also the defense mechanism. When Metchnikoff started to develop on this astonishing finding, many pathologists believed that phagocytes represent malicious cells since they provide suitable environment for multiplication of microbes and that they transport the bacteria throughout the body to the lymph nodes (Klebs, 1872; Koch, 1878). At that time, inflammation has been perceived as a pathological process and thus Metchnikoff's view of inflammation as beneficial to the host was in contrast to the prevailing opinion (Teti, Biondo and Beninati, 2016). Despite numerous confrontations and doubts about Metchnikoff's discoveries and opinions across the 19th century, it becomes more and more obvious that he was a true pioneer in understanding of multiple eminent aspects of life that can be summarized as homeostasis and his work remains inspirational up to now.

1.3 FUNCTIONAL VERSATILITY OF MACROPHAGES

1.3.1 SPECIAL FEATURES OF MACROPHAGES

Macrophages are endowed with certain unique features which enable them to stand for a variety of roles and which distinguish them from other cells in the body. They are equipped with numerous molecules for recognition of various chemoattractants, i.e. chemical signals derived from compromised cells of the organism, pathogens or other immune cells. Chemokine receptors, a family of G protein-coupled receptors (GPCRs), which identify chemokines, small chemotactic cytokines, are an example of chemoattractant receptors. These receptors include CCR1, CCR2, CCR5, CXCR1, CXCR2, or CX3CR1 (Sokol and Luster, 2015). Formyl peptide receptors are GPCRs that recognize formylated peptides derived from bacteria or mitochondria. Several complement receptors recognize the components of the complement and mediate the chemoattraction of macrophages to areas where complement activation has occurred, such as during inflammation or immune responses. Folate receptor, adenosine receptor, purinergic receptors, leukotriene receptors or sphingosine-1-phosphate receptors are another example of chemoattractant receptors (Kim, Song and Lee, 2020; O'Callaghan *et al.*, 2021). Whilst macrophages reside in a tissue in a quiescent state for most of time, chemoattractant recognition leads to activation of specific intracellular signaling cascades, such as PKC, PI3K-Akt, MAPK-ERK, AP, or JAK-STAT, and activation of transcriptional programs resulting in increased cytoskeleton reorganization allowing for macrophage migration against concentration gradient of the chemoattractant (Wang *et al.*, 2019).

As opposed to most cell types in the mammalian organism, macrophages display active migration, namely amoeboid and mesenchymal. Amoeboid migration is a rapid movement driven by an actin-rich pseudopod at the leading edge, hydrostatically generated blebs, and a highly contractile

uropod at the trailing edge. This movement is characterized by weak or absent adhesion to the substrate and low-level proteolysis of the extracellular matrix (ECM). In contrast, mesenchymal movement is characterized by cell adhesion to the substrate *via* integrins, cadherins, or fibronectins and requires enzymatic disruption of binding to the ECM (Pizzagalli *et al.*, 2022).

Another specific features of macrophages is the possession of evolutionary ancient pattern recognition receptors (PRRs) such as toll-like receptor (TLR) family, scavenger receptors, c-type lectins, or cytoplasmic nucleotide-binding oligomerization domain-containing proteins (NOD) like receptors, which recognize pathogen-associated molecular patterns (PAMPs) or damage-associated molecular patterns (DAMPs) (Mogensen, 2009; Amarante-Mendes *et al.*, 2018). Antigen binding to a PRR activates specific immune-related cascades, such as NFκB, ERK, JNK, or p38, which activate downstream signaling cascades that allow the macrophage to cope with the new situation, e.g. by formation of membrane invaginations to engulf the particle/cell or by secretion of various cytokines and signaling factors to inform other tissues of the body about nature of the new conditions (Amarante-Mendes *et al.*, 2018) (Fig. 3).

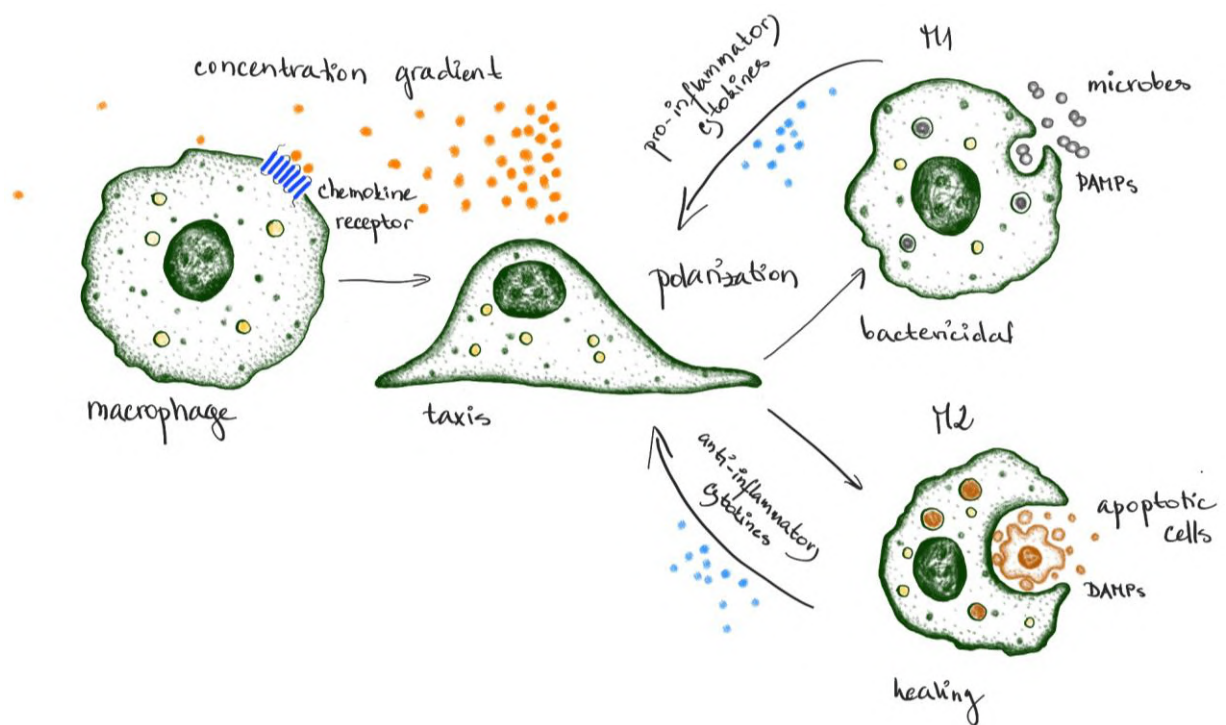


Figure 3: Schematic representation of the unique macrophage features. The picture was drawn in PENUP.

1.3.2 ROLES IN FIGHTING THE PATHOGEN

Macrophages are best known for their role in combating pathogens. Although the particular steps in fight against intruders can vary substantially between types of pathogen or context of the response, general response of macrophages to microbe invasion can be described as follows.

Invading pathogens release multiple secondary metabolites that are recognized by macrophages as chemoattractants, such as N-formylmethionine peptides, since bacteria transcribe proteins starting with N-formylmethionine whereas eukaryotic cells mostly initiate protein synthesis with non-formylated methionine. N-formylmethionine-leucyl-phenylalanine (fMLF) is a soluble element of low molecular weight released by both gram negative and gram positive bacteria and recognized by macrophages *via* Formyl peptide receptor 1 (FPR1) (Harris, 1954; Schiffmann, Corcoran and Wahl, 1975). Another example of how macrophages distinguish bacteria from eukaryotic cells is *via* recognition of unmethylated CpG dinucleotide motifs on bacterial DNA by TLR9 (Scheule, 2000; Krieg, 2002). Components of bacterial cell wall represent another group of potent antigens. Lipoteichoic acid is a component of the cell wall of Gram positive bacteria recognized by TLR2, while lipopolysaccharide (LPS) present in the wall of Gram negative bacteria is recognized by TLR4 (Schröder *et al.*, 2003). Peptidoglycans are detected by NOD-like receptors and other PRRs. Some bacteria can also produce certain chemokine-like molecules such as chemokine-like protein A released by *Staphylococcus aureus*, which interact with macrophage chemokine receptors (Yung, Parenti and Murphy, 2011).

Recognition of the pathogen subsequently leads to activation of signaling pathways allowing for phagocytosis of the microbe. Activation of TLRs results in induction of downstream signaling cascade through adapter molecules such as myeloid differentiation primary response 88 (MyD88) leading to activation of transcription factors such as NF- κ B, resulting in the induction of gene expression (Mogensen, 2009). Recognition of the pathogen is immediately followed by cytoskeletal rearrangements and membrane remodeling so the macrophage can extend around the bacteria. Activation of Rho family GTPases, such as Rac1 and Cdc42, leads to actin polymerization and the formation of membrane protrusions called pseudopodia. Activation of PI3K is another crucial step in phagocytosis since it generates phosphatidylinositol (3,4,5)-trisphosphate (PIP3) at the site of the formation of the phagocytic cup, leading to the recruitment and activation of downstream effector proteins. Once the pathogen is internalized within the membrane-bound vesicle called phagosome, the pathogen must be neutralized. Activation of phospholipase C leads to the production of diacylglycerol and inositol trisphosphate, which subsequently triggers the release of calcium ions important for phagosome maturation. Next, the membrane of the phagosome fuses with the lysosome, together creating a phagolysosome. Lysosomes are organelles containing a cocktail of various enzymes such as acidic nucleases, lipases, sulfatases, phosphatases or glycosidases, which cleave and degrade the engulfed bacteria. Since the optimum pH of these enzymes is quite low, the phagolysosome is acidified by proton pumps on its membrane, which actively transport protons into the compartment. NADPH oxidase NOX2 bound in the phagolysosome

membrane and inducible nitric oxide synthase 2 (NOS2) further contribute to pathogen neutralization as they pump reactive oxygen species (ROS) and reactive nitrogen species (RNS), respectively into the phagolysosome (Rosales and Uribe-Querol, 2017). Such rapid and intense production of ROS is called oxidative burst (Slauch, 2011).

Interestingly, a macrophage can internalize its entire cell membrane in 20 min, but recycle the membrane components equally rapidly to maintain homeostasis (Muller, Steinman and Cohn, 1983). Less is known about recycling of the cleaved pathogen compounds either for use by the macrophage itself or by other cells although it is to be anticipated to avoid nutrient waste. It has been reported that once the phagolysosome contents have been neutralized, a residual body, also called telolysosome, that contains the indigestible waste products from the phagolysosome, is formed and expelled by the cell either via exocytosis or the waste products turn into lipofuscin granules (Hartenstein and Martinez, 2019). Residual bodies can be subsequently engulfed by other immune cells or cleared by the lymphatic system or liver (Kajihara, Totović and Gedigk, 1975; Hendriks and Eestermans, 1986).

Since macrophages belong to antigen presenting cells, recognition of bacteria also leads to synthesis of major histocompatibility complex class II (MHCII), which binds antigenic fragments of the digested bacteria. This complex is subsequently transported to the macrophage membrane and presented to CD4⁺ helper T cells, which detect it *via* specific T cell receptors (Fig. 4). Once activated, T cells secrete pro-inflammatory cytokines, differentiate into various T cell subsets and provide positive feedback loop to macrophages, leading to amplification of the immune response (Mantegazza *et al.*, 2013).

Recognition of bacteria is also connected with secretion of pro-inflammatory cytokines, various signaling molecules and anti-microbial compounds by activated macrophages. Cathelicidins, such as LL-37, are family of cationic antimicrobial peptides primarily stored in macrophage lysosomes. They bind and disrupt negatively charged microbial membranes, but also have immunomodulatory effects since they can enhance chemotaxis, modulate cytokine production, or promote wound healing (Agier, Efenberger and Brzezińska-Błaszczuk, 2015). Defensins are also responsible for lysis of the bacterial wall and neutralization of bacterial toxins (Lichtenstein, 1991). Another compound that disrupts bacterial cell wall is lysozyme. Lysozyme is an antimicrobial enzyme present in macrophage granules and it hydrolyzes the beta linkages between N-acetylmuramic acid and N-acetyl-D-glucosamine residues in a bacterial peptidoglycan (Ragland and Criss, 2017). Peroxidases further contribute to the aforementioned macrophage oxidative burst. Secreted peroxidases, such as myeloperoxidase, generate ROS and RNS, leading to protein oxidation and nitration in the engulfed pathogen (Frangie and Daher, 2022). Another approach how to destroy the invading bacteria is to sequester iron, e.g. by lipocalin-2, since iron represents an essential nutrient for bacterial growth, thereby limiting replication of the pathogen (Xiao, Yeoh and Vijay-Kumar, 2017). Macrophages also secrete opsonins, small molecules that bind to the microbe and thus facilitate the recognition and enhance phagocytosis of the pathogen. Although C reactive protein, serum amyloid A, and complement proteins are mainly produced by

hepatocytes, liver macrophages have been shown to synthesize these proteins as well (Acharya *et al.*, 2020).

An alternate approach of pathogen neutralization is the formation of macrophage extracellular traps (METs). METs are extracellular web-like structures, which compose of double-stranded DNA, histones, elastase, and myeloperoxidase. Some studies also reported the presence of lysozyme and matrix metalloproteases (MMPs) (Liu *et al.*, 2014; King *et al.*, 2015, 2017). METs serve for trapping, immobilizing and killing the pathogen. Although the mechanism of its production is not yet well known, researchers anticipate that it will resemble formation of neutrophil ETs and include chromatin decondensation and DNA release as a result of programmed cell death either *via* apoptosis or NETosis (Rada, 2019).

Nonetheless, after engulfment, elimination of the pathogen and activation of the adaptive immune system, the macrophage duties are not fulfilled yet since the tissue homeostasis needs to be restored.

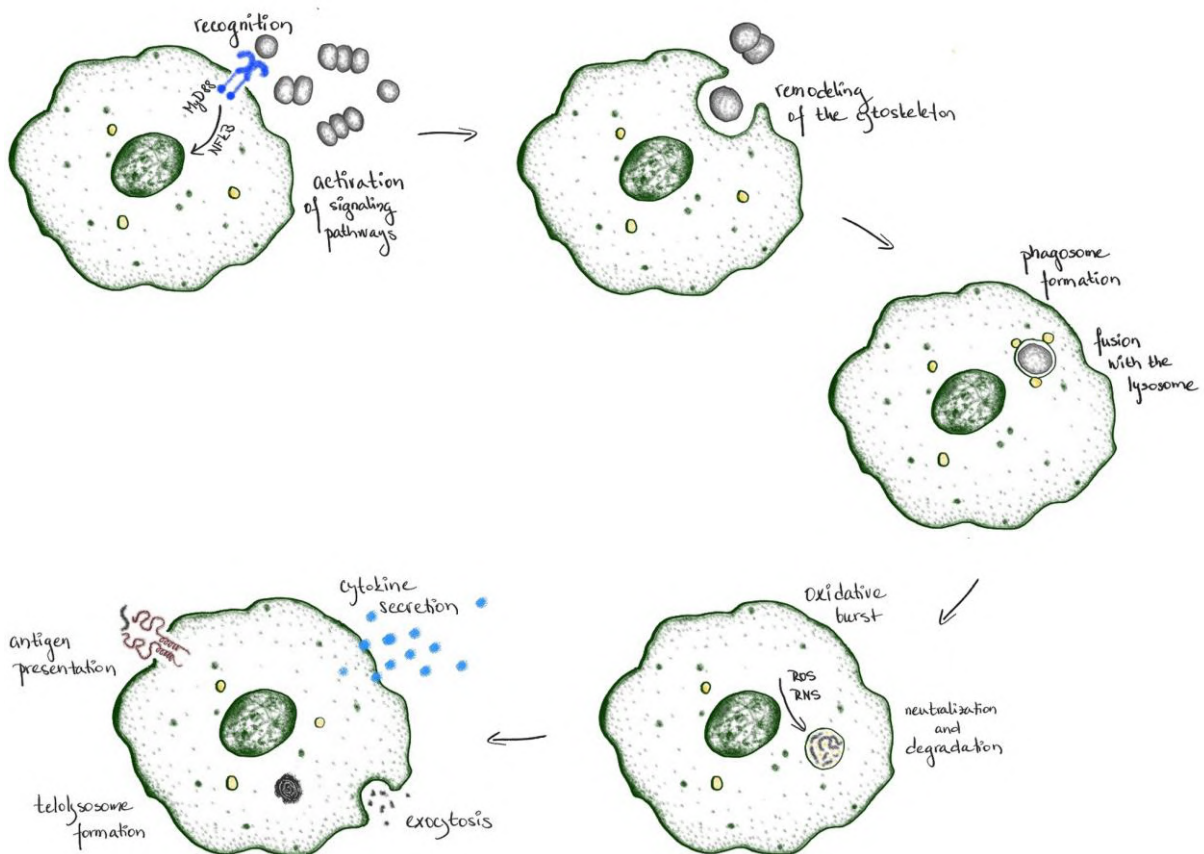


Figure 4: Schematic representation of the process of pathogen elimination by a macrophage. The picture was drawn in PENUP.

1.3.3 NON-CANONICAL ROLES

While much effort has been invested in studying the roles of macrophages in host defense, it has not been generally appreciated that macrophage activities extend far beyond their “immunological” roles. Expression of a broad spectrum of surface and intracellular receptors together with their capability to enter and crawl within virtually all tissues predisposes them to act as a dispersed organ system that is able to respond to and regulate every other system in the animal body. The macrophages maintain tissue and systemic homeostasis through mechanisms similar to those exploited during infection to detect pathogens and trigger inflammation. Tissue resident macrophages display a striking repertoire of functions during normal physiological conditions. Each population substantially differs in their gene expression profile, which is related to the specific tissue environment and is largely determined by distinct “chromatin landscape” (Gautier *et al.*, 2012; Lavin *et al.*, 2014). Interestingly, even fully differentiated tissue resident macrophages retain the ability to undergo reprogramming and alter their expression profile and thus their function when exposed to a new stimulus (Lavin *et al.*, 2014). Newcomers to the field of tissue resident macrophages are often surprised to learn that various tissues contain a significant proportion of macrophage even in the healthy state. For example, tissue resident macrophages of liver, denoted as Kupffer cells, account for approximately 15% of the total liver cell population (Sitia *et al.*, 2011). Since the functions of tissue resident macrophages are so diverse, the following paragraphs are not comprehensive and their aim is only to illustrate the immense macrophage functional versatility (Fig. 5).

To understand where the macrophages in various tissues of the body came from, I will briefly summarize their origin in a mammalian organism. Primitive embryonic hematopoiesis starts in extraembryonic yolk sack of mice at embryonic day 7.0, generating erythro-myeloid progenitors, from which the primitive macrophages as well as primitive erythrocytes and granulocytes differentiate at embryonic day 8.5. Subsequently, these cells migrate and colonize various developing tissues such as brain, where they will give rise to future microglia. They also seed fetal liver where they later expand rapidly to generate the pool of monocyte-derived macrophages. These cells also invade numerous peripheral tissues e.g. lung, heart, peritoneum, gut, heart, kidney or skin. In these tissues the monocytes differentiate into macrophages. Eventually, the fetal monocyte-derived macrophages will be replaced by monocytes generated in bone marrow around embryonic day 17.0 except for macrophages in lung and liver, which maintain the capacity to self-renew (Hoeffel and Ginhoux, 2015). Contrary to that, almost no proliferation of yolk sack macrophages and fetal monocytes has been observed in adults as it slowly declines during the course of development (Hoeffel *et al.*, 2015). The level of proliferation of bone marrow-derived tissue resident macrophages differs between tissues. While gut macrophages display barely any proliferative activity, heart macrophages maintain significant proliferative potential (Bain *et al.*, 2014; Molawi *et al.*, 2014). Nonetheless, the rate of proliferation can be influenced by local

conditions such as the presence of infection or increased level of certain signaling factors (Jenkins *et al.*, 2011).

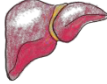



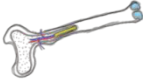
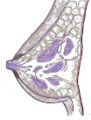

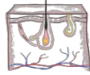
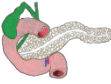

tissue	specific macrophage name	function
 liver	Kupffer cell	clearance of debris from blood liver tissue regeneration liver development?
 brain	microglial cell	neuronal survival connectivity repair after injury
 kidney	-	ductal development
 intestine	crypt macrophage	immune surveillance
 bone	bone marrow macrophage osteoclast	erythropoiesis bone remodeling providing a stem cell niche
 mammary gland	osteomacs	pro-anabolic support of osteoblasts
 ovary	-	branching morphogenesis ductal development
 epidermis	-	ovulation steroid hormone production
 pancreas	Langerhans cell	? immune surveillance
 testis	-	islet development
		steroid hormone production Leydig cell development?

Figure 5: Tissue resident macrophages and their roles. The figure was created in PENUP.

1.3.3.1 RESOLUTION OF INFECTION AND WOUND HEALING

While the previous paragraphs describe the roles of macrophages upon pathogen invasion, their roles are not fulfilled even after the microbes are cleared. Once the invaders are destroyed, it is essential to regenerate the damaged tissue and re-establish the lost homeostasis.

To do so, the macrophages shift their function toward anti-inflammatory phenotype and participate in resolution of inflammation. They remove cellular debris, dead cells, remnants of the pathogen and secrete MMPs, enzymes that degrade the disrupted ECM to create space for a new tissue

growth (Viola *et al.*, 2019). While collagenases (e.g., MMP-1, MMP-8, MMP-13) specifically degrade collagen, gelatinases (e.g., MMP-2, MMP-9) target gelatin, a denatured form of collagen (Klein and Bischoff, 2011). Simultaneously, the affected tissue must be regenerated and therefore the macrophages accelerate angiogenesis to form new blood supplies in order to deliver sufficient amount of nutrients and oxygen. Macrophages instruct endothelial cells to proliferate, migrate and form new blood vessels *via* secretion of various factors, e.g. vascular endothelial growth factor, fibroblast growth factor, interleukin-8 (IL-8), tumor necrosis factor α (TNF- α) or angiopoietin-1 (Hong and Tian, 2020). By positioning themselves nearby newly forming blood vessels, they aid their stabilization and fusion (Fantin *et al.*, 2010; Ogle *et al.*, 2016) *Via* secretion of platelet-derived growth factor, they also stimulate the recruitment and proliferation of pericytes and smooth muscle cells, which play important roles in stabilizing and supporting newly formed blood vessels (Corliss *et al.*, 2016).

Macrophages also mediate activation of fibroblasts, keratinocytes and endothelial cells to restore the dermis, epidermis and vasculature, respectively, *via* secretion of cytokines such as transforming growth factor beta (Ueshima *et al.*, 2019). Activated fibroblasts then produce collagen, fibronectin and elastin, major components of ECM and contribute to formation of a dense scar tissue (Kendall and Feghali-Bostwick, 2014). Macrophages also trigger the differentiation of myofibroblasts, which pull the edges of the wound closer together and thus facilitate contraction of the wound and its regeneration (Wynn and Barron, 2010). In line with that, studies on wounded mice have shown that macrophage depletion results in delayed re-epithelialization, reduced collagen formation and impaired angiogenesis (Goren *et al.*, 2009; Mirza, DiPietro and Koh, 2009).

1.3.3.2 CLEARANCE OF SENESCENT AND APOPTOTIC CELLS

Macrophage clearance of dead host cells is not restricted only to resolution of infection. Billions of senescent or apoptotic cells die and are replaced in our bodies every day. This burden of dying cells must be recognized, engulfed and eliminated by professional phagocytes, which is a selective and immunologically silent process denoted as efferocytosis (from *effero*, ‘to carry to the grave’, ‘to bury’) (Korns *et al.*, 2011).

Once apoptotic pathway is triggered, the dying cell secretes various chemoattractants, which attract and guide motile macrophages to their location and thus act as “find me” signals. Examples of such “find me” signals are lysophosphatidylcholine, CX3CL1/fractalkine, and extracellular nucleotides such as ATP (Pontejo and Murphy, 2022). Since originated by bacterial endosymbiosis, mitochondrial genome also codes for N-formyl-methionine proteins, so when N-formyl-methionyl-containing peptides are released from dead or dying cells, it leads to macrophage recruitment to the damaged cells and their engulfment (Carp, 1982). Certain lipids can also act as “find me” signals, such as bioactive molecule sphingosine-1-phosphate, which is released by apoptotic cells, and it is recognized by specific GPCRs (Pontejo and Murphy, 2022).

Another class of molecules important for the machinery of engulfment of dying cells has been denoted as “eat me” signals, which are surface-bound molecules that promote recognition by the phagocytes. Upon programmed cell death, the dying cell undergoes structural and biochemical changes that expose specific molecules on its surface (Li, 2012). In healthy cells, phosphatidylserine is restricted to the inner side of the plasma membrane but its concentration rises 300-fold on the outside leaflet of dying cells and thus acts as a key “eat me” signal recognized by phosphatidylserine receptors on macrophages (Borisenko *et al.*, 2003). Another examples of “eat me” signals are calreticulin and oxidized phospholipids (Li, 2012). Macrophages can also detect dead cells *via* scavenger receptors, which bind modified lipids and proteins such as oxidized or acetylated LDLs and other various motifs on the surface of dying cells (Li, 2012).

The ligand/receptor interaction subsequently triggers signaling cascades resulting in cytoskeletal rearrangements allowing for internalization of the dying host cell and secretion of various anti-inflammatory factors to promote tissue regeneration, e.g. TGF- β , IL-10, and prostaglandin E2 (Li, 2012). Once the apoptotic cells are degraded within the phagolysosome, it would be reasonable to recycle or utilize some of the components by the phagocyte to avoid nutrient wasting. Nonetheless, studies targeting this issue are rather scarce.

1.3.3.3 REBUILDING OF BODY PLAN

Extreme examples of apoptosis are events of re-building of the body plan such as during the metamorphosis of amphibians or regeneration of various body parts in certain animal species. Salamanders display a remarkable ability to regenerate complex body structures such as tail, limbs, spinal cord or retina (Tanaka and Reddien, 2011).

A study conducted on axolotl aquatic salamander has demonstrated that macrophages are absolutely crucial for a regeneration of the limb (Godwin, Pinto and Rosenthal, 2013). Macrophages infiltrate the regenerating limb blastema already the first day post amputation and are located immediately around and within the developing wound epithelium. Their numbers peak between day 4 and 6. Depletion of macrophages by clodrosome, a commonly used tool for macrophage ablation consisting of liposome-encapsulated clodronate, one day prior to the amputation leads to altered expression of cytokines, chemokines, and key regenerative genes in the regenerating tissue such as TGF- β 1, IL-1 β , MMP3, MMP9, or fibronectin. Unexpectedly, depletion of the macrophages also leads to decreased expression of wound epithelial marker WE3, which suggests that the wound epithelium is not functional. In addition, BrdU incorporation has not been detected in the underlying mesenchyme and the mesenchymal progenitors do not undergo the activation as suggested by staining for the classic blastemal progenitor marker 22/18. These data thus suggest that macrophage depletion disrupts pathways important for the progression from wound healing to regeneration within the first 6 days after limb amputation, which results in complete blockade of limb regeneration. Although wound closure still

happens, the limb does not regenerate. Instead, fibrotic stumps form and contain permanent scar tissue. Although the macrophage numbers are restored within two weeks after the clodrosome injection, the stumps persist and no blastema is formed. In concordance to decreased expression levels of MMP9 and MMP3 measured in the regenerating tissue after macrophage depletion, the tissue displays extensive collagen deposition and fibrosis. The authors have also examined the role of macrophages in later stages of the limb regeneration. For this purpose, the clodrosome has been injected at day 10 to day 13 after the amputation. This treatment has not blocked the regeneration entirely, but delayed it significantly (Godwin, Pinto and Rosenthal, 2013). Another study has shown that TGF- β is essential for successful axolotl limb regeneration (Lévesque *et al.*, 2007). Therefore, this work brings another piece of indication of the importance of macrophages for the regenerative processes.

Similarly to amphibians, macrophages are required for digit tip regeneration in mice. Even these authors working on mammalian models have shown that after ablation of macrophages, bone histolysis does not occur, wound re-epithelialization is inhibited and the blastema does not form, thus suggesting a conserved principle (Simkin *et al.*, 2017).

Another example of massive changes in the body shape is resorption of the tadpole tail during metamorphosis of amphibians, which is triggered by thyroid hormone (Fu, Wen and Shi, 2018). Interestingly, the tail of *Xenopus tropicalis* is resorbed within three days and given that it is twice as long as the trunk of the frog, it represents an immense mass of tissue that must be somehow degraded. Electron microscopy has revealed that first, longitudinal clefts appear between myofibrils of the tail and the sarcoplasmic reticulum dilates. Then, the muscle fibers undergo fragmentation into many apoptotic bodies, which are engulfed by the macrophages as evidenced by the presence of inclusion bodies, which differ in size, electron opacity, and content of enzymes in the macrophage cytosol (Nakai, Nakajima and Yaoita, 2017). Some of the inclusion bodies also contain myelin figures, also known as multilamellar bodies or patches of loose fibrillar elements (Weber, 1964).

1.3.3.4 ERYTHROPHAGOCYTOSIS, ERYTHROPOIESIS AND IRON RECYCLING

Approximately 2 to 3 million erythrocytes must be cleared from the circulation every second since their average life span is only about 120 days (Kaufman, 2017). This equates to about 200 billion red blood cells every day, which represents a vast amount. Notably, macrophages are not only responsible for their removal but also for iron recycling since dietary availability of iron is usually very low (Ganz, 2012). Strikingly, iron flux from macrophages exceeds iron adsorption through diet and from iron stored in hepatocytes in humans. Senescent or damaged erythrocytes are engulfed mainly by red pulp macrophages in spleen, liver resident and bone marrow macrophages, which not only degrade the no longer necessary cells but also majorly contribute to iron recycling (Ganz, 2012). Studies on rats have shown that macrophages in liver engulf about one erythrocyte per day (Kondo *et al.*, 1988). Upon erythrocyte efferocytosis and formation of the phagolysosome, the erythrocyte is subjected to

degradation by ROS and various enzymes, resulting in delamination of hemoglobin. Next, heme is degraded *via* heme oxygenase, transported from the phagolysosome to the cytoplasm *via* natural resistance-associated macrophage protein (NRAMP) transporters (Ganz, 2012). Iron travels through the cytoplasm with the participation of chaperons to avoid the chemical reactivity and toxicity of iron. Subsequently, ferrous iron is exported from the cytoplasm by plasma membrane ferroportin and loaded onto its plasma carrier transferrin and eventually it is supplied to erythrocyte precursors in the bone marrow for synthesis of hemoglobin and it is used also for synthesis of other iron-containing proteins (Ganz, 2012). In addition, macrophages engulf nuclei expelled during the final step of erythrocyte differentiation on the account of exposure of phosphatidylserine on the surface of the membrane of the nucleus (de Back *et al.*, 2014). Indeed, genetic knockout of DNase II, a nuclease expressed by macrophages, results in the macrophage inability to degrade the ejected nuclei, leading to blockage of erythropoiesis and lethal anaemia (Kawane *et al.*, 2001).

An intriguing notion has been reported decades ago that macrophages in spleen are able to remove intracellular inclusions in red blood cells, presumably caused by oxidative damage, while leaving the erythrocytes undamaged and intact (Crosby and Benjamin, 1957; Schnitzer *et al.*, 1972). It has been shown that red blood cells of patients who underwent splenectomy or who have non-functional spleen display a retention of a variety of intracellular inclusions, such as Howell-jolly bodies (inclusions of nuclear chromatin remnants), Heinz bodies (inclusions of denatured hemoglobin caused by oxidative damage) or Pappenheimer bodies (inclusion bodies formed by phagosomes that have been engulfing excessive amounts of iron) (Wilkins and Wright, 2000).

In terms of iron handling, macrophages do not only have trophic function but also contribute to pathogen elimination by depriving them of iron. Increased levels of inflammatory cytokines such as IL-6 result in synthesis of hepcidin, which is a hormone inducing iron sequestration by macrophages (Nemeth *et al.*, 2004). The bond between hepcidin and ferroportin in macrophage membrane leads to its endocytosis and subsequent degradation, which traps iron in cytoplasmic ferritin. These events result in hypoferremia and anemia of inflammation. Decrease in iron availability in the affected tissue limits pathogen growth. In addition, NRAMP transporters of divalent ions decrease the availability of iron to the engulfed bacteria, preventing their escape from the phagolysosome (Nemeth *et al.*, 2004).

1.3.3.5 STIMULATION OF THERMOGENESIS

Brown adipose tissue is known for its ability to generate heat. Despite it has been initially considered to be present only in mammalian neonates and small mammalian hibernators, subsequent studies showed that it is present even in adults, dispersed in the supraclavicular, para-aortic and suprarenal regions (Cypess *et al.*, 2009; van Marken Lichtenbelt *et al.*, 2009). The adipocytes of the brown adipose tissue contain multilocular lipid droplets and possess a large number of mitochondria, which gives it a characteristic brownish appearance (Sell, Deshaies and Richard, 2004). The main role

of brown adipose tissue is thermogenesis and uncoupling protein 1 plays an indispensable role in this process since it uncouples electron transport in mitochondrial membrane to promote heat instead of ATP generation (Sell, Deshaies and Richard, 2004). Despite uncoupling of mitochondrial metabolism from ATP generation is a cell-autonomous process of the adipocytes, macrophages have been shown to play an unexpected role in this process.

Macrophages have been shown to be crucial for adaptation to cold exposure. A study published in *Nature* in 2011 reported that in response to IL-4/IL-13, macrophages polarize towards anti-inflammatory phenotype and increase the expression of tyrosine hydroxylase, a key enzyme in production of catecholamines (van Marken Lichtenbelt *et al.*, 2009). Hence, the macrophages secrete norepinephrine, which in turn induces thermogenic gene expression in brown adipocytes and lipolysis in white adipose tissue. Indeed, mice lacking the anti-inflammatory macrophages exhibit drop in core body temperature and lack of upregulated expression of thermogenic and beta oxidation genes when exposed to cold conditions (van Marken Lichtenbelt *et al.*, 2009). In addition, they remove damaged mitochondria ejected from the brown adipocytes, thus ensuring optimal thermogenesis (Rosina *et al.*, 2022).

Beige fat cells have been found to be dispersed in clusters throughout white adipose tissue in mice (Wu *et al.*, 2012). Their functions comprise those of both white and brown adipocytes as they are able to switch from storage of energy to generation of heat upon cold exposure (Kajimura, Spiegelman and Seale, 2015). It has been documented that acute cold exposure leads to an adaptive increase of cholinergic macrophages in the beige adipose tissue, which secrete thermogenesis-promoting acetylcholine that activates neighboring beige adipocytes within the white adipose tissue (Knights *et al.*, 2021). Another study reported that macrophage-secreted factor Slit3 promotes cold adaptation by stimulating sympathetic innervation, norepinephrine release and thermogenesis in mice. Concordantly, overexpression of Slit3 in anti-inflammatory macrophages promotes adipose tissue beiging and thermogenesis, while Slit3 deficient mice are cold-intolerant and tend to gain weight (Y.-N. Wang *et al.*, 2021). Macrophages thus play major roles in regulation of systemic metabolism and energy expenditure.

1.3.3.6 CHOLESTEROL RECYCLING

The previous chapter describing the role of macrophages in thermogenesis is a harbinger of their role in the regulation of metabolism and energy handling. Similar mechanisms that macrophages use to protect the body from pathogens make them key players in lipid metabolism. As macrophages readily take up lipoproteins from dying cells, they must have evolved mechanism to eliminate it from the cell (Remmerie and Scott, 2018).

Macrophages play major role in reverse cholesterol transport, a process by which excess cholesterol is eliminated from peripheral tissues to the liver (Glomset, 1968). Excess cholesterol packed

in low density lipoprotein (LDL) particles is taken up by macrophages located in arterial walls and subendothelial space *via* scavenger receptors such as CD36 (Remmerie and Scott, 2018). Upon the receptor-mediated endocytosis of LDL and its transfer to the lysosome, cholesterol carried by LDL is digested to free cholesterol and free fatty acids (Jeong, Lee and Oh, 2017). As free cholesterol is toxic for the cell, it is esterified by acyl-CoA:cholesterol acyltransferase, converting it to cholesterol esters in the endoplasmic reticulum. Esterified cholesterol is stored in the macrophage lipid droplets. Cholesterol recycling by macrophages is enabled by activation of several transcription factors such as liver X receptor α and β and the retinoid X receptor, which form a heterodimer and activate the transcription of ATP-binding cassette transporter A1 and ATP-binding cassette transporter G1 (Cuchel and Rader, 2006; Jeong, Lee and Oh, 2017). These membrane-bound transporters mediate the efflux of cholesterol from the macrophage to lipid-poor apolipoprotein A-I, the major protein component of high density lipoprotein (HDL) secreted by the liver and intestine (Jeong, Lee and Oh, 2017). Subsequently, the HDL particle matures and it is eventually transported through the bloodstream back to the liver, where it is either excreted into bile, used for synthesis of bile acids, or re-enters the circulation (Remmerie and Scott, 2018). The role of macrophages in reverse cholesterol transport is of particular importance during atherosclerosis as discussed later in this thesis (Ross and Glomset, 1973).

1.3.3.7 DESTRUCTION OF TUMORS

In addition to recognition and elimination of pathogenic invaders and dying or senescent cells, macrophages can also recognize and destroy altered cells of the host such as tumors. Macrophages distinguish neoplastic cells due to the differences in the composition of the plasma membrane. These alterations include increased prevalence of phosphatidylserine on the outer membrane leaflet, altered carbohydrate structures or various tumor antigens, e.g. carcinoembryonic antigen or Tn antigen recognized by lectin-like receptors (Klimp *et al.*, 2002). Subsequently, the macrophages can destroy the tumor cells by several mechanisms.

The pro-inflammatory macrophages are able to kill the target cell via production of ROS and RNS, which cause the nitrosative/oxidative stress, induction of DNA damage, cytotoxicity, and apoptosis (Garbán and Bonavida, 1999). The pro-inflammatory macrophages also secrete a cocktail of cytokines, including IL-1 β and TNF- α , which activate other immune cells (NK and T cells). As a result, the NK cells destroy the tumor cells marked by antibodies secreted by the lymphocytes *via* release of cytotoxic granules, which contain perforin and granzymes. This process is denoted as antibody-dependent cellular cytotoxicity (ADCC) (Pinto *et al.*, 2022).

In addition, TNF- α can induce apoptosis of the cancer cells through activation of the tumor necrosis factor receptor 1 (TNFR1) signaling pathway, which ultimately results in activation of caspases and production of ROS (Wang and Lin, 2008; Kim *et al.*, 2010). Nonetheless, tumor cells evolve a plethora of strategies how they escape the immune cells.

1.3.3.8 MORPHOGENESIS AND ORGANOGENESIS

Macrophages play important roles during embryonic development of animals as they sculpt and shape various tissues by efferocytosis of apoptotic cells. In addition, the macrophages are involved in branching morphogenesis, angiogenesis, neuronal patterning, bone morphogenesis, and generation of adipose tissue, i.e. the macrophages have a trophic role, meaning that they sustain production of signaling factors that prevent apoptosis of the surrounding cells.

To reveal the position and thus potentially the function of macrophages in the developing embryo, the researchers employed a transgenic mouse strain expressing GFP under the myelomonocyte-specific *Colony-stimulating factor 1 receptor (Csf-1r)* (Rae *et al.*, 2007). In the 11.5 day old mouse embryo, the macrophages represent 3-10% of all embryonic cells, whilst their majority prevails in the developing limbs, lens, thymus and olfactory bulbs (Rae *et al.*, 2007; Nucera, Biziato and De Palma, 2011). Their role in shaping of the limb is readily apparent. They engulf the apoptotic cells in the remodeling interdigital zones of the developing mouse footplate to transform it into a foot with separate digits (Hopkinson-Woolley *et al.*, 1994).

Tissue resident macrophages of the brain, microglia, play major roles in synaptic pruning. A surplus of synaptic connection is formed during early brain development, but many of these are not useful for optimal brain function. Therefore, the excess, weak or unnecessary synapses need to be removed by a process called synaptic pruning. Microglia thus sculpt the neuronal circuit, contribute to neuronal patterning, and maintain optimal synapse density to enhance brain efficiency during postnatal development (Paolicelli *et al.*, 2011). In addition, microglia also produce various signaling and neurotrophic factors such as insulin-like growth factor 1, nerve growth factor and neurotrophin 3, which may further contribute to the establishment of normal neuronal development (Yin *et al.*, 2017).

In the embryo, the macrophages also associate with developing renal tubules and blood vessels, presumably enabling their invasion and expansion into the surrounding connective tissue (Rae *et al.*, 2007). They also contribute to the development of the reproductive systems as it has been documented that at the onset of the morphogenesis of testis, fetal macrophages associate with the gonadal and mesonephric vasculature, where they mediate vascular reorganization and pruning of the germ cells (DeFalco *et al.*, 2014).

Nonetheless, macrophages do not contribute to organogenesis only in embryonic development, but their function is crucial even in postnatal periods of life. Such an example may be their role in regulation of ductal branching in mammary glands during puberty. At the onset of puberty, the murine mammary ducts develop multilaminar bulbous termini known as terminal end buds that grow out through the adipose tissue. During this period the macrophages are recruited and align along the shaft of the terminal end bud, which is allowed by collagenous fibers that run parallel to the direction of the outgrowth of the terminal end bud (Gouon-Evans, Rothenberg and Pollard, 2000; Ingman *et al.*, 2006). The macrophages are also present within the terminal end bud itself, where they engulf the dying

epithelial cells, leading to the formation of the lumen (Gouon-Evans, Rothenberg and Pollard, 2000). Similar phenomenon has been observed also in mammary glands during pregnancy, when the ducts further outgrow and the lobuloalveolar structures that produce milk during lactation extensively proliferate (Pollard and Hennighausen, 1994).

Macrophages are also involved in the development and maintenance of the gonadal tissues in adults. They are intimately associated with Leydig cells in the testes, and their ablation by clodrosome leads to suppression of testosterone synthesis in mice (Pollard and Hennighausen, 1994). In an analogous manner, macrophages are also associated with the developing ovarian follicle, especially just before ovulation, and their ablation disrupts steroidogenesis and prevents ovulation (Brännström and Norman, 1993; Cohen, Zhu and Pollard, 1997; Wu, 2004)

Macrophages are also responsible for tissue shaping in senescent individuals. In the brain of adult mammals, microglia constitute about 15% of brain's cellularity (Carson *et al.*, 2006). A protective role of microglia in adults lies in their ability to wrap around amyloid- β plaques and thus protect against extension of amyloid fibrils in Alzheimer's disease mouse models (Condello *et al.*, 2015). Microglia cells also contribute to myelin regeneration, a process of repairing and restoring damaged myelin sheaths in the central nervous system (CNS) after demyelinating insult, disease or inflammation. *Via* secretion of various signaling and growth factors, microglia are able to promote differentiation, proliferation, and maturation of oligodendrocyte precursor cells, which are responsible for the generation of new myelin (Kalafatakis and Karagogeos, 2021).

Formation and degradation of bone must be tightly balanced to avoid osteoporosis (loss of bone mass) or osteopetrosis (excess bone mineralization). This regulation is controlled by osteal macrophages, osteoclasts, which are located immediately adjacent to osteoblasts (Sinder, Pettit and McCauley, 2015). Recently, the researchers found another population of bone macrophages and denoted them as osteomacs, which comprise about 15% of the bone marrow. They are located in a close vicinity to osteoblasts, indicating that osteomacs may provide proanabolic support to osteoblasts and promote bone formation (Hume *et al.*, 1983). This hypothesis has been supported by an observation of Chang *et al.*, who showed that the mineralization of osteoblasts was highly decreased upon osteomacs depletion from the culture and that osteomacs can maintain the maturation of osteoblasts *in vivo* (Chang *et al.*, 2008). Interestingly, it has been suggested that osteomacs play a role in bone regeneration via secretion of type I collagen and bone mineralization (Jilka *et al.*, 2007). In addition, it has been documented that macrophages play a role in bone formation as mice with depleted bone macrophages display reduced surface of osteoblasts and great reduction of bone mass (Chang *et al.*, 2008; Cho *et al.*, 2014). In concordance with these observations, amplification of macrophage population *via* systemic treatment with macrophage colony-stimulating factor leads to an increase in bone mass and bone formation (Lloyd *et al.*, 2009). The macrophages regulate the homeostasis and metabolism of the bone not only by secretion of various cytokines and growth factors, but also by secretion of extracellular vesicles (Chen *et al.*, 2020).

Bone macrophages are also heavily involved in bone fracture healing. Pro-inflammatory macrophages are recruited to the site of the fracture and participate in the clearance of dead cells and they also promote angiogenesis, formation of primary cartilaginous calluses and differentiation of the osteoblasts (Lee and Lorenzo, 2006; Yang *et al.*, 2007). Moreover, they can enhance osteogenesis *via* the production of cytokines such as bone morphogenetic protein 2, bone morphogenetic protein 4, and tumor growth factor β 1 (TGF- β 1) (Champagne *et al.*, 2002).

1.3.3.9 SURFACTANT HOMEOSTASIS

Lung resident macrophages, alveolar macrophages, contribute to homeostasis of the lung surfactant, which is necessary to prevent alveolar collapse during breathing cycle and creates a barrier from the inhaled pathogens. It is produced by alveolar epithelial cells and is composed mainly of lipids and proteins. Alveolar macrophages are responsible for surfactant catabolism and clearance as they hydrolyze the surfactant phospholipids and incorporate the fatty acids into cellular triacylglycerol (Stern *et al.*, 1986).

1.4 METABOLIC PLASTICITY OF MACROPHAGES

The previous paragraphs clearly demonstrate the immense array of functions the macrophages possess. As each macrophage can be focused on a completely different role in the host's body and the roles can also change in the macrophage lifetime, fulfillment of the various missions requires slightly different toolbox. For instance, macrophages dedicated to clearance of the invading pathogen must be able to rapidly engulf high number of the bacteria, while macrophages participating on the remodeling of ECM must be equipped for the secretion of collagen and other ECM components. The field of immunometabolism has come to the conclusion that such variability of macrophage function is enabled by their remarkable metabolic plasticity (Galván-Peña and O'Neill, 2014). After receiving a stimuli from the environment, quiescent macrophages become activated and adjust their metabolic setup accordingly (Martinez and Gordon, 2014). They can switch from an aerobic profile, based on production of energy in mitochondria, to an anaerobic one, characteristic by enhanced glycolytic pathway, an *vice versa* (Galván-Peña and O'Neill, 2014). Modifications of macrophage cellular metabolism have been best described for pro-inflammatory macrophages and many excellent review articles were dedicated to this issue (Pearce and Pearce, 2013; Galván-Peña and O'Neill, 2014; Mills and O'Neill, 2016; Van den Bossche, O'Neill and Menon, 2017).

1.4.1 M1 METABOLIC POLARIZATION

A hallmark of macrophage activation is a change in their metabolic setup. Pro-inflammatory metabolic polarization of macrophages, denoted also as M1, is characterized by utilization of aerobic glycolysis as predominate way for the generation of energy (Hard, 1970). Instead of pyruvate being

transported from the cytosol to the mitochondria, it is converted to lactate *via* lactate dehydrogenase (LDH) (Pearce and Pearce, 2013). To further ensure the diversion of pyruvate from mitochondrial metabolism, pyruvate dehydrogenase kinase inhibits pyruvate dehydrogenase (Pearce and Pearce, 2013). By these means, NAD⁺, which is produced in quiescent cells by malate aspartate shuttle located in the outer mitochondrial membrane, is regenerated from NADH to sustain the glycolytic flow in pro-inflammatory macrophages (Locasale and Cantley, 2011). M1 metabolic polarization is not restricted only to changes in glycolysis, but it stands for a complex rearrangement affecting a multitude of metabolic pathways. Enhanced flux through glycolysis is also connected with increased activity of pentose phosphate pathway (PPP), which branches off from glycolysis and enables the cell to scale up the production of ribose for nucleotides, which are subsequently used for the synthesis of biomolecules required for efficient immune response (Pearce and Pearce, 2013). Besides that, PPP generates NADPH, a cofactor used by NADPH oxidase for production of ROS dedicated to destroy the pathogen. Thus, mitochondria are often recruited to the vicinity of phagolysosomes in order to transport ROS inside these organelles (Wang *et al.*, 2021). In addition, NADPH has a protective role against oxidative stress as it provides reducing power for generation of the antioxidant glutathione (Winkler, DeSantis and Solomon, 1986).

Generation of ATP directly in the cytosol is a favored pathway for cells that require rapid bursts of energy, such as during intense exercise or by cancer cells. In this regard, M1 macrophages that must act quickly to prevent multiplication of the pathogen highly resemble cancer cells, which require significant energy for proliferation. Preferential use of aerobic glycolysis even under normoxic conditions has been first described by Otto Warburg in 1927 in tumor cells, and hence, such cellular metabolic setup is also known as the Warburg effect. He assumed that the cancer cells favor glycolysis due to defective mitochondria (Warburg, Wind and Negelein, 1927). However, some researchers have believed that impaired mitochondrial metabolism is a consequence of increased flux through glycolysis, a phenomenon known as the Crabtree effect (Crabtree, 1929; Weinhouse, 1951). Nowadays, it is evident that the mitochondrial metabolism is not simply impaired. Instead, the tricarboxylic (TCA) cycle is referred to as “rewired” or “broken” (O’Neill, 2015). The main flux does not come from the classical direction. It has been reported that similarly to cancer cells, activated macrophages consume high amounts of glutamine. Subsequently, glutamine is converted to glutamate in the cytosol and enters the TCA cycle at the position of α -ketoglutarate. Some of the TCA cycle intermediates were found to be accumulating in the mitochondria. Increased levels of citrate result from decreased expression of isocitrate dehydrogenase, an enzyme which converts citrate to α -ketoglutarate. Citrate is utilized by the cell for the production of itaconate, which possesses antimicrobial effects or can act as an anti-inflammatory agent, inhibiting succinate dehydrogenase (O’Neill, 2015). In addition, citrate can be used for protein acetylation or for synthesis of fatty acids (Williams and O’Neill, 2018). In order to do so, it must be transported to the cytosol *via* the mitochondrial citrate- carrier and transformed into acetyl-CoA and oxaloacetate. Subsequently, acetyl-CoA is converted to malonyl-CoA, and fatty acid synthase

elongates the nascent fatty acid chain, which represents a substrate for elongation and various degrees of saturation (Williams and O'Neill, 2018). Fatty acids are then available for membrane remodeling to facilitate phagocytosis, synthesis of triacylglycerides for energy storage or catecholamines and eicosanoids produced as signaling molecules (Röhrig and Schulze, 2016). Interestingly, a study conducted by Feingold et al. showed that macrophages (RAW 264.7 cells) enhance the conversion of glucose to lipids and uptake of fatty acids after LPS treatment (Feingold *et al.*, 2012).

α -ketoglutarate is used for production of 2-hydroxyglutarate, an important signaling molecule for maintenance of the M1 polarization (Jha *et al.*, 2015). Increased activity of arginine-succinate shunt results in accumulation of malate, another TCA cycle intermediate (O'Neill, 2015). Accumulation of TCA cycle intermediates has a very important signaling and regulatory role, which will be described later in this thesis.

Another hallmark of metabolic polarization of M1 macrophages besides alterations in pathways for energy production is the metabolism of arginine, a small non-essential amino acid molecule (Mills, 2001). The pro-inflammatory macrophages display increased expression of inducible nitric oxid synthase (iNOS), which can be induced by various pro-inflammatory cytokines, microbial products or hypoxia (Hibbs, Taintor and Vavrin, 1987). iNOS incorporates molecular oxygen, releases NO from the terminal guanidino-nitrogen group of arginine and generates citrulline as a by-product (MacMicking, Xie and Nathan, 1997). Subsequently, NO can be converted to RNS, such as dinitrogen trioxide, peroxyxynitrite or nitronium ion or it is utilized for protein nitrosylation (Ignarro, 1990). Interestingly, many enzymes involved in glycolysis, TCA cycle, electron transport chain and fatty acid metabolism were found to be nitrosylated, which likely affects their enzymatic activity (Doulias *et al.*, 2013). Moreover, there are pieces of evidence that NO dampens the mitochondrial electron transport chain, thereby increasing glycolysis and preventing the repolarization to M2 phenotype since experimental inhibition of iNOS restores regular mitochondrial respiration (Everts *et al.*, 2012). Although citrulline is generated by iNOS as a by-product, it can be exploited by the cell for increasing the pool of NO as it can be directed to the citrulline-NO cycle.

The necessity of metabolic reprogramming for macrophage function and efficient immune response is apparent from many studies. Aerobic glycolysis has been shown to fuel the ATP requirements for actin polymerization and thus formation of the phagocytic cup (Morioka *et al.*, 2018). Pioneering experiments concerning the importance of aerobic glycolysis have exploited 2-deoxyglucose, a D-glucose analog, which inhibits glycolysis at its onset, namely at the step of glucose phosphorylation by hexokinase. In addition, it has been shown to inhibit activation of Hypoxia inducible factor 1 α (HIF1 α), the central transcription factor governing M1 macrophage metabolism as discussed later in this thesis. Thus, 2-deoxyglucose treatment results in reduction of pro-inflammatory response due to decreased expression of pro-inflammatory cytokines (TNF α , IL-1 β , IL-6) and chemokines (CXCL1 and CXCL2), leading to decreased clearance of the pathogen (Francis *et al.*, 2020; Fan *et al.*, 2021; Pandey *et al.*, 2023). In addition, forcing oxidative metabolism in M1 macrophages attenuates

macrophage-mediated inflammation and leads to M2 polarization phenotype (Vats *et al.*, 2006). It can be thus concluded that metabolic polarization is superior to the functional polarization of macrophages and successful fulfillment of their roles. Hence, the rearrangement of cellular metabolic setup described above perfectly equips the M1 macrophages for the production of bactericidal compounds, secretion of pro-inflammatory cytokines, phagocytosis of the pathogen and its subsequent destruction (Michl, Ohlbaum and Silverstein, 1976; Freemerman *et al.*, 2014; Pavlou *et al.*, 2017).

The major regulator of the M1 metabolic polarization is HIF1 α , a transcriptional regulator of cellular and developmental responses to hypoxic conditions (Wang *et al.*, 2017). High activity of the HIF1 α signaling cascade has been described also in tumors, thus providing another evidence documenting the similarity of the metabolic setup between macrophages and cancer cells (Jun *et al.*, 2017). Under normoxic conditions, and in presence of sufficient levels of Fe²⁺ and α -ketoglutarate, HIF1 α is continuously hydroxylated by prolyl dehydrogenase, ubiquitinated by Von Hippel Lindau enzyme and consequently degraded by the proteasome. As molecular oxygen acts as a co-substrate for prolyl dehydrogenase, HIF1 α does not undergo hydroxylation in hypoxic conditions. Instead, HIF1 α is stabilized and acts as a transcription factor inducing expression of genes carrying hypoxia response element sequence in their promoter such as glycolytic enzymes, LDH, glucose transporters, pro-inflammatory cytokines, lactate transporter, various signaling molecules or pyruvate dehydrogenase kinase, leading to enhanced flux through glycolysis and diversion of pyruvate from entering the TCA cycle (Imtiyaz and Simon, 2010). Since stabilization of HIF1 α occurs in macrophages even under normoxic conditions, it is referred to as pseudohypoxia (Mohlin *et al.*, 2017). Hence, stabilization of HIF1 α must be achieved by other means than *via* decrease in molecular oxygen. It has been documented that stimulation of TLR leads to activation of NF- κ B, which in turn results in stabilization of HIF1 α (Kawai and Akira, 2007). However, it is much more complex and its stabilization is further secured by the TCA intermediates and associated metabolites, e.g. malate, succinate, fumarate, and 2-hydroxybutyrate (Fig. 6) (O'Neill, 2015). In addition, HIF1 α stabilization is further secured by iron sequestration. It has been shown that sensing of LPS induces ferritin expression in activated macrophages, which sequesters iron, resulting in lower prolyl dehydrogenase activity and thus stabilization of HIF1 α (Siegert *et al.*, 2015). The importance of HIF1 α signaling for metabolic reprogramming and efficient functioning of pro-inflammatory macrophages has been documented by an experiment conducted on HIF1 α knockout macrophages. Such cells display impaired expression of iNOS after IFN γ stimulation and decreased ability to eliminate both Gram positive and Gram negative bacteria (Peyssonnaud *et al.*, 2005; Takeda *et al.*, 2010).

Apart from stabilization of HIF1 α , the accumulating TCA intermediates and other biomolecules associated with M1 phenotype play another important role in maintenance of the pro-inflammatory polarization as they regulate the epigenetic landscape of the cell. The activity of chromatin-modifying enzymes has been shown to be regulated by the availability of these molecules (Baardman *et al.*, 2015). Whilst histone methyltransferases are α -ketoglutarate-, iron- and oxygen-dependent, histone

demethylases are inhibited by succinate, fumarate and ROS. Ten-eleven translocation methylcytosine dioxygenases, which mediate DNA demethylation, are known to be inhibited by fumarate and succinate and their require α -ketoglutarate, iron and oxygen as cofactors (Baardman *et al.*, 2015).

In conclusion, M1 metabolic polarization is a metabolic adaptation of pro-inflammatory macrophages, which results in their dependence on increased uptake of glucose and glutamate but in turn, it equips them with ATP, metabolites and precursors necessary to rapidly engulf and destroy the pathogen, and release pro-inflammatory molecules that inform rest of the organism about the encountered threat (Newsholme *et al.*, 1986).

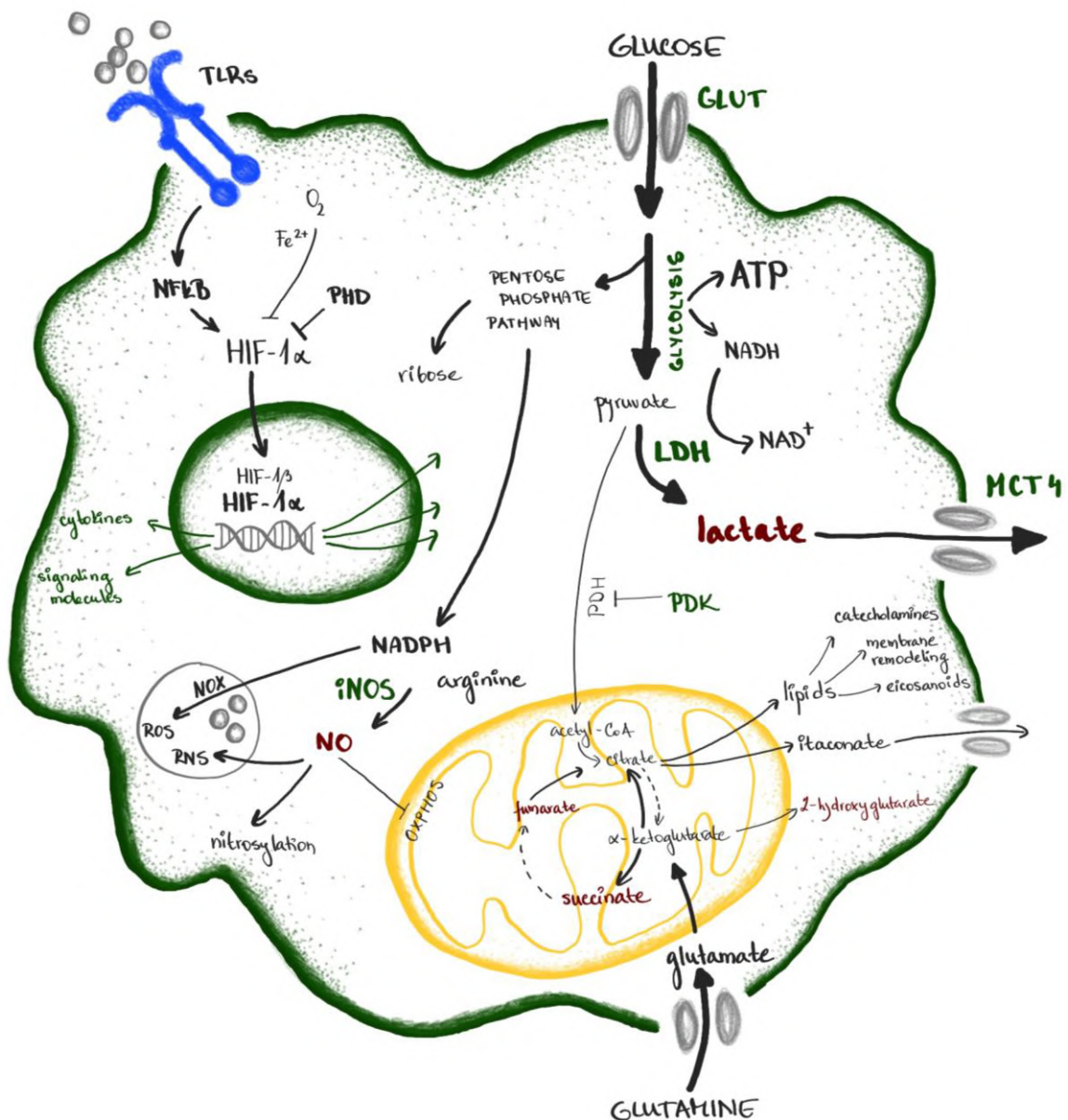


Figure 6: Schematic illustration of the metabolic setup of a M1 macrophage. The picture was drawn in PENUP.

1.4.2 M2 METABOLIC POLARIZATION

While M1 metabolic polarization is an adjustment of pro-inflammatory macrophages, M2 polarization is adopted by alternatively activated cells, also denoted as anti-inflammatory macrophages (Mills, 2001). In contrast to M1 macrophages, the main pathway for the production of energy in the form of ATP is oxidative phosphorylation. The TCA of M2 macrophages is intact, runs in a conventional direction and provides the substrates for the complexes of the electron transport chain (O'Neill, 2015). However, several studies report that glycolysis is also essential for M2 cells, especially those which engage in efferocytosis (Tan *et al.*, 2015; Van den Bossche *et al.*, 2016; Trzeciak, Wang and Perry, 2021).

The metabolism of arginine differs from M1 macrophages substantially. Arginine is catabolized by an enzyme arginase, thereby producing ornithine and urea. Subsequently, ornithine can be transformed by ornithine decarboxylase to polyamines (putrescine, spermidine, and spermine) that control cell growth and are important for tissue repair. In addition, ornithine can be exploited for synthesis of proline, which is used by the cell for collagen production, another molecule dedicated to tissue repair (Kelly and O'Neill, 2015).

As M2 macrophages often engulf dying cells or their fragments, they must deal with lipids these cells contain. Macrophages are capable of uptake of different forms of lipids such as LDL, VLDL, or oxidized lipoproteins *via* phagocytosis, macropinocytosis, and scavenger receptor-mediated uptake (Tabas and Bornfeldt, 2016). Subsequently, the ingested lipids are metabolized by acid lipases within lysosomes, leading to generation of cholesterol and fatty acids, which are subsequently transported into mitochondria and destined for fatty acid oxidation (Huang *et al.*, 2014).

Enhanced fatty acid oxidation is another hallmark of M2 polarization. During this process, the fatty acids are broken down by a series of steps to produce an alternative energy source to glucose. It begins with attachment of acetyl-CoA to the fatty acid chain *via* acyl-CoA synthetase, thus forming acyl-CoA. The actual oxidation takes place in mitochondria, and hence the acyl-CoA must be transported across the mitochondrial membrane *via* carnitine carrier. Once inside, acyl-CoA undergoes cycles of β -oxidation, which removes two carbon units from the fatty acid chain with each cycle, thereby becoming progressively shorter. Subsequently, the resulting acetyl-CoA molecules can enter the TCA (Nomura *et al.*, 2016).

Another metabolic feature displayed by M2 macrophages is glutaminolysis. Glutamine metabolism supports M2 polarization in several ways. Glutamine serves as a substrate for generation of α -ketoglutarate, which promotes the M2 phenotype at the level of epigenetic modifications, as it allows demethylation of H3K27 on the promoters of M2-specific marker genes (Liu *et al.*, 2017). Moreover, it supports activity of prolyl dehydrogenase, thereby inhibiting the activity of HIF1 α and thus maintaining the M2 phenotype. In addition, glutamine provides substrate for the synthesis of uridine diphosphate N-acetylglucosamine, which is crucial for glycosylation of M2 marker proteins (e.g., macrophage mannose

receptor and macrophage galactose binding lectin) (Jha *et al.*, 2015). Indeed, it has been documented that the pathway for UDP-GlcNAc synthesis is upregulated in M2 macrophages and that administration of N-glycosylation inhibitor abrogates the expression of M2 polarization markers in macrophages activated by IL-4, whilst it does not impact the expression of iNOS and several pro-inflammatory cytokines substantially (Jha *et al.*, 2015). While M1 macrophages display glutamine addiction, M2 cells do not have to rely on glutamine uptake. Instead, they are capable of glutamine synthesis from glutamate *via* glutamine synthetase, which is highly expressed in these macrophages contrary to the M1 state (Palmieri *et al.*, 2017). It has been shown by Palmieri and colleagues that inhibition of glutamate synthase leads to a repolarization to M1-like phenotype (Palmieri *et al.*, 2017).

Activation of the kynurenine pathway is a key metabolic route for tryptophan synthesis in M2 macrophages. Kynurenine is produced from tryptophan by indoleamine 2,3-dioxygenase, which is upregulated in response to anti-inflammatory cytokines. Subsequently, kynurenin produced to extracellular space has immunosuppressive effects and thus can prevent excessive inflammation and tissue damage. In addition, it can promote differentiation of regulatory T cells, which play roles in maintenance of immune tolerance and suppression of immune responses (Munn *et al.*, 1999; Yue *et al.*, 2015).

1.4.3 OTHER POLARIZATION STATES

Despite the literature distinguishes mainly the M1 and M2 polarization states, these are only the extremes of the whole polarization spectrum. It has been suggested that similarly to primary colors, these polarization phenotypes can blend into various other 'shades' of activation (Mosser and Edwards, 2008). For example, M2 macrophages can be further classified as M2a, M2b, M2c, and M2d, which can be distinguished mainly by the presence of various cluster of differentiation molecules (Ross, Devitt and Johnson, 2021). Some publications also propose the existence of M3 and M4 polarization phenotypes (Gleissner *et al.*, 2010; Kalish *et al.*, 2017). While Mhem polarization phenotype is induced in response to ingestion of heme by the cell, internalization of hemoglobin leads to M (Hb) macrophage polarization state (Gordon and Taylor, 2005; Boyle *et al.*, 2009). Macrophages exposed to oxidized lipids in atherosclerotic plaques have been denoted as Mox, and metabolically activated macrophages (MMe) have been described to be present in obese adipose tissue (Coats *et al.*, 2017). Besides potentiating inflammation, MMe macrophages contribute to clearance of dead adipocytes *via* exocytosis of their lysosomes. This metabolic profile is characterized by increased NADPH oxidase 2 (Nox2) expression. Since Nox2 knockout mice initially display improved metabolic profile, they have defective lysosomal exocytosis and accumulation of dead adipocytes after sixteen weeks of being fed high fat diet, the authors conclude that MMe macrophages have both detrimental and beneficial functions, depending on disease progression (Coats *et al.*, 2017).

1.5 INADEQUATE POLARIZATION UNDERLIES MANY DISEASES

As documented in the previous paragraphs, macrophages play a plethora of function within an organism. However, if they are unable to perform these roles or if a certain functional program is triggered in an inadequate context, this can lead to a serious pathology. It is mainly due to the adoption of a polarization state, which does not suit the situation and macrophages thus start to react inadequately to the condition. Since macrophages actively contribute to maintenance of tissue homeostasis under physiological conditions, they act as sensors of tissue dysfunction and may promote inflammation even in the absence of infection. Excessive number of macrophages polarized to M1 phenotype have been detected in patients suffering from maladies characterized by chronic inflammatory states.

Alternatively activated resident macrophages predominate in healthy white adipose tissue. They express IL-10, an anti-inflammatory cytokine which acts as insulin sensitizer. Chronic increase in energy uptake results in excessive accumulation of nutrients in the adipocytes, causing metabolic stress and homeostatic imbalance, which is sensed by resting monocytes. Once they recognize the signal, they are recruited to the adipose tissue and quickly differentiate to macrophages, which form crown-like structures around the dying adipocytes (Weisberg *et al.*, 2003; Cinti *et al.*, 2005; Murano *et al.*, 2008). Whilst in lean state the macrophages account for 5% of the cells in this organ, their number increases to 50% in obese individuals (Weisberg *et al.*, 2003). The infiltrating macrophages polarize to M1 phenotype, secrete pro-inflammatory genes such as IL-6 and *Nos2*, and thus induce low-grade chronic inflammation in adipose tissue (Lumeng *et al.*, 2007). Pro-inflammatory cytokines are considered major contributors to local and systemic insulin resistance. The central role of macrophages in the progression of metabolic syndrome lies in the negative impact of inflammation on signaling events downstream of the insulin receptor, resulting in insensitivity to insulin within the affected tissue (McNelis and Olefsky, 2014). Such state in turn results in maladaptation in glucose and lipid metabolism and increased production of insulin by pancreatic islet cells, which try to compensate for the lack of insulin signaling (Qatanani and Lazar, 2007). M1 macrophages thus significantly contribute to establishment of a pre-diabetic state.

Macrophages play major roles in other conditions associated with imbalance in lipid metabolism such as non-alcoholic fatty liver disease and non-alcoholic steatohepatitis. Inflammatory signals connected to fat accumulation in the liver lead to macrophage recruitment (Gadd *et al.*, 2014; Krenkel *et al.*, 2018). Subsequently, they release pro-inflammatory cytokines and other signaling factors that contribute to disease progression. Simultaneously, Kupffer cells become activated and further promote inflammation and tissue damage. Molecules produced by the pro-inflammatory macrophages in turn activate stellate cells, which start to release excess collagen and hence induce liver fibrosis, which may develop to cirrhosis, a state that adversely impacts liver function. Even in this case, secretion of pro-inflammatory cytokines by M1 macrophages has been associated with insulin resistance (Lefere and Tacke, 2019).

Similar situation arises in patients suffering from atherosclerosis. As cholesterol-rich particles, mainly LDLs accumulate within the wall of arteries, they readily become oxidized and thus attract the macrophages to the atherosclerotic plaques (Mushenkova *et al.*, 2021). Despite the macrophages initially help to eliminate the excess cholesterol, prolonged scavenging of modified LDLs results in formation of foam cells (Fig. 7), thereby triggering inflammatory response in the arterial wall, which acts as an attractant for more macrophages and thus amplification of the inflammatory process. Over time, as more cells, lipids, and debris accumulate within the arterial wall, the plaque becomes unstable and vulnerable to rupture. Such state is particularly dangerous as it can trigger a formation of a thrombus and obstruction of blood flow, progressing to myocardial infarction or stroke (von Ehr, Bode and Hilgendorf, 2022).

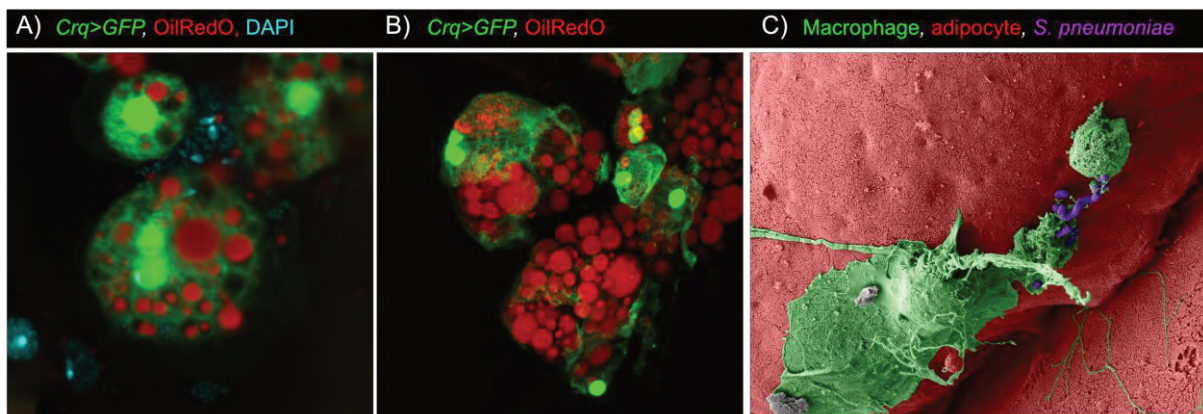


Figure 7: Macrophages display features of enhanced metabolism of lipids under certain conditions in adult fruit flies. (A) Confocal image of foamy macrophages (*Crq>GFP*, green) filled with lipid droplets (OilRedO, red). (B) Confocal image of macrophages (*Crq>GFP*) interacting with adipocytes in adult flies. (C) Scanning electron micrograph of a macrophage (pseudocolored in green) crawling on adult fat body (pseudocolored in red) and scavenging bacteria (pseudocolored in violet). Images in A and B were captured by FluoView3000 Olympus Confocal Microscope and in C by JSM-7401F JEOL Scanning Electron Microscope at the Biology Centre CAS.

Nonetheless, adverse roles of classically activated macrophages are not restricted to diseases associated with excessive energy intake and metabolic imbalances. Rheumatoid arthritis is an autoimmune disease characterized by responses to synovium, a tissue which lines the joints. Activated macrophages accumulate in synovium and contribute to inflammation, angiogenesis, fibrosis, auto-antigen presentation and degradation of cartilage and bone (Tu *et al.*, 2020). The imbalance in M1/M2 macrophages has been found to play crucial roles also in chronic obstructive pulmonary disease, allergic asthma, cachexia, inflammatory bowel disease, including Crohn's disease and ulcerative colitis, or cancer (Saradna *et al.*, 2018; Du *et al.*, 2021; Finicelli *et al.*, 2022).

Therefore, many efforts have been invested in the development of macrophage-specific tools designed to deliver drugs and various compounds that may lead to re-polarization of the cell without affecting the metabolic setup of other tissues (Fig. 8) (Du *et al.*, 2021). Nanoscale delivery systems have been recognized as particularly promising platforms thanks to their sufficient loading capacity and large

surface, while being able to penetrate into affected tissues (Shields *et al.*, 2020). In addition, these molecules can be further modified with ligands recognized by macrophage receptors, such as integrins, CD36 or mannose receptors, which further improves targeting efficacy (Nie *et al.*, 2015; Ye *et al.*, 2019).

Targeting macrophages of atherosclerotic lesions is a potent strategy to prevent plaque progression. The strategies focus mainly on enhancing cholesterol efflux, preventing foam cell formation, promoting efferocytosis or re-polarization from M1 to M2 phenotype (Moore and Tabas, 2011; Kamaly *et al.*, 2016; Bäck *et al.*, 2019). These effects can be achieved by administration of statins. Statins are inhibitors of 3-hydroxy-3-methylglutaryl coenzyme A reductase (HMGCR), a rate-limiting enzyme in cholesterol synthesis. Nonetheless, statins are usually commercially provided in a form of a capsule or tablet and the effects are thus not restricted to macrophages and are potentially cytotoxic to the liver. To improve their targeted delivery, HDL-mimicking nanoparticles, solid lipid nanoparticles, polymer micelles or electrospun fibers have been suggested (Tang *et al.*, 2015; Tsigkas *et al.*, 2016; Alaarg *et al.*, 2017). In addition to statins, administration of anti-oxidative agents has been proven as a suitable strategy to inhibit production of pro-inflammatory cytokines and induce atherosclerosis regression (Wang *et al.*, 2018). Increase in cholesterol efflux and thus reduction of lipid content in the macrophages may be achieved by the delivery of β -cyclodextrin, commonly used in pharmaceutical applications to deliver hydrophobic drugs, spherical HDL mimics or by chitosan particles loaded with microRNA (Zimmer *et al.*, 2016; Henrich *et al.*, 2019; Nguyen *et al.*, 2019).

Macrophage-targeting strategies also serve as a tool for the treatment of autoimmune diseases. Indeed, depletion of synovial macrophages is achieved by administration of clodronate encapsulated in liposomes in individuals suffering from rheumatoid arthritis (Van Lent *et al.*, 1998). Another example of beneficial effects of macrophage modulation is multiple sclerosis. Induction of anti-inflammatory polarization has been achieved by forskolin, which enhances the expression of arginase in macrophages and thus alleviates autoimmune encephalomyelitis (Veremeyko *et al.*, 2018).

Tumor associated macrophages are a promising target in the treatment of cancer. The researcher focus on inhibition of monocyte migration into the tumors and re-polarization or elimination of tumor-associated macrophages from the tumor milieu (Cassetta and Pollard, 2018). While recruitment of monocytes to solid tumors can be achieved by inhibition of the chemokine secretion, re-polarization of tumor associated macrophages to M1 phenotype includes agonists for TLRs, antibodies against CD47, inhibitors of histone deacetylase or blockages against macrophage receptor with collagenous structure (MARCO) (Loberg *et al.*, 2007; He *et al.*, 2020). CD47 is usually overexpressed by all solid tumors and acts as a 'do not eat me signal'. Unique liposome-like particles have been developed to deliver both anti-CD47 antibodies and inhibitors of CSF-1R (Kulkarni *et al.*, 2018).

Although metabolic setup of macrophages appears as very promising target for treatment of many maladies while avoiding the negative side effects resulting from non-specific administration, it is not clear yet whether it may have a negative impact on macrophage adaptive functions, such as

phagocytosis of the bacteria and elimination of the pathogen. This potential disadvantage thus should be tested in future studies.

As evident from the previous paragraphs, despite macrophages are primarily beneficial cells that play many crucial roles within the organism, there are situations when their actions can be maladaptive or even detrimental. Many researches thus wonder why their initially protective role turns against the host under certain conditions and what are the impulses invoking macrophage polarization in both adaptive and pathological conditions.

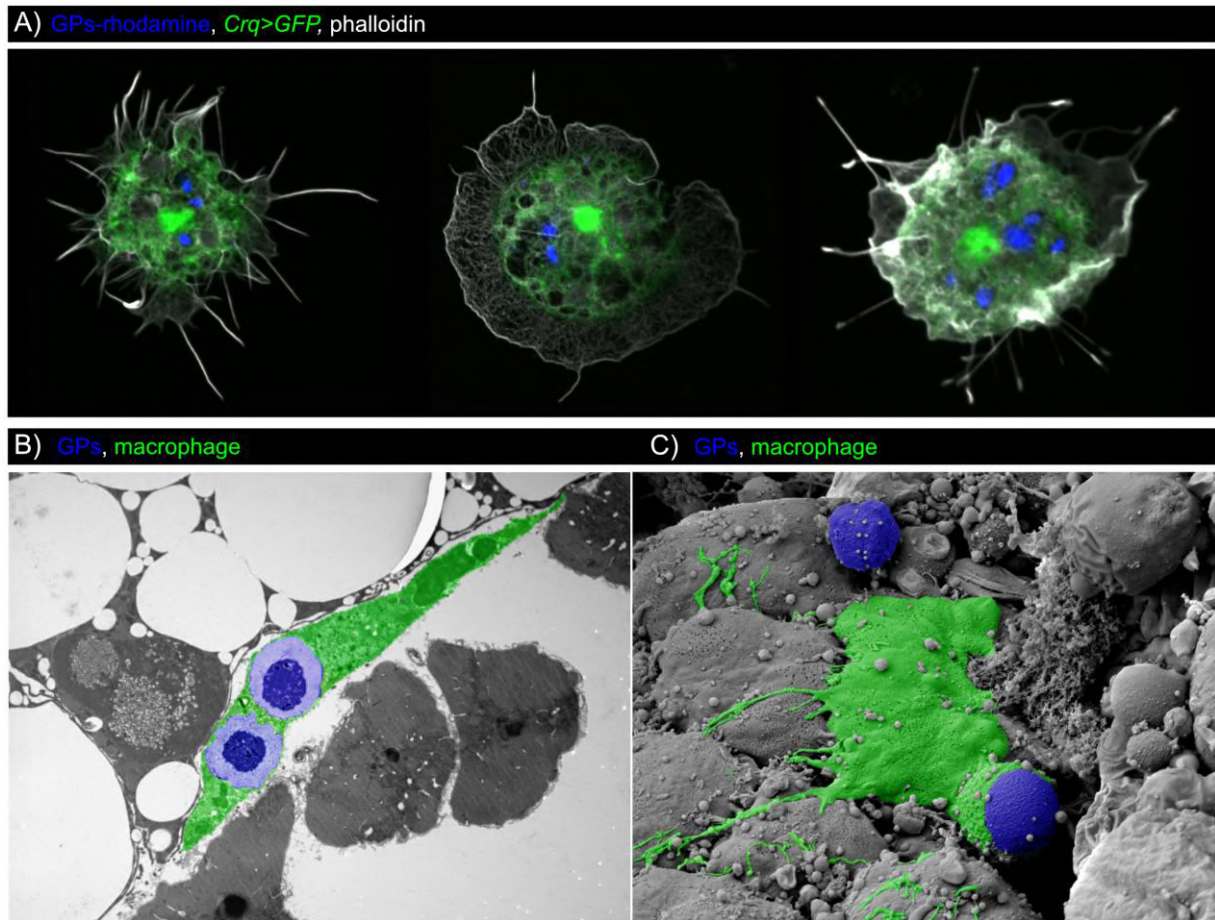


Figure 8: Yeast-derived glucan particles as a tool for macrophage-specific delivery in adult fruit flies developed in our laboratory. (A) Confocal images of macrophages (*Crq>GFP*; green) stained by phalloidin (white), which were dissected from adult *Drosophila* injected with glucan particles (GPs-rhodamine; blue). (B-C) Transmission (B) and scanning (C) electron micrograph depicting internalization of glucan particles (pseudocolored in blue) by macrophages (pseudocolored in green). Images in A were captured by FluoView3000 Olympus Confocal Microscope, in B by JEM-1400 JEOL Transmission Electron Microscope, and in C by JSM-7401F JEOL Scanning Electron Microscope at the Biology Centre CAS.

1.6 MACROPHAGE PLASTICITY AS A LEGACY OF THEIR ORIGIN

Strikingly, recent works note the similarities and interconnections of the signaling pathways activated upon recognition of pathogens and nutrient sensing (Hotamisligil and Erbay, 2008; Efeyan, Comb and Sabatini, 2015) This is particularly plausible in pathogenesis of chronic metabolic diseases

since TLRs, traditionally involved in pathogen recognition, can respond to the presence of lipids (Ajuwon and Spurlock, 2005; Shi *et al.*, 2006; Efeyan, Comb and Sabatini, 2015).

There are theories that the mechanisms and underlying signaling pathways involved in regulation of macrophage pathological actions may be rudiments of their evolutionary origin without retaining their initial adaptive function. Such vestigial pathways may underlie the pathological behavior of macrophages in complex organisms (Bajgar and Krejčová, 2023). For example, the folate receptor has been originally utilized by macrophage-like amoebocytes in *Dictyostelium* for bacterial hunting and thus obtaining nutrition since folate is a bacterial secondary metabolite (Driel, 1981). However, folate receptor β has been found to be highly expressed in macrophages in synovium of patients suffering from rheumatoid arthritis or macrophages or atherosclerotic plaques and its activation leads to their pro-inflammatory polarization and production of cytokines that further exacerbate the chronic inflammatory state (Xia *et al.*, 2009; Chandrupatla *et al.*, 2019). Another example may be formyl peptide receptor, which activation leads to enhanced directional motility, production of ROS, release of pro-inflammatory cytokines, and acceleration of phagocytosis and bactericidal actions (Liang *et al.*, 2020). Since formyl peptides are bacterial secondary metabolites, its receptors are essential for recognition of bacterial pathogens. However, formyl peptides may be released from damaged mitochondria of stressed tissues even under sterile conditions, leading to macrophage recruitment and induction of inflammation even without the presence of any bacteria (Wenceslau *et al.*, 2013). Excessive activation of formyl receptors has been connected to progressive development of many inflammatory states such as cardiovascular diseases and neurodegeneration (Trojan *et al.*, 2020; Caso *et al.*, 2021).

Notably, evolution can provide answers even for a question of the incredible versatile roles of macrophages and for the origin of M1/M2 polarization phenotypes. It has been assumed that macrophage functional versatility reflects the ancient origin of these cells and that their functional repertoire has further diversified with the emergence of multicellular organism and their further evolution into complex animals (Hartenstein and Martinez, 2019; Bajgar and Krejčová, 2023).

Strikingly, macrophages resemble many characteristics of free-living unicellular predatory amoebas. *Acanthamoeba*, a heterotrophic Protist relies on hunting of bacteria as a nutrition, which makes them professional phagocytic bactericidal omnivores (Rayamajhee *et al.*, 2022). Apart from the similarities between *Acanthamoeba* and mammalian macrophages in their behavior, size, and cellular ultrastructure, they both sense chemical signals from the environment, to which they are chemotactically attracted. These molecules represent mainly various bacterial metabolites such as formyl-methionyl-leucyl-phenylalanine, LPS, lipoteichoic acid, cAMP, or N-acetylglucosamine (Schuster and Levandowski, 1996). The social life stage of *Dictyostelium discoideum* closely resembles simple multicellular organisms. Suddenly, there is a demand for self-recognition and regulation. The social stage of *D. discoideum* (also called the slug) possesses four types of cells, from which sentinel cells resemble macrophages. They are freely moving, phagocytose bacteria and toxins to be subsequently eliminated and they highly express *Toll-interleukin receptor domain-containing protein*, a gene

analogous to mammalian toll-like receptors (Brock, Callison, *et al.*, 2016). Upon infection, the sentinel cells engulf the invaded cells, thus keeping the organism healthy. Moreover, the sentinel cells display high degree of tolerogenic behavior as they can recognize self- from non-self and they ensure the survival of commensal bacteria, in a specific form of nutritional symbiosis (Hirose *et al.*, 2011; Brock *et al.*, 2013; Brock, Jones, *et al.*, 2016).

Studying of the most ancestral relatives of metazoa, basal multicellular sponges with incomplete organs systems (Porifera), can unravel the origin of the striking macrophage versatility. Although they lack complex organs, they developed cells with specialized functions. Filtration of nutrients from the water is enabled by choanocytes, which are equipped with flagellum and internalize the food particles by nutritive phagocytosis and process it in food vacuoles (Laundon *et al.*, 2019). Subsequently, another lineage of professional phagocytes, motile amoebocytes called archaeocytes, distribute the particles to other cells of the sponge body (Hartenstein and Martinez, 2019). Interestingly, the mechanism of nutrient uptake and their distribution by freely motile amoebocytes is conserved across animals except for insects and vertebrates (Hartenstein and Martinez, 2019). Archaeocytes also play a protective role in sponges, and therefore, they are believed to represent the ancestors of macrophages of bilaterians (Nakanishi, Sogabe and Degnan, 2014). Indeed, they possess a broad spectrum of receptors homologous to PRRs such as GPCRs, NOD-like receptors, or scavenger receptors (Wiens *et al.*, 2005; Srivastava *et al.*, 2010). After recognition of the pathogen, activation of many molecules involved also in activation of mammalian immune response and production of several factors has been identified, e.g. activation of transcription factor NF κ B, IRAK, or TRAFs, and production of perforins and ROS (Müller, 2006). In addition, a study by Germer and colleagues documents the presence of the TLR-mediated signaling cascade (Germer, Cerveau and Jackson, 2017). On top of that, the archaeocytes of the sponge display tolerogenic behavior since commensal microbiota does not trigger bactericidal actions. They are also crucial for healing and tissue regeneration as they infiltrate the wound and engulf the damaged cells (Germer, Cerveau and Jackson, 2017). Subsequently, they secrete ECM components and differentiate into other cell types to replace the lost cells. Intriguingly, they represent the totipotent stem cells of the organism since they can give rise to any other cell type and thus regenerate the whole body of the sponge (Ereskovsky *et al.*, 2021). In addition, as evident from the transplantation studies, they ensure self-identification and immune tolerance (Carrier *et al.*, 2022).

Following the idea that the repertoire of functions of macrophage-like cells has broaden in evolution with the increasing complexity of the animal structures, immune cells of *Drosophila melanogaster* deserve closer attention.

1.7 DROSOPHILA MELANOGASTER FOR RESEARCH OF MACROPHAGE FUNCTIONS

D. melanogaster is a simple model organism with clearly defined tissues and complex organs. As a holometabolous hexapod, its life comprises of embryonic, three larval instars, pupal, and adult stages. It represents an excellent model organism for immunometabolic studies mainly thanks to its short

generation time, high reproductive rate, small size, well-characterized genome of only four chromosomes, well-characterized physiology and development. Moreover, it offers a wide range of various genetic tools which are kindly shared among the *Drosophila* research community. Thousands and thousands of fly lines bearing various genetic constructs are commercially available in *Drosophila* stock centers located mainly in Bloomington, Vienna and Kyoto. These include fly lines with balancer chromosomes, binary expression systems allowing for tissue-specific and time-limited genetic manipulations, mutant and RNAi lines, stocks for clonal analyses, FLP/FRT recombinases, genome editing stocks, reporter systems with fluorescent proteins or LacZ, etc. Notably, it is estimated that human and *Drosophila* genome is more than 60% homologous and approximately 75% of the genes known to cause human diseases have homologs in fruit flies (Ugur, Chen and Bellen, 2016).

D. melanogaster has been instrumental to one of the major discoveries in immunology, the discovery of Toll as a receptor involved in sensing of pathogenic bacteria and fungi in 1996, leading to a radiation of research on innate immunity (Lemaitre *et al.*, 1996). Since then, it became well established model organism for the research of host-microbe interactions, immune signaling pathways, phagocytosis, or wound healing (Razzell, Wood and Martin, 2011). Nonetheless, less attention has been dedicated to non-canonical roles of immune cells and to the relationship between immune activation and regulation of the systemic metabolism.

1.7.1 IMMUNE SYSTEM OF *DROSOPHILA*

Immune cells of *Drosophila*, called hemocytes, comprise of three distinct types. Although the composition of hemocytes varies through the fruit fly life, the predominant population are plasmatocytes, macrophage-like professional phagocytes. The second type of hemocytes are crystal cells, which make up to 5% of the immune cell population in embryo and larva. They contain crystalline structures composed of prophenoloxidasases, and hence are responsible for melanization. Besides deposition of black pigment melanin at the site of injury, melanization reaction produces toxic free radicals as a by-product during wound healing or infection (Meister and Lagueux, 2003). Finally, lamellocytes are present only during larval stages. Since their main role is encapsulation and subsequent destruction of parasitoid eggs, they differentiate massively only upon infestation. Indeed, almost no lamellocytes can be found in healthy larvae. When eggs of parasitoid wasps are laid in the body cavity of larvae, the lamellocytes differentiate from undifferentiated prohemocytes and plasmatocytes, and form successive layers around the parasitoid egg, resulting in its encapsulation and melanization (Fig. 9) (Meister and Lagueux, 2003).

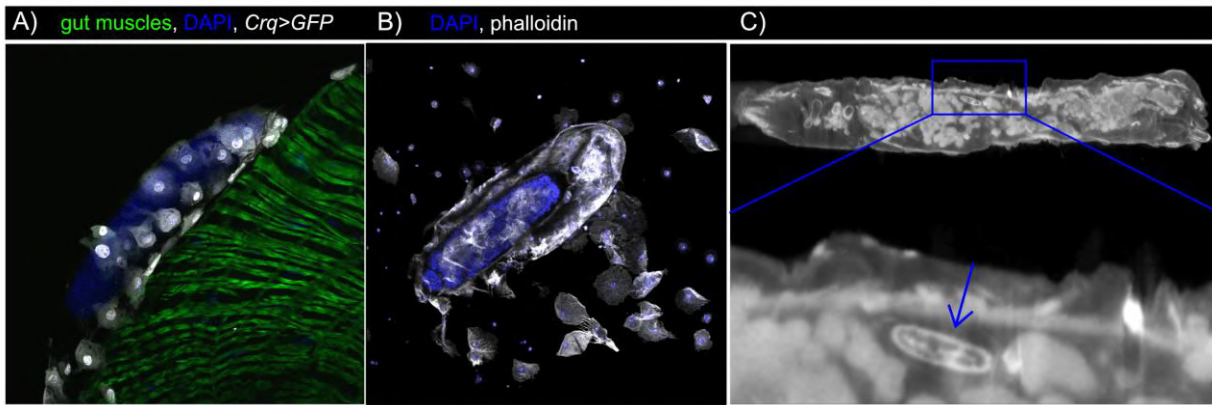


Figure 9: **Immune cells are responsible for the encapsulation and subsequent melanization of parasitoid eggs in fruit fly larvae.** (A) Confocal image of plasmatocytes (white) attaching to parasitoid wasp egg (blue), which hides in the folds of intestine (green) shortly after infestation. (B) Confocal image of lamellocytes forming thick layers around the parasitoid wasp egg. (C) Micro-computed tomography image of larva infected by parasitoid wasp *Leptopilina boulardi*. The arrow shows parasitoid wasp egg laid inside the body cavity of the host larva. The image was reconstructed from 3600 projections. Images in A and B were captured by FluoView3000 Olympus Confocal Microscope, and image in C by Bruker SkyScan 1272 μ CT Scanner.

Although the immune cell types and their function is less varied than in vertebrates, key signaling pathways and transcription factors involved in hematopoiesis, proliferation, and immune defense are conserved through 550 years of evolution. Vertebrates alike, the hematopoiesis in *Drosophila* occurs in two waves. The first population of immune cells is specified from the head mesoderm during embryogenesis and gives rise to about 700 macrophage-resembling plasmatocytes, which migrate throughout the embryo at the end of embryonic stage 10 (Crozatier and Meister, 2007). The movement of these cells is facilitated by large, polarized protrusions, filopodia and lamellipodia, formation of which is driven by *SCAR*, which regulates actin polymerization and influences cell shape and motility (Evans and Wood, 2014). In addition, it has been described that the expression and activity of the PDGF/VEGF receptor related (*Pvr*) on the plasmatocytes is required for their migration along specific pathways throughout the embryo since they are attracted by PDGF- and VEGF-related factor 2 (*Pvf2*) and *Pvf3* expressed along the ventral nerve chord (Cho *et al.*, 2002). By these means, the cells disperse throughout the embryo. The first wave also gives rise to approximately 30 crystal cells, which are later located around the proventriculus (Lebestky, Jung and Banerjee, 2003; Zaidman-Rémy *et al.*, 2012).

The second hematopoietic wave occurs in third instar larvae. In larva, the hemocytes reside in circulation, in the hematopoietic organ located alongside the aorta and in sessile compartment, which is represented by hemocytes residing in segmentally repeating lateral epidermal-muscular pockets and adhering to the epidermis in a dorsal patch. Distinct hemocytes also accumulate at the folds of intestine and become enriched mainly at the proventriculus (Zaidman-Rémy *et al.*, 2012). They maintain homeostasis of the gut and gut microbiota, protect the host against oral infection and participate in regeneration of gut injury. The hematopoietic organ called lymph gland forms during embryogenesis

and it consists of a single pair of lobes (i.e. anterior or primary lobes) until the second instar. At the beginning of third instar, another pairs of lobes (called posterior or secondary lobes) develop and hematopoiesis occurs almost exclusively in the primary lobes. However, upon infestation, it can occur also in the secondary lobes (Crozatier and Meister, 2007).

At the onset of metamorphosis, the lymph gland disintegrates, the plasmatocytes are released into the circulation and persist throughout the metamorphosis to the adult stage. The adults possess mainly these plasmatocytes, hereafter denoted as macrophages, no lamellocytes are present in mature *Drosophila*. Interestingly, some works document the presence of crystal cells also in adults (Kurucz *et al.*, 2007; Ghosh *et al.*, 2015; Boulet *et al.*, 2021). The number of macrophages decline as the adult ages since there is no hematopoietic organ present and the prevailing view of the field is that the macrophages do not divide in imagoes (Woodcock *et al.*, 2015; Sanchez Bosch *et al.*, 2019). Nonetheless, two publications dispute this observation (Ghosh *et al.*, 2015; Boulet *et al.*, 2021).

Whilst there is a significant number of circulating macrophages in larval stages, the vast majority of them are attached to various structures in adults, which complicates their isolation. In adults, the majority of macrophages are located in dorsal regions alongside the aorta and in the proximity of pericardial cells entangled into ECM composed of Pericardin and LamininA with accumulations on the transition between body segments (Ghosh *et al.*, 2015). They are also frequently found in association with the respiratory epithelia, where they function as sentinels of infection. Potentially, it may be a convenient position for them to convey information about infection to the epithelia and other neighboring cells (Sanchez Bosch *et al.*, 2019).

When introducing the immune system of *Drosophila*, the humoral branch cannot be omitted. It depends mainly on the production of antimicrobial peptides (AMPs), which are potent against Gram-positive and Gram-negative bacteria, fungi (yeasts and filamentous), some parasites and even some species of enveloped viruses. Although AMPs are constitutively expressed in certain tissues (salivary glands, reproductive tract), they become rapidly produced by the fat body, hemocytes and surface epithelia in a tissue-specific manner under systemic infection (Lemaitre and Hoffmann, 2007; Lemaitre and Miguel-Aliaga, 2013). Due to their positive charge, they get embedded in the hydrophobic portion of the bacterial or fungal membrane, leading to its destabilization and eventually cell death. Currently, seven families of antimicrobial peptides have been well characterized, out of which 21 AMP/AMP-like genes have been reported (Hanson, Lemaitre and Unckless, 2019). Since their expression is regulated either by Toll or Immune deficiency (Imd) signaling pathways, which become activated upon systemic infection of the host, they have been used as readouts of their activation. In general, whilst Gram-positive bacteria and fungi activate the Toll pathway, activation of Imd pathway follows after infection by Gram-negative bacteria (De Gregorio, 2002). In addition, after more than 15 years since their discovery, several peptides have been grouped under a designation 'Bomanins'. They are regulated by the Toll pathway, have been shown to have antimicrobial properties *in vivo* and are essential for combating Gram-positive bacteria and fungi (Lindsay, Lin and Wasserman, 2018).

Nonetheless, AMPs are not the only peptides whose expression is enhanced by immune challenge. It has been documented that immune response is followed by rapid activation of JNK signaling pathway, which controls the expression of cytoskeletal proteins and genes involved in the remodeling of cytoskeleton such as *myosin31DF*, *actin88F*, *flightin* or *ninjurin*. JAK/STAT signaling pathway is another such example, and its activation leads to expression of thioester-containing proteins (TEPs) or Turandots (TotA, TotB, TotC, TotF, TotM, TotX, and TotZ) (Yu *et al.*, 2022).

Despite *D. melanogaster* lacks the adaptive arm of the immune system, several studies have documented that the innate branch displays features of immune memory. This concept is known as innate immune priming and has been supported by several publications conducted on various insect species (Gomes *et al.*, 2022). One of the first studies documenting the “memory” features of innate immune system in insects has been conducted on *Periplaneta americana*, which displays protection against live *Pseudomonas aeruginosa* after prior immunization with heat-killed bacteria of the same species, which lasts for 14 days (Faulhaber and Karp, 1992). Since then, multiple studies have reported similar effects in other insect species. In 2007, Pham and colleagues showed that sublethal dose of *Streptococcus pneumoniae* protects against an otherwise lethal second encounter of *S. pneumoniae*, while this effect last for a life time of the fly (Pham *et al.*, 2007). Although analogous results have been obtained for natural fungal pathogen *Beauveria bassiana*, not all inspected pathogens evoked immune priming. In addition, the authors showed that while Toll pathway is indispensable for evoking the immune priming, imd pathway is not required, but experimental activation of Toll pathway is not sufficient to elicit immune memory. Moreover, while neither humoral immune response (AMPs) nor melanization seem to be the underlying mechanisms behind immune priming, the action of macrophages is crucial. Indeed, blocking of phagocytosis by injection of polystyrene beads results in abrogated immune response to second dose of *S. pneumoniae* (Pham *et al.*, 2007). In 2018, another research shed light on the features of *Drosophila* innate immune memory. The authors showed that oral infection of larvae with *Drosophila C* virus had improved the survival of a subsequent lethal dose of this virus in adults (Mondotte *et al.*, 2018). Strikingly, there are indices even about the transgenerational immune priming as the enhanced protection against viral infection is passed to the offspring for up to five generations in a sequence-specific and RNA-dependent manner (Mondotte *et al.*, 2020). An extensive review summarizing current knowledge on *Drosophila* primed immunity has been published by Arch and colleagues (Arch *et al.*, 2022). Yet, the underlying mechanisms remain to be determined.

In doing so, we may find an inspiration in research conducted on vertebrate models by the scientific group led by prof. Mihai Netea. In 2011, he introduced the term “trained immunity”, denoting the features of immunological memory possessed by mammalian innate immune cells (Netea, Quintin and van der Meer, 2011). Few years later, he showed that the trained immunity is heavily dependent on epigenetic reprogramming through histone modifications. On the molecular level, immune training is dependent on elevated glycolytic rate induced by mTOR-HIF1 α pathway, reduced basal respiration rate, increased consumption of glucose and lactate production (Cheng *et al.*, 2014). Additionally, it has been

show that innate immune memory also relies on metabolic signals, as activation of mevalonate pathway is essential for immune training. However, it is not because of synthesis of cholesterol itself, but due to mevalonate-induced activation of IGF1-R and mTOR signaling and subsequent histone modifications in inflammatory pathways (Bekkering *et al.*, 2018). Nonetheless, the molecular features of primed immunity are yet to be revealed in insects.

1.7.1.1 VARIOUS FUNCTIONS OF *DROSOPHILA* MACROPHAGES

As evidenced by the advances in the past years, *Drosophila* macrophages take on a strikingly wide variety of roles, ranging from phagocytosis of the pathogens, production of antimicrobial peptides and other bactericidal compounds to organogenesis, tissue remodeling, healing, and anti-tumorigenic function. In addition, there are indices that they contribute to regulation of the systemic metabolism under various conditions. Since mammalian macrophages possess very similar functions, often conserved even at the molecular level, *Drosophila* offers a powerful model for the study of their functional versatility *in vivo*. Interestingly, *Drosophila* macrophages are not diverse only functionally, but we can distinguish certain features of tissue residency in various macrophage subpopulations already in this holometabolous insect as evidenced by recent single-cell RNA sequencing (Cattenoz *et al.*, 2020; Cho *et al.*, 2020; Fu *et al.*, 2020; Tattikota *et al.*, 2020; Hirschhäuser *et al.*, 2023).

1.7.1.1.1 ROLES IN FIGHTING THE PATHOGEN

Since fruit flies live in a microbe-rich environment, they heavily rely on phagocytic defense (Fig. 10). In analogy to mammals, professional phagocytes in *Drosophila* are represented by macrophages. Phagocytosis is initiated after recognition of molecules exposed at the surface of the pathogen such as peptidoglycans, lipopolysaccharides, or fungal β -1,3 glucans by specialized phagocytic receptors. Namely, these are scavenger receptors (class B and class C Scavenger receptor families, e.g. *croquemort*), peptidoglycan recognition proteins (PGRPs), Nimrods (e.g. NimC1, NimC4, eater, draper (*drpr*)), or integrins (also involved in cell spreading and motility) (Lu *et al.*, 2020). Several molecules structurally related to the mammalian complement factor C3 family, which might thus act as opsonins, have been detected in the *Drosophila* genome. These are six TEPs, which are specifically expressed on macrophages, fat body, and some barrier epithelia. Four of them possess a signal peptide, suggesting that they are secreted from these tissues (Bou Aoun *et al.*, 2011). In addition, Dscam1 has been implicated to function as opsonin as well (Watson *et al.*, 2005). Active and dynamic remodeling of the plasma membrane allows for internalization of the particle and it is mainly guided by the actin cytoskeleton. Several molecules required for this process are homologous to those mediating the cytoskeletal reorganization in mammalian systems, such as *SCAR* and *WASP*, *Drosophila* homologues of *WAVE* and *WASP*, which activate the Arp2/3 complex responsible for F-actin generation at the engulfment site (Evans and Wood, 2014). This results in formation of the phagocytic cup and once the phagocytic protrusions fuse at the leading edges, a new phagosome is formed. Subsequently, it

undergoes maturation and eventually fusion with lysosome, which requires small GTPases of the Rab family. In order to activate the lysosomal hydrolases, the phagosome must be acidified by V-ATPases (Melcarne, Lemaitre and Kurant, 2019).

Another prominent role of *Drosophila* macrophages in immune defense is the secretion of various antimicrobial agents such as the aforementioned AMPs, lysozymes, ROS or clotting proteins. Coagulation of hemolymph is referred to as clotting and it is essential to prevent dissemination of pathogens. At first, the wound is covered by proteins that are cross-linked by transglutaminase, which is homologous to factor XIIIa, an essential component of the vertebrate coagulation cascade (Wang *et al.*, 2010). The soft cloth then hardens thanks to phenoloxidase-dependent cross-linking. Some of the clotting proteins are secreted by the immune-challenged macrophages such as hemolectin, which is also frequently used as a strong macrophage-specific Gal4 driver and which resembles human von Willebrand factor (Goto *et al.*, 2001; Goto, Kadowaki and Kitagawa, 2003). Nonetheless, the majority of clotting proteins are secreted by crystal cells and fat body. *Lipophorin*, hexamerins (*larval serum protein 1* and *2*) and their receptor *fat body protein 1*, *fondue* and phenoloxidases have been identified in pull-down and proteomics experiments as the most abundant proteins found in the clot (Wang *et al.*, 2010).

Another approach for immobilization of the pathogen is casting of extracellular traps. Despite it has been described to be formed by macrophages in *Drosophila suzukii*, it has not been reported as a tool for combating pathogens in *D. melanogaster* so far (Carrau *et al.*, 2021).



Figure 10: **Phagocytic capability of *Drosophila* macrophages.** (A) Confocal image of a macrophage (Crq>GFP, green) dissected from a fly injected with *S.a.*-pHrodo, depicting its phagocytic potential. (B) Scanning electron micrograph showing *S. pneumoniae* (pseudocolored in violet) attached to the macrophage surface. (C) Transmission electron micrograph of a macrophage (pseudocolored in green) with engulfed *S. pneumoniae* (pseudocolored in violet). Image in A was captured by FluoView3000 Olympus Confocal Microscope, in B by JSM-7401F JEOL Scanning Electron Microscope, and in C by JEM-1400 JEOL Transmission Electron Microscope at the Biology Centre CAS.

1.7.1.1.2 WOUND HEALING AND REGENERATION IN *DROSOPHILA*

Upon wounding, the macrophages not only clear the environment from the invading pathogens but also contribute to wound healing and tissue regeneration (Kelsey *et al.*, 2012). Mammals alike, the

macrophages engulf the damaged tissue and necrotic debris. Laser-induced wounding of *Drosophila* embryos serves as a model for investigation of macrophage roles in tissue healing (Stramer *et al.*, 2005). Using this approach, it has been shown that tissue damage induces a calcium flash, which spreads as a wave throughout the damaged epithelium. In turn, NADPH oxidase (*Duox*) generates hydrogen peroxide, which is sensed by the macrophages, resulting in their rapid and highly directional recruitment (Roddie *et al.*, 2019). *Six-microns-under (simu)* (also known as Nimrod C4) has been shown as a crucial molecule involved in this process as *simu* mutant embryos exhibit significant defects in macrophage recruitment to wounds (Roddie *et al.*, 2019). Moreover, it is considered as a general detector of damaged host tissues and an important molecule regulating macrophage function during resolution of inflammation (Roddie *et al.*, 2019).

Similarly, laser-induced wound of *Drosophila* pupae leads to recruitment of macrophages and their participation in tissue regeneration as they engulf the damaged tissue and cellular debris (Pastor-Pareja, Wu and Xu, 2008; Katsuyama *et al.*, 2015). Nonetheless, it has been shown that macrophages are not the only cells that participate in this process. They intimately cooperate with the larval adipocytes, which display an unusual adhesion-independent, actomyosin-driven motility and tightly seal the wound. In addition, they clear the cellular debris and secrete antimicrobial peptides (Franz, Wood and Martin, 2018). This work has thus unraveled another similarity between macrophages and adipocytes.

Regenerative role of macrophages has been described upon wounding of the gut in adult flies. It has been shown that the macrophages secrete unpaired 3 (upd3), presumably in response to elevated ROS levels, which activates JAK/STAT cascade in the gut and the fat body, leading to stimulation of intestinal stem cell proliferation and expression of *Drosomycin*-like genes in the gut, thus ensuring optimal survival of septic injury (Chakrabarti *et al.*, 2016; Chakrabarti and Visweswariah, 2020). In addition, production of ROS by macrophages at the site of sterile injury provides the flies with another advantage as it protects the flies on subsequent infection, suggesting training of the innate immune system (Chakrabarti *et al.*, 2016). On the other hand, another study has shown that the macrophages are attracted to the damaged intestine and produce the Bone morphogenetic protein (BMP) homologue *decapentaplegic*, which induces intestinal stem cell proliferation by activating the type I receptor Saxophone and the Smad homologue SMOX (Ayyaz, Li and Jasper, 2015). Although such interaction between macrophages and the gut promotes infection resistance, it also contributes to the development of intestinal dysplasia in ageing flies (Ayyaz, Li and Jasper, 2015). This study thus suggests that an initially adaptive role of macrophages may become detrimental in other situations. In addition, it has been suggested that similar inter-organ communication may play a significant role in certain pathologies such as inflammatory bowel disease and colorectal cancer in humans (Ayyaz, Li and Jasper, 2015).

1.7.1.1.3 CLEARANCE OF *DROSOPHILA* APOPTOTIC CELLS AND REBUILDING OF BODY PLAN

During the embryonic stage, the macrophages perform a plethora of “non-immune” functions. Extensive events of programmed cell death is a common phenomenon of embryogenesis. Apoptosis of the unwanted cells begins at stage 11 of embryogenesis (approximately 7 hours) and thereafter becomes widespread. Hence, the anlage of the embryonic immune cells must be determined early in the development to later remove the dying cells and thus shape various tissues and organs. Indeed, this happens strikingly early, already before formation of a blastoderm, which is in contrast to all other mesodermal cells (Holz *et al.*, 2003). A vast majority of macrophages (70-80%) contains at least one engulfed apoptotic body by the end of embryogenesis (Tepass *et al.*, 1994). Engulfment of apoptotic cells is enabled by several molecules. One of them is a scavenger receptor *croquemort*, a homolog of the mammalian CD36 (Franc *et al.*, 1996, 1999). In addition, two transmembrane proteins of the Nimrod family, DRPR and SIMU, and one secreted protein, Nimrod B4, have been shown to also mediate the recognition and internalization of apoptotic corpses, and it is presumably involved in phagosome maturation, more specifically in the fusion between the phagosome and lysosomes (Manaka *et al.*, 2004; Kurant *et al.*, 2008; Petrignani *et al.*, 2021). Similarly to vertebrates, these receptors recognize “eat me” epitopes such as phosphatidylserine on the surface of their apoptotic prey.

Clearance of apoptotic cells is also facilitated by the migratory abilities of macrophages. Regulation of macrophage cytoskeleton and formation of protrusions is a complex mechanism involving plethora of crucial molecules. These include *Enabled (Ena)*, which regulates lamellipodial protrusions, and the actin bundling protein fascin, which stabilizes these structures (Tucker, Evans and Wood, 2011; Zanet *et al.*, 2012). In addition, *SCAR* has been shown as primary regulator of the Arp2/3 complex, which promotes actin polymerization and influences cell shape and motility (Evans and Wood, 2014).

Interestingly, efferocytosis of apoptotic corpses by naïve macrophages during the embryonic stage of the individual is essential for priming of the macrophages to tissue damage and infection at later stages of life. The underlying mechanism is calcium-induced activation of JNK signaling, leading to upregulation of *drpr*, which facilitates rapid phagocytosis of bacterial pathogens or recruitment to injured tissues (Weavers *et al.*, 2016). Although macrophages display huge phagocytic capacity, it is not infinite and the capacity can become fully saturated. The researchers have developed a model for the study of macrophage-apoptotic cell interactions in the embryo employing individuals with mutation in transcription factor *reversed polarity (repo)* (Armitage, Roddie and Evans, 2020). Under normal conditions, *repo* is specifically expressed in glial cells, and loss of *repo* prevents these cells from contributing to apoptotic cell clearance. As a result, the macrophages must deal with excessive numbers of apoptotic cells, become highly vacuolated and their migration is perturbed. Moreover, their inflammatory response to injury is impaired (Armitage, Roddie and Evans, 2020). These results thus suggest that even these remarkable cells can be ‘overtasked’.

During the *Drosophila* life time, another period of extensive cell death occurs during metamorphosis and hence this period may potentially also serve to investigate the macrophage-apoptotic cell interaction *in vivo*. While the adult structures are built from imaginal discs, epithelial structures found inside the larva, vast majority of the larval tissues undergo histolysis. The mass of dying cells represents an immense burden for the organism and the debris must be thus promptly removed. During the pupal development, the lymph gland disintegrates and macrophages accumulate at the boundaries between the larval fat body cells (Fig. 11) (Nelliot, Bond and Hoshizaki, 2006). Indeed, macrophages are responsible for macroendocytosis and efferocytosis of mainly muscle and fat cells (Regan *et al.*, 2013; Ghosh, Ghosh and Mandal, 2020). The movement of macrophages towards the apoptotic cells in pupa is an actin-dependent process. A study by Regan and colleagues showed that upregulation of macrophage actin dynamics, motility and subsequent phagocytosis of apoptotic cells is regulated by the steroid hormone ecdysone. Indeed, overexpression of dominant-negative allele of ecdysone receptor specifically in immune cells resulted in defective bacterial phagocytosis and fatal susceptibility to infection by bacteria ingested at larval stages, although the production of antimicrobial peptides remains unchanged (Regan *et al.*, 2013).

Potentially, at this life stage lipid-loaded macrophages may serve as a model to dissect out the mechanisms and consequences of enhanced engulfment of adipocytes and leaking lipids. Despite that the presence of engulfed muscle sarcolemmas and adipocyte corpses inside the phagolysosomes is well described, the subsequent fate of this nutrient-rich debris and how the energy is transformed from larval stages to the adult remains to be understood (Ghosh, Ghosh and Mandal, 2020).

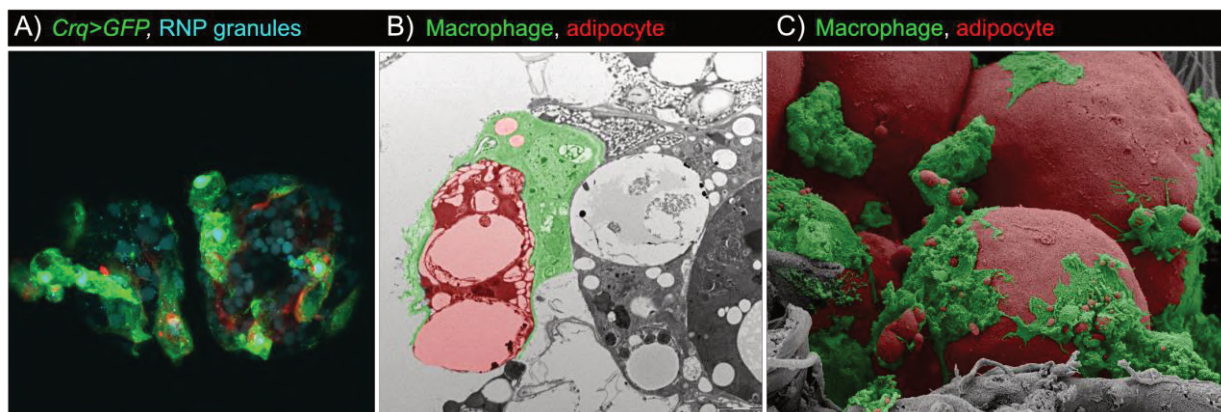


Figure 11: **Macrophages infiltrate larval adipose tissue during *Drosophila* metamorphosis.** (A) Macrophages (Crq>GFP, green) attached to adipocytes (visualized by autofluorescent RNP granules) dissected from freshly emerged flies. (B) Transmission electron micrograph depicting a macrophage (pseudocolored in green) engulfing a dying larval adipocyte (pseudocolored in red) in freshly emerged flies. (C) Scanning electron micrograph illustrating macrophages (pseudocolored in green) in close association with larval adipocytes in freshly emerged virgins (pseudocolored in red). Image in A was captured by FluoView3000 Olympus Confocal Microscope, in B by JEM-1400 JEOL Transmission Electron Microscope, and in C by JSM-7401F JEOL Scanning Electron Microscope at the Biology Centre CAS.

1.7.1.1.4 ADJUSTMENT OF *DROSOPHILA* SYSTEMIC METABOLISM

As already mentioned in the preceding paragraph, activated macrophages represent significant producers of AMPs *via* activation of Toll or Imd pathway, which eventually leads to destruction of the invading bacteria. Importantly, however, activation of immune-related signaling pathways is accompanied not only by AMP secretion, but also by production of signaling factors that may adjust the function of other organs and tissues. Thus, the macrophages play important role in propagating the information about infection to other tissues *via* inter-organ communication. Notably, some of the factors mediating this cross-talk are homologous to factors secreted by activated mammalian macrophages and hence can be denoted as true cytokines. For instance, *upd3* has been recognized as an ortholog of mammalian IL-6 and *eiger* (*egr*) has been identified as ortholog of TNF- α (Igaki, 2002; Oldefest *et al.*, 2013). Secretion of Upd3 documents the intimate interconnection between the immune cells and the fat body during immune challenge. Upon septic injury with Gram-negative bacteria, the immune cells secrete Upd3, which activates the JAK/STAT pathway in the larval fat body *via* the receptor domeless. Activation of Imd and JAK/STAT pathway then leads to the secretion of TotA by the adipocytes. Another example may be infection by Gram negative bacteria of domino mutant larvae (larvae devoid of immune cells), which fail to increase the expression of Diptericin in the fat body (Imler and Bulet, 2005; Sanchez Bosch *et al.*, 2019).

Interestingly, the macrophages can influence other tissues not only by stimulating them to secrete AMPs, but also by acting as potent regulators of cellular metabolism of various organs. It has been well documented that the infection is accompanied by significant changes in the systemic metabolism and systemic energy handling. While glycogen stores become depleted in muscles, the titer of glucose rises during the acute phase of infection (Bajgar *et al.*, 2015; Bajgar and Dolezal, 2018). Analogous effects have been also documented in septic patients, which experience hyperglycemia and hyperlipidemia (Gallin, Kaye and O’Leary, 1969; Sammalkorpi *et al.*, 1988; Wernly *et al.*, 2016). These effects can be explained by the “selfish immune system” theory (Straub, 2014). According to this concept, the macrophages have a superior position upon immune challenge and adjust the metabolism of other organs to secure enough energy for themselves (Bajgar *et al.*, 2015; Bajgar and Dolezal, 2018). There are two possible mechanisms how to do that, i.e. suppress nutrient consumption by “non-immune” tissues or induce mobilization of energy stores to the circulation to make them available for the immune system. Thus, from the perspective of inter-organ communication, the activated macrophages behave seemingly selfishly to ensure survival of the individual. Nonetheless, such adjustment of systemic metabolism must be restricted to the acute phase of infection, otherwise leading to nutrient wasting and cachexia-like effects.

The relevance of this theory may be documented on extracellular adenosine (eAdo). Bajgar and colleagues have experimentally demonstrated that upon wasp infestation of *Drosophila* larvae, the activated macrophages release eAdo, which in turn silences consumption of glucose by “non-immune” tissues, resulting in decreased growth of imaginal wing discs and delayed metamorphosis of the

individuals (Bajgar *et al.*, 2015). Similar effect of macrophage-derived eAdo was observed also in adult fruit flies challenged by streptococcal infection. Indeed, acting on its receptor, eAdo influences the expression level of glycogen-metabolizing enzymes, leading to depletion of glycogen stores in the fat body, thereby inducing hyperglycemia (Bajgar and Dolezal, 2018). Nonetheless, increased availability of nutrients caused either by decreased consumption by “non-immune” tissues or enhanced mobilization of nutrients from the storage organ may become detrimental upon infection by intracellular bacteria. It is well established that the nutrients usurped by the activated macrophages may be highjacked by the intracellular pathogens, which become literarily nourished. Indeed, knockdown of enzymes involved in triglyceride synthesis leads to reduction of bacterial burden in host cells due to reduction of lipid droplets (Péan *et al.*, 2017). The negative effect of increased titer of nutrients in circulation upon infection by intracellular bacteria may be documented on the production of eAdo. Whilst its secretion by activated macrophages is required for efficient resistance to streptococcal infection, its production is detrimental in flies infected by intracellular bacteria *Listeria monocytogenes* (Bajgar and Dolezal, 2018). Moreover, as eAdo has an effect on nutrient mobilization and thus its production must be time-limited. Indeed, when produced chronically, it results in nutrient wasting. Therefore, its titer in the circulation must return to the base level during the resolution phase of infection (Bajgar and Dolezal, 2018).

Another macrophage-derived molecule displaying the potential to adjust the systemic metabolism is *upd3*. It has been experimentally demonstrated that upon infection of *Drosophila* larvae, increased expression of *upd3* by activated macrophages enhances JAK/STAT signaling in muscles, thereby reducing their insulin sensitivity and thus glucose consumption, which is required by the activated macrophages to combat the pathogen (Yang *et al.*, 2015; Yang and Hultmark, 2017).

Another molecule which may have the potential to adjust the systemic metabolism upon infection is *egr*. Indeed, its expression has been shown to increase in macrophages upon immune stimulation and it is essential for resistance to extracellular bacteria, presumably due to its requirement for efficient phagocytosis (Brandt *et al.*, 2004; Johansson, Metzendorf and Soderhall, 2005; Schneider *et al.*, 2007). However, its effects may be detrimental upon infection by intracellular pathogens, analogously to eAdo. In concordance, it has been shown that blockade of mammalian *egr* ortholog TNF- α prevents muscle wasting in septic rats (Agrawal *et al.*, 2016). Nonetheless, the situation is far more complex as *egr* is produced also by the fat body upon immune challenge and it suppresses expression of *Drosophila* insulin-like peptides in the insulin-producing cells via JNK signaling (Agrawal *et al.*, 2016). Nonetheless, its effects on systemic energy handling has been documented mainly during other stress situations than infection and its role upon immune challenge remains to be fully explored (Hull-Thompson *et al.*, 2009; Pasco and Léopold, 2012; Agrawal *et al.*, 2016).

Despite the discoveries made in the past few years, the molecular mechanisms underlying the macrophage-induced silencing of systemic metabolism are not fully understood. Abrogation of insulin signaling in the peripheral tissues may represent a potent strategy how to ensure sufficient nutritional supplementation of the immune cells. Hence, insulin resistance may represent an adaptive mechanism

for energy mobilization upon immune challenge. Yet, the relevance of this idea has not been satisfactorily tested so far.

Interestingly, metabolic role of macrophages may not be restricted exclusively to immune challenge. Recent advances in the *Drosophila* immunological research describe many subpopulations of the immune cells and it is now thus clear that *Drosophila* macrophages are much more diverse than considered previously (Cattenoz *et al.*, 2020; Cho *et al.*, 2020; Fu *et al.*, 2020; Tattikota *et al.*, 2020). Cho *et al.* (2020) identified adipohemocyte population in their single cell transcriptome map of unchallenged larval immune cells characterized based on high expression of phagocytic receptors (*crq*, *eater*), lipid metabolism-related (*LpR2*, *Lsd-2*) genes and starvation-induced (*Sirup*) genes. In addition to gene expression, they have described a few macrophages containing neutral lipids, suggesting the role of macrophages in coordination of immunity and metabolism (Cho *et al.*, 2020). The involvement of macrophages in the metabolism of lipids has been further supported by identifying a subpopulation of macrophages with high expression of genes connected with lipid transport in another study (Cattenoz *et al.*, 2020). Moreover, this subpopulation designated as PL-Lsp is characterized by the expression of the storage proteins larval serum protein (*Lsp*) and odorant binding protein *Obp99b*, which were originally described to be secreted by the fat body (Cattenoz *et al.*, 2020). These data thus further document certain similarities between the immune cells and the fat body and suggest nutritional role of macrophages.

1.7.1.1.5 DESTRUCTION OF *DROSOPHILA* TUMORS

In 2008, it was first reported that macrophages of the fruit fly also respond to tumors. *Via Drosophila*-specific genetic tools, researchers generated tumors in eye-antennal imaginal discs of *Drosophila* larvae (*Ras^{VI2}/scrib^{-/-}* tumors), which displayed degeneration of basement membrane (Pastor-Pareja, Wu and Xu, 2008). As components of the basement membrane are remarkably conserved throughout the animal kingdom, it is not surprising that even insect macrophages detect its disruption and attach to the surface of the tumor, preferably to the sites of basement membrane disruption (Pastor-Pareja, Wu and Xu, 2008). The damaged tissue displays activation of JNK signaling, leading to the expression of JAK/STAT-activating cytokines *upd2* and *upd3*. Subsequently, the signals are amplified by their expression in the macrophages and the fat body, resulting in macrophage proliferation. As larvae with reduced number of macrophages exhibit increased size of tumors compared to controls, it has been proposed that macrophages play a significant role in elimination of tumor growth (Pastor-Pareja, Wu and Xu, 2008).

However, in the next years, it has been documented that tumor associated macrophages can lead to both tumor regression and tumor promotion and invasive migration, depending on the genetic makeup of the tumor. Another macrophage-derived factor involved in response to tumors is *egr*, as its production simultaneously leads to death of the simple neoplastic tumors cells and stimulation of Pvf1 expression, eventually resulting in macrophage proliferation *via* PVR signaling (Parisi *et al.*, 2014). However, it

these tumors also express oncogenic form of the Ras protein (Ras^{V12}), macrophage-derived *egr* induces tumor overgrowth and invasion driven by MMPs (Cordero *et al.*, 2010). These data thus experimentally showcase similarities to vertebrates, in which tumor-associated macrophages support tumor growth *via* TNF α and pro-inflammatory cytokines (Ostuni *et al.*, 2015).

1.7.1.1.6 MORPHOGENESIS AND ORGANOGENESIS IN *DROSOPHILA*

Vertebrate macrophages alike, macrophages of the fruit fly are also responsible for organ morphogenesis, mainly due to their role in deposition of the ECM components.

During the embryonic development, the macrophages synthesize and secrete high levels of *Secreted protein, acidic, cysteine-rich* (SPARC) and other basal lamina components such as collagen IV, laminin and perlecan. It has been documented that the migrating macrophages are responsible for deposition of ECM components to ventral nerve chord. In addition, they also engulf the apoptotic ventral nerve chord cells and are thus crucial for proper development of CNS. In embryos in which the migration of macrophages was blocked by mutation of *Pvr* and which thus lack of the deposition of the ECM proteins, CNS failed to condensate, resulting in perturbed function of the nervous tissue (Olofsson and Page, 2005). In addition, lack of clearance of the apoptotic debris results in mispositioning of the glial cells and affected CNS morphogenesis (Sears, Kennedy and Garrity, 2003). Clearance of the impaired neurons and neuronal debris is facilitated by *simu* and *drpr*, as their lack leads to delayed clearance of apoptotic neurons and ultimately to neurodegeneration (Awasaki *et al.*, 2006; MacDonald *et al.*, 2006; Kurant *et al.*, 2008; Purice *et al.*, 2017). Interestingly, reduced expression of *drpr* has been detected in aged flies, resulting in declined engulfment of the injured axons (Purice, Speese and Logan, 2016).

Glial cells are resident macrophages of the mammalian nervous system and are responsible both for immune protection and proper development of the CNS. In *Drosophila*, glial cells are often considered as professional phagocytes in addition to macrophages, although they arise from a distinct cell lineage. *Drosophila* macrophages and glial cells display molecular parallels regarding their phagocytic receptors *Simu* and *drpr* (MacDonald *et al.*, 2006; Kurant *et al.*, 2008; Weavers *et al.*, 2016; Davidson and Wood, 2020). In *Drosophila* embryo, mainly subperineural glial cells are also responsible for the engulfment of the apoptotic neurons (Sonnenfeld and Jacobs, 1995). Besides their role in tissue shaping, it has been suggested that glial cells do not act in the *Drosophila* brain as mere cleaners. It is hypothesized that they produce lactate from glucose and shuttle to the neurons for nutrition (Pellerin and Magistretti, 1994; Allaman, Bélanger and Magistretti, 2011; Limmer *et al.*, 2014; McMullen *et al.*, 2023).

Macrophages are also involved in proper development of the wings in freshly emerged adults. It has been suggested that they reside between the dorsal and ventral surfaces of newly opened wings and they are responsible for deposition of ECM that bonds the two wing surfaces together and phagocytosis of the apoptotic epithelial cells. Indeed, induction of cell death in these cells by

overexpression of catalytic subunit of the toxin Ricin A prevents expansion of the wings (Kiger, Natzle and Green, 2001).

The secretion of ECM components by macrophages has been further documented by the work of Yarnitzky and Volk who showed that lack of the deposition of the ECM protein Laminin results in impaired gut, heart, and muscle morphogenesis (Yarnitzky and Volk, 1995). Another work has shown that in the developing embryo, renal tubules produce VEGF/PDGF ligands, which in turn attract macrophages. Subsequently, the macrophages accumulate in the vicinity of the Malpighian tubules and secrete components of the basement membrane to ensheath them. Indeed, upon experimental abrogation of macrophage migration or loss of collagen IV, the renal tubules are misrouted, resulting in a defective organ shape and positioning (Bunt *et al.*, 2010).

Interestingly, macrophages also contribute to proper morphogenesis of the gonads and thus reproductive fitness of the flies. Distinct pool of macrophages were shown to be tightly associated with the ovaries and are also responsible for the formation of the basement membrane of the larval gonad via deposition of collagen IV. In addition, these ovarian macrophages thus tightly control the ovarian stem cell niche microenvironment and homeostasis. Hence, lack of the macrophage-secreted collagen may ultimately lead to decreased reproductive fitness (Van De Bor *et al.*, 2015).

As evident from the previous paragraphs, *Drosophila* macrophages take on a strikingly wide variety of roles, ranging from immune defense to organogenesis, tissue remodeling, healing, and regulation of the systemic metabolism under healthy physiological conditions, stress, and aging. Strikingly, we can also speculate on the existence of certain features of tissue residency and various macrophage subpopulations. To accomplish such distinct roles, it would be logical to assume that even *Drosophila* macrophages fine tune their metabolic setup similarly to their vertebrate counterparts. Nonetheless, not much research has been conducted to elucidate the potential of metabolic polarization of fruit fly macrophages.

1.7.2 METABOLIC SETUP OF *DROSOPHILA* MACROPHAGES

Whilst the concept of macrophage metabolic polarization toward M1 or M2 phenotype is well established in connotation with mammals, there are certain indices that also immune cells of fruit flies display features of metabolic switch.

Indeed, the proliferation and differentiation of lamellocytes upon parasitoid wasp infestation is accompanied by hemocyte-specific increase in glucose consumption, lactate production, and expression of glycolytic enzymes (Bajgar *et al.*, 2015; Dolezal *et al.*, 2019). Besides these studies, the implications of pro-inflammatory metabolic polarization are rather indirect (Fig. 12). Indeed, elevated expression of glycolytic enzymes including *Ldh* can be found in transcriptomic analyses of larval immune cells in response to wasp infestation and *Escherichia coli* infection (Irving *et al.*, 2005; Johansson, Metzendorf and Söderhäll, 2005). A recently published single cell RNA-seq data revealed that immune cells isolated

from the embryonic stage E16 display features of metabolic reliance on aerobic glycolysis rather than oxidative phosphorylation and silenced beta-oxidation in non-infectious conditions (Cattenoz *et al.*, 2020).

Similar indices can be found also in other insect species. Transcriptomics profiling of activated hemocytes isolated from mosquitoes *Anopheles gambiae*, *Aedes aegypti* and *Armigeres subalbatus*, and tobacco budworm *Heliothis virescens* has also revealed changes associated with the increased expression of glycolytic enzymes including *Ldh* (Bartholomay *et al.*, 2004; Pinto *et al.*, 2009; Shelby and Popham, 2012).

Concerning the analogy to M2 phenotype, a unique polarization setup of *Drosophila* macrophages has been described after ultraviolet light-induced retinal injury. In this scenario, the damaged tissue produces Pvf1. In turn, the macrophages promote repair mechanisms of the injured retina *via* expression of the mesencephalic astrocyte-derived neurotrophic factor (MANF). These cells also highly express the *Drosophila* homolog of the mammalian M2 marker *arginase1*, suggesting that these cells may be able to acquire phenotypes resembling alternative polarization (Neves *et al.*, 2016). Whether the fruit fly macrophages enter the M2-like phenotype also during other situations, such as efferocytosis of apoptotic cells or deposition of ECM during tissue differentiation in the embryonic stage is yet to be explored.

Despite these indications about the existence of various metabolic phenotypes, the concept of metabolic polarization of insect immune cells is far from complete. Hence, this issue represents an obvious gap in the field of insect immunometabolism and must be resolved in order to deeply understand how immune cells shape the systemic metabolic setup. In addition, a specific metabolic polarization state is linked to the production of specific signaling factors, and thus determining the setup of the immune cells may thus predict the systemic outcomes.

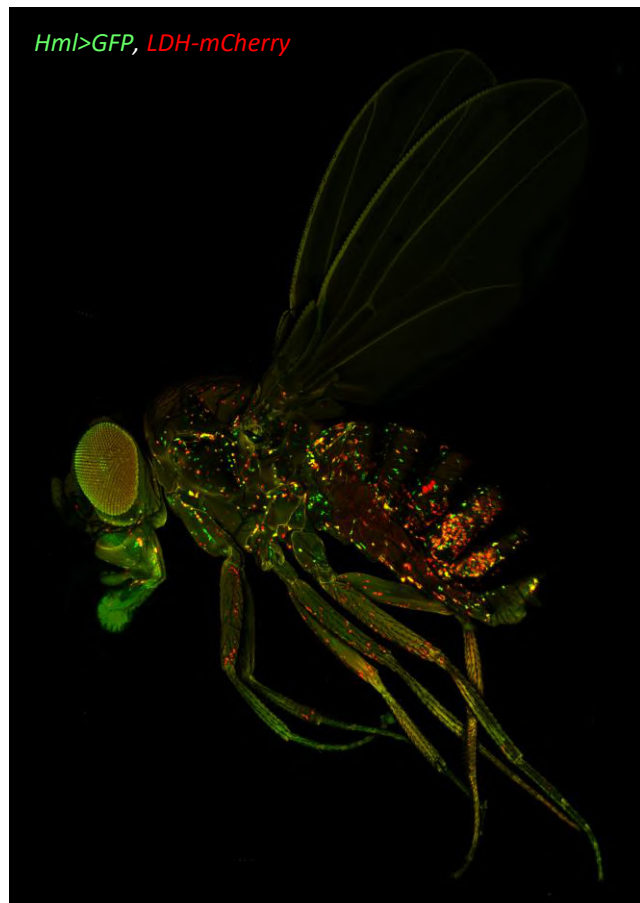


Figure 12: Confocal image of adult *Drosophila* infected by *S. pneumoniae* documenting colocalization of *LDH-mCherry* signal (red) with macrophage-specific marker (*Hml>GFP*; green). The image was captured by *FluoView3000 Olympus Confocal Microscope* at the *Biology Centre CAS*.

2 AIMS OF THE THESIS

The fact that macrophages represent a harmonizing force in developing embryos and adult animals by inducing physiological inflammation was already obvious to Elie Metchnikoff more than a century ago (Teti, Biondo and Beninati, 2016). Nonetheless, this perception has been slightly overshadowed by the discoveries of the roles of these cells in pathogen elimination. This function has been the focus of attention in the past decades. However, nowadays we come back to Metchnikoff's thoughts equipped with modern methods and approaches. *Drosophila* represent an excellent model organism for *in vivo* immunometabolic studies. Nonetheless, a key aspect of macrophage polarization has not been addressed in this organism up to now. Hence, the overarching goal of this thesis is to better understand the metabolic setup of activated *Drosophila* macrophages and identify their role in the regulation of systemic metabolism during various situations such as bacterial infection or metamorphosis and post-metamorphic maturation.

Severe bacterial infection represents a substantial metabolic burden on the host. Macrophages represent the front line of defense against bacterial intruders and it is well established that they switch the metabolic setup toward aerobic glycolysis in vertebrate species. Moreover, septic states are also accompanied by significant changes in systemic metabolism and energy handling. Indeed, increased serum triglyceride levels, characterized by an increase in VLDL levels, is an early metabolic alteration during infectious states and inflammatory conditions (Gallin, Kaye and O'Leary, 1969; Sammalkorpi *et al.*, 1988; Grunfeld *et al.*, 1992; Hardardóttir, Grunfeld and Feingold, 1995). Interestingly, these are also accompanying signs of chronic states such as obesity and metabolic syndrome or cancer (Teti, Biondo and Beninati, 2016). Nonetheless, the cause of these metabolic imbalances is poorly understood. Interestingly, previous research conducted in the laboratory revealed changes in systemic metabolism, such as elevated levels of glucose and reduced glycogen stores, also during wasp infestation and streptococcal infection in both larvae and adult *D. melanogaster* (Bajgar *et al.*, 2015; Bajgar and Dolezal, 2018). Following the "selfish immune system" theory, we hypothesize that macrophages may be the driving force of these changes due to their high metabolic demands and their privileged position in an organism stressed by infection. Nonetheless, despite the field of immuno-metabolism is gaining substantial attention and becoming a hot topic among *Drosophila* researchers in the past few years, the concept of macrophage polarization in insects has not yet been explored, and the metabolic needs of activated *Drosophila* macrophages are only indirectly assumed. Hence, it is first necessary to **describe the metabolic setup of *Drosophila* macrophages challenged with extracellular bacterial infection and to dissect the mechanism of its regulation.** Further, we aim to **identify potential molecules secreted by bacteria-challenged macrophages that may be responsible for the induction of the systemic metabolic changes and their mechanism of action.**

Yet, the role of macrophages is not limited to infection. Vertebrates alike, macrophages in *Drosophila* are responsible for maintaining tissue homeostasis and engulfing senescent and apoptotic cells (Sears, 2003; Kurant *et al.*, 2008; Van De Bor *et al.*, 2015). Previously, the members of our laboratory have noticed that macrophages in freshly emerged flies form crown-like structures around remaining larval adipocytes. Interestingly, these structures resembled those known from mammalian adipose tissue. Nonetheless, the number of publications mentioning the macrophage-adipocyte interaction during insect metamorphosis is very scarce, and limited efforts have been invested in exploring the role of macrophages in adipose tissue remodeling during *Drosophila* metamorphosis. Therefore, the next aim of the thesis is to **describe the phenotype of infiltrating macrophages during metamorphosis and early post-metamorphic development in *Drosophila* and to reveal their role in these life periods.**

Nonetheless, despite initially adaptive, dysregulation of macrophage role can result in pathology (Lumeng *et al.*, 2008; McNelis and Olefsky, 2014). As an imbalance in metabolic polarization is connected with the progression of many civilization and autoimmune diseases, there is a demand for macrophage-specific delivery of various drugs and metabolic inhibitors to avoid potential side effects (Kamaly *et al.*, 2016; Du *et al.*, 2021). For this reason, we also aim to **develop universal vehicles suitable for macrophage-specific delivery *in vivo***, which can potentially also serve as a research tool, e.g. for visualization or isolation of phagocytes and manipulation of macrophage metabolism in non-model insect species in subsequent research.

3 OUTLINE OF RESEARCH

This thesis consists of several published research and review papers and manuscripts still awaiting publication. **Chapter I** is devoted to exploring the metabolic setup of macrophages challenged by bacterial infection *in vivo*. To this end, severe infection was invoked by precise injection of 20,000 extracellular *S. pneumoniae* bacteria into the abdominal region of adult male *Drosophila*. We revealed that such infection leads to increased uptake of the glucose analog 2-NBDG by activated macrophages and that they increase the expression and activity of glycolytic enzymes including LDH during the acute phase of infection. In concordance, the titer of lactate is elevated in the circulation of infected flies, suggesting that macrophages preferentially convert pyruvate to lactate upon infection. Employing flies bearing a LacZ reporter construct for the activation of hypoxia response elements suggested that the transcription factor HIF1 α is stabilized in macrophages upon infection. Moreover, macrophage-specific knockdown of HIF1 α prevents the infection-induced increase in glucose uptake bacteria-challenged macrophages. Simultaneously, it also prevents the increase in expression and activity of glycolytic enzymes in macrophages, elevated levels of circulating glucose and lactate, and the depletion of glycogen in the fat body otherwise observed during the acute phase of infection. The importance of

HIF1 α -induced aerobic glycolysis for resistance to infection was confirmed by experimental macrophage-specific knockdown of LDH or HIF1 α , leading to elevated pathogen load and thus reduced survival of the infection. Importantly, these data suggest that *Drosophila* macrophages take up higher amount of glucose to sustain elevated flow through aerobic glycolysis, which is predominate program for the generation of energy in bacteria-challenged *Drosophila* macrophages. Nonetheless, this metabolic adaptation is temporary, as the metabolic switch to aerobic glycolysis is not present during the resolution phase of the infection. A major takeaway from this work is that the metabolic setup of M1 macrophages and its regulation is conserved between *Drosophila* and mammals, establishing the fruit fly as a powerful model for investigating the molecular mechanisms regulating the metabolism of immune cells.

Chapter II is a review article devoted to describing the molecular regulation of metabolism during the immune response in insects. It describes the metabolic reprogramming of activated immune cells and its link to adjustments in systemic metabolism resulting in physiological trade-offs during the immune response. In the last chapter, it discusses that once the pathogen has been eliminated, the metabolic setup and energy handling must return to the initial state, otherwise leading to chronic wasting.

Chapter III represents the major focus of research during my PhD studies. To find macrophage-derived signaling factors that may be responsible for inducing systemic metabolic changes, we performed RNA-seq analysis of macrophages isolated from adult flies injected with *S. pneumoniae* using a cell sorter. Of the cytokines that are highly expressed upon infection, we selected *Imaginal morphogenesis protein-late 2 (ImpL2)* as a potential candidate since it displays the most significant increase in response to infection and has previously been shown to affect systemic metabolism. Indeed, it has been shown by Kwon and colleagues that overproliferating intestinal stem cells secrete IMPL2, which is responsible for the induction of hyperglycemia and the depletion of glycogen and triglycerides, presumably due to abrogation of systemic of insulin signaling, leading to nutrient wasting in the ovary, fat body, and muscle (Kwon *et al.*, 2015). Similar results were obtained by Figueroa-Clarevega and Bilder, who showed that neoplastic tumors produce IMPL2, which is responsible for reduced insulin activity in peripheral tissues, high circulating sugar levels, and cancer cachexia (Figueroa-Clarevega and Bilder, 2015).

In our work, we demonstrated that the expression of *ImpL2* is directly regulated by HIF1 α as revealed by Chip-qPCR analysis. Employing the fly lines bearing the *ImpL2* knockdown and overexpression constructs showed that the production of IMPL2 by bacteria-challenged macrophages leads to elevated levels of circulating carbohydrates and lipids, their depletion in the fat body, and their accumulation in macrophages as determined by lipidomic analyses and tissue incorporation of ¹³C-labelled free fatty acids. Exploring the underlying mechanism of such change in systemic metabolism, we found that IMPL2 production leads to silencing of insulin signaling in the fat body, presumably due to its high affinity for *Drosophila* insulin-like peptides, resulting in nuclear translocation of the

transcription factor FOXO. As a result, activation of the FOXO-transcription program leads to the secretion of lipoproteins by the fat body into the circulation. The circulating lipoproteins are subsequently utilized by activated macrophages to fight the pathogen. Indeed, flies lacking the expression of *ImpL2* in macrophages or expression of lipases and lipoprotein-assembly genes in the fat body display abrogated phagocytic capability, elevated pathogen load, and thus reduced survival rate of the infection. These data thus document that *ImpL2* is produced by activated macrophages in reflection of their M1 metabolic switch and that this molecule thus translates the cellular metabolic demands to the systemic metabolism, thereby securing sufficient nutrients for an efficient immune response.

Interestingly, we found out that THP-1 cell lines of human macrophages increase the expression and production of the mammalian *ImpL2* homolog *IGFBP7* in response to LPS treatment in a HIF1 α -dependent manner. Similarly, it is also highly expressed in s human liver macrophages after LPS treatment. Moreover, administration of recombinant IGFBP7 to 3D liver spheroids leads to an increased titer of LDL and VLDL in the culture medium, and its silencing leads to a decrease in apolipoprotein expression in murine hepatocytes. These data thus suggest that macrophage-induced silencing of insulin signaling represents an evolutionarily conserved adaptive mechanism by which macrophages secure nutrients for their function upon bacterial infection.

In **Chapter IV**, we can see that macrophage-derived cytokines which are primarily beneficial mean become maladaptive under certain conditions. The study was conducted mostly under the baton of our collaborators from Karolinska Institutet and it shows that liver macrophages in obese mammals secrete IGFBP7, which binds to the insulin receptor on hepatocytes and induces lipogenesis and gluconeogenesis *via* the activation of ERK signaling. Interestingly, IGFBP7 in obese insulin resistant individuals is more frequently subjected to RNA editing than in obese insulin-sensitive patients, leading to the production of an IGFBP7 isoform with potentially higher capacity to bind to the insulin receptor. Thus, IGFBP7 may represent a new drug target for the treatment of metabolic diseases. Our laboratory contributed to this research by showing that expression of the IGFBP7 homolog *ImpL2* is also increased in fruit flies fed a high fat diet. In addition, these flies display elevated levels of circulating glucose and triglycerides, whereas such systemic metabolic imbalances can be prevented by macrophage-specific knockdown of *ImpL2*. This study is thus an example of the pathological action of a molecule conserved between insects, mice and humans.

Chapter V is a review article that attempts to present *Drosophila* as a model organism for immuno-metabolic studies and summarizes current knowledge of macrophage-derived signaling molecules that have the potential to shape the systemic metabolism. In addition to describing their mechanism of action, this paper also seeks to determine whether these molecules have mammalian homologs and whether their roles may be conserved across evolution. In addition, it also discusses that the immune cell-mediated metabolic changes are not always beneficial.

Chapter VI represents a Hypothesis and Theory article devoted to the evolutionary origins of macrophage functional versatility. It was written as a reflection of our astonishment at the various roles

macrophages play in the multicellular organism. Following evolution, it seeks to find when macrophage-like cells acquired functions that predisposed them to later acquire M1 and M2-related roles. It begins by describing the features unique to macrophages that distinguish them from other cell types in the body. Next, it discusses the parallels between macrophages in vertebrates and unicellular *Acanthamoeba*, sentinel cells of facultatively multicellular organism *Dictyostelium*, archaeocytes in Porifera, simple multicellular organisms with several distinct cell lineages, and macrophage-like plasmatocytes in *Drosophila* as a complex multicellular animal with clearly defined organs.

As a result, it suggests that M1 polarization is ancestral and that it evolved from the nutritional hunting of bacteria performed by *Acanthamoeba*. We also hypothesize that M2-like traits were acquired later in evolution and developed as a result of the need for harmonizing and tolerogenic forces in multicellular organisms. Last, but not least, we investigate the possibility that the origin of macrophage functions may explain the pathological action of macrophages in mammals.

Chapter VII consists of a project in which we aimed to develop a tool for macrophage-specific delivery *in vivo*. In this project, we tested the feasibility of glucan particles (GPs) prepared from baker's yeast in collaboration with VSCHT, Prague on the fruit fly model. We show that these particles can spread through the body of both adult flies and larvae after injection and that after 30 minutes they accumulate at sites where macrophages normally reside in adults. To confirm that they are indeed engulfed by the macrophages, GPs were modified with the pH-sensitive fluorescent dye pHrodo, which begins to shine brightly in the acidic environment of the phagolysosome. To test whether the GPs could be used for protein delivery, they were loaded with the transcription protein Gal4, as it is commonly used in *Drosophila* to study targeted gene expression and hence allows for easy monitoring. Indeed, injection of the Gal4 protein encapsulated in GPs into adult flies bearing the UAS-mCherry transgenic reporter leads to the production of a red fluorescent signal in macrophages, while injection of empty GPs or co-injection of GPs and Gal4 does not induce any fluorescence. GPs thus represent a potent macrophage-specific delivery tools since they have a negligible effect on immune response activation when compared to injection by *S. pneumoniae*. We thus believe that GPs are an efficient tool for intracellular drug delivery to phagocytes and that *Drosophila* model organism represents a unique opportunity for *in vivo* testing in the context of cancer, immunity, and metabolism research.

The section of unpublished manuscripts begins with **Chapter VIII**, which delves into the role of macrophages infiltrating larval adipose tissue in freshly emerged flies. Infiltration of the larval fat body by macrophages during metamorphosis and the first few days of adult life was documented by Nelliott, Bond and Hoshizaki when monitoring fat body remodeling in *D. melanogaster* (Nelliott, Bond and Hoshizaki, 2006). However, these authors claimed that it is a macrophage-independent process and their role is dispensable for successful metamorphosis.

In our manuscript, we show that genetic constructs used previously for macrophage ablation are not efficient enough and that macrophages are indispensable for pupal-to-adult transition and maturation of the young adult. In addition, employing confocal and electron microscopy we determine the time

frame of infiltration of macrophages into larval fat body and describe their morphology and their functional interaction. We show that the macrophages form crown-like structures around adipocytes and that they engulf the leaking lipids and RNA-protein granules from these cells. In turn, they acquire a foamy phenotype and display increased lipid and lipoprotein metabolic processes and increased cellular respiration and energy derivation as revealed by transcriptomic analysis. In addition, the combination of proteomic analysis with genetic tools for labeling of macrophage-derived protein by biotin ligase identified several unexpected macrophage-secreted proteins such as lipoproteins and storage peptides, which are traditionally produced by the fat body. Hence, we suggest that the macrophages adopt a unique secretory adipohemocyte-like profile in freshly emerged flies. Moreover, in this work we revealed that macrophage-derived apolipoprotein (apolpp) is essential for post-metamorphic development of ovaries and the achievement of early fecundity. We therefore believe that macrophages recycle components of engulfed histolyzing cells and cellular debris during insect metamorphosis and convert them into an exploitable form to prevent nutrient wasting. In this manner, the role of macrophages during post-metamorphic maturation resembles nutritive phagocytosis.

Chapter IX is dedicated to macrophage-specific delivery of the small-molecule metabolic inhibitor atorvastatin. In this study, we tested the function of atorvastatin, the most prescribed statin in U.S., encapsulated in GPs. We show that injection of GPs loaded with atorvastatin into abdomen of adult flies inhibits the enzymatic activity of HMGCR, the rate-limiting enzyme in the mevalonate pathway specifically in macrophages. Indeed, it does not affect enzymatic activity in any other tissue tested. Besides the potential of GPs for the delivery of metabolic inhibitors, this manuscript also demonstrates that the mevalonate pathway including HMGCR are elevated in macrophages after infection. Moreover, the expression and enzymatic activity of HMGCR in macrophages is essential for survival of infection, as flies injected with GPs loaded with atorvastatin or bearing genetic constructs for macrophage-specific silencing of *Hmgcr* display increased pathogen load and reduced survival of streptococcal infection, presumably since they fail to induce expression of AMPs and glycolytic enzymes. These data thus suggest that macrophages fail to switch to a pro-inflammatory phenotype when HMGCR is inhibited. We hypothesize that the mevalonate pathway may be essential for the synthesis of molecules that allow macrophages to enhance their motility and generate sufficient capacity for bacterial killing and inter-organ signaling. Since *Drosophila* is a cholesterol auxotroph, we suggest that *Drosophila* macrophages do not exploit the mevalonate pathway to synthesize cholesterol, but rather to produce the terpenoid backbone used for the synthesis of steroid compounds, or for farnesyl pyrophosphate, which serves as a substrate for synthesis of isoprenoids and posttranslational modifications of proteins by prenylation (Jing and Behmer, 2020). In addition, since the mevalonate pathway has been shown to be essential for the formation of innate immune memory in mammalian macrophages, our data implicate that it is essential for immune response in insect and its relevance to the insect immune priming should be tested in following research.

Chapter X represents a research paper exploring the potential of GPs for antibody-free magnetic separation of macrophages. We demonstrate in this manuscript that GPs loaded with paramagnetic nanoparticles represent an attractive bait for *Drosophila* macrophages and that they become readily internalized. These particles then allow the isolation of phagocytes from the fly homogenate, and the separated cells display comparable viability, expression of macrophage markers, AMPs and genes associated with macrophage activation when compared to macrophages isolated by cell sorter based on the endogenously expressed GFP. Since this method does not require any antibodies and is based on an ability common to all macrophages across species, we believe that it can potentially also serve to isolate of phagocytes from non-model insects and thus enable various studies including -omic analyses of macrophages in these organisms.

CHAPTER I:

***Drosophila* macrophages switch to aerobic glycolysis to mount effective antibacterial defense**

Gabriela Krejčová, Adéla Danielová, Pavla Nedbalová, Michalina Kazek, Lukáš Strych, Geetanjali Chawla, Jason M Tennessen, Jaroslava Lieskovská, Marek Jindra, Tomáš Doležal, and Adam Bajgar

eLife, 2019, **8**:e50414

Drosophilamacrophages switch to aerobic glycolysis to mount effective antibacterial defense

Gabriela Krejčová^{1*}, Adéla Danielová¹, Pavla Nedbalová¹, Michalina Kazek¹, Lukáš Strych¹, Geetanjali Chawla^{2†}, Jason M Tennessen², Jaroslava Lieskovská^{3,4}, Marek Jindra^{1,5}, Tomáš Doležal¹, Adam Bajgar^{1,5*}

¹Department of Molecular Biology and Genetics, University of South Bohemia, Ceske Budejovice, Czech Republic; ²Department of Biology, Indiana University, Bloomington, United States; ³Department of Medical Biology, University of South Bohemia, Ceske Budejovice, Czech Republic; ⁴Institute of Parasitology, Biology Centre CAS, Ceske Budejovice, Czech Republic; ⁵Institute of Entomology, Biology Centre CAS, Ceske Budejovice, Czech Republic

Abstract Macrophage-mediated phagocytosis and cytokine production represent the front lines of resistance to bacterial invaders. A key feature of this pro-inflammatory response in mammals is the complex remodeling of cellular metabolism towards aerobic glycolysis. Although the function of bactericidal macrophages is highly conserved, the metabolic remodeling of insect macrophages remains poorly understood. Here, we used adults of the fruit fly *Drosophila melanogaster* to investigate the metabolic changes that occur in macrophages during the acute and resolution phases of *Streptococcus*-induced sepsis. Our studies revealed that orthologs of Hypoxia inducible factor 1a (HIF1a) and Lactate dehydrogenase (LDH) are required for macrophage activation, their bactericidal function, and resistance to infection, thus documenting the conservation of this cellular response between insects and mammals. Further, we show that macrophages employing aerobic glycolysis induce changes in systemic metabolism that are necessary to meet the biosynthetic and energetic demands of their function and resistance to bacterial infection.

DOI: <https://doi.org/10.7554/eLife.50414.001>

*For correspondence:
krejcovagabriela@seznam.cz (GK);
bajgaa00@prf.jcu.cz (AB)

Present address: [†]Regional
Centre for Biotechnology,
Faridabad, India

Competing interests: The
authors declare that no
competing interests exist.

Funding: [See page 19](#)

Received: 25 July 2019
Accepted: 12 October 2019
Published: 14 October 2019

Reviewing editor: Utpal
Banerjee, University of California,
Los Angeles, United States

© Copyright Krejčová et al. This
article is distributed under the
terms of the [Creative Commons
Attribution License](#), which
permits unrestricted use and
redistribution provided that the
original author and source are
credited.

Introduction

Macrophages represent a highly specialized and versatile population of cells that occur in all animals and perform a diversity of functions (Lim et al., 2017). In the absence of an activating stimulus, macrophages reside as quiescent sentinel cells that have minimal metabolic requirements (Davies and Taylor, 2015). In response to extracellular triggers, however, macrophages undergo a dramatic change in behavior that coincides with an enhanced metabolic rate and increased energy demands (Pearce and Pearce, 2013). In this regard, the manner by which macrophages mount a response is dictated by the activating stimuli, which include tissue-damage-, pathogen- or microbe-associated molecular patterns (DAMPs, PAMPs and MAMPs, respectively), as well as signaling molecules that are secreted by other cells, such as cytokines. Each challenge requires the induction of specific metabolic and physiological processes that allow for an adequate immune response (Kawai and Akira, 2011) – cellular changes that are collectively known as a polarization phenotype.

Macrophages polarize into bactericidal (M1) or healing (M2) functional phenotypes characterized mainly by metabolism (Mills et al., 2000). M1 and M2 polarization phenotypes utilize distinct ways of generating ATP (glycolysis vs. oxidative phosphorylation) and metabolizing arginine (NO synthesis vs. the ornithine cycle) (O'Neill and Pearce, 2016). Nowadays, the whole spectrum of polarization

eLife digest Macrophages are the immune system's first line of defense against infection. These immune cells can be found in all tissues and organs, watching for signs of disease-causing agents and targeting them for destruction. Maintaining macrophages costs energy, so to minimize waste, these cells spend most of their lives in 'low power mode'. When macrophages sense harmful bacteria, they rapidly awaken and trigger a series of immune events that protect the body from infection. However, to perform these protective tasks macrophages need a sudden surge in energy.

In mammals, activated macrophages get their energy from aerobic glycolysis – a series of chemical reactions normally reserved for low oxygen environments. Switching on this metabolic process requires a protein called hypoxia inducible factor 1a (HIF-1a), which switches on the genes that macrophages need to generate energy as quickly as possible. Macrophages then maintain their energy supply by sending out chemical signals which divert glucose away from the rest of the body.

Fruit flies are regularly used as a model system for studying human disease, as the mechanisms they use to defend themselves from infections are similar to human immune cells. However, it remains unclear whether their macrophages undergo the same metabolic changes during an infection.

To address this question, Krejčová et al. isolated macrophages from fruit flies that had been infected with bacteria. Experiments studying the metabolism of these cells revealed that, just like human macrophages, they responded to bacteria by taking in more glucose and generating energy via aerobic glycolysis. The macrophages of these flies were also found to draw in energy from the rest of the body by raising blood sugar levels and depleting stores of glucose. Similar to human macrophages, these metabolic changes depended on HIF1a, and flies without this protein were unable to secure the level of energy needed to effectively fight off the bacteria.

These findings suggest that this metabolic switch to aerobic glycolysis is a conserved mechanism that both insects and mammals use to fight off infections. This means in the future fruit flies could be used as a model organism for studying diseases associated with macrophage mis-activation, such as chronic inflammation and autoimmune diseases.

DOI: <https://doi.org/10.7554/eLife.50414.002>

phenotypes corresponding to particular functions has been described (Mosser and Edwards, 2008; Martinez and Gordon, 2014). Perhaps the most dramatic change in macrophage metabolism associates with the M1 bactericidal phenotype, in which cells increase both glucose consumption and lactate production independently of oxygen concentration - a phenomenon known as aerobic glycolysis (AG) (Warburg et al., 1927; Warburg, 1956). The resulting metabolic program promotes increased glucose catabolism, thus allowing M1 macrophages to generate enough of the ATP and glycolytic intermediates necessary for elevated phagocytic cell activity (Liberti and Locasale, 2016). This shift in cellular metabolism towards AG appears to be a determining factor in macrophage function and in the development of the pro-inflammatory phenotype (Galván-Peña and O'Neill, 2014).

Hypoxia inducible factor 1a (HIF1a) is a key regulator of AG within macrophages. Although this transcription factor is normally degraded in the presence of oxygen, the triggering of either Toll-like receptor (TLR) or Tumor necrosis factor receptor (TNFR) signaling within macrophages activates Nuclear factor kappa-B (NFkB) and stabilizes HIF1a independently of oxygen availability (Siegert et al., 2015; Jung et al., 2003). This normoxic HIF1a stabilization promotes the expression of genes that are under the control of hypoxia response elements (HREs), many of which are involved in cellular metabolism, cell survival, proliferation, and cytokine signaling (Dengler et al., 2014). In this regard, two of the key HIF1a target genes encode the enzymes pyruvate dehydrogenase kinase (PDK) and lactate dehydrogenase (LDH), which together shunt pyruvate away from the mitochondria and maintain NAD⁺/NADH redox balance independently of oxidative phosphorylation. Inhibition of both HIF1a and LDH represents an efficient experimental strategy to direct cellular metabolism from AG to oxidative phosphorylation in both mice and *Drosophila* (Allison et al., 2014; Geeraerts et al., 2017), demonstrating the crucial role of these enzymes in this metabolic switch.

Although pyruvate metabolism within the tricarboxylic acid (TCA) cycle is limited during AG, the TCA intermediates are essential for many cellular processes. Therefore, cells under AG rely on

feeding the TCA cycle with glutamine, causing a TCA cycle to be 'broken' (Langston et al., 2017). Such a dramatic change in mitochondrial metabolism leads to significant imbalances in the cytosolic accumulation of TCA metabolites (such as NO, succinate, fumarate, L-2-hydroxyglutarate) that further contribute to HIF1a stabilization (Bailey and Nathan, 2018). While this feedback maintains AG, it simultaneously makes it dependent on a sufficient supply of nutrients from the environment (Iommarini et al., 2017).

Macrophages employing AG must consume sufficient carbohydrates to support biosynthesis and growth. In order to ensure an adequate supply of sugar and other nutrients, these cells produce signaling molecules that affect systemic metabolism in order to secure enough energy for themselves – a concept recently defined as selfish immune theory (Jeong et al., 2003; Straub, 2014). According to this theory, signaling molecules released by immune cells induce systemic metabolic changes such as hyperglycemia and systemic insulin resistance to increase the titer of nutrients that are available for the immune response and to limit their consumption by other tissues and processes (Dolezal, 2015). As many of these signaling molecules are direct HIF1a transcriptional targets, HIF1a stabilization directs the cellular metabolism while it simultaneously induces the expression of genes that have an impact on the whole systemic metabolism (Peyssonnaud et al., 2007; Imtiyaz and Simon, 2010). Thus, macrophages not only phagocytose cells but they also regulate the systemic metabolism of an organism.

Drosophila macrophages, like those of mammals, serve an essential role in the immune system and are capable of responding to a wide array of stimuli, ranging from pathogenic bacteria and fungi to the corpses of apoptotic cells (Wood and Martin, 2017; Searset et al., 2003; Govind, 2008). The mechanism of the bactericidal function itself is highly conserved at the molecular level between *Drosophila* and mammalian macrophages. In both *Drosophila* and mammals, two central signaling pathways, Toll and Imd (TLR and TNFR functional homologs) are triggered in response to pathogenic stimuli (Valanne et al., 2011; Buchonet et al., 2014; Lemaitre et al., 1996). The Toll and Imd pathways induce the NF κ B signaling in *Drosophila*, so we can assume that the phagocytic role of macrophages could be accompanied by stabilization of the HIF1a ortholog, *Similar* (*Sima*), hereafter referred to as Hif1a (van Uden et al., 2011). Indeed, normoxic stabilization of Hif1a followed by its nuclear localization and increased expression of HRE-controlled genes can induce metabolic changes that are typical of AG (Romero et al., 2008; Li et al., 2013; Liu et al., 2006; Herranz and Cohen, 2017; Eichenlaub et al., 2018). Even though the HRE-controlled genes frequently appear in transcriptomic data for activated insect macrophages (Irving et al., 2005; Johansson et al., 2005), the direct role of Hif1a in the macrophages has not yet been tested.

Considering that the molecular mechanisms that control macrophage activation are similar in both *Drosophila* and humans, it seems logical that the metabolic changes that occur within these cells would also be comparable, but the metabolism of insect macrophages remains poorly understood. Here, we address this question by analyzing in vivo metabolic and transcriptional changes in adult *Drosophila* phagocytic macrophages by employing a model of *Streptococcus pneumoniae*-induced sepsis. The well-defined progress of this infection allowed us to distinguish three phases of the immune response according to the changing dynamics of bacterial growth (acute, plateau, and resolution phase) (Figure 1A). The acute phase lasts for the first 24 hr, during which the streptococcal population is rapidly growing and its abundance must be limited by phagocytosis to avert early death (Pham et al., 2007; Bajgar and Dolezal, 2018). The established equilibrium between continuous bacterial growth and host bacterial killing results in the plateau phase lasting for the next four days. At the end of this period, the immune system of the host surmounts the infection and clears the majority of the pathogens. The following resolution phase (120 hr post-infection (hpi) and later) is essential for macrophage-mediated clearance of bacterial residues and for the reestablishment of homeostasis (Bajgar and Dolezal, 2018; Chambers et al., 2012).

To analyze processes that are characteristic of highly active phagocytic macrophages in *Drosophila*, we compared the attributes of acute phase macrophages (APMFs) with those of macrophages from uninfected individuals and resolution-phase macrophages (RPMFs). Using a previously described hemolymph-driven GFP (*HmlGal4 >UAS eGFP*) (Jung et al., 2005), we isolated *Drosophila* adult macrophages (approximately 15,000 cells/replicate) and analyzed the metabolic and transcriptional responses that are induced within these cells upon infection (Figure 1B). Our approach revealed that *Drosophila* macrophages respond to the acute phase of bacterial infection by increasing glucose uptake, elevating glycolytic flux, and producing lactate. Moreover, as in mammals, the

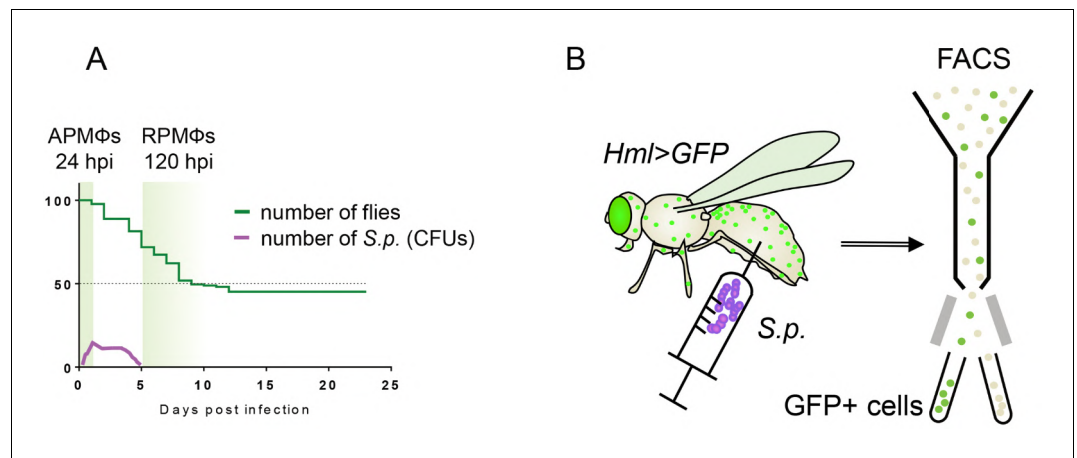


Figure 1. Graphical representation of the experimental approach. (A) The natural progress of streptococcal infection, with highlighted sampling times during the acute and resolution phases of infection. The Y axis indicates the percentage of surviving adults. (B) The approach used to isolate hemocytes, which are subsequently assayed for gene expression and enzymatic activities. Macrophages sorted from flies at the respective time points post-infection represent acute-phase macrophages (APMFs; 24 hpi) and resolution-phase macrophages (RPMFs; 120 hpi). Control flies were analyzed at the same time points after receiving injection of phosphate-buffered saline (PBS). hpi, hours post-infection; FACS, fluorescence-activated cell sorting; S.p., *Streptococcus pneumoniae*.

DOI: <https://doi.org/10.7554/eLife.50414.003>

activation and maintenance of AG within *Drosophila* macrophages depend on Hif1a, and require elevated Ldh activity. We also demonstrate that the induction of AG within *Drosophila* macrophages leads to a change in systemic carbohydrate metabolism. Overall, our findings demonstrate that *Drosophila* macrophages must induce both autonomous and systemic changes in carbohydrate metabolism to mount a proper bactericidal function and to resist infection.

Results

Drosophila macrophages undergo a metabolic shift to aerobic glycolysis during the acute phase of bacterial infection

Since the bactericidal function of phagocytic cells is connected with AG in mice (Mills et al., 2000), we analyzed *Drosophila* macrophages for the occurrence of AG hallmarks, such as increased glucose uptake, an increase in glycolytic flux, and the generation of an NADH pool facilitating the Ldh-mediated reduction of pyruvate to lactate (Langston et al., 2017). The distribution of fluorescently labeled deoxyglucose (NBDG) in an organism, frequently used in cancer research, reflects the competitive potential of tissues in glucose internalization (Cox et al., 2015). We tested the effect of immune response activation on glucose distribution among tissues in *Drosophila* by feeding the infected or control flies with NBDG during a 24-hr period before the signal detection. Infected flies displayed prominent NBDG accumulation in APMFs compared to other tissues, which is in contrast to the distribution of NBDG seen in uninfected controls or in flies fed during the resolution phase of infection, which displayed no such accumulation (Figure 2A,B). These results indicate an increased potential of phagocytosing macrophages to consume glucose in direct competition with other tissues during the acute phase of bacterial infection.

The increased NBDG uptake by macrophages was further supported by gene expression analysis, which revealed that the transcription of genes encoding both glycolytic enzymes and LDH, but not TCA cycle enzymes, was significantly upregulated in APMFs (Figure 2C). Moreover, these changes in glycolytic genes were restricted to the acute phase of infection as most glycolytic genes returned to a basal level of expression during the resolution phase, whereas hexokinase and enolase (similarly to all analyzed TCA cycle genes) even showed decreased expression (Figure 2C and Figure 2—figure supplement 1), which can be ascribed to the global suppression of metabolism in these cells.

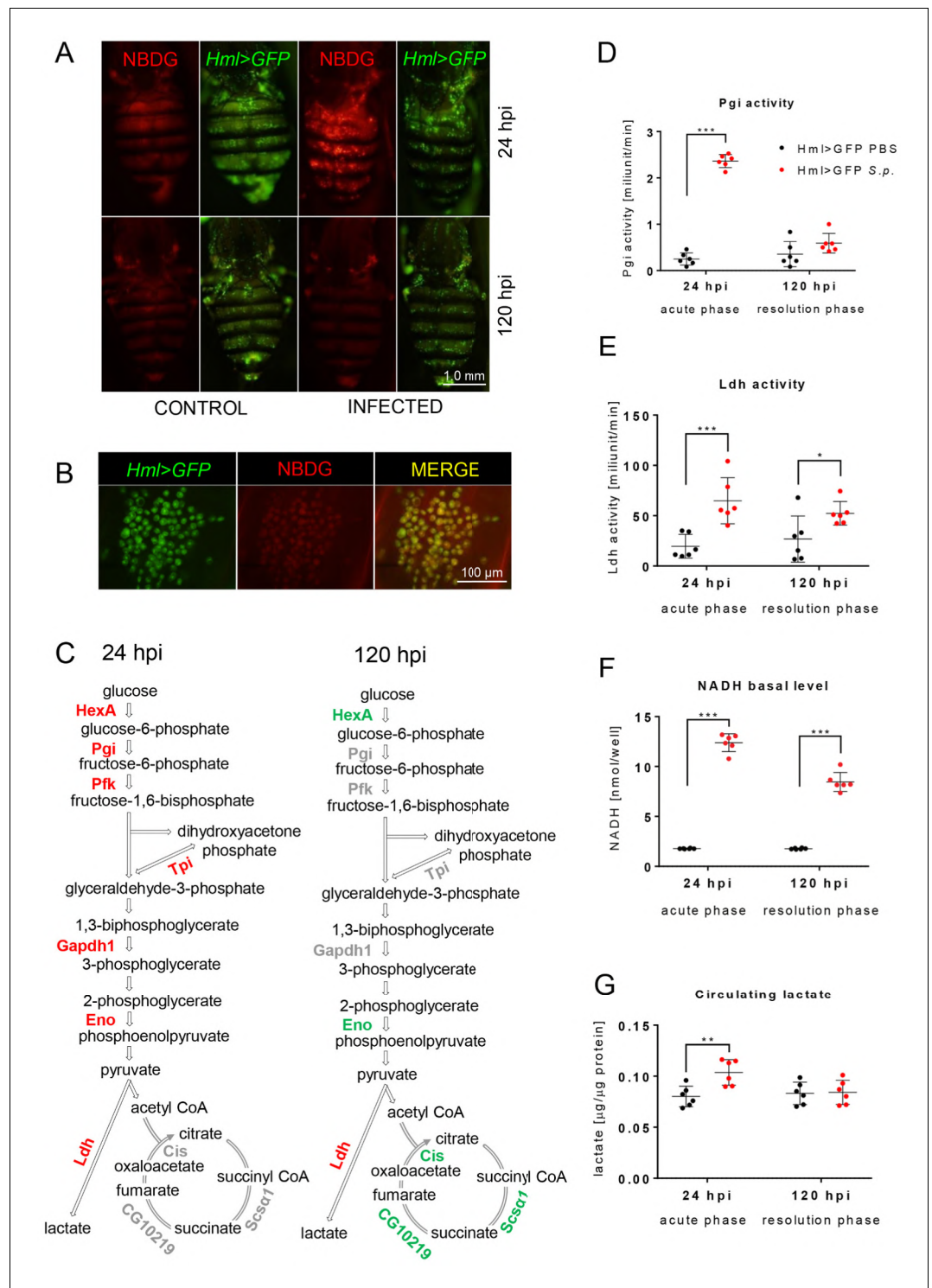


Figure 2. Streptococcal infection enhances glycolysis in acute-phase macrophages. (A–B) Fluorescent images of the dorsal view of the abdomens of infected and control (both Hml >GFP) flies at 24 and 120 hpi, showing NBDG the distribution among the tissues (A) and at a higher magnification (B). Images represent a minimum of ten observations of a similar pattern. (C) Scheme of glycolysis and the TCA cycle, highlighting significant changes in the quantified expression of the indicated genes at 24 and 120 hpi. The expression levels of the mRNA were measured relative to that of the ribosomal protein 49 (rp49), and the statistical significance ($p < 0.05$) was tested using ANOVA (for data see Figure 2—figure supplement 1). Upregulated genes are shown in red, downregulated genes in green; gray indicates no statistically significant difference. (D–F) Enzymatic activities of

Figure 2 continued on next page

Figure 2 continued

phosphoglucose isomerase (Pgi) (D) and lactate dehydrogenase (Ldh) (E), as well as the level of NADH (F), at 24 and 120 hpi measured in the homogenate of hemocytes isolated from infected and control flies. The levels of enzymatic activity and NADH concentration were normalized per ten thousand cells per sample. (G) The concentration of circulating lactate measured in the hemolymph of infected and control flies at 24 and 120 hpi. In all plots (D–G), individual dots represent biological replicates. Values are mean \pm SD, asterisks mark statistically significant differences (* p <0.05; ** p <0.01; *** p <0.001).

DOI: <https://doi.org/10.7554/eLife.50414.004>

The following source data and figure supplements are available for figure 2:

Source data 1. Metabolic characterization of macrophages post-infection.

DOI: <https://doi.org/10.7554/eLife.50414.007>

Figure supplement 1. Gene expression of glycolytic enzymes is increased in acute-phase macrophages.

DOI: <https://doi.org/10.7554/eLife.50414.005>

Figure supplement 1—source data 1. Expression of metabolic genes in macrophages post-infection.

DOI: <https://doi.org/10.7554/eLife.50414.006>

Overall, these results indicate that macrophages specifically upregulate glucose metabolism in response to *S. pneumoniae* infection.

Increased glucose uptake and expression of glycolytic genes, including *Ldh*, suggest an increased glycolytic flux and preferential reduction of pyruvate to lactate in APMFs. To confirm this, we measured the enzymatic activity of LDH, as an enzyme responsible for the diversion of pyruvate from TCA, and phosphoglucose isomerase (Pgi), as a glycolytic enzyme representative. In agreement with the expression data, Pgi enzymatic activity was significantly increased in APMFs compared to control and compared to the situation observed during the resolution phase of infection (Figure 2D). The activity of *Ldh* increased not only in APMFs but also in RPMFs (Figure 2E). Moreover, the observed increase in *Ldh* activity was directly correlated with increased lactate production in vivo, as the hemolymph of infected individuals during both the acute and the resolution phases of infection contained significantly elevated lactate levels as compared to controls (Figure 2G). Overall, our results demonstrate that *Drosophila* macrophages respond to *S. pneumoniae* infection by upregulating lactate production.

The primary reason why cells produce lactate as a byproduct of AG is to maintain NAD⁺/NADH redox balance. High levels of glycolytic flux produce excess NADH as a result of glyceraldehyde-3-phosphate dehydrogenase 1 (*Gapdh1*) activity (Olenchock et al., 2017). Consistently, we observed that NADH levels were significantly increased in APMFs and, to a lesser extent, in RPMFs when compared with controls (Figure 2F). When considered in the context of gene expression and enzyme activity assays, these results support a model in which activated *Drosophila* macrophages undergo a dramatic metabolic remodeling towards AG during bacterial infection.

Hif1a and *Ldh* activities are increased in *Drosophila* macrophages during the acute phase of infection

Since Hif1a can induce AG in both murine and *Drosophila* cells (Peyssonnaud et al., 2007; Herranz and Cohen, 2017; Eichenlaub et al., 2018), we examined the possibility that this transcription factor also promotes glucose catabolism within activated macrophages. Although Hif1a is known to be expressed continuously in almost all tissues and regulated predominantly at the post-translational level, we observed that *Hif1a* mRNA was significantly elevated in APMFs (Figure 3D). To determine whether this increase correlates with the elevated expression of Hif1a target genes, we used a transgenic b-galactosidase reporter under the control of a HRE (*HRE-LacZ*), which is primarily induced by HIF1a (Lavista-Llanos et al., 2002) although the involvement of other transcription factors cannot be entirely excluded. Although some cells exhibited *HRE-LacZ* expression in uninfected individuals, the number of b-galactosidase-positive macrophages rose dramatically in flies during the acute phase of infection (Figure 3A). These results suggest that Hif1a activity is increased in APMFs and confirms the previously reported expression pattern of glycolytic genes (see Figure 2—figure supplement 1A–F).

As increased lactate production is a hallmark of AG, we examined *Ldh* expression in macrophages using a transgene that expresses a *Ldh*-mCherry fusion protein from an endogenous *Ldh* promoter.

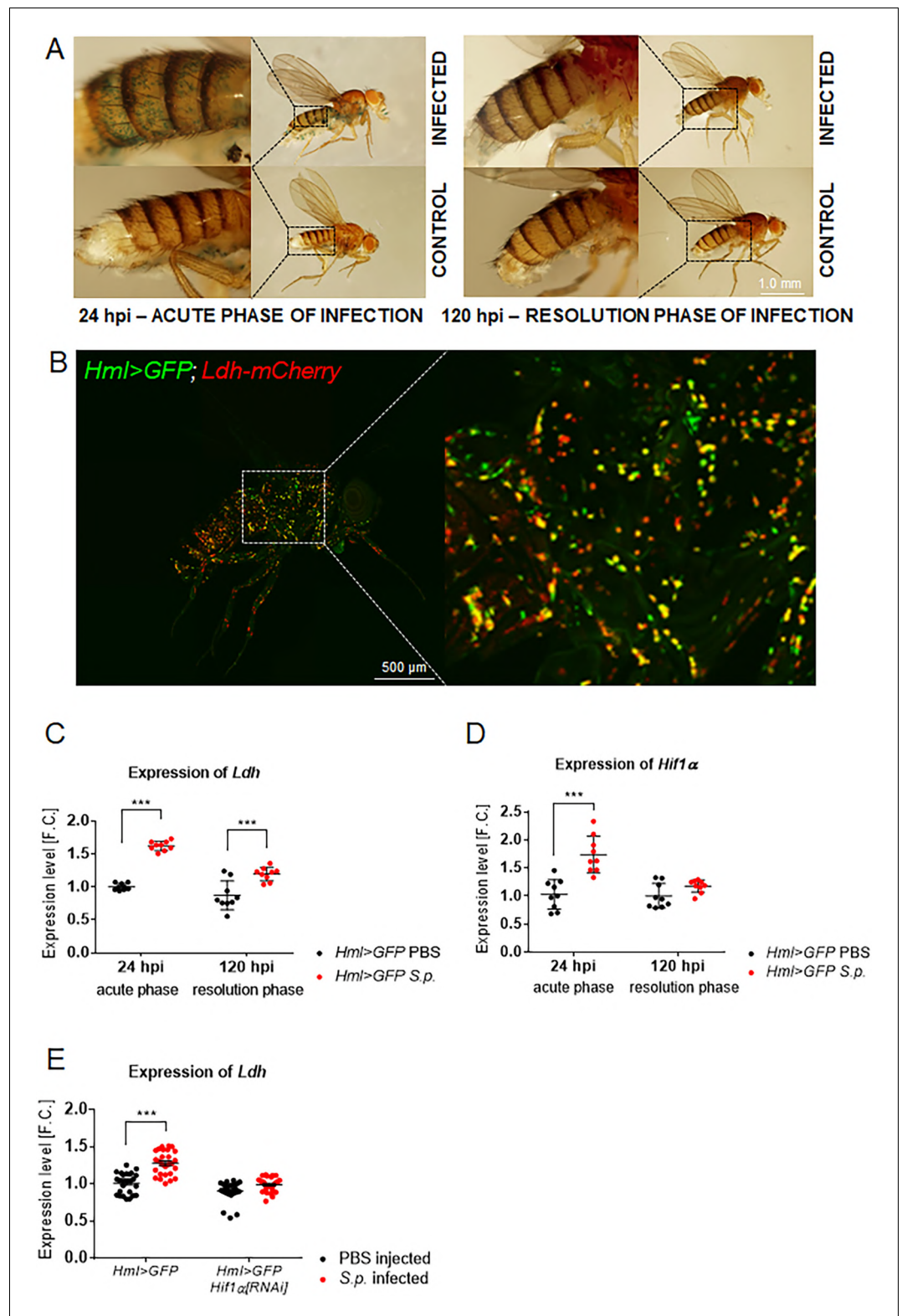


Figure 3. Macrophage-specific activities of Hif1a and Ldh increase upon infection. (A) X-gal staining of infected and control flies bearing the HRE-LacZreporter construct. Images represent a minimum of ten observations of a similar pattern. (B) An uninfected *Hml >GFP*, *Ldh-mCherry* adult fly (24 hpi) shows localization of the *Ldh* reporter activity (red) in many of the immune cells (green). The image is a Z-stack at maximal projection of 25 confocal slices. (C, D) Expression of *Ldh* (C) and *Hif1α* (D) mRNAs in hemocytes isolated from infected and control flies. Figure 3 continued on next page

Figure 3 continued

(both *Hml >GFP*; 24 and 120 hpi). (E) Expression of *Ldh* mRNA in hemocytes of infected and control *Hml >GFP* flies with and without a hemocyte-specific knockdown of *Hif1a* at 24 hpi. In all plots (C–E), expression levels, normalized against *rp49*, are given as fold change (F.C.) relative to levels in PBS-injected *Hml >GFP* controls (24 hpi), which were arbitrarily set to 1. Individual dots represent biological replicates. Values are mean \pm SD, asterisks mark statistically significant differences (* $p < 0.05$; ** $p < 0.01$; *** $p < 0.001$).

DOI: <https://doi.org/10.7554/eLife.50414.008>

The following source data is available for figure 3:

Source data 1. Expression pattern of *Hif1a* and *Ldh* genes.

DOI: <https://doi.org/10.7554/eLife.50414.009>

The expression of *Ldh*-mCherry in adult flies harboring the *HmlGal4 >UAS eGFP* reporter revealed that macrophages from uninfected adults expressed *Ldh* at levels that markedly exceeded the expression of this reporter in other tissues. This perhaps indicates that these cells are primed to generate lactate prior to infection (Figure 3B), as the *Ldh*-mCherry pattern did not change significantly after infection (data not shown). *Ldh* expression, however, was significantly upregulated in APMFs (Figure 3C), further supporting our observation that *S. pneumoniae* induces *Ldh* activity (Figure 2E), which is in agreement with elevated NADH levels (Figure 2G). The regulation of *Ldh* expression by *Hif1a* in activated immune cells was verified by knocking down *Hif1a* expression in macrophages 24 hr before infection (*Hml >Hif1a[RNAi]*). This strategy not only reduced *Hif1a* expression within APMFs (Figure 4—figure supplement 1G), but also led to the loss of the ability to increase *Ldh* expression in APMFs, indicating that *Hif1a* is essential for the elevated *Ldh* activity in APMFs (Figure 3E).

Hif1a promotes aerobic glycolysis in *Drosophila* macrophages during bacterial infection

To determine whether the observed increase in *Hif1a* activity is necessary to trigger AG in stimulated macrophages, we used *Hml >Hif1a[RNAi]* and examined the metabolic consequences. This treatment led to the abrogation of the metabolic changes associated with AG. Following infection, APMFs expressing *Hif1a[RNAi]* did not accumulate NBDG (Figure 4A), and failed to show increased expression of glycolytic genes (with the exception of *Gpdh1*) (Figure 4B). Moreover, these *Hml >Hif1a[RNAi]*-expressing cells exhibited no increase in either *Pgi* or *Ldh* enzyme activity and displayed decreased NADH levels when compared with controls (Figure 4D,E,F). These results indicate that *Hif1a* activity is essential for inducing AG in macrophages during the immune response.

As a complement to these cell-specific studies of *Hif1a*, we also used *Hml-Gal4* driving *UAS-Ldh [RNAi]* (*Hml > Ldh[RNAi]*) to reduce *Ldh* expression within APMFs. Intriguingly, although this approach successfully reduced *Ldh* activity in macrophages (Figure 4G), the metabolic consequences were relatively mild. Within APMFs, *Hml > Ldh[RNAi]* did not disrupt NBDG uptake and *Pgi* activity remained elevated (Figure 4C and I). Twenty-four hours after infection, however, we observed that NADH in *Hml > Ldh[RNAi]* macrophages failed to increase to the levels observed in infected controls (Figure 4H), thus revealing that increased *Ldh* activity is required for full metabolic reprogramming of *Drosophila* macrophages in response to bacterial infection.

Hif1a-mediated aerobic glycolysis in APMFs causes systemic metabolic changes

As we have shown previously (Bajgar and Dolezal, 2018), the systemic metabolic adaptation of carbohydrate metabolism is intimately linked to the effective function of the immune system during streptococcal infection. Therefore, we focused on the characterization of systemic carbohydrate metabolism during the acute phase of infection in *Hml >Hif1a[RNAi]* and *Hml >Ldh[RNAi]* flies (Figure 5). Both control genotypes underwent the expected metabolic response during the acute phase of streptococcal infection: a significantly raised level of circulating glucose was accompanied by a strong depletion of glycogen stores in tissues. The *Hif1a* silencing completely suppressed the infection-induced changes in carbohydrate metabolism, but infected *Hml >Ldh[RNAi]* flies still significantly increased circulating glucose, albeit to a lesser extent than in the infected controls

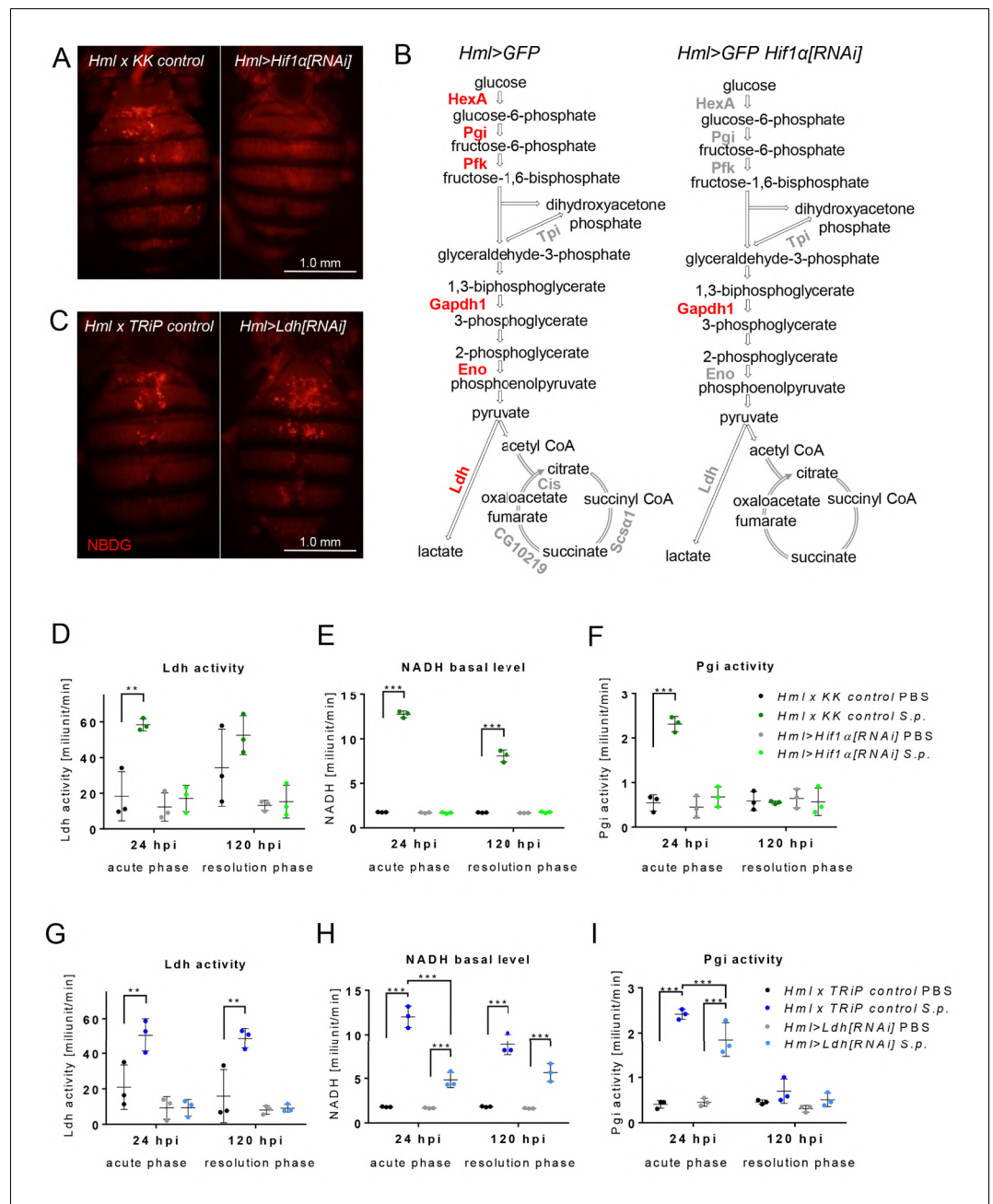


Figure 4. Effects of Hif1a and Ldh hemocyte-specific knockdown on macrophage metabolism. (A) Dorsal view of the abdomens of *S.p.*-infected flies (24 hpi) showing the distribution of the fluorescent NBDG probe. Controls (left) are compared to flies subjected to hemocyte-specific knockdown of Hif1a. Images represent a minimum of ten observations of a similar pattern. (B) Schematic representation of the expression of genes encoding metabolic enzymes in the hemocytes of infected control flies (left) and of flies with Hif1a hemocyte-specific knockdown (right) at 24 hpi. The expression levels of the mRNAs were measured relative to that of *rp49*, and the statistical significance ($p < 0.05$) was tested using ANOVA (for data see Figure 4—figure supplement 1). Upregulated genes are shown in red; gray indicates no statistically significant difference. (C) Dorsal view of the abdomens of *S.p.*-infected flies (24 hpi) showing the distribution of the fluorescent NBDG probe. Controls (left) are compared to flies subjected to hemocyte-specific knockdown of Ldh. Images represent a minimum of ten observations of a similar pattern. (D–F) Enzymatic activity of Ldh (D), level of NADH (E), and enzymatic activity of Pgi (F) at 24 and 120 hpi measured in lysates of hemocytes isolated from infected and non-infected control flies and from flies with Hif1a hemocyte-specific knockdown. (G–I) Enzymatic activity of Ldh (G), level of NADH (H), and enzymatic activity of Pgi (I) at 24 and 120 hpi measured in lysates of hemocytes isolated from infected and non-infected control flies and

Figure 4 continued on next page

Figure 4 continued

from flies with *Ldh* hemocyte-specific knockdown. In all plots (D–I), the enzyme activities and NADH concentrations were normalized per ten thousand cells per sample. Individual dots represent biological replicates. Values are mean \pm SD, asterisks mark statistically significant differences (* p <0.05; ** p <0.01; *** p <0.001).

DOI: <https://doi.org/10.7554/eLife.50414.010>

The following source data and figure supplements are available for figure 4:

Source data 1. Effect of macrophage-specific *Hif1a* knockdown on metabolic features of macrophages.

DOI: <https://doi.org/10.7554/eLife.50414.013>

Figure supplement 1. Expression of genes encoding glycolytic enzymes is not increased in acute-phase macrophages with *Hif1a* knock-down.

DOI: <https://doi.org/10.7554/eLife.50414.011>

Figure supplement 1—source data 1. Effect of macrophage-specific *Hif1a* knockdown on expression of metabolic genes.

DOI: <https://doi.org/10.7554/eLife.50414.012>

(**Figure 5A**). Although the glycogen stores appeared to be lowered in *Hml >Ldh[RNAi]* flies upon infection, the decrease was statistically insignificant (**Figure 5B**). Importantly, the macrophage-specific knockdown of either *Hif1a* or *Ldh* suppressed the occurrence of an infection-induced increase in circulating lactate titer (**Figure 5C**). These results show that APMFs are prominent lactate producers during the acute phase of the infection, and suggest that only full activation of APMFs with *Hif1a*-induced metabolic changes leads to reprogramming of systemic carbohydrate metabolism.

Hif1a- and Ldh-mediated metabolic remodeling of APMFs is essential for mounting a successful immune response

Our results suggest that *Drosophila* macrophages activate AG and systemic metabolic changes in order to mount a successful immune response. In support of this hypothesis, we observed a significant decrease in the viability of adult flies expressing either *Hml >Hif1a[RNAi]* or *Hml >Ldh[RNAi]* following *S. pneumoniae* infection. By 72 hr post infection, 25% of *Hml >Hif1a[RNAi]* flies died compared to 7% of controls, and the median time to death (MTD) in *Hml >Hif1a[RNAi]* flies was 10 days compared to 23 days in controls (**Figure 6A**). Moreover, pathogen load in *Hml >Hif1a[RNAi]* flies was substantially elevated when compared with that in controls at the second and third day post-infection (**Figure 6C**). We observed similar effects in *Hml >Ldh[RNAi]* flies, in which *S. pneumoniae* infection resulted in a decreased survival rate, a MTD of 9 days relative to the 18 days observed in controls, and elevated bacterial load during days 2 and 3 post-infection (**Figure 6B and D**). These results reveal that *Hif1a* and *Ldh* serve essential roles in both survival of infection and bacterial killing, and demonstrate how shift towards AG associated with systemic metabolic changes in activated macrophages is required to mount a successful immune response.

Discussion

Mammalian macrophages stimulated by bacteria have been shown to rewire their metabolism temporarily towards AG in order to develop an adequate bactericidal response (Olenchock et al., 2017; Nonnenmacher and Hiller, 2018; Browne et al., 2013). Although well established in mammals, such metabolic adaptation has not been experimentally tested in insect macrophages to date. We show here that *Drosophila* macrophages that are activated by bacterial infection undergo a dramatic remodeling of cellular metabolism. We demonstrate that acute-phase macrophages exhibit hallmarks of AG, such as elevated uptake of glucose, increased expression and activity of glycolytic genes, elevation of NADH levels, and preferential LDH-mediated conversion of pyruvate to lactate. Through macrophage-specific gene knockdown, we identified *Hif1a* to be essential for the induction of increased glycolytic flux as well as for the increased activity of LDH. Both *Hif1a* and *Ldh* are necessary for the full development of infection-induced changes in systemic carbohydrate metabolism and for resistance to bacterial infection.

A major takeaway of our work is that the cellular response to bacterial infection is an energetically challenging process that imposes significant metabolic demands upon the host. Our findings demonstrate that *Drosophila* macrophages meet these metabolic demands by inducing AG during the

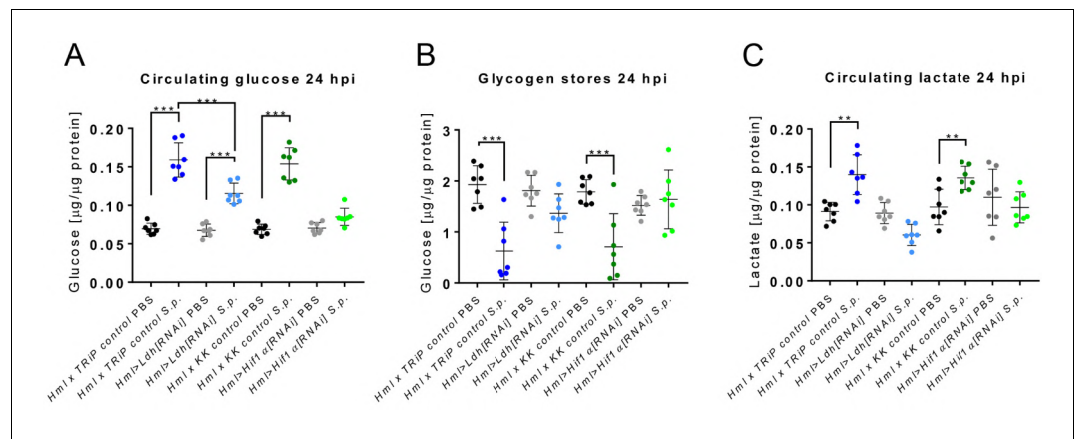


Figure 5. Systemic effects of Hif1a and Ldh hemocyte-specific knockdown. (A–C) The concentration of circulating glucose (A), glycogen stores (B) and circulating lactate (C) in infected and non-infected flies with Hif1a or Ldh hemocyte-specific knockdown and their respective controls at 24 hpi. The concentrations of metabolites were normalized to the amount of proteins in each sample. Individual dots in the plot represent biological replicates. Values are mean \pm SD, asterisks mark statistically significant differences (* $p < 0.05$; ** $p < 0.01$; *** $p < 0.001$).

DOI: <https://doi.org/10.7554/eLife.50414.014>

The following source data is available for figure 5:

Source data 1. Effect of macrophage-specific Hif1a and Ldh knockdown on systemic carbohydrate metabolism.

DOI: <https://doi.org/10.7554/eLife.50414.015>

acute phase of *S. pneumoniae* infection, as evidenced by the increased expression of glycolytic enzyme genes and elevated NADH levels. This increase in LDH enzyme activity in the absence of elevated TCA cycle activity suggests that macrophages preferentially convert pyruvate to lactate and is consistent with the elevated concentration of lactate observed in hemolymph. However, we find that this metabolic adaptation is temporary, as AG is terminated during the resolution phase of infection. This latter observation is important because it reveals that macrophages temporally regulate metabolic flux throughout an infection and because it establishes *Drosophila* as a powerful model for exploring the molecular mechanisms that control immune cell metabolism.

Our findings also extend the similarities between fly and mammalian models of macrophage polarization, as we identified Hif1a and Ldh as being crucial for the establishment and maintenance of AG in acute-phase macrophages. The importance of these factors is demonstrated by the macrophage-specific *Hif1a* knockdown experiment described above, in which many of the hallmark characteristics of AG, including expression of the *Ldh* gene, were abolished. This finding highlights the conserved and ancient role for Hif1a in regulating the switch between glycolytic and oxidative metabolism (Webster, 2003), and suggests that this function evolved as a means of allowing cells to adapt quickly to changing physiological conditions and cell-specific metabolic needs. The role of Hif1a in regulating this switch is of significant interest because, although this transcription factor is classically associated with the response to hypoxia, our study adds to the growing list of examples in which Hif1a remodels cellular metabolism in the context of cell proliferation, activation, and competition, even under normoxic conditions (Miyazawa and Aulehla, 2018). Moreover, our finding is particularly intriguing in light of the fact that Hif1a also serves a key role in promoting AG in neoplastic tumor cells (Herranz and Cohen, 2017; Eichenlaub et al., 2018; Wang et al., 2016). Therefore, our studies of fly macrophages provide a new *in vivo* system in which we can study how Hif1a promotes cell activity by modulating central carbon metabolism.

While Hif1a drives AG in *Drosophila* macrophages via transcriptional regulation of target genes, the role of Ldh in these cells is more complicated. Although acute-phase macrophages still consume more glucose upon *Ldh* knockdown, these cells exhibit significantly lower Pgi activity and NADH levels, and the titer of circulating lactate also drops. Our results suggest that even though Ldh acts only at the last step of AG, its role is essential for full metabolic reprogramming and efficient function of immune cells. *Drosophila* Ldh, like its mammalian ortholog, is responsible for the reduction of

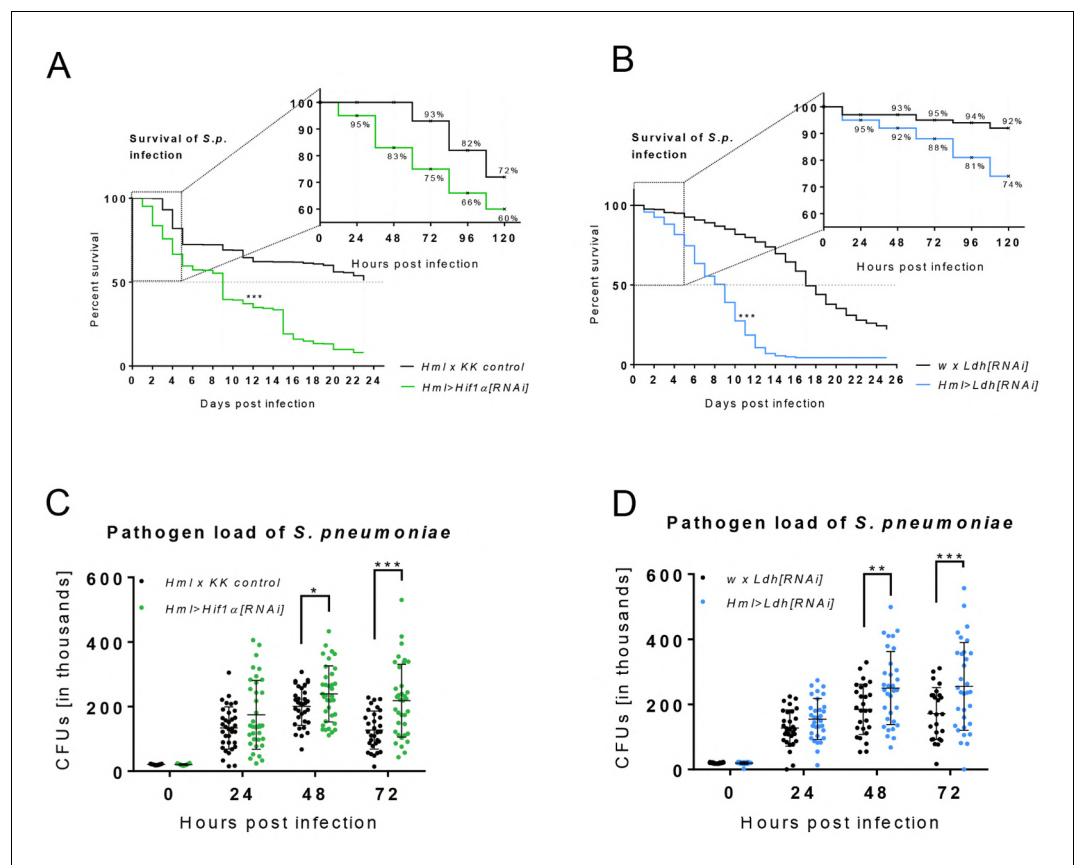


Figure 6. Effects of Hif1a and Ldh hemocyte-specific knockdown on resistance to infection. (A–B) The survival rate of infected flies of the control genotype and of flies with hemocyte-specific Hif1a (A) and Ldh (B) knockdown. Vertical dotted lines denote medium time to death for each genotype; survival rate during the first 120 hr is shown in detail. Three independent experiments were performed and combined into one survival curve. The average number of individuals per replicate was more than 500 for each genotype. (C, D) Colony forming units (CFUs) obtained from infected flies of control genotype and from flies with hemocyte-specific Hif1a (C) and Ldh (D) knockdown at 0, 24, 48, and 72 hpi. Individual dots in the plot represent the number of bacteria raised from one individual. The data show results merged from three independent biological replicates.

DOI: <https://doi.org/10.7554/eLife.50414.016>

The following source data is available for figure 6:

Source data 1. Effect of macrophage-specific Hif1a and Ldh knockdown on the resistance to bacterial infection.

DOI: <https://doi.org/10.7554/eLife.50414.017>

pyruvate to lactate, which is linked with the regeneration of NAD^+ from NADH. However, this single reaction has an immense impact on cellular metabolism. Both the accumulation of pyruvate and the lack of NAD^+ can become limiting in cells with high glycolytic flux (Olenchock et al., 2017). In addition, Ldh-dependent removal of cytosolic pyruvate was recently found to be essential to prevent pyruvate entry into mitochondria and a subsequent change of TCA cycle course (Eichenlaub et al., 2018; Wang et al., 2016).

Although not addressed in our study, changes in mitochondrial metabolism are also closely associated with AG and should be the focus of future studies of activated *Drosophila* macrophages. The interconnection between the transcriptional activity of Hif1a and the change of mitochondrial metabolism in *Drosophila* has recently been elucidated. The activation of several direct targets of Hif1a transcriptional activity leads to an inhibition of the classical course of the TCA cycle (Wang et al., 2016; Eichenlaub et al., 2018). One of the well-understood mechanisms is the prevention of pyruvate entry into the TCA cycle, which is caused by increased kinase activity of pyruvate dehydrogenase kinase 1 (PDK1). PDK1-mediated phosphorylation of pyruvate

dehydrogenase (PDH) directly inhibits its enzymatic function, which is essential for pyruvate conversion to acetyl-CoA (Wang et al., 2016). This event causes a cytoplasmic accumulation of TCA cycle intermediates and thus promotes a secondary wave of Hif1a stabilization through inhibition of prolyl hydroxylase dehydrogenase (PHD) under normoxic conditions (Koivunen et al., 2007; Freije et al., 2012). The change in the TCA cycle is further needed for mitochondrial production of ROS that are transferred to the phagolysosome for bacterial killing (Forrester et al., 2018; Williams and O'Neill, 2018).

We further demonstrate that both Hif1a and Ldh are crucial not only for full macrophage activation, but also for the bactericidal function of the immune cells, with the rearrangement of macrophage metabolism towards AG being essential for resistance to infection and host survival. An important aspect of AG is the functional dependence of macrophages on sufficient supply of external energy resources, as demonstrated in both mammalian and insect phagocytes (Bajgar and Dolezal, 2018; Anderson et al., 1973a; Anderson et al., 1973b; Langston et al., 2017; Newsholme et al., 1986) and documented here by increased consumption of glucose. Immune cells therefore generate systemic factors to secure sufficient supply of nutrients by altering the function of other organs and by regulating systemic metabolism (Bajgar et al., 2015; Bajgar and Dolezal, 2018). While the identification of specific signaling factors is beyond the scope of this work, there are several candidate molecules in *Drosophila* that are known to be produced by activated macrophages as a reaction to the metabolic state of the cell. Although it is likely that multiple factors will be involved in this process, we can presume that these factors will reflect the metabolic state of the cells (e.g., extracellular adenosine), or that they will be linked to the transcriptional program that causes the switch towards AG (e.g., Imaginal morphogenesis protein late 2 (ImpL2)). In our previous work, we showed that the systemic metabolic switch upon infection depends on extracellular adenosine, which is produced by the activated immune cells (Bajgar and Dolezal, 2018; Bajgar et al., 2015). The production of adenosine directly reflects a metabolic state of the cell, such as increased consumption of ATP (Worku and Newby, 1983), as well as the accelerated occurrence of methylation events (German et al., 1983; Wu et al., 2005). Expression of ImpL2 was shown to be regulated by Hif1a (Li et al., 2013), and as ImpL2 was previously identified as a mediator of cancer-induced loss of energy reserves in flies due to its anti-insulin role (Kwon et al., 2015; Figueroa-Claresvega and Bilder, 2015), it could represent another link between AG in macrophages and changes in systemic metabolism that ensure sufficient supply of energy resources.

Finally, our findings raise an interesting question regarding the links between AG and the ability of immune cells to respond quickly to infection. Recent studies of mammalian macrophage metabolism revealed that AG is essential for the development of innate immune memory - called trained immunity (Netea et al., 2016). The mechanism of trained immunity relies on chromatin remodeling by epigenetic factors that enable cells to react with higher efficiency in response to re-infection by a particular pathogen (Kim et al., 2019). As many chromatin remodeling enzymes need cofactors (such as acetyl-CoA, NAD⁺, α -KG) for the remodeling of the epigenetic landscape, their function can be influenced by the metabolic state of the cell. Induction of AG leads to the accumulation of many cofactors that are essential for a proper function of these enzymes (Kim et al., 2019; Baardman et al., 2015). The concept of trained immunity not only is valid for mammals, but is rather present in many invertebrate clades (where it is called immune priming; Milutinović and Kurtz, 2016; Pham et al., 2007). Our observation of AG as a characteristic feature of activated *Drosophila* macrophages thus raises a question of its importance for the development of trained immunity in insects and other invertebrates. Taken together, our findings demonstrate how the molecular mechanisms that control AG induction in *Drosophila* macrophages exhibit a surprisingly high level of evolutionary conservation between mammals and insects, thus emphasizing that this metabolic switch is essential for survival of infection and hinting at the potential role for AG in the development of immune memory.

In conclusion, we have shown that infection-induced systemic changes in carbohydrate metabolism are associated with changes of macrophage cellular metabolism, and that both can be affected by macrophage-specific *Hif1a* and *Ldh* knockdown. Our data thus link the metabolic state of macrophages with the systemic metabolic changes. On the basis of our previous research on the selfish nature of the immune system under challenge (Straub, 2014), we envision that the shift in the cellular metabolism of macrophages leads to the production of signals that alter the systemic metabolism, thereby securing the sufficient energy supply necessary to allow the macrophages to fight the

infection. By linking the induction of macrophage polarization with systemic metabolism and systemic outcomes in vivo, our experimental system can aid future research towards better understanding of the immune system and of diseases related to its malfunction.

Materials and methods

Key resources table

Reagent type (species) or resource	Designation	Source reference	Identifier	Additional information
Strain, strain background (<i>Streptococcus pneumoniae</i>)	<i>EJ1</i> strain	Provided by David Schneider		Dilution 20,000 units
Chemical compound, drug	TRIzol Reagent	Invitrogen	Cat# 15-596-018	
Chemical compound, drug	Superscript III Reverse Transcriptase	Invitrogen	Cat# 18080044	
Chemical compound, drug	2x SYBRMaster Mix	Top-Bio	Cat# T607	
Chemical compound, drug	2-NBDG	Thermo Fisher Scientific	Cat# N13195	
Chemical compound, drug	X-gal	Sigma	Cat# B4252	
Commercial assay, kit	Glucose (GO) Assay Kit	Sigma	Cat# GAGO20-1KT	
Commercial assay, kit	Bicinchoninic Acid Assay Kit	Sigma	Cat# BCA1	
Commercial assay, kit	Lactate Assay Kit	Sigma	Cat# MAK064	
Commercial assay, kit	Lactate Dehydrogenase Activity Assay Kit	Sigma	Cat# MAK066	
Commercial assay, kit	Phosphoglucose Isomerase Colorimetric Assay Kit	Sigma	Cat# MAK103	
Genetic reagent (<i>Drosophila melanogaster</i>)	<i>HmlG4G80: w[*]; HmlD-Gal4[*]; P{tubPGal80ts}[*]</i>	Cross made in our laboratory by Tomas Dolezal		
Genetic reagent (<i>D. melanogaster</i>)	<i>Hml > GFP: w; HmlD-Gal4 UAS-eGFP</i>	Provided by Bruno Lemaitre		
Genetic reagent (<i>D. melanogaster</i>)	<i>Hif1a[RNAi]: P{KK110834}VIE-260B</i>	Vienna Drosophila Resource Center	VDRC: v106504	FBst0478328
Genetic reagent (<i>D. melanogaster</i>)	<i>TRiP control: y(1) v(1); P{y[+7.7]=CaryP}attP2</i>	Bloomington Drosophila Stock Center	BDSC: 36303	FBst0036303
Genetic reagent (<i>D. melanogaster</i>)	<i>KK control: y, w[1118]; P{attP,y[+],w[3]}</i>	Bloomington Drosophila Stock Center	BDSC: 60100	FBst0060100
Genetic reagent (<i>D. melanogaster</i>)	<i>Ldh[RNAi]: y(1) v(1); P{y[+7.7] v[+1.8]=TRiP.HMS00039}attP2</i>	Bloomington Drosophila Stock Center	BDSC: 33640	FBst0033640
Genetic reagent (<i>D. melanogaster</i>)	<i>HRE-LacZ: HRE-HRE-CRE-LacZ</i>	Provided by Pablo Wappner (Lavista-Llanos et al., 2002)		
Genetic reagent (<i>D. melanogaster</i>)	<i>Ldh-mCherry</i>	Provided by Jason Tennesen		

Continued on next page

Continued

Reagent type (species) or resource	Designation	Source reference	Identifier	Additional information
Genetic reagent (<i>D. melanogaster</i>)	w: w ¹¹¹⁸	Genetic background based on CantonS		
Sequence-based reagent	Cis forward: 5 ⁰ TTCGATTGACTCCAGCCTGG3 ⁰	KRD	CG14740	FBgn0037988
Sequence-based reagent	Cis reverse: 5 ⁰ AGCCGGGAACCACCTGTCC3 ⁰	KRD	CG14740	FBgn0037988
Sequence-based reagent	Ldh forward: 5 ⁰ CAGAGAAGTGAACGAGCTG3 ⁰	KRD	CG10160	FBgn0001258
Sequence-based reagent	Ldh reverse: 5 ⁰ CATGTTCCGCCAAAACGGAG3 ⁰	KRD	CG10160	FBgn0001258
Sequence-based reagent	Eno forward: 5 ⁰ CAACATCCAGTCCAACAAGG3 ⁰	KRD	CG17654	FBgn0000579
Sequence-based reagent	Eno reverse: 5 ⁰ GTTCTTGAAGTCCAGATCGT3 ⁰	KRD	CG17654	FBgn0000579
Sequence-based reagent	Gapdh1 forward: 5 ⁰ TTG TGG ATC TTA CCG TCC GC3 ⁰	KRD	CG12055	FBgn0001091
Sequence-based reagent	Gapdh1 reverse: 5 ⁰ CTCGAACACAGACGAATGGG3 ⁰	KRD	CG12055	FBgn0001091
Sequence-based reagent	HexA forward: 5 ⁰ ATATCGGGCATGTATATGGG3 ⁰	KRD	CG3001	FBgn0001186
Sequence-based reagent	HexA reverse: 5 ⁰ CAATTCGCTCACATACTTGG3 ⁰	KRD	CG3001	FBgn0001186
Sequence-based reagent	Pfk forward: 5 ⁰ AGCTCACATTTCCAAACATCG3 ⁰	KRD	CG4001	FBgn0003071
Sequence-based reagent	Pfk reverse: 5 ⁰ TTTGATACCAGAATCACTGC3 ⁰	KRD	CG4001	FBgn0003071
Sequence-based reagent	Pgi forward: 5 ⁰ ACTGTCAATCTGTCTGTCCA3 ⁰	KRD	CG8251	FBgn0003074
Sequence-based reagent	Pgi reverse: 5 ⁰ GATAACAGGAGCATTCTTCTCG3 ⁰	KRD	CG8251	FBgn0003074
Sequence-based reagent	Rp49 forward: 5 ⁰ AAGCTGTGCGACAAATGGCG3 ⁰	KRD	CG7939	FBgn0002626
Sequence-based reagent	Rp49 reverse: 5 ⁰ GACGTTGTGCACCAGGAAC3 ⁰	KRD	CG7939	FBgn0002626
Sequence-based reagent	Hif1a forward: 5 ⁰ CCAAAGGAGAAAAGAAGGAAC3 ⁰	KRD	CG45051	FBgn0266411
Sequence-based reagent	Hif1a reverse: 5 ⁰ GAATCTTGAGGAAAGCGATG3 ⁰	KRD	CG45051	FBgn0266411
Sequence-based reagent	CG10219 forward: 5 ⁰ GAGATCTCCGTGAGTGCGC3 ⁰	KRD	CG10219	FBgn0039112
Sequence-based reagent	CG10219 reverse: 5 ⁰ CTCCACGCCCAATGGG3 ⁰	KRD	CG10219	FBgn0039112
Sequence-based reagent	Scsa1 forward: 5 ⁰ TCACAAGCGCGCAAGATC3 ⁰	KRD	CG1065	FBgn0004888
Sequence-based reagent	Scsa1 reverse: 5 ⁰ TTGATGCCCGAATTGACTCG3 ⁰	KRD	CG1065	FBgn0004888
Sequence-based reagent	Tpi forward: 5 ⁰ AGATCAAGGACTGGAAGAACG3 ⁰	KRD	CG2171	FBgn0086355
Sequence-based reagent	Tpi reverse: 5 ⁰ ACCTCCTTGAGATGTTGTC3 ⁰	KRD	CG2171	FBgn0086355
Software, algorithm	Graphpad Prism	https://www.graphpad.com/	Graphpad Prism	RRID: SCR_002798

Continued on next page

Continued

Reagent type (species) or resource	Designation	Source reference	Identifier	Additional information
Software, algorithm	Microsoft Excel	https://www.microsoft.com/	Microsoft Excel	
Software, algorithm	Fiji	ImageJ - https://fiji.sc	ImageJ	RRID: SCR_002285
Other	S3e Cell Sorter	BioRad - http://www.bio-rad.com/	BioRad	
Other	Olympus FluoView 1000	Olympus - https://www.olympus-global.com/	Olympus	RRID: SCR_017015 RRID: SCR_014215
Other	Olympus SZX12	Olympus - https://www.olympus-global.com/	Olympus	
Other	Olympus IX71	Olympus - https://www.olympus-global.com/	Olympus	

Drosophila melanogaster strains

Flies were raised on a diet containing cornmeal (80 g/l), agar (10 g/l), yeast (40 g/l), saccharose (50 g/l) and 10% methylparaben (16.7 mL/l) and were kept in a controlled humidity environment with natural 12 hr/12 hr light/dark periods at 25°C, except for those used in temperature-controlled Gal80 experiments. Flies bearing Gal80 were transferred at 29°C 24 hr prior to infection in order to degrade temperature-sensitive Gal 80 protein. Prior to experiments, flies were kept in plastic vials on 0% glucose diet (cornmeal 53.5 g/l, agar 6.2 g/l, yeast 28.2 g/l and 10% methylparaben 16.7 mL/l) for 7 days and transferred into fresh vials every second day without CO₂ in order to ensure good condition of the food. Infected flies were kept on 0% glucose diet in incubators at 29°C due to the temperature sensitivity of *S. pneumoniae*. Drosophila Stock Centre in Bloomington provided TRiP control and Ldh[RNAi] flies. Hif1a[RNAi] and KK control flies were obtained from Vienna Drosophila Resource Center. Ldh-mCherry strain was kindly provided by Jason Tennesen, HRE-LacZ by Pablo Wappner and Hml > GFP by Bruno Lemaitre. The w1118 strain has a genetic background based on CantonS.

Bacterial strain and fly injection

The *S. pneumoniae* strain EJ1 was stored at 80°C in Tryptic Soy Broth (TSB) media containing 16% glycerol. For the experiments, bacteria were streaked onto agar plates containing 3% TSB and 100 mg/mL streptomycin and subsequently incubated at 37°C + 5% CO₂ overnight. Single colonies were inoculated into 3 mL of TSB liquid media with 100 mg/mL of streptomycin and 100,000 units of catalase and incubated at 37°C + 5% CO₂ overnight. Bacterial density was measured after an additional 4 hr so that it reached an approximate 0.4 OD₆₀₀. Final bacterial cultures were centrifuged and dissolved in phosphate-buffered saline (PBS) so the final OD reached A = 2.4. The *S. pneumoniae* culture was kept on ice prior to injection and during the injection itself. Seven-day-old males (survival experiments, qPCR assays, measurement of metabolites and enzymatic activity) or females (X-gal staining, NBDG assay) were anaesthetized with CO₂ and injected with 50 nL culture containing 20,000 *S. pneumoniae* bacteria or 50 nL of mock buffer (PBS) into the ventrolateral side of the abdomen using an Eppendorf Femtojet Microinjector.

Pathogen load measurement

Sixteen randomly chosen flies per genotype and treatment were anaesthetized with CO₂ and individually homogenized in 200 μL PBS using a motorized plastic pestle. Serial dilutions were plated onto TSB agar plates and incubated at 37°C overnight. The number of colonies was counted at 0, 24, 48 and 72 hpi. Collected data were compared using Tukey's multiple comparisons test in Graphpad Prism software. Sidak's multiple comparison correction was performed.

Survival analysis

Injected flies were kept at 29°C in vials with approximately 30 individuals per vial and were transferred onto a fresh food every other day. Dead flies were counted daily. At least three independent experiments were performed and combined into one survival curve created in Graphpad Prism software; the individual experiments showed comparable results. Average number of individuals was more than 500 for each genotype. Data were analyzed by Log-rank and Grehan-Breslow-Wilcoxon tests (which gave more weight to deaths at early time points).

Isolation of hemocytes

GFP-labeled hemocytes were isolated from HmlD-Gal4 UAS-eGFP male flies using fluorescence-activated cell sorting (FACS). Approximately 200 flies were anaesthetized with CO₂, washed in PBS and homogenized in 600 mL of PBS using a pestle. Homogenate was sieved through a nylon cell strainer (<40 μm). This strainer was then additionally washed with 200 mL of PBS, which was added to the homogenate subsequently. Samples were centrifuged (3 min, 6°C, 3500 RPM) and the supernatant was washed in ice cold PBS after each centrifugation (3x). Prior to sorting, samples were transferred to polystyrene FACS tubes using a disposable bacterial filter (<50 μm, Sysmex) and sorted into 100 mL of TRIzol Reagent (Invitrogen) using a S3TM Cell Sorter (BioRad). Sorted cells were verified by fluorescent microscopy and by differential interference contrast (DIC).

Gene expression

Sorted hemocytes were homogenized using a DEPC-treated pestle and RNA was extracted by TRIzol Reagent (Invitrogen) according to the manufacturer's protocol. Superscript III Reverse Transcriptase (Invitrogen) and oligo(dT)20 primer was used for reverse transcription. Amounts of mRNA of particular genes were quantified on a CFX 1000 Touch Real-Time Cycler (Bio-Rad) using the TP 2x SYBR Master Mix (Top-Bio) in three technical replicates with the following conditions: initial denaturation for 3 min at 95°C, then amplification for 15 s at 94°C, 30 s at 54°C, 40 s at 72°C for 40 cycles and melting curve analysis at 65–85°C/step 0.5°C. Primer sequences are listed in the Key Resources Table. qPCR data were analyzed with double delta Ct analysis, and expressions of particular genes were normalized to the expression of Ribosomal protein 49 (Rp49) in the same sample. Relative values (fold change) to control were compared and are shown in the graphs. Samples for gene expression analysis were collected from three independent experiments. Data were compared with Tukey's multiple comparisons test in Graphpad Prism software. Sidak's multiple comparison correction was performed.

Glucose uptake

HmlD-Gal4 UAS-eGFP adults were placed on a cornmeal diet with an added 200 mL of 2-NBDG (excitation/emission maxima of ~465/540 nm, 5 mg/mL stock (used 10,000x diluted), Thermo-Fisher), which was soaked into the surface of food, immediately after infection (flies analyzed at 24 hpi) or 96 hpi (flies analyzed at 120 hpi). After 1 day, flies were prepared for microscopy (Olympus IX71). Flies for glucose uptake analysis were collected from three independent experiments.

Activation of the hypoxia response element (HRE)

X-gal staining was performed on infected HRE-HRE-CRE-LacZ females. Flies were dipped in 75% EtOH for 1 s in order to make their cuticle non-hydrophobic and dissected in PBS. Fixation was performed with 2.5% glutaraldehyde/PBS on a LabRoller rotator for 7 min at room temperature. Adults were then washed three times in PBS. Next, two washings were performed with a PT solution (1 mL 10x PBS (Ambion), 100 mL 1M MgCl₂ · 6H₂O, 300 mL 10% Triton, 8 mL dH₂O, 320 mL 0.1M K₄[Fe(CN)₆], 320 mL 0.1 M K₃[Fe(CN)₆]) for 10 min. Finally, PT solution with few grains of X-gal (Sigma) was added. Samples were placed in a thermoblock at 37°C and occasionally mixed, and the colorimetric reaction was monitored. The reaction was stopped with three PBS washings at the same time for all samples. Samples for HRE activation evaluation were collected from four independent experiments.

Concentration of metabolites

Five flies were homogenized in 200 mL of PBS and centrifuged (3 min, 4°C, 8000 RPM) for glycogen measurement. For lactate and glucose measurement, hemolymph was isolated from 25 adult males

by centrifugation (14,000 RPM, 5 min) through a silicagel filter into 50 mL PBS. Half of all samples were used for the quantification of proteins. Samples for glucose, glycogen and lactate measurement were denatured at 75°C for 10 min, whereas samples for protein quantification were stored in 80°C. Glucose was measured using a Glucose (GO) Assay (GAGO-20) Kit (Sigma) according to the manufacturer's protocol. Colorimetric reaction was measured at 540 nm. For glycogen quantification, sample was mixed with amyloglucosidase (Sigma) and incubated at 37°C for 30 min. A Bicinchoninic Acid Assay (BCA) Kit (Sigma) was used for protein quantification according to the supplier's protocol and the absorbance was measured at 595 nm. A Lactate Assay Kit (Sigma) was used for lactate concentration quantification according to the manufacturer's protocol. The absorbance was measured at 570 nm. Samples for metabolite concentration were collected from six independent experiments. Measured data were compared in Graphpad Prism using Tukey's multiple comparisons test. Sidak's multiple comparison correction was performed.

Enzymatic activity

The enzymatic activities of lactate dehydrogenase and phosphoglucose isomerase were measured using a Lactate Dehydrogenase Activity Assay Kit (Sigma) or a Phosphoglucose Isomerase Colorimetric Assay Kit (Sigma), respectively, according to the supplier's protocol in 10,000 FACS-sorted hemocytes for each sample. Colorimetric reaction was measured at 450 nm. Samples for enzymatic activity detection were collected from six independent experiments. Measured values were compared in Graphpad Prism software using Tukey's multiple comparisons test. Sidak's multiple comparison correction was performed.

Genotypes of experimental models

Figure 1

(B) Hml >GFP refers to HmlID-Gal4 UAS-eGFP/HmlID-Gal4 UAS-eGFP; +/+

Figure 2

(A–B, D–G) Hml >GFP refers to HmlID-Gal4 UAS-eGFP/HmlID-Gal4 UAS-eGFP; +/+

Figure 3

(A) HRE-LacZ refers to HRE-HRE-CRE-LacZ/HREHRE-CRE-LacZ; +/+

(B) Hml >GFP Ldh-mCherry corresponds to HmlID-Gal4 UAS-eGFP, Ldh-mCherry/HmlID-Gal4 UAS-eGFP, Ldh-mCherry; +/+

(C–E) Hml >GFP refers to HmlID-Gal4 UAS-eGFP/HmlID-Gal4 UAS-eGFP; +/+

(E) Hml >GFP Hif1a[RNAi] corresponds to HmlID-Gal4 UAS-eGFP/UAS-Hif1a[RNAi]; +/+

Figure 4

(A, D–F) Hml x KK control corresponds to HmlID-Gal4 UAS-eGFP/KKcontrol; +/+; and Hml >Hif1a[RNAi] refers to HmlID-Gal4 UAS-eGFP/UAS-Hif1a[RNAi]; +/+

(B) Hml >GFP refers to HmlID-Gal4 UAS-eGFP/HmlID-Gal4 UAS-eGFP; +/+; and Hml >Hif1a[RNAi] refers to HmlID-Gal4 UAS-eGFP/UAS-Hif1a[RNAi]; +/+

(C, G–I) Hml x TRiP control corresponds to HmlID-Gal4 UAS-eGFP/+; TRiP control/+; and Hml >Ldh[RNAi] refers to HmlID-Gal4 UAS-eGFP/+; UAS-Ldh[RNAi]/ +

Figure 5

(A, B, C) Hml x TRiP control corresponds to HmlID-Gal4 UAS-eGFP/+; TRiP control/+; and Hml >Ldh[RNAi] corresponds to HmlID-Gal4 UAS-eGFP/+; UAS-Ldh[RNAi]/ +; and Hml >Hif1a[RNAi] refers to HmlID-Gal4 UAS-eGFP/UAS-Hif1a[RNAi]; +/+; and Hml x KK control corresponds to HmlID-Gal4 UAS-eGFP/KKcontrol; +/+

Figure 6

(A, C) Hml >Hif1a[RNAi] refers to HmlID-Gal4/+; P{tubPGal80ts}/UAS-Hif1a[RNAi]; and Hml x KK control corresponds to HmlID-Gal4/KK control; P{tubPGal80ts}/+ (B, D) w x Ldh[RNAi] refers to +/+; UAS-Ldh[RNAi]/+; and Hml >Ldh[RNAi] corresponds to HmlID-Gal4/+; P{tubPGal80ts}/UAS-Ldh[RNAi]

Acknowledgements

The authors acknowledge funding from the Grant Agency of the Czech Republic to TD (Project 17–16406S; www.gacr.cz). JMT and GC were supported by R35 MIRA 1R35GM119557 from NIGMS/NIH. The *S. pneumoniae* bacterial strain was obtained from David Schneider. We thank to Pablo Wappner and Bruno Lemaitre, who kindly provided us with HRE-HRE-CRE-LacZ and HmlID-Gal4 UAS-eGFP transgenic fly lines. Other fly stocks were obtained from the Bloomington Center (Bloomington, IN) and the VDRC (Vienna, Austria). We are thankful to the reviewing editors Prof. Utpal Banerjee and Prof. Ulrich Theopold for interesting comments on our work and hints for improvement of the discussion.

Additional information

Funding

Funder	Grant reference number	Author
Czech Science Foundation	Project 17-16406S	Tomaš Doležal
National Institute of General Medical Sciences	R35 MIRA 1R35GM119557	Jason M Tennessen

The funders had no role in study design, data collection and interpretation, or the decision to submit the work for publication.

Author contributions

Gabriela Krejčova´, Conceptualization, Data curation, Formal analysis, Investigation, Methodology, Writing—original draft, Writing—review and editing; Ade´la Danielova´, Pavla Nedbalova´, Michalina Kazek, Luka´s Strych, Data curation, Formal analysis; Geetanjali Chawla, Jaroslava Lieskovska´, Data curation; Jason M Tennessen, Resources, Data curation, Funding acquisition, Writing—original draft, Writing—review and editing; Marek Jindra, Validation, Writing—original draft, Writing—review and editing; Tomaš Doležal, Resources, Supervision, Funding acquisition, Validation, Writing—original draft, Writing—review and editing; Adam Bajgar, Conceptualization, Data curation, Formal analysis, Supervision, Validation, Investigation, Methodology, Writing—original draft, Project administration, Writing—review and editing

Author ORCIDs

Jason M Tennessen  <http://orcid.org/0000-0002-3527-5683>

Marek Jindra  <https://orcid.org/0000-0002-2196-9924>

Tomaš Doležal  <https://orcid.org/0000-0001-5217-4465>

Adam Bajgar  <https://orcid.org/0000-0002-9721-7534>

Decision letter and Author response

Decision letter <https://doi.org/10.7554/eLife.50414.020>

Author response <https://doi.org/10.7554/eLife.50414.021>

Additional files

Supplementary files

· Transparent reporting form DOI: <https://doi.org/10.7554/eLife.50414.018>

Data availability

All data generated or analysed during this study are included in the manuscript and supporting files. Source data have been provided for Figures 2 and 4.

References

- Allison SJ, Knight JRP, Granchi C, Rani R, Minutolo F, Milner J, Phillips RM. 2014. Identification of LDH-A as a therapeutic target for cancer cell killing via (i) p53/NAD(H)-dependent and (ii) p53-independent pathways. *Oncogenesis* 3:102–111. DOI: <https://doi.org/10.1038/oncsis.2014.16>
- Anderson RS, Holmes B, Good RA. 1973a. In vitro bactericidal capacity of *Blaberus craniifer* hemocytes. *Journal of Invertebrate Pathology* 22:127–135. DOI: [https://doi.org/10.1016/0022-2011\(73\)90021-9](https://doi.org/10.1016/0022-2011(73)90021-9), PMID: 4719276
- Anderson RS, Holmes B, Good RA. 1973b. Comparative biochemistry of phagocytizing insect hemocytes. *Comparative Biochemistry and Physiology Part B: Comparative Biochemistry* 46:595–602. DOI: [https://doi.org/10.1016/0305-0491\(73\)90099-0](https://doi.org/10.1016/0305-0491(73)90099-0)
- Baardman J, Licht I, de Winther MP, Van den Bossche J. 2015. Metabolic-epigenetic crosstalk in macrophage activation. *Epigenomics* 7:1155–1164. DOI: <https://doi.org/10.2217/epi.15.71>, PMID: 26585710
- Bailey P, Nathan J. 2018. Metabolic regulation of Hypoxia-Inducible transcription factors: the role of small molecule metabolites and iron. *Biomedicines* 6:60. DOI: <https://doi.org/10.3390/biomedicines6020060>
- Bajgar A, Kucerova K, Jonatova L, Tomcala A, Schneedorferova I, Okrouhlik J, Dolezal T. 2015. Extracellular adenosine mediates a systemic metabolic switch during immune response. *PLoS Biology* 13:e1002135. DOI: <https://doi.org/10.1371/journal.pbio.1002135>, PMID: 25915062
- Bajgar A, Dolezal T. 2018. Extracellular Adenosine modulates host-pathogen interactions through regulation of systemic metabolism during immune response in *Drosophila*. *PLoS Pathogens* 14:e1007022. DOI: <https://doi.org/10.1371/journal.ppat.1007022>, PMID: 29702691
- Browne N, Heelan M, Kavanagh K. 2013. An analysis of the structural and functional similarities of insect hemocytes and mammalian phagocytes. *Virulence* 4:597–603. DOI: <https://doi.org/10.4161/viru.25906>, PMID: 23921374
- Buchon N, Silverman N, Cherry S. 2014. Immunity in *Drosophila melanogaster*—from microbial recognition to whole-organism physiology. *Nature Reviews Immunology* 14:796–810. DOI: <https://doi.org/10.1038/nri3763>, PMID: 25421701
- Chambers MC, Lightfield KL, Schneider DS. 2012. How the fly balances its ability to combat different pathogens. *PLoS Pathogens* 8:e1002970. DOI: <https://doi.org/10.1371/journal.ppat.1002970>, PMID: 23271964
- Cox BL, Mackie TR, Eliceiri KW. 2015. The sweet spot: fdg and other 2-carbon glucose analogs for multi-modal metabolic imaging of tumor metabolism. *American Journal of Nuclear Medicine and Molecular Imaging* 5:1–13. PMID: 25625022
- Davies LC, Taylor PR. 2015. Tissue-resident macrophages: then and now. *Immunology* 144:541–548. DOI: <https://doi.org/10.1111/imm.12451>, PMID: 25684236
- Dengler VL, Galbraith M, Espinosa JM. 2014. Transcriptional regulation by hypoxia inducible factors. *Critical Reviews in Biochemistry and Molecular Biology* 49:1–15. DOI: <https://doi.org/10.3109/10409238.2013.838205>, PMID: 24099156
- Dolezal T. 2015. Adenosine: a selfish-immunity signal? *Oncotarget* 6:32307–32308. DOI: <https://doi.org/10.18632/oncotarget.4685>, PMID: 26427038
- Eichenlaub T, Villadsen R, Freitas FCP, Andrejeva D, Aldana BI, Nguyen HT, Petersen OW, Gorodkin J, Herranz H, Cohen SM. 2018. Warburg effect metabolism drives neoplasia in a *Drosophila* genetic model of epithelial Cancer. *Current Biology* 28:3220–3228. DOI: <https://doi.org/10.1016/j.cub.2018.08.035>, PMID: 30293715
- Figueroa-Claevega A, Bilder D. 2015. Malignant *Drosophila* tumors interrupt insulin signaling to induce cachexia-like wasting. *Developmental Cell* 33:47–55. DOI: <https://doi.org/10.1016/j.devcel.2015.03.001>, PMID: 25850672
- Forrester SJ, Kikuchi DS, Hernandez MS, Xu Q, Griendling KK. 2018. Reactive oxygen species in metabolic and inflammatory signaling. *Circulation Research* 122:877–902. DOI: <https://doi.org/10.1161/CIRCRESAHA.117.311401>, PMID: 29700084
- Freije WA, Mandal S, Banerjee U. 2012. Expression profiling of attenuated mitochondrial function identifies retrograde signals in *Drosophila*. *G3: Genes|Genomes|Genetics* 2:843–851. DOI: <https://doi.org/10.1534/g3.112.002584>, PMID: 22908033
- Galván-Peña S, O'Neill LA. 2014. Metabolic reprogramming in macrophage polarization. *Frontiers in Immunology* 5:420. DOI: <https://doi.org/10.3389/fimmu.2014.00420>, PMID: 25228902
- Geeraerts X, Bolli E, Fendt SM, Van Ginderachter JA. 2017. Macrophage metabolism as therapeutic target for Cancer, atherosclerosis, and obesity. *Frontiers in Immunology* 8:289. DOI: <https://doi.org/10.3389/fimmu.2017.00289>, PMID: 28360914
- German DC, Bloch CA, Kredich NM. 1983. Measurements of S-adenosylmethionine and L-homocysteine metabolism in cultured human lymphoid cells. *The Journal of Biological Chemistry* 258:10997–11003. PMID: 6885808
- Govind S. 2008. Innate immunity in *Drosophila*: pathogens and pathways. *Insect Science* 15:29–43. DOI: <https://doi.org/10.1111/j.1744-7917.2008.00185.x>, PMID: 20485470

- Herranz H, Cohen S. 2017. Drosophila as a model to study the link between metabolism and Cancer. *Journal of Developmental Biology* 5:15. DOI: <https://doi.org/10.3390/jdb5040015>
- Imtiyaz HZ, Simon MC. 2010. Hypoxia-inducible factors as essential regulators of inflammation. *Current Topics in Microbiology and Immunology* 345:105–120. DOI: https://doi.org/10.1007/82_2010_74, PMID: 20517715
- Iommarini L, Porcelli AM, Gasparre G, Kurelac I. 2017. Non-Canonical mechanisms regulating Hypoxia-Inducible factor 1 alpha in Cancer. *Frontiers in Oncology* 7:1–9. DOI: <https://doi.org/10.3389/fonc.2017.00286>, PMID: 29230384
- Irving P, Ubeda J-M, Doucet D, Troxler L, Lagueux M, Zachary D, Hoffmann JA, Hetru C, Meister M. 2005. New insights into Drosophila larval haemocyte functions through genome-wide analysis. *Cellular Microbiology* 7: 335–350. DOI: <https://doi.org/10.1111/j.1462-5822.2004.00462.x>
- Jeong HJ, Chung HS, Lee BR, Kim SJ, Yoo SJ, Hong SH, Kim HM. 2003. Expression of proinflammatory cytokines via HIF-1alpha and NF-kappaB activation on desferrioxamine-stimulated HMC-1 cells. *Biochemical and Biophysical Research Communications* 306:805–811. DOI: [https://doi.org/10.1016/S0006-291X\(03\)01073-8](https://doi.org/10.1016/S0006-291X(03)01073-8), PMID: 12821113
- Johansson KC, Metzendorf C, Söderhäll K. 2005. Microarray analysis of immune challenged Drosophila hemocytes. *Experimental Cell Research* 305:145–155. DOI: <https://doi.org/10.1016/j.yexcr.2004.12.018>, PMID: 15777795
- Jung Y, Isaacs JS, Lee S, Trepel J, Liu ZG, Neckers L. 2003. Hypoxia-inducible factor induction by tumour necrosis factor in Normoxic cells requires receptor-interacting protein-dependent nuclear factor kappa B activation. *Biochemical Journal* 370:1011–1017. DOI: <https://doi.org/10.1042/bj20021279>, PMID: 12479793
- Jung SH, Evans CJ, Uemura C, Banerjee U. 2005. The Drosophila lymph gland as a developmental model of hematopoiesis. *Development* 132:2521–2533. DOI: <https://doi.org/10.1242/dev.01837>, PMID: 15857916
- Kawai T, Akira S. 2011. Toll-like receptors and their crosstalk with other innate receptors in infection and immunity. *Immunity* 34:637–650. DOI: <https://doi.org/10.1016/j.immuni.2011.05.006>, PMID: 21616434
- Kim MY, Lee JE, Kim LK, Kim T. 2019. Epigenetic memory in gene regulation and immune response. *BMB Reports* 52:127–132. DOI: <https://doi.org/10.5483/BMBRep.2019.52.2.257>
- Koivunen P, Hirsilä M, Remes AM, Hassinen IE, Kivirikko KI, Myllyharju J. 2007. Inhibition of Hypoxia-inducible factor (HIF) Hydroxylases by citric acid cycle intermediates. *Journal of Biological Chemistry* 282:4524–4532. DOI: <https://doi.org/10.1074/jbc.M610415200>
- Kwon Y, Song W, Droujinine IA, Hu Y, Asara JM, Perrimon N. 2015. Systemic organ wasting induced by localized expression of the secreted insulin/IGF antagonist ImpL2. *Developmental Cell* 33:36–46. DOI: <https://doi.org/10.1016/j.devcel.2015.02.012>, PMID: 25850671
- Langston PK, Shibata M, Horng T. 2017. Metabolism supports macrophage activation. *Frontiers in Immunology* 8:1–7. DOI: <https://doi.org/10.3389/fimmu.2017.00061>, PMID: 28197151
- Lavista-Llanos S, Centanin L, Irisarri M, Russo DM, Gleadle JM, Bocca SN, Muzzopappa M, Ratcliffe PJ, Wappner P. 2002. Control of the hypoxic response in Drosophila Melanogaster by the basic helix-loop-helix PAS protein similar. *Molecular and Cellular Biology* 22:6842–6853. DOI: <https://doi.org/10.1128/MCB.22.19.6842-6853.2002>, PMID: 12215541
- Lemaître B, Nicolas E, Michaut L, Reichhart JM, Hoffmann JA. 1996. The dorsoventral regulatory gene cassette spätzle/Toll/cactus controls the potent antifungal response in Drosophila adults. *Cell* 86:973–983. DOI: [https://doi.org/10.1016/S0092-8674\(00\)80172-5](https://doi.org/10.1016/S0092-8674(00)80172-5), PMID: 8808632
- Li Y, Padmanabha D, Gentile LB, Dumur CI, Beckstead RB, Baker KD. 2013. HIF- and non-HIF-regulated hypoxic responses require the estrogen-related receptor in Drosophila Melanogaster. *PLOS Genetics* 9:e1003230. DOI: <https://doi.org/10.1371/journal.pgen.1003230>, PMID: 23382692
- Liberti MV, Locasale JW. 2016. The warburg effect: how does it benefit Cancer cells? *Trends in Biochemical Sciences* 41:211–218. DOI: <https://doi.org/10.1016/j.tibs.2015.12.001>
- Lim JJ, Grinstein S, Roth Z. 2017. Diversity and versatility of phagocytosis: roles in innate immunity, tissue remodeling, and homeostasis. *Frontiers in Cellular and Infection Microbiology* 7:1–12. DOI: <https://doi.org/10.3389/fcimb.2017.00191>
- Liu G, Roy J, Johnson EA. 2006. Identification and function of hypoxia-response genes in Drosophila melanogaster. *Physiological Genomics* 25:134–141. DOI: <https://doi.org/10.1152/physiolgenomics.00262.2005>, PMID: 16403841
- Martinez FO, Gordon S. 2014. The M1 and M2 paradigm of macrophage activation: time for reassessment. *F1000Prime Reports* 6:1–13. DOI: <https://doi.org/10.12703/P6-13>
- Mills CD, Kincaid K, Alt JM, Heilman MJ, Hill AM. 2000. M-1/M-2 macrophages and the Th1/Th2 paradigm. *The Journal of Immunology* 164:6166–6173. DOI: <https://doi.org/10.4049/jimmunol.164.12.6166>, PMID: 10843666
- Milutinović B, Kurtz J. 2016. Immune memory in invertebrates. *Seminars in Immunology* 28:328–342. DOI: <https://doi.org/10.1016/j.smim.2016.05.004>, PMID: 27402055
- Miyazawa H, Aulehla A. 2018. Revisiting the role of metabolism during development. *Development* 145: dev131110. DOI: <https://doi.org/10.1242/dev.131110>
- Mosser DM, Edwards JP. 2008. Exploring the full spectrum of macrophage activation. *Nature Reviews Immunology* 8:958–969. DOI: <https://doi.org/10.1038/nri2448>, PMID: 19029990
- Netea MG, Joosten LA, Latz E, Mills KH, Natoli G, Stunnenberg HG, O'Neill LA, Xavier RJ. 2016. Trained immunity: a program of innate immune memory in health and disease. *Science* 352:aaf1098. DOI: <https://doi.org/10.1126/science.aaf1098>, PMID: 27102489

- Newsholme P, Curi R, Gordon S, Newsholme EA. 1986. Metabolism of glucose, glutamine, long-chain fatty acids and ketone bodies by murine macrophages. *Biochemical Journal* 239:121–125. DOI: <https://doi.org/10.1042/bj2390121>, PMID: 3800971
- Nonnenmacher Y, Hiller K. 2018. Biochemistry of proinflammatory macrophage activation. *Cellular and Molecular Life Sciences* 75:2093–2109. DOI: <https://doi.org/10.1007/s00018-018-2784-1>, PMID: 29502308
- O'Neill LA, Pearce EJ. 2016. Immunometabolism governs dendritic cell and macrophage function. *The Journal of Experimental Medicine* 213:15–23. DOI: <https://doi.org/10.1084/jem.20151570>, PMID: 26694970
- Olenchok BA, Rathmell JC, Vander Heiden MG. 2017. Biochemical underpinnings of immune cell metabolic phenotypes. *Immunity* 46:703–713. DOI: <https://doi.org/10.1016/j.immuni.2017.04.013>, PMID: 28514672
- Pearce EL, Pearce EJ. 2013. Metabolic pathways in immune cell activation and quiescence. *Immunity* 38:633–643. DOI: <https://doi.org/10.1016/j.immuni.2013.04.005>, PMID: 23601682
- Peyssonnaud C, Cejudo-Martin P, Doedens A, Zinkernagel AS, Johnson RS, Nizet V. 2007. Cutting edge: essential role of hypoxia inducible factor-1alpha in development of lipopolysaccharide-induced Sepsis. *The Journal of Immunology* 178:7516–7519. DOI: <https://doi.org/10.4049/jimmunol.178.12.7516>, PMID: 17548584
- Pham LN, Dionne MS, Shirasu-Hiza M, Schneider DS. 2007. A specific primed immune response in Drosophila is dependent on phagocytes. *PLoS Pathogens* 3:e26. DOI: <https://doi.org/10.1371/journal.ppat.0030026>, PMID: 17352533
- Romero NM, Irisarri M, Roth P, Cauerhff A, Samakovlis C, Wappner P. 2008. Regulation of the Drosophila hypoxia-inducible factor alpha sima by CRM1-dependent nuclear export. *Molecular and Cellular Biology* 28:3410–3423. DOI: <https://doi.org/10.1128/MCB.01027-07>, PMID: 18332128
- Sears HC, Kennedy CJ, Garrity PA. 2003. Macrophage-mediated corpse engulfment is required for normal Drosophila CNS morphogenesis. *Development* 130:3557–3565. DOI: <https://doi.org/10.1242/dev.00586>, PMID: 12810602
- Siegert I, Schödel J, Nairz M, Schatz V, Dettmer K, Dick C, Kalucka J, Franke K, Ehrenschrwender M, Schley G, Beneke A, Sutter J, Moll M, Hellerbrand C, Wielockx B, Katschinski DM, Lang R, Galy B, Hentze MW, Koivunen P, et al. 2015. Ferritin-Mediated iron sequestration stabilizes Hypoxia-Inducible Factor-1a upon LPS activation in the presence of ample oxygen. *Cell Reports* 13:2048–2055. DOI: <https://doi.org/10.1016/j.celrep.2015.11.005>, PMID: 26628374
- Straub RH. 2014. Insulin resistance, selfish brain, and selfish immune system: an evolutionarily positively selected program used in chronic inflammatory diseases. *Arthritis Research & Therapy* 16:S4. DOI: <https://doi.org/10.1186/ar4688>
- Valanne S, Wang JH, Rämetsä M. 2011. The Drosophila toll signaling pathway. *Journal of Immunology* 186:649–656. DOI: <https://doi.org/10.4049/jimmunol.1002302>
- van Uden P, Kenneth NS, Webster R, Müller HA, Mudie S, Rocha S. 2011. Evolutionary conserved regulation of HIF-1b by NF-kB. *PLOS Genetics* 7:e1001285. DOI: <https://doi.org/10.1371/journal.pgen.1001285>, PMID: 21298084
- Wang CW, Purkayastha A, Jones KT, Thaker SK, Banerjee U. 2016. In vivo genetic dissection of tumor growth and the warburg effect. *eLife* 5:e18126. DOI: <https://doi.org/10.7554/eLife.18126>, PMID: 27585295
- Warburg O, Wind F, Negelein E. 1927. The metabolism of tumors in the body [English reprint]. *The Journal of General Physiology* 8:519–530. DOI: <https://doi.org/10.1085/jgp.8.6.519>
- Warburg O. 1956. On the origin of Cancer cells. *Science* 123:309–314. DOI: <https://doi.org/10.1126/science.123.3191.309>, PMID: 13298683
- Webster KA. 2003. Evolution of the coordinate regulation of glycolytic enzyme genes by hypoxia. *Journal of Experimental Biology* 206:2911–2922. DOI: <https://doi.org/10.1242/jeb.00516>, PMID: 12878660
- Williams NC, O'Neill LAJ. 2018. A role for the Krebs cycle intermediate citrate in metabolic reprogramming in innate immunity and inflammation. *Frontiers in Immunology* 9:141. DOI: <https://doi.org/10.3389/fimmu.2018.00141>, PMID: 29459863
- Wood W, Martin P. 2017. Macrophage functions in tissue patterning and disease: new insights from the fly. *Developmental Cell* 40:221–233. DOI: <https://doi.org/10.1016/j.devcel.2017.01.001>, PMID: 28171746
- Worku Y, Newby AC. 1983. The mechanism of adenosine production in rat polymorphonuclear leucocytes. *Biochemical Journal* 214:325–330. DOI: <https://doi.org/10.1042/bj2140325>, PMID: 6311180
- Wu QL, Fu YF, Zhou WL, Wang JX, Feng YH, Liu J, Xu JY, He PL, Zhou R, Tang W, Wang GF, Zhou Y, Yang YF, Ding J, Li XY, Chen XR, Yuan C, Lawson BR, Zuo JP. 2005. Inhibition of S-Adenosyl-L-homocysteine hydrolase induces immunosuppression. *The Journal of Pharmacology and Experimental Therapeutics* 313:705–711. DOI: <https://doi.org/10.1124/jpet.104.080416>, PMID: 15640397

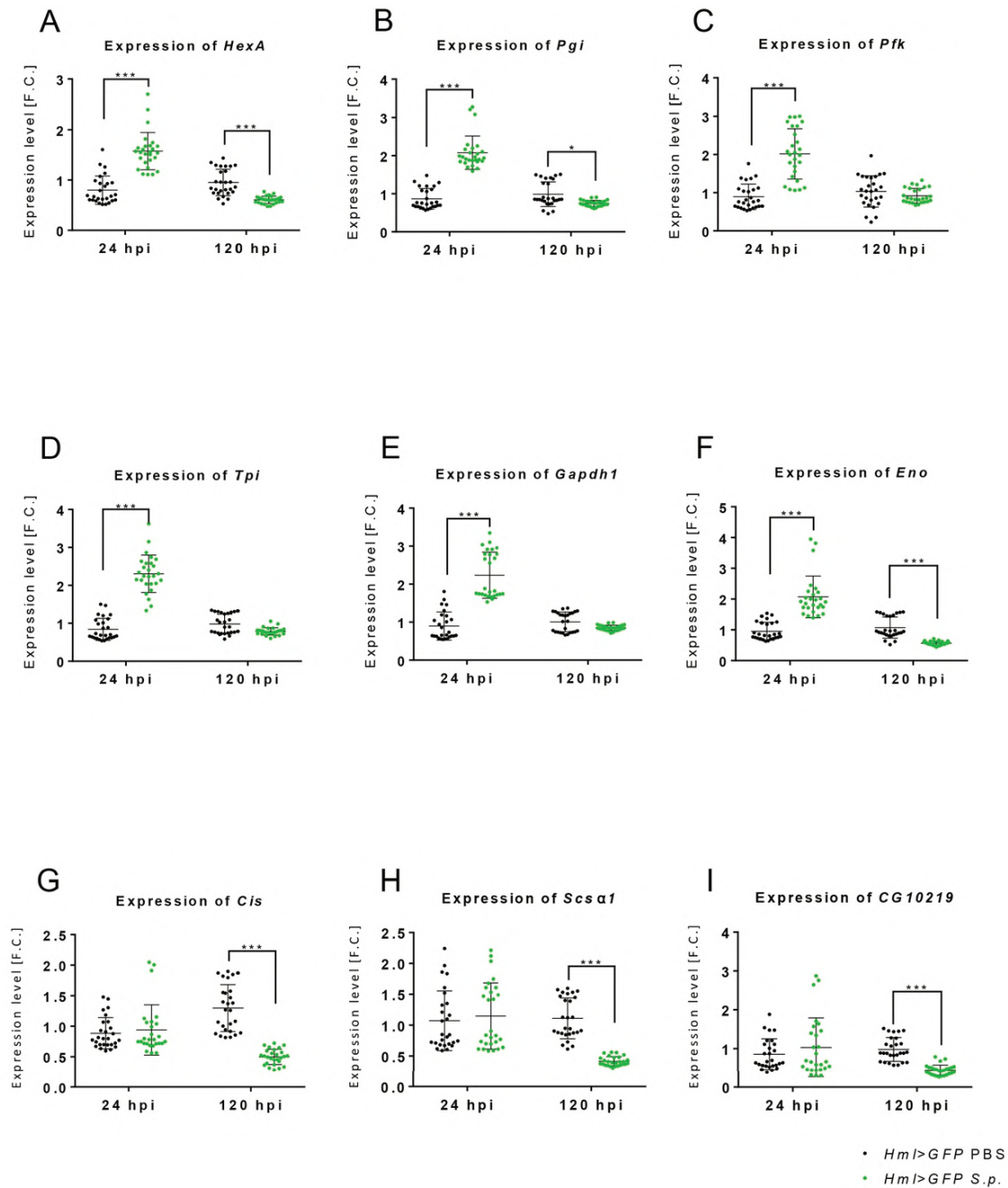
Supplementary information

***Drosophila* macrophages switch to aerobic glycolysis to mount effective antibacterial defense**

Gabriela Krejčová, Adéla Danielová, Pavla Nedbalová, Michalina Kazek, Lukáš Strych, Geetanjali Chawla, Jason M Tennessen, Jaroslava Lieskovská, Marek Jindra, Tomáš Doležal, and Adam Bajgar

eLife, 2019, **8**:e50414

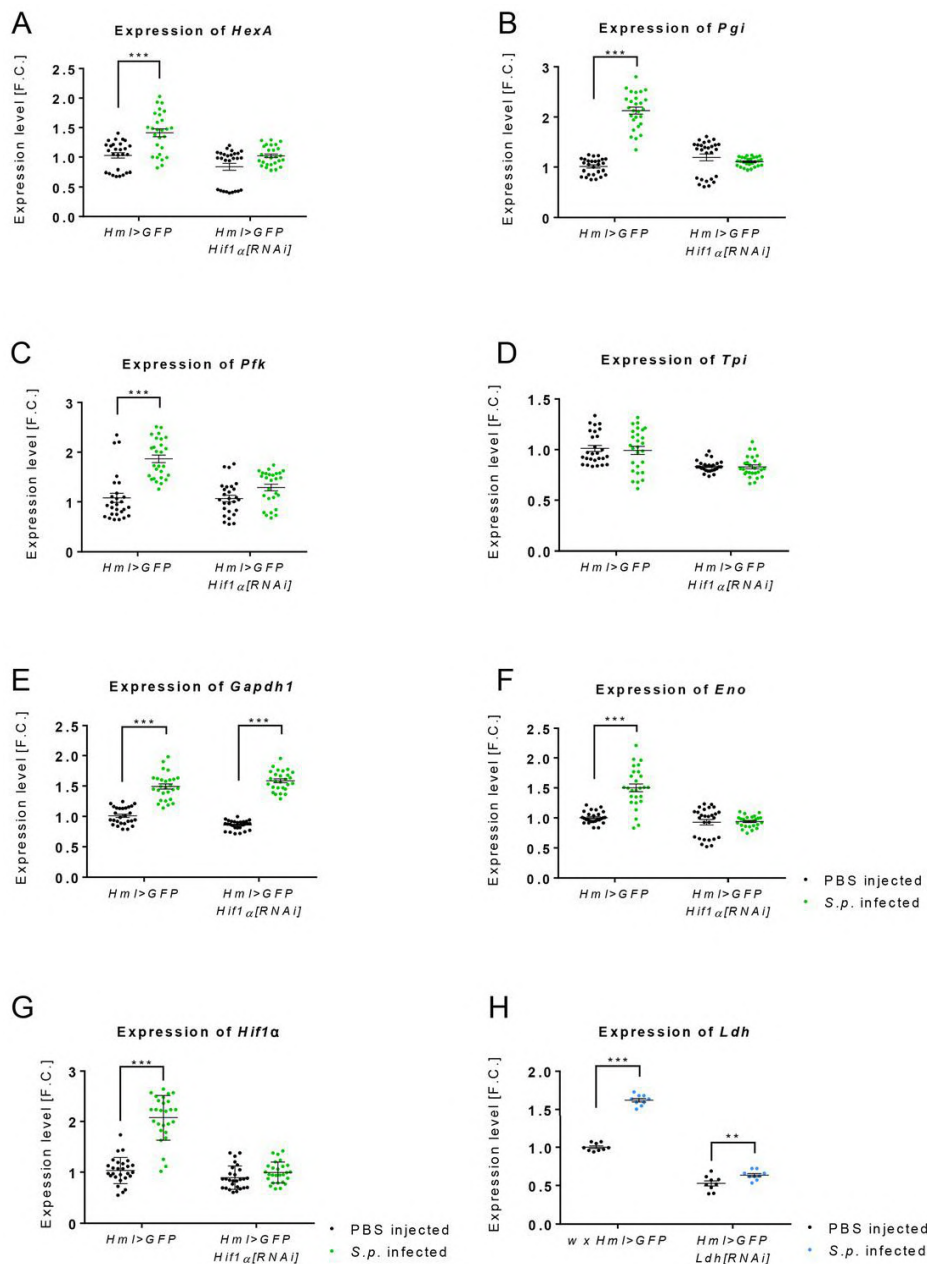
Figure 2 - Figure Supplement 1



Gene expression of glycolytic enzymes is increased in acute-phase macrophages.

Gene expression of glycolytic (HexA (A), Pgi (B), Pfk (C), Tpi (D), Gapdh1 (E), Eno (F)) and TCA (Cis (G), Scs α 1 (H), CG10219 (I)) genes in the hemocytes of infected and control flies (both Hml >GFP) at 24 and 120 hpi. The mRNA expression levels, normalized against rp49, are given as fold change (F.C.) relative to the expression of noninfected controls. Individual dots represent biological replicates. Values are mean \pm SD, asterisks mark statistically significant differences (*p<0.05; **p<0.01; ***p<0.001).

Figure 4 - Figure Supplement 1



Expression of genes encoding glycolytic enzymes is not increased in acute-phase macrophages with *Hif1α* knock-down.

(A–F) Gene expression of glycolytic genes (*HexA* (A), *Pgi* (B), *Pfk* (C), *Tpi* (D), *Gapdh1* (E) and *Eno* (F)) in the hemocytes of infected and control *Hml >GFP* flies and of flies with hemocyte-specific *Hif1α* knockdown at 24 hpi. (G, H) Gene expression of *Hif1α* (G) and *Ldh* (H) at 24 hpi in infected and control *Hml >GFP* flies and in flies with hemocyte-specific *Hif1α* knockdown representing the efficiency of RNAi treatment. The mRNA expression levels, normalized against *rp49*, are given as fold change (F.C.) relative to the expression in noninfected controls. Individual dots represent biological replicates. Values are mean \pm SD, asterisks mark statistically significant differences (* $p < 0.05$; ** $p < 0.01$; *** $p < 0.001$).

CHAPTER II:

Molecular regulations of metabolism during immune response in insects

Tomáš Doležal, **Gabriela Krejčová**, Adam Bajgar, Pavla Nedbalová, Paul Strasser

Insect Biochemistry and Molecular Biology, 2019, **109**:31-42



Molecular regulations of metabolism during immune response in insects

Tomas Dolezal^{*}, Gabriela Krejcová, Adam Bajgar, Pavla Nedbalová, Paul Strasser

Department of Molecular Biology and Genetics, Faculty of Science, University of South Bohemia in Ceske Budejovice, Branisovska 31, 37005, Ceske Budejovice, Czech Republic

ARTICLE INFO

Keywords:

Immunometabolism
Adenosine signaling
Disease tolerance
Warburg effect
Privileged immunity
Insulin resistance

ABSTRACT

Mounting an immune response is an energy-consuming process. Activating immune functions requires the synthesis of many new molecules and the undertaking of numerous cellular tasks and it must happen rapidly. Therefore, immune cells undergo a metabolic switch, which enables the rapid production of ATP and new biomolecules. Such metabolism is very nutrient-demanding, especially of glucose and glutamine, and thus the immune response is associated with a systemic metabolic switch, redirecting nutrient flow towards immunity and away from storage and consumption by non-immune processes. The immune system during its activation becomes privileged in terms of using organismal resources and the activated immune cells usurp nutrients by producing signals which reduce the metabolism of non-immune tissues. The insect fat body plays a dual role in which it is both a metabolic organ, storing energy and providing energy to the rest of the organism, but also an organ important for humoral immunity. Therefore, the internal switch from anabolism to the production of antimicrobial peptides occurs in the fat body during infection. The mechanisms regulating metabolism during the immune response ensure adequate energy for an effective response (resistance) but they must be properly regulated because energy is not unlimited and the energy needs of the immune system thus interfere with the needs of other physiological traits. If not properly regulated, the immune response may in the end decrease fitness via decreasing disease tolerance.

1. Physiological trade-offs during immune response that requires increased energy supply

The ability to mount an immune response belongs to the most fundamental of evolutionary traits among all organisms, insects being no exception. Organisms are usually equipped with an array of pre-existing, innately present immune mechanisms, ready to take immediate action. These mechanisms quiescently await activation by the pathogen, using no more energy than is needed for their basal functioning (maintenance costs—(McKean et al., 2008)). For example, developing and maintaining hematopoietic cells in *Drosophila* larva, which are important for cellular immunity, requires around 10% of the whole organismal glucose (Bajgar et al., 2015). Activation of the immune system rapidly increases its energy needs, depending of course on the extent of the response; the induction of immune response is associated with so called deployment costs (McKean et al., 2008). Merely triggering immune cell motility and executing, for example, phagocytosis already requires an increased amount of energy (Anderson et al., 1973). Detecting a pathogen however induces a plethora of additional immune reactions, which require the synthesis of many new molecules with signaling and antimicrobial functions, the undertaking of various

cellular tasks and often the proliferation of additional immune cells (for example lamellocytes for encapsulation); all this must happen rapidly. Therefore, the energy requirements of immune cells may rise from 10% to almost one third of overall glucose consumption, for example in the case of the mounting of an immune response to parasitoid infection in *Drosophila* larva (Bajgar et al., 2015).

Such an increase in energy consumption by the activated immune system affects other processes within the organism competing for the available resources, which is well documented in eco-physiological studies of insects. During infection, the immune response, as an essential life-preserving process, becomes privileged regarding energy supply over other processes. Therefore, activating the immune response leads to a reduced overall metabolic rate during infection (Arnold et al., 2013; Bashir-Tanoli and Tinsley, 2014; Chambers et al., 2012; Gray and Bradley, 2005; Ibrahim et al., 2018), associated with slower development and reduced growth (Bajgar et al., 2015; Diamond and Kingsolver, 2011; DiAngelo et al., 2009) and can also lead to an extensive loss of energy reserves during chronic infection (Bajgar and Dolezal, 2018; Dionne et al., 2006). The immune response may also compete with another energy consuming process, reproduction. Especially during the acute phase of infection, a decline in fecundity has been observed

^{*}Corresponding author.

E-mail address: tomas.dolezal@prf.jcu.cz (T. Dolezal).

<https://doi.org/10.1016/j.ibmb.2019.04.005>

Received 3 December 2018; Received in revised form 12 March 2019; Accepted 1 April 2019

Available online 05 April 2019

0965-1748/ © 2019 Elsevier Ltd. All rights reserved.

Abbreviations

Ado	adenosine
AMPs	antimicrobial peptides
JNK	c-Jun N-terminal kinase
Dilps	Drosophila insulin-like peptides
Grnd	Grindelwald
GBP	growth-blocking peptide
Imd	Immunodeficiency

InR	insulin receptor
LDH	lactate dehydrogenase
OXPHOS	oxidative phosphorylation
PPP	pentose phosphate pathway
PDH	pyruvate dehydrogenase
PDK	pyruvate dehydrogenase kinase
TCA	tricarboxylic acids
Upd	Unpaired

(Bashir-Tanoli and Tinsley, 2014; Gray and Bradley, 2005; Howick and Lazzaro, 2014; McKean et al., 2008; Nystrand and Dowling, 2014). On the other hand, active reproduction may negatively affect resistance to infection (McKean et al., 2008; Siva-Jothy et al., 1998).

Another process, which may compete with the immune response for energy, is the acute stress response (fight-or-flight). They both represent life-preserving reactions and they share certain attributes – they are energy consuming processes and they are associated with a release of energy required for the reaction. Therefore, transient acute hyperglycemia as a marker of energy release is present during both reactions. However, the actual use of energy differs profoundly. In contrast to immunity, the overall metabolic rate during fight-or-flight increases because tissues, such as muscles and the nervous system, which are not negligible on the whole organismal level, need to process the released energy to fight or escape. Stress induces the production of the stress hormones octopamine and adipokinetic hormone, which cause the

release of energy required in muscles and the nervous system (Gäde and Auerswald, 2003; Verlinden et al., 2010). These hormones reduce resistance, which may be explained by their activating effects on systemic metabolism, which is not favorable for the immune response (Adamo, 2017; Adamo and Parsons, 2006; Goldsworthy et al., 2005; Ibrahim et al., 2018). This is in agreement with the observation that chronic exposure to predators, which increases levels of stress hormones and metabolic rates, leads to a chronic reduction in disease resistance (reviewed in Adamo, 2017). On the other hand, the immune response increases susceptibility to predation stress (Otti et al., 2012).

The regulation of resource distribution during development and the maintenance of various systems within the organism as well as during the activation of the stress response is a fundamental theme in the evolution of organisms. The trade-offs between different systems have been beautifully demonstrated by the artificial selection of increased resistance to parasitoids (Kraaijeveld and Godfray, 1997). The

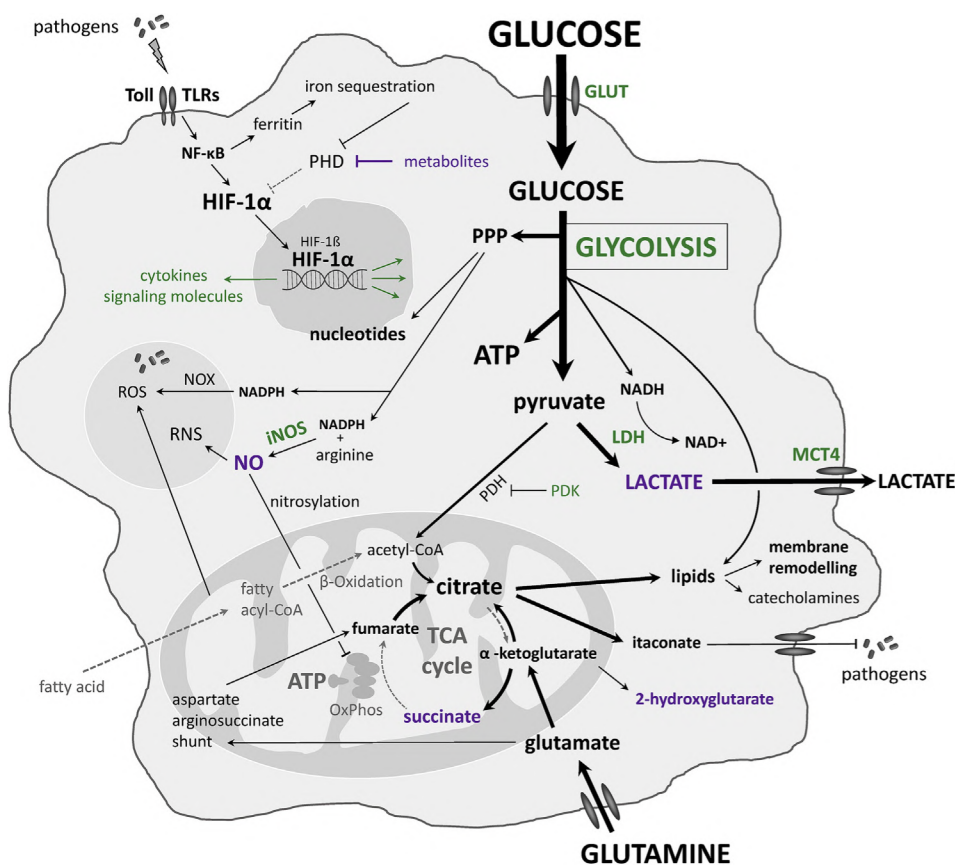


Fig. 1. Metabolic changes in the activated macrophage based on studies of mammalian cells. Grey arrows and letters represent pathways and metabolites that are important in the quiescent immune cell but are rather suppressed in the activated immune cell. Black arrows and black/colored letters represent enhanced pathways, metabolites and enzymes in the activated immune cell. Activation of the Toll-like receptors and NF-κB signaling leads to stabilization of HIF-1α (by the ferritin-mediated inhibition of prolyl hydroxylase dehydrogenase - PHD). The stabilized HIF-1α works as a master switch, which promotes a glucose uptake and increases expression of several glycolytic genes. The green color shows the targets of activated HIF-1α. ATP is generated by increased glycolysis, which also feeds glucose carbons into the pentose phosphate pathway (PPP) for a production of nucleotides and NADPH. By pyruvate dehydrogenase kinase (PDK)-mediated inhibition of pyruvate dehydrogenase (PDH) and by simultaneous increase of lactate dehydrogenase (LDH) and lactate transporter MCT4, HIF-1α diverts pyruvate from mitochondrial metabolism. The mitochondrial metabolism is substantially changed in activated immune cells. Inflammatory macrophages largely reduce OXPHOS via the nitrosylation of the electron transport chain by iNOS-generated NO and by itaconate produced from citrate. In inflammatory macrophages, the TCA cycle is broken when citrate is not converted to isocitrate but is primarily used for fatty acid synthesis, membrane biosynthesis, and the production of antimicrobial metabolite itaconate. When pyruvate is not fed into the TCA cycle and/or the TCA cycle is broken at the citrate step, glutamine is anaplerotically metabolized in the mitochondria to replenish TCA intermediates. It is first converted to glutamate, which is used in mitochondria to produce α-ketoglutarate and either succinate or citrate in a reversed mode, reductively carboxylated by NADPH-dependent isoforms of isocitrate dehydrogenase. Citrate can also be produced, using glutamate, through an aspartate-argininosuccinate shunt. Purple color shows metabolites that increase due to the HIF-1α-reprogrammed metabolism and which further stabilize HIF-1α (by inhibiting PHD) to reinforce changes induced by initial stabilization of HIF-1α. (For interpretation of the reference to color in this figure legend, the reader is referred to the Web version of this article.)

duction of antimicrobial metabolite itaconate. When pyruvate is not fed into the TCA cycle and/or the TCA cycle is broken at the citrate step, glutamine is anaplerotically metabolized in the mitochondria to replenish TCA intermediates. It is first converted to glutamate, which is used in mitochondria to produce α-ketoglutarate and either succinate or citrate in a reversed mode, reductively carboxylated by NADPH-dependent isoforms of isocitrate dehydrogenase. Citrate can also be produced, using glutamate, through an aspartate-argininosuccinate shunt. Purple color shows metabolites that increase due to the HIF-1α-reprogrammed metabolism and which further stabilize HIF-1α (by inhibiting PHD) to reinforce changes induced by initial stabilization of HIF-1α. (For interpretation of the reference to color in this figure legend, the reader is referred to the Web version of this article.)

increased resistance was associated with an increased number of immune cells and thus with increased maintenance costs, which decreased, on the other hand, the competitiveness of larvae in obtaining food (Kraaijeveld et al., 2001).

2. What are the energy needs of immunity?

The immune system of insects can be divided into the cellular and the humoral components, which are however interconnected at many levels. Insects occupy a wide variety of ecological niches where they inevitably face trauma and frequent attack by pathogens. After a pathogen crosses the first physical immune barriers, integument, or the gut peritrophic membrane, immune cells are usually the first to react to it. They can phagocytose the invading pathogen or they can initiate nodulation, netosis, or the encapsulation response associated with melanization (Rosales, 2017). During nodulation, hemocytes form multicellular aggregates, entrapping groups of microorganisms, and ultimately performing melanization (Satyavathi et al., 2014). It seems that insect hemocytes can also release nucleic acids to facilitate the extracellular trapping of bacteria (Altincicek et al., 2008) similar to mammalian NETosis (Branzk and Papayannopoulos, 2013). Larger objects such as parasitoid eggs, which are too large to be phagocytosed, are encapsulated in the multilayered capsule of hemocytes and destroyed by melanization. This may involve the proliferation and differentiation of specialized cells known as lamellocytes. These cellular responses are accompanied by humoral processes such as the above mentioned melanization, which requires the activation of prophenoloxidases transforming them into phenoloxidases, and acts on tyrosine, forming melanin in multiple steps. Another humoral response involves the production of various antimicrobial peptides (AMPs), which are produced mainly in the fat body and usually follow the cellular response several hours later.

The activation of cellular immunity leads to a metabolic switch within the immune cells, which become dependent on a massive supply of glucose and glutamine (see section 3 below). The energy costs of the humoral arm of immunity are associated with the synthesis of AMPs, whose expressions might increase even several hundred times during the immune response. The question is whether the induced synthesis of numerous AMPs and other immune molecules among all other synthetic processes normally happening in the fat body represents a significant cost to the overall metabolism (Wagner, 2005). For example, flies overexpressing Drosomycin have reduced glycogen and triglyceride stores and reduced activity (Rera et al., 2012) suggesting that the induced expression of AMPs might indeed represent an energy burden upon the organism. In addition, the induction of AMPs expression is directly linked to the suppression of anabolism in the fat body through the switching of MEF2 (Clark et al., 2013). However, the fat body plays a dual role in which it expresses AMPs on the one hand, but on the other hand also provides energy to the rest of the organism, including cellular immunity. The observed metabolic costs thus might be primarily associated with the energy-demanding cellular immunity; it is hard to separate the metabolic costs of the cellular and humoral arms due to this dual role of the fat body. It may also be hard to estimate metabolic costs of the other humoral part of immunity, the melanization cascade, which is often again linked with actions of immune cells. Prophenoloxidases are constitutively present prior to defense activation, so the metabolic costs of mounting the melanization response are mainly associated with the depletion of the amino acid tyrosine (Chambers et al., 2012).

3. Cellular immunity activation leads to a metabolic reprogramming resembling the Warburg effect

3.1. Warburg effect in immune cells is based on studies of mammalian immunity

To understand the metabolic needs of cellular immunity, we must look at mammalian immune cells studies, which describe the process of metabolic reprogramming with sufficient depth (summarized and described with additional details on Fig. 1). However as described below, it is likely for the most part to also be valid for insect cells. As shown on Fig. 1, quiescent immune cells, awaiting immune stimulation, use glycolysis for the production of pyruvate, which enters the mitochondria and is converted into acetyl-CoA. Acetyl-CoA, which is also produced by the β -oxidation of fatty acid, is used in the tricarboxylic acids (TCA) cycle linked to oxidative phosphorylation (OXPHOS) to produce ATP by the most efficient means—theoretically up to 38 ATP molecules are generated per one molecule of glucose. Glycolysis and β -oxidation are thus linked to active OXPHOS and primarily used for effective ATP production to cover the basal maintenance of quiescent immune cells (reviewed in Palsson-McDermott and O'Neill, 2013). Although this is a very efficient metabolism for energy generation, it is too slow for ATP generation during the immune response. Upon immune stimulation, the immune cells switch from this state of low nutrient uptake to the metabolism optimized to a rapid production of ATP and a large amount of newly-synthesized molecules, which are required to mount the immune response. ATP is primarily produced by glycolysis, ineffectively (merely 2 ATP molecules per glucose) but much faster compared to the glycolysis-TCA-OXPHOS axis. Glucose carbons are also used to a much greater extent for the production of new macromolecules, required for the functioning of the activated immune cell, not being lost as CO_2 in OXPHOS. The pentose phosphate pathway (PPP) branches off from glycolysis, generating ribose for nucleotides and NADPH for the production of reactive oxygen species (Bergin et al., 2005; Rybicka et al., 2010). Pyruvate is converted to lactate to regenerate NAD^+ from NADH by lactate dehydrogenase (LDH). Lipids are used for a dynamic remodeling of the cellular membrane and for the synthesis of eicosanoids and other lipid based metabolites in lipid bodies (Péan et al., 2017; Remmerie and Scott, 2018).

Metabolic changes in inflammatory immune cells thus resemble a situation where cells prefer glycolysis over OXPHOS even with sufficient oxygen supply, the process known as the Warburg effect. This metabolic adaptation was originally described for yeast and cancer cells (Warburg, 1925), but recently found also in mammalian immune cells in their proinflammatory state (Mills, 2015) and in rapidly proliferating cells (Burns and Manda, 2017). The mitochondrial metabolism is substantially changed in activated immune cells; pyruvate is diverted from the TCA cycle, which is broken at the citrate step and glutamine is anaerobically metabolized in the mitochondria to replenish TCA intermediates, becoming thus another important metabolite for activated immune cells (Jha et al., 2015). In summary, the activation of the immune cell is associated with massively increased glycolysis (feeding PPP, lipid synthesis, and resulting in lactate production) and the re-wired mitochondrial metabolism (broken TCA cycle and suppressed OXPHOS), which make the cell dependent on high doses of glucose and glutamine (Van den Bossche et al., 2017).

3.2. Metabolic reprogramming is present also in insect immune cells

Although the metabolic reprogramming of activated immune cells is studied mostly in mammalian systems and is much less studied in insects, the Warburg effect has also been described in insects both in normal proliferation and cancer (Herranz and Cohen, 2017; Slaninova et al., 2016; Tennessen et al., 2014; Wang et al., 2016) as well as in activated immune cells. For example, the activation of phagocytic cells of *Blaberus* was associated with changes resembling the Warburg effect

(Anderson et al., 1973). The transcriptome profiling of activated hemocytes of mosquitoes, fruit flies, and tobacco budworms also reveals changes associated with the increased expression of glycolytic genes and LDH (Bartholomay et al., 2004; Choi et al., 2012; Irving et al., 2005; Johansson et al., 2005; Pinto et al., 2009; Shelby et al., 2012). We have shown that the proliferation and differentiation of lamellocytes during the parasitoid infestation of *Drosophila* larvae were associated with a hemocyte-specific increase in the expression of glycolytic genes, accompanied by increased glucose consumption (Bajgar et al., 2015) and the production of lactate (Fig. 2 and Strasser, 2016). Although it is clear that various insect immune cells significantly increase glucose consumption, glycolysis and lactate production upon activation, further detailed characterization of metabolic changes is necessary to bridge the gap between insect and mammalian studies.

3.3. Myc and hypoxia inducible factor 1 α induce the metabolic reprogramming, both in insects and mammals

The above described complex reprogramming of many metabolic pathways, which supports the activated immune functioning of the cell, requires a coordinated change of expression and the activity of hundreds of metabolic enzymes. It is then adaptive to have a master regulator, quickly reacting to the immune activating signals and triggering the whole complex reprogramming (Metallo and Heiden, 2013). The metabolic switch in proliferating immune cells is connected to the activation of Myc, as has been shown, for example, for proliferating T lymphocytes in mammals (Gnanaprakasam and Wang, 2017; Wang et al., 2011). In insects, Myc was shown to be strongly upregulated in highly proliferative hopTum-I hemocytes (Anderson et al., 2017). The metabolic changes of activated macrophages and the subsequent pro-inflammatory phenotype are dependent on Hypoxia inducible factor 1 α (HIF-1 α). Contrary to the proliferating precursors of macrophages, the pro-inflammatory stimulation of macrophages in mammals suppresses Myc while engaging HIF-1 α (Gnanaprakasam and Wang, 2017).

The role of HIF-1 α was originally described during hypoxia, where it is responsible for changes of cellular metabolism induced by the lack of oxygen which is otherwise necessary for OXPHOS in mitochondria (Wenger et al., 2005). The signaling pathway, activated in response to hypoxia in the insect, is conserved and mediated by a homolog of HIF-1 α , known in *Drosophila* as Similar, or Sima for short (Lavista-Llanos et al., 2002). Without hypoxia, HIF-1 α is continuously translated, followed by an immediate hydroxylation by enzyme prolyl hydroxylase dehydrogenase (PHD), which marks HIF-1 α for degradation; in *Drosophila*, the respective enzyme is called Fatiga and mutation in the Fatiga gene has been shown to lead to an accumulation of the Sima protein in normoxia (Centanin et al., 2005). HIF-1 α stabilization leads to nuclear translocation, heterodimerization with HIF-1 β (Tango in flies), and the activation of the specific transcriptional program of genes under the control of HRE elements (Dengler et al., 2014; Romero et al., 2008). HIF-1 α thus works as a central transcription factor regulating the expression of many metabolic genes leading to the complex rewiring of cellular metabolism.

Various other inputs besides the lack of oxygen may lead to a stabilization of HIF-1 α , including immunostimulatory signals, linking the activation of immune cells with metabolic changes. In mammals, activation of the Toll-like receptors and NF- κ B signaling results in an increased expression and stabilization of HIF-1 α (Jung et al., 2003; Siegert et al., 2015). This mechanism of normoxic stabilization and the expression of HIF factors by NF- κ B signaling has also been described in *Drosophila*. Bandarra et al. (2015) and Uden et al. (2011) showed that HIF-1 α can be induced by both Toll and Imd-induced NF- κ B signaling, either genetically or by infection. Bandarra et al. (2015) showed that the Sima/Tango induction during infection is dependent on Imd/IKK/Rel and that the knockout of Sima resulted in increased mortality during *Serratia marcescens* infection. Uden et al. (2011) showed that Sima/Tango are activated by the overexpression of *Drosophila* NF- κ B factor

Dorsal or by the cactus mutation, both mimicking activated Toll signaling.

4. Effects of immune response activation on systemic metabolism

As described above, activated immune cells undergo a metabolic switch associated with increased glycolysis and glucose uptake. The increased demands of activated immune cells for glucose raise a question of the impact on overall metabolism. The impact likely depends on the extent of the response. For example, using radioactively-labeled glucose, we were able to quantify the glucose demands of the activated immune cells during the parasitoid attack—glucose consumption by immune cells raised from 11% to 27% of total glucose (Bajgar et al., 2015). In such cases, immune activation can lead to a significant suppression of the metabolism in the rest of the organism during infection. The generation of energy reserves (triglycerides and glycogen) during larval development was suppressed by wasp infection (Bajgar et al., 2015) and, in adult flies, the reserves decreased during bacterial infection, providing energy to phagocytes (Bajgar and Dolezal, 2018). Larval development slowed down, resulting in slower imaginal disc growth and in developmental delay (Bajgar et al., 2015). The overall metabolism was documented to be suppressed by various types of infection (Chambers et al., 2012; Schlenke et al., 2007). These results demonstrate that the activation of the immune system leads to a systemic metabolic switch redirecting the energy/nutrients flow from growth/storage to the activated immune system.

The fat body plays a dual role in such energy redirection since it is both an immune and a metabolic organ at the same time. The fat body is important for storage and overall metabolic homeostasis on the one hand, but it is also responsible for the humoral immune response on the other. Therefore, the switch from anabolism to immunity also operates within the fat body itself, which is beautifully demonstrated by the dual

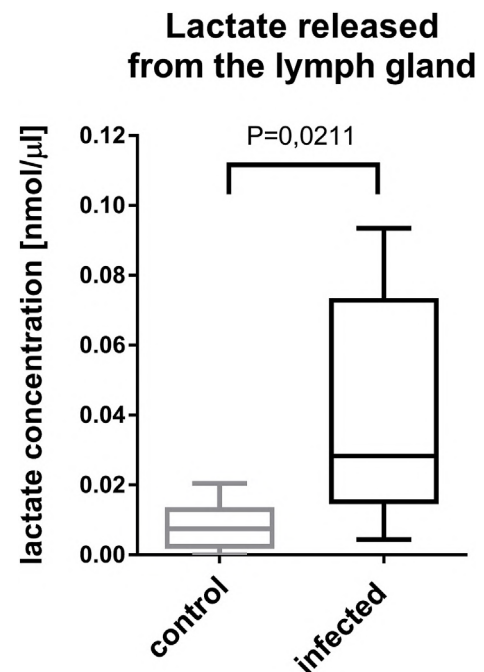


Fig. 2. Lactate production is increased in the lymph glands of *Drosophila* larvae infected by parasitoid wasps. Six lymph glands were dissected from larvae of *Drosophila melanogaster* infected with parasitoid wasp *Leptopilina boulardi* 6 h post-infection (black) and from uninfected control (grey). Lymph glands were incubated *ex vivo* for 50 min in 20 μ l of PBS supplemented with 200 μ M glucose and 6 mM trehalose. Lactate was determined in supernatant by Lactate Assay Kit (Sigma Aldrich). The difference was tested by Welch's t-test ($n = 8$). Further details can be found in (Strasser, 2016).

role of MEF2. Phosphorylated MEF2 activates the expression of genes involved in anabolic processes, however infection leads to its dephosphorylation, thus lowering anabolic processes and at the same time dephosphorylated MEF2 activates AMPs expression (Clark et al., 2013). Immune system activation is, therefore, linked to the suppression of systemic metabolism and to a redirection of energy flow from the anabolic and non-immune processes towards immunity. Since immune cells require an increased supply of nutrients upon their activation, it seems logical that they obtain nutrients by suppressing their consumption by other processes.

It is not easy to test the importance of such suppression for the effectivity of the response since the manipulations of inducers of metabolic changes often simultaneously affect immune induction. These processes are intricately linked and regulators often suppress metabolism and induce immune response at the same time (Clark et al., 2013; DiAngelo et al., 2009). It is then hard to say whether the resulting reduced resistance is due to the lack of metabolic switch or due to the lack of immune induction. When the processes are manipulated throughout the development, it is hard to say whether the effects are caused by the state of metabolism before the immune response starts, for example by low energy stores as reported in (Clark et al., 2013; Yang and Hultmark, 2017). However, when the inducible knockdown of glycogen phosphorylase (i.e. merely a metabolic manipulation blocking the release of glucose from glycogen) was performed just prior to infection, the glycogen levels in manipulated flies were comparable to the control and the glycogen breakdown was suppressed only upon infection (Bajgar and Dolezal, 2018). In such a case, the reduced resistance to *Streptococcus pneumoniae* in flies with such manipulation clearly demonstrated the importance of the metabolic switch to the effectivity of the immune response.

5. Adenosine mediates the privileged behavior of the immune system

The importance of the systemic metabolic switch for immune response can be demonstrated in the *adoR* mutant with a deficiency in adenosine (Ado) signaling (Dolezal et al., 2005). The *adoR* mutation allows normal development with no effect on metabolism under normal conditions (Bajgar et al., 2015; Bajgar and Dolezal, 2018). However, extracellular Ado mediates the systemic metabolic switch via *AdoR* during infection and the switch does not occur or is severely delayed in the *adoR* mutant. The mutant simply keeps developing as if there were no infection (Bajgar et al., 2015) and the hyperglycemia associated with glycogen breakdown (markers of the switch) is suppressed (Bajgar and Dolezal, 2018). This inability of the *adoR* larvae or flies to reroute energy from storage and growth towards immunity results in a markedly decreased resistance against parasitoid and bacterial infections. These results demonstrate that the Ado-mediated systemic metabolic switch,

associated with hyperglycemia at the expense of stores and with an overall suppression of the metabolism, supplies immune cells with the required energy either for their rapid proliferation and the differentiation of lamellocytes and effective encapsulation of parasitoid eggs, or for their effective phagocytosis of bacteria.

Ado is not only an important metabolite but it also serves as an important stress signaling molecule. It is formed during intracellular metabolic stress when ATP levels drop and AMP increases. Ado is then formed from AMP and is released from a stressed cell to inform the surrounding tissues or the whole organism of the stress (Antonoli et al., 2008). It can also be formed upon tissue damage from leaking ATP by ectoenzymes converting ATP to ADP, AMP, and Ado (Fenckova et al., 2011). A common response at the organismal level to the increased level of Ado is a slowing down of metabolism to overcome the stress. This Ado role is very ancient, being present in “social bacteria” (Shimkets and Dworkin, 1981) to vertebrates (Buck, 2004). The Ado role in the systemic metabolic switch during infection perfectly fits into this ancient role. Interestingly, knocking down the transporter of Ado *ENT2* specifically in hemocytes demonstrated that it is actually immune cells themselves that produce this important regulator of systemic metabolism (Bajgar et al., 2015). Therefore we can say that the activated immune system becomes privileged, hierarchically placed above other systems, and the immune cells release Ado to usurp energy from the rest of the organism (Fig. 3).

The privileged behavior of immunity, mediated by Ado, represents an experimental verification of a theoretical concept of the “selfish immune system”, first articulated by Rainer Straub (2014) inspired by the “selfish brain theory” (Peters et al., 2004). These concepts put brain and immune system hierarchically above the rest of the organism in allocating energy. During the fight-or-flight response or trauma/infection, the organism depends vitally on either the central nervous system or the immune system and thus these organs are privileged in energy allocation. According to Straub, insulin resistance, leading to the lower consumption of glucose and hyperglycemia, is a physiological means for the brain or immune system to usurp energy from the rest of the organism during acute stress because the brain and immune cells themselves do not become insulin resistant. Chronic insulin resistance, caused by chronic inflammation or by chronic mental activation, then leads to various pathologies such as diabetes, obesity, metabolic syndrome, or chronic inflammatory diseases.

Such Ado effects clearly demonstrate that the global metabolic switch is crucial for an effective immune response. How this global effect is achieved by Ado signaling in *Drosophila* is not well understood. Ado modulates fat body metabolism, for example the expression of glycogen synthase/phosphorylase (Bajgar and Dolezal, 2018); *AdoR* is expressed in imaginal discs, the brain, and the ring gland (Dolezalova et al., 2007) and thus it could influence the target tissues directly or via the production of hormones. Hyperglycemia and growth/storage

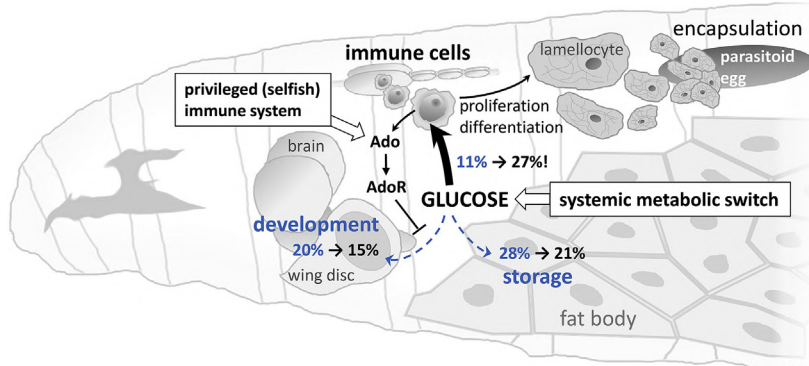


Fig. 3. Adenosine-mediated systemic metabolic switch during parasitoid wasp infection of *Drosophila* larva. Parasitoid egg is first recognized by circulating hemocytes that activate the proliferation and differentiation of specialized immune cells called lamellocytes. Lamellocytes eventually encapsulate and destroy the egg. Activated lamellocyte precursors increase glycolysis and glucose consumption. They usurp glucose from the rest of the organism by releasing adenosine (Ado). The extracellular Ado inhibits the metabolism of other tissues by signaling via the adenosine receptor *AdoR* and this slows down the larval development. By releasing Ado, which induces a systemic metabolic switch, the immune system becomes privileged over the rest of the organism. Percentage shows changes in overall glucose consumption by different systems from uninfected (blue) to infected (black) state (based on (Bajgar et al., 2015)). (For interpretation of the reference to color in this figure legend, the reader is referred to the Web version of this article.)

suppression mediated by Ado resembles a common response observed with different types of infection (Bajgar et al., 2015; Bajgar and Dolezal, 2018; Dionne et al., 2006; Ibrahim et al., 2018). Since insulin signaling is generally pro-growth/pro-storage, the systemic metabolic switch observed during infection is most likely associated with attenuation of insulin signaling, as observed for example in (Dionne et al., 2006). Reduced insulin signaling during the immune response seems to be at the core of the immune-metabolic interaction. In humans, insulin resistance-causing pro-inflammatory cytokines are believed to mediate the systemic metabolic switch (Straub, 2014). Pro-inflammatory cytokines-induced insulin resistance as a means to re-route energy towards immunity in mammals might have parallels in the insect world.

6. Molecular regulations of metabolism during immune response

Various research work, described in detail below, leads us to the following overall picture (Fig. 4) of the molecular regulation of the systemic metabolism during the immune response. Without immune stimulation, insulin signaling allows energy/nutrients to be used for storage, growth, and other non-immune processes. The fat body uses dietary nutrients in part to generate fat and glycogen stores, and releases other amounts for the needs of other tissues. The detection of pathogens activates the immune processes in immune cells and the fat body. The activation of immune cells leads to their internal metabolic switch (Warburg effect) associated with increased energy consumption. Activated immune cells release various signals and some of them suppress systemic metabolism. Others send the information to the fat body and mediate the switch from anabolism to humoral immunity. Many of these proinflammatory signals affect insulin signaling at various levels, from the release of insulin-like peptides (in *Drosophila* known as Dilps such as *Drosophila* insulin-like peptides), to blocking insulin signaling downstream of the insulin receptor (InR) in target tissues. Toll, Imd, Eiger/TNF- α , JNK, and JAK-STAT are the most important signals/signaling cascades for the immune response. They are activated by various immune stimuli and besides being crucial to the induction of immune processes, they also affect metabolism at various levels. Therefore, they can be seen as the key players in immunometabolism. Toll signaling, which is predominantly activated by G-positive bacteria or fungi, was shown to reduce insulin signaling in the fat body. Imd (Immunodeficiency) signaling, activated mainly by G-negative bacteria, induces an MEF2-mediated switch from anabolism to immunity in the fat body. JNK (c-Jun N-terminal kinase) is a master regulator of metabolism during various types of stress. It can be activated by both Eiger and Imd and it can possibly mediate the Imd-induced MEF2 switch in the fat body, it activates FOXO in various tissues and it reduces Dilps expression in insulin-producing cells. JAK-STAT is activated by many different pathogens, including viruses, bacteria, and parasitoids, and it has been shown to interact with insulin signaling in muscles. There is probably a certain degree of redundancy among these signals but they might also be engaged with different strengths and with different impacts on tissues, fine tuning thus both metabolic and immune responses according to the type of infection. Possible molecular interactions are depicted in Fig. 5 and described in details below.

6.1. Toll and insulin signaling

DiAngelo et al. (2009) clearly showed that bacterial/fungal infection reduces insulin signaling at the level of the Akt phosphorylation in the fat body via Toll activation. Imd, predominantly activated by G-negative bacteria, leads to JNK activation in the fat body but it does not affect the Akt phosphorylation. However, G-negative bacteria also activate Toll signaling in the fat body, leading to the suppression of Akt phosphorylation, suggesting that this metabolic regulation by Toll is not restricted to G-positive bacterial or fungal infection but also includes those associated with the activation of the Imd pathway. The activation of Toll in the fat body reduces triglycerides stores and has a global

impact on organismal growth, demonstrating that immune activation in the fat body can lead to a systemic metabolic switch via the reduction of insulin signaling. This is further supported by (Roth et al., 2018) demonstrating that Toll-induced growth suppression can be rescued by the expression of the phospho-mimicking version of Akt in the fat body. Such research work thus quite clearly demonstrates that infection can lead to an acute suppression of insulin signaling in the fat body and the global suppression of growth. However, how important this suppression is for the effectivity of the immune response was not tested. The work of Libert et al. (2008) may support the role of the suppression of insulin signaling for the effectivity of the immune response when mutation in InR substrate Chico actually increased the survival of *Pseudomonas aeruginosa* and *Enterococcus faecalis* infections. However, the resistance was tested in the chico mutant when its function was lacking throughout the whole development and therefore the effect on resistance cannot simply be attributed to insulin signaling suppressed by infection. Chico mutant flies might simply be better prepared for coming infection, for example by the pre-existing expression of AMPs due to lowered insulin activity and increased FOXO activation of AMPs as reported by Becker et al. (2010). Toll activation was also shown to block the S6K-mediated phosphorylation of MEF2, leading to a switch from anabolism to immunity in the fat body (Clark et al., 2013). This work, together with the work of DiAngelo et al. (2009), demonstrates that Toll and Imd

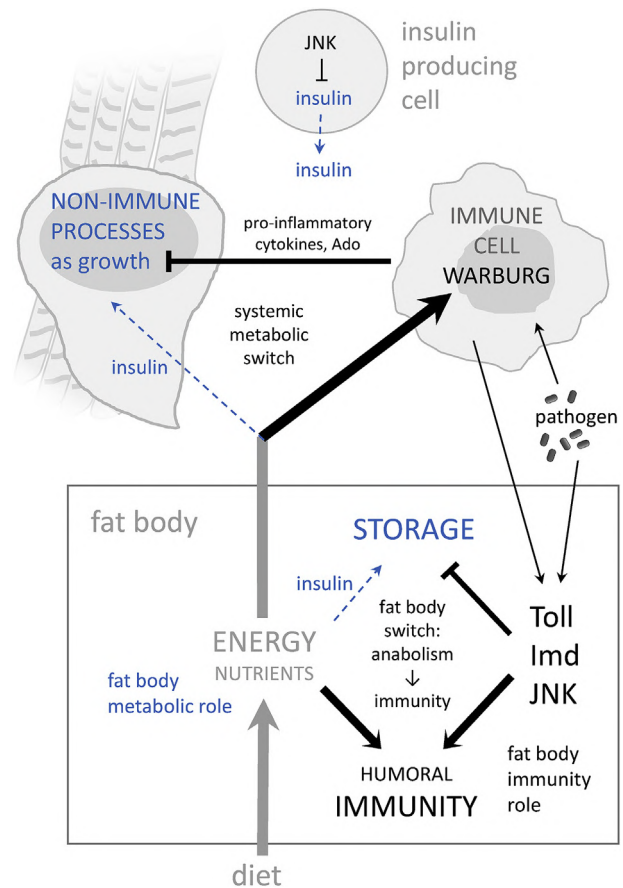


Fig. 4. Overall scheme of change of energy flow during immune response. Normally (blue), insulin signaling directs dietary nutrients towards storage and non-immune processes, such as growth. During immune response (black), immune signaling, as Toll, Imd and JNK, activates humoral immunity in the fat body while reducing insulin signaling, diverting energy flow from storage to humoral immune response and releasing energy for the needs of immune cells. Activated immune cells alter their own metabolism (similar to Warburg effect) and release signals that suppress energy consumption by non-immune processes. (For interpretation of the references to color in this figure legend, the reader is referred to the Web version of this article.)

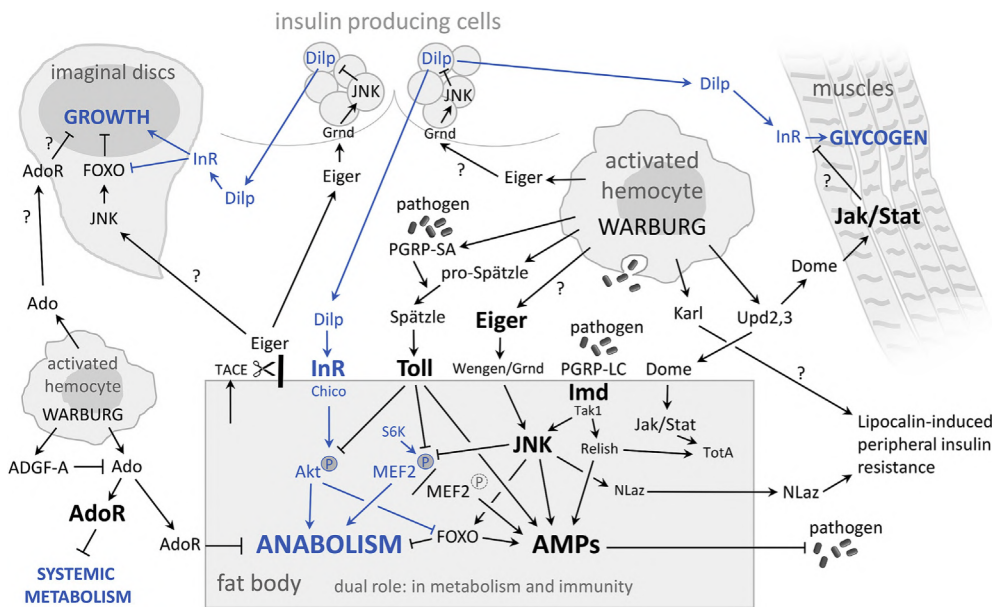


Fig. 5. Scheme of possible molecular interactions between immune signaling and metabolism. Signaling during an uninfected state is shown in blue and during infection in black. Arrows represent a known induction (although not necessarily tested for the suggested immunometabolic interaction), bars represent a known suppression, and arrows/bars with question marks represent suggested induction/suppression. See the text for a detailed description of the depicted interactions. (For interpretation of the references to color in this figure legend, the reader is referred to the Web version of this article.)

signaling, the core immune activators, are directly linked at the molecular level to a switch redirecting nutrients away from anabolic processes. This inevitable switch away from anabolism associated with immune activation means that the immune response is hardwired with the expected metabolic costs of the response in the genetic program.

PGRP-SA and Spätzle are crucial to Toll activation in the fat body. They are expressed by hemocytes and the expression increases upon infection (Boutros et al., 2002; Irving et al., 2005; Shia et al., 2009). Therefore, hemocytes are somehow involved in setting up the magnitude of this crucial activation – the magnitude is determined by the number of bacteria, but also by the pool of molecules able to detect the pathogen (PGRP-SA) and by the molecules mediating the signal (Spätzle). Since activation of Toll leads not only to AMPs expression, but also to the suppression of insulin signaling, it can be said that hemocytes, by expressing PGRP-SA and Spätzle, play a role in the activation of humoral immunity associated with a metabolic switch. In this regard, PGRP-SA and Spätzle resembles the pro-inflammatory cytokines of mammals released by immune cells and causing insulin resistance.

6.2. Eiger, Imd and JNK

Another important signaling for antibacterial response is the Imd pathway, which is primarily associated with the response to G-negative bacteria. Similarly to Toll, Imd was associated with the MEF2-mediated switch from anabolism to immunity (Clark et al., 2013). Although it is not clear how, the likely explanation for the Imd-MEF2 interaction is TAK1-dependent JNK activation (Boutros et al., 2002; Delaney et al., 2006). JNK (c-Jun N-terminal kinase) signaling can influence metabolism and immunity in many different ways and in many different tissues. Besides being activated by Imd, it is also activated by another important pro-inflammatory cytokine Eiger. Eiger is a TNF- α orthologue in insect (Igaki et al., 2002; Tang et al., 2019), which has also been shown to influence both the immune response and metabolism, representing thus another potential link between immune activation and systemic metabolism. TNF- α causes insulin resistance in mammals when the administration of TNF- α can induce cachexia (Moldawer and Copeland, 1997), and the blockade of TNF- α in rats with either cancer or sepsis prevents muscle wasting (Combaret et al., 2002). In *Drosophila* larvae, a low-protein diet induces Eiger secretion from the fat body into the hemolymph, Eiger binds to insulin-producing cells through the Grindelwald (Grnd) receptor, which acts through JNK to inhibit Dilp2/5 mRNA expression and reduces larval growth (Agrawal et al., 2016).

Under high-sugar diet conditions, Grnd signaling in the fat body induces a lipocalin NLaz-mediated peripheral insulin resistance by inducing NLaz expression via JNK in the fat body (Agrawal et al., 2016; Hull-Thompson et al., 2009; Pasco and Léopold, 2012). Eiger is thus able to reduce insulin signaling either by lowering Dilps expression remotely in insulin-producing cells or by inducing the expression of lipocalin NLaz.

Eiger was shown to be expressed upon immune stimulation both in hemocytes (Johansson et al., 2005) and in the fat body (Mabery and Schneider, 2010) and was shown to influence the immune response to various infections (Bastos et al., 2017; Brandt et al., 2004; Schneider et al., 2007; Tang et al., 2019). Eiger signaling is required for resistance to extracellular pathogens but may cause complications to the host when infected with intracellular pathogens (Brandt et al., 2004; Schneider et al., 2007). Eiger is required for an effective phagocytosis (Schneider et al., 2007), which could explain the resistance defect regarding extracellular pathogens. Although it is not known why Eiger is important for phagocytosis, one possible explanation is the effect of Eiger on the systemic metabolism being similar to that of AdoR, namely that the AdoR-mediated metabolic switch was shown to be crucial to effective phagocytosis (Bajgar and Dolezal, 2018). Likewise, some of the complications, the reduced survival rate of the host with intracellular infection, may be explained by the wasteful effects of Eiger on metabolism (Brandt et al., 2004; Schneider et al., 2007). In this light, an Eiger-induced systemic metabolic switch (Agrawal et al., 2016) would be required to mount an effective response, for example phagocytosis (Bajgar and Dolezal, 2018). However, it may become counterproductive in the case of intracellular pathogens which have escaped immune destruction, and removing Eiger would rather increase disease tolerance (Schneider et al., 2007) similarly to the blockade of TNF- α in rats with sepsis where it prevents muscle wasting (Combaret et al., 2002). Eiger-mediated effects during intracellular infection have been shown to be dependent on Eiger expressed in the fat body (Mabery and Schneider, 2010). Eiger released from the fat body has been shown to suppress Dilp2 and Dilp3 expression via Grnd-activated JNK signaling in the insulin-producing cells (Agrawal et al., 2016). Similarly, Eiger released by infection from the fat body or hemocytes upon infection (Johansson et al., 2005; Mabery and Schneider, 2010) may suppress the expression of Dilps in the same way. Since Eiger activates JNK, the effects of Eiger are potentially much broader. JNK activates FOXO and induces insulin resistance in peripheral tissues, as in larval imaginal discs (Wang et al., 2005) and as mentioned above, it might also be

associated with the MEF2 mediated switch from anabolism to immunity in the fat body (Clark et al., 2013). It was shown that activating JNK increased the survival of *Pseudomonas aeruginosa* and *Enterococcus faecalis* infections (Libert et al., 2008) but the potential role of Eiger in metabolic regulation through JNK during immune response has yet to be tested.

A high-sugar diet activates JNK through Grnd in the fat body (Agrawal et al., 2016) which leads to the expression of lipocalin NLaz (Hull-Thompson et al., 2009) and NLaz-mediated peripheral insulin resistance. Although Imd activation in the fat body leads to JNK activation (DiAngelo et al., 2009), Hull-Thompson et al. (2009) showed that NLaz is not important for immune resistance. However, they used G-positive *E. faecalis* to test resistance, which might not lead to a strong activation of IMD-JNK-NLaz in the fat body; it would be interesting to test the importance of NLaz with G-negative bacteria. Interestingly, they also showed that another lipocalin, Karl, was released from hemocytes and was important for an efficient immune response (Hull-Thompson et al., 2009); it is not clear what activates the secretion of Karl upon infection and whether or not it leads to peripheral insulin resistance similarly to NLaz.

6.3. JAK-STAT

JAK-STAT signaling activated by the Unpaired 3 (Upd3) cytokine in *Drosophila* can be seen as parallel to JAK-STAT activation by type 1 cytokines in mammalian systems, such as for example IL-6 (Vanha-aho et al., 2016; Woodcock et al., 2015). Yang et al. (2015) showed that the activation of JAK-STAT in muscles by hemocytes-derived cytokines Upd2 and Upd3 is required for an effective response against parasitoid wasp infection. Yang and Hultmark (2017) further showed that insulin signaling is reduced both in muscles and the fat body upon this type of infection. This effect of Upd3 cytokine is similar to the effect found by Woodcock et al. (2015) who showed that hemocyte-secreted Upd3 activates Jak-Stat signaling in muscles and the gut, which reduces insulin sensitivity. Although in this case, Upd3 was stimulated by a high-fat diet in adult flies, the potency of Upd3 derived from hemocytes to cause insulin resistance in muscles would nicely explain the results of Yang and Hultmark (2017) and would fit the suggested role of pro-inflammatory cytokine IL-6 in insulin resistance in mammals (Kim et al., 2013; Straub, 2014). Upd3 released from hemocytes upon infection could lower insulin sensitivity in muscles by activating JAK-STAT, lowering thus glucose consumption by muscles and leaving the required energy to hemocytes. Although Yang and Hultmark (2017) tried to explore the relationship of JAK-STAT and insulin signaling during wasp infection, genetic manipulations of both these pathways led to reduced feeding throughout the larval development, which affected the immune response but did not clarify the role of JAK-STAT in insulin signaling post-infection. Thus the role of Upd cytokines and JAK-STAT effects on insulin signaling during the immune response in *Drosophila* remain to be clarified.

(Agaïsse et al., 2003) showed that bacterial infection can also trigger the hemocyte-specific expression of upd3 that was necessary for the JAK-STAT + Relish-dependent activation of the TotA-mediated immune response in the *Drosophila* fat body. However the knockdown of stat92E, the transcription factor that mediates JAK-STAT pathway activity, in the fat body did not affect triglycerides storage, suggesting that JAK-STAT does not modulate metabolism in the fat body (Rajan and Perrimon, 2012) and the metabolic role of JAK-STAT might be rather associated with muscles. JAK-STAT effects are quite complicated, having for example both pro-proliferative functions in imaginal discs earlier in development and anti-proliferative effects later in development (Mukherjee et al., 2005). Ectopic activation of JAK-STAT leading to the premature cell cycle arrest in the wing imaginal disc in third instar larva (Mukherjee et al., 2005) offers another possibility of how hemocyte-released Upd3 during infection (Agaïsse et al., 2003; Yang et al., 2015) could lead to the redirection of energy by slowing down

the development.

6.4. GBP

Although growth-blocking peptide (GBP) signaling through Methuselah-like receptor-10 was shown to influence both the immune response and metabolism (Sung et al., 2017), the role of GBP in this intersection remains unclear. GBP from the fat body increases expression of Dilps (rather an opposite effect to that described above) and this is more likely important for nutritional signaling (Koyama and Mirth, 2016; Sunget al., 2017). The effect of GBP on immunity might be rather associated with a direct effect of GBP signaling on hemocytes, inducing their spreading during activation (Sung et al., 2017; Tsuzuki et al., 2014). It was not distinguished whether the lower resistance associated with systemic Mth10 knockdown was due to the hemocyte activation defect, or due to the expression of Dilps, or both (Sung et al., 2017).

6.5. Crosstalk and specificities of immune-metabolic pathways

Both Toll and Imd shift MEF2 activity from anabolism to immunity in the fat body, but only Toll reduces phosphorylation of Akt. Both G-positive and G-negative bacteria can activate Toll but G-positive bacteria and fungi are stronger inducers of Toll while G-negative bacteria predominantly activates Imd (DiAngelo et al., 2009; Lemaitre et al., 1997). So although the metabolic effects of Toll and Imd are partly redundant (effect on Mef2), different types of infection can probably differ in the metabolic response they induce. In addition, Eiger can further modulate the response of Toll, Imd, and JNK. Tang et al., (2019) showed that while Eiger can enhance Toll-mediated responses, it actually reduces the Imd-Relish arm, and while the full melanization response to G-negative bacteria requires Eiger/JNK, there is no effect of Eiger on the melanization response to G-positive bacteria. Similarly, Schneider et al. (2007) showed that eiger mutants produced more Imd-stimulated AMPs. Although metabolic effects were not analyzed in these works, modulating the Toll-Imd-JNK immune response most likely also affects Toll-Imd-JNK metabolic responses, suggesting a fine-tuning according to the type of infection. Parasitoid wasp infections differ in many aspects from the immune response induced by bacterial challenges and this is also probably reflected in metabolic modulation. JNK does not seem to be strongly activated by wasp attack (Schlenke et al., 2007). While co-activation of Toll and EGFR signaling in the lymph gland is important for the response to parasitoid wasp infection (Louradour et al., 2017), Toll is not required in the fat body for an effective immune response against parasitoid wasps (Schmid et al., 2014) although it is activated there (Schlenke et al., 2007). JAK-STAT is not strongly activated in the fat body by parasitoid infection and it is not required for an effective response (Yang and Hultmark, 2016). While Toll and JNK activation might not play a strong role, the release of Ado as well as Upd2 and Upd3 from hemocytes and Upd-activation of JAK-STAT signaling in muscles might have the most important roles during this type of infection. However, bacterial infection also leads to Ado and Upd3 release, being important during the immune response to this type of infection (Agaïsse et al., 2003; Bajgar and Dolezal, 2018), suggesting that these signals are not specific to a response to parasitoids. There are not many studies primarily focusing on the metabolic role in the immune response and each usually focuses on one or a few specific types of infection as viral, bacterial (and often only a particular strain) or parasitoid. To get a clearer picture, it will be necessary to analyze particular signaling cascades or processes and compare their importance across different types of infection, as shown for example by (Troha et al., 2018).

7. Keeping the response within limits and turning it off

The effect of infection on the global suppression of storage, growth, and other non-immune processes is now well established. Enhancing

the Ado effect, associated with a more extensive impact on energy stores, can even lead to a more efficient phagocytosis (Bajgar and Dolezal, 2018). The suppression of insulin signaling at various levels during the immune response is also well documented, however its actual importance for the effectivity of the acute immune response still remains to be tested. What has actually been shown is the adverse effects of the prolonged suppression of insulin signaling during chronic infections (Dionne et al., 2006).

The immune reaction, although life-saving for the host in its task in killing the pathogen, is also more or less harmful to the host, and thus keeping the response within a certain range and its eventual down regulation are necessary (Schneider, 2007). Sometimes, the immune response itself is more harmful to the host than the pathogen. The host cannot be prepared for every possible pathogen. Sometimes, the host just cannot get rid of the pathogen since it does not possess an effective immune response against that particular infection. Disease tolerance is now being recognized as an integral part of the defense mechanisms—it is a host strategy that reduces the negative impact of infection on host fitness without affecting the pathogen load (Schneider and Ayres, 2008). This includes limiting the tissue damage caused by the host's own immune response, but it most likely also includes limiting the metabolic effects of the activated immune response. Energy stores are limited and the energy supply for the immune system may also be exploited by the pathogen. For example, Howick and Lazzaro (2018) found that SNPs associated with disease tolerance were enriched in the genes involved, among others, in the regulation of the metabolism.

Although lowering insulin signaling is a common response and probably important for an effective immune response as discussed above, in the case of chronic, intracellular pathogen infections, which cannot be effectively removed by the host, the suppression of insulin becomes eventually harmful to the host. For example in case of mycobacterial infection, compensating for the negative regulation of insulin signaling during infection by the hypomorphic foxo mutation reduces the negative impacts of infection, such as wasting, and improves the survival of the flies, without changing bacteria numbers (Dionne et al., 2006). This is an example of a chronically provoked immune response and reducing the long-term impact on the metabolism may actually help to increase disease tolerance, even though initially lowering insulin might be important for effective resistance. Another such example is the dual effect of Eiger. Eiger is important for resistance against extracellular pathogens but becomes harmful in the case of intracellular infection where removing Eiger actually improves survival (Schneider et al., 2007). One possible explanation is the extensive effect of Eiger on metabolism, which does not help the host to fight the intracellular infection and only does unnecessarily harm to the host. Removing Eiger in such a scenario may increase disease tolerance.

What are the molecular mechanisms limiting the impact of the immune response on metabolism? Is it a disappearance of the original immune stimulatory (pro-inflammatory) signals? The disappearance would eventually unblock insulin signaling. For example, Toll activation suppresses insulin signaling in the fat body (DiAngelo et al., 2009) and it is logical that, with no pathogen around to activate Toll, insulin will no longer be suppressed. An active autoregulatory loop is mediated by the Toll-activated WntD expression, which in turn blocks Toll activation by binding to the Frizzled 4 receptor (Gordon et al., 2005; Lamielle et al., 2016). Zaidman-Rémy et al. (2006) beautifully demonstrated a negative feedback loop downregulating Imd signaling by peptidoglycan degradation by amidase PGRP-LB, which is activated by Imd itself. PGRP together with Pirk represent very important regulators of Imd (Paredes et al., 2011).

In the case of immunometabolic regulatory loops, one such regulating mechanism was uncovered in the case of the Ado-induced metabolic switch. ADGF-A is the fly adenosine deaminase, which removes extracellular Ado from circulation by converting it to inosine (Dolezal et al., 2005). ADGF-A is strongly expressed in fully differentiated lamellocytes, encapsulating parasitoid wasp eggs (Novakova and Dolezal,

2011), suggesting that Ado, initially important in inducing the metabolic switch, is degraded once the egg is in the process of being successfully encapsulated. Removing one copy of the ADGF-A gene or knocking it down specifically in hemocytes lowers glycogen stores during bacterial infection of the adult flies (Bajgar and Dolezal, 2018) demonstrating that ADGF-A limits the use of energy reserves. Rising ADGF-A expression in hemocytes beautifully coincides with the hyperglycemic peak upon *S. pneumoniae* infection; upon knocking-down ADGF-A, hyperglycemia continues beyond this peak at the expense of glycogen stores. This has interesting consequences. Enhancing energy supply to hemocytes, by downgrading ADGF-A and thus enhancing Ado effects on metabolism, increases their phagocytic activity and reduces thus the *S. pneumoniae* load. However, in the case of intracellular *L. monocytogenes* infection, which a fly cannot clear, the chronic lowering of glycogen stores is associated with an increased intracellular pathogen load. One possible explanation is that enhancing the Ado effects and the release of energy does not help to kill intracellular bacteria and instead leads to feeding it. Summarizing these effects, privileged immune cells first release Ado upon their activation to suppress the systemic metabolism so that the energy is available in higher quantities to the immune system. Later, the same immune cells limit their own privilege (or selfishness) by releasing the regulator of Ado levels, the ADGF-A adenosine deaminase. ADGF-A limits the actions of Ado, preventing its excessive effects on the systemic metabolism and thus preventing a larger loss of energy reserves, and maybe also the unnecessary feeding of the pathogen.

The regulation of metabolism during the immune response is crucial. It ensures adequate energy for an effective response (resistance) but it must also be kept under tight check because it interferes with other physiological traits. Energy is not unlimited and it may also be exploited by the pathogen. If the energy release is not properly regulated, it may, in the end, decrease fitness via a lowering of disease tolerance. Understanding the regulation of immunometabolism is thus important for both resistance and tolerance mechanisms.

8. Concluding remarks

Molecular immunometabolic interactions have become an intensively studied subject in recent years and although studies on insects have been somewhat lagging behind the studies on mammalian systems, recent research is now uncovering the parallels between insects and mammals both in metabolic reprogramming of the activated immune cells and in the regulation of systemic metabolism during the immune response. Insect-based studies of the metabolic reprogramming of immune cells are still rather scarce. Technological advances such as cell sorting and metabolomics (Cox et al., 2017) may soon change this. There are many well established infection models *in vivo* using insects as models, which might be combined with these technological advances in the future to study the metabolism of immune cells *in vivo*. Insects, being relatively simple compared to mice, and especially *Drosophila* with the excellent genetic tools available to work with them, already serve as great models to study inter-organ communication (Droujinine and Perrimon, 2016) and thus can also be used to study the regulation of systemic metabolism and inter-organ communication during the immune response. There are many interesting results linked to immunometabolic interactions already available, but the studies were often focused either on the immune or metabolic function of the molecule under study, but not both. No less interesting is the dietary influence of immunometabolism and the relationship to microflora and gut immunity, which can be expected to affect metabolic regulations during immune response to a large extent. Although this review did not cover these topics, studies are now emerging even in these areas and have been recently covered in (Galenza and Foley, 2019).

- Aerobic Glycolysis. G3 BethesdaMd. . <https://doi.org/10.1534/g3.114.010652>.
- Troha, K., Im, J.H., Revah, J., Lazzaro, B.P., Buchon, N., 2018. Comparative transcriptomics reveals CrebA as a novel regulator of infection tolerance in *D. melanogaster*. *PLoS Pathog.* 14, e1006847. <https://doi.org/10.1371/journal.ppat.1006847>.
- Tsuzuki, S., Matsumoto, H., Furihata, S., Ryuda, M., Tanaka, H., Jae Sung, E., Bird, G.S., Zhou, Y., Shears, S.B., Hayakawa, Y., 2014. Switching between humoral and cellular immune responses in *Drosophila* is guided by the cytokine GBP. *Nat. Commun.* 5, 4628. <https://doi.org/10.1038/ncomms5628>.
- Uden, P., van, Kenneth, N.S., Webster, R., Müller, H.A., Mudie, S., Rocha, S., 2011. Evolutionary conserved regulation of HIF-1 β by NF- κ B. *PLoS Genet.* 7, e1001285. <https://doi.org/10.1371/journal.pgen.1001285>.
- Van den Bossche, J., O'Neill, L.A., Menon, D., 2017. Macrophage immunometabolism: where are we (going)? *Trends Immunol.* 38, 395–406. <https://doi.org/10.1016/j.it.2017.03.001>.
- Vanha-aho, L.-M., Valanne, S., Rämetsä, M., 2016. Cytokines in *Drosophila* immunity. *Immunol. Lett.* 170, 42–51. <https://doi.org/10.1016/j.imlet.2015.12.005>.
- Verlinden, H., Vleugels, R., Marchal, E., Badisco, L., Pflüger, H.-J., Blenau, W., Broeck, J.V., 2010. The role of octopamine in locusts and other arthropods. *J. Insect Physiol.* 56, 854–867. <https://doi.org/10.1016/j.jinsphys.2010.05.018>.
- Wagner, A., 2005. Energy constraint on the evolution of gene expression. *Mol. Biol. Evol.* 22, 1365–1374. <https://doi.org/10.1093/molbev/msi126>.
- Wang, C.-W., Purkayastha, A., Jones, K.T., Thaker, S.K., Banerjee, U., 2016. In vivo genetic dissection of tumor growth and the Warburg effect. *eLife* 5, e18126. <https://doi.org/10.7554/eLife.18126>.
- Wang, M.C., Bohmann, D., Jasper, H., 2005. JNK extends life span and limits growth by antagonizing cellular and organism-wide response to insulin signaling. *Cell* 121, 115–125. <https://doi.org/10.1016/j.cell.2005.02.030>.
- Wang, R., Dillon, C.P., Shi, L.Z., Milasta, S., Carter, R., Finkelstein, D., McCormick, L.L., Fitzgerald, P., Chi, H., Munger, J., Green, D.R., 2011. The transcription factor Myc controls metabolic reprogramming upon T lymphocyte activation. *Immunity* 35, 871–882. <https://doi.org/10.1016/j.immuni.2011.09.021>.
- Warburg, O., 1925. über den Stoffwechsel der Carcinomzelle. *Klin. Wochenschr.* 4, 534–536. <https://doi.org/10.1007/BF01726151>.
- Wenger, R.H., Stiehl, D.P., Camenisch, G., 2005. Integration of Oxygen Signaling at the Consensus HRE. *Sci STKE* 2005, Re12–Re12. <https://doi.org/10.1126/stke.3062005re12>.
- Woodcock, K.J., Kierdorf, K., Pouchelon, C.A., Vivancos, V., Dionne, M.S., Geissmann, F., 2015. Macrophage-derived upd3 cytokine causes impaired glucose homeostasis and reduced lifespan in *Drosophila* fed a lipid-rich diet. *Immunity* 42, 133–144. <https://doi.org/10.1016/j.immuni.2014.12.023>.
- Yang, H., Hultmark, D., 2017. *Drosophila* muscles regulate the immune response against wasp infection via carbohydrate metabolism. *Sci. Rep.* 7. <https://doi.org/10.1038/s41598-017-15940-2>.
- Yang, H., Hultmark, D., 2016. Tissue communication in a systemic immune response of *Drosophila*. *Fly* 10, 115–122. <https://doi.org/10.1080/19336934.2016.1182269>.
- Yang, H., Kronhamn, J., Ekström, J.-O., Korkut, G.G., Hultmark, D., 2015. JAK/STAT signaling in *Drosophila* muscles controls the cellular immune response against parasitoid infection. *EMBO Rep.* 16, 1664–1672. e201540277. <https://doi.org/10.15252/embr.201540277>.
- Zaidman-Rémy, A., Hervé, M., Poidevin, M., Pili-Floury, S., Kim, M.-S., Blanot, D., Oh, B.-H., Ueda, R., Mengin-Lecreux, D., Lemaître, B., 2006. The *Drosophila* amidase PGRP-LB modulates the immune response to bacterial infection. *Immunity* 24, 463–473. <https://doi.org/10.1016/j.immuni.2006.02.012>.

CHAPTER III:

Macrophage-derived insulin antagonist *ImpL2* induces lipoprotein mobilization upon bacterial infection

Gabriela Krejčová, Cecilia Morgantini, Helena Zemanová, Volker M. Lauschke, Julie Kovářová, Jiří Kubásek, Pavla Nedbalová, Nick Kamps-Hughes, Martin Moos, Myriam Aouadi, Tomáš Doležal, Adam Bajgar

The EMBO Journal, 2023, e114086

SOURCE
DATATRANSPARENT
PROCESSOPEN
ACCESS

Macrophage-derived insulin antagonist ImpL2 induces lipoprotein mobilization upon bacterial infection

Gabriela Krejčová¹ , Cecilia Morgantini², Helena Zemanová¹, Volker M Lauschke^{2,3,4}, Julie Kovařova⁵ , Jiří Kubasek⁶, Pavla Nedbalová¹, Nick Kamps-Hughes⁷, Martin Moos⁸, Myriam Aouadi², Tomáš Doležal^{1,*} & Adam Bajgar^{1,**}

Abstract

The immune response is an energy-demanding process that must be coordinated with systemic metabolic changes redirecting nutrients from stores to the immune system. Although this interplay is fundamental for the function of the immune system, the underlying mechanisms remain elusive. Our data show that the pro-inflammatory polarization of *Drosophila* macrophages is coupled to the production of the insulin antagonist ImpL2 through the activity of the transcription factor HIF1 α . ImpL2 production, reflecting nutritional demands of activated macrophages, subsequently impairs insulin signaling in the fat body, thereby triggering FOXO-driven mobilization of lipoproteins. This metabolic adaptation is fundamental for the function of the immune system and an individual's resistance to infection. We demonstrated that analogically to *Drosophila*, mammalian immune-activated macrophages produce ImpL2 homolog IGFBP7 in a HIF1 α -dependent manner and that enhanced IGFBP7 production by these cells induces mobilization of lipoproteins from hepatocytes. Hence, the production of ImpL2/IGFBP7 by macrophages represents an evolutionarily conserved mechanism by which macrophages alleviate insulin signaling in the central metabolic organ to secure nutrients necessary for their function upon bacterial infection.

Keywords *Drosophila*; ImpL2; insulin resistance; lipoproteins; macrophage polarization

Subject Categories Metabolism; Microbiology, Virology & Host Pathogen Interaction

DOI 10.15252/embj.2023114086 | Received 22 March 2023 | Revised 6 September 2023 | Accepted 12 September 2023

The EMBO Journal (2023) e114086

Introduction

Rapid activation of the mononuclear phagocytic system is critical for limiting bacterial burden and promoting resistance to infection (Chow et al, 2011). However, the activation of the immune system is an energetically and nutritionally demanding process requiring a coordinated response of almost all organs and tissues within the organism (Rankin & Artis, 2018). Although metabolic reprogramming accompanies virtually any immune response and can profoundly affect patient health (Chi, 2022), the mechanism coordinating the immune response with systemic metabolism remains poorly understood.

Upon recognition of a pathogen, macrophages adopt a pro-inflammatory polarization to enhance their bactericidal capacity and secrete pro-inflammatory cytokines that propagate information about the pathogenic threat to other tissue in the body (Mills et al, 2000). This polarization is achieved by stabilizing the transcription factor HIF1 α that governs the complex rewiring of macrophage cellular metabolism, which is generally referred to as aerobic glycolysis (Galvan-Pena & O'Neill, 2014). However, this metabolic adaptation leads to the rapid depletion of macrophage intracellular stores and makes them functionally dependent on external sources of nutrients (Ganeshan & Chawla, 2014).

Along with the rewiring of the cellular metabolism of the immune cells, systemic metabolism also exhibits substantial adjustments. For example, altered hormonal signaling, and subsequent disruption of metabolic homeostasis manifested by loss of nutritional stores and their enhanced level in circulation (hyperglycemia, hyperlipidemia), are commonly observed accompanying signs in patients suffering from severe bacterial infections (Wasylyuk & Zwolak, 2021).

Recently, insulin resistance has been considered an adaptive mechanism of energy redistribution during acute metabolic stress

1 Department of Molecular Biology and Genetics, Faculty of Science, University of South Bohemia, Ceske Budejovice, Czech Republic

2 Department of Medicine, Integrated Cardio Metabolic Center (ICMC), Karolinska Institutet, Huddinge, Sweden

3 Dr Margarete Fischer-Bosch Institute of Clinical Pharmacology, Stuttgart, Germany

4 University of Tübingen, Tübingen, Germany

5 Biology Centre CAS, Institute of Parasitology, Ceske Budejovice, Czech Republic

6 Department of Experimental Plant Biology, Faculty of Science, University of South Bohemia, Ceske Budejovice, Czech Republic

7 Institute of Molecular Biology, University of Oregon, Oregon City, OR, USA

8 Institute of Entomology, Biology Centre CAS, Ceske Budejovice, Czech Republic

*Corresponding author. Tel: +420 384 772229; E-mail: tomas.dolezal@prf.jcu.cz

**Corresponding author. Tel: +420 774 912172; E-mail: bajgaradam@seznam.cz; bajgaa00@prf.jcu.cz

(Tsatsoulis et al, 2013). However, this concept is in stark contrast to the common perception of insulin resistance as a pathological process associated with obesity, atherosclerosis, arthritis, and cachexia (Akhtar et al, 2019), and the possible adaptive role of insulin resistance has been neglected so far. Interestingly, the increased production of pro-inflammatory cytokines by the activated immune system plays a central role in the induction of insulin resistance and the progression of the diseases mentioned above (Al-Mansoori et al, 2022).

In this work, we aim to investigate the factors inducing the mobilization of nutrients required to supplement the nutritional demands of the activated immune system.

To reveal the role of macrophages in the regulation of systemic metabolism during the immune response, we employed an established experimental model of streptococcal infection in *Drosophila* (Bajgar & Dolezal, 2018). Exploiting this experimental system, we have previously demonstrated that *Drosophila* macrophages undergo pro-inflammatory polarization in response to bacterial infection associated with HIF1 α -driven aerobic glycolysis in a manner analogous to that observed in mammals (Krejčová et al, 2019). Moreover, streptococcal infection in this model is accompanied by substantial remodeling of systemic carbohydrate and lipid metabolism (Dionne & Schneider, 2008; Bajgar & Dolezal, 2018).

Here we demonstrate that pro-inflammatory macrophage polarization is coupled with the production of the signaling factor IMPL2, which alleviates insulin signaling in the central metabolic organ of flies, the fat body. Macrophage-derived IMPL2 is required for the mobilization of lipid stores in the form of lipoproteins, which is fundamental for the nutritional supplementation of bactericidal macrophages and resistance to infection. Our data further imply that this mechanism is evolutionarily conserved in mammals. Indeed, mammalian macrophages produce the mammalian ImPL2 homolog Insulin growth factor binding protein 7 (IGFBP7), which induces the mobilization of lipoproteins from hepatocytes during bacterial infection.

Results

Infection leads to systemic redistribution of lipids

To elicit an immune response, adult fruit flies (*Drosophila melanogaster*) were injected with 20,000 extracellular bacteria (*Streptococcus pneumoniae*). In our experimental model, acute streptococcal infection leads to rapid activation of macrophages, called plasmatocytes in *Drosophila*, and their pro-inflammatory polarization (Bajgar & Dolezal, 2018; Krejčová et al, 2019). The infection culminates during the first 24 h of infection, which determines whether or not an individual survives the infection. Although all pathogenic bacteria in surviving flies are eliminated within the first 5 days, the flies continue to decline due to the long-term effects of the infection experienced (Bajgar & Dolezal, 2018; Krejčová et al, 2019). This treatment offers a standardized course of immune response in which macrophage pro-inflammatory polarization and their bactericidal activity is crucial for limiting the bacterial burden (Bajgar & Dolezal, 2018). To determine how the ongoing immune response is reflected by rearrangement of the systemic metabolism, we analyzed metabolic changes in infected individuals 24 h post-infection (hpi).

We found that the acute phase of infection is accompanied by a depletion of two major storage molecules, glycogen (GLY) and triglycerides (TG) when measured on the whole-individual level (Fig 1A). This is consistent with the pattern observed in the fat body, organ comprising the functionalities of mammalian liver and adipose tissue. In this tissue, the levels of all analyzed carbohydrates and lipids are significantly reduced upon infection (Fig 1B). Depletion of lipid stores is further documented by a significantly decreased diameter of lipid droplets and the area they occupy in adipocytes of infected flies (Fig 1C) as quantified from the confocal images of the fat body stained for neutral lipids (Fig 1D).

Examination of the fat body lipid content using lipidomic analysis revealed that depletion of lipid stores in this organ is accompanied by a significant shift in lipid composition. While the main storage lipids, triglycerides, prevail in the fat body of control flies, their relative amounts decrease significantly after infection in favor of polar lipids (phosphatidylcholine, PC; phosphatidylethanolamine, PE) and diglycerides (DG; Figs 1E and EV1A), a transport form of lipids in insects (Palm et al, 2012).

Contrary to that, the titer of carbohydrates and lipids rises significantly in circulation upon infection (Fig 1F). These observations imply that the infection is accompanied by depletion of energy stores and redistribution of nutrients between tissues via circulation. To investigate whether mobilized nutrients serve as metabolic support for the activated immune system, we analyzed the metabolic profile of macrophages at 24 hpi. Macrophages isolated from infected individuals display elevated levels of all analyzed carbohydrates and lipids when compared to uninfected controls (Fig 1G).

Lipidomic analysis revealed that the overall lipid content is 3.5-fold increased in infection-activated macrophages compared to controls (Fig EV1B). Moreover, the infection affects the lipid composition in these cells displaying a significantly enhanced fraction of hydrolyzed forms of polar lipids (lysophosphatidylcholine, LPC; lysophosphatidylethanolamine, LPE; Figs 1H and EV1C) that may be attributed to increased endocytosis of circulating lipoproteins and eicosanoid production (Lee et al, 2020; Liu et al, 2020).

To further characterize the infection-induced redistribution of lipids from the fat body to macrophages, we fed flies with a mixture of ^{13}C -labeled free fatty acids (^{13}C -FFAs) and monitored their immediate incorporation into tissues. While in control subjects, most of the ^{13}C -FFAs are destined for the fat body, and only a small fraction incorporates into macrophages, this ratio is completely reversed upon infection (Fig 1I). Since the control and infected flies display comparable dietary intake, the possibility that the observed differences may be accounted to infection-induced anorexia can be excluded (Fig EV1D). Overall, our data show that infection is accompanied by a rearrangement of systemic metabolism that leads to a redistribution of lipids from the central metabolic organ toward the circulation and the activated immune system. To explore the possibility that the observed metabolic changes are induced by signaling factors originating from macrophages, we proceeded to a detailed analysis of these cells after infection (Fig 1J).

Infection-activated macrophages increase ImPL2 expression in a HIF-1 α -dependent manner

To better understand the ongoing processes in infection-activated macrophages, we performed a comparative analysis of their

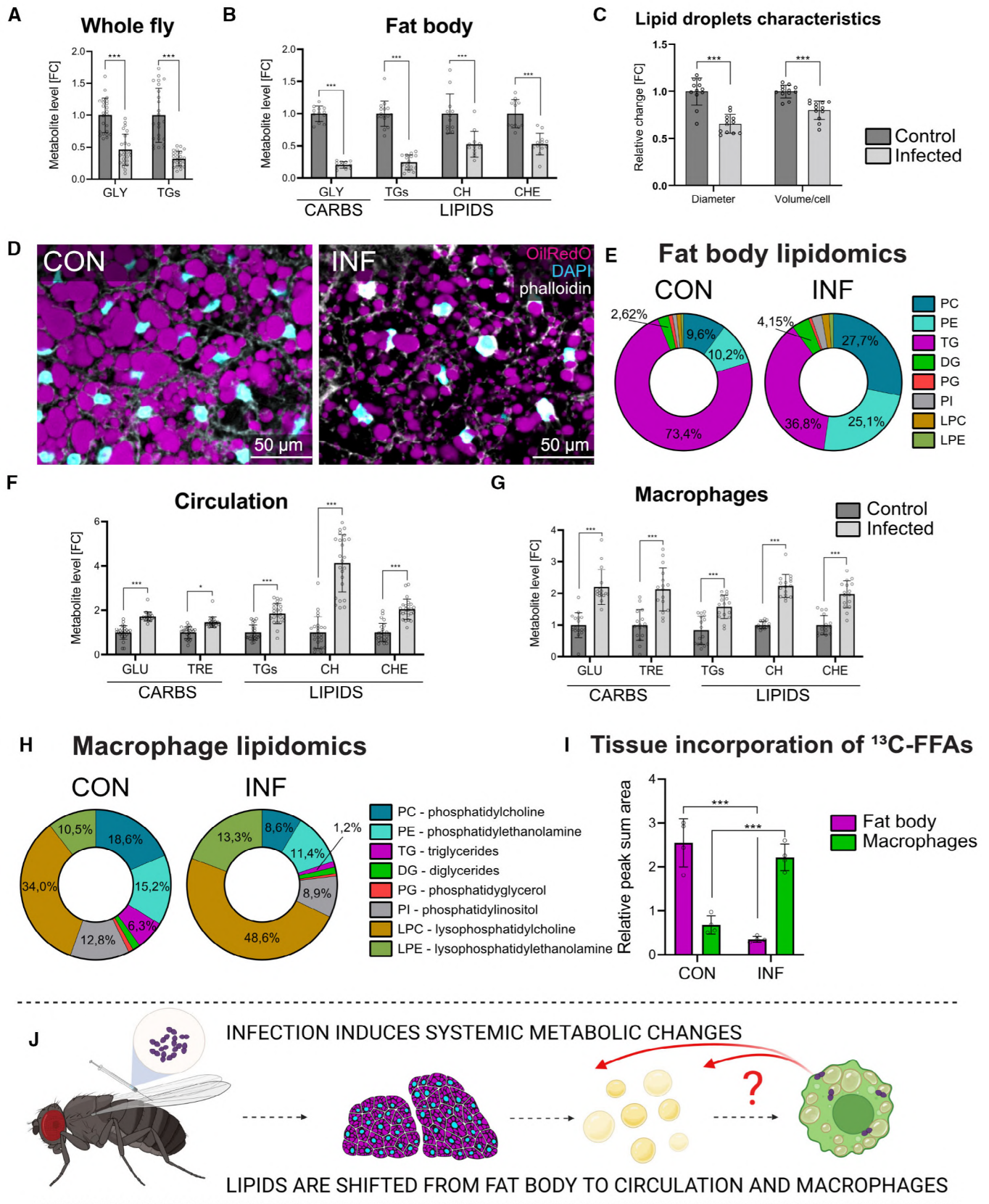


Figure 1.

Figure 1. Infection leads to systemic redistribution of lipids.

- A Whole body amounts of glycogen (GLY) and triglycerides (TG) after infection, expressed as fold change in infected flies compared to control.
- B The level of glycogen (GLY) and lipids (CH, cholesterol; CHE, cholesteryl-ester; TGs, triglycerides) in the fat body after infection, expressed as fold change in infected flies compared to controls.
- C Lipid droplet diameter and volume of lipid droplets per adipocyte in the fat body expressed as fold change in infected flies compared to controls. Data were obtained from the quantification of lipid droplet characteristics in confocal images of dissected fat body tissues (shown in D).
- D Representative confocal images documenting the morphology of lipid droplets in the fat body whole mounts of control (CON) and infected (INF) flies. Lipids stained by OilRedO (magenta); DAPI (cyan) labels nuclei; membranes stained by phalloidin (white).
- E Lipidomic analysis showing the proportional change in lipid species in the fat body dissected from control (CON) and infected (INF) flies. Samples were collected in six independent experiments; data was expressed as a percent of the total amount of lipids in the sample.
- F A titer of carbohydrates (GLU, glucose; TRE, trehalose) and lipids (CH, cholesterol; CHE, cholesteryl-ester; TGs, triglycerides) in the circulation after infection, expressed as fold change in infected flies compared to controls.
- G The amounts of carbohydrates (GLU, glucose; TRE, trehalose) and lipids (CH, cholesterol; CHE, cholesteryl-ester; TGs, triglycerides) in macrophages after infection, expressed as fold change in infected flies compared to control.
- H Lipidomics analysis showing the proportional change in lipid species in macrophages isolated from control (CON) and infected (INF) flies. In five biological replicates; normalized to the number of isolated cells.
- I Incorporation of dietary ^{13}C -labeled free fatty acids into the fat body and macrophages in control (CON) and infected (INF) flies, expressed as relative incorporation of ^{13}C free fatty acids normalized to ^{12}C free fatty acids in the sample.
- J Schematic representation of the results obtained. Infection leads to a systemic redistribution of lipids in the body, indicating a mobilization of resources to be available for the immune response. The role of potential macrophage-derived signaling factors in this process is unknown.

Data information: Fat bodies from six individuals and macrophages from 160 flies were used for each biological replicate. The plots display data obtained 24 h post-infection. For (A–C, F and G), data are reported as fold change relative to controls arbitrarily set to 1. Metabolite concentrations in A, B, F and H were normalized to protein level in the sample. For analysis of metabolites; six whole flies, fat bodies from six individuals, hemolymph from 25 flies, and macrophages from 160 flies were used for each biological replicate. For lipidomic analysis; fat bodies from six individuals and macrophages from 300 flies were used for each biological replicate. Individual dots in the plots represent biological replicates. Samples for lipidomics were obtained in five biological replicates for macrophages and in six biological replicates for the fat bodies. Results were compared by 2way ANOVA followed by Šidak's multiple comparisons test. Values are displayed as mean SD, asterisks mark statistically significant differences (* $P < 0.05$; *** $P < 0.001$).

Sourcedata are available online for this figure.

transcriptomic profile at 24 hpi. Gene set enrichment analysis revealed that along with the activation of immune-related processes, macrophages undergo remarkable changes in their cellular metabolism (Figs 2A and EV2A). Infection-activated macrophages attenuate the expression of genes involved in the mitochondrial generation of ATP and simultaneously enhance the expression of genes involved in the regulation of lipid and cholesterol metabolism (Fig 2A). These data further extend our previous observations that bactericidal polarization of *Drosophila* macrophages is coupled with the remodeling of their cellular metabolism toward aerobic glycolysis (Krejčová et al, 2019). We have previously shown that the adoption of aerobic glycolysis by *Drosophila* macrophages is fundamental for their bactericidal function and that this metabolic remodeling is analogous to mammalian macrophages governed by the master regulator Hif1 α , which controls the expression of many metabolic genes (Galvan-Pena & O'Neill, 2014; Krejčová et al, 2019).

We further identified several signaling factors whose induction goes hand in hand with infection-induced macrophage polarization (Fig 2B). From several candidates, we chose ImpL2 for further investigation since it is highly expressed in macrophages, displays the most significant increase in response to infection (Figs 2C and EV2B), and has been previously shown to have a potential to affect systemic lipid metabolism (Kwon et al, 2015). Other potential candidates, the signaling factors Unpaired 3 (Upd3) and Eiger (Egr) were tested together with ImpL2, but already the initial experiments showed that neither Upd3 nor Egr had a rather negligible effect on lipid mobilization from the fat body during infection (Appendix Figs S1–S6).

To investigate the spatial pattern of ImpL2 expression, we employed a fly strain bearing a fluorescent ImpL2 reporter (ImpL2-Gal4 > UASmCherry). We found that ImpL2 promoter activity is

almost exclusive to macrophages, as evidenced by the strong production of the ImpL2-mCherry signal in cells positive for the *Drosophila* macrophage marker NimC1 (Fig 2D and Appendix Fig S7).

Next, we investigated the mechanism controlling ImpL2 expression in these cells. Given that HIF1 α is the master regulator of macrophage metabolic remodeling during infection, we assessed its effect on ImpL2 expression. Macrophage-specific knockdown of Hif1 α (Crq > Gal4; UAS-GFP, Hif1 α^{RNAi}) abolished the infection-induced increase in ImpL2 expression in these cells (Fig 2E; see Fig EV2C for Hif1 α^{RNAi} efficiency; see Fig EV2D for genotype explanations). This interaction is further confirmed by the direct binding of HIF1 α to the ImpL2 promoter, as revealed by Chip-qPCR analysis (Fig 2F).

Taken together, the presented data show that metabolic rearrangement of pro-inflammatory macrophages is coupled to ImpL2 expression since both processes are governed by the same transcription factor, HIF1 α . This implies a possible role of ImpL2 as a signal produced by pro-inflammatory macrophages in reflection of their newly adopted metabolic program associated with specific nutritional demands (Fig 2G).

Macrophage-derived IMPL2 directs the infection-induced mobilization of lipid stores

To investigate the effect of macrophage-derived IMPL2 on the redistribution of lipids during infection, we generated flies carrying genetic constructs for time-limited macrophage-specific ImpL2 knockdown ($M\phi$ -ImpL2 $^{\text{RNAi}}$) or overexpression ($M\phi$ -ImpL2 $^{\text{CDS}}$). Using these fly strains, we experimentally manipulated ImpL2 expression macrophage-specifically 24 h before the infection and compared the effect of these interventions to control lines of the

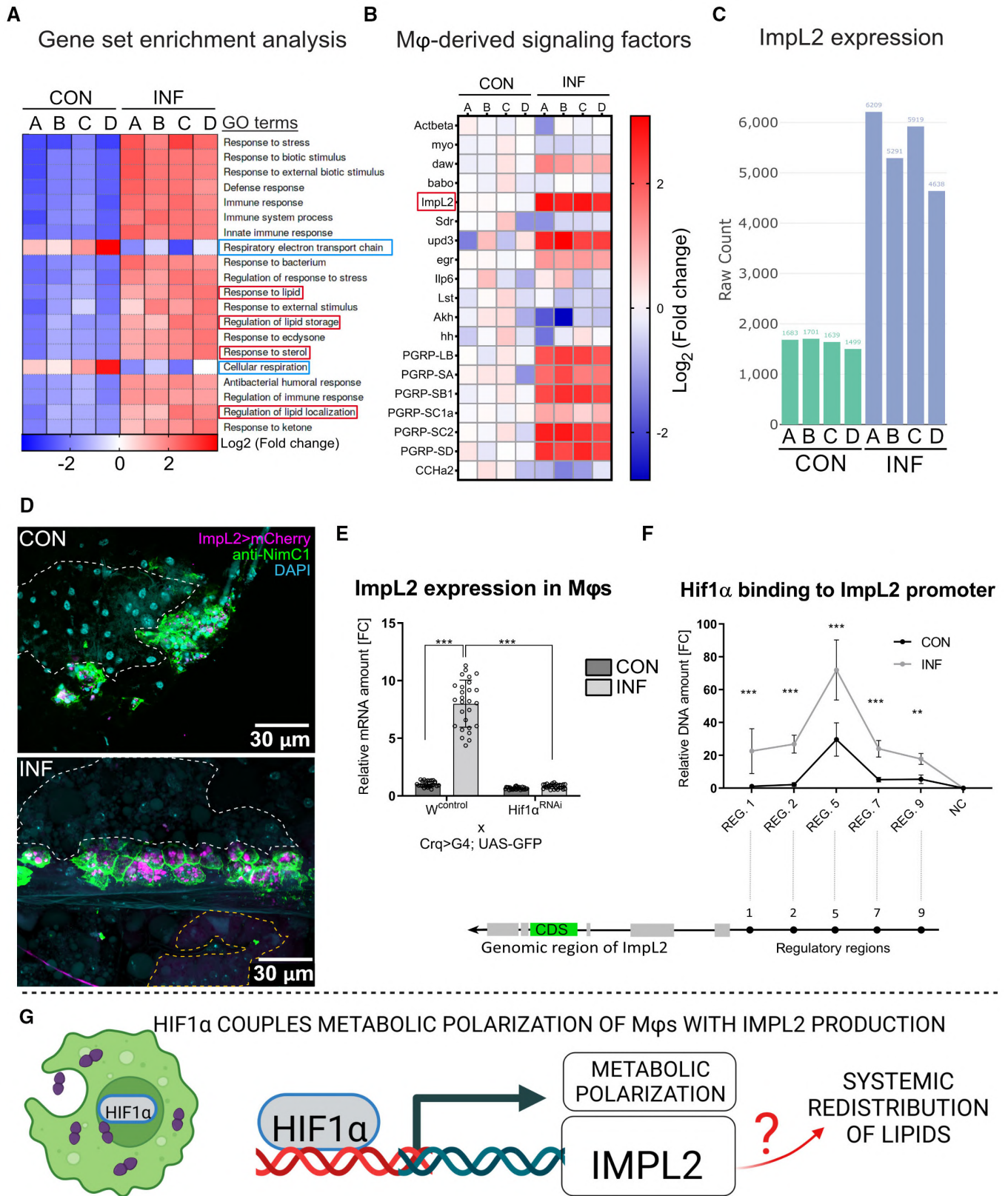


Figure 2.

Figure 2. Infection-activated macrophages increase the Impl2 expression in a Hif1 α -dependent manner.

- A Geneset enrichment analysis of transcriptomic data from macrophages isolated from infected flies (INF) compared to controls (CON). Heat map displays the top 20 significantly altered gene sets, GeneOntology (GO) terms retrieved from KEGG pathways. Silenced mitochondrial respiration (blue rectangles) and upregulation of lipid-related pathways (red rectangles) are highlighted.
- B Heat map documenting the differential expression of secreted signaling factors in macrophages isolated from infected individuals (INF) compared to controls (CON), expressed as Log₂ fold change in infected flies compared to control.
- C Expression level of Impl2 in macrophages isolated from infected individuals compared to controls, data presented as raw count level (counts per million).
- D Representative confocal microscopy images of abdominal whole mounts, illustrating Impl2 expression (Impl2>mCherry; magenta) in macrophages (stained by an anti-NimC1 antibody; green) of control and infected flies compared to the surrounding tissues (fat body, white dashed line; oenocytes, yellow dashed line). Nuclei stained by DAPI (cyan). From Z-stack consisting of a maximum projection of 11 layers.
- E Expression of Impl2 in macrophages isolated from infected (INF) and control (CON) in flies with macrophage-specific Hif1 α knockdown (Hif1 α ^{RNAi}) and their respective control (W^{control}). Expression levels normalized against rp49 are reported as fold change relative to Impl2 levels in uninfected W^{control} flies arbitrarily set to 1. Results compared by 2way ANOVA/Tukey's multiple comparisons test.
- F ChIP-qPCR analysis showing the abundance of arbitrarily preselected regions in Impl2 promoter bound by the transcription factor HIF1 α in control (CON) and infected flies (INF). The genomic region of S-adenosylmethionin synthetase with no predicted HIF1 α -binding sites was used as a negative control (NC). Data normalized to the number of detected fragments in the slurry before chromatin immunoprecipitation. Data are reported as fold change relative to REG.1 level in uninfected W^{control} flies arbitrarily set to 1. Results compared by 2way ANOVA/Tukey's multiple comparisons test.
- G Schematic representation of the obtained results. The transcription factor HIF1 α binds to the Impl2 promoter to increase its expression in macrophages after infection. Thus, Impl2 production is coupled to the metabolic polarization of pro-inflammatory macrophages toward aerobic glycolysis via HIF1 α activity. Whether macrophage-derived IMPL2 induces systemic lipid redistribution will be addressed in the following sections.

Data information: All data presented in this figure were obtained 24 h post-infection. Data were obtained from four independent experiments if not stated otherwise. For qPCR analysis, the dots in the plots represent biological replicates. For transcriptomic analysis, macrophages from 300 flies were used for each biological replicate. For qPCR analysis, macrophages from 90 flies were used for each biological replicate. Values are displayed as mean SD, asterisks mark statistically significant differences (**P < 0.01; ***P < 0.001).

Sourcedata are available online for this figure.

respective genetic background (TRiP^{control}, W^{control}; see Fig EV2D for an explanation of the genotypes and Fig EV3A for efficiency of macrophage-specific Impl2 manipulations).

First, we evaluated the impact of M ϕ -Impl2 manipulations on the morphology of the fat body. While flies of the control genotypes (TRiP^{control}, W^{control}) display the characteristic infection-induced changes in the morphology of lipid droplets in adipocytes, M ϕ -Impl2^{RNAi} abrogates these changes. Accordingly, macrophage-specific overexpression of Impl2 (M ϕ -Impl2^{CDS}) is sufficient to mimic the infection-induced changes even under control conditions (Figs 3A and EV3B and C). These morphological changes can be attributed to the redistribution of lipids from the fat body to the circulation, as evidenced by triglyceride, cholesterol, and cholesteryl-ester levels, which are decreased in the fat body and elevated in circulation upon infection. Since all these metabolites show an identical pattern in response to treatments and genetic manipulations, they are displayed in the main Figures as "Lipids" for simplicity and presented individually in the ExpandedView file (Fig EV3D–F).

While M ϕ -Impl2^{RNAi} prevents the infection-induced depletion of lipids in the fat body and their subsequent rise in circulation, these changes are invoked by mere M ϕ -Impl2^{CDS} even without infection (Figs 3B and C, and EV3D–F).

Fat body lipidomics provides further indications that macrophage-derived IMPL2 plays a central role in the mobilization of lipids upon infection. M ϕ -Impl2^{RNAi} suppresses the characteristic infection-induced changes in the proportion of lipid species in the fat body as manifested by increased abundance of PC, PE, and DG, whereas enrichment of these lipid classes can be observed in the fat body of flies carrying M ϕ -Impl2^{CDS} even under control conditions (Fig 3D and E).

To comprehend the mechanism of the Impl2-induced changes in the fat body, we measured the expression pattern of genes involved in lipolysis (brummer, bmm; Hormone-sensitive lipase, Hsl) and the production of lipoproteins (Apolipoprotein lipid transfer particle, Apoltp; apolipophorin, apolpp; Neuropeptide-like precursor 2, Nplp2;

Microsomal triacylglycerol transfer protein, Mtp). Expression of all these genes is significantly elevated in the fat body upon infection, and the expression pattern of bmm, Apoltp, apolpp, and Mtp seems to be dependent on macrophage-derived Impl2 (Figs 3F and EV4A). Interestingly, all these genes are known FOXO targets (Brankatschk et al, 2014), which implicates the involvement of this transcription factor in the mediation of IMPL2 effects. This notion is supported by the expression of two commonly used FOXO readouts (Thor, 4EBP; eukaryotic translation initiation factor 4E1, eIF4E1; Santalla et al, 2022), showing analogous expression patterns with respect to infection and M ϕ -Impl2 manipulations (Fig 3F). Consistent with metabolic effects attributed to M ϕ -Impl2 manipulations, identical metabolic effect has been achieved also by using an alternative Impl2^{RNAi} fly line (Appendix Figs S16–S18). Infection also leads to increased expression of Hsl and the exchange lipoprotein Nplp2 in the fat body, however, their expression is not affected by M ϕ -Impl2 manipulations, suggesting an alternative mechanism for their regulation.

Macrophage-derived IMPL2 drives lipid mobilization via alleviation of fat body insulin signaling

To determine whether FOXO plays a role in the manifestation of IMPL2 effects in the fat body, we decided to analyze its subcellular localization and its contribution to the infection-induced changes in lipid droplet morphology. While FOXO may be found distributed evenly between the nucleus and cytosol under normal physiological conditions, it becomes predominantly nuclear in response to metabolic stress (Koyama et al, 2014). This translocation also occurs during bacterial infection; however, it is impaired by M ϕ -Impl2^{RNAi} and can be induced by M ϕ -Impl2^{CDS} even in uninfected individuals (Figs 4A and EV5A). Moreover, flies carrying the hypomorphic foxo allele together with M ϕ -Impl2^{CDS} do not exhibit lipid depletion observed otherwise in M ϕ -Impl2^{CDS} flies, as documented by lipid

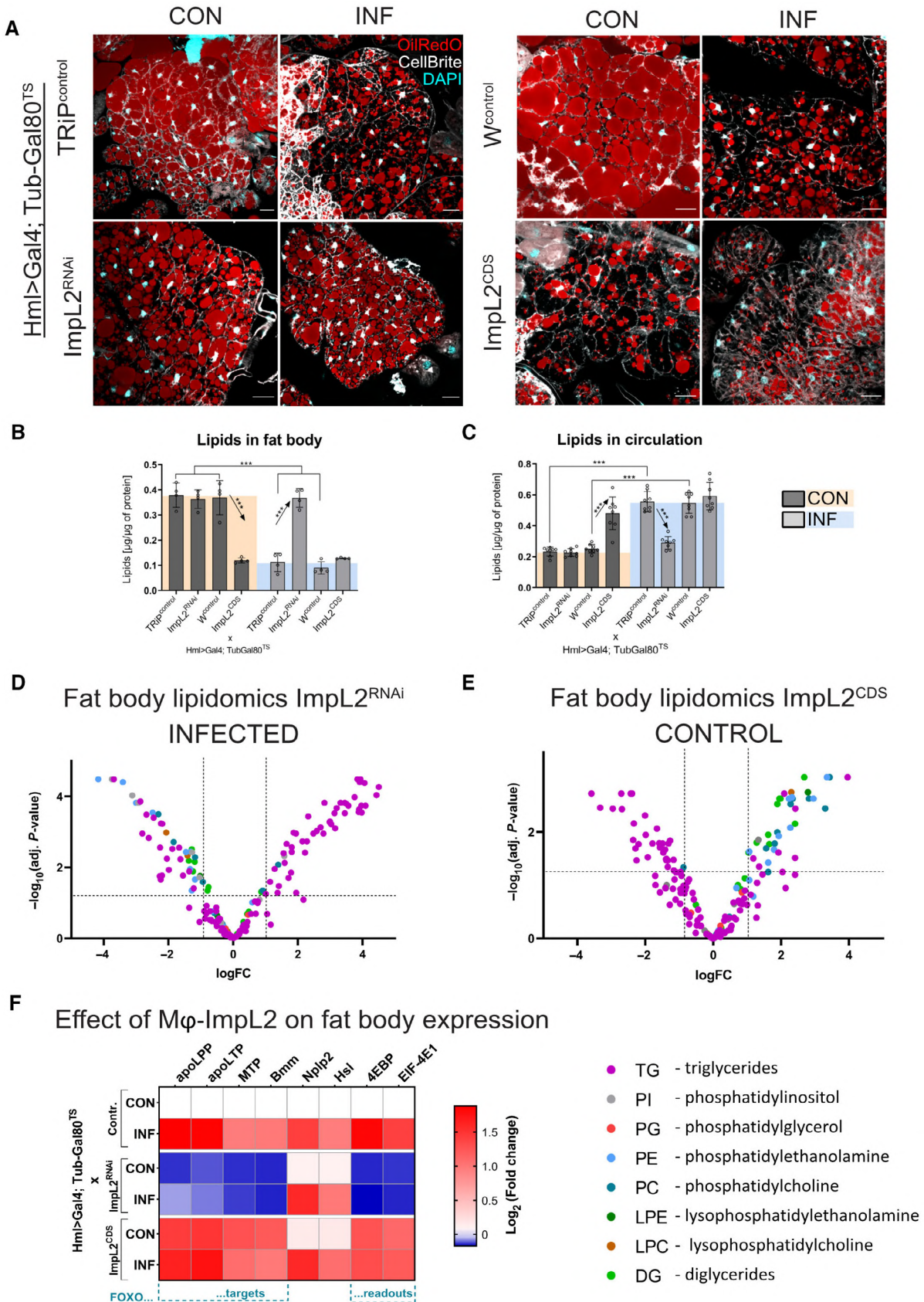


Figure 3.

Figure 3. Macrophage-derived IMPL2 directs the infection-induced mobilization of lipid stores.

- A Representative confocal microscopy images of the dissected fat body whole mounts of non-infected (CON) and infected (INF) flies with macrophage-specific *Impl2* knockdown (*Impl2^{RNAi}*), overexpression (*Impl2^{CDS}*) and their respective controls (*TRiP^{control}, W^{control}*). The images illustrate the morphological changes of lipid droplets stained with OilRedO (red); nuclei are labeled by DAPI (cyan), CellBrite marks membranes (white). Scalebar represents 20 μ m. Images of *TRiP* controls have been reused in Appendix Fig S15.
- B, C Lipid levels in the fat body (B) and circulation (C) of non-infected (CON) and infected (INF) flies with macrophage-specific *Impl2* knockdown (*Impl2^{RNAi}*), overexpression (*Impl2^{CDS}*) and their respective controls (*TRiP^{control}, W^{control}*). Results compared by 2way ANOVA Tukey's multiple comparisons test. The individual dots represent biological replicates with line/bar showing mean SD, asterisks mark statistically significant differences (***) $P < 0.001$.
- D Volcano plot showing the relative abundance of lipid classes in the fat body of infected flies with macrophage-specific *Impl2* knockdown (*Impl2^{RNAi}*) compared to their infected controls (*TRiP^{control}*). Data were obtained from six independent experiments.
- E Volcano plot showing the relative abundance of lipid classes in the fat body of non-infected (CON) flies with macrophage-specific *Impl2* knockdown (*Impl2^{CDS}*) compared to their non-infected controls (*W^{control}*). Data were obtained from six independent experiments.
- F Heat map showing the \log_2 -fold change in mRNA expression of genes of interest in the fat bodies dissected from non-infected (CON) and infected (INF) flies with macrophage-specific *Impl2* knockdown (*Impl2^{RNAi}*), overexpression (*Impl2^{CDS}*) and their respective controls (*TRiP^{control}, W^{control}*). Differential expression is displayed as a \log_2 -fold change with respect to the gene expression level in control flies (average change for *TRiP^{control}* and *W^{control}*) under control conditions.

Data information: Expression levels normalized against *rp49*. All data presented in this figure were obtained 24 h post-infection. Data were obtained from four independent experiments if not stated otherwise. For analysis of metabolites; fat bodies from six individuals and hemolymph from 25 flies were used for each biological replicate. For lipidomic analysis, fat bodies from six individuals were used for each biological replicate. For qPCR analysis, fat bodies from six individuals were used for each biological replicate. 4EBP, Thor; apoLPP, apolipoprotein lipoprotein; apoLTP, apolipoprotein lipid transfer particle; Bmm, brummer; EIF-4E1, eukaryotic translation initiation factor 4E1; Hsl, hormone sensitive lipase; MTP, microsomal triacylglycerol transfer protein; Nplp2, Neuropeptide-like precursor 2. Sourcedata are available online for this figure.

droplet morphology in adipocytes (Fig 4B–D). In conclusion, the effects of macrophage-derived IMPL2 on lipid metabolism in the fat body are mediated by the transcription factor FOXO, which is required for the mobilization of lipid stores upon infection.

Given that FOXO nuclear translocation is controlled by PI3K activity in situations of metabolic stress (Zhao et al, 2021), we analyzed the effect of M ϕ -*Impl2* manipulations on PI3K activity in the fat body. For this purpose, we employed a fly strain carrying in vivo PI3K reporter based on pleckstrin homology domain fused with GFP (tGPH; Britton et al, 2002). The signal, which is predominately localized to the plasma membrane in control flies, becomes more cytosolic in infected individuals, documenting decreased PI3K signaling in the fat body of infected flies. Since M ϕ -*Impl2^{CDS}* phenocopies tGPH localization during infection even under control conditions (Fig 5A and B), we postulate that macrophage-derived *Impl2* silences PI3K enzymatic activity in the fat body upon infection.

The impact of macrophage-derived *Impl2* on FOXO and PI3K activity in the fat body indicates that the *Impl2* effects may be mediated via silencing of insulin signaling since both these factors play a central role in insulin signaling in *Drosophila* (DiAngelo et al, 2009). This is consistent with the previously described function of *Impl2* as an insulin signaling antagonist with a high affinity to circulating insulin and *Drosophila* insulin-like peptides (Honegger et al, 2008; Kwon et al, 2015).

Therefore, we aim to investigate the effects of insulin signaling on the redistribution of lipid stores upon infection. For this purpose, we generated flies with constitutively active (FB > *InR^{CA}*) or genetically abrogated (FB > *InR^{DN}* and FB > *PTEN^{CDS}*) insulin signaling exclusively in the fat body by using a fat body-specific Gal4 driver (FB-Gal4; Grönke et al, 2003; see Fig EV2D for genotype explanations). While mere silencing of insulin signaling in the fat body of uninfected flies (FB > *InR^{DN}* and FB > *PTEN^{CDS}*) results in the depletion of lipid stores in this organ and their accumulation in the circulation, constitutive activation of insulin receptor (FB > *InR^{CA}*) does not allow for the redistribution of lipids between these two compartments otherwise observed upon infection (Fig 5C and D and Appendix Fig S8A and B). In concordance with the previously observed morphology of

lipid droplets in the fat body, the flies bearing the foxo hypomorphic allele (*foxo^{hyppo}*) were not able to induce mobilization of lipids from the fat body into the circulation upon infection as well as flies with foxo hypomorphic allele and macrophage-specific overexpression of *Impl2* (*Hml* > *Impl2^{CDS}*; *foxo^{hyppo}*; Fig 5C and D and Appendix Fig S8A and B). These data further support our conclusion that the metabolic effects of *Impl2* are mediated by the activation of the FOXO transcriptional program.

Moreover, manipulation of insulin signaling in the fat body also affects the expression of genes involved in the assembly and mobilization of lipoproteins (*Apoltp*, *apolpp*, *Mtp*) in this tissue, which has been demonstrated above to respond to M ϕ -*Impl2* manipulations (Fig 5E and Appendix Fig S8C).

As anticipated, fat body-specific knockdown of genes involved in the assembly and mobilization of lipoproteins (*Apoltp*, *apolpp*, *Mtp*; see Appendix Fig S8D for RNAi efficiency and Fig EV2D for genotype descriptions) intervenes with the infection-induced depletion of lipid stores in the fat body and their mobilization into circulation (Fig 5F and G and Appendix Fig S9A and B).

Although the epistatic effect of macrophage-derived IMPL2 on insulin signaling in the fat body has not been explicitly demonstrated here, the data suggest that the effect of IMPL2 on the mobilization of lipid stores is likely mediated by attenuation of insulin signaling in the fat body, leading to increased production of lipoproteins into the circulation via a FOXO-induced transcriptional program (Fig 5H).

Redistribution of lipids toward activated macrophages is essential for resistance to bacterial infection

To address the question of whether *Impl2*-induced lipoprotein mobilization is required for the redistribution of lipids toward infection-activated macrophages (Fig 1G and I), we assessed the incorporation of dietary ¹³C-FFAs and macrophage lipid content in flies with M ϕ -*Impl2* manipulations (see Appendix Fig S19 for experimental setup).

While infection in flies of control genotypes leads to the enhanced ¹³C-FFAs accumulation in activated macrophages at

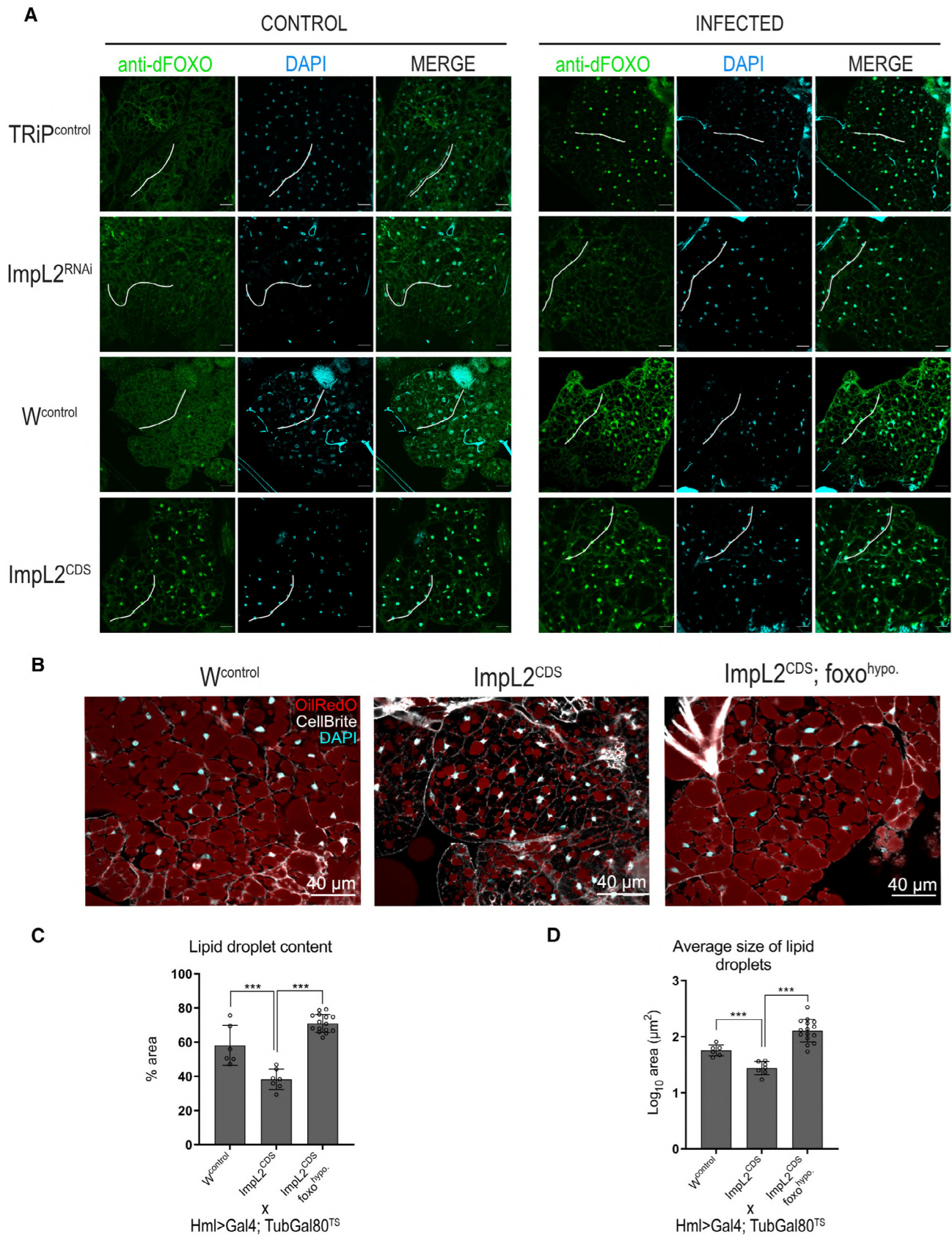


Figure 4.

Figure 4. Macrophage-derived IMPL2 affects FOXO signaling in the fat body.

- A Representative confocal images showing subcellular localization of FOXO (stained by anti-dFOXO; green) in the fat body whole mounts dissected from non-infected (CON) and infected (INF) flies with macrophage-specific *Impl2* knockdown (*Impl2^{RNAi}*), overexpression (*Impl2^{CDS}*) and their respective controls (*TriP^{control}* and *W^{control}*). DAPI (cyan) marks nuclei. A white freehand line indicates the section for which the colocalization of DAPI and anti-dFOXO signals is displayed in intensity histograms in Fig EV5. Scale bar represents 20 μ m.
- B Representative confocal images showing the morphology of lipid droplets in the dissected fat body whole mounts dissected from noninfected control flies (*W^{control}*), flies with macrophage-specific *Impl2* overexpression (*Impl2^{CDS}*), and flies with macrophage-specific *Impl2* overexpression in the hypomorphic Fox mutant background (*Impl2^{CDS}; foxo^{hyp}*). Neutral lipids stained by OilRedO (red), CellBrite marks membranes (white), and DAPI nuclei (cyan).
- C Percentage of the area occupied by lipid droplets in the fat body of non-infected control flies (*W^{control}*), flies with macrophage-specific *Impl2* overexpression (*Impl2^{CDS}*), and flies with macrophage-specific *Impl2* overexpression in the hypomorphic Fox mutant background (*Impl2^{CDS}; foxo^{hyp}*).
- D The average size of lipid droplets in the fat body of non-infected control flies (*W^{control}*), flies with macrophage-specific *Impl2* overexpression (*Impl2^{CDS}*), and flies with macrophage-specific *Impl2* overexpression in the hypomorphic Fox mutant background (*Impl2^{CDS}; foxo^{hyp}*).

Data information: All data presented in this figure were obtained 24 h post-infection. In (C) and (D), data were obtained by analysis of dissected fat body whole mounts stained for neutral lipids (OilRedO). Images were captured by a confocal microscope. Data were obtained from six independent experiments. Results were compared by 2way ANOVA followed by Šidak's multiple comparisons test. The individual dots represent biological replicates with line/bar showing mean SD, asterisks mark statistically significant differences (** $P < 0.001$).

Sourcedata are available online for this figure.

the expense of the fat body, this effect is diminished significantly in flies with $M\phi$ -*Impl2^{RNAi}*. Contrary to that, mere $M\phi$ -*Impl2^{CDS}* leads to enhanced ^{13}C -FFAs levels in macrophages in both infected and control flies (Fig 6A). Notably, we have not observed any marks of infection-induced anorexia as documented by comparable dietary uptake in flies regardless of treatment or their genotypes (Appendix Fig S10A).

That is consistent with elevated lipid content in macrophages of infected flies of control genotypes, which is not present in flies with $M\phi$ -*Impl2^{RNAi}* but can be induced in uninfected flies by $M\phi$ -*Impl2^{CDS}* (Fig 6B and Appendix Fig S10B). These data imply that macrophage-derived *Impl2* is required for enhanced availability of lipids for the immune system and their accumulation in activated macrophages.

Further, we evaluated the importance of *IMPL2*-induced metabolic changes for immune function and resistance to infection. In this regard, we assessed the survival rate of flies with manipulated *IMPL2* production in macrophages and flies with knockdown of genes required for the assembly and production of lipoproteins from the fat body.

$M\phi$ -*Impl2^{RNAi}* leads to a significantly reduced phagocytic capacity of macrophages as documented by the decreased number of phagocytic events upon injection of a phagocytic marker (pHrodo-*S. aureus*; Fig 6C and D). In line with that, $M\phi$ -*Impl2^{RNAi}* leads to increased pathogen load in these flies and decreased survival of infection, whereas flies with $M\phi$ -*Impl2^{CDS}* display lower pathogen load and improved infection resistance (Fig 6E and F and Appendix Fig S10C). Cell-autonomous effects of $M\phi$ -*Impl2* manipulations on the function of these cells were found to be insignificant since macrophages isolated from these flies show normal production of antimicrobial peptides, markers of metabolic polarization, and macrophage numbers (Appendix Figs S11–S15).

The importance of enhanced mobilization of lipoproteins during infection is documented by the decreased survival rate of flies with the fat body-specific knockdown of genes involved in lipoprotein assembly (Apoltp, apolpp, Mtp; Fig 7A and Appendix Fig S10D). Inhibition of mobilization of lipoproteins by fat body-specific knockdown of apolpp leads to decreased phagocytic capability of macrophages resulting in enhanced pathogen load in these flies at 24 hpi (Fig 7B–D). This is in concordance with enhanced lipoprotein

uptake by infection-activated macrophages compared to uninfected controls, as documented by the number of endocytic events of pHrodo-labeled low-density lipoproteins (LDL; Fig 7E and F), the enhanced proportion of macrophages containing lipid droplets in their cytosol as well as by accumulation of fluorescently-labeled FFAs (Appendix Figs S20 and S21). Increased uptake of lipids by activated macrophages and their subsequent processing is further supported by enhanced expression of genes involved in these processes (Appendix Figs S22 and S23).

Infection-activated mammalian liver macrophages release IGFBP7 to induce the mobilization of lipids from hepatocytes

The presented data demonstrate that the pro-inflammatory polarization of *Drosophila* macrophages is associated with the production of the signaling factor *IMPL2* through the activity of the transcription factor HIF1 α . *IMPL2* subsequently triggers the mobilization of lipoproteins in the fat body to nutritionally supplement the immune system.

To investigate whether an analogous mechanism may be evolutionarily conserved and relevant in mammals, we focused on mammalian *Impl2* homolog Insulin growth factor binding protein 7 (Igfbp7; Honegger et al, 2008). *Igfbp7* is a member of insulin growth factors with high affinity to human insulin and its functional and sequence homology to *Impl2* has been described previously (Sloth Andersen et al, 2000; Roed et al, 2018).

First, we analyzed the production of IGFBP7 in human monocyte-derived macrophages (THP1 cells) during their bactericidal polarization. Pro-inflammatory polarization of THP1 cells induced by administration of *S. pneumoniae* or LPS leads to significant upregulation of IGFBP7 at both mRNA (Fig 8A) and protein levels (Fig 8B). Moreover, we revealed that IGFBP7 production in THP1 cells is controlled by the transcription factor HIF1 α since the application of its inhibitor (KC7F2) or agonist (DMOG) has a major effect on IGFBP7 production in these cells regardless of their activation state (Fig 8A and B). Next, we investigated the effects of bacterial endotoxins (LPS) on IGFBP7 expression in liver macrophages (see Appendix Fig S24A for experimental design). Consistently with the data from THP1 cells, LPS induces IGFBP7 expression in liver macrophages isolated from mice and humans (Fig 8C and D).

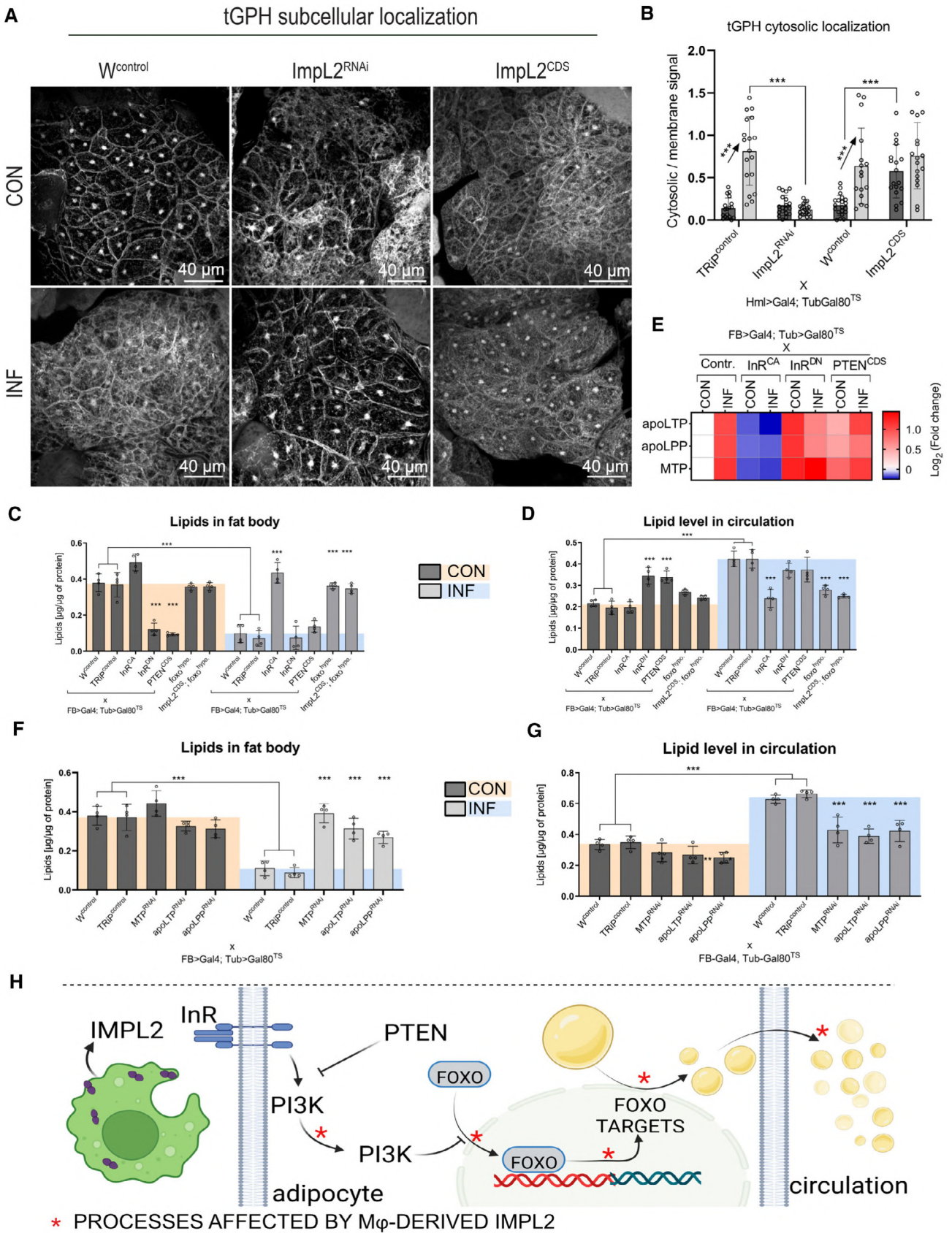


Figure 5.

Figure 5. Macrophage-derived IMPL2 drives lipid mobilization in the fat body.

- A Representative confocal images showing subcellular localization of the PI3K-activity reporter (tGPH; white) in the fat body whole mounts dissected from non-infected (CON) and infected (INF) control flies ($W^{control}$), flies with macrophage-specific *ImpL2* knockdown ($ImpL2^{RNAi}$) and overexpression ($ImpL2^{CDS}$). Images reconstructed from Z-stack consisting of a maximum projection of 10 layers.
- B tGPH cytosolic localization in the fat body of non-infected (CON) and infected (INF) flies with macrophage-specific *ImpL2* knockdown ($ImpL2^{RNAi}$), overexpression ($ImpL2^{CDS}$) and their respective controls ($TRiP^{control}$ and $W^{control}$) quantified as a proportion of the amount of signal in the membrane and cytosol regions. Individual dots in the plot represent biological replicates.
- C, D The concentration of lipids in the fat body (C) and circulation (D) in non-infected (CON) and infected (INF) flies with fat body-specific overexpression of constitutively active or dominant negative form of insulin receptor (InR^{CA} , InR^{DN}), *PTEN* ($PTEN^{CDS}$), flies bearing *foxo* hypomorphic allele ($foxo^{hypo}$), and in flies with a combination of *foxo* hypomorphic allele and macrophage-specific overexpression of *ImpL2* ($Hml > ImpL2^{CDS}; foxo^{hypo}$) compared to their respective controls ($W^{control}$, $TRiP^{control}$).
- E Heat map showing the \log_2 -fold change in mRNA expression of involved in mobilization of lipoproteins (*MTP*, *apoLTP*, *apoLPP*) in the fat body of noninfected (CON) and infected (INF) flies with fat body-specific overexpression of constitutively active or dominant negative form of insulin receptor (InR^{CA} , InR^{DN}), *PTEN* ($PTEN^{CDS}$), flies bearing *foxo* hypomorphic allele ($foxo^{hypo}$), and in flies with a combination of *foxo* hypomorphic allele and macrophage-specific overexpression of *ImpL2* ($Hml > ImpL2^{CDS}; foxo^{hypo}$) compared to their respective controls ($W^{control}$, $TRiP^{control}$). Differential expression is displayed as a \log_2 -fold change with respect to the gene expression level in control flies (average change for $TRiP^{control}$ and $W^{control}$) under control experimental conditions. Expression levels normalized against *rp49*.
- F, G The concentration of lipids in the fat body (F) and circulation (G) in non-infected (CON) and infected (INF) control flies ($W^{control}$, $TRiP^{control}$) and flies with fat body-specific knockdown of genes involved in the mobilization of lipoproteins (*MTP*, *apoLTP*, *apoLPP*).
- H Schematic representation of the obtained results. Macrophage-derived *IMPL2* silences insulin signaling in the fat body, resulting in decreased PI3K enzymatic activity, FOXO nuclear translocation, and enhanced mobilization of lipids from the fat body to the circulation.

Data information: All data presented in this figure were obtained 24 h post-infection. Data were obtained from four independent experiments if not stated otherwise. For analysis of metabolites; fat bodies from six individuals and hemolymph from 25 flies were used for each biological replicate. For qPCR analysis, fat bodies from six individuals were used for each biological replicate. In (C, D) and (F, G), the metabolite concentrations were normalized to the number of proteins in each sample. Results were compared by 2way ANOVA Tukey's multiple comparisons test. The individual dots represent biological replicates with line/bar showing mean SD, asterisks mark statistically significant differences ($***P < 0.001$). *apoLPP*, apolipoprotein; *apoLTP*, Apolipoprotein lipid transfer particle; *InR*, insulin receptor; *MTP*, microsomal triacylglycerol transfer protein; *PTEN*, Phosphatase and tensin homolog. Sourcedata are available online for this figure.

To induce gene-specific knockdown exclusively in murine liver macrophages *in vivo*, we employed glucan particles as a macrophage-specific delivery tool that was developed for this purpose (Tencerova, 2020). Intravenously administered glucan particles loaded with siRNA against *Igfbp7* are specifically scavenged by liver macrophages and significantly reduce *Igfbp7* expression exclusively in these cells (Tencerova et al, 2015; Morgantini et al, 2019). Knockdown of *Igfbp7*, specifically in murine liver macrophages, results in decreased expression of apolipoprotein genes in hepatocytes *in vivo*, as revealed by their transcriptomic analysis (Fig 8F and Appendix Fig S24B).

To further test the IGFBP7 potential to induce lipoprotein production in human hepatocytes, we employed an organotypic 3D model of primary human liver cells in which cellular phenotypes closely resemble liver cells at the transcriptomic, proteomic, and metabolomic level *in vivo* (Bell et al, 2017; Vorrink et al, 2017; Oliva-Vilarnau et al, 2020). Indeed, the administration of human recombinant IGFBP7 on hepatocellular spheroids leads to elevated LDL and VLDL titers in culture media (Fig 8E).

Overall, our data indicate that *Igfbp7* may play an analogous role to *Drosophila ImpL2* since it is produced by liver macrophages in response to their pro-inflammatory polarization in a HIF1 α -

Figure 6. Redistribution of lipids toward activated macrophages is essential for resistance to bacterial infection.

- A Incorporation of dietary ^{13}C -labeled free fatty acids into the fat body, gut, and macrophages of non-infected (CON) and infected (INF) flies with macrophage-specific *ImpL2* knockdown ($Crq-Gal4 > ImpL2^{RNAi}$), overexpression ($Crq-Gal4 > ImpL2^{CDS}$) and their respective controls ($Crq-G4 > UASGFP$). Data are expressed as relative incorporation of ^{13}C free fatty acids normalized to ^{12}C free fatty acids in the sample. Arrows indicate treatment- or genotype-induced changes compared to uninfected controls. Guts from six flies, fat bodies from six individuals, and macrophages from 160 flies were used for each biological replicate.
- B The concentration of lipids in macrophages isolated from non-infected (CON) and infected (INF) flies with macrophage-specific *ImpL2* knockdown ($ImpL2^{RNAi}$), overexpression ($ImpL2^{CDS}$) and their respective controls ($TRiP^{control}$, $W^{control}$).
- C The phagocytic capability of pHrodo-*S. aureus* in macrophages of infected flies with macrophage-specific *ImpL2* knockdown ($ImpL2^{RNAi}$), overexpression ($ImpL2^{CDS}$), and their respective controls ($TRiP^{control}$, $W^{control}$). The individual dots represent the \log_{10} -normalized numbers of the phagocytic events per cell. Results were analyzed by Ordinary one-way ANOVA Dunnett's multiple comparisons test.
- D Representative confocal images of macrophages ($Crq > GFP$; green) of abdominal whole mounts dissected from infected flies with macrophage-specific *ImpL2* knockdown ($ImpL2^{RNAi}$), overexpression ($ImpL2^{CDS}$) and their respective controls ($TRiP^{control}$, $W^{control}$) injected with pHrodo-*S. aureus* (magenta).
- E Pathogen load in flies with macrophage-specific knockdown of *ImpL2* ($ImpL2^{RNAi}$), overexpression ($ImpL2^{CDS}$), and their respective controls ($TRiP^{control}$, $W^{control}$) at 48 hpi. Results were compared by Ordinary one-way ANOVA Dunnett's multiple comparisons test.
- F Survival of bacterial infection of flies with macrophage-specific knockdown of *ImpL2* ($ImpL2^{RNAi}$), overexpression ($ImpL2^{CDS}$), and their respective controls ($TRiP^{control}$, $W^{control}$). Survival curves for the respective uninfected genotypes are shown in dashed lines.

Data information: All data presented in this figure were obtained 24 h post-infection if not stated otherwise. In (B), (C), and (E), the individual dots represent biological replicates with line/bar showing mean SD. In (B), macrophages from 160 flies were used for each biological replicate; results were compared by 2way ANOVA Tukey's multiple comparisons test. In (F), three independent experiments were performed and combined into each survival curve; the number of individuals per replicate was at least 600 for each genotype; results were analyzed by Log-rank and Gehan-Breslow Wilcoxon tests. In (E), the individual dots in the plot represent the number of bacteria (colony forming units—CFUs) in thousands per fly. Asterisks mark statistically significant differences ($***P < 0.001$). Sourcedata are available online for this figure.

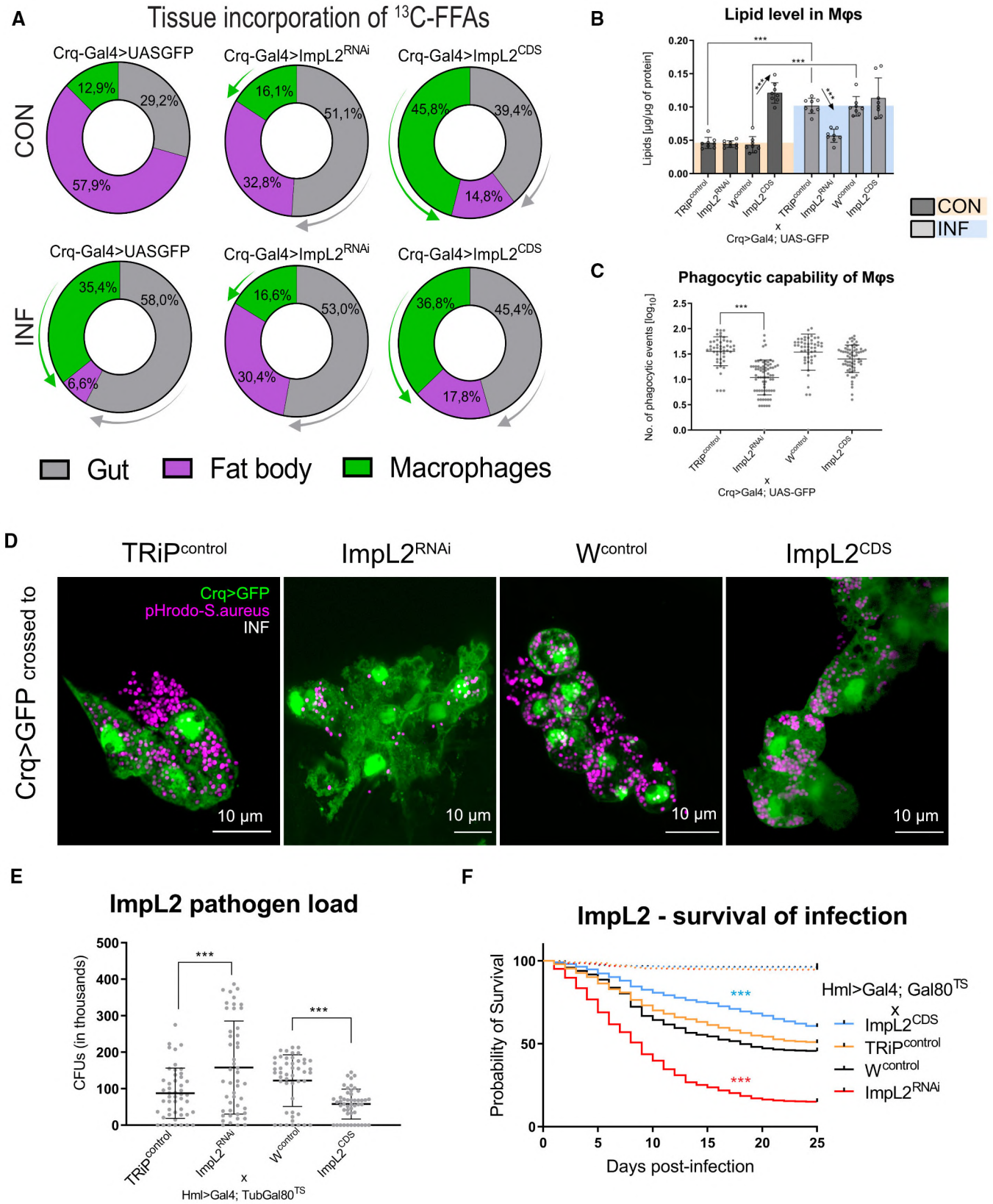


Figure 6.

dependent manner and that IGFBP7 production by macrophages can elicit the production of lipoproteins from neighboring hepatocytes (Fig 8G).

Discussion

The pro-inflammatory polarization of macrophages is associated with extraordinary energy and nutritional demands that must be

supplemented from external sources (Newsholme, 2021). To fight infection, an organism must significantly adjust systemic metabolism and relocate nutrients from stores toward the immune system (Ganeshan et al, 2019). In this regard, induction of insulin resistance has been proposed as a potentially adaptive mechanism for metabolic adaptation to infection (DiAngelo et al, 2009). However, the signal reflecting the nutritional demands of the activated immune system and the mechanism underlying the systemic metabolic changes remain largely unknown. In this work, we employed

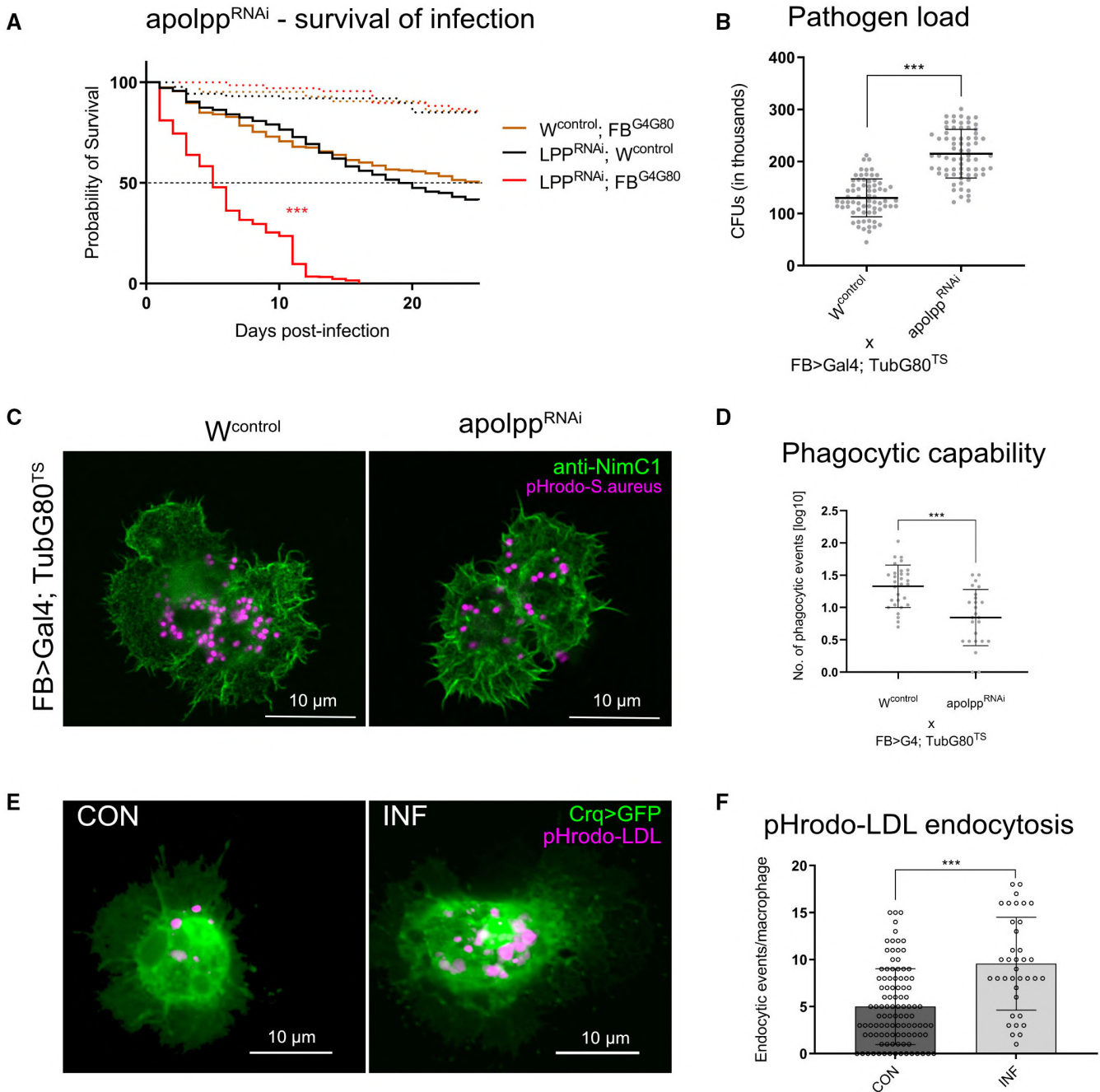


Figure 7.

Figure 7. Mobilization of lipoproteins from the fat body is required for efficient phagocytosis.

- A Survival of bacterial infection of flies with fat body-specific knockdown of apolpp (LPP^{RNAi}; FB^{G4G80}) and their respective controls (W^{control}; FB^{G4G80} and LPP^{RNAi}; FB^{G4G80}). Survival curves for the respective uninfected genotypes are shown in dashed lines.
- B Pathogen load in flies with fat body-specific knockdown of apolpp (apolpp^{RNAi}) and their respective controls (W^{control}) at 48 hpi. Results were compared by Ordinary one-way ANOVA Dunnett's multiple comparisons test.
- C Representative confocal images of macrophages (Crq>GFP; green) dissected from flies with fat body-specific knockdown of apolpp (apolpp^{RNAi}) and their respective controls (W^{control}) injected with pHrodo-*S. aureus* (magenta).
- D The phagocytic capability of pHrodo-*S. aureus* in macrophages of flies with fat body-specific knockdown of apolpp (apolpp^{RNAi}) and their respective controls (W^{control}). The individual dots represent the log₁₀-normalized numbers of the phagocytic events per cell. Results were analyzed by Ordinary one-way ANOVA Dunnett's multiple comparisons test.
- E Representative confocal images of macrophages (green) in non-infected (CON) and infected (INF) control flies (Crq>GFP; TRiP^{control}) injected with pHrodo-LDL depicting events of LDL endocytosis (magenta).
- F The number of endocytic events of low-density lipoproteins (LDL) per macrophage in non-infected (CON) and infected (INF) control flies (Crq>GFP; TRiP^{control}) injected with pHrodo-LDL. The individual dots mark the number of phagocytic events per cell. Results were analyzed by Ordinary one-way ANOVA Dunnett's multiple comparisons test.

Data information: Data were obtained from four independent experiments if not stated otherwise. In A, three independent experiments were performed and combined into each survival curve; the number of individuals per replicate was at least 600 for each genotype. Results were analyzed by Log-rank and Gehan-Breslow Wilcoxon tests. In (B), the individual dots in the plot represent the number of bacteria (colony forming units—CFUs) in thousands per fly; data were obtained from three independent experiments. Asterisks mark statistically significant differences (***) $P < 0.001$. In (B), (D), and (F), individual dots in the plots represent biological replicates with line/bar showing mean SD. apolpp, apolipoprotein.

Sourcedata are available online for this figure.

a model of bacterial infection in *Drosophila* to reveal the mechanism connecting the metabolic remodeling of activated macrophages to a systemic metabolic switch.

In our previous work, we described that infection-activated *Drosophila* macrophages adopt aerobic glycolysis driven by the transcription factor HIF1 α as a predominant metabolic pathway for energy production (Kedia-Mehta & Finlay, 2019; Krejčova et al, 2019). Here, we extend this observation and show that infection-activated macrophages exhibit increased lipid uptake and utilization in addition to aerobic glycolysis. Moreover, here we found that HIF1 α activity leads to increased production of the signaling factor IMPL2 in these cells. Given that HIF1 α is a crucial transcription factor governing the M1 metabolic shift (Corcoran & O'Neill, 2016), IMPL2 can be perceived as a signal translating the increased nutritional demands of activated macrophages to systemic metabolism.

It has been documented that IMPL2 is also secreted by genetically induced neoplastic tumors (Kwon et al, 2015), hypoxic muscles (Owusu-Ansah et al, 2013), and inflamed guts (Hang et al, 2014). Thus, IMPL2 production is not under all circumstances restricted exclusively to immune cells and may be coupled to strong metabolic activity and suddenly increased nutritional demands of virtually any tissue. Thus, the regulatory role of ImpL2 may be crucial for the redistribution of resources during metabolic stress, and IMPL2 activity is not limited to pathological stress situations but may also have adaptive evolutionary significance.

Enhanced IMPL2 production has been shown to invoke systemic metabolic changes resembling cachexia-like wasting, leading to the depletion of lipid stores in the central metabolic organ (Figueroa-Claresvega & Bilder, 2015; Kwon et al, 2015). Bacterial infection and subsequent activation of immune-related cascades in the fat body leads to dramatic changes in its physiology and metabolism leading to mobilization of lipids as a part of the antibacterial immune response (Martinez et al, 2020; Zhao & Karpac, 2021). Consistent with this, we found that the production of IMPL2 by activated macrophages induces the mobilization of lipid stores from the fat body, leading to an elevated level of lipids in circulation and their subsequent accumulation in activated immune cells. The mechanism

underlying the effects of IMPL2 can be attributed to the alleviation of insulin signaling in the fat body, resulting in enhanced FOXO-induced mobilization of lipoproteins. This is consistent with the previous observation that IMPL2 exhibits a high affinity for circulating *Drosophila* insulin-like peptides, thus acting as a potent inhibitor of insulin signaling and coordinating larval growth and development (Honegger et al, 2008). Even though our data indicate that macrophage-derived IMPL2 induces mobilization of lipoproteins from the fat body, the participation of direct transport of dietary lipids toward activated immune cells cannot be excluded. Some of our data, however, do not support this eventuality. Analysis of lipid content in the gut indicates that infection leads to enhanced retention of lipids in this organ. Moreover, although genetic manipulation of ImpL2 expression in macrophages affects the expression of Apoltp in the fat body, which is thought to be responsible for lipid transport from the gut, this manipulation does not affect gut lipid content significantly. We may thus speculate that in *Drosophila*, Apoltp may play a role in both lipid transport from the gut and mobilization of lipids from the fat body, as has been shown in other insect species (Arrese et al, 2001; Canavoso et al, 2004). Nevertheless, further investigation is needed in this regard.

Recently, it has been proposed that IMPL2 activity may cause the metabolic adaptations observed in the reproductive cast of ants that are required for the maturation of the ovaries, but the mechanism underlying this process has not been fully elucidated (Yan & Horng, 2020). Thus, our proposed mechanism of action of IMPL2 explains this phenomenon well.

We found that IMPL2 production interconnects the metabolic switch of activated macrophages to the mobilization of lipoproteins to supplement the metabolic needs associated with the bactericidal function of the immune system. Interventions of this mechanism at the level of IMPL2 production by macrophages, or lipoprotein mobilization from the fat body compromise the ability of macrophages to fight the bacterial pathogen, resulting in deterioration of the individual's resistance to infection. Thus, IMPL2-mediated metabolic changes are essential for an adequate immune response to extracellular bacteria. The presented data indicate that activated macrophages must be supplemented by lipids from external sources to

fight the pathogen efficiently. The increased uptake and accumulation of lipids by infection-activated macrophages may be attributed to their use for cell membrane remodeling, catecholamine synthesis, and epigenetic reprogramming (Remmerie & Scott, 2018; Yan & Horng, 2020). Nonetheless, the link between increased lipid utilization and the bactericidal activity of *Drosophila* macrophages has not yet been satisfactorily elucidated.

Our data from mice and human experimental systems suggest that an analogous mechanism may be evolutionarily conserved. The Impl2 homolog IGFBP7 is produced by liver macrophages upon

their proinflammatory polarization and possesses the potential to induce the mobilization of LDL and VLDL from hepatocytes. Although the mechanism of IGFBP7 action on hepatocytes was not addressed in this study, we have previously shown that IGFBP7 binds directly to the insulin receptor in hepatocytes and induces systemic metabolic changes via regulation of ERK signaling in the liver (Roed et al, 2018). Our model is analogous to observations in obese mice and humans in which hepatic insulin resistance induces constitutive FOXO activation leading to increased lipoprotein production (Yan & Horng, 2020). Nonetheless, the effect of IGFBP7 and other

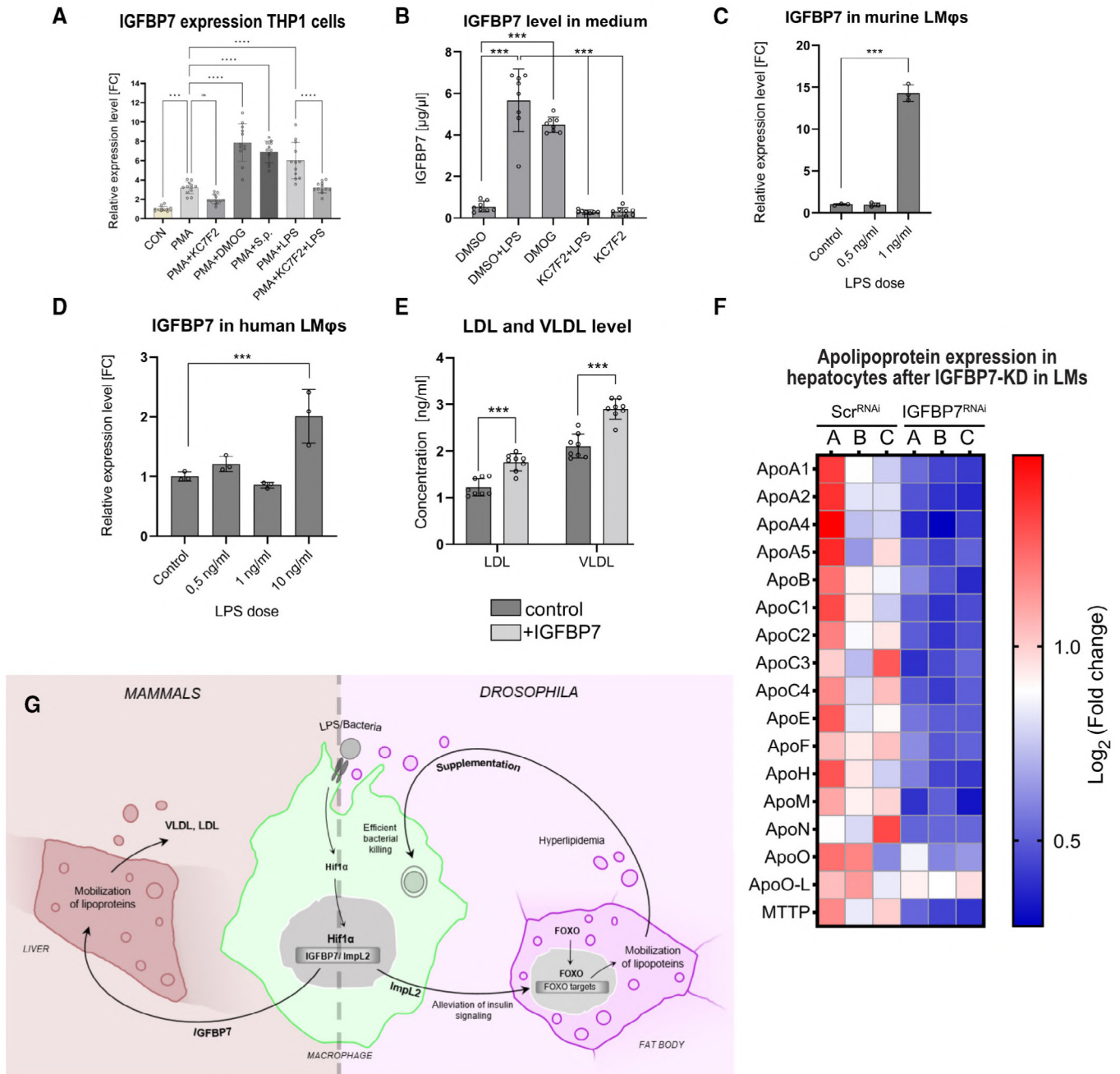


Figure 8.

Figure 8. Infection-activated liver macrophages release IGFBP7 to induce the mobilization of lipids from hepatocytes.

- A Expression of IGFBP7 in the culture of THP-1 cells after administration of heat-killed streptococcus or LPS in combination with HIF1 α inhibitor (KC7F2) or agonist (DMOG) and respective controls as measured by RT-qPCR. Expression levels normalized against ACTB are shown as a fold change relative to levels of IGFBP7 in non-activated THP1 cells (Mo) that were arbitrarily set to 1.
- B The concentration of IGFBP7 in culture media of THP-1 cells after administration of lipopolysaccharide (LPS) in combination with HIF1 α inhibitor (KC7F2) or agonist (DMOG) and their respective control as measured by ELISA.
- C Expression of IGFBP7 in mouse liver macrophages in response to lipopolysaccharide treatment (LPS; 0.5 and 1 ng/ml) and their respective control. Expression levels are shown as a fold change relative to ACTB mRNA in buffer-treated controls that were arbitrarily set to 1.
- D Gene expression of IGFBP7 in human liver macrophages in response to lipopolysaccharide treatment (LPS; 0.5, 1, 10 ng/ml) and their respective control. Expression levels are shown as a fold change relative to ACTB mRNA in buffer-treated controls that were arbitrarily set to 1.
- E Concentration of low-density lipoproteins (LDL) and very-low-density lipoproteins (VLDL) in culture media obtained from the culture of human hepatocellular spheroids treated by human recombinant IGFBP7 protein (+IGFBP7) compared to buffer treated controls.
- F Heat map of transcriptomic data showing a log₂-fold change in mRNA expression of apolipoproteins and lipoprotein synthesizing gene (Mtp) in hepatocytes isolated from mice with liver macrophage-specific knockdown of IGFBP7 (IGFBP7_KD) compared to scramble RNAi (Scr_RNAi) used as a control. Differential expression is displayed as a log₂-fold change with respect to the average gene expression level in control replicates (Scr_RNAi).
- G Schematic representation of the proposed model. Foxo, forkhead box O; Hif1 α , hypoxia-inducible factor 1 α ; IGFBP7, insulin growth factor binding protein 7; Impl2, imaginal morphogenesis protein-late 2.

Data information: All data presented in this figure were obtained 24 h post-infection. Data were obtained from four independent experiments if not stated otherwise. In (A, B), the results were compared by 2way ANOVA Tukey's multiple comparisons test and by Ordinary one-way ANOVA Dunnett's multiple comparisons test in (C, D). The individual dots represent biological replicates with a line/bar showing mean. Samples from mice and humans, displayed in (C), (D) and (F), were isolated in three biological replicates. SD, asterisks mark statistically significant differences (* $P < 0.05$; ** $P < 0.001$; *** $P < 0.0001$). DMOG, dimethylallyl glycine; IGFBP7, insulin-like growth factor-binding protein 7; HIF-1 α , hypoxia-inducible factor 1 α ; KC7F2, N,N'-(disulfanediy)bis(ethane-2,1-diy)bis(2,5-dichlorobenzenesulfonamide). Sourcedata are available online for this figure.

cytokines on the mobilization of lipoproteins from the liver during bacterial infection requires further investigation.

Of particular note is the control of Impl2/IGFBP7 by the transcription factor HIF1 α . In addition to the role of HIF1 α in macrophage polarization during infection, increased activity of this transcription factor is a hallmark of progressive obesity and obesity-related diseases such as non-alcoholic fatty liver disease and atherosclerosis (Izquierdo et al, 2022). Therefore, the initially adaptive production of pro-inflammatory cytokines under HIF1 α control may become maladaptive in the case of chronic macrophage polarization in adipose tissue and the liver.

In the context of the presented results, the cytokine-induced alleviation of insulin signaling in the liver may represent an initially adaptive mechanism by which macrophages secure nutrients for the function of the immune system during bacterial infection. However, chronic activation of this signaling in an infection-independent context may lead to the development of metabolic diseases.

Materials and Methods

Drosophila melanogaster strains and culture

The flies were raised on a diet containing cornmeal (80 g/l), sucrose (50 g/l), yeast (40 g/l), agar (10 g/l), and 10%-methylparaben (16.7 ml/l) and maintained in a humidity-controlled environment with a natural 12 h/12 h light/dark cycle at 25°C. Flies carrying Gal80 protein were raised at 18°C and transferred to 29°C 24 h before infection in order to degrade temperature-sensitive Gal80. Prior to the experiments, both experimental and control flies were kept in plastic vials on a sucrose-free cornmeal diet (cornmeal 53.5 g/l, yeast 28.2 g/l, agar 6.2 g/l and 10%-methylparaben 16.7 ml/l) for 7 days. Flies infected with *S. pneumoniae* were kept on a sucrose-free cornmeal diet in incubators at 29°C due to the temperature sensitivity of *S. pneumoniae*. Infected individuals were transferred to fresh vials every other day without the use of CO₂ to ensure good food conditions.

HmlG4Gal80:w ¹¹¹⁸ ; Hml Δ -Gal4; P{tubPGal80ts}	Crossed by Tomas Dolezal	
w ¹¹¹⁸ ; Hml Δ -Gal4 P{tubPGal80ts}/+; P{w[+mGT]=GT1}foxo ^{BG01018} /UAS-Impl2 ^{cds}	Crossed by Tomas Dolezal	
w ¹¹¹⁸ ; Hml Δ -Gal4 P{tubPGal80ts}/+; tGPHGFP/TRiP ^{control}	Crossed by Tomas Dolezal	
w ¹¹¹⁸ ; PBac{simA-GFPAC.FPTB}VK00037	Bloomington Drosophila Stock Center	BDSC:42672
FbGal4/FbGal4; Tub-Gal80 ^{TS} /Tub-Gal80 ^{TS}	Provided by Katrin Kierdorf	
MTP RNAi	Bloomington Drosophila Stock Center	BDSC:51872
ApoLP ^{RNAi}	Bloomington Drosophila Stock Center	BDSC:28946
ApoLTP ^{RNAi}	Bloomington Drosophila Stock Center	BDSC:51937
yw; UAS-PTEN	Provided by Prof. Marek Jindra	
InR ^{CA}	Bloomington Drosophila Stock Center	BDSC:8263
InR ^{DN}	Bloomington Drosophila Stock Center	BDSC:8253
KK control	Vienna Drosophila Resource Center	
Impl2 ^{RNAi}	Bloomington Drosophila Stock Center	BDSC:55855
Impl2 ^{RNAi}	Bloomington Drosophila Stock Center	BDSC:64936

Impl2-RA-Gal4	Provided by Hugo Stocker	
Impl2 ^{CDS}	Provided by Hugo Stocker	
20xUAS-6xmCherry	Bloomington Drosophila Stock Center	BDSC:52267
CrqGal4 > 2xeGFP	Provided by Marc C. Dionne	
Hif1α[RNAi]: P{KK110834}VIE-260B	Vienna Drosophila Resource Center	VDRC:v106504
TRiP ^{control} :y(1)w(1); P{y[+t7.7]=CaryP}attP2	Bloomington Drosophila Stock Center	BDSC:36303
w: w ¹¹¹⁸	Genetic background based on CantonS	

Bacterial strain and fly injection

The *Streptococcus pneumoniae* strain EJ1 was stored at 80°C in Tryptic Soy Broth (TSB) media containing 10% glycerol. For the experiments, bacteria were streaked onto agar plates containing 3% TSB and 100 mg/ml streptomycin and subsequently incubated at 37°C in 5% CO₂ overnight. Single colonies were inoculated into 3 ml of TSB liquid media with 100 mg/ml of streptomycin and 100,000 units of catalase and incubated at 37°C + 5% CO₂ overnight. Bacterial density was measured after an additional 4 h so that it reached an approximate 0.4 OD₆₀₀. Final bacterial cultures were centrifuged and dissolved in PBS so the final OD reached 2.4. The *S. pneumoniae* culture was kept on ice before injection and during the injection itself. Seven-day-old males were anesthetized with CO₂ and injected with a 50 nl culture containing 20,000 *S. pneumoniae* bacteria or 50 nl of mock buffer (PBS) into the ventrolateral side of the abdomen using an Eppendorf Femtojet microinjector.

Survival analysis

Streptococcus-injected flies were kept at 29°C in vials with approximately 30 individuals per vial and were transferred to fresh food every other day. Dead flies were counted daily. At least three independent experiments were performed and combined into a single survival curve generated in GraphPad Prism software; individual experiments showed comparable results. The average number of individuals was more than 500 for each genotype and replicate.

Pathogen load measurement

Single flies were homogenized in PBS using a motorized plastic pestle in 1.5 ml tubes. Bacteria were plated in spots onto TSB (*S. pneumoniae*) agar plates containing streptomycin in serial dilutions and incubated overnight at 37°C before manual counting. Pathogen loads of 16 flies were determined for each genotype and treatment in each experiment; at least three independent infection experiments were conducted and the results were combined into one graph (in all presented cases, individual experiments showed comparable results).

Isolation of macrophages

GFP-labeled macrophages were isolated from Crq > Gal4 UAS-eGFP male flies using fluorescence-activated cell sorting (FACS; Krejčová et al, 2019). Approximately 200 flies were anesthetized with CO₂, washed in PBS, and homogenized in 600 ml of PBS using a pestle. The homogenate was sieved through a nylon cell strainer (40 μm).

This strainer was then additionally washed with 200 μl of PBS, which was added to the homogenate subsequently. The samples were centrifuged (3 min, 4°C, 3,500 rpm) and the supernatant was washed with ice-cold PBS after each centrifugation (three times). Before sorting, samples were transferred to FACS polystyrene tubes using a disposable bacterial filter (50 μm, Sysmex) and macrophages were sorted into 100 μl of PBS using an S3™ Cell Sorter (BioRad). Isolated cells were verified by fluorescence microscopy and differential interference contrast. Different numbers of isolated macrophages were used in different subsequent analyses. To this end, different numbers of flies were used for their isolation, specifically 90 flies were used to isolate 20,000 macrophages for qPCR analysis; approximately 160 flies were used to isolate 50,000 macrophages for metabolic analysis; approximately 300 flies were used to isolate 100,000 and 200,000 macrophages for lipidomic and transcriptomic analyses.

Gene expression analysis

Gene expression analyses were performed on several types of samples: six whole flies, six thoraxes, six fat bodies, or 20,000 isolated macrophages. For a description of the dissection procedure see Appendix Fig S25. Macrophages were isolated by a cell sorter (S3e Cell Sorter, BioRad) as described previously (Krejčová et al, 2019) while dissections were made in PBS, transferred to TRIzol Reagent (Invitrogen), and homogenized using a DEPC-treated pestle. Subsequently, RNA was extracted by TRIzol Reagent (Invitrogen) according to the manufacturer's protocol. Superscript III Reverse Transcriptase (Invitrogen) primed by oligo(dT)₂₀ primer was used for reverse transcription. Relative expression rates for particular genes were quantified on a 384CFX 1000 Touch Real-Time Cycler (BioRad) using the TP 2x SYBR Master Mix (Top-Bio) in three technical replicates with the following protocol: initial denaturation—3 min at 95°C, amplification—15 s at 94°C, 20 s at 56°C, 25 s at 72°C for 40 cycles. Melting curve analysis was performed at 65–85°C/step 0.5°C. The primer sequences are listed in the Key Resources Table. The qPCR data were analyzed using double delta Ct analysis, and the expressions of specific genes were normalized to the expression of Ribosomal protein 49 (Rp49) in the corresponding sample. The relative values (fold change) to control are shown in the graphs.

Metabolite measurement

To measure metabolite concentration, isolated macrophages, whole flies, fat bodies, or hemolymph (circulation) were used. Hemolymph was isolated from 25 adult males by centrifugation (14,000 rpm,

5 min) through a silica-gel filter into 50 μ l of PBS. For measurement of metabolites from whole flies, five flies were homogenized in 200 μ l of PBS and centrifuged (3 min, 4°C, 8,000 rpm) to discard insoluble debris. 50,000 macrophages were isolated by cell sorter (S3e Cell Sorter, BioRad) as described in the section Isolation of macrophages. For analysis of fat body metabolites, the fat body from six flies was dissected and homogenized in ice-cold PBS. Fraction of fat body was used for quantification of carbohydrates and part was used for isolation of lipid fraction by adapted Bligh and Dyer method for assaying of cholesterol, cholesteryl-ester, and triglycerides. The concentration of metabolites was normalized per protein in the sample. Half of all samples were used for the quantification of proteins. Samples for glucose, glycogen, trehalose, and glyceride measurement were denatured at 75°C for 10 min, whereas samples for protein quantification were frozen immediately at -80°C . Glucose was measured using a Glucose (GO) Assay (GAGO-20) Kit (Sigma) according to the manufacturer's protocol. The colorimetric reaction was measured at 540 nm. For glycogen quantification, a sample was mixed with amyloglucosidase (Sigma) and incubated at 37°C for 30 min. A Bicinchoninic Acid Assay (BCA) Kit (Sigma) was used for protein quantification according to the supplier's protocol and the absorbance was measured at 595 nm. Cholesterol and cholesteryl esters were measured on isolated lipid fractions by using Cholesterol/Cholesteryl Ester Quantitation Kit (Sigma) according to the supplier's protocol. Glycerides were measured using a Triglyceride quantification Colorimetric/Fluorometric Kit (Sigma). For trehalose quantification, a sample was mixed with trehalase (Sigma) and incubated at 37°C for 30 min. Samples for metabolite concentration were collected from three independent experiments.

Staining of lipid droplets

Flies were dissected in Grace's Insect Medium (Sigma) and subsequently stained with DAPI and Cell Brite Fix Membrane Stain 488 (Biotium) diluted with Grace's Insect Medium according to the manufacturer's protocol at 37°C. Tissues were washed in PBS and then fixed with 4% PFA (Polysciences). After 20 min, the tissues were washed in PBS and pre-washed with 60% isopropanol. Dissected abdomens were then stained with OilRedO dissolved in 60% isopropanol for 10 min. The tissues were then washed with 60% isopropanol and mounted in an Aqua Polymount (Polysciences). Tissues were imaged using an Olympus FluoView 3000 confocal microscope (Olympus). The content of lipids in adipose tissue and the size of lipid droplets were analyzed using Fiji software. Flies for the analysis of lipid droplets in the fat body were collected from three independent experiments and representative images are shown.

Lipidomic analysis

Fat bodies from six flies and one hundred thousand isolated macrophages were obtained for each analyzed group. Tissue lipid fraction was extracted by 500 μ l of cold chloroform: methanol solution (v/v; 2:1). The samples were then homogenized by a Tissue Lyser II (Qiagen, Prague, Czech Republic) at 50 Hz, -18°C for 5 min and kept further in an ultrasonic bath (0°C, 5 min). Further, the mixture was centrifuged at 10,000 rpm at 4°C for 10 min followed by the removal of the supernatant. The extraction step was repeated under the same conditions. The lower layer of pooled supernatant was

evaporated to dryness under a gentle stream of Argon. The dry total lipid extract was re-dissolved in 50 μ l of chloroform: methanol solution (v/v; 2:1) and directly measured using previously described methods (Bayley et al, 2020). Briefly, high-performance liquid chromatography (Accela 600 pump, Accela AS autosampler) combined with mass spectrometry LTQ-XL (all Thermo Fisher Scientific, San Jose, CA, USA) were used. The chromatographic conditions were as follows: Injection volume 5 μ l; column.

Gemini 3 μM C18 HPLC column (150 \times 2 mm ID, Phenomenex, Torrance, CA, USA) at 35°C; the mobile phase (A) 5 mM ammonium acetate in methanol with ammonia (0.025%), (B) water and (C) isopropanol: MeOH (8:2); gradient change of A:B:C as follows: 0 min: 92:8:0, 7 min: 97:3:0, 12 min: 100:0:0, 19 min: 93:0:7, 20–29 min: 90:0:10, 40–45 min: 40:0:60, 48 min: 100:0:0, and 50–65 min: 92:8:0 with flow rate 200 μ l/min. The mass spectrometry condition: positive (3 kV) and negative (-2.5 kV) ion detection mode; capillary temperature 200°C. Eluted ions were detected with full scan mode from 200 to 1,000 Da with the collisionally induced MS2 fragmentation (NCE 35). Data were acquired and processed by means of XCalibur 4.0 software (Thermo Fisher). The corrected areas under individual analytical peaks were expressed in percentages assuming that the total area of all detected is 100%. Lipidomics data were subsequently analyzed in the online platform LipidSuite (<https://suite.lipid.org/>; Mohamed & Hill, 2021). Data were inputted by the K-Nearest Neighbors method (KNN), and normalization was performed by the PQN algorithm. Subsequently, data were explored by PCA and OPLS-DA methods. Differential analysis of lipidomic data was done by univariate analysis and visualized in Volcano plots.

Immunostaining

Flies were dissected in ice-cold PBS and fixed with 4% PFA in PBS (Polysciences) for 20 min. After three washes in PBS-Tween (0.1%), nonspecific binding was blocked by 10% NGS in PBS for 1 h at RT. Tissues were then incubated with primary antibodies (for NimC1: Mouse anti-NimC1 antibody P1a + b, 1:100, kindly provided by Istvan Ando (Kurucz et al, 2007); for Foxo: Rabbit anti-Foxo, CosmoBio, 1:1,000; for tGPH: Rabbit anti-GFP, ABfinity, 1:100) at 4°C overnight. After washing the unbound primary antibody (three times for 10 min in PBS-Tween), the secondary antibody was applied at a dilution of 1:250 for 2 h at RT (Goat anti-Mouse IgG (H + L) Alexa 555, Invitrogen or Goat anti-Rabbit IgG (H + L) Cy2, Jackson-ImmunoResearch). Nuclei were stained with DAPI. Tissues were mounted with Aqua Polymount (Polysciences). Tissues were imaged using an Olympus FluoView 3000 confocal microscope (Olympus) and images were reconstructed using Fiji software. Foxo localization was detected by Plot-Profile analysis using Fiji software. For tGPH activity, confocal images were analyzed by using a plot profile (FIJI) under an arbitrarily defined line connecting two nuclei of neighboring cells and crossing the membrane in the middle. The ratio between cytosolic and membrane signals is displayed in the plot.

Incorporation of ^{13}C free fatty acids

For assaying ^{13}C -FFA distribution post-infection, males were fed standard fly food covered on its surface with 50 μ l ^{13}C Fatty Acid

Mix (Cambridge Isotope Laboratories), 5 mg/ml in chloroform per each vial for 5 h. After 5 h FFAs can be detected in the gut, but are not incorporated into other body compartments (as documented by Bodipy-labeled FFAs). Thereafter, the flies were split into control and experimental groups and injected with buffer or *S. pneumoniae*, and transferred to a fresh vial containing unlabeled food. After 24 h, six guts and six fat bodies were dissected in PBS and 50,000 macrophages were isolated by cell sorter from 160 individuals. Lipid fraction from the samples was isolated through the standard Bligh and Dyer procedure and free fatty acids were liberated from complexes by a lipase from *Aspergillus niger*. Homogenized and filtered chloroform extracts (100 μ l) were put in glass inserts in 2 ml chromatographic vials and their ^{13}C enrichment was analyzed compound-specific. 1 μ l was injected in a split/splitless injector of a gas chromatograph, GC (Trace 1310, Thermo, Bremen, Germany), injector at 250°C. The injection was splitless for 1.5 min, then split with flow 100 ml/min for the next 1 min, and 5 ml/min (gassaver) for the rest of the analysis. Semipolar capillary column Zebron, ZB-FFAP (Phenomenex, Torrance CA, USA, 30 m \times 0.25 mm \times 0.25 μ m film thickness) with a flow rate of 1.5 ml/min of helium was used as a carrier. The temperature program was: 50°C during injection and for the next 2 min, then 50–200°C with a slope of 30°C/min, 200–235°C with a slope of 3°C/min, and hold at 235°C for the rest 32 min (total run time ca 51 min). Eluting compounds were oxidized to CO_2 via IsoLink II interphase (Thermo, Bremen, Germany) at 1000°C and introduced to continuous-flow isotope ratio MS (Delta V Advantage, Thermo, Bremen, Germany). Compounds were identified using retention times of fatty acid standards. ^{13}C sample abundance was expressed in At-% ^{13}C and “ ^{13}C excess” calculated as follow:

$$^{13}\text{C excess} = \frac{A_{13\text{Cs}} - A_{13\text{Cn}}}{A_{13\text{Cs}}}$$

where $A_{13\text{Cs}}$ is the absolute ^{13}C abundance of labeled samples and $A_{13\text{Cn}}$ absolute ^{13}C abundance of natural lipids.

Transcriptomic analysis

For transcriptomic analysis, macrophages from flies infected by *S. pneumoniae* or injected with PBS were isolated by cell sorter as described in the section “Isolation of macrophages”. Two hundred thousand macrophages were used for the isolation of RNA by TRIzol (Ambion). Sequencing libraries were prepared by using siTOOLS riboPOOL *D. melanogaster* RNA kit (EastPort) followed by subtraction of ribosomal fraction by NEBNext Ultra II Directional RNA kit (Illumina). The quality of prepared RNA libraries was assayed by Bioanalyzer and all samples reached a RIN score over the threshold of 7. Sequencing analysis was performed by using the NovaSeq instrument (Illumina). Raw sequencing data were processed by standard bioinformatics workflow for trimming barcodes and adapters. Trimmed reads were aligned to reference *D. melanogaster* genome BDGP6.95 (Ensembl release). Trimming, mapping, and analysis of quality were performed in CLC Genomic Workbench 21.0.5 software via standard workflow for RNA-seq and differential gene expression analysis. A subsequent search of transcriptomic data for enhanced and silenced pathways and biological processes was done by using TCC (Sun et al, 2013), and iDep94 (Ge et al, 2018) platforms combined with String and FlyMine databases.

Chip-qPCR assay

The Pro-A *Drosophila* CHIP Seq Kit (Chromatrap) was used to co-immunoprecipitate genomic regions specifically bound by the transcription factor HIF1 α . A transgenic fly strain carrying the Hif1 α protein fused to GFP (BDSC: 42672) was used for this purpose. The procedure was performed according to the supplier's instructions. Briefly, the slurry was prepared by homogenizing 10 infected or PBS-injected males in three biological replicates. The Rabbit Anti-GFP antibody (ABfinity) was bound to the chromatographic column. Genomic DNA was fragmented to an approximate size of 500 bp by three cycles of 60-s sonication. The fragment size was verified by gel electrophoresis. All samples were tested with positive and negative controls. The amount of precipitated genomic fragments was normalized to the number of fragments in the slurry before precipitation. The ImpL2-RA promoter sequence was covered with seven primer pairs corresponding to the 500-bp bins upstream of the transcription start site previously assessed in the *in silico* analysis. The genomic region of *S*-adenosylmethionine synthetase was used as a negative control since it does not contain any sequences of hypoxia response elements. Primer sequences are listed in the Key Resources Table. The amount of HIF1 α -bound regions of the ImpL2 promoter was quantified on a 96CFX 1000 Touch Real-Time Cycler (BioRad) using TP 2 \times SYBR Master Mix (Top-Bio) in three technical replicates with the following protocol: initial denaturation—3 min at 95°C, amplification—15 s at 94°C, 20 s at 56°C, 25 s at 72°C for 40 cycles. Melting curve analysis was performed at 65–85°C/step 0.5°C. The qPCR data were analyzed using double delta Ct analysis.

Phagocytic activity

To analyze the phagocytic rate, flies were infected with 20,000 *S. pneumoniae* and after 24 h, they were injected with 50 nl of pHrodo™ Red *S. aureus* (Thermo Fischer Scientific). After 1 h, the abdomens of flies were dissected in PBS and then fixed for 20 min with 4% PFA. Aqua Polymount (Polysciences) was used to mount the sample. Macrophages were imaged using an Olympus FluoView 3000 confocal microscope and red dots depicting phagocytic events were manually counted per cell.

Lipoprotein uptake

To analyze lipoprotein uptake by *Drosophila* macrophages, Buff injected or infected Crq > GFP flies were injected at 24 hpi with pHrodo™ Red LDL (Invitrogen) into the ventrolateral side of the abdomen using an Eppendorf Femtojet microinjector. After 1 h, the fly abdomens were opened in PBS and subsequently fixed for 20 min with 4% PFA in PBS (Polysciences). Aqua Polymount (Polysciences) was used to mount the sample. Macrophages were imaged using an Olympus FluoView 3000 confocal microscope. LDL pHrodo signal was counted manually from 10 flies for each group.

THP-1 cell lines

THP-1 cells were cultured at 37°C, 5% CO_2 , in RPMI-1640 medium (Sigma), supplemented with 2 mM glutamine (Applichem), 2 g/l sodium bicarbonate (J&K Scientific), 10% FBS (Biosera) and 100 mg/l streptomycin (Sigma). Prior to the experiment, cells were

transferred to 24-well plates at 10^5 cells/well in four biological replicates. THP-1 cells were activated with phorbol-12-myristate-13-acetate (200 ng/ml, MedChemExpress). After 24 h, *S. pneumoniae* bacteria were added (MOI 50 bacteria/macrophage) or LPS (100 ng/ml; and the plate was centrifuged briefly (2 min, 200 g). Following 6-h incubation, the cells were washed with RPMI-1640 medium, and fresh RPMI-1640 supplemented with gentamycin (0.1 mg/ml, Sigma) was added. After 1 h incubation, the medium was replaced with RPMI-1640 supplemented with penicillin–streptomycin (1%, Biosera). After another 17 h, the cells were harvested into TRIzol Reagent (Invitrogen) followed by RNA isolation. In experiments with Hif1 α agonist (DMOG—50 mg/ml) and antagonist (KC7F2—25 mg/ml), the Hif1 α -affecting drugs were administered 24 h before exposure of cells to LPS. DMSO was used instead of drug treatments in controls. For quantification of IGFBP7 concentration, the media were harvested and diluted 1:10. IGFBP7 protein level was quantified according to the manufacturer's protocol (Human IGFBP7/Igfbp Rp1 ELISA Kit PicoKine, BosterBio).

Expression analysis of IGFBP7 in mice and human LMs and transcriptomic analysis of hepatocytes

Isolation of RNA, real-time qPCR and RNA library preparation
RNA extraction and purification were performed by using TRIzol reagent according to the manufacturer's instructions (Thermo Fisher Scientific, 15596018). For real-time qPCR, cDNA was synthesized from 0.5 μ g of total RNA with the iScript cDNA Synthesis kit (Bio-Rad) according to the manufacturer's instructions. Synthesized cDNA along with forward and reverse primers and Advanced Universal SYBR Green Supermix was run on a CFX96 Real-Time PCR System (Bio-Rad). β -actin (Actb) was used as a reference gene in mice and humans. RNA integrity was determined with an Agilent Bioanalyzer. Libraries from mouse RNA were prepared with the TruSeq Stranded mRNA kit (Illumina) and libraries from human RNA were prepared with the SMARTer Ultra-Low RNA kit (Clontech). The concentration of the indexed libraries was determined by real-time qPCR using the Universal Kapa Library Quantification kit (KAPA Biosystems). Final libraries were normalized and sequenced on an Illumina HiSeq 2000 sequencer.

Isolation of liver macrophages and hepatocytes from mice

Liver macrophages and hepatocytes were isolated as previously described. Briefly, the livers of anesthetized mice were first perfused with calcium-free Hank's balanced salt solution (HBSS), followed by collagenase digestion. After digestion, hepatocytes were released by mechanical dissociation of the lobes and underwent several steps of filtration with calcium-containing HBSS and centrifugation at 50 g for 3 min. The resulting hepatocyte pellet was washed twice and plated. The supernatant containing non-parenchymal cells was loaded onto a Percoll gradient (25 and 50%) and centrifuged at 2,300 rpm for 30 min at 4°C. The interphase ring with enriched liver macrophages was collected. Cells were then plated for 30 min and washed twice before RNA or protein was extracted for subsequent analyses.

Isolation of liver macrophages from humans

Freshly obtained liver biopsies were cut into small pieces and immediately digested in RPMI medium containing collagenase II

(0.25 mg/ml; Sigma, C6885) and DNase I (0.2 mg/ml; Roche, 1010415900) at 37°C for 30 min. Single-cell suspensions were filtered through a cell strainer (75 μ m) and centrifuged at 50 g for 3 min. The supernatant containing non-parenchymal cells was loaded onto a Percoll gradient and liver macrophages were isolated as described above. For details concerning this experiment view part Methods and Supplementary Methods in (Tencerova, 2020).

GeRP administration by intravenous injection in vivo

Glucan shells (GS) were prepared by using a previously published protocol (Tesz et al, 2011). Briefly, 100 g of baker's yeast (*Saccharomyces cerevisiae*, SAF-Mannan, Biospringer) was heated at 80–85°C for 1 h in 1 l of NaOH (0.5 M) to hydrolyze the outer cell wall and intracellular components. This step was repeated after a water wash. Following centrifugation (15,000 g for 10 min), the resulting pellet was washed at least three times with water and three times with isopropanol. This yielded approximately 3–4 mg of purified, porous 2- to 4- μ m, hollow β 1,3-d-glucan particles. One gram of empty β 1,3-d-glucan particles resuspended in 100 ml of sodium carbonate buffer was then labeled with FITC by incubation with 10 mg of 5-(4,6-dichlorotriazinyl) amino fluorescein (DTAF) dissolved in 10 ml of ethanol for 16 h protected from light. Labeled GS were then washed at least five times in water. Wild-type mice fed an HFD for 8 weeks were first randomized according to their body weight and glucose tolerance. Mice were then treated with 12.5 mg/kg GeRPs loaded with siRNA (247 μ g/kg) and Endoport (2.27 mg/kg). Mice received six doses of fluorescently labeled GeRPs by intravenous injection over 15 days. For details concerning this experiment view part Methods and Supplementary Methods in (Tencerova, 2020).

Human liver spheroids and IGFBP7 administration

Cryopreserved primary human hepatocytes (Bioreclamation IVT) were cultured in 96-well ultra-low attachment plates (Corning) as previously described (Tencerova, 2020). Briefly, 1,500 cells/well were seeded in culture medium (Williams' medium E containing 11 mM glucose supplemented with 2 mM l-glutamine, 100 U/ml penicillin, 100 μ g/ml streptomycin, 10 μ g/ml insulin, 5.5 μ g/ml transferrin, 6.7 ng/ml sodium selenite, and 100 nM dexamethasone) with 10% FBS as described previously. Following aggregation, cells were transitioned into serum-free Williams' medium E (PAN-Biotech) containing 5.5 mM glucose and 1 nM insulin for 7 days. On the day of the treatment, after 2 h of starvation, cells were exposed to recombinant human IGFBP7 (200 ng/ml; K95R, R&D Systems, 1334-B7-025 or wild type, R&D Systems, custom made) or insulin (100 nM) as reported previously (Tencerova, 2020). Protein was collected for immunoprecipitation assays and western blot analysis. Spheroid viability was controlled by ATP quantification using the CellTiter-Glo Luminescent Cell Viability Assay (Promega) with values normalized to the corresponding vehicle control on the same plate. No statistically significant differences in viability were observed between IGFBP7- and vehicle-treated controls when using heteroscedastic two-tailed t-tests ($n = 8$ spheroids) and $P < 0.05$ as the significance threshold (Morgantini et al, 2019). For analysis of lipoprotein production, the media were harvested and the level of LDL and VLDL was measured according to the manufacturer's protocol (Human Very Low-Density Lipoprotein [LDL] and Human

Very Low-Density Lipoprotein [VLDL] Elisa Kit, respectively; Abbexa).

Statistics

Box plots, heat maps, and donut graphs were generated in GraphPad Prism9 software. 2way ANOVA was used for multiple comparison testing, followed by Tukey's or Šidak's multiple comparisons tests. Ordinary one-way ANOVA followed by Dunnett's multiple comparisons test was used to compare the results with the corresponding control group. An unpaired t-test was used for pair reciprocal comparison of datasets. Bar plots display mean and standard deviation. The statistical significance of the test is depicted in plots by using the following GP code ($P < 0.05 = *$; $P < 0.001 = **$; $P < 0.0001 = ***$). Normality and homogeneity of variations were tested by the Anderson-Darling test, D'Agostino

Pearson's test, and Shapiro–Wilk test. Data showing significant deviances from normal distribution was normalized by Log₂-transformation. For survival analyses, the data sets were compared by Log-rank and Grehan-Breslow Wilcoxon test. For complex differential analysis of omics data, we processed the data through an online platform for transcriptomic data analysis TCC (Sun et al, 2013)—based on the following R-packages (edgeR, DESeq, baySeq, and NBPSec), iDep95 (Ge et al, 2018)—based on the following R-packages (limma, DESeq2, GSEA, PAGE, GACE, RactomePA, Kallisto, Galaxy) followed by subsequent analysis of assigned biological processes in Kegg pathways (www.genome.jp/kegg/pathway) and Flymine databases (<https://www.flymine.org/flymine>). An online platform for lipidomic data analysis (LipidSuite (Mohamed & Hill, 2021) – based on the R-package lipidr) was employed for differential comparison of obtained lipidomic datasets.

List of primers and other nucleotide sequences used in this work:

4EBP Forward: CCATGATCACCAGGAAGTTGTCA	CG8846	FBgn0261560
4EBP Reverse: AGCCCGCTCGTAGATAAGTTTGGT	CG8846	FBgn0261560
EIF-4E Forward: AAGAAGAACATTCGCCCATGT	CG4035	FBgn0015218
EIF-4E Reverse: GGAAGTCCGACGAAACAAC	CG4035	FBgn0015218
MTP Forward: GAATCGAAATGCCAGACG	CG9342	FBgn0266369
MTP Reverse: AACGTTGTTTGTGAGAAGC	CG9342	FBgn0266369
HSL Forward: CAGTCTACGAGATTCACGG	CG11055	FBgn0034491
HSL Reverse: GGCTTCGTTGGATAACATTGTG	CG11055	FBgn0034491
Bmm Forward: CACCGCGCCGAATGAATGTATAA	CG5295	FBgn0036449
Bmm Reverse: TTCAATCACTGTTTGTGCGGTCGGC	CG5295	FBgn0036449
apoLTP Forward: TGGGTGGATTGAAGCCACAG	CG15828	FBgn0032136
apoLTP Reverse: TGAGTGGATTTCTCTCACTGC	CG15828	FBgn0032136
apoLPP Forward: TTGGAATCCTAGCTTCTGTGCT	CG11064	FBgn0087002
apoLPP Reverse: AGTCATAGTAGTTGCCGGTAT	CG11064	FBgn0087002
Hif1a Forward: AGCCATCCATCTATGTGCC	CG45051	FBgn0266411
Hif1a Reverse: TCAAACGCCACGAGACGAC	CG45051	FBgn0266411
Nlp2 Forward: ATGGCCAAAGCTCGCAATTTG	CG11051	FBgn0287423
Nlp2 Reverse: TCAACCTTCTTCGCGTCCAA	CG11051	FBgn0287423
Rp49 Forward: AAGCTGTGCGACAATGGCG	CG7939	FBgn0002626
Rp49 Reverse: GCACGTTGTGCCACGGAAC	CG7939	FBgn0002626
ImpL2 Forward: TTCGCGTTCCTGGGACCC	CG15009	FBgn0001257
ImpL2 Reverse: GCGCGTCCGATCGTCGATA	CG15009	FBgn0001257
Dlp3 Forward: ACCAAAAAGACCCGGCTCG	CG14167	FBgn0036046
Dlp3 Reverse: TGCAGCTGTCTTAACGCC	CG14167	FBgn0036046
Dlp6 Forward: CGGAATACGAACAGAGACGC	CG8167	FBgn0044047
Dlp6 Reverse: ACTGTTGGGAAATACATCGCC	CG8167	FBgn0044047
Upd3 Forward: AGAACACCTGCAATCTGAAGC	CG33542	FBgn0053542
Upd3 Reverse: TCITGGTCTCACTGTGGCC	CG33542	FBgn0053542
Egr Forward: AGCTGATCCCCCTGGTTTTG	CG12919	FBgn0033483
Egr Reverse: GCCAGATCGTTAGTGCGAGA	CG12919	FBgn0033483
Reg 1 Forward: GAGCAAATGGACTCTACAGG	3L:4221582..4238579	

Reg 1 Reverse: GGGGAGCAACAAGTAACTCG	3L:4221582..4238579	
Reg 2 Forward: CTTTGGGCTGATAATCCGG	3L:4221582..4238579	
Reg 2 Reverse: TACATATATCCATAGAACCACG	3L:4221582..4238579	
Reg 5 Forward: AGCCATCCATCTATGTGCC	3L:4221582..4238579	
Reg 5 Reverse: TCAAACGCACGAGACGAC	3L:4221582..4238579	
Reg 7 Forward: GCAACTCAAATCTTCAAACCTCG	3L:4221582..4238579	
Reg 7 Reverse: TCGGACCACTTGTCTTGTGT	3L:4221582..4238579	
Reg 9 Forward: GAACCGTCGCCCTTCCAG	3L:4221582..4238579	
Reg 9 Reverse: TGCCATGCCATTTGTTTGC	3L:4221582..4238579	
Sam-S Forward: CAAATCAGCGACGCTATCTTGG	CG2674	FBgn0005278
Sam-S Reverse: TGTCTCACGAACAACCTTCTGG	CG2674	FBgn0005278
Human IGFBP7 Forward: GCCATCACCCAGGTCAGCAAG	GC04M057030	
Human IGFBP7 Reverse: GGATTCGGATGACCTCACAGCT	GC04M057030	
Human ACTB Forward: ATTGCCGACAGGATGCAGAA	GC07M005527	
Human ACTB Reverse: GCTGATCCACATCTGCTGGAA	GC07M005527	
Murine IGFBP7 Forward: TGCCCTCCATGAAATACCAC	ENSMUSG00000036256	
Murine IGFBP7 Reverse: GGCTGTCTGAGAGCACCTTT	ENSMUSG00000036256	
Murine Actb Forward: TCTACAATGAGCTGCGTGTGG	ENSMUSG00000029580	
Murine Actb Reverse: GTACATGGCTGGGGTGTGAA	ENSMUSG00000029580	
Murine 36B4 Reverse: TCCAGGCTTTGGGCATCA	ENSMUSG00000067274	
Murine 36B4 Reverse: CTTTATCAGCTGCACATCACTCAGA	ENSMUSG00000067274	
IGFBP7-si 1 GCAAGAGCGGAAGGUAA	ENSMUSG00000036256	
IGFBP7-si 2 GGAGGACGCGGAGAGUAA	ENSMUSG00000036256	
IGFBP7-si 3 AGGUGAAGGUGCUCAGUAA	ENSMUSG00000036256	

Genotypes of experimental models

Figure 1

(A–F) Hml>Gal4; TubGal80^{TS} x TRiP^{control} refers to w¹¹¹⁸/+; HmlΔ-Gal4/+; P{tubPGal80ts}/TRiP^{control}
 Hml>Gal4; TubGal80^{TS} x W^{control} corresponds to w¹¹¹⁸/w¹¹¹⁸; HmlΔ-Gal4/+; P{tubPGal80ts}/+
 (H, I) Crq>Gal4; UAS2xGFPxTRiP^{control} refersto +/+; +/+; Crq-Gal4, UAS-2xeGFP/TRiP^{control}
 Crq>Gal4; UAS2xGFP x W^{control} corresponds to w¹¹¹⁸/w¹¹¹⁸; Crq-Gal4, UAS-2xeGFP/+

Figure 2

(A–C) Crq>Gal4; UAS-GFP correspondsto +/+; +/+; Crq-Gal4, UAS-2xeGFP/Crq-Gal4, UAS-2xeGFP
 (D) ImpL2>mCherry corresponds to w¹¹¹⁸/w¹¹¹⁸; 20xUAS-6xmCherry/+; ImpL2-Gal4/+
 (E) Crq>Gal4; UAS-GFP x W^{control} correspondsto w¹¹¹⁸/+; +/+; Crq-Gal4,UAS-2xeGFP/+
 Crq>Gal4; UAS-GFP x Hif1α^{RNAi} corresponds to w¹¹¹⁸/+; +/+; UAS-Hif1α^{RNAi}/Crq-Gal4UAS-2xeGFP
 (F) Crq>Gal4; UAS-SimaGFP refers to w¹¹¹⁸/w¹¹¹⁸; +/PBac {sima-GFP.AC.FPTB}VK00037; Crq-Gal4 UAS-2xeGFP/+

Figure 3

(A–F) Hml>Gal4; TubGal80^{TS} x TRiP^{control} refers to w¹¹¹⁸/+; HmlΔ-Gal4/+; P{tubPGal80ts}/TRiP^{control}
 Hml>Gal4; TubGal80^{TS} x W^{control} corresponds to w¹¹¹⁸/w¹¹¹⁸; HmlΔ-Gal4/+; P{tubPGal80ts}/+
 Hml>Gal4; TubGal80^{TS} > ImpL2^{CDS} corresponds to w¹¹¹⁸/w¹¹¹⁸; HmlΔ-Gal4/+; P{tubPGal80ts}/UAS-ImpL2^{CDS}
 Hml>Gal4; TubGal80^{TS} > ImpL2^{RNAi} correspondsto w¹¹¹⁸/+; HmlΔ-Gal4/UAS-ImpL2^{RNAi}; P{tubPGal80ts}/+

Figure 4

(A) Hml>Gal4; TubGal80^{TS} x TRiP^{control} refers to w¹¹¹⁸/+; HmlΔ-Gal4/+; P{tubPGal80ts}/TRiP^{control}
 Hml>Gal4; TubGal80^{TS} x W^{control} corresponds to w¹¹¹⁸/w¹¹¹⁸; HmlΔ-Gal4/+; P{tubPGal80ts}/+
 Hml>Gal4; TubGal80^{TS} > ImpL2^{CDS} corresponds to w¹¹¹⁸/w¹¹¹⁸; HmlΔ-Gal4/+; P{tubPGal80ts}/UAS-ImpL2^{CDS}
 Hml>Gal4; TubGal80^{TS} > ImpL2^{RNAi} correspondsto w¹¹¹⁸/+; HmlΔ-Gal4/UAS-ImpL2^{RNAi}; P{tubPGal80ts}/+
 (B–D) Hml>Gal4 TubGal80^{TS} xW^{control} correspondsto w¹¹¹⁸/w¹¹¹⁸; HmlΔ-Gal4P{tubPGal80ts}/+; +/+
 Hml>Gal4 TubGal80^{TS} x ImpL2^{CDS} correspondsto w¹¹¹⁸/w¹¹¹⁸; HmlΔ-Gal4P{tubPGal80ts}/+; UAS-ImpL2^{CDS}/+

Hml>Gal4 TubGal80^{TS} x foxo^{BG01018} ImpL2^{CDS} refers to w¹¹¹⁸/w¹¹¹⁸; HmlΔ-Gal4 P{tubPGal80ts}/+; P{w[+mGT]=GT1} foxo^{BG01018} UAS-ImpL2^{CDS}/+

Figure 5

(A, B) Hml>Gal4 TubGal80^{TS}; tGPH-GFPx w¹¹¹⁸ corresponds to w¹¹¹⁸/w¹¹¹⁸; HmlΔ-Gal4P{tubPGal80ts}/+; tGPH/+ Hml>Gal4 TubGal80^{TS}; tGPH-GFPx ImpL2^{CDS} corresponds to w¹¹¹⁸/w¹¹¹⁸; HmlΔ-Gal4 P{tubPGal80ts}/+; tGPH/UAS-ImpL2^{CDS} Hml>Gal4 TubGal80^{TS}; tGPH-GFPx ImpL2^{RNAi} corresponds to w¹¹¹⁸/w¹¹¹⁸; HmlΔ-Gal4 P{tubPGal80ts}/+; tGPH/ImpL2^{RNAi} (C, D) FB>Gal4 TubGal80^{TS}xW¹¹¹⁸ correspondsto w¹¹¹⁸/+; FB-Gal4/+; P{tubPGal80ts}/+ FB>Gal4 TubGal80^{TS}x TRiP^{control} refersto +/+; FB-Gal4/+; P{tubPGal80ts} / TRiP^{control} FB>Gal4 TubGal80^{TS}x InR^{CA} correspondsto+/+; FB-Gal4/+; P{tubPGal80ts}/P{w[+mC]=UAS-InR.K1409A}3 FB>Gal4 TubGal80^{TS} x InR^{DN} refers to +/+; FB-Gal4/P{w[+mC]=UAS-InR.A1325D}2; P{tubPGal80ts}/+ FB>Gal4 TubGal80^{TS} x PTEN^{CDS} correspondsto to +/+; FB-Gal4/+; P{tubPGal80ts}/M{UAS-Pten.ORF.3xHA}ZH-86Fb Hml>Gal4 TubGal80^{TS} x foxo^{BG01018} ImpL2^{CDS} refers to w¹¹¹⁸/w¹¹¹⁸; HmlΔ-Gal4 P{tubPGal80ts}/+; P{w[+mGT]=GT1} foxo^{BG01018} UAS-ImpL2^{CDS}/+ Hml>Gal4 TubGal80^{TS} x foxo^{BG01018} refers to w¹¹¹⁸/w¹¹¹⁸; HmlΔ-Gal4P{tubPGal80ts}/+; P{w[+mGT]=GT1}foxo^{BG01018} / P{w[+mGT]=GT1}foxo^{BG01018} (F, G) FB>Gal4 TubGal80^{TS} x TRiP^{control} refers to +/+; FB-Gal4/+; P{tubPGal80ts}/TRiP^{control} FB>Gal4 TubGal80^{TS}x InR^{CA} correspondsto+/+; FB-Gal4/+; P{tubPGal80ts}/P{w[+mC]=UAS-InR.K1409A}3 FB>Gal4 TubGal80^{TS} x Mtp^{RNAi} refers to +/+; FB-Gal4/P{y[+t.7] v[+t1.8]=TRiP.HMC03446}attP40; P{tubPGal80ts}/+ FB>Gal4 TubGal80^{TS}x apoLTP^{RNAi} refersto +/+; FB-Gal4/+; P{tubPGal80ts}/P{y[+t.7]v[+t1.8]=TRiP.HMC03294}attP2 FB>Gal4 TubGal80^{TS} x apoLPP^{RNAi} correspondsto +/+; FB-Gal4/+; P{tubPGal80ts}/P{y[+t.7]v[+t1.8]=TRiP.HM05157}attP2

Figure 6

(A-D) Crq> GFPx ImpL2^{RNAi} refersto w¹¹¹⁸/+; UAS-ImpL2^{RNAi}/+; Crq-Gal4, UAS-2xeGFP/+ Crq> GFP x ImpL2^{CDS} correspondsto w¹¹¹⁸/w¹¹¹⁸; +/+; Crq-Gal4, UAS-2xeGFP/UAS-ImpL2^{CDS} Crq> GFP x TRiP^{control} refers to +/+; +/+; Crq-Gal4,UAS-2xeGFP/TRiP^{control} Crq> GFP x W¹¹¹⁸ corresponds to w¹¹¹⁸/w¹¹¹⁸; Crq-Gal4, UAS-2xeGFP/+ (E-F) Hml>Gal4; TubGal80^{TS} x TRiP^{control} refers to w¹¹¹⁸/+; HmlΔ-Gal4/+; P{tubPGal80ts}/TRiP^{control} Hml>Gal4; TubGal80^{TS} xW^{control} correspondsto w¹¹¹⁸/w¹¹¹⁸; HmlΔ-Gal4/+; P{tubPGal80ts}/+ Hml>Gal4; TubGal80^{TS} x ImpL2^{CDS} corresponds to w¹¹¹⁸/w¹¹¹⁸; HmlΔ-Gal4/+; P{tubPGal80ts}/UAS-ImpL2^{CDS} Hml>Gal4; TubGal80^{TS} x ImpL2^{RNAi} correspondsto w¹¹¹⁸/+; HmlΔ-Gal4/UAS-ImpL2^{RNAi}; P{tubPGal80ts}/+

Figure 7

(A) FB>Gal4 TubGal80^{TS} x LPP^{RNAi} correspondsto +/+; FB-Gal4/+; P{tubPGal80ts}/P{y[+t.7] v[+t1.8]}=TRiP.HM05157}attP2 W^{control} x FB>Gal4 TubGal80^{TS} correspondsto w¹¹¹⁸/+; FB-Gal4/+; P{tubPGal80ts}/+ LPP^{RNAi} x W^{control} correspondsto w¹¹¹⁸/+; +/+; +/P{y[+t.7] v[+t1.8]}=TRiP.HM05157}attP2 (B–D) FB>Gal4 TubGal80^{TS} x LPP^{RNAi} correspondsto +/+; FB-Gal4/+; P{tubPGal80ts}/P{y[+t.7] v[+t1.8]}= TRiP.HM05157} attP2 W^{control} x FB>Gal4 TubGal80^{TS} correspondsto w¹¹¹⁸/+; FB-Gal4/+; P{tubPGal80ts}/+ (E, F) Crq>Gal4; UAS-GFPcorrespondsto +/+; +/+; Crq-Gal4, UAS-2xeGFP/Crq-Gal4, UAS-2xeGFP

Data availability

The datasets produced in this study are available in the following databases:

RNA-Seq data: Gene Expression Omnibus; GSE237617 (<https://www.ncbi.nlm.nih.gov/geo/query/acc.cgi?acc=GSE237617>).

Lipidomic data: DRYAD; DOI: [10.5061/dryad.9zw3r22kw](https://doi.org/10.5061/dryad.9zw3r22kw).

Expanded View for this article is available [online](#).

Acknowledgements

The authors acknowledge funding from the Grant Agency of the Czech Republic to AB (Project 20-14030S and 23-06133S; www.gacr.cz) and to TD (Project 20-09103S; www.gacr.cz). GK was supported by USB Grant Agency (Project 050/2019/P). We thank to Lucie Hradkova for laboratory services, enthusiasm and support, Alena Krejčí-Bruce and Lenka Chodakova for critical comments and inspiring discussions, Pavel Branny and Linda Doubravova for their help with the preparation of the S.p.-GFP strain. We thank to Tracey Hurrel for her assistance in obtaining media from human liver spheroids. We thank to Hana Sehadova, Lucie Pauchova, Jitka Pfliegerova for their help with microscopy imaging. We thank to Hugo Stocker for the ImpL2^{RNAi}, ImpL2^{CDS}, and ImpL2^{RA-Gal4} fly lines, and Marc Dionne for Crq > GFP fly line. Other fly stocks were obtained from the Bloomington Center (Bloomington, IN) and the VDRC (Vienna, Austria). The S.pneumoniae bacterial strain was obtained from Dr. David Schneider. We also thank Petra Berkova and Petr Šimek for the lipidomics service, the Department of Medical Biology (USB) for allowing us to use the S3eBio Radsorter, Biology Centre CAS for allowing us to use a confocal microscope, and a laboratory equipment to maintain human tissue cultures. We are also grateful to developers of Fiji: an open-source platform for biological-image analysis (doi: [10.1038/nmeth.2019](https://doi.org/10.1038/nmeth.2019)), LipidSuite: a suitable platform for lipidomics analysis, TCC: online platform for transcriptomic data processing and iDep94: an alternative online platform for transcriptomic data analysis. Graphical summarizations were done by using BioRender as online graphical platform for making biological schemes.

Author contributions

Gabriela Krejčová: Conceptualization; resources; data curation; formal analysis; supervision; funding acquisition; validation; investigation; visualization; methodology; writing – original draft; project administration;

writing – review and editing. Cecilia Morgantini: Conceptualization; data curation; investigation. Helena Zemanová: Validation; investigation. Volker M Lauschke: Conceptualization; data curation; formal analysis; investigation. Julie Kovářová: Conceptualization; data curation; validation; investigation. Jiří Kubásek: Conceptualization; data curation; validation; investigation. Pavla Nedbalová: Data curation; validation; investigation. Nick Kamps-Hughes: Data curation; formal analysis; validation; investigation. Martin Moos: Conceptualization; data curation; formal analysis; validation; investigation. Myriam Aouadi: Conceptualization; data curation; formal analysis; supervision; validation; investigation. Tomáš Doležal: Resources; data curation; formal analysis; funding acquisition; validation; investigation; project administration. Adam Bajgar: Conceptualization; resources; data curation; formal analysis; supervision; funding acquisition; validation; investigation; visualization; methodology; writing – original draft; project administration; writing – review and editing.

Disclosure and competing interests statement

The authors declare that they have no conflict of interest.

References

- Akhtar DH, Iqbal U, Vazquez-Montesino LM, Dennis BB, Ahmed A (2019) Pathogenesis of insulin resistance and atherogenic dyslipidemia in nonalcoholic fatty liver disease. *J Clin Transl Hepatol* 7: 1–9
- Al-Mansoori L, Al-Jaber H, Prince MS, Elrayess MA (2022) Role of inflammatory cytokines, growth factors and adipokines in adipogenesis and insulin resistance. *Inflammation* 45: 31–44
- Arrese EL, Canavoso LE, Jouni ZE, Pennington JE, Tsuchida K, Wells MA (2001) Lipid storage and mobilization in insects: current status and future directions. *Insect Biochem Mol Biol* 31: 7–17
- Bajgar A, Doležal T (2018) Extracellular adenosine modulates host-pathogen interactions through regulation of systemic metabolism during immune response in *Drosophila*. *PLoS Pathog* 14:e1007022
- Bayley JS, Sørensen JG, Moos M, Košťál V, Overgaard J (2020) Cold acclimation increases depolarization resistance and tolerance in muscle fibers from a chill-susceptible insect, *Locusta migratoria*. *Am J Physiol Integr Comp Physiol* 319:R439–R447
- Bell CC, Lauschke VM, Vorriuk SU, Palmgren H, Duffin R, Andersson TB, Ingelman-Sundberg M (2017) Transcriptional, functional, and mechanistic comparisons of stem cell-derived hepatocytes, HepaRG cells, and three-dimensional human hepatocyte spheroids as predictive in vitro systems for drug-induced liver injury. *Drug Metab Dispos* 45: 419–429
- Brankatschk M, Dunst S, Nemetschke L, Eaton S (2014) Delivery of circulating lipoproteins to specific neurons in the *Drosophila* brain regulates systemic insulin signaling. *Elife* 3:e02862
- Britton JS, Lockwood WK, Li L, Cohen SM, Edgar BA (2002) *Drosophila*'s insulin/PI3-kinase pathway coordinates cellular metabolism with nutritional conditions. *Dev Cell* 2: 239–249
- Canavoso LE, Yun HK, Jouni ZE, Wells MA (2004) Lipid transfer particle mediates the delivery of diacylglycerol from lipophorin to fat body in larval *Manduca sexta*. *J Lipid Res* 45: 456–465
- Chi H (2022) Immunometabolism at the intersection of metabolic signaling, cell fate, and systems immunology. *Cell Mol Immunol* 19: 299–302
- Chow A, Brown BD, Merad M (2011) Studying the mononuclear phagocyte system in the molecular age. *Nat Rev Immunol* 11: 788–798
- Corcoran SE, O'Neill LAJ (2016) HIF1 α and metabolic reprogramming in inflammation. *J Clin Invest* 126: 3699–3707
- DiAngelo JR, Bland ML, Bambina S, Cherry S, Bimbaum MJ (2009) The immune response attenuates growth and nutrient storage in *Drosophila* by reducing insulin signaling. *Proc Natl Acad Sci USA* 106: 20853–20858
- Dionne MS, Schneider DS (2008) Models of infectious diseases in the fruit fly *Drosophila melanogaster*. *Dis Model Mech* 1: 43–49
- Figuerola-Clavevega A, Bilder D (2015) Malignant *Drosophila* tumors interrupt insulin signaling to induce cachexia-like wasting. *Dev Cell* 33: 47–55
- Galvan-Pena S, O'Neill LAJ (2014) Metabolic reprogramming in macrophage polarization. *Front Immunol* 5: 420
- Ganeshan K, Chawla A (2014) Metabolic regulation of immune responses. *Annu Rev Immunol* 32: 609–634
- Ganeshan K, Nikkanen J, Man K, Leong YA, Sogawa Y, Maschek JA, Van Ry T, Chagwedera DN, Cox JE, Chawla A (2019) Energetic trade-offs and hypometabolic states promote disease tolerance. *Cell* 177: 399–413.e12
- Ge SX, Son EW, Yao R (2018) iDEP: an integrated web application for differential expression and pathway analysis of RNA-Seq data. *BMC Bioinformatics* 19: 534
- Grönke S, Beller M, Fellerl S, Ramakrishnan H, Jockle H, Kühnlein RP (2003) Control of fat storage by a *Drosophila* PAT domain protein. *Curr Biol* 13: 603–606
- Hang S, Purdy AE, Robins WP, Wang Z, Mandal M, Chang S, Mekalanos JJ, Watnick PI (2014) The acetate switch of an intestinal pathogen disrupts host insulin signaling and lipid metabolism. *Cell Host Microbe* 16: 592–604
- Honegger B, Galic M, Köhler K, Wittwer F, Brogiolo W, Hafen E, Stocker H (2008) Imp-L2, a putative homolog of vertebrate IGF-binding protein 7, counteracts insulin signaling in *Drosophila* and is essential for starvation resistance. *J Biol* 7: 10
- Izquierdo MC, Shanmugarajah N, Lee SX, Kraakman MJ, Westerterp M, Kitamoto T, Harris M, Cook JR, Gusarova GA, Zhong K et al (2022) Hepatic FoxO links insulin signaling with plasma lipoprotein metabolism through an apolipoprotein M/sphingosine-1-phosphate pathway. *J Clin Invest* 132: e146219
- Kedia-Mehta N, Finlay DK (2019) Competition for nutrients and its role in controlling immune responses. *Nat Commun* 10: 2123
- Koyama T, Rodrigues MA, Athanasiadis A, Shingleton AW, Mirth CK (2014) Nutritional control of body size through FoxO-Ultraspire mediated ecdysone biosynthesis. *Elife* 3:e03091
- Krejčova G, Danielova A, Nedbalova P, Kazek M, Strych L, Chawla G, Tennesen JM, Lieskovska J, Jindra M, Doležal T et al (2019) *Drosophila* macrophages switch to aerobic glycolysis to mount effective antibacterial defense. *Elife* 8:e50414
- Kurucz E, Markus R, Zsomboki J, Folki-Medzihradsky K, Darula Z, Vilmos P, Udvardy A, Krausz I, Lukacsovich T, Gateff E et al (2007) Nimrod, a putative phagocytosis receptor with EGF repeats in *Drosophila* plasmatocytes. *Curr Biol* 17: 649–654
- Kwon Y, Song W, Droujinine IA, Hu Y, Asara JM, Perrimon N (2015) Systemic organ wasting induced by localized expression of the secreted insulin/IGF antagonist ImpL2. *Dev Cell* 33: 36–46
- Lee H-J, Hong W-G, Woo Y, Ahn J-H, Ko H-J, Kim H, Moon S, Hahn T-W, Jung YM, Song D-K et al (2020) Lysophosphatidylcholine enhances bactericidal activity by promoting phagosomal maturation via the activation of the NF- κ B pathway during *Salmonella* infection in mouse macrophages. *Mol Cells* 43: 989–1001
- Liu P, Zhu W, Chen C, Yan B, Zhu L, Chen X, Peng C (2020) The mechanisms of lysophosphatidylcholine in the development of diseases. *Life Sci* 247: 117443
- Martinez BA, Hoyle RG, Yeudall S, Granade ME, Harris TE, Castle JD, Leitinger N, Bland ML (2020) Innate immune signaling in *Drosophila* shifts anabolic

- lipid metabolism from triglyceride storage to phospholipid synthesis to support immune function. *PLoSGenet* 16:e1009192
- Mills CD, Kincaid K, Alt JM, Heilman MJ, Hill AM (2000) M-1/M-2 macrophages and the Th1/Th2 paradigm. *J Immunol* 164: 6166–6173
- Mohamed A, Hill MM (2021) LipidSuite: interactive web server for lipidomics differential and enrichment analysis. *Nucleic Acids Res* 49: W346–W351
- Morgantini C, Jager J, Li X, Levi L, Azzimato V, Sulen A, Bareby E, Xu C, Tencerova M, Nilsson E et al (2019) Liver macrophages regulate systemic metabolism through non-inflammatory factors. *Nat Metab* 1: 445–459
- Newsholme P (2021) Cellular and metabolic mechanisms of nutrient actions in immune function. *Nutr Diabetes* 11: 22
- Oliva-Vilarnau N, Vorrink SU, Ingelman-Sundberg M, Lauschke VM (2020) A 3D cell culture model identifies Wnt/ β -catenin mediated inhibition of p53 as a critical step during human hepatocyte regeneration. *Adv Sci* 7: 2000248
- Owusu-Ansah E, Song W, Perrimon N (2013) Muscle mitohormesis promotes longevity via systemic repression of insulin signaling. *Cell* 155: 699–712
- Palm W, Sampaio JL, Brankatschk M, Carvalho M, Mahmoud A, Shevchenko A, Eaton S (2012) Lipoproteins in *Drosophila melanogaster*—assembly, function, and influence on tissue lipid composition. *PLoSGenet* 8: e1002828
- Rankin LC, Artis D (2018) Beyond host defense: emerging functions of the immune system in regulating complex tissue physiology. *Cell* 173: 554–567
- Remmerie A, Scott CL (2018) Macrophages and lipid metabolism. *Cell Immunol* 330: 27–42
- Roed NK, Viola CM, Kristensen O, Schluckebier G, Norman M, Sajid W, Wade JD, Andersen AS, Kristensen C, Ganderton TR et al (2018) Structures of insect Imp-L2 suggest an alternative strategy for regulating the bioavailability of insulin-like hormones. *Nat Commun* 9: 3860
- Santalla M, Garcia A, Mattiazzi A, Valverde CA, Schiemann R, Paululat A, Hernandez G, Meyer H, Ferrero P (2022) Interplay between SERCA, 4E-BP, and eIF4E in the *Drosophila* heart. *PLoSOne* 17:e0267156
- Sloth Andersen A, Hertz Hansen P, Schiffer L, Kristensen C (2000) A new secreted insect protein belonging to the immunoglobulin superfamily binds insulin and related peptides and inhibits their activities. *J Biol Chem* 275: 16948–16953
- Sun J, Nishiyama T, Shimizu K, Kadota K (2013) TCC: an R package for comparing tag count data with robust normalization strategies. *BMC Bioinformatics* 14: 219
- Tencerova M (2020) Glucan-encapsulated siRNA particles (GeRPs) for specific gene silencing in Kupffer cells in mouse liver. *Methods Mol Biol* 2164: 65–73
- Tencerova M, Aouadi M, Vangala P, Nicoloso SM, Yawe JC, Cohen JL, Shen Y, Garcia-Menendez L, Pedersen DJ, Gallagher-Dorval K et al (2015) Activated Kupffer cells inhibit insulin sensitivity in obese mice. *FASEB J* 29: 2959–2969
- Tesz GJ, Aouadi M, Prot M, Nicoloso SM, Boutet E, Amano SU, Goller A, Wang M, Guo C-A, Salomon WE et al (2011) Glucan particles for selective delivery of siRNA to phagocytic cells in mice. *Biochem J* 436: 351–362
- Tsatsoulis A, Mantzaris MD, Bellou S, Andrikoula M (2013) Insulin resistance: an adaptive mechanism becomes maladaptive in the current environment — An evolutionary perspective. *Metabolism* 62: 622–633
- Vorrink SU, Ullah S, Schmidt S, Nandania J, Velagapudi V, Beck O, Ingelman-Sundberg M, Lauschke VM (2017) Endogenous and xenobiotic metabolic stability of primary human hepatocytes in long-term 3D spheroid cultures revealed by a combination of targeted and untargeted metabolomics. *FASEB J* 31: 2696–2708
- Wasyluk W, Zwolak A (2021) Metabolic alterations in sepsis. *J Clin Med* 10: 2412
- Yan J, Horng T (2020) Lipid metabolism in regulation of macrophage functions. *Trends Cell Biol* 30: 979–989
- Zhao X, Karpac J (2021) Glutamate metabolism directs energetic trade-offs to shape host-pathogen susceptibility in *Drosophila*. *Cell Metab* 33: 2428–2444.e8
- Zhao P, Huang P, Xu T, Xiang X, Sun Y, Liu J, Yan C, Wang L, Gao J, Cui S et al (2021) Fat body Ire1 regulates lipid homeostasis through the Xbp1s-FoxO axis in *Drosophila*. *iScience* 24: 102819



License: This is an open access article under the terms of the [Creative Commons Attribution-NonCommercial-NoDerivs](https://creativecommons.org/licenses/by-nc-nd/4.0/) License, which permits use and distribution in any medium, provided the original work is properly cited, the use is non-commercial and no modifications or adaptations are made.

Expanded View Figures

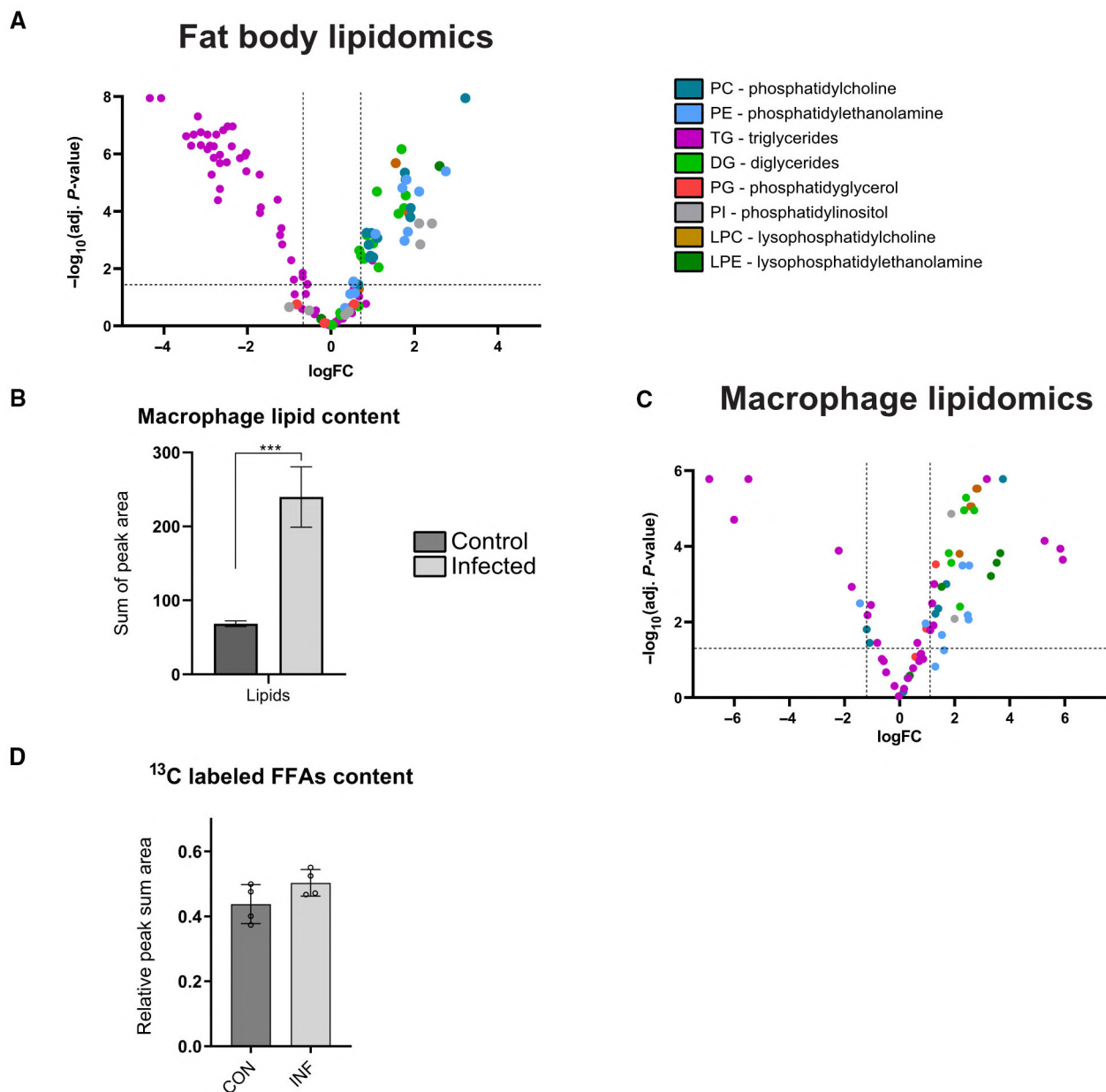


Figure EV1. *Drosophila* macrophages accumulate lipids in response to infection.

- A Volcano plot showing the relative abundance of the lipid species in the fat body dissected from infected vs. non-infected flies as determined by the lipidomic analysis (data obtained from six independent experiments; normalized to total lipid content).
- B The total lipid content is increased in macrophages after infection compared to the non-infected control flies as determined by the lipidomic analysis (data obtained from five independent experiments; normalized to the number of cells). Results were compared by unpaired t-test. Values are displayed as mean SD, asterisks mark statistically significant differences (** $P < 0.001$).
- C Volcano plot depicting the relative abundance of lipid species in macrophages isolated from non-infected vs. infected flies as determined by the lipidomic analysis (data obtained from five independent experiments; normalized to the number of cells).
- D Total dietary ^{13}C -labeled FFAs as a sum of their amount in guts, fat bodies, and macrophages, documenting comparable dietary intakes in infected and control flies.

Figure EV2. Transcriptomic analysis of activated macrophages and overview of the experimental strategy.

- A Generally applicable gene set enrichment (GAGE) analysis of transcriptomic data of macrophages isolated from non-infected and infected flies. The plot displays the top 30 significantly altered gene sets. The data illustrate the remodeling of macrophage cellular metabolism. GO Cellular component was used as an enrichment analysis for DEGs.
- B Volcano plot of differentially expressed genes in macrophages isolated from non-infected and infected flies as determined by the transcriptomic analysis. Significantly up-regulated signaling factors are highlighted with respect to reference spots in the volcano plot.
- C Gene expression of Hif1 α measured by RT-qPCR in macrophages isolated from non-infected and infected control flies (HmlGal4>GFP;KK^{control}) and flies with macrophage-specific Hif1 α knockdown (HmlGal4>GFP;Hif1 α ^{RNAi}) documenting the efficiency of RNAi interference in macrophages. Data obtained from three independent experiments. Expression levels normalized to rp49 are reported as fold change relative to Hif1 α levels in non-infected HmlGal4>GFP;KK^{control} arbitrarily set to 1. Results compared by 2way ANOVA Tukey's multiple comparisons test; values displayed as mean SD; asterisks mark statistically significant differences (**P < 0.01).
- D Schematic overview of the experimental strategy with an explanation of genotypes included in the work.

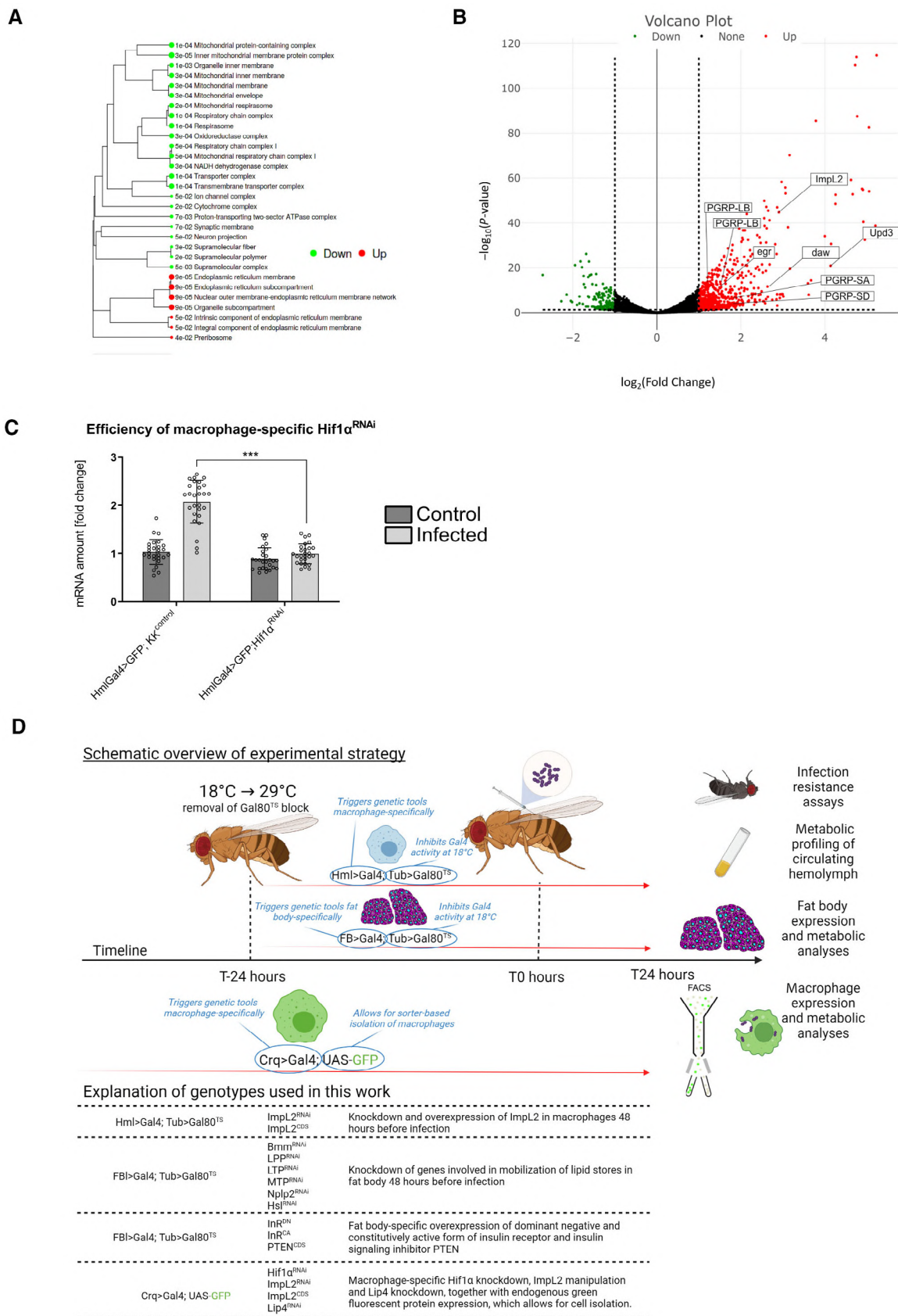


Figure EV2.

Figure EV3. Metabolic change induced by infection and genetic manipulations.

- A Gene expression of *ImpL2* measured by RT-qPCR in macrophages isolated from non-infected and infected control flies (TRiP^{control} and *W*^{control}), flies with macrophage-specific *ImpL2* knockdown (*ImpL2*^{RNAi}) and flies with macrophage-specific *ImpL2* overexpression (*ImpL2*^{CDS}) documenting the efficiency of the genetic tools used for manipulation of *ImpL2* expression. Expression levels normalized against *rp49* are reported as fold change relative to *ImpL2* levels in non-infected TRiP^{control} arbitrarily set to 1.
- B Percentage of the area occupied by lipid droplets in the fat body of non-infected (CON) and infected (INF) control flies (TRiP^{control} and *W*^{control}), flies with macrophage-specific *ImpL2* knockdown (*ImpL2*^{RNAi}) and flies with macrophage-specific *ImpL2* overexpression (*ImpL2*^{CDS}). Data obtained by analysis of dissected fat body whole mounts stained for neutral lipids (OilRedO). Images were captured by a confocal microscope.
- C Log₁₀ of an average size of lipid droplets in the fat body of non-infected (CON) and infected (INF) control flies (TRiP^{control} and *W*^{control}), flies with macrophage-specific *ImpL2* knockdown (*ImpL2*^{RNAi}), and flies with macrophage-specific *ImpL2* overexpression (*ImpL2*^{CDS}). Data obtained by analysis of dissected fat body whole mounts stained for neutral lipids (OilRedO). Images were captured by a confocal microscope.
- D Relative level of cholesterol, cholesteryl-ester, and triglycerides in the fat body of non-infected (CON) and infected (INF) control flies (TRiP^{control} and *W*^{control}), flies with macrophage-specific *ImpL2* knockdown (*ImpL2*^{RNAi}) and flies with macrophage-specific *ImpL2* overexpression (*ImpL2*^{CDS}).
- E Relative level of cholesterol, cholesteryl-ester, and triglycerides in the circulation of non-infected (CON) and infected (INF) control flies (TRiP^{control} and *W*^{control}), flies with macrophage-specific *ImpL2* knockdown (*ImpL2*^{RNAi}) and flies with macrophage-specific *ImpL2* overexpression (*ImpL2*^{CDS}).
- F Concentration of selected metabolites measured either from the whole flies or in the circulation of non-infected and infected flies bearing additional control genotypes. Results compared by 2way ANOVA Šidak's multiple comparisons test. In (D–F), the metabolite concentrations were normalized to the protein level in each sample. Results compared by 2way ANOVA Tukey's multiple comparisons test. All data presented in this figure were obtained 24 h post-infection. Data were obtained from four independent experiments if not stated otherwise. The line/bar shows mean SD, asterisks mark statistically significant differences (**P* < 0.05; ***P* < 0.01; ****P* < 0.001).

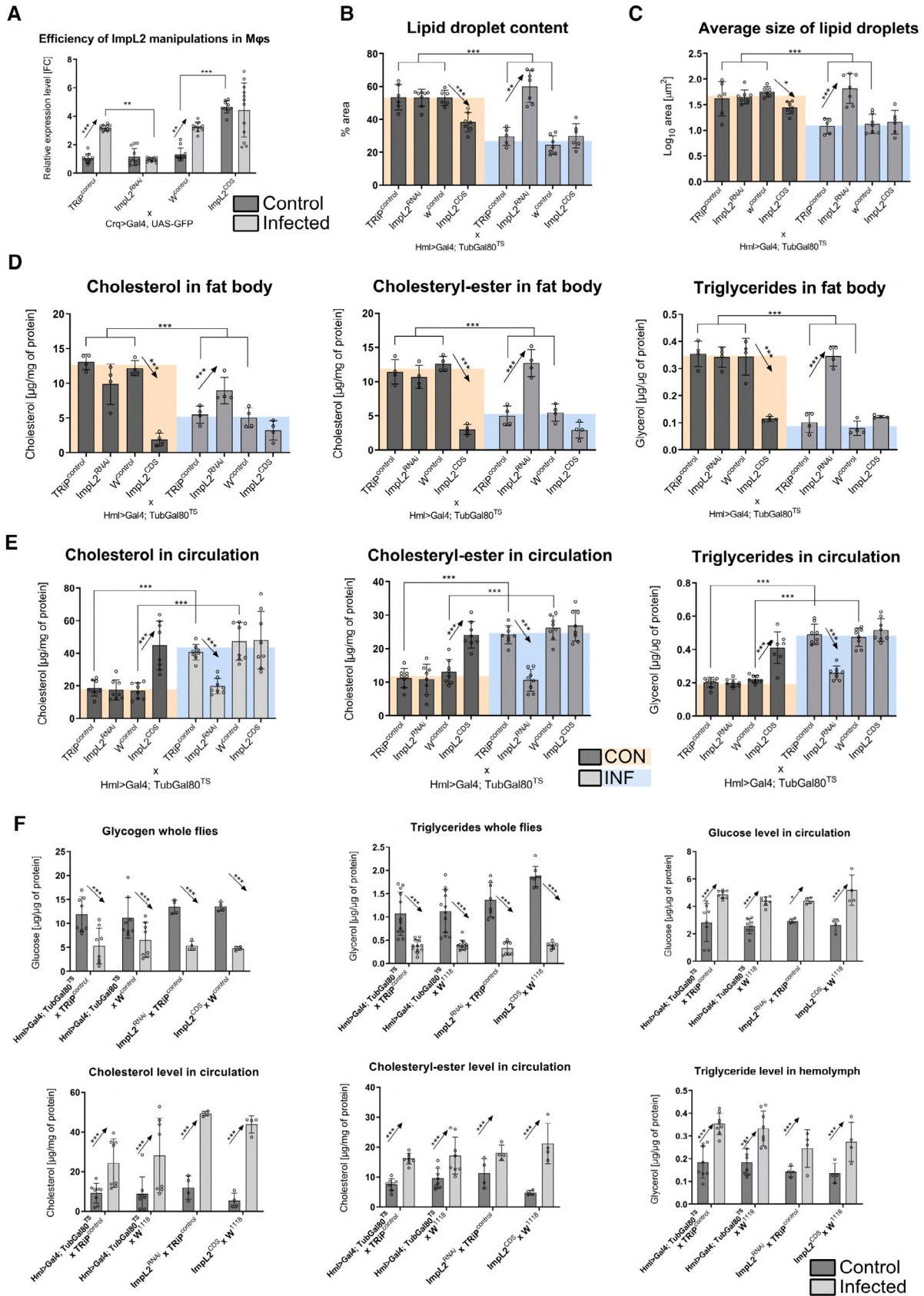


Figure EV3.

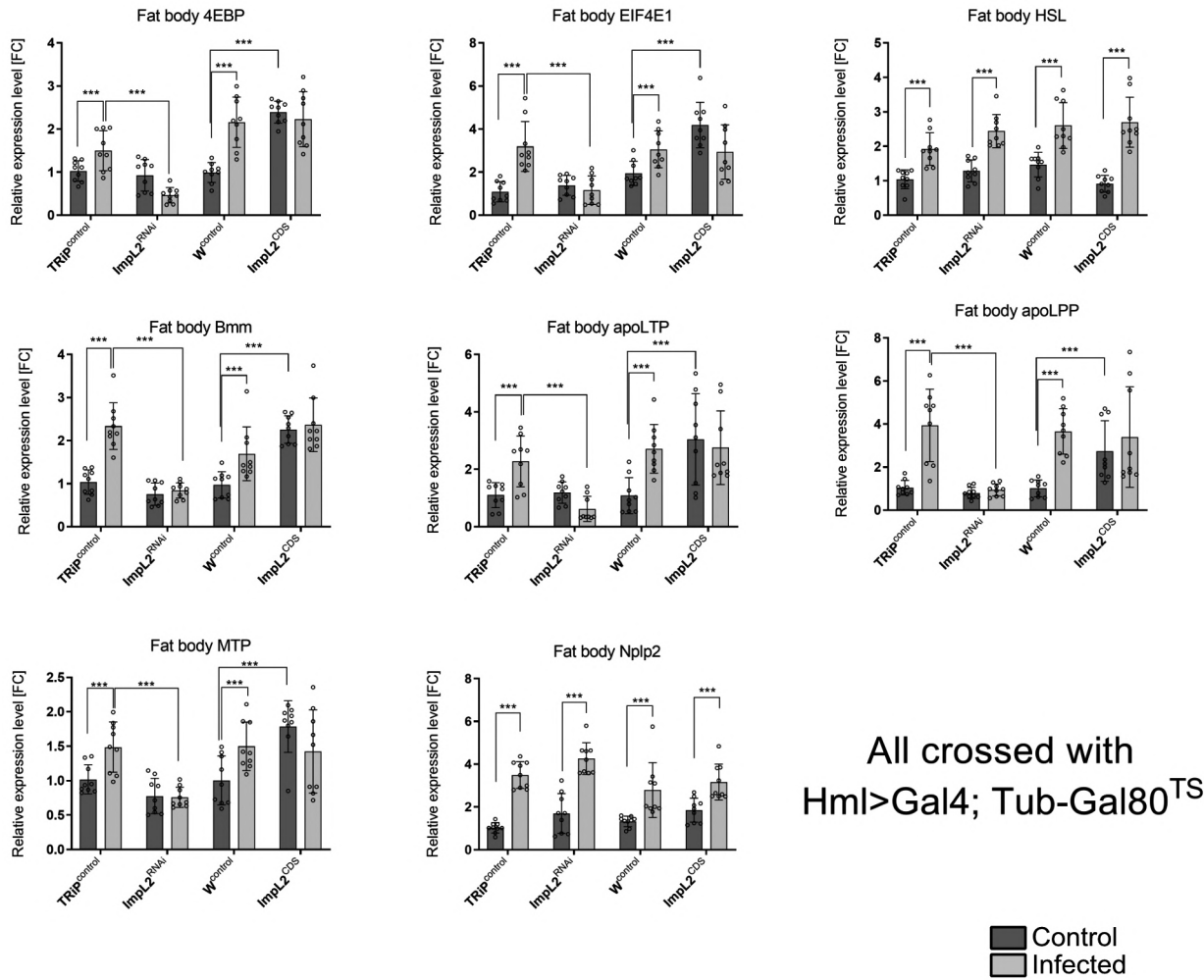


Figure EV4. Expression level of lipid metabolism-related genes in the fat body.

Gene expression of 4EBP, EIF4E1, HSL, Bmm, apoLTP, apoLPP, MTP, and Nplp2 in the fat body of non-infected and infected flies with macrophage-specific *Impl2* knockdown (*Impl2^{RNAi}*), overexpression (*Impl2^{CDS}*) and their respective controls (*TRIP^{control}* and *W^{control}*). Expression levels normalized against *rp49* are presented as a fold-change relative to the levels in the non-infected *TRIP^{control}*, which was arbitrarily set to 1. Presented data were obtained 24 h post-infection. Data were obtained from four independent experiments. Results were compared by 2-way ANOVA Tukey's multiple comparison test. Bars show mean SD, asterisks mark statistically significant differences (* $P < 0.05$; ** $P < 0.01$; *** $P < 0.001$).

FOXO NUCLEAR LOCALIZATION

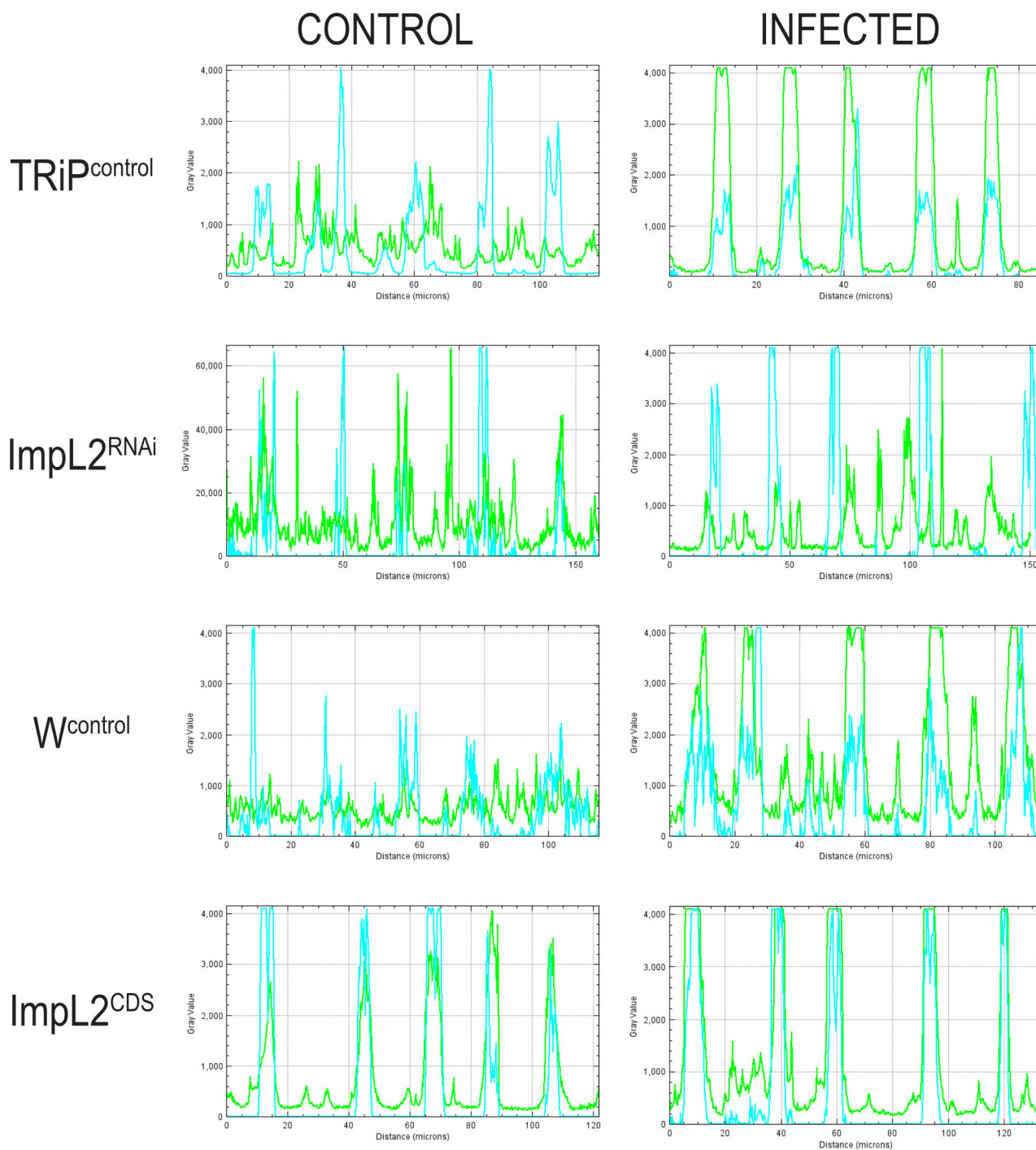


Figure EV5. Histograms documenting FOXO nuclear translocation in response to infection.

Histograms plotting colocalization of Foxo (green) and DAPI (cyan) signal intensity in sections indicated by a white freehand line in confocal images of fat bodies dissected from non-infected (CON) and infected (INF) flies with macrophage-specific *ImpL2* knockdown (*ImpL2*^{RNAi}), overexpression (*ImpL2*^{CDS}) and their respective controls (*TRiP*^{control} and *W*^{control}) as shown in Fig 4.

Appendix

Macrophage-derived insulin antagonist *ImpL2* induces lipoprotein mobilization upon bacterial infection

Author list

Gabriela Krejčová¹, Cecilia Morgantini², Helena Zemanová¹, Volker M. Lauschke^{2,3,4}, Julie Kovářová⁵, Jiří Kubásek⁶, Pavla Nedbalová¹, Nick Kamps-Hughes⁷, Martin Moos⁸, Myriam Aouadi², Tomáš Doležal^{1*}, Adam Bajgar^{1*}

Affiliation

¹Department of Molecular Biology and Genetics; Faculty of Science; University of South Bohemia; Ceske Budejovice, 37005, Czech Republic.

²Integrated Cardio Metabolic Center (ICMC); Department of Medicine; Karolinska Institutet; Huddinge, 14157, Sweden.

³Dr Margarete Fischer-Bosch Institute of Clinical Pharmacology, Stuttgart, Germany.

⁴University of Tübingen, Tübingen, Germany.

⁵Institute of Parasitology; Biology Centre CAS; Ceske Budejovice, 37005, Czech Republic.

⁶Department of Experimental Plant Biology; Faculty of Science; University of South Bohemia; Ceske Budejovice, 37005, Czech Republic.

⁷Institute of Molecular Biology; University of Oregon; Oregon, OR 97403, United States.

⁸Institute of Entomology; Biology Centre CAS; Ceske Budejovice, 37005, Czech Republic.

*Correspondence: bajgaradam@seznam.cz, bajgaa00@prf.jcu.cz, tomas.dolezal@prf.jcu.cz

This PDF file includes:

Six supplementary notes and 25 Appendix figures further supporting the data.

TABLE OF CONTENTS

I.) SUPPLEMENTARY NOTES

	Page
I.) The observed effects cannot be explained by either <i>Upd3</i> or <i>Egr</i> signaling	3
II.) Macrophage-specific <i>ImpL2</i> manipulations have no autonomous effects on macrophages	4
III.) Alternative <i>ImpL2</i> RNAi fly line phenocopies the originally observed metabolic effects	4
IV.) Graphical representation of experiment using ¹³ C-labeled FFAs	5
V.) Uptake and utilization of lipids in macrophages upon bacterial infection	5
VI.) Description of the technique used for dissection of the fat body from an adult fly abdomen	6

II.) APPENDIX FIGURES

Appendix Figure S1	7
Appendix Figure S2	7
Appendix Figure S3	8
Appendix Figure S4	9
Appendix Figure S5	9
Appendix Figure S6	10
Appendix Figure S7	11
Appendix Figure S8	12
Appendix Figure S9	13
Appendix Figure S10	14
Appendix Figure S11	15
Appendix Figure S12	15
Appendix Figure S13	15
Appendix Figure S14	16
Appendix Figure S15	16
Appendix Figure S16	16
Appendix Figure S17	17
Appendix Figure S18	18
Appendix Figure S19	19
Appendix Figure S20	19
Appendix Figure S21	20
Appendix Figure S22	20
Appendix Figure S23	21
Appendix Figure S24	22
Appendix Figure S25	23

In the Appendix information file, we address several points that further strengthen the hypothesis proposed in the main manuscript but are not essential to understanding the story. The data presented here provide answers to essentially three separate questions: I. Could be the observed effects of *ImpL2* manipulations attributed to the activity of another intermediate signaling factor (*Upd3*, *Egr*, *DILPs* production) rather than *ImpL2*-induced insulin resistance in the fat body? II. Is there a possible cell-autonomous effect of *ImpL2* knockdown on macrophage function? III. What is the assumed mechanism behind observed increased lipid accumulation in infection-activated macrophages?

In addition, we have provided a schematic representation describing the procedure of dissection of the fat body from the abdomens of adult flies and details on the experimental design for monitoring ¹³C-FFA distribution during infection.

I.) The observed effects of macrophage *ImpL2* manipulation on the fat body metabolism cannot be explained by either *Upd3* or *Egr* signaling

In the presented manuscript we conclude that *ImpL2* produced by macrophages causes insulin resistance in the fat body and the induction of subsequent systemic metabolic changes. However, *ImpL2* is not the only signaling factor that is upregulated in macrophages in our experimental system and there is a certain possibility that *ImpL2* manipulations influence the production of another unrecognized factor that is responsible for the induction of the observed phenotypes. In this respect, signaling factors *Unpaired3* (*Upd3*) and *Eiger* (*Egr*) are the most interesting alternative candidates. *Upd3* is significantly upregulated in infection-activated macrophages and is known to induce insulin resistance in various tissues through activation of the Jak-STAT signaling cascade. In parallel, enhanced production of *Egr* has been shown to directly control the production of *drosophila insulin-like peptides* in the cells of pars intercerebralis under metabolic stress. Thus both factors may substantially contribute to the induction of systemic insulin resistance in infected individuals and their importance cannot be ruled out without adequate experimental validation. Here we focused on the eventuality that one of these factors may be responsible for the induction of metabolic changes attributed in our original manuscript to *ImpL2*.

For this reason, we have performed a series of experiments that should reliably confirm or exclude the participation of *Upd3* and *Egr* in observed infection-induced mobilization of lipids in the form of lipoproteins. Both factors are significantly elevated in infection-activated macrophages in our experimental system. First, we analyzed whether their expression is affected by *ImpL2* manipulations (knockdown and overexpression) in these cells. We found that neither macrophage-specific *ImpL2* knockdown nor overexpression significantly affect the expression of these factors in macrophages (Appendix Figure S1 and Appendix Figure S4). Next, we focused on the activation of *Upd3* and *Egr* downstream signaling in the fat body of infected flies. While *Upd3* is known to enhance the activity of Jak-STAT signaling, *Egr* is expected to trigger JNK signaling, while both may lead to alleviated insulin signaling in the target tissue. For detection of the activity of these signaling cascades, we employed flies bearing reporter constructs (10xSTAT-GFP, TRE-GFP respectively) and analyzed the strength of these signals on confocal images of whole mounts of the abdominal fat body. We have not found data indicating that infection leads to strong activation of either of these stress pathways in the fat body. These experiments did not reveal increased activation of either of these signaling cascades in the fat body after infection (Appendix Figure S2 and Appendix Figure S5).

Next, we decided to test whether knockdown of *Upd3* or *Egr* expression in infection-activated macrophages leads to an infection-induced rise in the expression of FOXO-target genes in the fat body, as

observed in flies with macrophage-specific *ImpL2* knockdown. Nevertheless, even these experiments do not indicate that any of these factors produced by macrophages may be responsible for the induction of metabolic changes attributed to *ImpL2* in this publication (Appendix Figure S3 and Appendix Figure S6).

While *ImpL2* presumably suppresses insulin signaling by binding to circulating insulin-like peptides, *Upd3* intervenes in the insulin signaling cascade downstream of the insulin receptor. Thus, their action may be synergistic in some cases and a certain contribution of the *Upd3* gene to metabolic changes during bacterial infection in the fat body or other tissues cannot be entirely excluded. Similarly, the same can be said for *Egr*, which may be responsible for mitigating the production of DILPs in the brain during the acute phase of infection. To test the potential impact of *Egr* on the production of DIPLS upon infection, we have measured the expression of DILP2, DILP3, and DILP6 in the brains of infected and control flies and flies with macrophage-specific knockdown of *Egr* and respective controls. Our data show negligible effects of Streptococcal infection and macrophage-derived *Egr* on DILPs expression in brains (Appendix Figure S6).

II.) Macrophage-specific *ImpL2* manipulations have no autonomous effects on macrophage viability, metabolic activation, or proinflammatory polarization

In this paper, we show that the downregulation of *ImpL2* in macrophages leads to a reduced ability of individuals to resist infection. In our presented model we attribute these effects to the impact of *ImpL2* on systemic metabolism and the need to induce the redistribution of lipoproteins toward the activated immune cells. To exclude the possibility that the experimental intervention negatively affects the cells themselves, we performed a series of experiments for their characterization at 24 hours post-infection. Our data show that flies possess a comparable number of immune cells regardless of genetic manipulations of *ImpL2* in macrophages (Appendix Figure S11), nor do these manipulations lead to a reduced ability to produce antimicrobial peptides (Appendix Figure S12) or undergo metabolic polarization (Appendix Figure S13). Together with this, we have shown that *ImpL2* manipulation in macrophages does not significantly affect the expression of antimicrobial peptides in the fat body (Appendix Figure S14). Since it has been shown in previous work that gut infection leads to increased expression of *ImpL2* in the gut³⁹, we analyzed the expression of *ImpL2* in the gut in our experimental model for completeness. However, our data do not indicate that streptococcal infection leads to a significant increase in *ImpL2* gene expression in this tissue (Appendix Figure S7). Finally, we have addressed the possibility that macrophage-derived *ImpL2* affects insulin signaling in the fat body by alleviation of DILPs production in the brain. Nevertheless, we have found negligible effects of macrophage-specific *ImpL2* manipulations on their expression (Appendix Figure S15).

III.) The intervention of macrophage-induced metabolic effects may be achieved also by using alternative *ImpL2* RNAi fly line

Our data indicate that macrophage-derived factor *ImpL2* remotely controls metabolic changes induced by infection in the fat body as manifested by the redistribution of lipids within an organism. Even though our claims are supported by the ability of macrophage-induced *ImpL2*-RNAi (BDSC: 55855) to intervene in these effects and the ability to mimic these effects by *ImpL2* macrophage-specific overexpression, there might be a potential risk that these effects may be attributed to off-targets. To test this eventuality, we used an alternative *ImpL2*-RNAi (BDSC: 64936) strain and experimentally tested whether macrophage-specific knockdown of *ImpL2* by this RNAi line displays analogous phenotypes. Our data indicate that the

knockdown of *ImpL2* invoked by the alternative RNAi line (see Appendix Figure S16 for RNAi efficiency) intervenes with the infection-induced rise in the expression of FOXO-target genes responsible for the mobilization of lipoproteins from the fat body (Appendix Figure S16). Moreover, this treatment abrogates infection-induced changes in the structure of lipid droplets, mobilization of lipids from the fat body, and their rise in circulation (Appendix Figures S17 and S18). These data strongly support our original claim that observed infection-induced metabolic effects can be attributed to macrophage-derived factor *ImpL2* and that these effects are not caused by the off-target effect of the initially used *ImpL2* RNAi line.

IV.) Graphical representation of experimental setup for analysis of the momentary distribution of ¹³C-labeled FFAs

To analyze the momentary lipid distribution after infection, we first fed the flies ¹³C-labeled lipids for five hours. From a previous experiment with fluorescently labeled lipids, we know that five hours after the start of feeding, the fluorescent signal of lipids can only be detected in the digestive tract. Then the flies were divided into control and infected groups and treated accordingly. The fat body, macrophages, and intestine were then isolated from the experimental subjects 24 hours post-infection. FFAs are metabolized to diacylglycerols in the fly gut and subsequently distributed to other tissues as lipoproteins via the open circulatory system. It is not clear whether there is direct transport of lipids from the gut to the immune system or whether they are always processed through the fat body. To determine the distribution of labeled FFAs, tissues were homogenized and lipids were cleaved with a mixture of lipases to deliberate FFAs. The instantaneous lipid distribution was analyzed as the ratio of ¹³C-labeled FFAs to natural FFAs in the analyzed tissues. Thus, the ¹³C content does not necessarily reflect the total amount of lipids in the tissue of interest, but rather the proportion of lipids destined for a given tissue during the first 24 hours of infection (Appendix Figure S19).

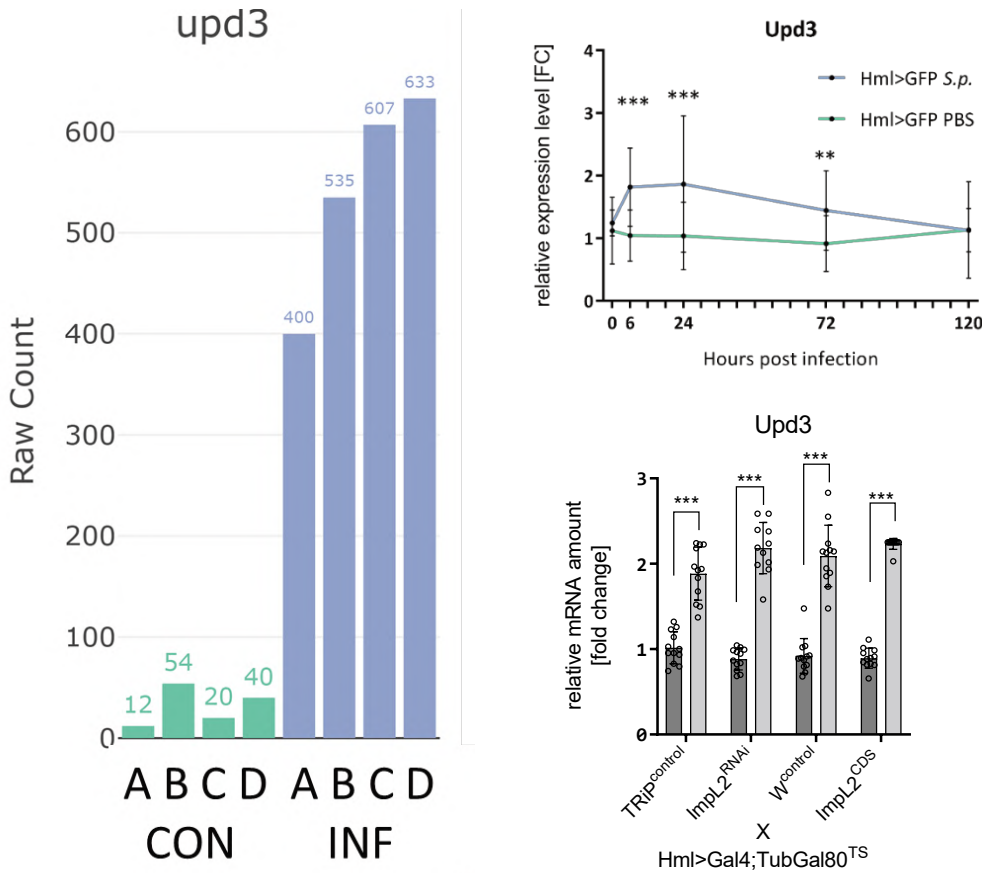
V.) Uptake and utilization of lipids in macrophages upon bacterial infection

The data presented in the manuscript suggest that macrophages induce lipoprotein mobilization to their advantage through the production of the signaling factor *ImpL2*. This is consistent with the observed mobilization of lipids from the fat body, their increased titer in the circulation, and the subsequent accumulation in macrophages. However, the mechanism by which lipids accumulate in macrophages activated by infection has not yet been fully resolved. Although there is no simple answer to this question, our data suggest a possible explanation. Lipid accumulation in activated macrophages has been observed by several independent mechanisms. In addition to the quantitative analysis of lipids and the increased momentary allocation of ¹³C-labeled FFAs to activated macrophages, we observed that more than 80% of all macrophages analyzed showed significant accumulation of lipids that showed positive staining for neutral lipids (OilRedO) (Appendix Figure 17). An alternative experimental approach in which we analyzed the fate of fluorescently labeled dietary lipids (Bodipy-FFAs; ThermoFisher) revealed that activated macrophages are able to accumulate more lipids from the circulation compared to surrounding tissues such as oenocytes, adipose tissue, or muscle. Although difficult to quantify, these data suggest that macrophages are prominent cells that uptake lipids during infection (Appendix Figure S21). This is consistent with transcriptomic data showing strong upregulation of scavenger receptors involved in lipid uptake (Appendix Figure S22) and their lysosomal processing (Appendix Figure S23). It is common for mammalian macrophages that lipids in the form of lipoproteins are recognized by scavenger receptors, leading to lipid uptake by endocytosis independent of lipoprotein lipase (PMID: 34626791).

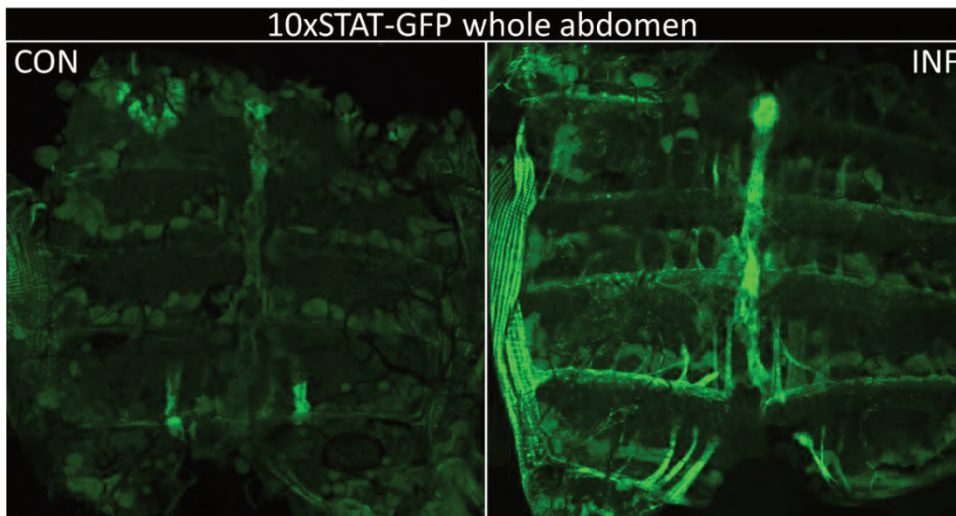
VI.) Description of the technique used for dissection of the fat body from an adult fly abdomen

Fat body dissection procedure: to isolate the fat body from the abdomen, subjects were dissected in ice-cold PBS. Individuals destined for dissection were attached with tiny entomological pins to a Sylgard polymer-coated dish. The abdomen was opened with spring scissors in five sections and the abdomen was spread and secured at the corners with additional pins. The adult abdominal fat sheets were released with a small needle by disrupting the trachea and the fat body plates were carefully scraped off the dorsal cuticle (Appendix Figure S25). The entire procedure takes a trained experimenter about five minutes, and twelve individuals can be dissected on a three-centimeter-diameter dish.

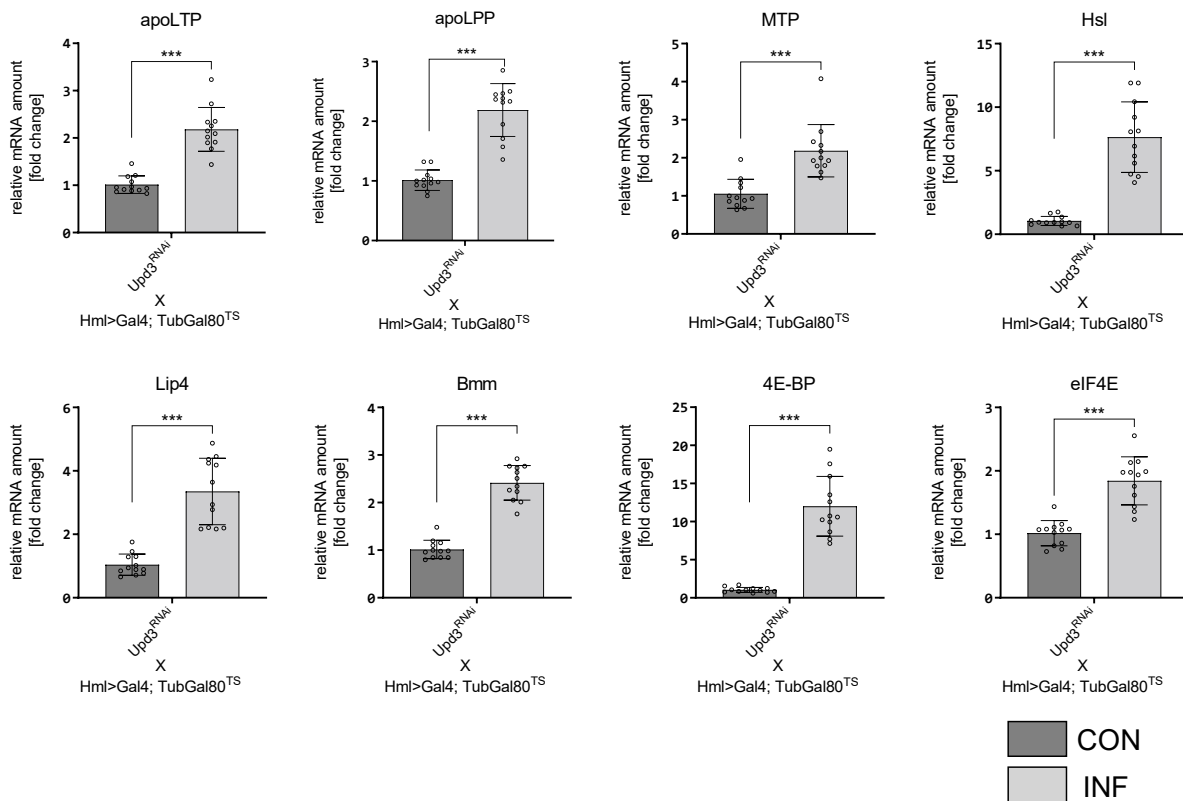
We admit that samples may contain negligible amounts of other cell types such as oenocytes, small branches of the trachea, or associated macrophages. However, adipocytes represent the vast majority of the tissue. Dissection of adult adipose tissue was performed analogously to the procedure described here for oenocytes (PMID: 20689503).



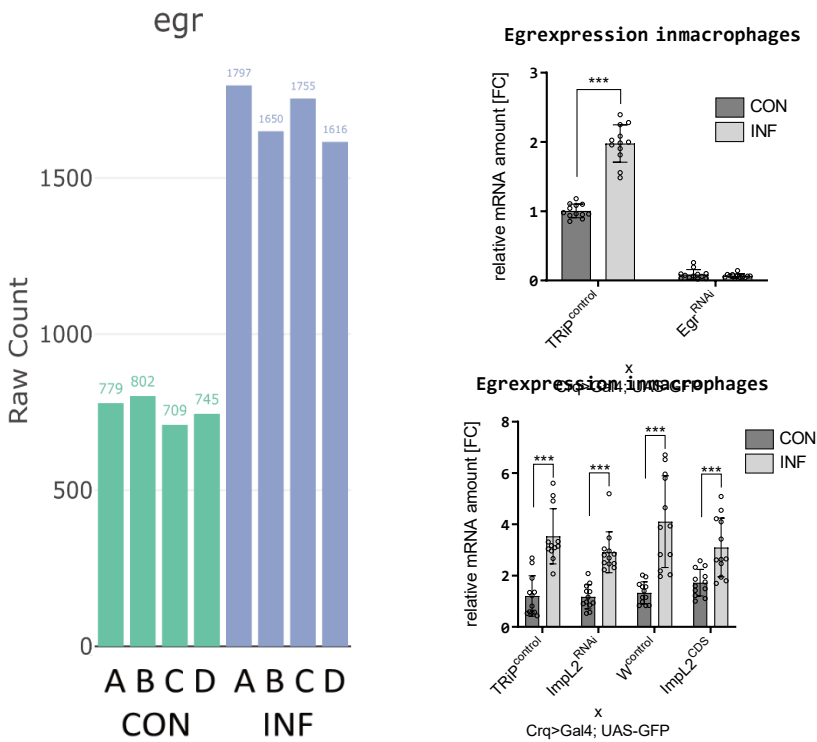
Appendix Figure S1. Transcriptomic and expression data demonstrating that the expression of *Upd3* is increased by activated macrophages after infection, however, this expression is not significantly affected by macrophage-specific manipulations of *ImpL2*.



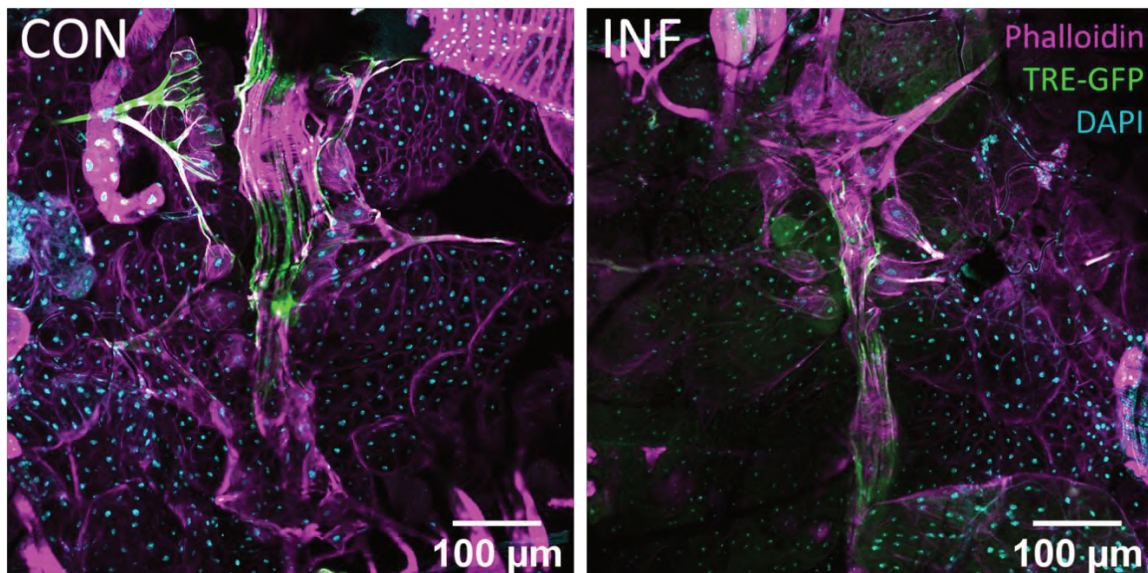
Appendix Figure S2. Representative confocal images of STAT activity in the abdominal segment of control and infected flies bearing 10xSTAT-GFP reporter (green) at 24 hours post-infection. We may observe increased GFP signal localized predominantly to muscles and aorta but a rather scarce signal in the abdominal fat body.



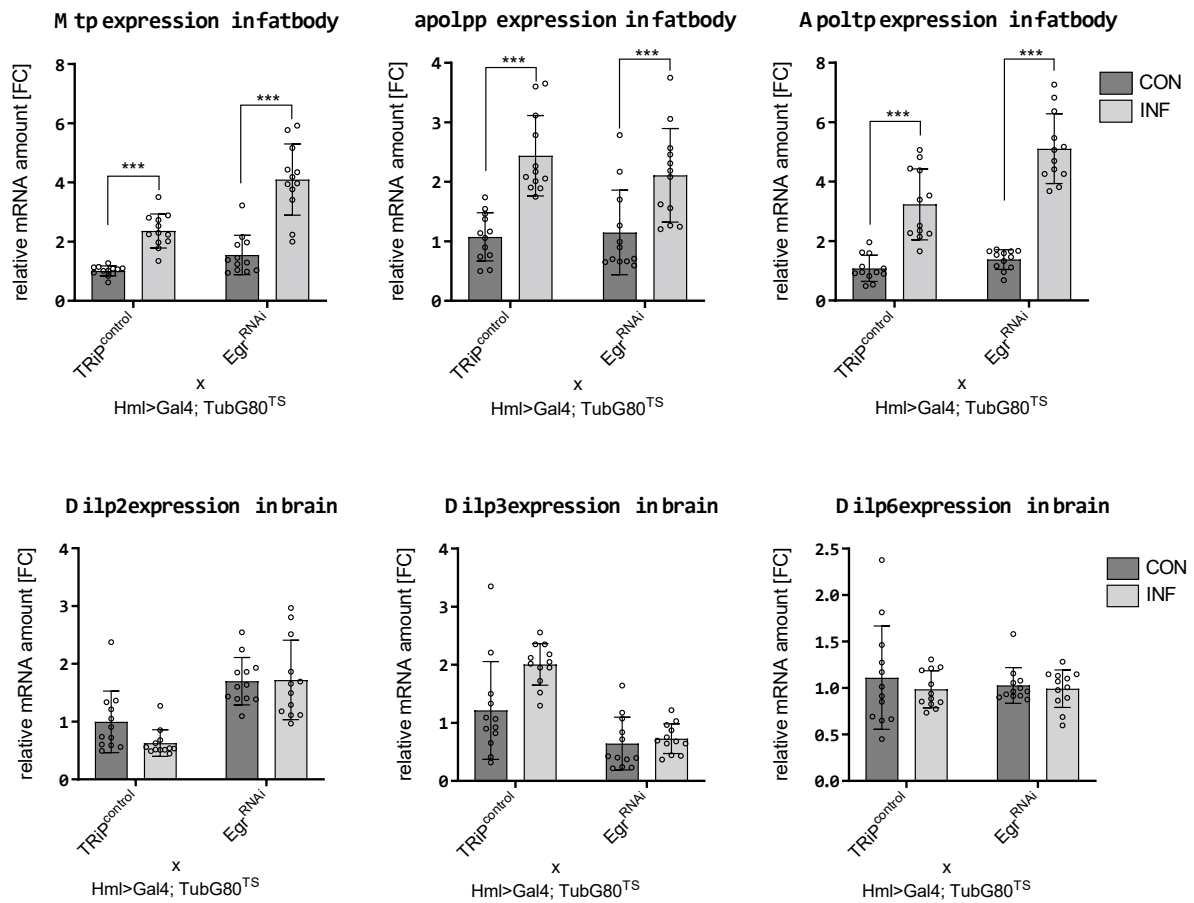
Appendix Figure S3. Expression pattern of FOXO target genes responsible for enhanced production of lipoproteins upon infection (*apolipoprotein lipid transfer particle*, *apoLTP*; *apolipoprotein*, *apoLPP*; *microsomal triacylglycerol transport protein*, *MTP*; *hormone sensitive lipase*, *Hsl*; *Lysosomal acid lipase*, *Lip4*; *Brummer*, *Bmm*; *Thor*, *4E-BP*; *Eukaryotic translation initiation factor 4E*, *eIF4E*). While the rise of expression of these genes is intervened by macrophage *ImpL2* manipulations this effect was not observed in flies with macrophage-specific knockdown of the signaling factor *Upd3*.



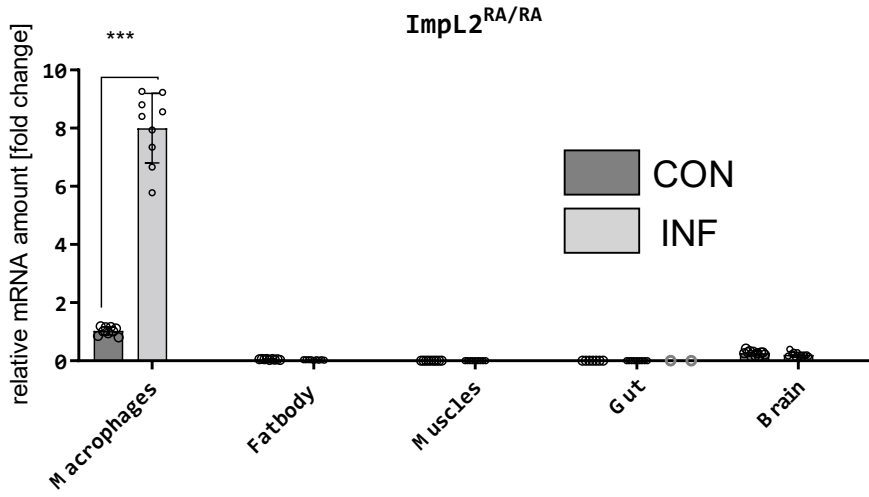
Appendix Figure S4. Transcriptomic and expression data demonstrating that expression of *Egr* is increased by activated macrophages after infection, however, this expression is not significantly affected by macrophage-specific manipulations of *ImpL2*.



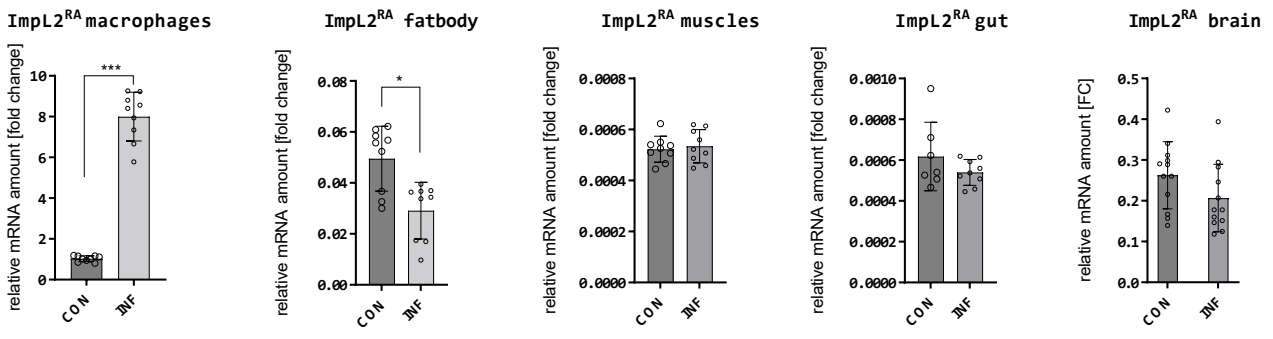
Appendix Figure 5. Representative confocal images of JNK activity in the abdominal segment of control and infected flies bearing TRE-GFP reporter (green) at 24 hours post-infection. We may observe increased GFP signal localized predominantly to the tracheas and aorta but a rather scarce signal in the abdominal fat body.

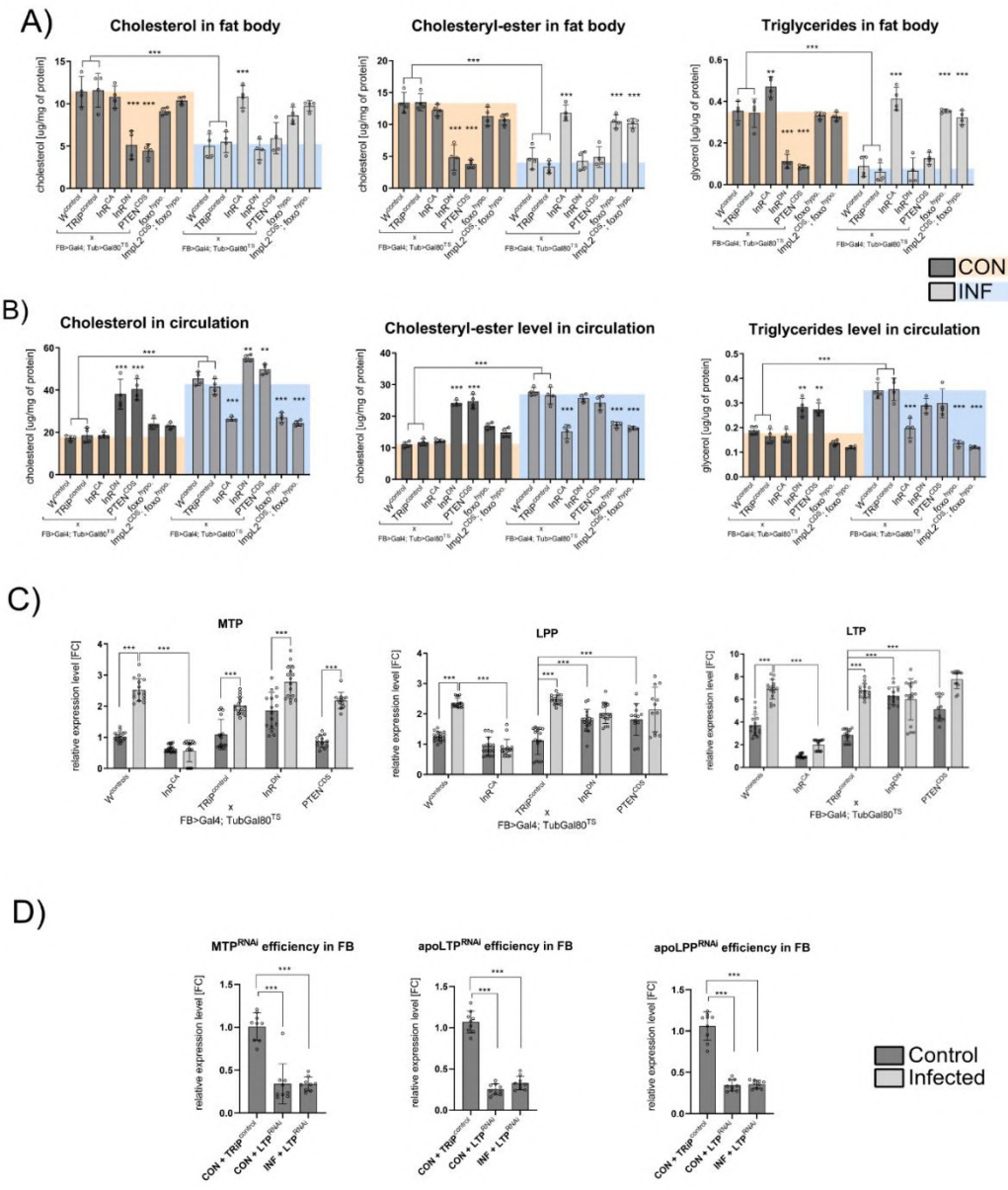


Appendix Figure S6. Expression pattern of FOXO target genes responsible for enhanced production of lipoproteins upon infection (*apolipoprotein lipid transfer particle, apoLTP*; *apolipoporphin, apoLPP*; *microsomal triacylglycerol transport protein, MTP*). While the rise of expression of these genes is intervened by macrophage *Impl2* manipulations this effect was not observed in flies with macrophage-specific knockdown of the signaling factor *Upd3*. Similarly, neither infection nor macrophage-specific manipulations of *Egr* seem to have a significant effect on the transcription of selected *drosophila insulin-like peptides* (DILP2; DILP3; and DILP6).



Appendix Figure S7. Gene expression of *ImpL2^{RA}* in macrophages, fat body, muscles, gut, and brain obtained from control and infected flies at 24 hours post-infection.

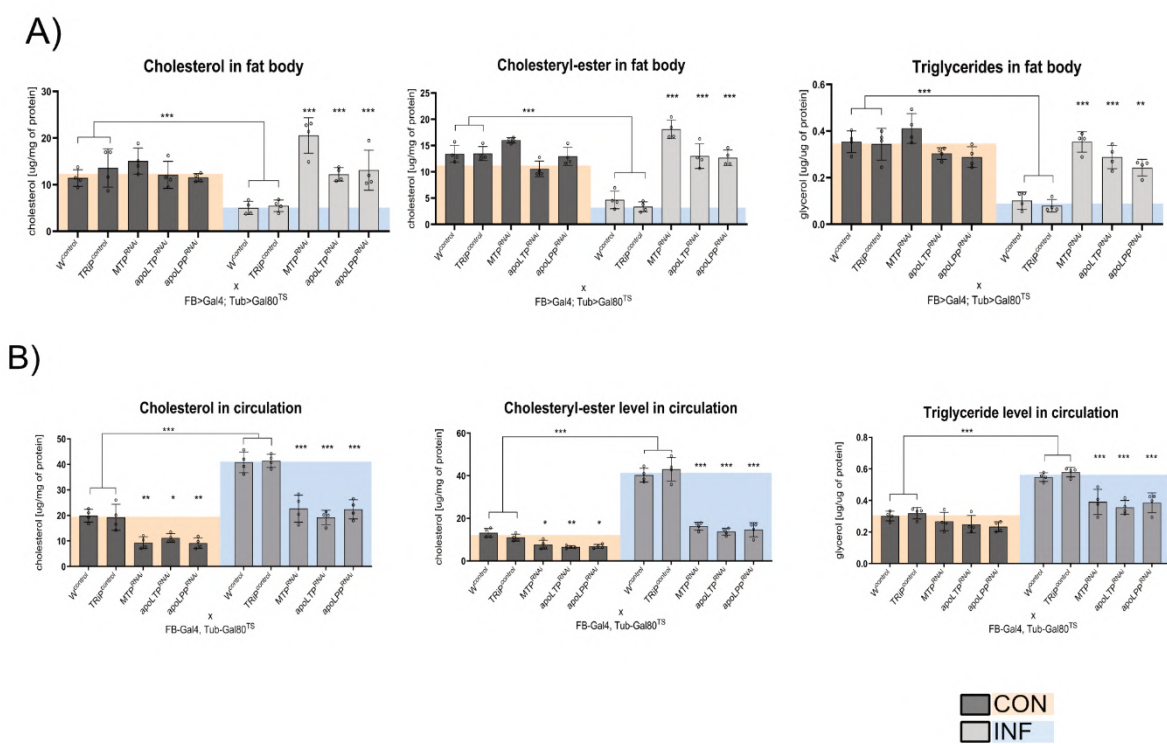




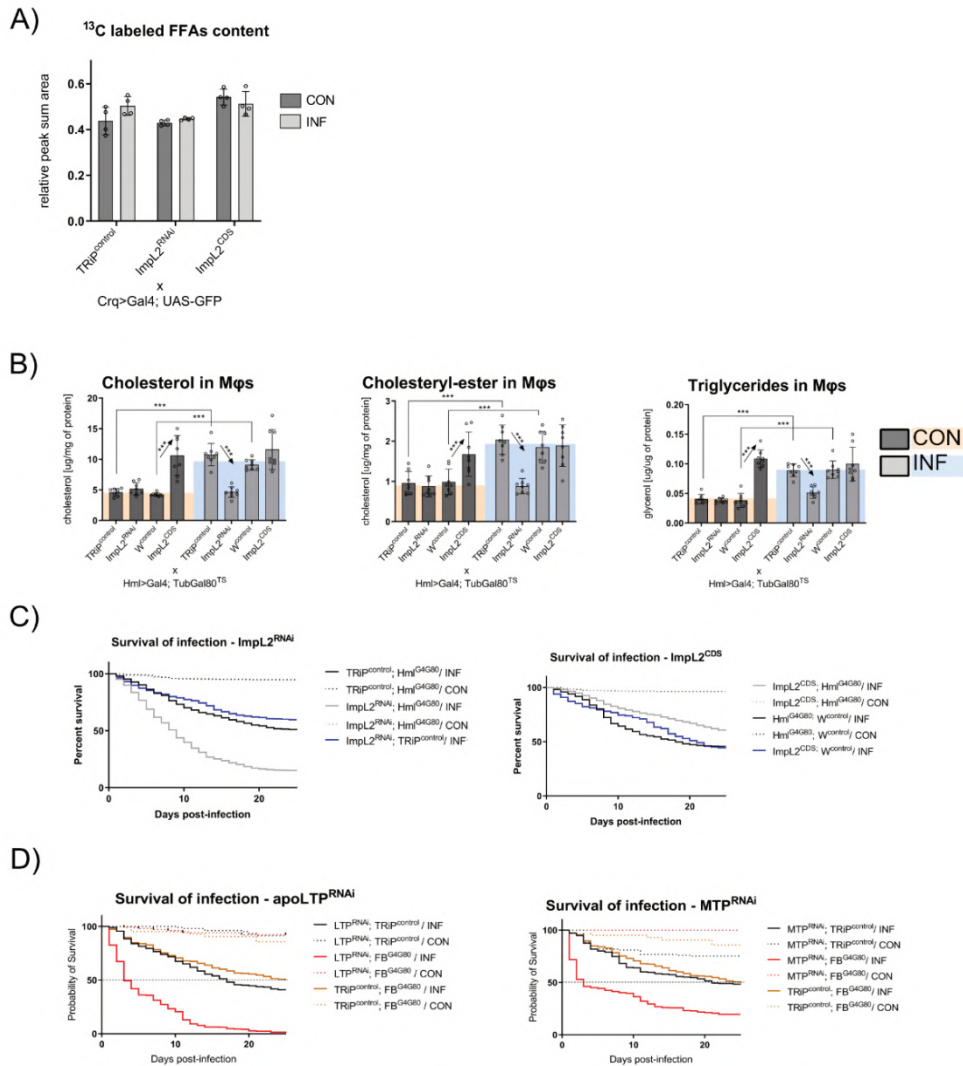
all crossed to FB>Gal4; TubGal80^{TS}

Appendix Figure S8. (A) Concentration of cholesterol, cholesteryl-ester and triglycerides in the fat body of non-infected (CON) and infected (INF) control flies with fat body-specific overexpression of constitutively active or dominant negative forms of insulin receptor (*InR^{CA}*, *InR^{DN}*), *PTEN* (*PTEN^{CDS}*), flies bearing *foxo* hypomorphic allele (*foxo^{hyppo.}*), and in flies with a combination of *foxo* hypomorphic allele and macrophage-specific overexpression of *ImpL2* (*Hml>ImpL2^{CDS}*; *foxo^{hyppo.}*) compared to their respective controls (*W^{control}*; *TriP^{control}*). (B) Concentration of cholesterol, cholesteryl-ester, and triglycerides in the circulation of non-infected (CON) and infected (INF) control flies with fat body-specific overexpression of constitutively active or dominant negative form of insulin receptor (*InR^{CA}*, *InR^{DN}*), *PTEN* (*PTEN^{CDS}*), flies bearing *foxo* hypomorphic allele (*foxo^{hyppo.}*), and in flies with a combination of *foxo* hypomorphic allele and macrophage-specific overexpression of *ImpL2* (*Hml>ImpL2^{CDS}*; *foxo^{hyppo.}*) compared to their respective

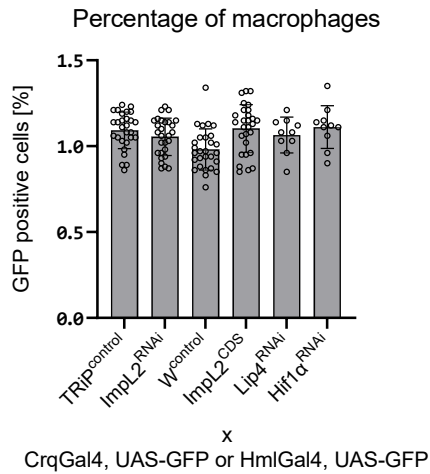
controls ($W^{control}$; $TRiP^{control}$). (C) Gene expression of MTP , $apoLPP$, and $apoLTP$ measured by RT-qPCR in the fat body dissected from non-infected (CON) and infected (INF) control flies with fat body-specific overexpression of constitutively active or dominant negative form of insulin receptor (InR^{CA} , InR^{DN}) or $PTEN$ ($PTEN^{CDS}$) compared to their respective controls ($W^{control}$; $TRiP^{control}$). (D) Gene expression of MTP , $apoLTP$, and $apoLPP$ measured by RT-qPCR in the fat body dissected from non-infected control flies (CON + $TRiP^{control}$) and non-infected (CON) and infected (INF) flies with fat body-specific knockdown of the measured gene documenting the efficiency of the RNA interference. Results compared by unpaired t-test. In A-B, the metabolite concentrations were normalized to protein levels in each sample. Expression levels normalized against $rp49$ are reported as fold change relative to the levels in the non-infected control genotype arbitrarily set to 1. In A-C, the results were compared by 2way ANOVA Tukey's multiple comparisons test. The individual dots represent biological replicates with line/bar showing mean \pm SD, asterisks mark statistically significant differences (* p <0.05; ** p <0.01; *** p <0.001).



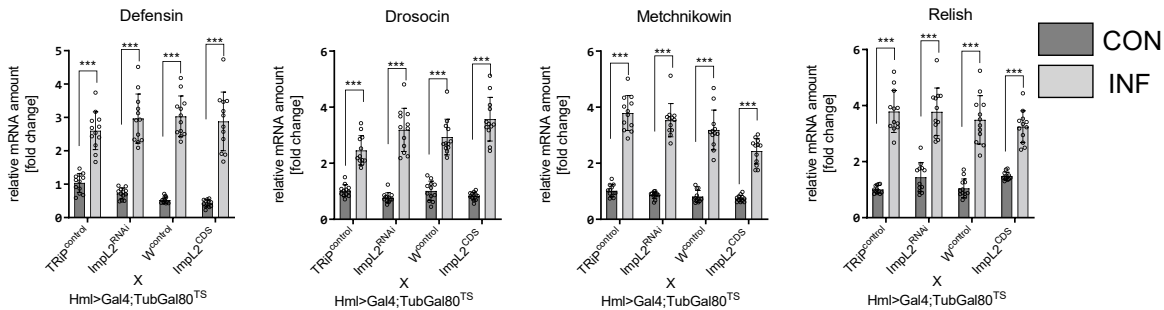
Appendix Figure S9. (A) Concentration of cholesterol, cholesteryl-ester, and triglycerides in the fat body of non-infected (CON) and infected (INF) control flies ($TRiP^{control}$ and $W^{control}$) and flies with fat body-specific knockdown of genes involved in the mobilization of lipoproteins (MTP , $apoLTP$, $apoLPP$). (B) Concentration of cholesterol, cholesteryl-ester, and triglycerides in the circulation of non-infected (CON) and infected (INF) control flies ($TRiP^{control}$ and $W^{control}$) and flies with fat body-specific knockdown of genes involved in the mobilization of lipoproteins (MTP , $apoLTP$, $apoLPP$). The metabolite concentrations were normalized to the protein level in each sample. Results compared by 2way ANOVA Tukey's multiple comparisons test. The individual dots represent biological replicates with line/bar showing mean \pm SD, asterisks mark statistically significant differences (* p <0.05; ** p <0.01; *** p <0.001).



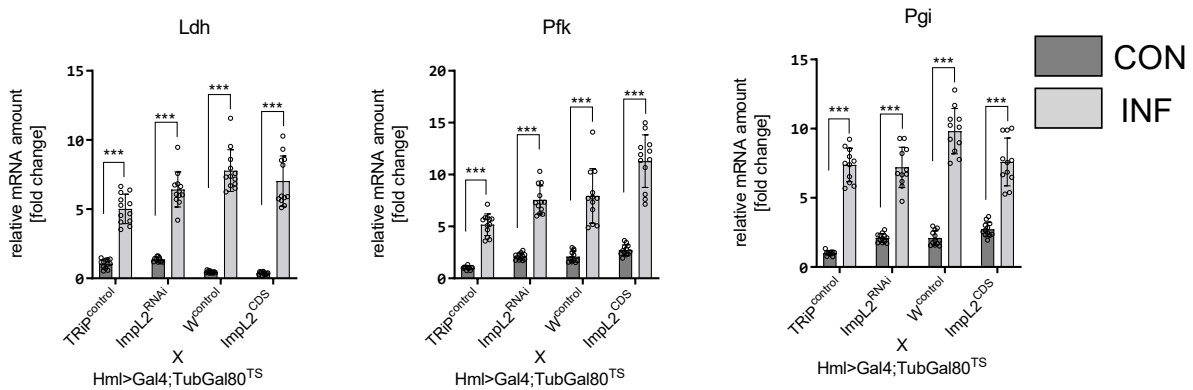
Appendix Figure S10. (A) Total dietary ^{13}C -labeled FFAs as a sum of their amount in guts, fat bodies, and macrophages in non-infected (CON) and infected (INF) control flies ($TRIP^{control}$), flies with macrophage-specific $Impl2$ knockdown ($Impl2^{RNAi}$) and flies with macrophage-specific $Impl2$ overexpression ($Impl2^{CDS}$), documenting comparable dietary intakes in infected and control flies of these genotypes. (B) Concentration of cholesterol, cholesteryl-ester, and triglycerides in macrophages isolated from non-infected (CON) and infected (INF) control flies ($TRIP^{control}$ and $W^{control}$), flies with macrophage-specific $Impl2$ knockdown ($Impl2^{RNAi}$) and flies with macrophage-specific $Impl2$ overexpression ($Impl2^{CDS}$). Data obtained from four independent experiments. Results compared by 2way ANOVA Tukey's multiple comparisons test. (C-D) Survival of bacterial infection of non-infected (CON) and infected (INF) flies bearing additional control genotypes for macrophage-specific manipulations of $Impl2$ and flies with fat-body specific knockdown of genes involved in the mobilization of lipoproteins (MTP and $apoLTP$). The number of individuals per replicate was at least 600 for each genotype. Results analyzed by Log-rank and Grehan-Breslow Wilcoxon tests. Data were obtained from four independent experiments. The metabolite concentrations were normalized to the protein level in each sample. Results compared by 2way ANOVA Tukey's multiple comparisons test. The line/bar shows mean \pm SD, asterisks mark statistically significant differences (* $p < 0.05$; ** $p < 0.01$; *** $p < 0.001$).



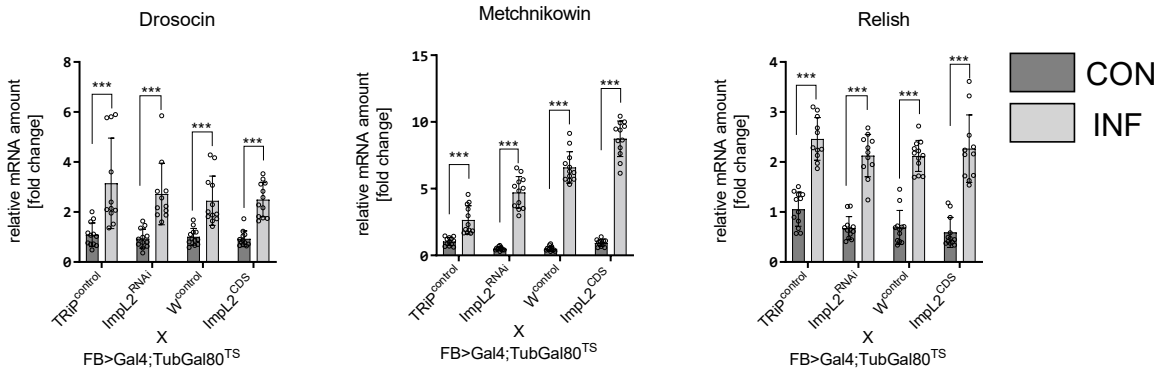
Appendix Figure S11. Percentage of GFP-positive cells (macrophages) sorted from control fly lines and fly lines with macrophage-specific genetic manipulations used in this manuscript. Data were obtained from the cell sorter as the proportion of GFP-positive cells out of the total number of cells in suspension.



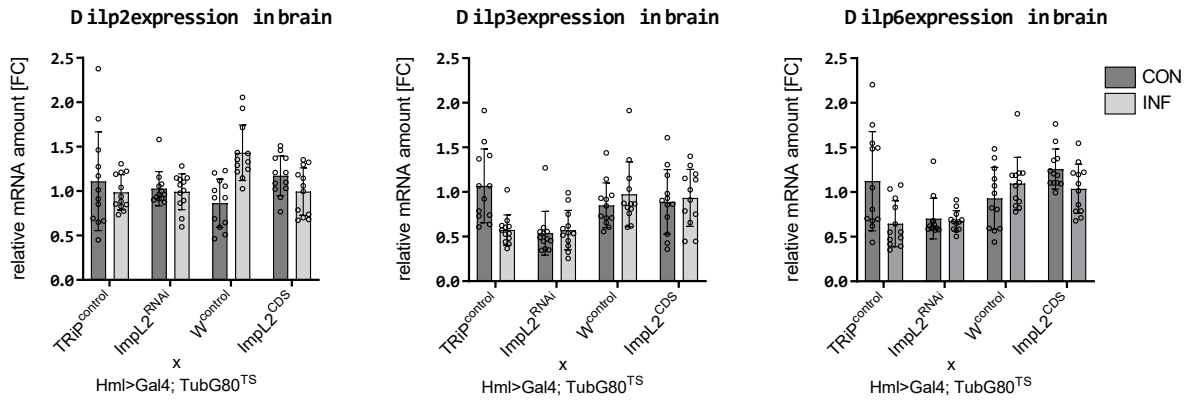
Appendix Figure S12. Expression pattern of antimicrobial peptides (*Defensin*, *Drosocin*, *Metchnikowin*, and *Relish*) in macrophages isolated from control and infected flies with macrophage-specific manipulations of *Impl2* and their respective controls.



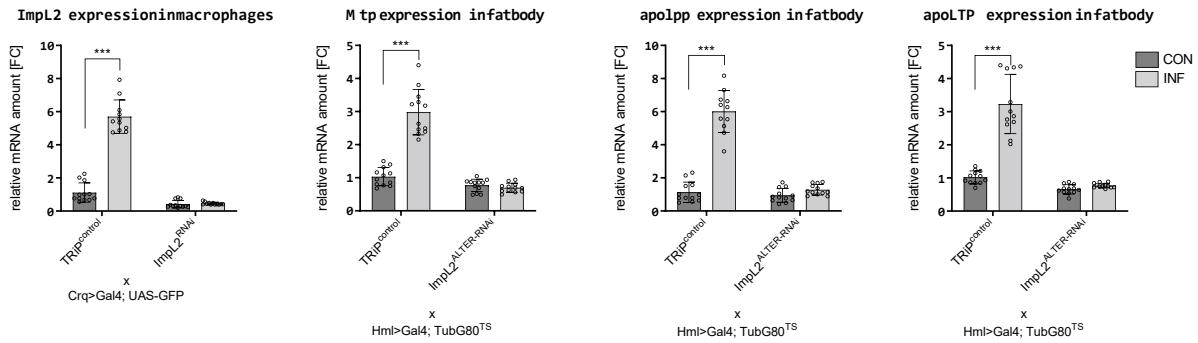
Appendix Figure S13. Expression pattern of glycolytic enzymes (*Lactate dehydrogenase*, *Ldh*; *Phosphofructose kinase*, *Pfk*; and *Phosphoglucose isomerase*, *Pgi*) in macrophages isolated from control and infected flies with macrophage-specific manipulations of *Impl2* and their respective controls.



Appendix Figure S14. Expression pattern of antimicrobial peptides (*Drosocin*, *Metchnikowin*, and *Relish*) in the fat body dissected from control and infected flies with macrophage-specific manipulations of *Impl2* and their respective controls.

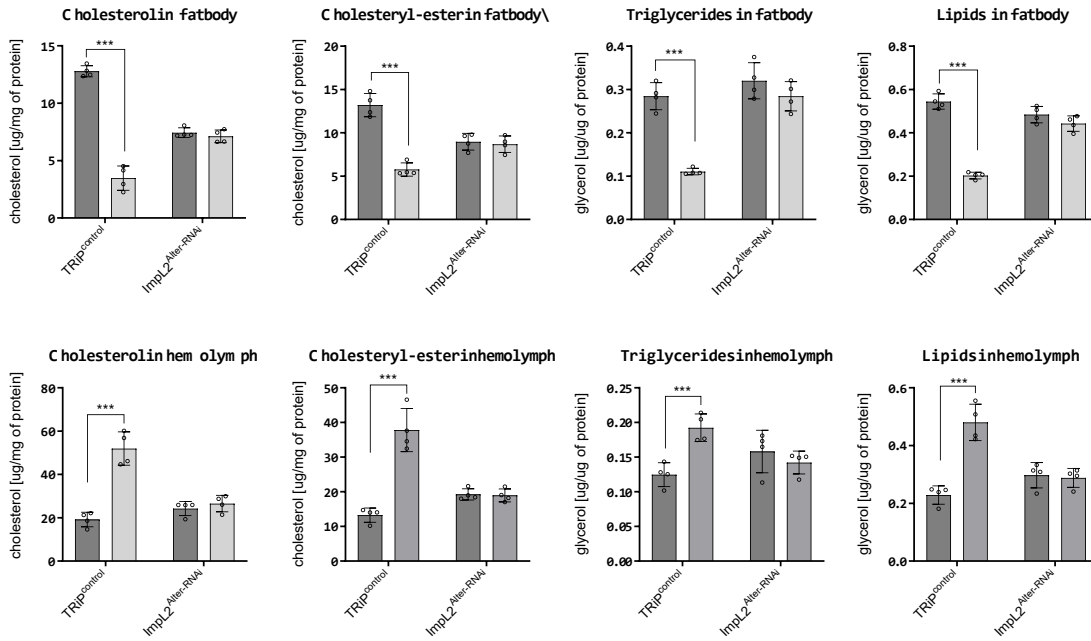


Appendix Figure S15. Expression pattern of drosophila insulin-like peptides (*DILP2*, *DILP3*, and *DILP6*) in the brains dissected from control and infected flies with macrophage-specific manipulations of *Impl2* and their respective controls.

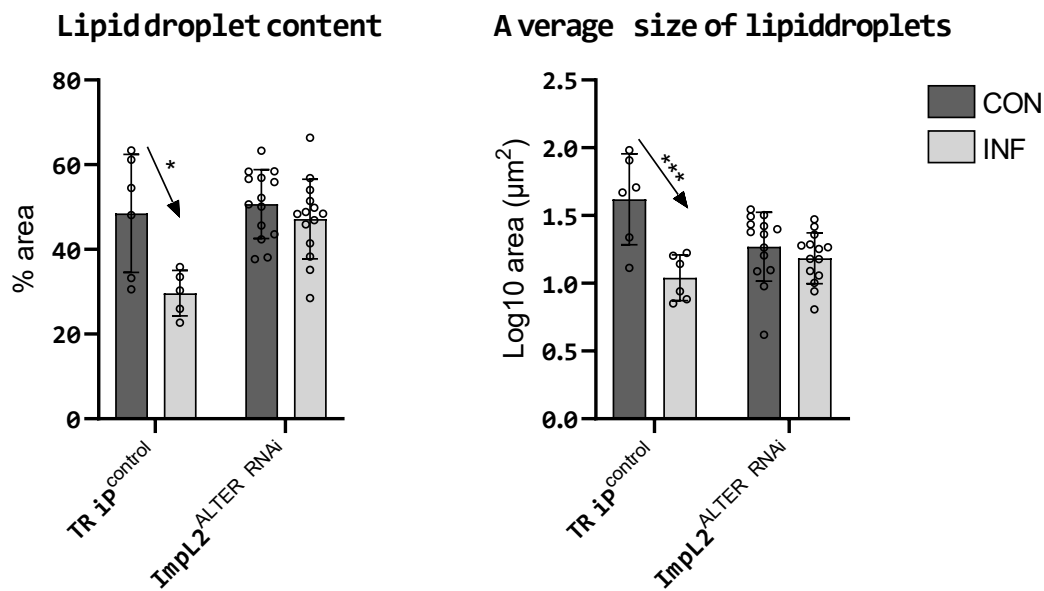
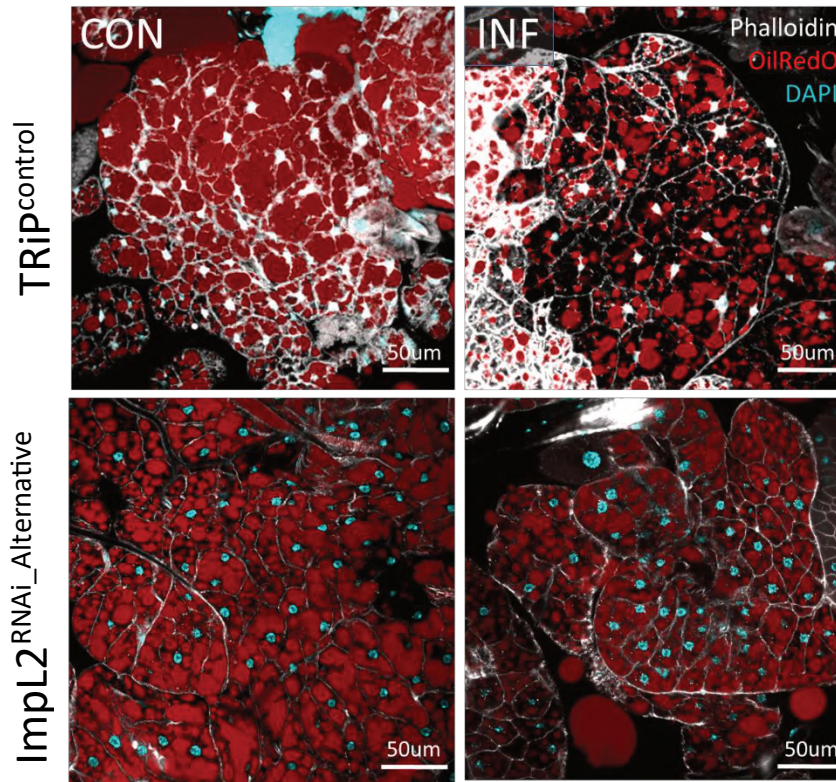


Appendix Figure S16. Expression pattern of FOXO target genes responsible for enhanced production of lipoproteins upon infection (*apolipoprotein lipid transfer particle*, *apoLTP*; *apolipoporphin*, *apoLPP*; *microsomal triacylglycerol transport protein*) in the fat body dissected from infected and control

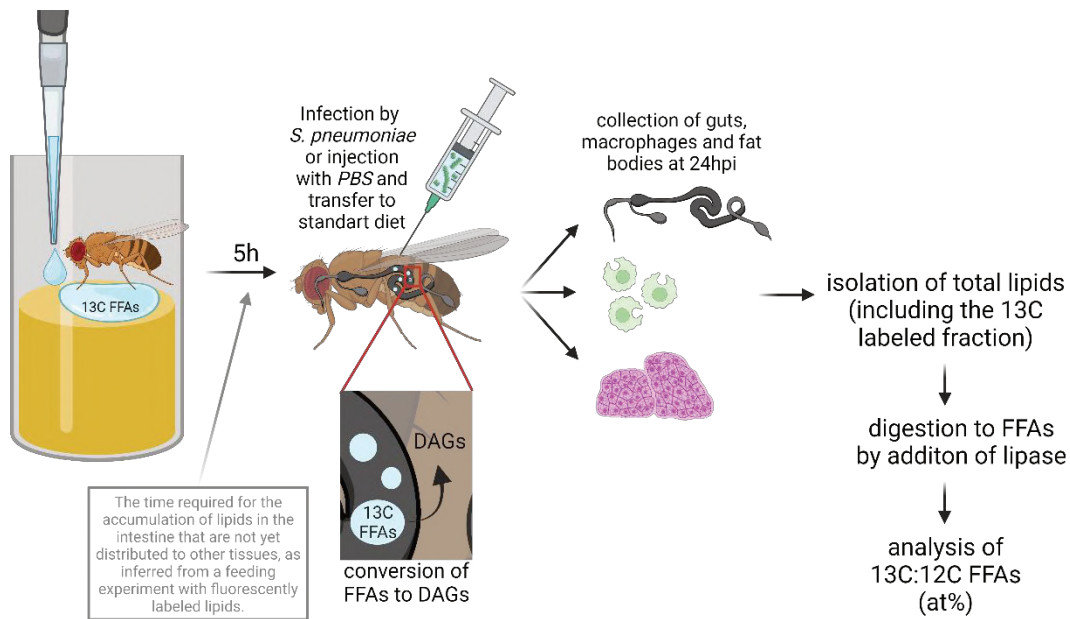
individuals bearing macrophage-specific *Impl2* knockdown induced by alternative RNAi and respective controls.



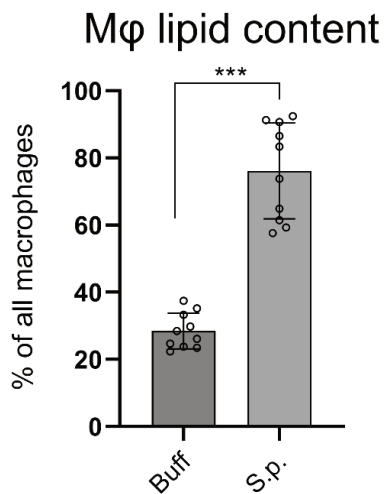
Appendix Figure S17. Titer of cholesterol, cholesteryl-ester, triglycerides, and their summarization as total lipids in the fat body and hemolymph isolated from control and infected flies bearing macrophage-specific *Impl2* knockdown induced by alternative RNAi and respective controls.



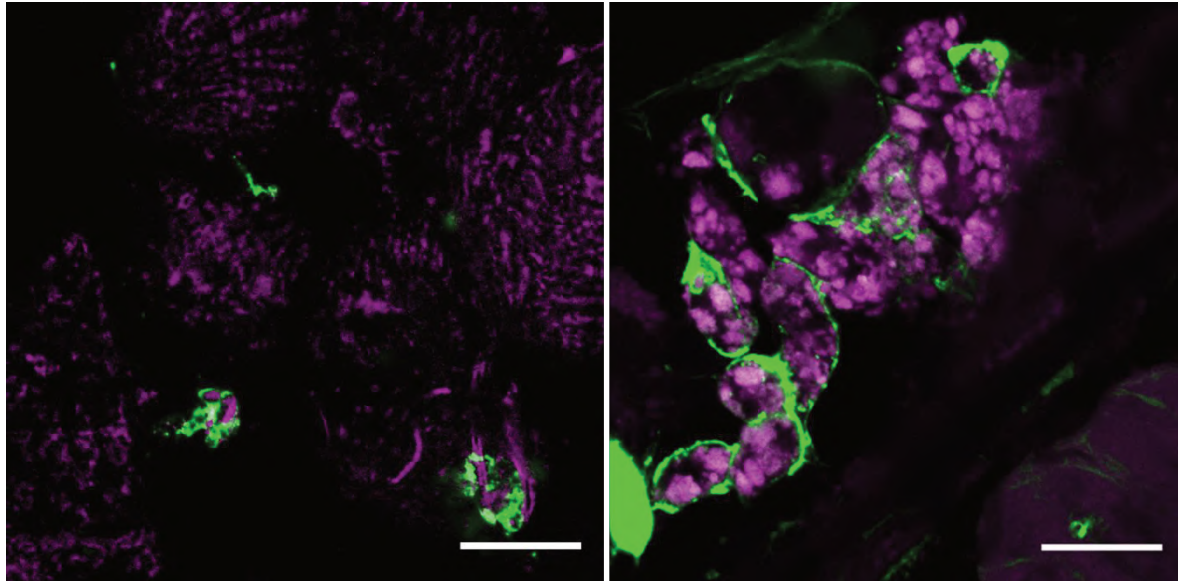
Appendix Figure S18. Representative confocal images documenting the structure of lipid droplets in the fat body dissected from control and infected flies with macrophage-specific knockdown of *Impl2* by alternative RNAi fly line and its respective control. Structural changes of lipid droplets were quantified as the area occupied by lipid droplets and the average size of lipids droplets in adipocytes as quantified from confocal images. Images of TRiP controls have been previously used in Figure 3A.



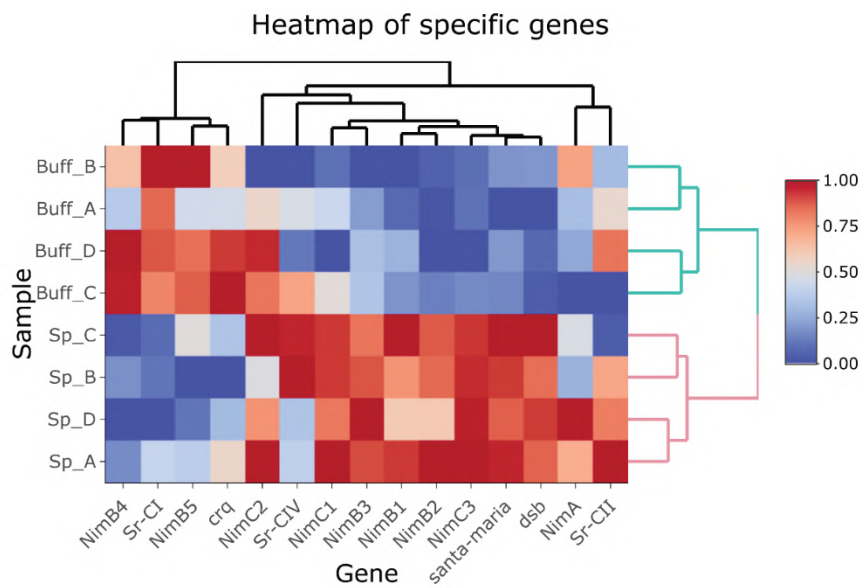
Appendix Figure S19. Graphical representation of the experimental procedure for analysis of the distribution of ^{13}C -labeled FFAs in control and infected flies.



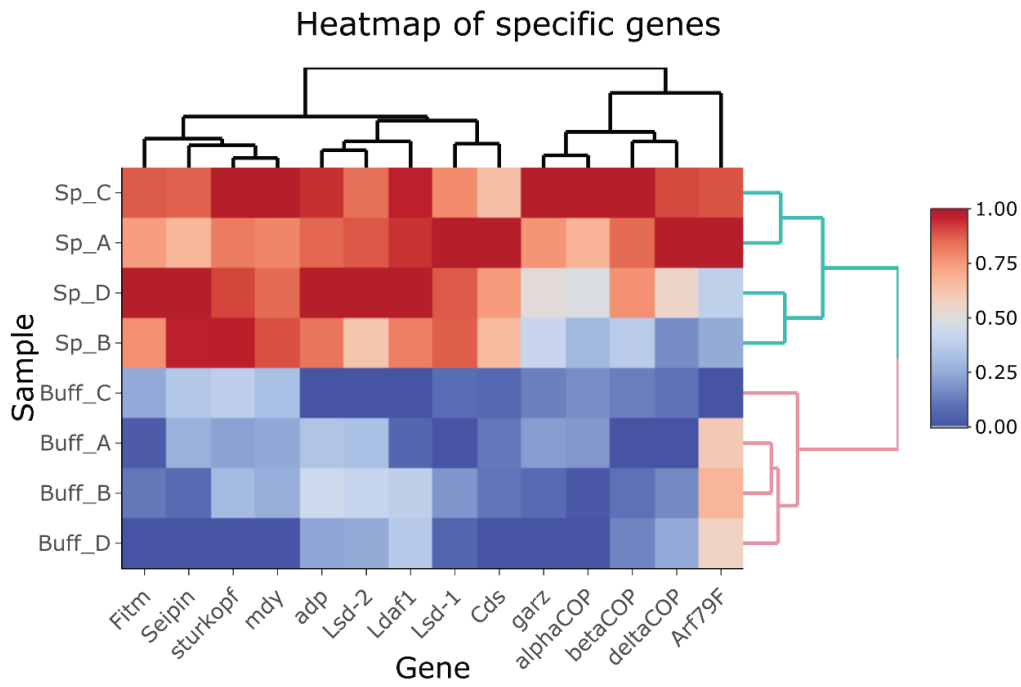
Appendix Figure S20. Percentage of macrophages containing at least one lipid droplet in their cytosol at 24 hours post-infection.



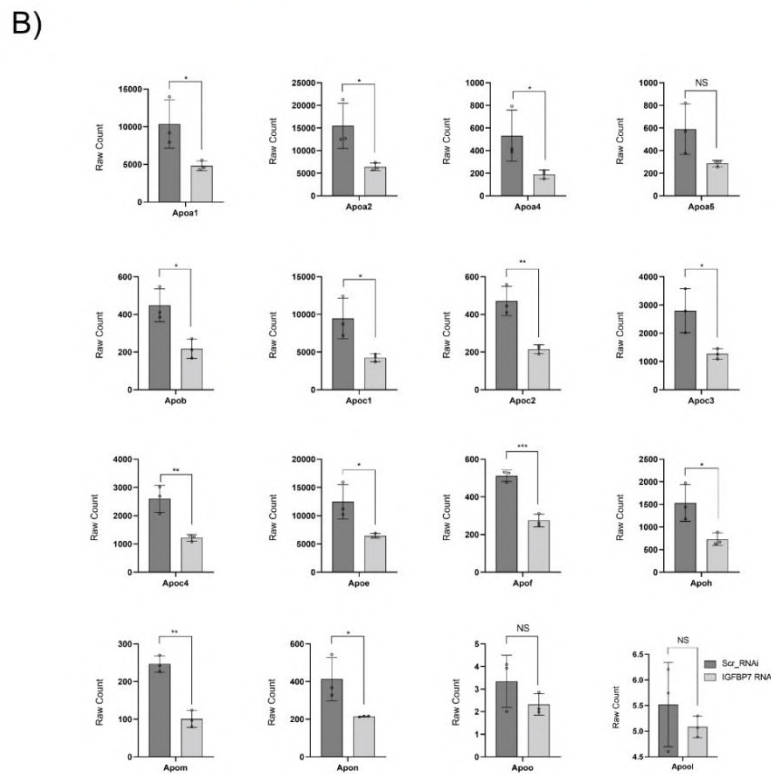
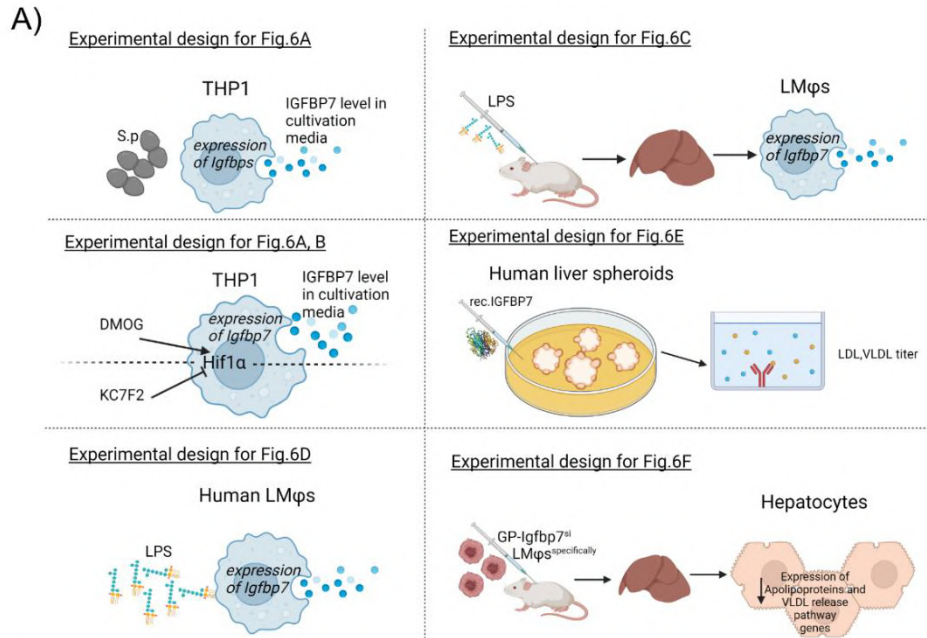
Appendix Figure S21. Representative confocal images documenting enhanced accumulation of fluorescently labeled FFAs (FFAs-Bodipy (magenta), ThermoScientific) in infection-activated macrophages (green; right) compared to controls (left). The scale bar represents 15um.



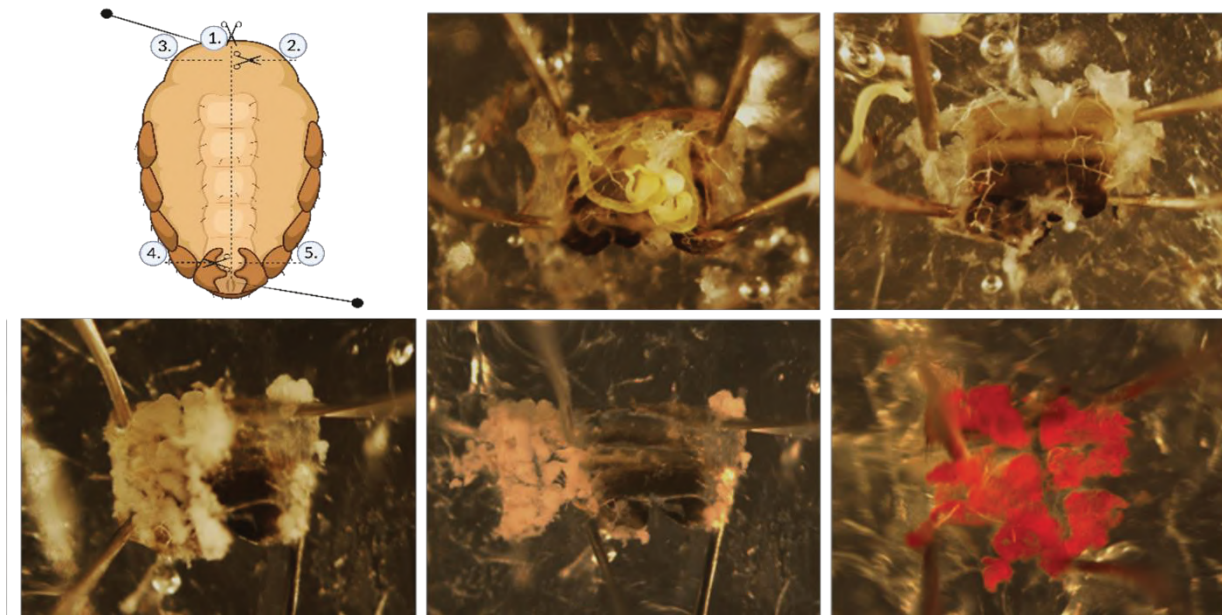
Appendix Figure S22. Heat map documenting the altered expression of scavenger receptors in macrophages post-infection.



Appendix Figure S23. Heat map documenting the enhanced expression of genes involved in lipid processing and regulation of lipid storage.



Appendix Figure S24. (A) Schematic overview of the experimental strategy used in the subsequent experiments performed on mammalian models. (B) Raw count mRNA level of the apolipoprotein genes in hepatocytes isolated from control mice (Scr_RNAi) and mice with liver macrophage-specific knockdown of *IGFBP7* (IGFBP7 RNAi). Data were obtained from four independent experiments. *The line/bar shows mean ± SD, asterisks mark statistically significant differences (*p<0.05; **p<0.01; ***p<0.001). Results compared by unpaired t test.*



Appendix Figure S25. Graphical documentation of the process of the fat body dissection from the adult fly abdomen. The dissected fat body was subsequently stained by OilRedO (right bottom image).





CHAPTER IV:

Liver macrophages regulate systemic metabolism through non-inflammatory factors

Cecilia Morgantini, Jennifer Jager, Xidan Li, Laura Levi, Valerio Azzimato, André Sulen, Emelie Barreby, Connie Xu, Michaela Tencerova, Erik Näslund, Chanchal Kumar, Francisco Verdeguer, Sara Straniero, Kjell Hultenby, Niklas K Björkström, Ewa Ellis, Mikael Rydén, Claudia Kutter, Tracey Hurrell, Volker M Lauschke, Jeremie Boucher, Aleš Tomčala, **Gabriela Krejčová**, Adam Bajgar, Myriam Aouadi

Nature Metabolism, 2019, 4:445-459

Liver macrophages regulate systemic metabolism through non-inflammatory factors

Cecilia Morgantini ¹, Jennifer Jager^{1,17}, Xidan Li¹, Laura Levi¹, Valerio Azzimato¹, André Sulen¹, Emelie Barreby¹, Connie Xu¹, Michaela Tencerova², Erik Näslund³, Chanchal Kumar^{1,4}, Francisco Verdeguer⁵, Sara Straniero⁶, Kjell Hultén⁷, Niklas K. Björkström ⁸, Ewa Ellis⁹, Mikael Rydén ¹⁰, Claudia Kutter¹¹, Tracey Hurrell¹², Volker M. Lauschke¹³, Jeremie Boucher^{13,14}, Aleš Tomčala¹⁵, Gabriela Krejčová¹⁶, Adam Bajgar¹⁶ and Myriam Aouadi ^{1*}

Liver macrophages (LMs) have been proposed to contribute to metabolic disease through secretion of inflammatory cytokines. However, anti-inflammatory drugs lead to only modest improvements in systemic metabolism. Here we show that LMs do not undergo a proinflammatory phenotypic switch in obesity-induced insulin resistance in flies, mice and humans. Instead, we find that LMs produce non-inflammatory factors, such as insulin-like growth factor-binding protein 7 (IGFBP7), that directly regulate liver metabolism. IGFBP7 binds to the insulin receptor and induces lipogenesis and gluconeogenesis via activation of extracellular-signal-regulated kinase (ERK) signalling. We further show that IGFBP7 is subject to RNA editing at a higher frequency in insulin-resistant than in insulin-sensitive obese patients (90% versus 30%, respectively), resulting in an IGFBP7 isoform with potentially higher capacity to bind to the insulin receptor. Our study demonstrates that LMs can contribute to insulin resistance independently of their inflammatory status and indicates that non-inflammatory factors produced by macrophages might represent new drug targets for the treatment of metabolic diseases.

The liver has a major role in maintaining normal blood glucose levels¹. In metabolic diseases, such as obesity-associated insulin resistance, impaired hormonal regulation of liver glucose production leads to fasting hyperglycaemia, a hallmark of type 2 diabetes (T2D)². Liver inflammation has been implicated in dysregulation of hepatic glucose production in insulin resistance and progression from simple steatosis to steatohepatitis and liver fibrosis^{3,4}. In obesity, LMs have been reported to undergo a phenotypic switch from an anti-inflammatory (M2) state to a proinflammatory (M1) activation state, consequently having a central role in liver inflammation and the emergence of insulin resistance⁵. Activated LMs are thought to directly inhibit the ability of insulin to block hepatic glucose production via production of inflammatory cytokines³.

However, the metabolic effects of anti-inflammatory drugs have remained modest in most clinical trials^{6–8}, suggesting a limited role for inflammation in metabolic regulation. Conversely, LM depletion has been reported to impact metabolism in obese mice^{9–13}, suggesting an unknown contribution of macrophages to the regulation

of insulin sensitivity. To test this possibility, we performed unbiased transcriptomic analyses of human LMs, encompassing both resident and infiltrating macrophages, isolated from insulin-sensitive and insulin-resistant obese patients as well as lean individuals. Surprisingly, obesity and insulin resistance were not associated with a proinflammatory phenotypic switch in LMs. However, we found that LMs regulated hepatocyte function via production of non-inflammatory factors such as Igfbp7, encoded by a gene previously shown to regulate insulin signalling in mammalian cells and flies^{14–16}. Taken together, the findings of this study indicate that LM-derived non-inflammatory factors, rather than inflammatory cues, underlie LM-dependent metabolic remodelling.

Results

Obesity is not associated with LM activation. To investigate the inflammatory status of LMs in obesity, we measured the expression of genes encoding proinflammatory cytokines (*Il18*, *Tnf*, *Il1b*, *Il12a* and *Infγ*), anti-inflammatory cytokines (*Il10*, *Tgfb1*, *Infba1*,

¹Integrated Cardio Metabolic Center (ICMC), Department of Medicine, Karolinska Institutet, Huddinge, Sweden. ²Department of Molecular Endocrinology, KMEB, University of Southern Denmark, Odense University Hospital and Danish Diabetes Academy, Odense, Denmark. ³Division of Surgery, Department of Clinical Sciences, Danderyd Hospital, Karolinska Institutet, Stockholm, Sweden. ⁴Translational Sciences, Cardiovascular, Renal and Metabolic Diseases, IMED Biotech Unit, AstraZeneca, Gothenburg, Sweden. ⁵Department of Molecular Mechanisms of Disease, University of Zurich, Zurich, Switzerland.

⁶Metabolism Unit C2:94, Department of Medicine, and Center for Innovative Medicine, Department of Biosciences and Nutrition, Karolinska Institutet, Huddinge, Stockholm, Sweden. ⁷Department of Laboratory Medicine, Clinical Research Center, Karolinska Institutet, Huddinge, Sweden. ⁸Center for Infectious Medicine, Department of Medicine Huddinge, Karolinska Institutet, Karolinska University Hospital, Stockholm, Sweden. ⁹Division of Transplantation Surgery, CLINTEC, Karolinska Institutet, Huddinge, Sweden. ¹⁰Unit of Endocrinology, Department of Medicine, Karolinska Institutet, Huddinge, Sweden. ¹¹Department of Microbiology, Tumor and Cell Biology, Science for Life Laboratory, Karolinska Institutet, Stockholm, Sweden. ¹²Section of Pharmacogenetics, Department of Physiology and Pharmacology, Karolinska Institutet, Solna, Sweden. ¹³Bioscience, Cardiovascular, Renal and Metabolism, IMED Biotech Unit, AstraZeneca, Gothenburg, Sweden. ¹⁴Wallenberg Centre for Molecular and Translational Medicine, Lundberg Laboratory for Diabetes Research, University of Gothenburg, Gothenburg, Sweden. ¹⁵Laboratory of Evolutionary Protistology, Institute of Parasitology, Biology Centre, Czech Academy of Sciences, Ceske Budejovice, Czech Republic. ¹⁶Faculty of Science, University of South Bohemia, and Institute of Entomology, Biology Centre, Czech Academy of Sciences, Ceske Budejovice, Czech Republic. ¹⁷Present address: Université Nice Côte d'Azur, INSERM U1065, C3M, Team Cellular and Molecular Physiopathology of Obesity, Nice, France. *e-mail: myriam.aouadi@ki.se

Il4 and *Il13*), chemokines (*Ccl8*, *Cxcl10*, *Ccl3*, *Ccl2* and *Ccl5*), LM markers (*Cd68*, *Adgre1*, *Clec4f* and *Ilgam*), M1 markers (*Ilgax*, *Gpr18*, *Fpr2*, *Tlr2*, *Socs3*, *Cd80*, *Cd86*, *Tlr4*, *Cd38* and *Nos2*) and M2 markers (*Il1r1*, *Chil3*, *Arg1*, *Myc*, *Mrc1*, *Cd200r1*, *Egr2* and *Tgm2*) by RNA-seq in LMs from lean and obese patients (for clinical data, see Supplementary Table 1a–c). We also measured the expression of markers for metabolically activated (MMe) macrophages (*Abca1*, *Cd36* and *Plin2*), which have been found in the adipose tissue of obese humans and animals¹⁷.

In contrast to the current paradigm in which LMs switch to an inflammatory state in obesity, we did not observe a proinflammatory transcriptomic profile for LMs from obese individuals in comparison to lean controls (Fig. 1a and Supplementary Table 2). Similarly, we did not observe differential expression of MMe markers¹⁷. Because previous studies demonstrated an association between insulin resistance and inflammation when patients were matched for body mass index (BMI)^{18,19}, we compared the expression of inflammatory markers in insulin-resistant versus insulin-sensitive obese patients. However, insulin resistance was not associated with increased expression of inflammatory markers in LMs from obese patients matched for BMI (Fig. 1a and Supplementary Table 2). Because most studies on the contribution of liver inflammation to insulin resistance have been based on gene expression in whole liver rather than in isolated macrophages, we analysed the inflammatory status of whole liver by using previously published datasets comparing lean individuals to obese individuals or patients with nonalcoholic fatty liver disease (NAFLD)^{20,21}. Similarly to the findings for isolated LMs, whole-liver transcriptomic analyses did not show a proinflammatory profile in obese individuals or patients with NAFLD in comparison to healthy individuals (Supplementary Table 3).

Obesity-induced liver inflammation in mice has primarily been studied following long-term high-fat feeding. We therefore examined whether metabolic impairment and LM activation occurred simultaneously in mice by analysing the kinetics of macrophage activation during development of obesity. We first measured the expression of four inflammatory cytokine genes (*Il1b*, *Il18*, *Tnf* and *Ccl2*) in LMs isolated from mice fed a normal diet (ND) or a high-fat diet (HFD) for 3, 9 or 12 weeks. Weight gain, liver lipid accumulation, fasting hyperglycaemia and glucose intolerance were observed as early as 9 weeks for HFD-fed mice (Fig. 1b–d and Supplementary Fig. 1a–c). Interestingly, expression of *Tnf* in LMs was significantly increased only after 12 weeks of HFD feeding, whereas no significant difference was observed in expression of the other cytokines (Fig. 1e). In addition, flow cytometry analyses showed that recruitment of infiltrating macrophages occurred after 12 weeks of HFD feeding, but not after 9 weeks (Supplementary Fig. 1d,e). In line with previous studies, *Tnf* expression was significantly increased in adipose tissue macrophages in mice fed a HFD at as early as 9 weeks (Supplementary Fig. 1f). These results are consistent with those from previous studies reporting that liver inflammation following long-term high-fat feeding in mice is due to the recruitment of monocytes/macrophages²². More notably, these results indicate that macrophage activation in the liver is not required for the initiation of metabolic impairment induced by obesity in mice.

By using glucan-encapsulated RNAi particles (GeRPs)^{23,24} to silence gene expression specifically in LMs²⁵, we previously demonstrated that silencing of *Nfkb* (p65, encoded by *Rela*) in LMs improved insulin sensitivity in obese (*ob/ob*) mice. We had hypothesized that these effects were due to reduced expression of the inflammatory cytokine gene *Il1b* in LMs²⁵. However, NF- κ B is known as a major regulator of not only inflammatory responses but also broader cellular activities, including cell proliferation, death and survival²⁶. We therefore sought to determine whether the beneficial effects of *Nfkb* silencing on metabolism in obese mice were indeed due to decreased transcription of inflammatory cytokines in LMs. GeRP-mediated *Nfkb* silencing in LMs was thus performed according to the protocol

previously used to improve insulin sensitivity in obese mice²⁵. Thereafter, global run-on sequencing (GRO-seq), which allows for measurement of nascent rather than steady-state transcript levels²⁷, was performed in LMs. Surprisingly, although obese mice exhibited improved glucose tolerance with GeRP treatment, transcription of the majority of inflammatory cytokines, including *Il1b* transcription, remained unaffected by *Nfkb* silencing in LMs (Supplementary Fig. 1g–i). In addition, *Il1b* silencing with GeRPs did not affect glucose tolerance in obese mice (Supplementary Fig. 1j). These data strongly suggest that *Nfkb* expressed by LMs does not regulate insulin sensitivity in obese mice via inflammatory gene regulation and that *Il1b* expressed by LMs does not contribute to obesity-induced insulin resistance in mice. Similarly, specific silencing of another major regulator of inflammation, c-Jun N-terminal kinase (JNK1/JNK2; encoded by *Mapk8/Mapk9*), in LMs had no impact on glucose tolerance in obese mice (Supplementary Fig. 1k). Collectively, these results suggest that obesity-associated insulin resistance occurs independently of LM inflammatory pathway activation.

On the basis of these observations, we further analysed the phenotype of LMs from mice fed a HFD for 9 weeks, which, like obese humans, displayed metabolic impairments without a change in *Tnf* expression. To determine the transcriptomic profile of LMs, we first compared the gene expression profiles of macrophages isolated from the livers of mice by using two different methods: gradient centrifugation/adherence²⁸ and FACS sorting with antibodies specific for the macrophage markers CD11b and F4/80 (ref. 22). The transcriptomic profiles of LMs isolated via these two different methods were extremely similar (Supplementary Fig. 1l). Most notably, expression remained unchanged for the majority of inflammatory markers in LMs during the emergence of metabolic impairments induced by HFD feeding (gradient/adherence method, Fig. 1f and Supplementary Table 4; sorted cells, Supplementary Fig. 1m). In addition, in both humans and mice, pathway analyses showed that activation of many inflammatory processes was actually decreased in LMs with insulin resistance and obesity (Fig. 1g,h and Supplementary Data 1 and 2). These results demonstrate that obesity does not cause LM activation in mice and humans. In addition, obesity-induced insulin resistance occurs independently of LM activation.

***Igfbp7* expression and editing in LMs.** Although LMs did not undergo a proinflammatory phenotypic switch in obesity, they could still have an important role in the regulation of insulin sensitivity, as their depletion before or during high-fat feeding prevents the development of insulin resistance in obese mice^{11,13,29}. To test this possibility, we applied our unbiased transcriptomic data to compare the gene expression of whole liver and LMs for mice fed a HFD to expression in the corresponding tissue in ND-fed mice. Obesity resulted in a significant difference in the expression of 1,690 genes in LMs and 169 genes in whole liver (Fig. 2a and Supplementary Data 3). These data suggest that, despite failing to show inflammatory activation, LMs undergo major changes in transcriptional regulation during obesity.

Igfbp7 was the most highly expressed and upregulated gene in LMs isolated from HFD-fed mice in comparison to ND-fed mice (Fig. 2b and Supplementary Data 4). In line with this, IGFBP7 protein levels were also increased in LMs from HFD- as compared to ND-fed mice isolated by the two different methods described above (Fig. 2c and Supplementary Fig. 2a). Furthermore, IGFBP7 protein secretion by LMs was increased with obesity, whereas blood levels were slightly decreased, suggesting local upregulation of IGFBP7 in the liver (Fig. 2d and Supplementary Fig. 2b). Interestingly, although expressed in most tissues (Supplementary Fig. 2c), *Igfbp7* was highly expressed in LMs in comparison to hepatocytes as well as adipose tissue and peritoneal macrophages (Fig. 2e), suggesting tissue-macrophage-specific regulation of *Igfbp7*. The increase in IGFBP7

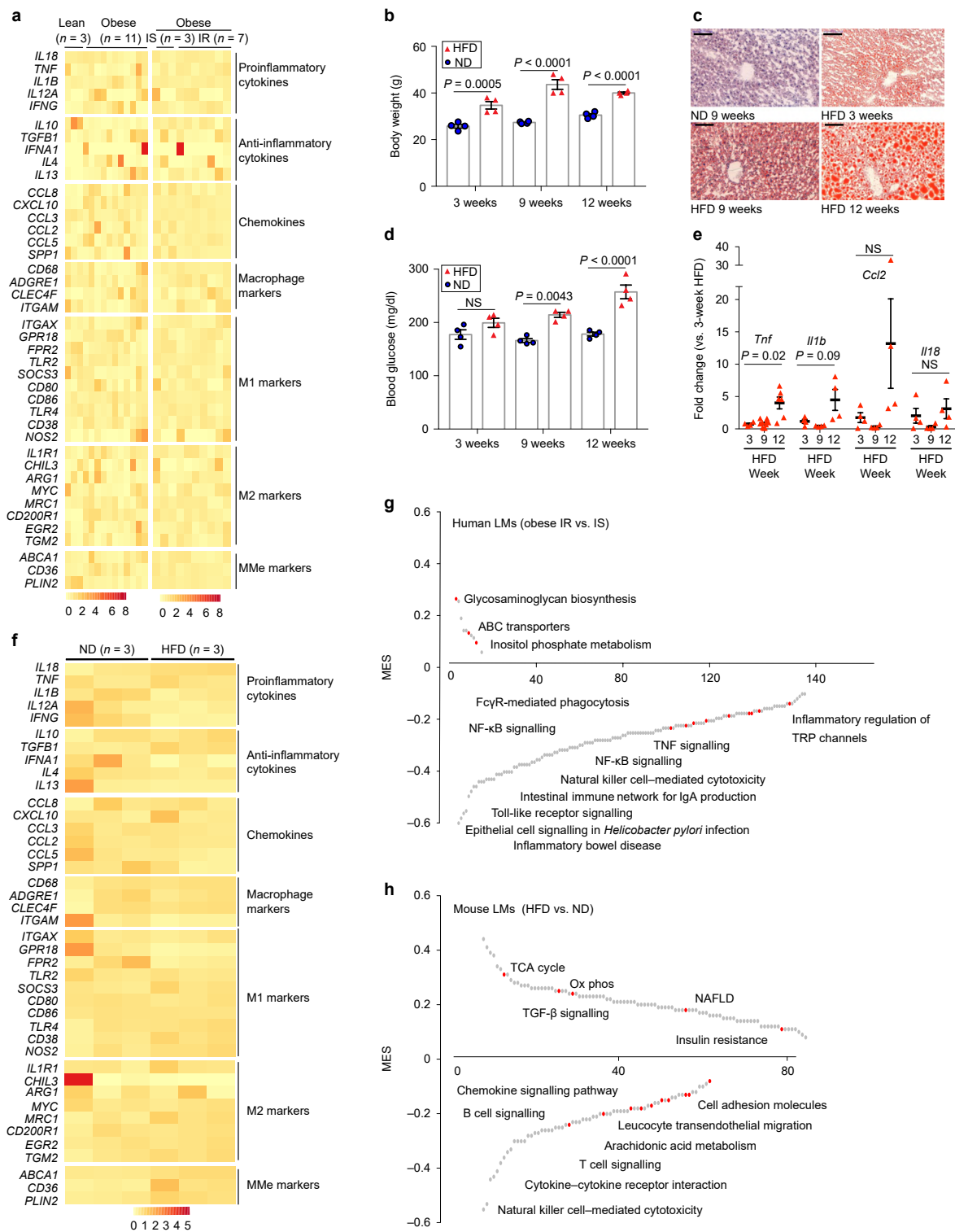


Fig. 1 | obesity-induced insulin resistance occurs independently of inflammation. **a**, Gene expression (normalized RPKM) in human LMs; *n* corresponds to the number of subjects. IR, insulin resistant; IS, insulin sensitive. **b**, Body weight of HFD-fed and ND-fed mice at the indicated times after starting the diet; *n* = 4 mice per condition. **c**, Liver Oil Red O staining (scale bars, 100 μm); five random images were acquired from five mice per group with similar results. **d**, Fasting glycaemia; *n* = 4 mice per condition. **e**, Fold change (FC) in expression of *Tnf*, *Il1b*, *Ccl2* and *Il18* in LMs isolated from mice fed a HFD for 9 weeks (*n* = 10 mice for *Tnf*; *n* = 4 mice for the other genes) or 12 weeks (*n* = 6 mice for *Tnf*; *n* = 4 mice for the other genes) relative to LMs from mice fed a HFD for 3 weeks (*n* = 4). **f**, Gene expression (normalized RPKM) in mouse LMs; *n* corresponds to the number of mice. **g, h**, GeneSet enrichment analysis depicting up- and downregulated pathways in human (**g**) and mouse (**h**) LMs according to maximum estimate score (MES). The x axis indicates the rank of the pathways according to MES. *P* value was calculated by permutation test. To set the significance threshold, the adjusted *P* value was calculated by using the Benjamini–Hochberg method with false-discovery rate (FDR) < 0.1. Data are shown as the mean ± s.e.m. *P* values were calculated by one-way ANOVA with adjustment for multiple comparisons in **b** and **d** and by unpaired two-tailed Student’s *t* test in **e**; NS, not significant.

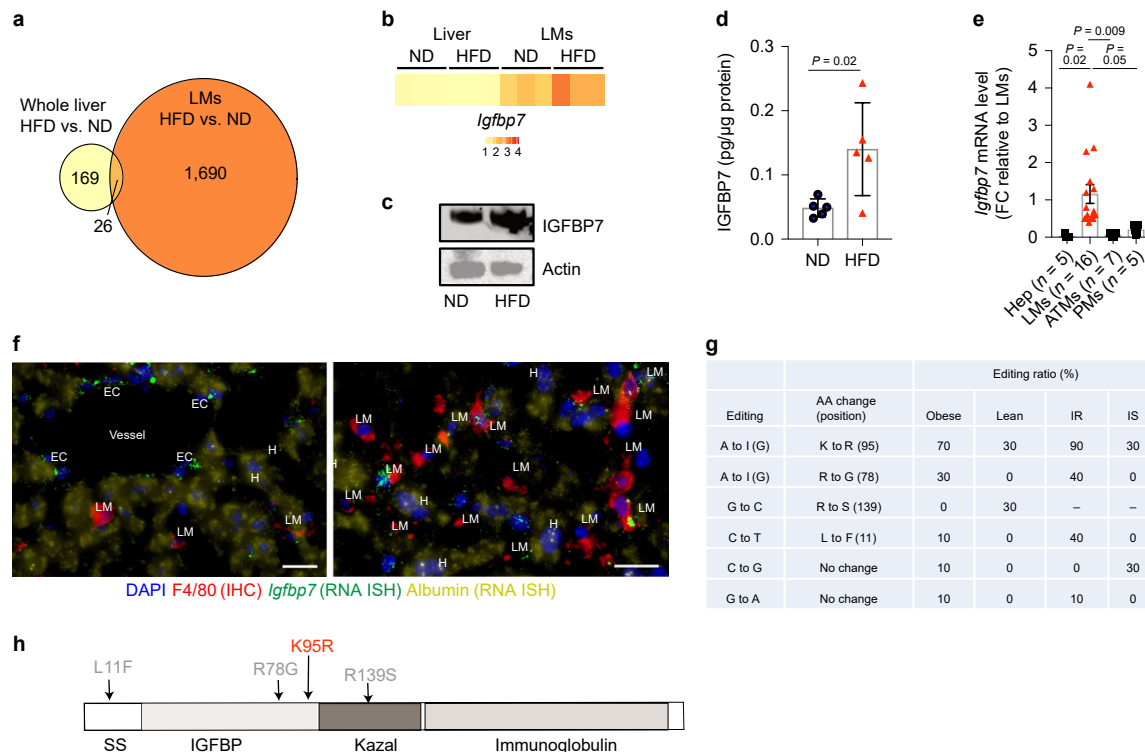


Fig. 2 | High-fat feeding increases *Igfbp7* expression in LMs. **a**, Diagram showing genes with significant differences in expression in mice with HFD versus ND feeding; $n = 3$ mice per condition. P value was calculated by Wald test with DESeq2. To set the significance threshold, the adjusted P value was calculated by the Benjamini–Hochberg method with $FDR < 0.05$. **b**, Comparison of *Igfbp7* expression (normalized RPKM) in mouse liver and LMs; $n = 3$ mice per condition. **c**, IGFBP7 protein expression in mouse LMs; $n = 3$ pooled mice/condition. **d**, IGFBP7 secretion from mouse LMs assessed by ELISA; $n = 5$ mice per condition. **e**, *Igfbp7* expression in different cell types in mice; the number of mice (n) is indicated. Hep, hepatocytes; ATMs, adipose tissue macrophages; PM, peripheral macrophages. **f**, RNA ISH combined with immunohistochemistry (IHC) for mouse liver (scale bars, 20 μ m); $n = 3$ independent experiments with similar results. EC, endothelial cell; H, hepatocyte. **g**, *IGFBP7* RNA editing in human LMs. AA, amino acid. **h**, Representation of the positions at which RNA editing occurs with respect to the IGFBP7 protein domains. Data are shown as the mean \pm s.e.m. P values were calculated by unpaired two-tailed Student's t test.

expression induced by high-fat feeding was not due to hyperinsulinaemia or higher levels of nutrients in the extracellular environment, as treatment of LMs with glucose, insulin or palmitate did not induce expression of IGFBP7 (Supplementary Fig. 2d). Further investigation using RNA in situ hybridization (ISH) confirmed the absence of *Igfbp7* expression in hepatocytes, although expression was recorded in endothelial cells as previously described³⁰ and in macrophages (Fig. 2f and Supplementary Fig. 2e). Although *Igfbp7* is known to be expressed at similar levels in infiltrating and resident LMs³¹, expression of *Igfbp7* was not detected in all F4/80⁺ cells.

Similarly to observations in mice, levels of circulating IGFBP7 in humans were slightly but significantly decreased with obesity (Supplementary Fig. 2f). However, *IGFBP7* expression in LMs remained unchanged in obesity or insulin resistance in comparison to controls (Supplementary Fig. 2g and Supplementary Data 5). Because *IGFBP7* mRNA has previously been described as a target of adenosine deaminase acting on RNA (ADAR) enzymes^{32,33}, we analysed the sequence of *IGFBP7* in human LMs. *IGFBP7* was subject to adenosine-to-inosine RNA editing, which changed codon 95 from AAG to AIG in 90% of insulin-resistant obese patients (83% \pm 9%, mean transcripts edited \pm s.e.m.) in comparison to 30% of insulin-sensitive obese patients and lean individuals (Fig. 2g). This editing event was absent in mice (data not shown). As inosine is interpreted by the translational machinery as guanosine, *IGFBP7* RNA editing leads to an amino acid substitution of arginine for lysine, p.Lys95Arg, in the IGFBP domain of the protein (Fig. 2h). Previous studies have reported that this RNA editing of *IGFBP7* leads to production of distinct protein isoforms with different ligand affinities^{33,34}.

Altogether, these results show that obesity-associated insulin resistance increases *Igfbp7* expression in mouse LMs and results in RNA editing of *IGFBP7* in human LMs.

IGFBP7 does not directly regulate inflammation. To investigate the role of IGFBP7 in the regulation of LM phenotype, we applied GeRP technology^{23,24}, which delivers short interfering RNA (siRNA) and silences genes specifically in LMs, without affecting gene expression in other liver cells or the rest of the body²⁵. After screening for the most potent siRNA sequences in vitro (Supplementary Fig. 3a,b), we intravenously injected GeRPs loaded with either a control scrambled siRNA (GeRP-Scr) or *Igfbp7*-targeting siRNA (GeRP-*Igfbp7*) over a 15-d period into HFD-fed mice (protocol for treatment in Fig. 3a). Immunohistochemistry using an antibody against F4/80 showed specific delivery of FITC-labelled GeRPs to LMs following the 15-d treatment (Fig. 3a). Treatment with GeRP-*Igfbp7* significantly decreased *Igfbp7* expression in and secretion of the encoded protein from LMs in comparison to treatment with GeRP-Scr, whereas expression of *Igfbp7* remained unchanged in hepatocytes, which did not contain GeRPs (Fig. 3b,c and Supplementary Fig. 3c). Circulating levels of IGFBP7 remained unchanged following GeRP-mediated silencing (Supplementary Fig. 3d). These data confirm our previously published findings showing that GeRPs deliver siRNA to and silence genes specifically in LMs, but not in hepatocytes or other non-parenchymal cells (NPCs), when administered intravenously.

To investigate the effect of *Igfbp7* silencing on LM phenotype, we first performed RNA-seq on LMs isolated from mice treated with

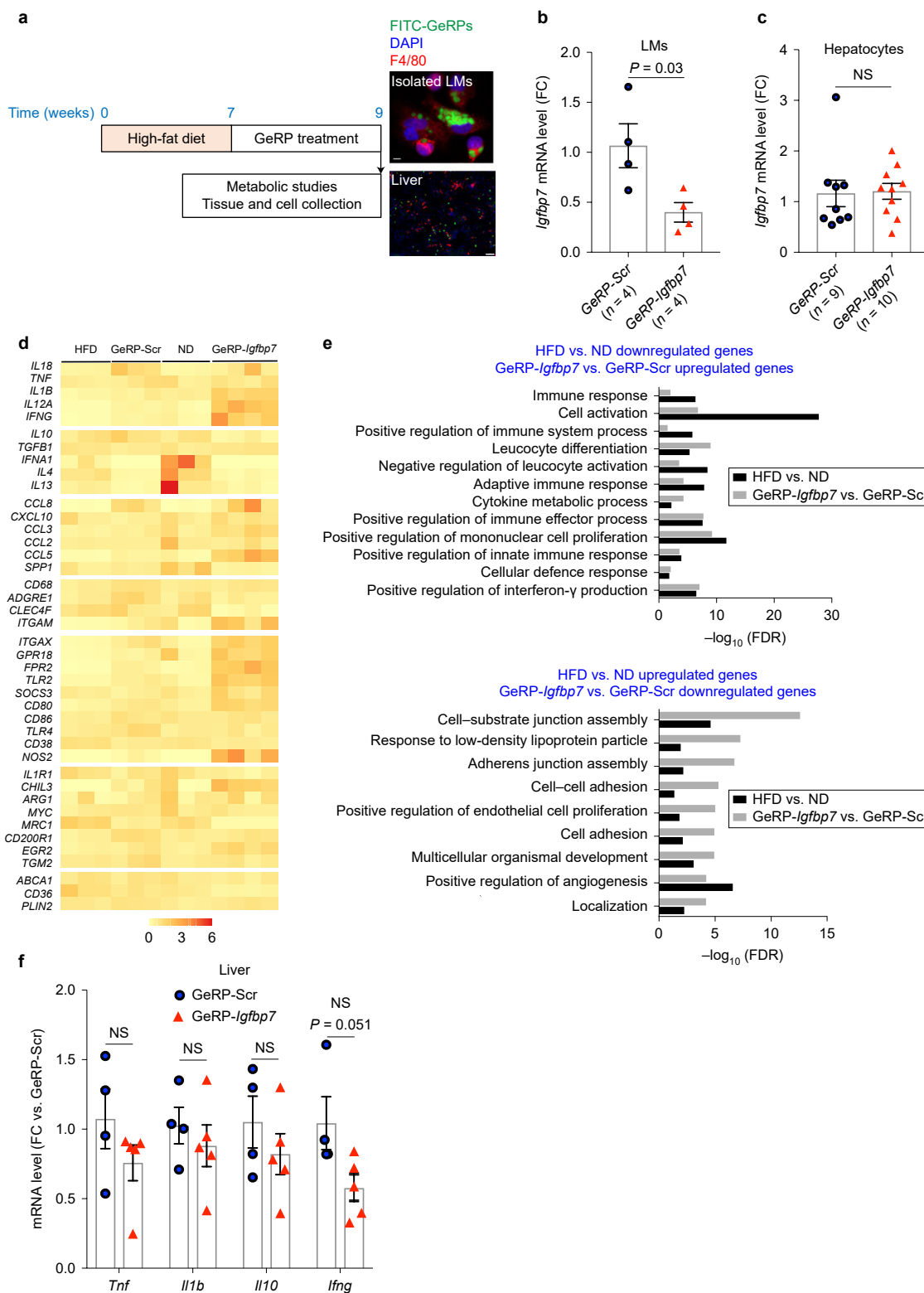


Fig. 3 | Phenotype of *Igfbp7*-deficient LMs. **a**, Protocol for GeRP treatment. Images show FITC-labelled GeRPs in isolated F4/80⁺ liver cells (top; scale bar, 5 μ m) and in liver (bottom; scale bar, 50 μ m); $n = 3$ independent experiments with similar results. **b, c**, *Igfbp7* expression in LMs (**b**) and hepatocytes (**c**) treated with GeRP-*Igfbp7*; the number of mice (n) is indicated. **d**, Gene expression pattern for selected genes (normalized RPKM) in LMs from mice treated with GeRP-*Igfbp7* ($n = 4$ mice) versus GeRP-Scr ($n = 3$ mice). **e**, Gene ontology enrichment analysis of genes inversely regulated in LMs from mice with HFD versus ND feeding and mice treated with GeRP-*Igfbp7* versus GeRP-Scr. P value was calculated by conditional hypergeometric test. To set the significance threshold, adjusted P value was calculated by the Benjamini–Hochberg method with $FDR < 0.05$. **f**, Inflammatory gene expression in whole liver from mice treated with GeRP-Scr ($n = 4$ mice) or GeRP-*Igfbp7* ($n = 5$ mice). Data are shown as the mean \pm s.e.m. P values were calculated by unpaired two-tailed Student’s t test.

GeRP-Scr versus GeRP-*Igfbp7*. In this transcriptomic analysis, the expression of 1,403 genes was significantly changed following *Igfbp7* silencing in LMs (Supplementary Data 6). Whereas GeRP-Scr treatment in HFD mice had no effect on the expression of genes involved in immune response in LMs in comparison to untreated HFD-fed mice, *Igfbp7* knockdown in LMs was associated with increased expression of several proinflammatory cytokine genes, including *Il1b*, *Il12a* and *Infg*, as well as several markers of M1 macrophages (Fig. 3d and Supplementary Table 5). Conversely, the cytokine gene *Il10* and other markers of M2 macrophages, such as *Mrc1*, were significantly downregulated following *Igfbp7* silencing in comparison to mice treated with GeRP-Scr and HFD- or ND-fed untreated mice (Fig. 3d). Interestingly, treatment with recombinant mouse IGFBP7 or silencing of *Igfbp7* in vitro had no effect on the expression of *Il1b* and *Il10*, suggesting that IGFBP7 does not directly regulate the inflammatory phenotype of LMs (Supplementary Fig. 3e,f).

To further investigate the phenotype acquired by LMs following *Igfbp7* silencing, we studied biological processes inversely regulated in mice fed a HFD versus a ND in comparison to mice treated with GeRP-*Igfbp7* versus GeRP-Scr. In line with the observed differential inflammatory gene expression, gene set enrichment analysis showed that inflammatory pathways whose activity was decreased with HFD feeding had increased activity following *Igfbp7* silencing (Fig. 3e and Supplementary Data 7). In contrast, pathways involved in cell adhesion and angiogenesis, which showed increased activity in HFD-fed mice, were downregulated in *Igfbp7*-deficient LMs (Fig. 3e). We next investigated the cell composition of NPCs following *Igfbp7* silencing by flow cytometry. Lymphocyte subset composition (CD3⁺CD4⁺ and CD3⁺CD8⁺) remained unchanged (Supplementary Fig. 3g); the proportions of LMs (CD45⁺F4/80⁺CD11b⁺) and recruited macrophages were slightly decreased, although absolute numbers remained the same (Supplementary Fig. 3h,i). More notably, inflammatory gene expression in whole liver remained unchanged in mice treated with GeRP-*Igfbp7* as compared to controls treated with GeRP-Scr (Fig. 3f).

These data suggest that *Igfbp7* silencing does not have a major impact on inflammatory gene expression and immune cell content in the liver.

***Igfbp7* deficiency in LMs improves metabolism.** To study the role of IGFBP in regulation of metabolism in obesity, we performed metabolic studies following GeRP-mediated *Igfbp7* silencing specifically in LMs in obese mice (Fig. 3a). *Igfbp7* deficiency in LMs led to a significant improvement in glucose tolerance, independently of a change in body weight or adipose tissue distribution (Fig. 4a and Supplementary Fig. 4a–c). Although treatment with GeRP-*Igfbp7* significantly reduced overnight fasting glycaemia, insulin tolerance tests showed no significant difference in insulin regulation of circulating glucose levels (Fig. 4b,c). In agreement with this, pancreatic islet mass and insulin levels in the fasted state and during the glucose tolerance tests remained unchanged (Supplementary Fig. 4d,e). These results suggest a selective effect of *Igfbp7* knockdown in LMs on regulation of fasting glycaemia. In accordance with this hypothesis, although fasting glycaemia was significantly decreased in mice treated with GeRP-*Igfbp7*, glucose clearance (as measured by percentage of baseline) remained unchanged (Supplementary Fig. 4f). Furthermore, liver insulin sensitivity, as measured by AKT phosphorylation, was improved owing to reduced AKT phosphorylation in the basal fasted state, rather than in response to treatment with insulin (Supplementary Fig. 4g). Intriguingly, mice that were fed a HFD for an additional 2 weeks while undergoing GeRP-mediated *Igfbp7* silencing showed a trend towards improvement in fasting glycaemia (Supplementary Fig. 4h). This suggests that regulation by IGFBP7 of glucose homeostasis occurs in a tight time frame that corresponds to the initiation of metabolic impairment by high-fat feeding rather than its maintenance.

Notably, silencing of *Igfbp7* in LMs drastically reduced accumulation of total triglycerides (TGs) in liver, whereas circulating levels of free fatty acids (FFAs), glycerol, TGs and cholesterol remained unchanged (Fig. 4d–g and Supplementary Fig. 4i–k). This improvement in hepatic steatosis was due to decreased lipid content in hepatocytes rather than NPCs, as observed by electron microscopy and flow cytometry analysis using the lipid stain LipidTOX (Fig. 4h,i). This was not surprising given that lipid content in NPCs, as assessed by LipidTOX staining, was not affected by 9 weeks of HFD feeding (Supplementary Fig. 4l).

To further investigate the effect of *Igfbp7* silencing in LMs on hyperglycaemia and hepatic steatosis, we performed RNA-seq on hepatocytes isolated from mice treated with GeRP-Scr or GeRP-*Igfbp7* (Supplementary Data 8). In line with the metabolic studies, transcriptomic analyses showed that pathways and genes involved in lipid metabolism and glucose production had significantly decreased activity following *Igfbp7* silencing in LMs in vivo (Fig. 4j,k and Supplementary Data 9). qPCR analyses in hepatocytes confirmed that the expression of genes involved in lipogenesis, such as *Srebf1* (also known as *Srebp1c*; encoding sterol regulatory element-binding protein 1), and gluconeogenesis, such as *G6pc* (encoding glucose-6-phosphatase) and *Pck1* (also known as *Pepck*; encoding phosphoenolpyruvate carboxykinase), was significantly downregulated (Fig. 4l). Notably, levels of fasting glucogenic hormones such as glucagon, epinephrine, norepinephrine and corticosterone and the activity of their downstream signalling pathway (protein kinase A, PKA) remained unchanged (Supplementary Fig. 4m–q). These data suggest that *Igfbp7* silencing in LMs corrects hyperglycaemia and decreases hepatic steatosis by reducing the expression of genes involved in gluconeogenic and lipogenic pathways independently of hormonal regulation of lipid and glucose metabolism.

Because the homologue of *Igfbp7* in *Drosophila melanogaster*, *ImpL2*, has been extensively described to be produced by cancer cells and to regulate insulin signalling^{14,15}, we focused further investigation on studying the role of *ImpL2* in the regulation of metabolism in a fly model of obesity. We first assessed the expression of *ImpL2* in haemocytes under physiological conditions by using the phagocytic marker pHrodo Green. mCherry expressed under the control of the *ImpL2* promoter colocalized with the pHrodo Green signal, suggesting that *ImpL2* is expressed in haemocytes (Fig. 4m). Similarly to our observations in mice, *ImpL2* was also expressed by non-phagocytic cells, while some haemocytes did not express any *ImpL2* (Fig. 4m). More notably, we observed an increase in *ImpL2* expression in sorted haemocytes from HFD- as compared to ND-fed flies (Fig. 4n,o). In line with the human and mouse findings, adult *Drosophila* fed a HFD for 10 d, a protocol that induced glucose and lipid accumulation in whole-body homogenates (Fig. 4p,q), did not exhibit any change in the expression of inflammatory markers in haemocytes (Fig. 4r). Remarkably, the effect of *Igfbp7* silencing in LMs in mice was conserved in *Drosophila*, with *ImpL2* silencing in haemocytes significantly decreasing glucose accumulation and TG content in whole-body homogenates of flies fed a HFD (Fig. 4s,t and Supplementary Fig. 4r).

These data suggest that silencing of *Igfbp7* specifically in LMs and of *ImpL2* in haemocytes improves metabolism in mice and flies, respectively.

LM IGFBP7 regulates hepatocyte function. To investigate the mechanism through which the IGFBP7 produced by LMs regulates hepatic function, we first studied the effect of recombinant IGFBP7 on the insulin signalling pathway in healthy mouse hepatocytes in vitro. AKT phosphorylation was measured following treatment with recombinant IGFBP7 in the absence or presence of insulin. Surprisingly, whereas recombinant IGFBP7 had no effect on AKT activation in the absence of insulin, it enhanced the phosphorylation of AKT induced by insulin (Fig. 5a). Because treatment with

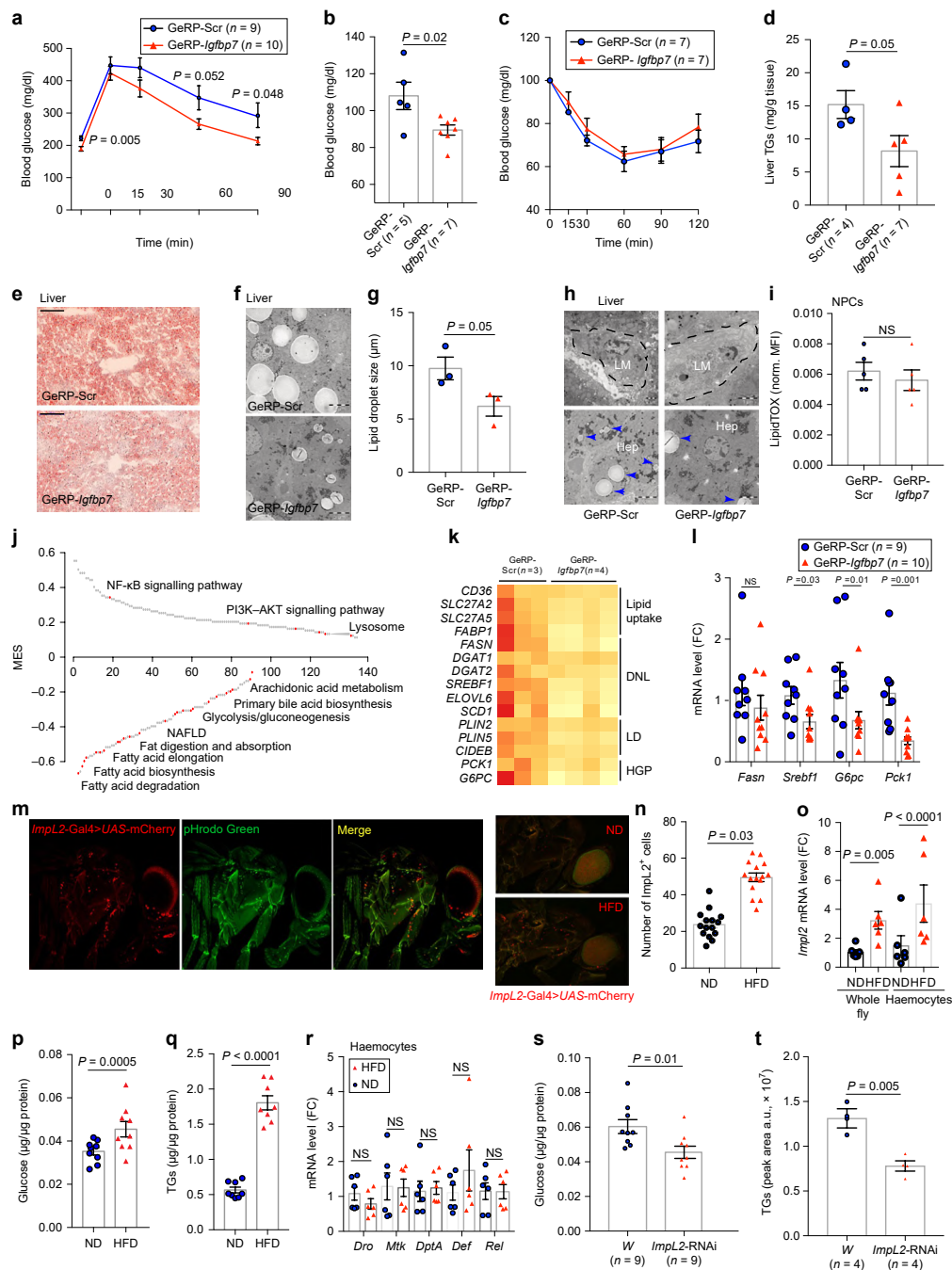


Fig. 4 | Silencing of *Igfbp7* in LMs decreases hyperglycaemia and hepatic steatosis. **a–d**, Glucose tolerance tests (**a**), overnight fasting glycaemia (**b**), insulin tolerance tests (**c**) and liver TG levels (**d**) in mice treated with GeRP-Scr or GeRP-*Igfbp7*; the number of mice (*n*) is indicated. **e**, Representative images of Oil Red O staining performed in mice treated with GeRP-Scr (*n* = 4) or GeRP-*Igfbp7* (*n* = 5) (scale bars, 100 μm); five random images were taken per mouse with similar results. **f, g**, Liver transmission electron microscopy (TEM) images (**f**) and lipid droplet size quantification (**g**). **h**, LM and hepatocyte TEM (blue arrowheads indicate lipid droplets); for all TEM experiments, 15 images were randomly acquired from 3 different mice treated with GeRP-Scr or GeRP-*Igfbp7*. **i**, NPC lipidTOX staining measured by flow cytometry; *n* = 5 mice per condition. MFI, median fluorescence intensity. **j**, GSEA enrichment analysis depicting up- and downregulated pathways in hepatocytes from mice treated with GeRP-Scr (*n* = 3) or GeRP-*Igfbp7* (*n* = 4) according to MES. The x axis indicates the rank of the pathways according to MES. *P* value was calculated by permutation test. To set the significance threshold, adjusted *P* value was calculated by the Benjamini–Hochberg method with FDR < 0.1. **k, l**, Gene expression pattern of selected genes (normalized RPKM) (**k**) and gene expression by qPCR (**l**) in isolated hepatocytes from mice treated with GeRP-Scr or GeRP-*Igfbp7*; the number of mice (*n*) is indicated. DNL, de novo lipogenesis; HGP, hepatic glucose production. **m**, Images of *ImpL2-Gal4>UAS-mCherry* flies showing *ImpL2*⁺ cells (red), pHrodo Green staining (green) and overlay (merge). Images to the right represent flies fed a ND or HFD. The green channel was used to visualize structure and for orientation; *n* = 8 independent experiments with similar results. **n, o**, *ImpL2*⁺ haemocytes counted in 15 randomly selected flies per condition (**n**) and *ImpL2* expression in *n* = 6 flies per condition (**o**). **p, q**, Glucose (**p**) and TG (**q**) levels in *n* = 9 flies per condition. **r**, Immune gene expression in haemocytes; *n* = 6 flies per condition. **s, t**, Glucose (**s**) and TG (**t**) levels in *ImpL2-RNAi* (*Hml-Gal4>ImpL2-RNAi*) versus *W* (*Hml-Gal4 × w*) *Drosophila* fed a HFD; the number of flies (*n*) is indicated. A.u., arbitrary units. Data are shown as the mean ± s.e.m. *P* values were calculated by unpaired two-tailed Student's *t* test in all panels except **o**, where one-way ANOVA was used with adjustment for multiple comparisons. DNL, de novo lipogenesis; LD, lipid droplets; HGP, hepatic glucose production.

recombinant IGFBP7 increased the AKT activation induced by insulin, we tested the effect of *Igfbp7* silencing in LMs on glucose homeostasis in healthy lean mice. Blood glucose levels were measured in a fasted state and following 2 h of refeeding, which induces insulin release and blockage of hepatic glucose production via AKT activation. Silencing of *Igfbp7* in LMs in lean mice resulted in increased blood glucose levels after refeeding, in agreement with a decreased ability of insulin to inhibit hepatic glucose production (Fig. 5b and Supplementary Fig. 5a). These results corroborate the hypothesis that in lean animals the IGFBP7 produced by LMs enhances insulin signalling.

IGFBP7 has been suggested to bind to insulin or its receptor and to regulate insulin signalling in mammalian cells and flies^{16,35}. We therefore tested whether IGFBP7 could enhance insulin activation of AKT through binding to the insulin receptor (IR). Coimmunoprecipitation assays showed that IGFBP7 could bind to the IR and induce its tyrosine phosphorylation as well as activation of insulin receptor substrate 2 (IRS2) (Fig. 5c and Supplementary Fig. 5b). Interestingly, treatment with insulin did not disrupt interaction of IGFBP7 with the IR in healthy hepatocytes (Fig. 5c). Furthermore, binding of IGFBP7 to the IR was specific, as coimmunoprecipitation experiments using an antibody against the LDL receptor did not show any IGFBP7 binding (Supplementary Fig. 5c). Treatment with an IR antagonist reduced the effect of insulin and recombinant IGFBP7 on insulin-induced AKT phosphorylation (Fig. 5d), confirming binding of IGFBP7 to the IR in the presence of insulin to enhance AKT phosphorylation in healthy hepatocytes.

Igfbp7 silencing in insulin-resistant animals improved glucose homeostasis, suggesting a detrimental role for IGFBP7 in metabolically impaired animals in comparison to healthy animals (Fig. 4). We therefore studied the effect of recombinant IGFBP7 on insulin signalling in insulin-resistant hepatocytes. To this end, we induced insulin resistance in hepatocytes through long-term insulin treatment (16 h), which blocks the ability of insulin to activate AKT. Under this condition, neither insulin nor recombinant IGFBP7 had an effect on AKT phosphorylation (Fig. 5e). These results suggest that the inability of insulin to activate AKT in insulin resistance cannot be rescued by recombinant IGFBP7. In coimmunoprecipitation experiments, insulin resistance reduced the ability of IGFBP7 to bind to the IR, which could at least partly explain the lack of effect of recombinant IGFBP7 on AKT phosphorylation (Fig. 5f). This raised the question of how silencing of IGFBP7 *in vivo* improves hepatic metabolic status in insulin-resistant obese animals. Some IGFBP family members have been reported to activate the MAPK pathway via ERK1 and ERK2 (ERK1/2)^{35,36}, and this activation has been implicated in pathological concomitant activation of lipogenesis and gluconeogenesis³⁶. Thus, we hypothesized that *Igfbp7* silencing in LMs in an insulin-resistant state could result in decreased hyperglycaemia and hepatic steatosis as a result of reduced ERK1/2 activation. In line with this hypothesis, phosphorylation of ERK1/2, which remained unchanged upon treatment with insulin, was increased by recombinant IGFBP7 treatment in insulin-resistant hepatocytes (Fig. 5g). We then studied the recruitment of an upstream regulator of the ERK pathway, Shc, to the IR. Recombinant IGFBP7 treatment was associated with higher recruitment of Shc to the IR under insulin resistance (Fig. 5h). Notably, inhibition of ERK1/2 phosphorylation by a MEK inhibitor (U0126) blocked induction of the expression of gluconeogenic (*G6Pc* and *Pck1*) and lipogenic (*Fasn* and *Srebf1*) genes, whose expression was induced by recombinant IGFBP7 in hepatocytes (Fig. 5i). Overall, these data suggest that in healthy, insulin-sensitive hepatocytes recombinant IGFBP7 binds to the IR and enhances AKT activation by insulin, leading to decreased gluconeogenesis. Conversely, in insulin-resistant hepatocytes, binding of recombinant IGFBP7 to the IR is reduced but still sufficient to activate ERK1/2 and induce expression of gluconeogenic and lipogenic genes.

As mentioned above, RNA editing of *IGFBP7* occurred at a higher frequency in insulin-resistant obese patients than in insulin-sensitive individuals (Fig. 2g). Because previous studies^{33,34} have suggested that this editing event leads to generation of a new isoform, we tested the effect of wild-type and edited IGFBP7 on insulin signalling in 3D cultures of primary human hepatocytes (liver spheroids; Fig. 5j). As expected, insulin induced both AKT and ERK1/2 phosphorylation, which was blocked under insulin resistance (Fig. 5k). Similarly to the effect observed in mouse hepatocytes with recombinant IGFBP7, treatment with wild-type or edited human IGFBP7 enhanced the AKT phosphorylation induced by insulin. Edited IGFBP7 by itself was able to increase AKT phosphorylation in the insulin-resistant state, although to a lesser extent than in the insulin-sensitive state (Fig. 5k). Because *IGFBP7* editing has been suggested to affect the binding affinity of IGFBP7 for ligands, and mouse experiments have shown that higher binding capacity of IGFBP7 for the IR is associated with elevated AKT phosphorylation by insulin, we tested whether wild-type and edited IGFBP7 bound to the IR with different affinity in human liver spheroids. In line with the previous studies, we found that edited IGFBP7 coimmunoprecipitated to a higher degree with the IR than wild-type IGFBP7 under insulin resistance, which could explain the ability of edited IGFBP7 to still activate AKT in the insulin-resistant state (Fig. 5l).

In summary, these results demonstrate that in mice LMs can produce factors such as IGFBP7 that can directly impair hepatic function, in particular gluconeogenesis and lipogenesis, by regulating ERK1/2 activation. In humans, IGFBP7 undergoes RNA editing, which confers a higher capacity to bind the IR and regulate its downstream signalling (Fig. 6).

Discussion

In this study, we investigated the relevance of LM proinflammatory activation in obesity-induced insulin resistance. We used unbiased transcriptomic profiling of isolated human LMs and determined that the expression of inflammatory genes remained unchanged in states of obesity and insulin resistance (Fig. 1). Similarly, initiation of metabolic impairment in obese mice occurred independently of LM activation (Fig. 1). High-fat feeding also failed to induce an immune response in a third species, *Drosophila* (Fig. 4). Although the measurements of inflammatory gene expression in human LMs need to be repeated in larger cohorts, our results suggest that the inflammatory phenotype of LMs does not contribute to diet-induced metabolic impairment.

Most studies in the literature describing LM activation in the context of obesity and insulin resistance are based on whole-liver^{37,38} or NPC³⁹ inflammatory gene expression, depletion approaches^{9–13,29} or myeloid-specific inflammatory gene ablation^{40,41}, and extrapolation of observations from adipose tissue macrophages. In addition to the lack of specificity inherent in using a whole organ or mixed cell populations to investigate the effect of obesity on a particular cell type, side effects intrinsic to macrophage depletion strategies could lead to overinterpretation. Furthermore, in mouse models with myeloid-specific deficiency, several macrophage populations in the body are affected, including adipose tissue macrophages, which also contribute to obesity-induced insulin resistance.

Although long-term high-fat feeding in mice leads to increased expression of inflammatory cytokines and recruitment of LMs, as previously reported^{22,39}, the recruited macrophages seem to have a limited role in obesity-induced insulin resistance, as their recruitment occurs after the development of insulin resistance and their depletion does not improve insulin sensitivity in obese mice⁴². In addition, although we have previously shown that silencing of *Nfkb* in LMs improves insulin sensitivity in obese mice²⁵, the beneficial effects of *Nfkb* knockdown seemed to be independent of inflammation (Supplementary Fig. 1).

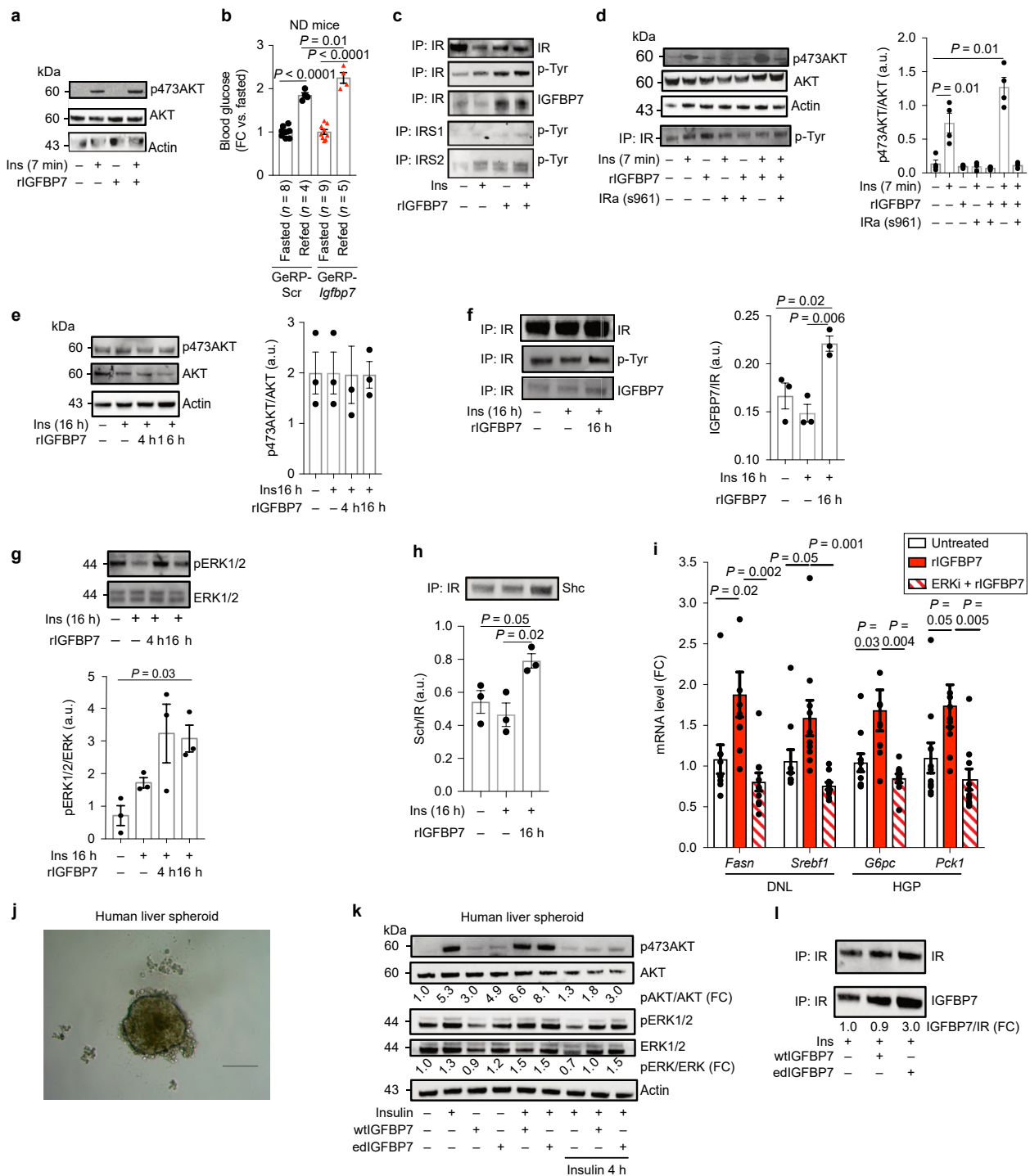


Fig. 5 | LM-derived iGFBP7 increases lipogenesis and gluconeogenesis. **a**, Western blots of AKT phosphorylation in primary mouse hepatocytes treated with recombinant IGFBP7 (rIGFBP7) and short-term insulin (Ins); $n = 4$ biological replicates. p473AKT, AKT phosphorylated at residue 473. **b**, Blood glucose levels for fasted and refed states in mice fed a ND and treated with GeRP-Scr or GeRP-*Igfbp7*; the number of mice (n) is indicated. **c**, Western blots of immunoprecipitations in primary mouse hepatocytes for IR, IRS1 and IRS2; $n = 3$ biological replicates. p-Tyr, phosphorylated tyrosine. **d**, Western blots and quantification (for **a** and **d**) of AKT phosphorylation in primary mouse hepatocytes treated with IR antagonist (IRa) s961, recombinant IGFBP7 and short-term insulin; $n = 4$ biological replicates. **e**, Western blots and quantification of AKT phosphorylation in primary mouse hepatocytes treated with recombinant IGFBP7 under hyperinsulinaemia; $n = 3$ biological replicates. **f**, Western blots and quantification showing immunoprecipitation of IGFBP7 with IR under hyperinsulinaemia; $n = 3$ biological replicates. **g, h**, Western blots and quantification of phosphorylated ERK1/2 (pERK1/2) (**g**) and immunoprecipitation of Shc with IR (**h**) in primary mouse hepatocytes treated with recombinant IGFBP7 under hyperinsulinaemia; $n = 3$ biological replicates. **i**, Gene expression in primary mouse hepatocytes treated with insulin, recombinant IGFBP7 and the ERK pathway inhibitor U0126 (ERKi); $n = 10$ technical replicates. **j**, Image of a human liver spheroid (scale bar, 200 μm). **k**, Western blots and quantification of AKT and ERK1/2 phosphorylation in human liver spheroid treated with short-term (7-min) or long-term (4-h) insulin and with wild-type (wt) or edited (ed) recombinant IGFBP7 for 4 h. Quantification is expressed as fold change in comparison to control. **l**, Western blots and quantification of coimmunoprecipitation of IGFBP7 with IR in human liver spheroids under hyperinsulinaemia. Quantification is expressed as fold change in comparison to control. Data are shown as the mean \pm s.e.m. P values were calculated by unpaired two-tailed Student's t test in **i** and by one-way ANOVA with adjustment for multiple comparisons in **b** and **d–h**.

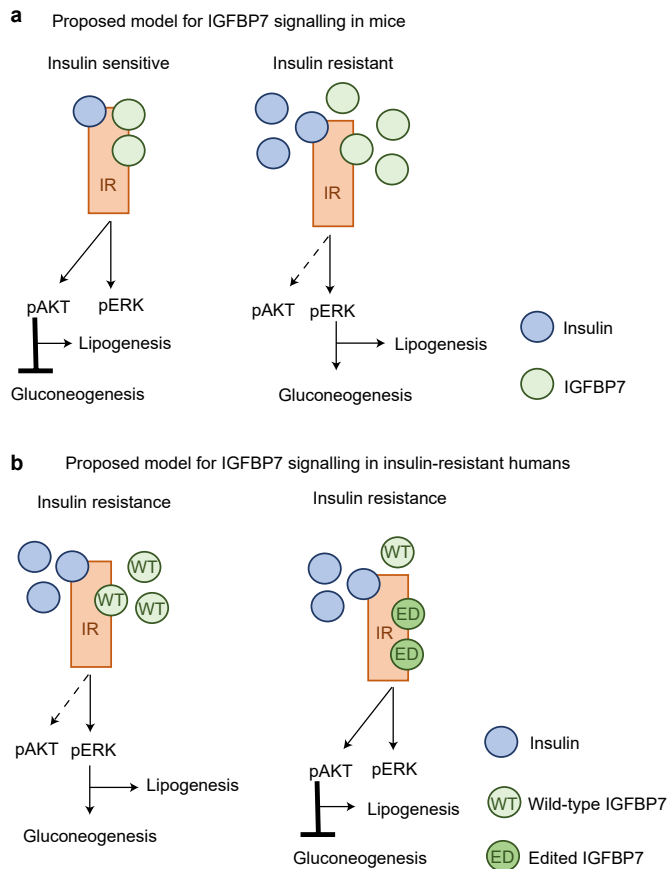


Fig. 6 | Proposed models for IGFBP7 signalling in mice and humans.

a, In mice, under insulin-sensitive conditions, the IGFBP7 produced by LMs binds to the hepatic IR and enhances AKT activation by insulin; under insulin-resistant conditions, in which AKT does not respond to insulin, IGFBP7 binds to the IR with lower affinity but can still activate the ERK pathway and induce gluconeogenesis and lipogenesis. **b**, In humans, edited *IGFBP7* is found more frequently in insulin-resistant states. Edited IGFBP7 has a higher capacity to bind the IR and activate AKT than wild-type IGFBP7.

Although obesity had no effect on the inflammatory profile of LMs, unbiased transcriptomic profiling notably showed that the expression of more than a thousand genes was significantly affected in mice. Among these genes was *Igfbp7*, encoding a secreted protein known to regulate insulin signalling in *Drosophila*⁴³. In the earlier studies, *Drosophila Igfbp7 (ImpL2)* was shown to be expressed by tumours and to prevent glucose uptake by the fat body and redirect it to tumour cells, thereby resulting in energy wasting^{14,15}. Here we demonstrate that, in mice and flies, *Igfbp7* is highly expressed in LMs and haemocytes, respectively, and its expression is significantly increased by high-fat feeding (Fig. 2). Taking advantage of GeRP technology to specifically manipulate gene expression in LMs, we report that silencing of *Igfbp7* expression in LMs significantly decreased hyperglycaemia and hepatic steatosis in mice (Fig. 4). Remarkably, the effect of *Igfbp7* silencing was also observed in flies, in which haemocyte-specific *ImpL2* knockdown significantly decreased glucose levels and lipid accumulation in adults fed a HFD (Fig. 4). Finally, we showed that IGFBP7 binds to the IR and enhances insulin signalling in insulin-sensitive hepatocytes. In contrast to another factor shown to bind the IR (glypican-4)⁴⁴, stimulation with insulin did not disrupt interaction of IGFBP7 with the IR. We induced insulin resistance in mouse hepatocytes through long-term treatment (16 h) by using the same concentration of insulin as

for the insulin-sensitive condition (100 nM). This insulin resistance completely blocked the ability of insulin to activate AKT, even in the presence of IGFBP7. In the insulin-resistant state, IGFBP7 was not able to overcome the resistance of the AKT pathway to activation by insulin. In addition, insulin resistance reduced the ability of IGFBP7 to bind to the IR. Because the same concentration of insulin was used in both conditions (insulin sensitive and resistant), the binding capacity of IGFBP7 for the IR does seem to be due not to the level of insulin but rather to insulin sensitivity. The different binding capacities of IGFBP7 for the IR in the insulin-sensitive and insulin-resistant states could be explained by reduced presence of the IR at the membrane under insulin resistance⁴⁵ or modification of the ratio of IR isoforms, which have different affinities⁴⁶. Interestingly, IGFBP7 was still able to activate ERK1/2 and recruit the upstream regulator Shc in insulin-resistant hepatocytes. Modification of IR isoforms has been shown to reroute insulin signalling from AKT to the ERK1/2 pathway⁴⁷, which suggests that the ability of IGFBP7 to activate ERK rather than AKT could be due to lower binding affinity for different IR isoforms. Finally, we cannot exclude the possibility that another IGFBP7 receptor is able to activate the ERK pathway. Although IGFBP7 has been shown to bind to IGF1R¹⁶, we were not able to observe any IGFBP7 binding to this receptor (data not shown), suggesting that activation of ERK1/2 by IGFBP7 is not mediated by IGF1R.

Although expression of *IGFBP7* was not affected by obesity or insulin resistance in human LMs, our transcriptomic study allowed the identification of a 'recoding' site at which adenosine-to-inosine editing resulted in a nonsynonymous substitution in the IGFBP7 protein-coding sequence in the LMs of insulin-resistant obese patients. This recoding site is not conserved in mice, suggesting that it has functional and evolutionary importance. Interestingly, this editing event is known to affect the binding affinity of IGFBP7 for its ligand^{33,34}. In addition, arginine has different electrostatic properties and abilities to form hydrogen bonds than lysine, which may increase the protein-binding capacity of the edited IGFBP7 (refs. 48,49). In agreement with these earlier studies, we demonstrated that edited IGFBP7 had a higher capacity to bind to the IR and activate AKT than wild-type IGFBP7 in insulin-resistant liver organoids. The role of edited IGFBP7 in enhancing insulin signalling and its higher levels in insulin-resistant human LMs may seem counterintuitive at first. However, insulin itself shows a similar distribution, with lower levels in insulin-sensitive than in insulin-resistant states. This suggests that RNA editing of *IGFBP7* could serve as a protective evolutionary mechanism, as has been suggested for other factors in other systems⁵⁰.

Anti-inflammatory drugs are currently being explored as therapeutic strategies to treat metabolic diseases^{5,51}. Our data clearly show that, although inflammation does not seem to directly contribute to obesity-induced insulin resistance, LMs could have multiple roles by producing non-inflammatory factors able to regulate metabolism. Our unbiased transcriptomic analyses offer the possibility to explore many factors that could influence LM phenotype and hepatic function. In addition, the ability of GeRP technology to manipulate gene expression specifically in LMs while leaving other cells and macrophages in the body unaffected provides a unique advantage in studying the direct role of LMs in the development of metabolic diseases. Finally, this study indicates that therapeutic strategies targeting LMs independently of their inflammatory phenotype might be more beneficial than strictly focusing on inflammation.

Methods

Human subjects. Liver samples were obtained from 11 volunteers, with BMI between 35 and 42 kg/m², undergoing laparoscopic Roux-en-Y gastric bypass surgery at Danderyd Hospital in Stockholm. None of the participants had a previous history of cardiovascular diseases, diabetes, gastrointestinal diseases, systemic illness, alcohol abuse, coagulopathy or chronic inflammatory diseases, clinical signs of steatohepatitis or liver damage, or surgical intervention within 6 months of the start of the studies. Patients did not follow any special diet

before the surgery. Two weeks before the intervention, blood was collected for subsequent biochemical tests and a 2-h 75-g oral glucose tolerance test (OGTT) was performed. Insulin sensitivity was assessed by homeostatic model assessment (HOMA-IR). One of the 11 obese patients recruited did not consent to the OGTT and additional blood sampling for insulin measurement and was therefore excluded from the second set of analyses (insulin sensitive versus insulin resistant). Hepatic steatosis index (HSI) was calculated as in Lee et al.³²: HSI = 8 × (ALT/AST ratio) + BMI (+2 if female; +2 if the individual had diabetes mellitus). The Regional Ethical Committee in Stockholm approved the study and all subjects gave written informed consent prior to their participation for all procedures.

Liver cells from non-obese individuals were obtained from liver donors and isolated by the Liver Cell Laboratory at the Unit of Transplantation Surgery, Department of Clinical Science, Intervention and Technology (CLINTEC) at Karolinska Institutet.

Blood samples for the measurement of serum IGF1P7 concentration were obtained from 30 obese volunteers (average BMI, 37.4 kg/m²; range, 32.6–45.2 kg/m²) and 23 age- and sex-matched lean controls (average BMI, 24.33 kg/m²; range, 21–27 kg/m²) recruited by the Endocrinology Unit, Karolinska Hospital, Huddinge.

Mice and diet. Four-week-old wild-type C57BL/6J and 5-week-old *ob/ob* (B6.Cg-Lep^{ob}/J) males were obtained from Charles River Laboratories International and maintained on a 12-h light/12-h dark cycle. Animals were given free access to food and water. Wild-type C57BL/6J mice were fed a HFD with 60% calories from fat, 20% from carbohydrates and 20% from protein (Research Diets, D12492) at 5 weeks of age. Control mice were fed a normal chow diet. All procedures were performed in accordance with guidelines approved by the Swedish Ethical Committee in Stockholm (Stockholm södra djurförsöksetiska nämnd).

Fly stocks and culture. All fly strains used in this work were first backcrossed ten times into the same *w¹¹¹⁸* strain with a genetic background based on Canton-S, which was used as a control. To visualize the site of *ImpL2* expression, fly strains carrying *ImpL2-Gal4* (kindly provided by H. Stocker, Department of Biology, Institute of Molecular Systems Biology, ETH Zurich) and *UAS-mCherry* (kindly provided by A. Krejci Bruce, Department of Molecular Biology and Genetics, University of South Bohemia, Czech Republic) constructs were crossed. For the phagocytosis assay, pHrodo Green (Thermo Fisher, P35367) was resuspended according to the manufacturer's instructions and 50 nl of solution was injected. After 45 min, animals were killed and fixed for further analysis. For experiments with haemocyte-specific silencing of *ImpL2*, flies carrying a haemocyte-specific *Gal4* driver (*Hml-Gal4*) in combination with ubiquitous expression of the thermosensitive *Gal80^{TS}* repressor protein (*w¹¹¹⁸; HmlΔ-Gal4; P{tubP-GAL80^{TS}}*) were crossed with an *ImpL2*-specific RNAi strain (kindly provided by H. Stocker). Haemocytes positive for *ImpL2* expression were counted in a morphologically defined part of the thorax in randomly selected flies.

All crosses and strains used in this study are described below.

Preparation of fly strains expressing an *ImpL2* RNAi construct under the control of the *UAS* promoter activated by *Gal4* under the control of the haemocyte-specific *Hml* promoter (temperature controlled through *Gal80^{TS}*)

Preparation of a reporter fly strain carrying *mCherry* under the control of the *UAS* promoter activated by *Gal4* under the control of the natural promoter of *ImpL2*

$$P: \frac{w}{w}; \frac{+}{+} \frac{ImpL2 \Delta Gal4}{Tm_6 Be Tb Hu} \times \frac{x}{x}; \frac{+}{+} \frac{UAS Hosein : Cherry}{UAS Hosein : Cherry}$$

$$F1: \frac{w}{w}; \frac{+}{+} \frac{ImpL2 \Delta Gal4}{UAS Hosein : Cherry} \times \frac{w}{x}; \frac{+}{+} \frac{+}{Tm_6 Be Tb Hu}$$

$$F2: \frac{w}{w}; \frac{+}{+} \frac{ImpL2 \Delta Gal4, UAS Hosein : Cherry}{Tm_6 Be Tb Hu} \times \frac{w}{x}; \frac{+}{+} \frac{+}{Tm_6 Be Tb Hu}$$

$$F3: \frac{w}{x}; \frac{+}{+} \frac{ImpL2 \Delta Gal4, UAS Hosein : Cherry}{ImpL2 \Delta Gal4, UAS Hosein : Cherry}$$

Preparation of fly strains expressing GFP and the *ImpL2* RNAi construct in haemocytes

$$P: \frac{w}{w}; \frac{HmlGal4, UAS-GFP}{HmlGal4, UAS-GFP} \times \frac{w}{x}; \frac{UAS- ImpL2 RNAi}{UAS- ImpL2 RNAi}; \frac{+}{+}$$

$$F1: \frac{w}{x}; \frac{HmlGal4, UAS-GFP}{UAS- ImpL2 RNAi}; \frac{+}{+}$$

For all experiments, fly lines with the nearest genetic background were used as the control. White control fly line

$$\frac{w}{x}; \frac{+}{+}; \frac{+}{+} \quad (5)$$

Control fly lines used for experiments with *Hml-Gal4* lines

$$P: \frac{w}{x}; \frac{+}{+}; \frac{x}{x}; \frac{HmlGal4}{CyO}; \frac{P\{tubPGal80ts\}}{Tm_6 Be Tb Hu}$$

$$F1: \frac{w}{x}; \frac{HmlGal4}{+}; \frac{P\{tubPGal80ts\}}{+}$$

Control fly lines used for experiments with *ImpL2*-RNAi lines

$$P: \frac{w}{w}; \frac{UAS ImpL2 RNAi}{UAS ImpL2 RNAi}; \frac{x}{x}; \frac{+}{+}; \frac{+}{+}$$

$$F1: \frac{w}{x}; \frac{UAS ImpL2 RNAi}{+}; \frac{+}{+}$$

Adult flies were fed a HFD (1% cornmeal, 10% fat (lard), 2.5% yeast, 5% glucose and 0.62% agar (Ambresco)) for 10 d. Control flies were fed a ND (8% cornmeal, 4% yeast, 5% glucose and 0.62% agar (Ambresco)) with the equivalent caloric content per gram of diet. Flies were grown under controlled conditions: approximately 50 larvae/vial were obtained from the same parents and split into equal numbers after emergence to be fed the different diets. Diet was replaced every second day. Males were used for quantification of metabolites and qPCR analysis.

GeRP administration by intravenous injection in vivo. Glucan shells (GS) were prepared by using a previously published protocol³⁴. Briefly, 100 g of baker's yeast (*Saccharomyces cerevisiae*, SAF-Mannan, Biospringer) was heated at 80–85°C for 1 h in 1 litre of NaOH (0.5 M) to hydrolyse the outer cell wall and intracellular components. This step was repeated after a water wash. Following centrifugation (15,000g for 10 min), the resulting pellet was washed at least three times with water and three times with isopropanol. This yielded approximately 3–4 mg of purified, porous 2- to 4-μm, hollow β 1,3-d-glucan particles. One gram of empty β 1,3-d-glucan particles resuspended in 100 ml of sodium carbonate buffer was then labelled with FITC by incubation with 10 mg of 5-(4,6-dichlorotriazinyl) amino fluorescein (DTAF) dissolved in 10 ml of ethanol for ~16 h protected from light. Labelled GS were then washed at least five times in water.

Wild-type mice were fed a HFD for 8 weeks and were first randomized according to their body weight and glucose tolerance. Mice were then treated with 12.5 mg/kg GeRPs loaded with siRNA (247 μg/kg) and Endoport (2.27 mg/kg). Mice received six doses of fluorescently labelled GeRPs by intravenous injection over 15 d. siRNA sequences are listed in Supplementary Table 7.

Isolation of LMs and hepatocytes from mice. LMs and hepatocytes were isolated as previously described³⁵. Briefly, the livers of anaesthetized mice were first perfused with calcium-free Hank's balanced salt solution (HBSS), followed by collagenase digestion. After digestion, hepatocytes were released by mechanical dissociation of the lobes and underwent several steps of filtration with calcium-containing HBSS and centrifugation at 50g for 3 min. The resulting hepatocyte pellet was washed twice and plated. The supernatant containing NPCs was loaded onto a Percoll gradient (25% and 50%) and centrifuged at 2,300 r.p.m. for 30 min at 4°C. The interphase ring with enriched LMs was collected. Cells were then plated for 30 min and washed twice before RNA or protein was extracted for subsequent analyses.

Isolation of LMs from humans. Freshly obtained liver biopsies were cut into small pieces and immediately digested in RPMI medium containing collagenase I (0.25 mg/ml; Sigma, C6885) and DNase I (0.2 mg/ml; Roche, 1010415900) at 37°C for 30 min. Single-cell suspensions were filtered through a cell strainer (75 μm) and centrifuged at 50g for 3 min. The supernatant containing NPCs was loaded onto a Percoll gradient and LMs were isolated as described above.

Haemocyte isolation from flies. Fluorescent cells were sorted from male flies endogenously producing GFP under the control of a haemocyte-specific promoter (*Hml-Gal4*). Together with *Hml-Gal4*>GFP flies, negative controls were used to ensure proper gate setting.

Flies were anaesthetized with carbon dioxide, washed several times in PBS and then homogenized with a sterile pestle in PBS. Cell homogenate was filtered through a 70-μm cell strainer and washed three times with ice-cold PBS, followed by centrifugation at 5,000 r.p.m. for 3 min at 4°C. Approximately 12,000 live cells were sorted starting from 100 male flies. Sorting was performed with the S3e Cell

Sorter (Bio-Rad); GFP⁺ cells represented approximately 1% of total cell number. Microscopy analyses of GFP signal and haemocyte-specific morphology confirmed the accuracy of FACS.

Metabolic analyses in mice. The glucose tolerance test and insulin tolerance test (IP-GTT and IP-ITT) were performed on the day of the last GeRP injection and following a 6-h fast. A dose of 1 g/kg glucose or insulin (0.25 IU/kg) was intraperitoneally injected, and blood glucose levels were measured with a glucometer at defined time points from the tail vein. The following day, mice were killed and tissues were collected for subsequent analyses.

Insulin-stimulated phosphorylation of AKT in vivo. Insulin-stimulated phosphorylation of AKT was measured 24 h after the last GeRP injection and 4 h of fasting. A dose of 0.25 U/kg insulin was injected intraperitoneally, and adipose tissue and liver samples were collected from GeRP-treated mice for further analyses, 15 min after injection.

Cell culture. Transfection of primary cells in vitro. Peritoneal exudate cells (PECs), isolated by washing the peritoneal cavity 4 d after an intraperitoneal injection with 4% thioglycolate broth using a previously described protocol²³, and LMs were transfected with a mixture of 120 picomoles of siRNA and 3 nanomoles of Endoporter, incubated for 15 min prior to addition to the cells. Medium was changed 24 h after transfection; 48 h after transfection, medium, mRNA and cell lysates were collected for subsequent analyses.

Treatment of primary mouse hepatocytes. For qPCR analysis, primary mouse hepatocytes were isolated from 8- to 12-week-old wild-type mice by liver perfusion as described above. Within a few minutes of isolation, cells were maintained in glucose-free DMEM in microcentrifuge tubes. Cells were then subjected to a 1-h preincubation with U0126, an inhibitor of the upstream kinase activating ERK1/2, MAPK kinase (MEK) (10 mM concentration; Cell Signaling Technology, 9903), or maintained in the same medium and subsequently treated with recombinant IGFBP7 (20 ng/ml; R&D Systems, 2120-B7-025) for 4 h. Cell pellets were washed and RNA was extracted.

For protein analysis, primary mouse hepatocytes were isolated from 8- to 12-week-old wild-type mice by liver perfusion as described above. Primary hepatocytes were plated on collagen-coated plates and kept overnight in adherence medium (M199 (Sigma, M4530) supplemented with 100 nM insulin, 100 nM dexamethasone (Sigma, D4902), 10% BSA and 10% FBS). The next morning, all experiments were performed following the same protocol: cells were (i) maintained for 2 h in starvation medium (M199 (Sigma, M4530) without FBS or BSA added), (ii) pretreated for 1 h with either IR antagonists 961 (100 nM; Phoenix Europe, ABIN2876379) or ERK inhibitor U0126 (10 mM; Cell Signaling Technology, 9903); and (iii) treated with recombinant IGFBP7 (20 ng/ml) for 4 h followed by 7-min co-incubation with insulin (100 nM; Thermo Fisher Scientific, 12585-014). Controls were maintained in starvation medium. For the hyperinsulinaemic condition, insulin at a concentration of 100 nM was maintained in the medium overnight (16 h). Protein lysates were collected for western blot analysis and immunoprecipitation assays.

Human liver spheroids. Cryopreserved primary human hepatocytes (Bioreclamation IVT) were seeded in 96-well ultra-low attachment plates (Corning) in culture medium (Williams' medium E containing 11 mM glucose supplemented with 2 mM L-glutamine, 100 U/ml penicillin, 100 µg/ml streptomycin, 10 µg/ml insulin, 5.5 µg/ml transferrin, 6.7 ng/ml sodium selenite and 100 nM dexamethasone) with 10% FBS as described previously²³. Following aggregation, cells were transitioned into serum-free Williams' medium E (PAN-Biotech) containing 5.5 mM glucose and 1 nM insulin for 7 d. The day of the treatment, after 2 h of starvation, cells were exposed to recombinant human IGFBP7 (200 ng/ml; K95R, R&D Systems, 1334-B7-025) or wild type, R&D Systems, custom made) or insulin (100 nM). Protein was collected for immunoprecipitation assays and western blot analysis. Spheroid viability was controlled by ATP quantification using the Cell Titer-Glo Luminescent Cell Viability Assay (Promega) with values normalized to the corresponding vehicle control on the same plate. No statistically significant differences in viability were observed between IGFBP7- and vehicle-treated controls when using heteroscedastic two-tailed *t* tests ($n = 8$ spheroids) and $P < 0.05$ as the significance threshold (data not shown).

Isolation of RNA, real-time qPCR and RNA library preparation. RNA extraction and purification were performed by using TRIzol reagent according to the manufacturer's instructions (Thermo Fisher Scientific, 15596018). For real-time qPCR, cDNA was synthesized from 0.5 µg of total RNA with the iScript cDNA Synthesis kit (Bio-Rad) according to the manufacturer's instructions. Synthesized cDNA along with forward and reverse primers and Advanced Universal SYBR Green Supermix was run on a CFX96 Real-Time PCR System (Bio-Rad). Ribosomal RNA (36B4) or β -actin (*Actb*) was used as a reference gene in mice and ribosomal protein 49 (*Rp49*) was used as a reference gene in flies. The primer sequences used for qPCR are listed in Supplementary Table 6.

For library preparation, RNA integrity was determined with an Agilent Bioanalyzer. Libraries from mouse RNA were prepared with the TruSeq Stranded mRNA kit (Illumina) and libraries from human RNA were prepared with the SMARTer Ultra-Low RNA kit (Clontech). The concentration of the indexed libraries was determined by real-time qPCR using the Universal Kapa Library Quantification kit (KAPA Biosystems). Final libraries were normalized and sequenced on an Illumina HiSeq 2000 sequencer.

Nuclei and library preparation for GRO-seq. GRO-seq was performed as previously described²⁷, with minor modifications for mouse LM samples. Nuclei were extracted from LMs (three or four pooled mice/group) by using hypotonic buffer and visually inspected for quality under a microscope with DAPI staining. The total number of nuclei was determined with a Countess Automated Cell Counter (Bio-Rad). Nuclear run-on was performed by Br-UTP followed by enrichment with anti-Br-UTP antibodies, reverse transcription and library preparation.

Western blot analysis and immunoprecipitation assays. Protein (30 µg) was fractionated by SDS-PAGE on precast 4–12% gradient gels (Thermo Fisher Scientific, NP0321BOX), transferred to PVDF membranes (Thermo Fisher Scientific, LC2005) and probed with the primary antibodies indicated below. This was followed by incubation with the appropriate HRP-conjugated secondary antibody (Abcam, ab6721 or ab6789). Finally, bound secondary antibodies were visualized with ECL detection reagent (Bio-Rad, 1705060) and images were acquired with an imaging system equipped with a CCD camera (ChemIDoc, Bio-Rad). Immunoprecipitation for IR, IRS1 and IRS2 was performed on 100 µg of protein. Lysates were incubated overnight with Agarose Protein G plus mixture (Pierce, 22851) and protein complexes were eluted in Laemmli buffer. Western blot analysis was then performed as described above. Primary antibodies to the following were used: Akt (Cell Signaling Technology, 4691), phosphorylated Akt (Ser473) (Cell Signaling Technology, 9271), p44/42 MAPK (Erk1/2) (Cell Signaling Technology, 4965), phosphorylated p44/42 MAPK (Erk1/2) (Thr202/Tyr204) (Cell Signaling Technology, 4370), phosphotyrosine (P-Tyr-100) (Cell Signaling Technology, 9411), IR β (4B8) (Cell Signaling Technology, 3025), IRS1 (Cell Signaling Technology, 2382), IRS2 (L1326) (Cell Signaling Technology, 3089), Igfbp7 (R&D Systems, MAB21201), actin (Abcam, ab179467) and Shc (Cell Signaling Technology, 2432). Quantification of signal was performed with ImageJ software. The antibody dilutions used are given in Supplementary Table 8.

Histology. Paraffin-embedded tissue sections of pancreas were used for haematoxylin and eosin staining, and frozen sections of the liver were used for Oil Red O staining. Slides were scanned with a Panoramic 250 Slide Scanner.

Immunofluorescence. Isolated LMs plated on coverslips were fixed in 4% paraformaldehyde, washed twice in PBS, and incubated with 0.1% Triton X-100 and 5% goat serum in PBS for 30 min at room temperature for blocking and permeabilization. F4/80 was visualized with rat anti-mouse monoclonal antibody (MCA497, AbD Serotec; 1:50 dilution in PBS) followed by goat anti-rat Alexa Fluor 555-conjugated antibody (Thermo Fisher Scientific, A21434; 1:1,000 dilution). Nuclei were counterstained with ProLong Gold antifade reagent with DAPI (Thermo Fisher Scientific).

Liver sections were blocked with 5% normal goat serum for 30 min at room temperature and incubated overnight with primary antibody to F4/80 (rat anti-mouse; Bio-Rad, MCA497; 1:50 dilution in 5% goat serum) at 4°C. Alexa Fluor 647-conjugated antibody (goat anti-rat; Thermo Fisher Scientific, A21247; 1:200 dilution in 5% goat serum) was used as secondary antibody. Nuclei were counterstained with DAPI reagent, and slides were mounted with SlowFade Gold Antifade Mountant (Thermo Fisher Scientific, S36936). Fluorescence microscopy images were acquired with an inverted Axio Observer.Z1 (Zeiss), equipped with an AxioCam 506 color (Zeiss). The antibody dilutions used are listed in Supplementary Table 8. Flies were fixed with 4% paraformaldehyde in PBS and imaged by confocal microscopy with maximal-intensity projections from five different layers; the same setting for the z-stack range as well as for the intensity of the lasers was used for all animals (Olympus, Fluoview FV1000). The number of *ImpL2*⁺ cells in adult flies was determined by counting mCherry⁺ cells visualized by confocal microscopy. The red signal for mCherry is driven by expression from the natural promoter of the *ImpL2* gene. The green laser was used just for differential visualization of structures. The exact number of cells was determined within a selected thorax region by using Fiji software, and results were compared by Student's *t* test in GraphPad Prism software.

Single-molecule RNA ISH (RNAscope). Expression of *Igfbp7*, *Adgre1* and *Alb* mRNA in frozen liver sections was assessed by multiplexed single-molecule fluorescence ISH using the RNAscope Fluorescent Multiplex Reagent kit (Advanced Cell Diagnostics) according to the manufacturer's instructions, with minor modifications. Tissue sections of 12-µm thickness were stained with probes against *Igfbp7*, *Adgre1* and *Alb*. *Apoe* probe was used as a positive control together with negative-control probes provided with the kit. Before mounting of slides, sections were stained with 0.25% Sudan Black B solution in 70% ethanol for 20 min and then washed twice for 5 min in deionized water.

The following probes were used: *Igf1bp7*: probe target region, nucleotides 12–1,113; fluorophore combination, C1–Alexa Fluor 488; *Adgre1*: probe target region, nucleotides 85–1,026; fluorophore combination, C2–ATTO 550; *ApoE*: probe target region, nucleotides 83–1,245; fluorophore combination, C1–Alexa Fluor 488; *Alb*: probe target region, 2–1,028; fluorophore combination, C2–ATTO 550.

Liver sections stained for *Igf1bp7* and *Alb* mRNA with RNAscope were also subsequently stained for F4/80 protein by immunohistochemistry as described above.

Samples were imaged with an inverted Axio Observer.Z1 (Zeiss), equipped with an Axiocam 506 color (Zeiss).

Transmission electron microscopy. To prepare samples for TEM, small pieces of liver were fixed in 2.5% glutaraldehyde + 1% paraformaldehyde in 0.1 M phosphate buffer, pH 7.4, at room temperature for 30 min and stored at 4°C. Specimens were rinsed in 0.1 M phosphate buffer, pH 7.4, and postfixed in 2% osmium tetroxide in 0.1 M phosphate buffer, pH 7.4, at 4°C for 2 h, dehydrated in ethanol followed by acetone, and embedded in LX-112 (Ladd). Semithin sections were cut and stained with Toluidine Blue O and were used for light microscopy analysis. Ultrathin sections (approximately 50–60 nm) were cut with a Leica EM UC 6 (Leica) and contrasted with uranyl acetate followed by lead citrate. They were then examined in a Hitachi HT 7700 at 80 kV. Digital images were acquired with a Veleta camera (Olympus Soft Imaging Solutions)⁵⁴.

Volume density measurements of lipids in transmission electron microscopy images. To measure the quantity of lipids in liver, digital images of liver cell cytoplasm were randomly taken at a final magnification of ×5,000. Printed digital images were used and the volume density (Vv) of lipids was calculated by point counting using a 1.5-cm square lattice as described by Weibel⁵⁵. A pilot study was performed to determine the number of images needed for an appropriate sample by using a cumulative mean plot for evaluation⁵⁵. As a result, 15 images were randomly collected from three different animals. The total areas for all lipids and liver cytoplasm were calculated. The total lipid area was divided by the total area of liver cytoplasm, generating the ratio of lipids/cytoplasm in each animal. In all images, the total number of lipid profiles was determined and the total lipids value was divided by the lipid profile number, giving a mean area (in μm²) for the lipids.

Flow cytometry. NPCs were stained with the following dyes and fluorophore-conjugated primary antibodies: Viability Dye SYTOX Blue (Thermo Fisher Scientific, S34857), F4/80-APC (Bio-Rad, CI:A3-1; MCA497 APC), CD11b-PerCP/Cy5.5 (BD Biosciences, MI170; 561114), Ly6C-BV605 (BioLegend, HK1.4; 128035), CD45-PE-CF594 (BD Biosciences, 30-F11; 562420), CD3-PE (BioLegend, 17A2; 100205), CD8-FITC (BD Biosciences, 56-6.7; 561966), CD4-APC (BD Biosciences, RM4-5; 561091), LipidTOX Neutral Lipid Stain (Thermo Fisher Scientific, Green (H34475) and DeepRed (H34477)). After staining, cells were washed three times with FACS buffer (1% BSA in PBS) and samples were analysed with a BD LSR II Fortessa instrument and FlowJo software (Tree Star). The gating scheme is shown in Supplementary Fig. 1. Flow cytometry determination of absolute liver cell numbers was performed by using CountBright Absolute Counting beads (Molecular Probes, C36950). The antibody dilutions used are listed in Supplementary Table 8.

Mouse biochemical parameters. Total serum cholesterol and TG levels were determined by colorimetric techniques using commercially available reagents (Roche/Hitachi; TGs, 12016648; cholesterol, 12016630).

Lipoprotein profiles were obtained after separation by fast-performance liquid chromatography (FPLC) using commercially available kits for cholesterol and TG determination (Roche/Diagnostic). Lipoprotein fractions were calculated from the FPLC curves by determining the area under the curve⁵⁶.

The following ELISA kits were used: insulin (Millipore, EZRMI-13K), norepinephrine (Biotech-IgG, LD-BA E-5200), epinephrine (Biotech-IgG, LD-BA E-5100), corticosterone (Abcam, ab108821), glucagon (R&D Systems, DGCG0) and IGFBP7 (Nordic Biosite, EKM1620).

FFAs were measured by colorimetric quantification assay (Abcam, ab65341).

PKA activity was measured in liver lysates with the PKA Kinase Activity kit (Enzo Life Sciences, ASI-EKS-390). TGs were measured in frozen livers according to the manufacturer's instructions (Cayman Chemical, CAYM1001303-96), and results were normalized by liver weight.

Metabolite measurements in flies. Glucose was measured as previously described⁵⁷. Briefly, flies were homogenized in PBST (PBS with 0.3% Tween-20) and large tissue fragments were pelleted by centrifugation at 800 g for 5 min at 4°C. Glucose was measured with a GAGO-20 kit (Sigma) according to the supplier's protocol. TGs were measured either by using a TG quantification kit (Sigma) according to the supplier's protocol (Fig. 2) or via HPLC ESIMS/MS (electrospray ionization tandem mass spectrometry) followed by multivariate statistical analysis as described by Sneedorferová et al.⁵⁸ (Fig. 4). Protein concentration was determined by Bradford assay.

Serum IGFBP7 concentration in humans. IGFBP7 concentration was measured in human serum by sandwich ELISA using a previously published protocol⁵⁹. Briefly, each well of a 96-well plate was coated with 50 ng of poly(L-histidine) (Sigma,

P4707) overnight at room temperature. Polyclonal anti-IGFBP7 antibody (R&D Systems, AF1334) was diluted to 1 μg/ml in PBS and incubated overnight at room temperature in the coated wells. The wells were then washed in PBST (PBS + 0.1% Tween-20) and blocked with 3% BSA in PBS for 1 h at room temperature. After washing with PBST, 90 μl of undiluted sample was added to each well. Recombinant human IGFBP7 (R&D Systems, 1334-B7-025) at a concentration of 100, 50, 25, 12.5, 3.1 and 1.5 ng/ml in PBS was also added as a standard. The plate was incubated for 90 min at 37°C and then washed with PBST. Monoclonal anti-IGFBP7 antibody (R&D Systems, MAB1334) at a concentration of 1 μg/ml in PBS was then added and the plate was incubated for 90 min at 37°C. The plate was washed again in PBST and incubated with goat anti-mouse IgG H&L HRP-conjugated antibody (Abcam, ab6789) diluted to 1 μg/ml for 30 min at 37°C and then washed again with PBST. Substrate reagent (100 μl) from R&D Systems (DY999) was added to each well and the chromogenic reaction was allowed to proceed for 10 min at 37°C. Stop solution (50 μl of 2N HCl) was then added to stop the reaction. The plate was read at 450 nm in a microtiter plate reader (Molecular Devices, SpectraMax i3).

Bioinformatics. Data analysis and storage. Signal intensities were converted into individual basecalls during a sequencing run by the system's real-time analysis (RTA) software. Sample demultiplexing and conversion to fastq files were performed by using Illumina's bcl2fastq software with all default options. The distribution of reads per sample in a lane was within the reasonable limits tolerated.

RNA-seq alignment and gene quantification. Raw fastq files were aligned against mouse genome version mm10 and human genome version hg38 by using TopHat version v2.0.13 (ref. ⁶⁰) with all default options. BAM files containing the alignment results were sorted according to mapping position. mRNA quantification was performed with FeatureCounts from the Subread package⁶¹ against GRCm38-genecode transcripts database version 7 (genecode.vM7.annotation.gtf) and GRCh38-genecode transcripts database version 24 (genecode.v24.annotation.gtf) to obtain read counts for each individual Ensembl gene.

GRO-seq data processing and gene quantification. Raw fastq files were aligned against mouse genome version mm10 by using BVAA⁶² with the same option. Uniquely mapped reads were extended to 150 bp in the 5'-to-3' direction and used for downstream analysis. Nascent transcription of genes was measured by using GRO-seq reads mapped to the sense strand of the gene in a 10-kb window (+2 kb to +12 kb relative to the transcription start site (TSS)) within the annotated gene body. Smaller genes between 2 kb and 12 kb in length were quantified by using a smaller window size, from +2 kb to the transcription end site (TES). For genes shorter than 2 kb, the entire gene body was used for quantification. The mapped reads within each gene quantification window were counted by using BEDTools with the intersect option⁶² and are expressed as reads per kilobase per million reads (RPKM). Genes with transcription levels greater than 0.3 RPKM were considered to be actively transcribed. Genes that were not transcribed throughout all conditions were eliminated before downstream analysis. A gene was defined as 'differential' for a given pair of conditions if it was transcribed in either condition and the fold change in expression was greater than 1.5 (either up or down).

Dataset composition and normalization. Five RNA-seq datasets containing different combinations of samples were collected. Datasets were as follows:

- Dataset I: LMs from mice fed a ND or HFD;
 - Dataset II: LMs from mice treated with GeRP-Scor Gerp-*Igf1bp7*;
 - Dataset III: hepatocytes from mice treated with GeRP-Scor Gerp-*Igf1bp7*;
 - Dataset IV: LMs from lean and obese human subjects;
 - Dataset V: LMs from obese insulin-resistant and insulin-sensitive subjects.
- The read count table for each dataset was normalized separately with DESeq2 (ref. ⁶³).

GRO-seq dataset composition and normalization. One GRO-seq dataset composed of nuclei from LMs (pooled samples from mice treated with GeRP-Scor Gerp-*Nfkb*) was collected. The read count table was normalized by the TMM⁶⁴ method.

Multiple-test corrections. Whenever stated in relation to differential expression analyses, FDR-adjusted *P* values were obtained with the Benjamini–Hochberg procedure to account for multiple testing⁶⁵.

Identification of differentially expressed genes. Differentially expressed genes from each dataset were identified by using DESeq2 with *P* values adjusted for multiple testing via Benjamini–Hochberg correction with FDR values less than 0.05.

Gene set enrichment analysis. The gene set enrichment analysis (GSEA)⁶⁶ method was performed by using the KEGG pathways database. First, genes were ranked in decreasing order according to log₂-transformed fold change (log₂(FC)) in expression. For each query pathway, if gene *i* was a member of the pathway, it was defined as

$$X_i = 2 \sqrt{\frac{N - G}{G}}$$

If gene i was not a member of the pathway, it was defined as

$$X_i = -2\sqrt{\frac{G}{N-G}}$$

where N corresponds to the total number of genes and G corresponds to the number of genes in the query pathway. Next, a maximum running sum across all N genes called the MES was calculated as

$$MES = \max_{1 \leq j \leq N} \sum_{i=1}^j X_i$$

A permutation test was then performed 500 times to evaluate the significance of MES values, where the null hypothesis stated that the pathway was not enriched in ranking. If the query pathway had a nominal P value of less than 0.05 and the adjusted P value after correction for multiple testing using the Benjamini–Hochberg method with FDR was less than 0.1, the null hypothesis was rejected and the query pathway was considered to be significantly enriched. MES value represents the direction of expression of a pathway, where a positive MES value indicates upregulation and a negative MES value indicates downregulation.

Gene ontology enrichment analysis. For any set of differentially expressed genes, enrichment analysis for GO biological processes was achieved with respect to the whole mouse genome by conditional hypergeometric test, available in the GOstats package⁶⁷ in the R statistical environment. Enrichment P values were adjusted by using the Benjamini–Hochberg method⁶⁵.

Comparison with human transcriptomic data. To compare the gene expression trends from Supplementary Table 3 with similar human-centric gene expression datasets, we surveyed the Gene Expression Omnibus (GEO)⁶⁸ and downloaded two relevant microarray datasets: (i) GSE48452 (ref. 20) and (ii) GSE61260 (ref. 21). For each of these datasets, we retained probe sets that had MAS5 'present' calls for at least 50% of the samples in one of the groups being compared for differential expression. Differential expression was calculated by using the limma package⁶⁹ and genes with FDR < 0.05 were deemed to be differentially regulated independently of \log_2 (fold change).

Statistical analyses. The data were analysed with GraphPad Prism software. The statistical significance of differences among groups was analysed by ANOVA or Student's t test whenever appropriate. Data are presented as mean \pm s.e.m. $P < 0.05$ was considered to be statistically significant. Sample size for each experiment was calculated on the basis of previous data collection and as described in ref. 70. For animal experiments, although we started every experiment with the same number of animals per group, if any individual animal showed signs of discomfort or an injection failed, we had to terminate the study for this particular animal in accordance with our ethical permit and the rigor of the study.

Reporting Summary. Further information on research design is available in the Nature Research Reporting Summary linked to this article.

Data availability

The data that support the plots within this paper and other findings of this study are available from the corresponding author upon reasonable request. Custom codes used for GSEA are available upon request. All sequenced data for this study have been deposited in the Sequence Read Archive (SRA) under accession numbers PRJNA483744 (mouse data) and PRJNA491664 (human data).

Received: 21 April 2018; Accepted: 12 February 2019;

Published online: 25 March 2019

References

- Moore, M. C., Coate, K. C., Winnick, J. J., An, Z. & Cherrington, A. D. Regulation of hepatic glucose uptake and storage in vivo. *Adv. Nutr.* **3**, 286–294 (2012).
- Petersen, M. C., Vatner, D. F. & Shulman, G. I. Regulation of hepatic glucose metabolism in health and disease. *Nat. Rev. Endocrinol.* **13**, 572–587 (2017).
- Lackey, D. E. & Olefsky, J. M. Regulation of metabolism by the innate immune system. *Nat. Rev. Endocrinol.* **12**, 15–28 (2016).
- Tilg, H. & Moschen, A. R. Evolution of inflammation in nonalcoholic fatty liver disease: the multiple parallel hits hypothesis. *Hepatology* **52**, 1836–1846 (2010).
- Jager, J., Aparicio-Vergara, M. & Aouadi, M. Liver innate immune cells and insulin resistance: the multiple facets of Kupffer cells. *J. Intern. Med.* **280**, 209–220 (2016).
- Esser, N., Paquot, N. & Scheen, A. J. Anti-inflammatory agents to treat or prevent type 2 diabetes, metabolic syndrome and cardiovascular disease. *Expert Opin. Investig. Drugs* **24**, 283–307 (2015).
- Pollack, R. M., Donath, M. Y., LeRoith, D. & Leibowitz, G. Anti-inflammatory agents in the treatment of diabetes and its vascular complications. *Diabetes Care* **39**(Suppl. 2), S244–S252 (2016).
- Everett, B. M. et al. Anti-inflammatory therapy with canakinumab for the prevention and management of diabetes. *J. Am. Coll. Cardiol.* **71**, 2392–2401 (2018).
- Chen, L. et al. Selective depletion of hepatic Kupffer cells significantly alleviated hepatosteatosis and intrahepatic inflammation induced by high fat diet. *Hepatology* **59**, 1208–1212 (2012).
- Clementi, A. H., Gaudy, A. M., van Rooijen, N., Pierce, R. H. & Mooney, R. A. Loss of Kupffer cells in diet-induced obesity is associated with increased hepatic steatosis, STAT3 signaling, and further decreases in insulin signaling. *Biochim. Biophys. Acta* **1792**, 1062–1072 (2009).
- Lanthier, N. et al. Kupffer cell activation is a causal factor for hepatic insulin resistance. *Am. J. Physiol. Gastrointest. Liver Physiol.* **298**, G107–G116 (2010).
- Papackova, Z. et al. Kupffer cells ameliorate hepatic insulin resistance induced by high-fat diet rich in monounsaturated fatty acids: the evidence for the involvement of alternatively activated macrophages. *Nutr. Metab.* **9**, 22 (2012).
- Stienstra, R. et al. Kupffer cells promote hepatic steatosis via interleukin-1 β -dependent suppression of peroxisome proliferator-activated receptor α activity. *Hepatology* **51**, 511–522 (2010).
- Figuroa-Clarevega, A. & Bilder, D. Malignant *Drosophila* tumors interrupt insulin signaling to induce cachexia-like wasting. *Dev. Cell* **33**, 47–55 (2015).
- Kwon, Y. et al. Systemic organ wasting induced by localized expression of the secreted insulin/IGF antagonist ImpL2. *Dev. Cell* **33**, 36–46 (2015).
- Evdokimova, V. et al. IGFBP7 binds to the IGF-1 receptor and blocks its activation by insulin-like growth factors. *Sci. Signal.* **5**, ra92 (2012).
- Kratz, M. et al. Metabolic dysfunction drives a mechanistically distinct proinflammatory phenotype in adipose tissue macrophages. *Cell Metab.* **20**, 614–625 (2014).
- Hardy, O. T. et al. Body mass index-independent inflammation in omental adipose tissue associated with insulin resistance in morbid obesity. *Surg. Obes. Relat. Dis.* **7**, 60–67 (2011).
- Haukeland, J. W. et al. Systemic inflammation in nonalcoholic fatty liver disease is characterized by elevated levels of CCL2. *J. Hepatol.* **44**, 1167–1174 (2006).
- Ahrens, M. et al. DNA methylation analysis in nonalcoholic fatty liver disease suggests distinct disease-specific and remodeling signatures after bariatric surgery. *Cell Metab.* **18**, 296–302 (2013).
- Horvath, S. et al. Obesity accelerates epigenetic aging of human liver. *Proc. Natl. Acad. Sci. USA* **111**, 15538–15543 (2014).
- Morinaga, H. et al. Characterization of distinct subpopulations of hepatic macrophages in HFD/obese mice. *Diabetes* **64**, 1120–1130 (2015).
- Aouadi, M. et al. Orally delivered siRNA targeting macrophage Map4k4 suppresses systemic inflammation. *Nature* **458**, 1180–1184 (2009).
- Tesz, G. J. et al. Glucan particles for selective delivery of siRNA to phagocytic cells in mice. *Biochem. J.* **436**, 351–362 (2011).
- Tencerova, M. et al. Activated Kupffer cells inhibit insulin sensitivity in obese mice. *FASEB J.* **29**, 2959–2969 (2015).
- Wan, F. & Lenardo, M. J. The nuclear signaling of NF- κ B: current knowledge, new insights, and future perspectives. *Cell Res.* **20**, 24–33 (2010).
- Fang, B. et al. Circadian enhancers coordinate multiple phases of rhythmic gene transcription in vivo. *Cell* **159**, 1140–1152 (2014).
- Aparicio-Vergara, M., Tencerova, M., Morgantini, C., Barreby, E. & Aouadi, M. Isolation of Kupffer cells and hepatocytes from a single mouse liver. *Methods Mol. Biol.* **1639**, 161–171 (2017).
- Huang, W. et al. Depletion of liver Kupffer cells prevents the development of diet-induced hepatic steatosis and insulin resistance. *Diabetes* **59**, 347–357 (2010).
- Halpern, K. B. et al. Single-cell spatial reconstruction reveals global division of labour in the mammalian liver. *Nature* **542**, 352–356 (2017).
- Scott, C. L. et al. Bone marrow-derived monocytes give rise to self-renewing and fully differentiated Kupffer cells. *Nat. Commun.* **7**, 10321 (2016).
- Levanon, E. Y. et al. Evolutionarily conserved human targets of adenosine to inosine RNA editing. *Nucleic Acids Res.* **33**, 1162–1168 (2005).
- Godfried Sie, C., Hesler, S., Maas, S. & Kuchka, M. IGFBP7's susceptibility to proteolysis is altered by A-to-I RNA editing of its transcript. *FEBS Lett.* **586**, 2313–2317 (2012).
- Ahmed, S. et al. Proteolytic processing of IGFBP-related protein-1 (TAF/angiomodulin/mac25) modulates its biological activity. *Biochem. Biophys. Res. Commun.* **310**, 612–618 (2003).
- Bader, R. et al. The IGFBP7 homolog ImpL2 promotes insulin signaling in distinct neurons of the *Drosophila* brain. *J. Cell Sci.* **126**, 2571–2576 (2013).
- Jiao, P., Feng, B., Li, Y., He, Q. & Xu, H. Hepatic ERK activity plays a role in energy metabolism. *Mol. Cell Endocrinol.* **375**, 157–166 (2013).
- Han, M. S. et al. JNK expression by macrophages promotes obesity-induced insulin resistance and inflammation. *Science* **339**, 218–222 (2013).
- Cai, D. et al. Local and systemic insulin resistance resulting from hepatic activation of IKK- β and NF- κ B. *Nat. Med.* **11**, 183–190 (2005).

39. Obstfeld, A. E. et al. C-C chemokine receptor 2 (CCR2) regulates the hepatic recruitment of myeloid cells that promote obesity-induced hepatic steatosis. *Diabetes* **59**, 916–925 (2010).
40. Arkan, M. C. et al. IKK- β links inflammation to obesity-induced insulin resistance. *Nat. Med.* **11**, 191–198 (2005).
41. Odegaard, J. I. et al. Alternative M2 activation of Kupffer cells by PPAR δ ameliorates obesity-induced insulin resistance. *Cell Metab.* **7**, 496–507 (2008).
42. Lanthier, N. et al. Kupffer cell depletion prevents but has no therapeutic effect on metabolic and inflammatory changes induced by a high-fat diet. *FASEB J.* **25**, 4301–4311 (2011).
43. Honegger, B. et al. Imp-L2, a putative homolog of vertebrate IGF-binding protein 7, counteracts insulin signaling in *Drosophila* and is essential for starvation resistance. *J. Biol.* **7**, 10 (2008).
44. Ussar, S., Bezy, O., Bluher, M. & Kahn, C. R. Glypican-4 enhances insulin signaling via interaction with the insulin receptor and serves as a novel adipokine. *Diabetes* **61**, 2289–2298 (2012).
45. Boothe, T. et al. Inter-domain tagging implicates caveolin-1 in insulin receptor trafficking and Erk signaling bias in pancreatic beta-cells. *Mol. Metab.* **5**, 366–378 (2016).
46. Belfiore, A., Frasca, F., Pandini, G., Sciacca, L. & Vigneri, R. Insulin receptor isoforms and insulin receptor/insulin-like growth factor receptor hybrids in physiology and disease. *Endocr. Rev.* **30**, 586–623 (2009).
47. Leibiger, B. et al. PI3K-C2 α knockdown results in rerouting of insulin signaling and pancreatic beta cell proliferation. *Cell Rep.* **13**, 15–22 (2015).
48. Kumar, S., Bradley, C. L., Mukashyaka, P. & Doerfler, W. T. Identification of essential arginine residues of *Escherichia coli* DedA/Tvp38 family membrane proteins YqjA and YghB. *FEMS Microbiol. Lett.* **363**, fnw133 (2016).
49. Dahms, S. O., Hades, K., Steinmetzer, T. & Than, M. E. X-ray structures of the proprotein convertase furin bound with substrate analogue inhibitors reveal substrate specificity determinants beyond the S4 pocket. *Biochemistry* **57**, 925–934 (2018).
50. Eisenberg, E. & Levanon, E. Y. A-to-I RNA editing—immune protector and transcriptome diversifier. *Nat. Rev. Genet.* **19**, 473–490 (2018).
51. Donath, M. Y. Targeting inflammation in the treatment of type 2 diabetes: time to start. *Nat. Rev. Drug Discov.* **13**, 465–476 (2014).
52. Lee, J. H. et al. Hepatic steatosis index: a simple screening tool reflecting nonalcoholic fatty liver disease. *Dig. Liver Dis.* **42**, 503–508 (2010).
53. Bell, C. C. et al. Transcriptional, functional, and mechanistic comparisons of stem cell-derived hepatocytes, HepaRG cells, and three-dimensional human hepatocyte spheroids as predictive in vitro systems for drug-induced liver injury. *Drug Metab. Dispos.* **45**, 419–429 (2017).
54. Wijkstrom, J. et al. Renal morphology, clinical findings, and progression rate in Mesoamerican nephropathy. *Am. J. Kidney Dis.* **69**, 626–636 (2017).
55. Weibel, E. R. Stereological methods in cell biology: where are we—where are we going? *J. Histochem. Cytochem.* **29**, 1043–1052 (1981).
56. Parini, P., Johansson, L., Broijersén, A., Angelin, B. & Rudling, M. Lipoprotein profiles in plasma and interstitial fluid analyzed with an automated gel-filtration system. *Eur. J. Clin. Invest.* **36**, 98–104 (2006).
57. Tennessen, J. M., Barry, W. E., Cox, J. & Thummel, C. S. Methods for studying metabolism in *Drosophila*. *Methods* **68**, 105–115 (2014).
58. Schneedorferova, I., Tomcala, A. & Valterova, I. Effect of heat treatment on the n-3/n-6 ratio and content of polyunsaturated fatty acids in fish tissues. *Food Chem.* **176**, 205–211 (2015).
59. Kutsukake, M. et al. Circulating IGF-binding protein 7 (IGFBP7) levels are elevated in patients with endometriosis or undergoing diabetic hemodialysis. *Reprod. Biol. Endocrinol.* **6**, 54 (2008).
60. Kim, D. et al. TopHat2: accurate alignment of transcriptomes in the presence of insertions, deletions and gene fusions. *Genome Biol.* **14**, R36 (2013).
61. Liao, Y., Smyth, G. K. & Shi, W. featureCounts: an efficient general purpose program for assigning sequence reads to genomic features. *Bioinformatics* **30**, 923–930 (2014).
62. Quinlan, A. R. & Hall, I. M. BEDTools: a flexible suite of utilities for comparing genomic features. *Bioinformatics* **26**, 841–842 (2010).
63. Love, M. I., Huber, W. & Anders, S. Moderated estimation of fold change and dispersion for RNA-seq data with DESeq2. *Genome Biol.* **15**, 550 (2014).
64. Robinson, M. D. & Oshlack, A. A scaling normalization method for differential expression analysis of RNA-seq data. *Genome Biol.* **11**, R25 (2010).
65. Benjamini, Y. & Hochberg, Y. Controlling the false discovery rate: a practical and powerful approach to multiple testing. *J. R. Stat. Soc.* **57**, 289–300 (1995).
66. Mootha, V. K. et al. PGC-1 α -responsive genes involved in oxidative phosphorylation are coordinately downregulated in human diabetes. *Nat. Genet.* **34**, 267 (2003).
67. Falcon, S. & Gentleman, R. Using GOstats to test gene lists for GO term association. *Bioinformatics* **23**, 257–258 (2007).
68. Barrett, T. et al. NCBI GEO: archive for functional genomics data sets—update. *Nucleic Acids Res.* **41**, D991–D995 (2013).
69. Ritchie, M. E. et al. limma powers differential expression analyses for RNA-sequencing and microarray studies. *Nucleic Acids Res.* **43**, e47 (2015).
70. Rosner, B. *Fundamental of Biostatistics* 7th edn (Brooks/Cole CENGAGE Learning, 2010).

Acknowledgements

We are grateful to R. Harris, S. Craige and B. Craige for their considerable input on the manuscript. We thank T. Dolezal and M. Jindra for helpful suggestions on the *Drosophila* work. We also thank T. Schröder and R. Kuiper for the tissue histology, M. Taipale and J. Liu for performing sequencing, and A. Krstic for providing flow cytometry support. We thank M. Nordstrand for organising the collection of human obese liver biopsies. This work was supported by research grants from AstraZeneca through the ICMC (M.A.), the Swedish Research Council (M.A.; 2015-03582), the Stockholm County Council (E.N.), the Novo Nordisk Foundation, including the Tripartite Immuno-metabolism Consortium (M.A. and TrIC; NNF15CC0018486), the Strategic Research Program in Diabetes at Karolinska Institutet (M.A. and E.N.), the Diabetes Wellness Foundation Sweden (J.J.) and the Ruth and Richard Julin Foundation (C.M.).

Author contributions

C.M. carried out most experiments. G.K. and A.B. performed and analysed the data from the *Drosophila* experiments. J.J., L.L., V.A., E.B., A.S., C.X., M.T., C.K. and F.V. helped with experiments and interpretation of the data. S.S. measured circulating lipid levels in mice. A.T. measured lipids in *Drosophila*. K.H. generated all electron microscopy images and measurements. N.K.B. and E.E. provided biopsies and liver cells from lean individuals. E.N. provided liver biopsies from obese human subjects. M.R. provided serum from obese and lean volunteers. T.H. and V.M.L. performed experiments in human liver spheroids. X.L. and C.K. performed the bioinformatics analysis and interpretation. J.B. contributed to the design of experiments related to IGFBP7 signalling. C.M. and M.A. conceived the project, analysed data and wrote the manuscript with input from all co-authors.

Competing interests

The authors declare no competing interests.

Additional information

Supplementary information is available for this paper at <https://doi.org/10.1038/s42255-019-0044-9>.

Reprints and permissions information is available at www.nature.com/reprints.

Correspondence and requests for materials should be addressed to M.A.

Publisher's note: Springer Nature remains neutral with regard to jurisdictional claims in published maps and institutional affiliations.

© The Author(s), under exclusive licence to Springer Nature Limited 2019

CHAPTER V:

Polarization of macrophages in insects: Opening gates for immuno-metabolic research

Adam Bajgar, **Gabriela Krejčová**, Tomáš Doležal

Frontiers in Cell and Developmental Biology, 2021, 9:10.3389/fcell.2021.629238



Polarization of Macrophages in Insects: Opening Gates for Immuno-Metabolic Research

Adam Bajgar*, Gabriela Krejčová and Tomáš Doležal

Department of Molecular Biology and Genetics, University of South Bohemia, Ceske Budejovice, Czechia

OPEN ACCESS

Edited by:

Katrin Kierdorf,
University of Freiburg, Germany

Reviewed by:

Dan Hultmark,
Umeå University, Sweden
Helen Weavers,
University of Bristol, United Kingdom

*Correspondence:

Adam Bajgar
bajgaradam@seznam.cz

Specialty section:

This article was submitted to
Cell Death and Survival,
a section of the journal
Frontiers in Cell and Developmental
Biology

Received: 13 November 2020

Accepted: 11 January 2021

Published: 15 February 2021

Citation:

Bajgar A, Krejčová G and
Doležal T (2021) Polarization
of Macrophages in Insects: Opening
Gates for Immuno-Metabolic
Research.
Front. Cell Dev. Biol. 9:629238.
doi: 10.3389/fcell.2021.629238

Insulin resistance and cachexia represent severe metabolic syndromes accompanying a variety of human pathological states, from life-threatening cancer and sepsis to chronic inflammatory states, such as obesity and autoimmune disorders. Although the origin of these metabolic syndromes has not been fully comprehended yet, a growing body of evidence indicates their possible interconnection with the acute and chronic activation of an innate immune response. Current progress in insect immuno-metabolic research reveals that the induction of insulin resistance might represent an adaptive mechanism during the acute phase of bacterial infection. In *Drosophila*, insulin resistance is induced by signaling factors released by bactericidal macrophages as a reflection of their metabolic polarization toward aerobic glycolysis. Such metabolic adaptation enables them to combat the invading pathogens efficiently but also makes them highly nutritionally demanding. Therefore, systemic metabolism has to be adjusted upon macrophage activation to provide them with nutrients and thus support the immune function. That anticipates the involvement of macrophage-derived systemic factors mediating the inter-organ signaling between macrophages and central energy-storing organs. Although it is crucial to coordinate the macrophage cellular metabolism with systemic metabolic changes during the acute phase of bacterial infection, the action of macrophage-derived factors may become maladaptive if chronic or in case of infection by an intracellular pathogen. We hypothesize that insulin resistance evoked by macrophage-derived signaling factors represents an adaptive mechanism for the mobilization of sources and their preferential delivery toward the activated immune system. We consider here the validity of the presented model for mammals and human medicine. The adoption of aerobic glycolysis by bactericidal macrophages as well as the induction of insulin resistance by macrophage-derived factors are conserved between insects and mammals. Chronic insulin resistance is at the base of many human metabolically conditioned diseases such as non-alcoholic steatohepatitis, atherosclerosis, diabetes, and cachexia. Therefore, revealing the original biological relevance of cytokine-induced insulin resistance may help to develop a suitable strategy for treating these frequent diseases.

Keywords: *Drosophila*, macrophages, insulin resistance, cachexia, cytokines, immuno-metabolism, aerobic glycolysis

INTRODUCTION

Both cachexia and insulin resistance are in the spotlight of immuno-metabolic research and represent the most important comorbidities that often accompany acute and chronic inflammatory states and complicate their treatment (Fonseca et al., 2020). Cachexia, literally meaning “bad condition,” is a metabolic syndrome of excessive weight loss and muscle wasting caused by alterations in appetite and the overall metabolic setup (Yang et al., 2020). The progressive development of insulin resistance to pre-cachexia and cachexia, which is defined as a loss of more than 5% of the cell body mass over 12 months or less, is known to be a hallmark for a wide range of seemingly unrelated diseases, such as obesity, cancer, chronic obstructive pulmonary disease, acute kidney disease, and sepsis (Mak and Cheung, 2006; Koehler et al., 2007; Srikanthan et al., 2010; Honors and Kinzig, 2012). Nevertheless, the mechanism of induction of these frequently occurring metabolic syndromes remains to be elucidated.

The origin of insulin resistance and cachexia relies on the activity of immune cell-derived signaling factors and is thus a result of excessive activation of the immune system (Olefsky and Glass, 2010). However, the biological relevance of such signaling has not been fully comprehended yet. It is mainly due to the prevailing perception of the cytokine-induced insulin resistance as a mere side effect of pathological syndromes and insufficient effort to reveal its adaptive meaning. The complexity of the mammalian immune system, as well as pleiotropic effects of most immune cell-derived factors, further complicate the resolution of this intricate relationship (Stenholm et al., 2008; Del Fabbro et al., 2011).

Recent progress in insect immuno-metabolic research revealed that cytokine-induced insulin resistance is not a mechanism occurring exclusively in vertebrates. Indeed, we may observe several physiological conditions in which immune cells release cytokines to affect the systemic metabolism via induction of insulin resistance in *Drosophila*, such as metabolic imbalance and development, as well as immune response (Rajan and Perrimon, 2011; Woodcock et al., 2015; Lee et al., 2018; Dolezal et al., 2019). These states document the preservation of this mechanism among such evolutionarily distant groups as insects and mammals. To be maintained in the evolution, we might presume that cytokine-induced insulin resistance represents an ancient adaptive process of systemic metabolic rearrangement.

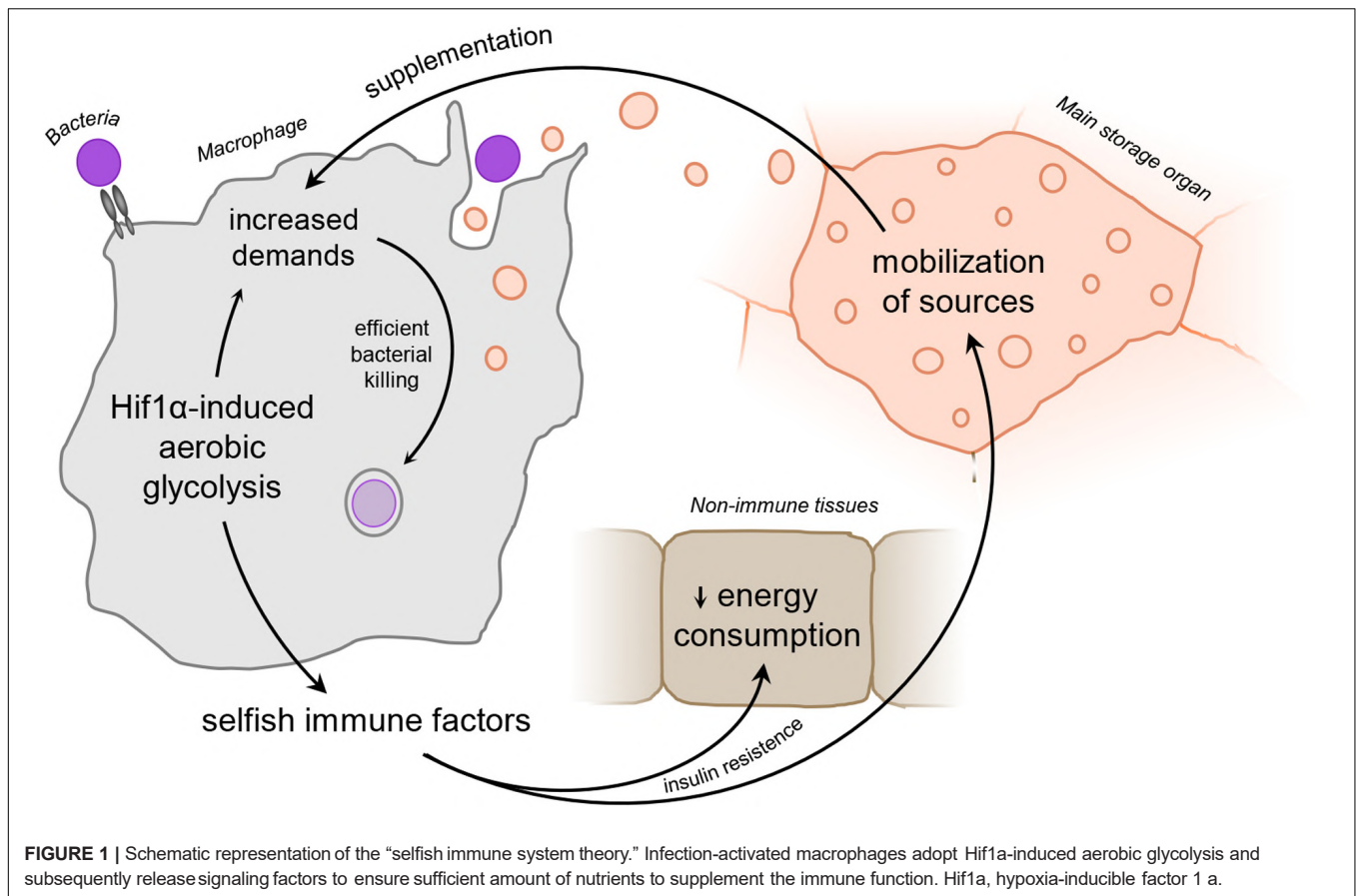
Here, we would like to present several recent observations depicting that *Drosophila* activated immune cells affect systemic metabolism via the induction of insulin resistance to ensure sufficient supplementation with nutrients for their function (Figure 1 and Box 1). Although this mechanism is necessary for the acute phase of the immune response (Yang et al., 2015; Bajgar and Dolezal, 2018; Dolezal et al., 2019), it may lead to nutrient wastage if chronic, and prolonged reallocation of sources may become the basis for the development of many serious pathological conditions.

Innate immune cells performing the phagocytic function represent the front line of protection against invading pathogens (Franken et al., 2016). Individuals, therefore, tend to maximize

the number of these protectors participating in phagocytosis and clearance of pathogen (Kacsóh and Schlenke, 2012; Mihajlovic et al., 2019). Nevertheless, the maintenance of an excessive number of metabolically demanding phagocytes would be highly energy-intensive with subsequent adverse impact on concurrent energy-consuming processes, such as growth and reproduction (Wolowczuk et al., 2008). Therefore, animals have developed a strategy to overcome these evolutionary constraints by maintaining a sufficient number of immune cells in a quiescent state as well as by proliferation of their progenitors upon immune challenge. Quiescent phagocytes exhibiting only a basal metabolic rate are thus waiting for the activation stimuli ready to be metabolically awakened and to participate in the acute immune response (Mosser and Edwards, 2008). In plentiful times, individuals can fully exploit the surplus energy to maintain homeostasis, growth, and reproduction as processes based mainly on anabolic metabolism (Wang et al., 2019). That is in sharp contrast to the situation of life-threatening infection. In response to the recognition of pathogen-associated molecular patterns, activated immune cells such as monocytes, macrophages, dendritic cells, and neutrophils, must react rapidly to limit the pathogen burden and adopt a bactericidal polarization phenotype (Galván-peña and O'Neill, 2014; Loftus and Finlay, 2016). However, the immediate activation of a large number of these cells toward the bactericidal phenotype (also known as pro-inflammatory) represents an immense energy load for the organism (Demas, 2004; Edholm et al., 2017). The nutritional investments connected with the acute phase response are further increased by the proliferation of immune cell progenitors and their differentiation toward effector cells upon activation of the immune response.

Professional phagocytes must rewire their cellular metabolism greatly to become efficient in bacterial killing (Pavliou et al., 2017). It is well established particularly for mammalian bactericidal macrophages that they undergo metabolic polarization toward aerobic glycolysis as a predominant source of energy and a precursor essential for bactericidal function (Benoit et al., 2008). Similarly to macrophages, the increased glycolytic rate and other metabolic adjustments were later confirmed also for neutrophils, dendritic cells, effector lymphocytes, and natural killer cells (Loftus and Finlay, 2016). Interestingly, adoption of aerobic glycolysis by immune cells may originate not only in response to bacterial invaders but can also be induced by excessive lipid uptake (Box 2).

Although the term “aerobic glycolysis” *sensu stricto* refers to lactic acid fermentation of glucose, here we perceive it as a complex phagocyte metabolic program including, in addition, increased pentose phosphate pathway, lipid synthesis, and the mevalonate pathway, as well as a rewired flow of the Krebs cycle (Mills and O'Neill, 2016; Nonnenmacher and Hiller, 2018). Such metabolic adaptation affects also nutritional demands of these cells and makes them functionally dependent on external supplementation. Since the availability of nutrients may become limiting for the adoption of bactericidal polarization (Nagy and Haschemi, 2015; Ganeshan et al., 2019), they have to secure sufficient availability of sources in circulation and gain an advantage over the surrounding tissues in their use.



Therefore, activated professional phagocytes release signaling factors regulating both local and systemic energy in order to usurp enough sources for an acute immune response (Khovidhunkit et al., 2004; Soeters and Soeters, 2012; Straub, 2014; Dolezal, 2015; **Figure 1** and **Box 1**).

Besides the mobilization of sources from central energy-storing organs, such as adipose tissue and the liver, it is fundamental to limit the consumption of nutrients by other processes unrelated to the immune response (Almajwal et al., 2019). The privileged status of immune cells in reaching the nutrients is justified since making the immune response the most efficient is often a question of life and death. Although such behavior of the immune cells is for the sake of the individual, the usurpation of sources may be interpreted as selfish if viewed from the perspective of inter-organ competition for sources. Immune cell-derived signaling

factors responsible for such systemic metabolic switch may be hence called selfish immune factors (SIFs) (Bajgar et al., 2015; Dolezal et al., 2019).

Insulin signaling is the central signaling pathway regulating the balance between anabolic and catabolic processes in the body (Schwartzburd, 2017). We may, therefore, presume that antagonism of insulin signaling is the most straightforward strategy to reroute energy flows from maintenance, growth, and reproduction to its fast utilization by the activated immune system. Cytokine-induced deterioration of insulin signaling leads to an increased titer of circulating energy-rich compounds such as glucose, lipoproteins, and amino acids (Felig et al., 1969; Salazaret al., 2018; Cho et al., 2019). The impact of infection-induced insulin insensitivity on the systemic metabolism highly resembles hyperglycemia and hyperlipidemia as hallmark states of chronic insulin resistance and cachexia (Khovidhunkit et al., 2004; de Luca and Olefsky, 2008; Shi et al., 2019). However, the regulation of energy homeostasis in mammals is substantially influenced also by other metabolism-related hormones such as cortisol and catecholamines, particularly noradrenalin and norepinephrine that should not be omitted for their effects on nutrient mobilization in situation of metabolic stress (Marik and Bellomo, 2013).

In the presented perspective, insulin resistance and subsequent pre-cachectic state induced by immune cell-derived factors may be perceived as an adaptive metabolic adjustment

BOX 1 | Hypothesis.

We hypothesize that activated phagocytes produce signaling factors to reflect their current nutritional demands upon adoption of aerobic glycolysis. These factors induce mobilization of nutrients and silence their consumption by non-immune tissues via insulin resistance, leaving thus enough of sources for the activated immune system. Release of these signaling factors is thus beneficial for the acute immune response; however, it may lead to energy wasting and development of severe pathologies if produced chronically (**Figure 1**).

BOX 2 | Excessive lipids induce adoption of macrophage pro-inflammatory phenotype.

It is of particular interest that the adoption of pro-inflammatory M1 polarization can be induced even without the presence of a pathogen. That is in concordance with the previously mentioned fact that HIF1 α stabilization, central for induction of bactericidal macrophage polarization, may be achieved either by TLR4 activation or by metabolic feedback from mitochondrial metabolism (Iommarini et al., 2017). It underpins many metabolically induced inflammatory diseases with a significant impact on human well-being, such as obesity, non-alcoholic fatty liver disease, atherosclerosis, and diabetes (Kraakman et al., 2014; Castoldi et al., 2016; Kazankov et al., 2019).

Exposure of macrophages to excessive amounts of lipids can lead to the adoption of pro-inflammatory polarization of macrophages. The effect of lipids on macrophages is dual. The increased concentration of lipids in the extracellular space is recognized by TLR4 and, analogically to infection, leads to the stabilization of HIF1 α via the NF κ B signaling pathway (Hubler and Kennedy, 2016; Korbecki and Bajdak-Rusinek, 2019). In addition, lipids are efficiently internalized by macrophages via receptor-mediated endocytosis (Park, 2014). Because there is no feedback on lipid uptake by macrophages, it leads to a massive accumulation of oxidized lipids and cholesterol in the cytosol of these cells, followed by disruption of mitochondrial function (Gibson et al., 2018). Lipid peroxidation catalyzed by free iron ions, together with ROS accumulation, leads to disruption of mitochondrial function by activating the transcription factor *nuclear factor erythroid 2-related factor 2* (NRF2) (Dodson et al., 2019). NRF2 triggers the expression of a number of genes responsible for the sequestration of free iron and enzymes that neutralize the oxidative potential of ROS (Tonelli et al., 2018). Therefore, the accumulation of both internal and external lipids results in HIF1 α stabilization and the adoption of AG. It seems that macrophages are predetermined for this detoxification function by exploiting a whole set of genes involved in lipid metabolism and thus help to cope with ectopic lipid deposition (Bobryshev et al., 2016).

Under conditions in which macrophages are exposed to excessive lipids for a time-restricted period, such as aerobic exercise, intermittent fasting, and caloric restriction, induction of mild mitochondrial stress may be beneficial for the organism. This phenomenon, called mitohormesis, alleviates systemic insulin signaling, which has a positive impact on lifespan (Ristow and Schmeisser, 2014). Nevertheless, prolonged exposure of macrophages to lipids leads to the adoption of pro-inflammatory phenotypes and chronic insulin resistance (Shin et al., 2017). During obesity, macrophages are thought to cause cytokine-induced insulin resistance in adipose tissue, the liver, and, subsequently, the whole organism (Marette, 2002; Tilg and Hotamisligil, 2006; Makki et al., 2013).

Activation of macrophages by excessive lipids may explain several metabolic syndromes such as adipose tissue inflammation, non-alcoholic liver steatosis, atherosclerosis, diabetes, and cachexia. This hypothesis is in concordance with clinical observations and experiments carried out on mice, in which the amelioration of macrophage polarization by anti-inflammatory agents and drugs affecting lipid metabolism leads to significant improvement of these syndromes in obese individuals (Bellucci et al., 2017; Koelwyn et al., 2018).

essential for the effective fight of invading pathogens. However, mobilization of nutrients and their altered distribution in the body may become detrimental if chronic and may progress to the development of several human pathological states.

In the following paragraphs, we would like to present several lines of evidence supporting this perspective. Although gained mostly by the research of immuno-metabolism in insects, these observations are in concordance with many data from mice models and humans. Since the metabolic switch of innate immune cells is best comprehended for macrophages, we will focus in this review mainly on these cells. The hypothetical model discussed in this review is based on knowledge of biology of both mammalian macrophages as well as *Drosophila* professional phagocytes, called plasmatocytes. Their basic characteristics and the features resembling mammalian macrophages and neutrophils are further described in **Box 3**. To specify that the presented information concerns *Drosophila* phagocytes, these cells will be always denoted here as plasmatocytes.

We believe that we present here a compelling set of information to change the general conception of insulin resistance and pre-cachexia as clearly pathological states. This may help to better comprehend medical treatment in many human diseases.

MACROPHAGE ADOPTION OF A BACTERICIDAL PHENOTYPE IS NUTRITIONALLY DEMANDING

Macrophages, as highly versatile cells, fulfill various tasks in the organism. Besides representing the front line of protection against invading pathogens, macrophages also clear apoptotic cellular debris, maintain tissue homeostasis, and participate in the formation of many morphological structures during

development (Wynn et al., 2013; Gordon and Martinez-Pomares, 2017; Theret et al., 2019).

Not surprisingly, the various macrophage tasks require specific settings of cellular metabolism to obtain the optimal amount of metabolites and precursors required for the desired function. That may be depicted, for instance, in the metabolism of amino acid arginine. While macrophages participating in wound healing metabolize arginine to generate growth-promoting ornithine essential for wound reconstruction, bactericidal macrophages use the same amino acid as a precursor for the production of nitric oxide later applied as an efficient bactericidal agent (Mills et al., 2015). This revelation led to later identification of the full spectrum of macrophage polarization states characterized by their metabolic program, with the extremes represented by healing and bactericidal polarizations (Mosser and Edwards, 2008). Interestingly, the metabolic settings are determinative of macrophage function, and a mere metabolic setting has the potential to change the polarization phenotype (Galván-peña and O'Neill, 2014).

Upon pathogen infiltration, macrophages have to recognize, entrap, engulf, and destroy the invaders in the phagolysosome (Diskin and Pålsson-McDermott, 2018). There is no doubt that these processes are connected with excessive energy expenditure and a need for a synthesis of a high amount of precursors for the production of bactericidal agents, signaling molecules, as well as remodeling of cytoskeleton and cellular membrane. It has been estimated that the cellular membrane of activated macrophage turns over completely every 30 min due to accelerated endocytosis and micropinocytosis (Werb and Cohn, 1972). Besides membrane remodeling, phagocytosis also requires a high amount of energy. The ATP required for phagocytosis of a single polystyrene particle has been estimated to cost about 10^9 ATP molecules (Kamovsky, 1962). The subsequent generation of a sufficient amount of ROS and myeloperoxidase for bacterial

BOX 3 | *Drosophila* as a model for immuno-metabolic research.

Over the last century, *Drosophila* has become a very universal and suitable model organism for the study of many human diseases. The simplicity of *Drosophila*, the existence of readily available transgenic strains, as well as the possibility of tissue-specific and time-limited knockdown of a particular gene make *Drosophila* one of the most suitable model organisms for the study of complex systemic metabolic syndromes (Duffy, 2002). In addition, approaches that previously could not be applied due to the lack of input material from such a small organism are now possible due to the greater sensitivity of analytical techniques in recent years (Cheng et al., 2018).

The *Drosophila* immune system consists of several layers of protection of an individual, which consist of two main branches of the humoral and cellular immune response. In addition to immune cells, the fat body also participates in immune responses, as the central metabolic organ supports the immune response by releasing resources and producing antimicrobial peptides (Melcarne et al., 2019). Although *Drosophila* may develop a characteristic immune response against underlying types of pathogens, such as gram-positive and gram-negative bacteria, viruses, and fungi, the adaptive immune response in *Drosophila* has not been reliably demonstrated (Ferrandon et al., 2007). The *Drosophila* and mammalian immune systems display a surprising level of homology in the major immune signaling pathways. The antibacterial response consists of the activation of the Toll and Imd signaling pathways, supported by the usual JNK and HIF1a stress response (De Gregorio et al., 2002).

Some observations suggest that the innate immune response to invading pathogens shows certain features of trainability, but the mechanism of this process remains unclear. *Drosophila* immune cells, called hemocytes, include prohemocytes, plasmatocytes, crystal cells, and lamellocytes. While crystal cells and plasmatocytes are mainly involved in the encapsulation and melanization of foreign objects in the hemolymph, plasmatocytes represent a population of professional phagocytes (Melcarne et al., 2019; **Figure 2**).

Plasmatocytes are the most abundant population of cells in both larvae and adult flies (**Figure 2A**). These functionally versatile cells are involved in many biological processes (**Figure 2F**), from embryonic morphogenesis, metamorphosis, and wound healing to protection against invading pathogens (Banerjee et al., 2019). Because phagocytosis and bacterial killing are highly conserved at the level of cell biology, *Drosophila* plasmatocytes show an exceptional level of similarity to cells of the mammalian innate immune system, especially macrophages and neutrophils. Indeed, plasmatocytes use the same metabolic and signaling pathways for pathogen uptake and destruction in phagolysosomes (**Figure 2C**) as their mammalian counterparts, including the involvement of a plethora of homologous genes (Browne et al., 2013).

Although plasmatocytes are predominantly considered in the literature as a homogeneous population of phagocytic cells, a single cell transcriptomic analysis of the immune-stimulated larval hemocytes revealed a surprising level of their variability. However, the research of the plasmatocyte subpopulation is still at the beginning and far from distinguishing tissue-resident or specifically primed plasmatocyte subsets (Cattenoz et al., 2020; Tattikota et al., 2020).

Recently, the concept of immuno-metabolism has been developed in mammals, which indicates that several populations of mammalian immune cells must adopt a specific cellular metabolism in order to perform the desired function (Galván-peña and O'Neill, 2014). Although there are still some doubts about an analogous mechanism for *Drosophila* plasmatocytes, several publications and transcriptomic data document this ability (Krejčová et al., 2019; Cattenoz et al., 2020; Ramond et al., 2020; Tattikota et al., 2020). These observations are necessary not only for a comprehensive understanding of the antibacterial immune response but may become a base for research of many other human diseases that are connected with the pathological metabolic polarization of mammalian immune cells.

Despite the undeniable benefits of the *Drosophila* model for the study of human diseases, there are certain limits because many *Drosophila* organs and tissues show a lower level of complexity than in mammals.

Drosophila is currently used extensively to study insulin resistance. *Drosophila* and mammalian insulin signaling share major components at the level of cell biology (Álvarez-Rendón et al., 2018). However, certain significant differences also need to be taken into account. *Drosophila* carries eight insulin-like peptides (DILP1-8) that show structural homology to either mammalian insulin or relaxin. Analogous to mammals, *Drosophila* insulin signaling also reflects the current metabolic status of the individual. DILPs 2, 3, and 5 are thus released by specialized neurosecretory cells in the *Drosophila* CNS to regulate reproduction, growth and lifespan. While most DILPs activate a single *Drosophila* insulin receptor, DILP8 binds to its own LGR3 receptor. The situation in humans is even more complicated because, in addition to insulin, we can recognize two insulin-like growth factors, relaxin, as well as several insulin-like peptides. Insulin signaling activity is affected by many convergent signaling pathways and factors, such as hormones of a lipophilic nature, as well as insulin-binding proteins and IGFs (Nässel et al., 2015; Nässel and Broeck, 2016). Thus, an analogy can also be observed in the manner of insulin resistance induction.

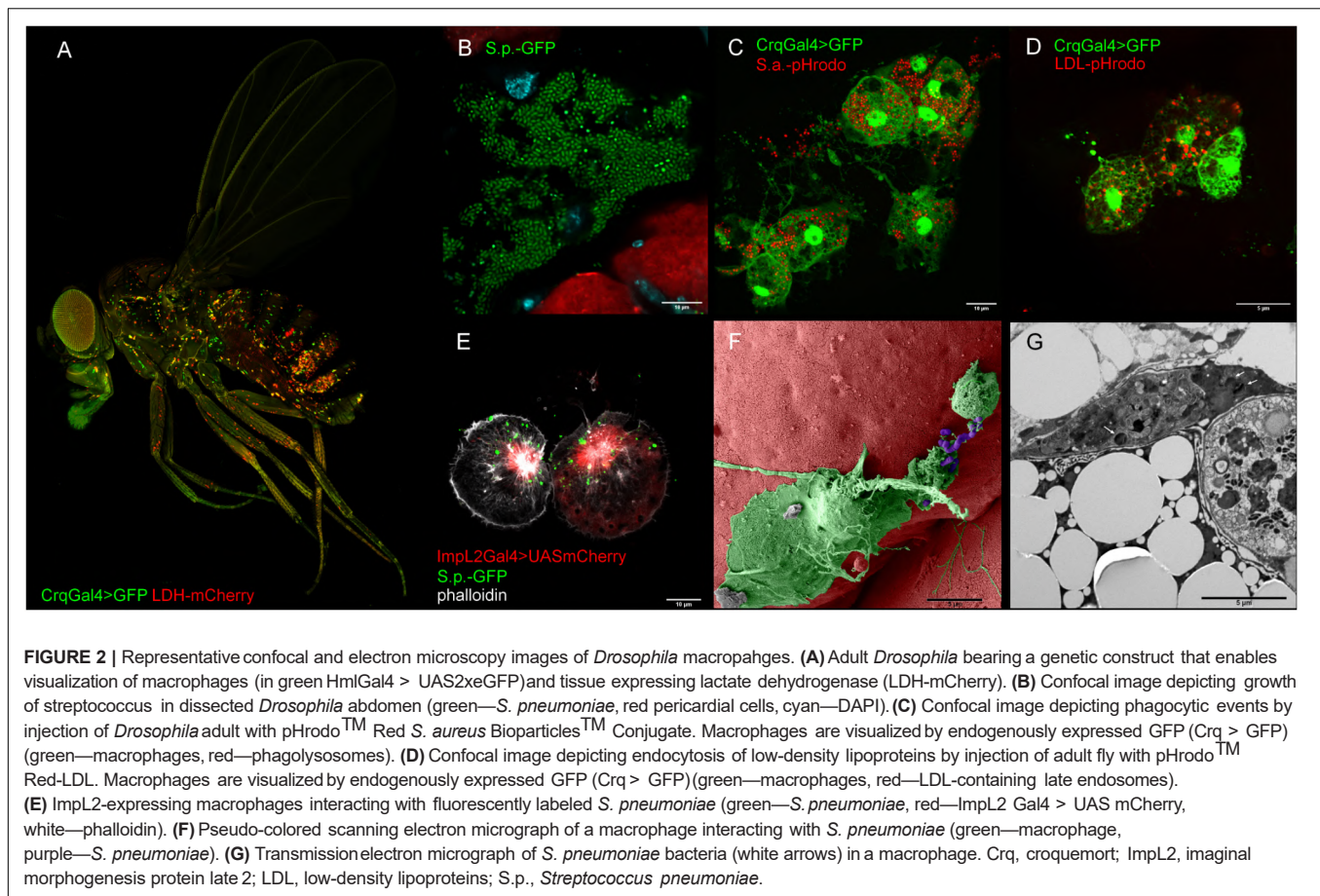
Therefore, we believe that ongoing research on the role of the *Drosophila* immune system in the regulation of systemic metabolism will lead to new discoveries that can be generalized to human medical research.

killing in the phagolysosome is another metabolically demanding process. The production of ROS, as well as compensation of its cytotoxicity, depends on sufficient availability of NADPH in cells. Therefore, macrophages must substantially increase the flow rate of the metabolic pathways producing this reducing agent (Panday et al., 2015).

To cover the sudden requirements arising from bactericidal function, macrophage has to adjust the overall metabolic setup, i.e., glycolysis, pentose phosphate pathway, mevalonate pathway, as well as the mitochondrial cycle of tricarboxylic acids and oxidative phosphorylation (Galván-peña and O'Neill, 2014). Such a complex rearrangement is orchestrated by central metabolic regulator Hypoxia-inducible factor 1 alpha—*Hif1a* (Corcoran and O'Neill, 2016; Wang et al., 2017). This stress-related transcription factor, originally discovered in research of hypoxia, is constitutively produced and degraded by all cells in the body (Marxsen et al., 2004). That is particularly important for immediate initiation of *Hif1a* activity since mere inhibition of its degradation suffices to stimulate expression of its target

genes (Watts and Walmsley, 2019). Stabilized HIF1a triggers the expression of more than a hundred genes under the control of the hypoxia response element (Dengler et al., 2014). The unique metabolic program established by the activity of HIF1a is generally called aerobic glycolysis. Between HIF1a-target genes, we can find mostly enzymes directly participating in metabolic pathways upregulated in aerobic glycolysis or regulating their flow rate, as will be mentioned below (**Figure 3**).

Many different signaling cascades converge on prolyl hydroxylase dehydrogenase (PHD), the enzyme responsible for HIF1a degradation. PHD requires several metabolic products as essential cofactors for its enzymatic activity. From the most prominent, we should mention oxygen, Fe²⁺ ions, and α -ketoglutarate as a product of canonically running Krebs cycle (Iommarini et al., 2017). Although originally described in hypoxia, HIF1a stabilization may be achieved even under normoxic conditions as may be observed in macrophages stimulated by pathogen-associated molecular patterns or pro-inflammatory cytokines (Iommarini et al., 2017). These ligands

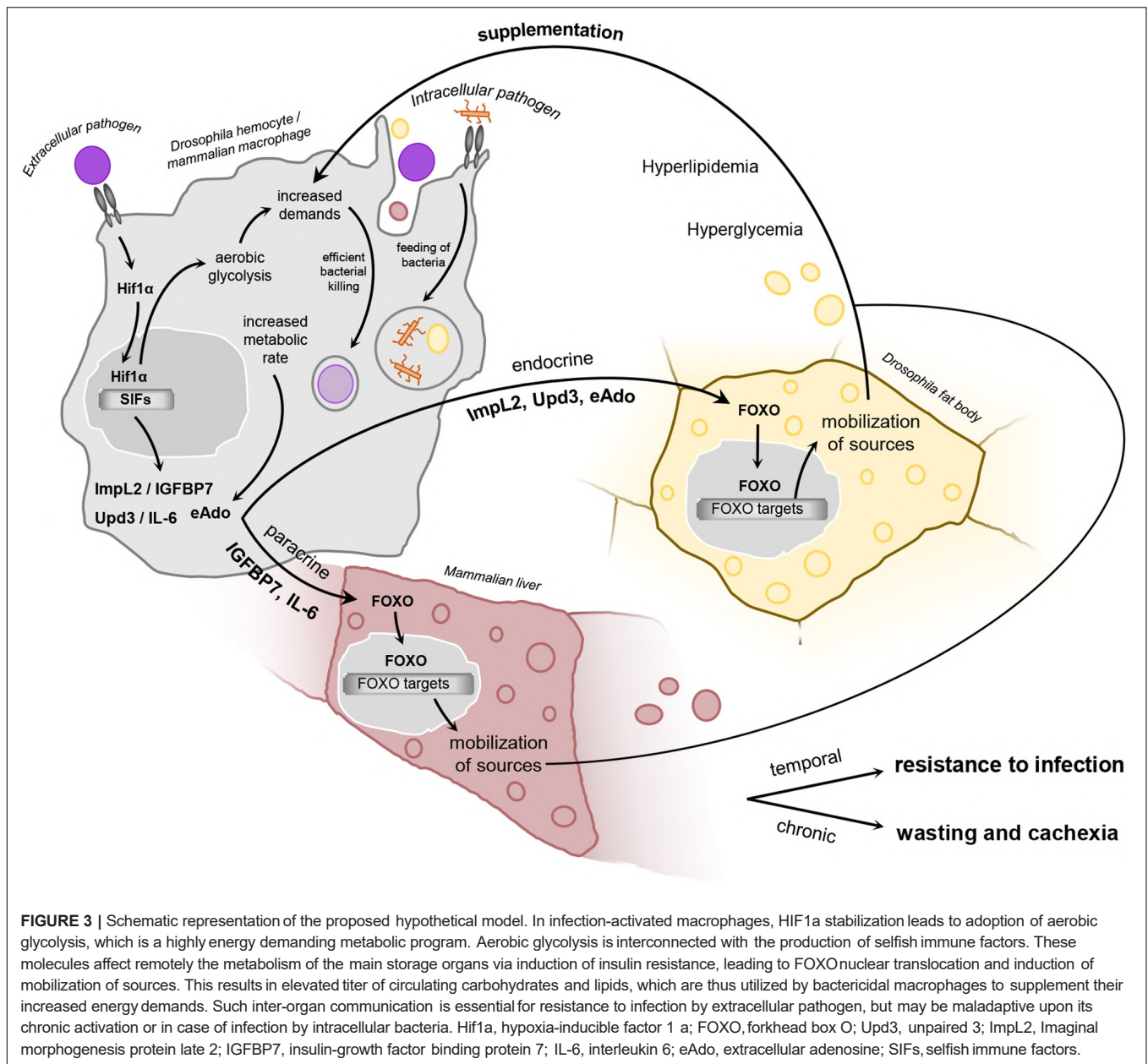


activate toll-like receptor 4 (TLR4), which further enhances a Nuclear Factor kappa B (NF- κ B)-signaling pathway. As an outcome of NF κ B activity, the cytosolic Fe²⁺ ions are sequestered by the major iron-storage protein ferritin. Lack of Fe²⁺ as a crucial cofactor of PHD thus causes HIF1a stabilization and substantial remodeling of overall cellular metabolism (Siegert et al., 2015). It should be noted that TLR4 may also be activated by endogenous ligands such as extracellular matrix components, oxidized lipids, and lipoproteins (Erridge, 2010).

Besides extracellular stimuli, HIF1a stabilization may be achieved by the cytosolic accumulation of several metabolic intermediates originating from the mitochondrial Krebs cycle. It has been documented that lactate, succinate, itaconate, pyruvate, and 2-hydroxyglutarate impair PHD ability to degrade HIF1a (Koivunen et al., 2007; Bailey and Nathan, 2018). This interconnection seems to be adaptive for overcoming hypoxic states since an accumulation of these metabolites in the cytosol is a hallmark of mitochondrial dysfunction (Garedew and Moncada, 2008; Prabakaran, 2015). Even though this mechanism enables cells to reflect their current metabolic state, it makes HIF1a stabilization dependent on elevated flow through metabolic pathways enhanced in aerobic glycolysis. Therefore, cells employing aerobic glycolysis are highly sensitive to the availability of sources. Early experiments using LPS as a classic way to activate macrophages showed that

macrophages functionally depend on sufficient concentrations of glucose, glutamine, and lipids in the culture medium (Newsholme et al., 1986). Further *in vitro* investigation of nutrient uptake and trafficking fully elucidated the complexity of HIF1a-mediated metabolic changes and the utilization of these nutrients by bactericidal macrophages (Stunault et al., 2018).

An immense uptake of glucose is one of the hallmarks of bactericidal macrophages. That may be explained by its utilization as a primary energy resource as well as a substrate for the generation of NADPH and nucleotides in the pentose phosphate pathway (Yamashita et al., 2014). Consistently, *glucose-6-phosphate dehydrogenase*, which catalyzes the first step in pentose phosphate pathway, is known to be triggered by HIF1a (Gao et al., 2004). Interestingly, the glucose energy potential is not fully exploited since pyruvate as the end-product of glycolysis not entering the mitochondria for its full oxidation. Due to HIF1a transcriptional activity, it is instead preferentially converted to lactate by *lactate dehydrogenase* and excluded from the cell through *monocarboxylate transporter 4* (Firth et al., 1995; Kim et al., 2006). Via increased glycolytic flux, cells avoid the time-consuming transport of pyruvate into the mitochondrial lumen that otherwise represents the rate-limiting step of ATP generation (Thomas and Halestrap, 1981). Thanks to that, the glycolytic flux may be increased even a hundred times, thus fully compensating for the lower efficiency of ATP generation.



The acceleration of glycolysis is also under the control of HIF1a, which regulates the expression of rate-limiting glycolytic enzymes *hexokinase II* and *phosphofructokinase-1* (Riddle et al., 2000; Obach et al., 2004). Pyruvate conversion into lactate, together with pentose phosphate pathway, serves as a mechanism generating sufficient amounts of NADPH to be utilized for ROS production as well as self-protection against its detrimental effects (Riganti et al., 2012).

Despite the generation of sufficient amounts of ATP by glycolysis, mitochondrial metabolism is still crucial for activated macrophages (Sancho et al., 2017). Indeed, many Krebs cycle intermediates have been shown to be essential for macrophage bactericidal function. Since HIF1a-elevated expression of *pyruvate dehydrogenase kinase* diverts the pyruvate

from entering the mitochondria, there must be an alternative way for Krebs cycle supplementation. The flow of the Krebs cycle is sustained by using glutamate as an initial precursor for the synthesis of Krebs cycle intermediates. To supplement the Krebs cycle by glutamate, HIF1a increases the expression of glutamine transporters SLC1A5 and SLC38A2 (Chen et al., 2001). Since the Krebs cycle is replenished from a different direction than usual, it produces several intermediates in opposite directions and was therefore referred to as the “broken Krebs cycle” (O’Neill, 2015). Consequently, the concentration of several Krebs cycle intermediates varies substantially in the cytosol. While overproduced itaconate and fumarate are used directly to fight the pathogen extracellularly, citrate is used as a substrate for the synthesis of fatty acids and glutathione (Rouzer et al., 1982).

However, the broken Krebs cycle does not generate enough precursors to fuel the oxidative phosphorylation. The canonical function of oxidative phosphorylation is thus disabled, and cells cannot employ cellular respiration (Ramond et al., 2019). Although bactericidal macrophages generate ATP independently from oxygen, their activity is often associated with a high oxygen consumption rate (OCR) when metabolically analyzed under controlled *in vitro* conditions (Van den Bossche et al., 2015). This can be explained by the massive utilization of oxygen for the generation of reactive oxygen and nitric species (ROS/RNS) later used for bacterial killing in phagolysosomes and oxidative burst (Forman and Torres, 2002). Indeed, an expressional increase in *Nitric oxide synthase* is triggered by the transcriptional activity of HIF1a (Matrone et al., 2004). ROS are produced by the NADPH-oxidase complex as well as the reversed mitochondrial electron transport chain. Production of ROS/RNS thus depends on the utilization of ATP, NADPH, and their effective regeneration (Xu et al., 2016; Scialò et al., 2017).

A considerable amount of ROS must be generated for bacterial killing in phagolysosomes. However, with increasing concentration of ROS, also the risk of lipid peroxidation and subsequent cell death rises. Bactericidal macrophages invest many sources to cascades producing a sufficient amount of neutralizing reductive compounds. Citrate and glutamate are exploited for the generation of glutathione, which protects thus macrophages from self-harming by otherwise bactericidal ROS (Kwon et al., 2019).

Finally, yet importantly, the difference can also be seen in the utilization of lipids if comparing quiescent and bactericidal macrophages. While resting macrophages use a relatively small amount of lipids mainly as a source of energy from fatty acid oxidation, upon infection, HIF1a-induced activity of sterol regulatory element-binding proteins and peroxisome proliferator-activated receptors lead to the accumulation of fatty acids and cholesterol (Shen and Li, 2017; Mylonis et al., 2019). That may be attributed to increased uptake of lipids in the form of lipoproteins as well as a rise in lipid synthesis. Uptake of lipoproteins [via scavenger receptor CD36, very-low-density lipoprotein receptor (VLDL-R) and low-density lipoprotein receptor-related protein 1 (LRP1)] as well as their synthesis increases in a HIF1a-dependent manner (Krishnan et al., 2009; Castellano et al., 2011; Mylonis et al., 2012; Shen et al., 2012; Maier et al., 2017), which further supports the perception of HIF1a as a master-regulator of aerobic glycolysis in bactericidal macrophages. However, the involvement of this regulation upon infection has not been fully comprehended yet. Contrary, the utilization of fatty acids for energy generation via fatty acid oxidation is significantly decreased upon HIF1a stabilization (Remmerie and Scott, 2018). Even though the use of lipids by macrophages upon infection has not been fully elucidated yet, we can presume their deployment for remodeling of the cellular membrane, formation of cholesterol rafts, synthesis of catecholamines, trained immunity, as well as inflammasome activation (Bekkering et al., 2018; Remmerie and Scott, 2018).

As we depicted above, the adjustment of macrophage central metabolic pathways is fundamental for the engulfment of bacteria and its killing. However, this relationship has been omitted for

a long time in insects. Nevertheless, phagocytosis and clearance of invading pathogens is an evolutionarily highly conserved process even on the molecular level and, therefore, plasmatocytes as *Drosophila* professional phagocytes (Figure 2 and Box 3) should have the same requirements for energy and precursors (Stuart and Ezekowitz, 2008; Browne et al., 2013). The position of plasmatocytes in fly's body (Figure 2A), their morphology (Figures 2C–G), as well as their ability to phagocytose bacteria (Figures 2C, E–G and Box 3) and uptake LDLs (Figure 2D) are depicted in Figure 2.

Thus, we can hypothesize that basically, all professional phagocytes performing bactericidal function should undergo the switch toward aerobic glycolysis upon their activation. This notion is supported by observations made by Anderson and his colleagues, who investigated the metabolic demands of cockroach hemocytes during phagocytosis *in vitro*. They revealed that insect hemocytes are functionally dependent on uptake of glucose, glutamine, and lipids from cultivation media (Anderson et al., 1973; Ratcliffe and Rowley, 1975). That may be supported by transcriptomic data characterizing *Drosophila* immune cells with various stimuli. In larvae, both differentiating and proliferating immune cells display hallmarks of increased glycolytic rate and conversion of pyruvate to lactate resembling aerobic glycolysis (Irving et al., 2005; Johansson et al., 2005; Bajgar et al., 2015; Ramond et al., 2020). The versatility of *Drosophila* immune cells and their metabolic response to the activating stimuli may be further documented by the single-cell transcriptomic analysis published recently (Tattikota et al., 2020), which shows the above-mentioned patterns in raw data. According to these data, larval hemocytes display increased expression levels of lipid-scavenging receptors and genes for import and metabolism of lipids in the Krebs cycle. Moreover, a subpopulation of immune cells bearing lamellocyte markers displays metabolic shift toward aerobic glycolysis upon wasp infestation.

It has been proven experimentally that even adult fly plasmatocytes perform the switch to aerobic glycolysis upon streptococcal infection *in vivo* (Krejčová et al., 2019). In analogy to their mammalian counterparts, *Drosophila* plasmatocytes require the activity of HIF1a for induction of aerobic glycolysis and, in response to infection, display substantially increased glucose and lipid uptake (Krejčová et al., 2019, 2020). In concordance with that, the rate of glycolysis, as well as the production of lactate, is increased in these cells. However, the complex metabolic characterization concerning particularly mitochondrial metabolism still remains to be fully explored. In this experimental setup, plasmatocyte function is central for limiting the bacterial burden during the first 24 h post-infection. Decreased efficiency of phagocytosis and bacterial killing leads to the death of the individuals. Interestingly, the cellular metabolic switch is accompanied by an adjustment of the systemic metabolism of flies when both adoption of aerobic glycolysis by plasmatocytes and induction of hyperglycemia and hyperlipidemia are essential for resistance during the acute phase of the infection. Since adoption of aerobic glycolysis by plasmatocytes is epistatic to adjustment of systemic metabolism, we may anticipate the existence of signaling factors

mediating this interorgan crosstalk (Bajgar and Dolezal, 2018; Krejčová et al., 2019, 2020; **Figure 1** and **Box 1**).

In conclusion, the adoption of aerobic glycolysis as a metabolic program fundamental for effective bactericidal function results in increased demands for external sources. Since these sources may be depleted rapidly in the local microenvironment (Kedia-Mehta and Finlay, 2019), we suggest that one of the possible ways how to ensure resource supplementation is the release of immune cell-derived signaling factors to affect systemic metabolism (**Figure 1** and **Box 1**). The character of these signaling factors will be considered in the following paragraphs.

ADOPTION OF AEROBIC GLYCOLYSIS IS CONNECTED WITH THE RELEASE OF SYSTEMIC SIGNALING FACTORS

As described in the previous paragraphs, macrophage activation is connected with enhanced nutritional demands due to the adoption of aerobic glycolysis and a high activity of these cells. Macrophages are expected to release signaling factors to usurp enough sources from other non-immune organs and tissues. Thus, the immune response becomes a privileged physiological process above other processes in the body. However, redistribution of sources may be limiting for concurrent physiological processes based mainly on anabolic metabolism (Ganeshan et al., 2019; Kedia-Mehta and Finlay, 2019). From the perspective of inter-organ signaling, the immune system behaves selfishly in competition for energy sources and releases SIFs that mediate this signaling (**Figure 1** and **Box 1**). Based on the knowledge of insect SIFs, we may propound several hypothetical features to be met by these factors. This approach may help to identify possible novel SIFs in mammals.

Firstly, we expect the SIFs to be released by activated immune cells as a reflection of their nutritional status and adoption of HIF1 α -driven aerobic glycolysis. There are two ways to

translate the information about the increased demands linked to the adoption of aerobic glycolysis into the production of SIFs. SIF production may be a part of the transcriptional program associated with the metabolic switch directed by either HIF1 α or other transcriptional factors involved in immune cell polarization—for example, JNK and NF κ B. Thus, the remodeling of cellular metabolism of these cells and concurrent production of SIFs may be intimately interlinked. Alternatively, certain metabolites, generated as a product of some highly active metabolic pathways in aerobic glycolysis, may serve as potential SIFs as well (**Figure 3**).

Whether or not SIFs are linked to a transcriptional program or to the metabolic status of the cells, they should be released during the early phase of the acute immune response. Although it has been shown that macrophages are endowed with certain nutritional stores, they barely suffice for the initial few hours of their activation (Ma et al., 2020). This fact has been documented by many clinical data as well as experimental studies describing the progress of infection (Imran and Smith, 2007; Scott et al., 2019). Last, but not least, we should consider the potential of SIFs to spread through the body and affect systemic nutrient expenditure.

Assuming that the nutritional requirements of activated immune cells are the primary motivation for SIF release, we can look for a parallel in neoplastic tumors and hypoxic tissues, because they all use HIF1 α -driven aerobic glycolysis (Escoll and Buchrieser, 2018; Miska et al., 2019; **Box 4**). Based on that presumption, we may preselect several cancer-derived cachectic factors that also occur in hypoxia. In the following paragraphs, we will address three immune signaling factors that meet the above criteria and represent the potential SIFs in *Drosophila* [extracellular adenosine (eAdo), insulin/IGF antagonist Imaginal morphogenesis protein late 2 (ImpL2), and cytokine Unpaired3 (Upd3)] (**Figure 3**).

Adenosine is a purine metabolite naturally occurring at low concentrations in all living cells. Nevertheless, its concentration

BOX 4 | Cancer and bactericidal macrophages display a similar cellular metabolic setup.

It is almost 100 years since the discovery that cancer cells preferentially employ glucose fermentation as an oxygen-independent source of ATP even when sufficiently supplied with oxygen (Warburg et al., 1927; Warburg, 1956). This metabolism was thought to be unique for cancer cells and was called the Warburg effect, named after its discoverer. Since the adoption of the Warburg effect yields eighteen times less ATP generated from one molecule of glucose compared to oxidative phosphorylation, the benefits arising from the use of such a metabolic program appeared unlikely. The adoption of the Warburg effect was thus attributed to disturbed mitochondrial function. However, this explanation cannot elucidate the similar observations made in yeasts that often use anaerobic metabolism despite the constant level of oxygen in the culture. This phenomenon is known as the Crabtree effect, which suggests an adaptive significance for such metabolic settings (de Deken, 1966; Diaz-Ruiz et al., 2011). Later research has shown that this mechanism is also utilized by other highly active or dividing cells, such as embryonic stem cells and activated bactericidal macrophages, and the term aerobic glycolysis has been introduced for this metabolic adaptation (Jones and Bianchi, 2015). This motivated scientists to find an explanation for why cells in certain situations prefer to switch to this metabolic regime and what the benefits are.

Using modern metabolomics techniques, it has been found that the lower yield of ATP is compensated by the increased glycolytic rate and that this metabolic setting represents an advantage in the production of essential precursors promoting cell growth, division, and active participation in many biological processes (Burns and Manda, 2017). As a result, these cells are dependent on an increased supply of nutrients. It is now clear that neoplastic cancer cells alter all major cellular metabolic pathways and that there is a high similarity in metabolism between cancer and bactericidal macrophages (Escoll and Buchrieser, 2018). It is generally accepted that neoplastic cancer cells represent a significant energy burden for patients compared to benign tumors of the same size. The malignancy of these tumors depends on the induction of systemic metabolic changes such as insulin resistance and cachexia (Nagao et al., 2019).

Interestingly, the pro-cachectic effect of tumors is interconnected with the adoption of HIF1 α -dependent aerobic glycolysis (Koltai, 2020). It has been outlined that cancer may be perceived as a metabolic syndrome comprising cancer-induced insulin resistance and cachexia as mechanisms to usurp enough nutrition from the host's anabolic processes to support tumor growth and metastatic spreading (Porporato, 2016). In concordance with that, cachexia is thought to cause about 20% of deaths in cancer patients and accompany up to 80% of advanced cancer states (Fonseca et al., 2020). Besides metabolic profile, cancer cells also share with bactericidal macrophages the production of several pro-inflammatory cytokines with impact on systemic metabolism (Liou, 2017). Therefore, research on these factors and their involvement in the induction of insulin resistance and cachexia upon infection should be considered.

may rise substantially as a reflection of increased activation of cellular metabolism (Eitzschig, 2013). Adenosine is formed in the cells as an outcome of the enormous consumption of ATP, the increased number of methylation events, as well as generation of reductive potential (Ham and Evans, 2012; Tehlivets et al., 2013; Sarkar et al., 2020). Accumulation of intracellular adenosine serves as a negative feedback signal on cellular metabolism via AMPK activation leading to quiescence (Aymerich et al., 2006). That is contradictory to the desired tasks of an activated immune system, and immune cells thus must expel excessive adenosine extracellularly (Sag et al., 2008). Since the quantification of intracellular adenosine is technically challenging under natural physiological conditions, its production by immune cells has to be presumed from indirect evidence. Nonetheless, the processes leading to the generation of intracellular adenosine are accelerated in activated macrophages employing aerobic glycolysis (Leonard et al., 1978; Vijayan et al., 2019; Silva et al., 2020). Aside from the intracellular source of adenosine, we should not omit its generation in an extracellular space, where it may be produced by ectonucleotidases bound to the surface of the immune cells (Zanin et al., 2012). Characteristic producers of adenosine in mammals are hypoxic endothelial and smooth muscle cells, activated immune cells, as well as cancerous tissues (Grenz et al., 2011; Silva-Vilches et al., 2018; Boison and Yegutkin, 2019). Recently, it has been shown that intracellular adenosine may be released by cultured human macrophages infected by *Leishmania* (Hsu et al., 2012). It is in concordance with an observation made in *Drosophila*, in which activated immune cells release adenosine via equilibrative nucleoside transporters upon an infestation of larvae by parasitoid wasps (Bajgar et al., 2015). Extracellular production of adenosine has also been described for murine macrophages upon their classic activation by LPS (Zanin et al., 2012). Although local rise in adenosine concentration has rather anti-inflammatory effects in mammals (Haskó and Cronstein, 2013), its systemic spreading may support immune response by mobilizing required energy substrates (Tadaishi et al., 2018). As an outcome of paracrine and systemic adenosine effects, we may observe overall metabolic suppression in the organism inducing thus, e.g., fatigue or hibernation (Davis et al., 2003; Olson et al., 2013). That is analogous to the observation made in infected *Drosophila* where adenosine directs mobilization of carbohydrates from adipose tissue and concurrently limits glucose consumption by other than immune tissues (Bajgar et al., 2015; Bajgar and Dolezal, 2018). Although the release of adenosine has not yet been experimentally linked to the adoption of aerobic glycolysis in activated immune cells, it is well established that many genes involved in adenosine signaling are HIF1a targets (Bowser et al., 2017). Thus, we hypothesize that adenosine production may be directly linked to the adoption of aerobic glycolysis. This is in concordance with the observation of eAdo release from cancer cells, hypoxic tissues, as well as activated immune system (Schrader et al., 1977; Alam et al., 2015; Bajgar and Dolezal, 2018; Arab and Hadjati, 2019).

The second SIF—Impl2—has been identified as a *Drosophila* cancer-derived cachectic factor (Kwon et al., 2015). This putative functional homolog of mammalian *insulin-like growth*

factor-binding protein 7 (IGFBP7) is known to be released from experimentally induced cancer cells in adult flies. Impl2 affects the metabolism of adipose tissue via insulin resistance and induces the mobilization of nutrients subsequently exploited by the tumor for its own growth (Kwon et al., 2015; Figueroa-Claresvega and Bilder, 2015). Impl2 is documented to be released from tumors, which growth was induced either by loss of cell polarity or overexpression of transcription coactivator *Yorkie* (Bunker et al., 2015; Kwon et al., 2015). Importantly, these tumors are known to rely metabolically on aerobic glycolysis (Wang et al., 2016).

A remarkable release of Impl2 was also observed from tissues undergoing experimentally-induced hypoxia and mitohormesis, where its expression reflected the mitochondrial dysfunction (Allee, 2011; Owusu-Ansah et al., 2013). The link between HIF1a and Impl2 production has been revealed by comparing Impl2 transcript abundance in response to hypoxia for wild-type and HIF1a homozygous mutant adult flies. Moreover, experimentally increased HIF1a expression is sufficient for enhanced Impl2 protein levels (Allee, 2011). The role of HIF1a in the regulation of Impl2 production has been suggested for infection-activated plasmacytes (Krejčová et al., 2020). It has been revealed that the rise in Impl2 expression in plasmacytes (**Figure 2E**) is dependent on HIF1a activity in these cells upon infection. Thus, HIF1a directs not only the metabolic switch to aerobic glycolysis but also Impl2 expression. That is further supported by the occurrence of four hypoxia response elements in the regulatory sequence of the Impl2 genomic region. We thus may claim that bactericidal plasmacytes produce Impl2 as a reflection of HIF1a-driven aerobic glycolysis (Krejčová et al., 2020). Interestingly, plasmacytes produce Impl2 not only in response to the recognition of invading pathogens but also in response to their exposure to excessive lipids, as it has been documented for high-fat-diet fed flies (Morgantini et al., 2019). Since Impl2 is known to bind *Drosophila* insulin-like peptides, its effects on systemic metabolism can be accounted to the abrogation of insulin signaling (Honegger et al., 2008).

The last SIF discussed here is a *Drosophila* cytokine Upd3. Based on its structural and functional similarities, it is considered to be a functional homolog of mammalian cytokine IL6 (Oldefest et al., 2013). In analogy to its mammalian counterpart, Upd3 also acts as a ligand for the JAK-STAT signaling pathway. Upd3 production is crucial in the regulation of many physiological processes, ranging from embryogenesis and larval growth and development to stress response, such as in tissue damage, loss of cell polarity, metabolic stress, and bacterial infection (Jiang et al., 2009; Wang et al., 2014; Woodcock et al., 2015). Under such situations, Upd3 production is triggered by the activation of JNK by loss of cell polarity, recognition of bacterial pathogens, or increased accumulation of ROS (Jiang et al., 2009). Immune cells are one of the prominent producers of Upd3 in adult flies. In response to tissue damage, bacterial infection, or exposure to oxidized lipids, Upd3 expression rises in these cells substantially (Agaisse et al., 2003; Woodcock et al., 2015; Chakrabarti et al., 2016; Shin et al., 2020). Systemic Upd3 subsequently triggers JAK-STAT signaling in non-immune tissues and activates a stress response primarily in the gut and the fat body. While in the

gut, Upd3 induces regenerative proliferation and maintenance of integrity, in the fat body, it induces a Foxo-driven transcriptomic program, leading to a mobilization of lipid stores (Chakrabarti et al., 2016; Shin et al., 2020).

Interestingly, Upd3 production is induced under a similar condition to Impl2. Indeed, both are produced from cancer and hypoxic cells as well as from plasmacytes responding to bacterial infection, excessive lipids, or tissue damage (Agaisse et al., 2003; Bunker et al., 2015; Shin et al., 2020). The interconnection of Upd3 production with HIF1a transcriptional activity has been observed for hypoxia-responsive neurons in the central nervous system of *Drosophila* larvae. Upd3 released by these cells has a remote impact on insulin signaling in adipose tissue and, thus, supports the proliferation of immune cell progenitors in lymph glands (Cho et al., 2018).

From the above-mentioned, we may suggest that Upd3 production reflects a situation of cellular metabolic stress. However, the direct link between plasmacyte aerobic glycolysis and Upd3 production has not been satisfactorily studied to date. A systemic effect of Upd3 may be attributed to the activation of a JAK-STAT cascade, which often leads to an alleviation of the insulin signaling pathway in target tissues (Yang et al., 2015; Kierdorf et al., 2020; Shin et al., 2020).

We propose that all three SIFs discussed here are produced by bactericidal immune cells due to their increased metabolic activity and the adoption of HIF1a-driven aerobic glycolysis. It is particularly interesting that the informing of metabolic demands is mediated by multiple factors involving the body's central metabolic organs. However, it seems that their cooperative action ensures the supplementation of the immune system with sources (Figure 3).

IMMUNE CELL-DERIVED FACTORS INDUCE MOBILIZATION AND TARGETED DELIVERY OF NUTRIENTS

The task of SIFs is to ensure sufficient supplementation of their producers with energy resources and nutrients necessary for their function.

The mechanism of resource redistribution consists of two parallel processes, the mobilization of resources from reserves and their subsequent delivery to the activated immune system. The energy suddenly required for protection against pathogen attack is usurped from anabolic processes such as the building of reserves, maintenance, growth, and reproduction. Therefore, SIFs are expected to mobilize the nutrients from central energy-storing organs and concurrently minimize their consumption by other immune response-unrelated tissues.

Since most physiological processes based on anabolism depend on the insulin signaling pathway (Schwartzburd, 2017), we can assume that the transition between insulin sensitivity and resistance may represent such a mechanism. We hypothesize here that Impl2, Upd3, and adenosine represent examples of possible SIFs. Therefore, their impact on systemic metabolism with emphasis on the induction of insulin resistance will be considered in the following paragraphs.

Recently, it has been deciphered that Impl2 is released from infection-activated plasmacytes during acute immune response in *Drosophila* (Krejčová et al., 2020; Figure 3). However, a recently published RNA-Seq analysis of *Drosophila* larval plasmacytes revealed neither an increase in Impl2 transcripts upon septic injury nor enriched expression of Impl2 in plasmacytes (Ramond et al., 2020). That is in concordance with other observations showing that larval Impl2 is expressed in the fat body rather than in circulating immune cells. That suggests a different role of Impl2 in larva and adult immune system since, in adult flies, the subpopulation of plasmacytes clearly displays a strong Impl2 expression level, particularly of Impl2 RA isoform (Krejčová et al., 2020). Interestingly, another single-cell analysis displays a clear subpopulation of larval plasmacytes denoted according to a high level of Impl2 expression as Impl2-positive (Cattenoz et al., 2020).

Krejčová shows that Impl2 subsequently affects the mobilization of carbohydrates and lipoproteins from the fat body, which results in their increased titer in circulation and their subsequent utilization by activated plasmacytes (Figure 3). Several independent approaches document its impact on nutrient mobilization. It was shown that Impl2 induces morphological changes in the fat body of infected individuals. The adipocytes display a significantly reduced amount of lipid stores, which are dispersed in the cytoplasm in an increased number of smaller lipid droplets. It is believed that the reduced diameter of the lipid droplets is advantageous for cells undergoing increased lipolysis since it makes the triglycerides more accessible to lipases located on their surface (Kühnlein, 2012). That is in concordance with the induction of Forkhead Box O (Foxo)-driven transcriptomic program, which triggers the expression of enzymes responsible for lipolysis and assembly and release of lipoproteins (Figure 3). Lipid mobilization in the form of lipoproteins is further supported by the change of relative representation of individual lipid classes in the fat body on behalf of phospholipids. Interestingly, a mere overexpression of Impl2 in plasmacytes is able to mimic the effects of infection in the fat body (Krejčová et al., 2020).

Foxo is known to regulate adipocyte metabolism upon metabolic stress conditions such as starvation, hypoxia, and elicitation of immune response. It has been reported that when starving or eliciting an immune response, Foxo is triggered by immune signaling cascades such as NF- κ B, Toll, and IMD in the fat body (Molaei et al., 2019; Texada et al., 2019). Nevertheless, adipocyte insulin signaling has the power to counteract this nutrient-deliberating mechanism completely (Lee and Dong, 2017). Therefore, it is central for the organism to alleviate insulin signaling in these cells to induce mobilization of stores. Impl2 is a perfect candidate for this role since it is known for its high affinity to *Drosophila* insulin-like peptides as well as experimentally administered human insulin (Honegger et al., 2008). Although the production of Impl2 by plasmacytes appears to be sufficient to induce changes in lipid metabolism of adipose tissue upon infection, another plasmacyte-derived factor, Upd3, surprisingly targets the same signaling pathway in this organ (Krejčová et al., 2020; Shin et al., 2020).

There is a striking similarity between the effects accounted for ImpL2 and Upd3. Contrary to ImpL2, Upd3 affects the FOXO nuclear translocation via activation of the JAK/STAT signaling pathway in the fat body and induces insulin resistance in adipocytes downstream of insulin receptor (Shin et al., 2020). That may be accomplished via affecting the phosphorylation status of effector kinase AKT. Interestingly, also Upd3 itself can induce mobilization of lipid stores into the circulation (Woodcock et al., 2015). Redundancy of ImpL2 and Upd3 effects suggests that it is adaptive to inhibit insulin signaling in adipose tissue by multiple SIFs to secure mobilization of sources upon infection. Also eAdo affects adipose tissue metabolism in response to infection in *Drosophila*. While the effects of ImpL2 and Upd3 are manifested mainly by the mobilization of lipid stores, eAdo affects the level of expression of glycogen metabolizing enzymes through its receptor. eAdo induces hyperglycemia upon infection via depletion of adipose tissue glycogen stores (Bajgar and Dolezal, 2018). However, its effect on lipid metabolism has not been sufficiently investigated yet.

We may conclude that immune cell-derived SIFs induce adipocyte insulin resistance leading to mobilization of sources from adipose tissue and their utilization by activated immune cells (Figure 3).

Besides mobilization of sources, SIFs also often silence the nutrient consumption of tissues that are not involved in the immune response. Interestingly, all the SIFs discussed here are known to silence anabolic processes in these tissues in certain situations. Production of one factor by macrophages thus regulates concurrently both mobilization of sources and suppression of physiological processes competing with the immune response for resources.

The effect of ImpL2 on anabolic processes has been observed during the fly's development and upon experimental induction of cancer. An increased titer of circulating ImpL2 alleviated insulin signaling and thus decreased metabolic muscle rate and caused fragmentation of muscle mitochondria (Figueroa-Claevega and Bilder, 2015; Kwon et al., 2015; Lee et al., 2018). In addition, these individuals displayed disrupted ovary maturation and mobilization of sources leading to wasting-induced cachexia (Figueroa-Claevega and Bilder, 2015; Kwon et al., 2015). We can hypothesize that plasmacyte-derived ImpL2 may have similar effects upon infection, although not with as significant phenotypes as in cancer because upregulation of the ImpL2 gene in these experimental systems resulted in concentrations far beyond those occurring naturally.

Also, the effects of Upd3 on muscle metabolism have been investigated. Plasmacyte-derived Upd3 has been shown to limit remote lipid accumulation in muscles to maintain lipid homeostasis in the tissue via alleviation of insulin signaling in these cells through activation of the JAK-STAT signaling pathway, which is documented by decreased pAKT occurrence (Kierdorf et al., 2020). We suggest that such a mechanism may also be involved in the regulation of muscle lipid uptake upon infection, during which Upd3 expression in plasmacytes is markedly elevated (Péan et al., 2017). A similar mechanism may be observed in larvae infested by wasp parasitoids, in which Upd3-induced JAK-STAT signaling in muscles is essential for

an effective immune response (Yang et al., 2015). This may indicate that muscle insulin resistance is essential to effectively combat wasp parasitic infestation. However, in their follow-up study, Yang and Hultmark (2017) showed that insulin signaling in muscles, in contrast to fat body and plasmacytes, is essential for the effective encapsulation of invaders. Muscle-specific knockdown of insulin receptor resulted in reduced resistance to infection and encapsulation rate. However, these effects can be explained by developmental defects caused by changes in feeding behavior and subsequent malnutrition, as this experimental treatment was induced throughout the life of individuals. Nonetheless, this publication nicely depicts the impact of experimentally induced muscle insulin resistance on systemic carbohydrate metabolism.

The impact of eAdo on decreased energy consumption by non-immune tissues has also been described in *Drosophila* larva upon wasp infestation. eAdo released by activated immune cells silences consumption of C¹⁴-labeled glucose by virtually all non-immune tissues, leading to decreased growth of imaginal wing discs and delayed metamorphosis. Consequently, this mechanism allows the glucose uptake by immune cells to be increased up to threefold. These effects were mediated by eAdo activation of the adenosine receptors in target tissues (Bajgar et al., 2015).

Based on the aforementioned data, we may say that the effects of macrophage-derived SIFs are dual. They induce nutrient mobilization from central storage organs and concurrently limit their consumption by non-immune tissues and physiological processes. While these effects are essential for the acute-phase response to infection, they may cause nutrient waste and cachexia if activated chronically (Figure 3).

IMMUNE CELL-MEDIATED METABOLIC CHANGES ARE NOT ALWAYS BENEFICIAL UPON INFECTION

Immune cell-derived SIFs increase the titer of circulating carbohydrates and lipids, which are then available to be exploited by the immune system. Subsequently, these nutrients are utilized by activate phagocytes to feed the suddenly increased energy and nutritional demands. Thus, we may presume that this signaling is important for resistance to infection.

Indeed, experimental knockdown of ImpL2 and Upd3 in infection-activated plasmacytes or systemic abrogation of adenosine signaling pathway leads to the reduced ability of plasmacytes to fight the pathogens. That manifests in decreased resistance to bacterial infection accompanied by elevated pathogen load in these individuals (Agaïsse et al., 2003; Bajgar and Dolezal, 2018; Krejčová et al., 2020). Further studies suggested that such a decrease in resistance to infection is due to reduced availability of nutrients for immune cells. Notably, a mere twofold increase in glucose concentration in fly diet is sufficient to rescue phenotypes caused by a lack of eAdo signaling (Bajgar et al., 2015).

Although SIF signaling is essential for an adequate immune response to acute bacterial infection, it may become maladaptive under certain conditions. Since SIFs mobilize sources primarily

for the needs of phagocytes, they may be exploited by the bacteria growing intracellularly. It is well documented that many intracellular pathogens affect the metabolic profile of macrophages to be literally nourished by the host cell (Teng et al., 2017). Indeed, it has been described for each of the SIFs discussed here that their effects have become maladaptive upon infection with intracellular pathogens such as *Listeria monocytogenes* or *Mycobacterium tuberculosis* (Péan et al., 2017; Bajgar and Dolezal, 2018; Krejčová et al., 2020).

Not only the type of bacterial threat but also the duration of SIF action seems to be central. Prolonged SIF production leads to uncontrolled wasting of nutrients, cachexia, and irreversible damage of tissues silenced by insulin resistance. Indeed, for instance, the production of eAdo by plasmacytes has to be time-restricted by eAdo degrading enzyme Adenosine deaminase-related growth factor A (Adgf-A). Interestingly, this enzyme is produced by plasmacytes as well, with an 8 h delay after adenosine. Lack of adgf-A function leads to wasting of glycogen stores and slow-down of development (Bajgar and Dolezal, 2018).

Also, the ImpL2 production by plasmacytes must be time-restricted. Chronically increased ImpL2 production by plasmacytes leads to developmental malformations, reduced body size of the individual, and excessive melanization of immune cells (Krejčová et al., 2020). Moreover, the overproduction of ImpL2 causes insulin resistance and cachexia in the *Drosophila* cancer model (Figueroa-Claevega and Bilder, 2015; Kwon et al., 2015).

Although eAdo, ImpL2, and Upd3 meet the criteria of a selfish immune factor released by the *Drosophila* plasmacytes, analogous signaling in mammals remains controversial. However, all of these factors have their signaling counterparts in mammals. While the Upd3 functional homolog has been identified as IL6, studied mostly for its signaling and metabolic effects in immune response, the ImpL2 mammalian putative functional homolog IGFBP7, known for its ability to attenuate insulin signaling, has not yet been explored in the context of infection. Therefore, we speculate about the evolutionary conservation of the role of these SIFs in the following paragraphs.

THE FUNCTION OF IMMUNE CELL-DERIVED SIFs MAY BE CONSERVED BETWEEN INSECTS AND MAMMALS

Experimental studies performed on insects demonstrate that plasmacytes release signaling factors to affect systemic metabolism and thus ensure a sufficient supply of resources. Here, we would like to consider the possibility that such a mechanism is also valid for mammals (Figure 3). The connection between aerobic glycolysis in activated phagocytic immune cells and the adjustment of systemic metabolism has been considered for mammals in recent review based mainly on clinical data of chronically ill patients (van Niekerk et al., 2017). Moreover, it

may represent the essence of many human diseases, as will be discussed later.

A plethora of cytokines and chemokines are released from activated immune cells upon the adoption of a bactericidal polarization state. These are generally known as “pro-inflammatory cytokines” due to their potential to guide other myeloid cells toward inflammatory polarization. Here, we suggest their role in the regulation of systemic metabolism via the induction of insulin resistance upon bacterial infection.

From several experimental and clinical studies, it is clear that macrophage production of pro-inflammatory cytokines is associated with HIF1a transcriptional activity and subsequent metabolic rearrangement toward aerobic glycolysis (Palazon et al., 2014; Corcoran and O'Neill, 2016). However, it is difficult to distinguish whether their production reflects either cellular metabolic switch or adopted pro-inflammatory state since both are intimately interconnected (Diskin and Pálsson-McDermott, 2018). To solve this problem, we must focus on the production of cytokines by cells utilizing HIF1a-mediated aerobic glycolysis in non-inflammatory context, such as neoplastic tumors and hypoxic tissues (He et al., 2014; Edwardson et al., 2017).

There is a compelling list of publications describing the release of pro-inflammatory cytokines from cancer and hypoxic tissues (Dinarello, 2006; Peyssonnaud et al., 2007; Popa et al., 2007; Heikkilä et al., 2008; Xing and Lu, 2016; Lewis and Elks, 2019; Kammerer et al., 2020). Recently, a transcriptomic meta-analysis of human cancers varying in degree of their pro-cachectic potential has been performed to identify new cachectic factors (Freire et al., 2020). Many of the identified factors were cytokines and chemokines well-known for their participation in the acute immune response. That is in concordance with other studies documenting the pro-cachectic features of Il1b, TNF α , and Il6 (Zhang et al., 2007; Narsale and Carson, 2014; Patel and Patel, 2017).

Consistent with this hypothesis, hypoxic tissues also release a number of cytokines with pro-cachectic properties. Surprisingly, the elicitation of hypoxic response employs several immune-related signaling pathways such as JNK, NF- κ B, and Hif1a (Jin et al., 2000; D'Ignazio and Rocha, 2016). Their activation leads to the adjustment of cellular metabolism to overcome periods of mitochondrial dysfunction. Although pro-inflammatory cytokines were originally investigated in the context of LSP-induced sepsis (Pizarro and Cominelli, 2007; Rossol et al., 2011), they also reflect the metabolic status and nutritional requirements of their producers and thus serve as potential regulators of systemic metabolism.

According to the proposed theory, the central mechanism that changes the systemic metabolism from anabolism to catabolism is the induction of insulin resistance. In adipose tissue, the lack of insulin signaling serves as a signal for potentiation of lipolysis and subsequent fatty acid mobilization (Langin, 2013). Therefore, infection-induced lipodystrophy results in a substantial release of lipid stores during the acute phase of the immune response. Deliberated fatty acids are further metabolized in the liver and enwrapped into lipoproteins as a lipid form suitable for transport to distant tissues on the periphery (Perry et al., 2014). The liver is

known to respond differently to a lack of insulin signaling from most tissues in the body, which is called the “liver insulin resistance paradox” (Santolero and Titchenell, 2019). Indeed, contrary to other tissues silenced by a lack of insulin signal, hepatic insulin resistance accelerates lipid synthesis, gluconeogenesis, and absorption of circulating amino acids (Biddinger et al., 2008). All of these metabolic changes lead to increased mobilization of lipoproteins and glucose into circulation, resulting in the development of hyperglycemia and hyperlipidemia (Lewis et al., 2002). It is known that stress-related hyperglycemia, as a result of insulin resistance in critically ill and septic patients, is beneficial under certain conditions. In the acute phase of stress response, hyperglycemia appears to support metabolically stressed tissues and immune cell function, whereas in context of its chronic activation, it may result in development of glucotoxicity, exaggerated glycosylation, and chronic inflammation. The function of mammalian immune cells is affected by insulin signaling with different context-dependent effects (Van den Berghe, 2002; Marik and Bellomo, 2013; van Niekerk et al., 2017).

An opposite effect of insulin resistance can be observed in muscles, where a lack of insulin signal leads to a significant reduction of its metabolic rate and induction of autophagy (Lim et al., 2014; Ryter et al., 2014). Autophagy covers basal nutritional demands of silenced cells and concurrently generates amino acids utilized for gluconeogenesis in hepatocytes (Cui et al., 2019). In line with the energy-saving program, insulin resistance in the brain also significantly reduces its energy consumption, leading to a lower intellectual capacity, bad moods, and depressions (Kullmann et al., 2020). Nevertheless, metabolic adaptation to metabolic stress is a tremendously complex process in mammals, which is affected by many hormonal and signaling cues. Particularly effect of several stress-related hormones, such as cortisol, noradrenaline, or norepinephrine on the mobilization of nutrients from adipose tissue and the liver is well established. In this context, the role of immune cell-derived factors on these signaling pathways should also be considered.

Besides the systemic impact on insulin resistance, we should also take into account the paracrine effects of cytokines in the liver. The liver is the central metabolic organ that coordinates the systemic metabolic changes upon infection (Bernal, 2016). In addition, the liver hosts a specialized population of tissue-resident macrophages known as Kupffer cells (KC). KCs serve as sentinel cells reflecting changes in the titers of metabolites and endotoxins in the blood. Although KCs tolerate some levels of endotoxins being permanently present in the circulation without eliciting an immune response, their increase above a certain limit leads to KC activation (Zeng et al., 2016). KCs recognize endotoxins via TLR4, which in turn leads to the activation of NF- κ B and its classical M1 polarization (Gandhi, 2020). This process is accompanied by the stabilization of HIF1 α and the adoption of aerobic glycolysis (Roth and Cople, 2015). Subsequently, KCs release the pro-inflammatory cytokines IL1 β , TNF α , and IL6 into the extracellular space. Consequently, these signaling factors induce hepatocyte insulin resistance via their paracrine signaling (Bartolomé et al., 2008). The lack of insulin signaling in hepatocytes leads to a nuclear translocation of

the transcription factor FOXO and the subsequent induction of its specific transcriptomic program. FOXO increases the expression of genes involved in lipogenesis and glycogenolysis, as well as the production and release of lipoproteins (Puigserver et al., 2003). This mechanism is strikingly reminiscent of the process observed in insect adipose tissue. Although the role of KC-derived IL1 β , IL6, and TNF α in inducing hepatocyte insulin resistance has been reliably demonstrated, their mere administration cannot fully mimic the effects of KCs (Bartolomé et al., 2008). This suggests the involvement of additional KC-derived signaling factors. IGFBP7, a mammalian putative functional homolog of *Drosophila* ImpL2, may be a potential candidate (Figure 3).

It has been shown that IGFBP7 expression increases fourfold in the culture of human THP-1 macrophages in response to their exposure to *Streptococcus pneumoniae* (Krejčová et al., 2020). In addition, IGFBP7 expression increases sixfold in response to the exposure of KCs to excessive lipids in obese mice. Subsequently, IGFBP7 induces hepatocyte insulin resistance, hyperlipidemia, and hyperglycemia prior to the production of KC-derived pro-inflammatory cytokines (Morgantini et al., 2019). Although the experimental data connecting the adoption of aerobic glycolysis by KCs to the production of IGFBP7 are missing, we suggest that this mechanism may be relevant for the mobilization of nutrients for immune cells, upon infection. The role of IGFBP7 and IL6 in the induction of insulin resistance and cachexia is further supported by their increased plasma titer in patients suffering from diseases often accompanied by cachexia, such as morbid obesity, cancer, chronic obstructive pulmonary disease, acute kidney diseases, and liver fibrosis (Liu et al., 2015; Gunnerson et al., 2016; Ruan et al., 2017; Martínez-Castillo et al., 2020). Although nowadays IGFBP7 is associated with diseases accompanied by chronic inflammatory and pathological conditions, we suggest that its beneficial role in nutrient mobilization during an acute immune response should also be considered (Figure 3).

SUMMARY

This review brings the new perspective that systemic insulin resistance represents an essential mechanism for overcoming the acute phase of bacterial infection. Insulin resistance is induced by immune cell-derived cytokines, which are produced as a reflection of their elevated metabolic demands resulting from the adoption of aerobic glycolysis. These cytokines induce both the mobilization of sources from the storage organs and their suppressed consumption by non-immune tissues. Titers of nutrients thus elevate in circulation to be utilized by the activated immune system. While such metabolic adaptation is fundamental for resistance to extracellular pathogens, it may become maladaptive upon infection by intracellular bacteria exploiting phagocyte cellular stores for its own benefits. Although cytokine-induced insulin resistance is beneficial during acute phase response, its chronic activation may progress into the wasting of nutrients and cachexia (Figure 3), which are severe metabolic disorders accompanying several serious diseases. Understanding

the adaptive significance of cytokine-induced insulin resistance may therefore provide new insights into these maladies.

Induction of insulin resistance in hepatocytes is central for the progress of obesity and obesity-associated diseases, such as non-alcoholic steatohepatitis, atherosclerosis, and diabetes. According to the presented hypothesis, liver and systemic insulin resistance are induced by chronically adopted aerobic glycolysis in activated liver macrophages. Reversal of macrophage metabolic switch may thus represent a powerful therapeutic strategy.

AUTHOR CONTRIBUTIONS

AB, GK, and TD discussed the topic, conceptualized, wrote, and revised the manuscript. GK created the figures. AB and GK captured the microscopy images. All authors contributed to the article and approved the submitted version.

REFERENCES

- Agaisse, H., Petersen, U.-M., Boutros, M., Mathey-Prevot, B., and Perrimon, N. (2003). Signaling role of hemocytes in *Drosophila* JAK/STAT-dependent response to septic injury. *Dev. Cell* 5, 441–450. doi: 10.1016/S1534-5807(03)00244-2
- Alam, M., Costales, M., Cavanaugh, C., and Williams, K. (2015). Extracellular adenosine generation in the regulation of pro-inflammatory responses and pathogen colonization. *Biomolecules* 5, 775–792. doi: 10.3390/biom5020775
- Allee, J. P. (2011). *ImpL2 Represses Insulin Signaling in Response to Hypoxia*, Thesis, University of Oregon, Eugene, OR.
- Almajwal, A., Alam, I., Zeb, F., and Fatima, S. (2019). Energy metabolism and allocation in selfish immune system and brain: a beneficial role of insulin resistance in aging. *Food Nutr. Sci.* 10, 64–80. doi: 10.4236/fns.2019.10.1006
- Álvarez-Rendón, J. P., Salceda, R., and Riesgo-Escovar, J. R. (2018). *Drosophila melanogaster* as a model for diabetes type 2 progression. *Biomed Res. Int.* 2018, 1–16. doi: 10.1155/2018/1417528
- Anderson, R. S., Holmes, B., and Good, R. A. (1973). Comparative biochemistry of phagocytizing insect hemocytes. *Comp. Biochem. Physiol. Part B Comp. Biochem.* 46, 595–602. doi: 10.1016/0305-0491(73)90099-0
- Arab, S., and Hadjati, J. (2019). Adenosine blockage in tumor microenvironment and improvement of cancer immunotherapy. *Immune Netw.* 19:e23. doi: 10.4110/in.2019.19.e23
- Aymerich, I., Foufelle, F., Ferré, P., Casado, F. J., and Pastor-Anglada, M. (2006). Extracellular adenosine activates AMP-dependent protein kinase (AMPK). *J. Cell Sci.* 119, 1612–1621. doi: 10.1242/jcs.02865
- Bailey, P., and Nathan, J. (2018). Metabolic regulation of hypoxia-inducible transcription factors: the role of small molecule metabolites and iron. *Biomedicines* 6:60. doi: 10.3390/biomedicines6020060
- Bajgar, A., and Dolezal, T. (2018). Extracellular adenosine modulates host-pathogen interactions through regulation of systemic metabolism during immune response in *Drosophila*. *PLoS Pathog.* 14:e1007022. doi: 10.1371/journal.ppat.1007022
- Bajgar, A., Kucerova, K., Jonatova, L., Tomcala, A., Schneederferova, I., Okrouhlik, J., et al. (2015). Extracellular adenosine mediates a systemic metabolic switch during immune response. *PLoS Biol.* 13:e1002135. doi: 10.1371/journal.pbio.1002135
- Banerjee, U., Girard, J. R., Goins, L. M., and Spratford, C. M. (2019). *Drosophila* as a genetic model for hematopoiesis. *Genetics* 211, 367–417. doi: 10.1534/genetics.118.300223
- Bartolomé, N., Arteta, B., Martínez, M. J., Chico, Y., and Ochoa, B. (2008). Kupffer cell products and interleukin 1 β directly promote VLDL secretion and apoB mRNA up-regulation in rodent hepatocytes. *Innate Immun.* 14, 255–266. doi: 10.1177/1753425908094718

FUNDING

The authors confirm funding from the Grant Agency of the Czech Republic AB (Project 20-14030S; www.gacr.cz) and TD (Project 20-09103S; www.gacr.cz).

ACKNOWLEDGMENTS

We would like to thank Lucie Hrádková, Pavla Nedbalová, Marcela Jungwirthová, and other members of our laboratory for stimulating discussions and eternal support for our work. We thank Hanka Sehadová and Lucie Pauchová for introducing us to the fascinating world of electron microscopy. We appreciate Rebecca Collier for her enthusiasm and positive mood, which helped us overcome difficult moments in the preparation of the manuscript.

- Bekkering, S., Arts, R. J. W., Novakovic, B., Kourtzelis, I., van der Heijden, C. D. C. C., Li, Y., et al. (2018). Metabolic induction of trained immunity through the mevalonate pathway. *Cell* 172, 135–146. doi: 10.1016/j.cell.2017.11.025
- Bellucci, P. N., González Bagnes, M. F., Di Girolamo, G., and González, C. D. (2017). Potential effects of nonsteroidal anti-inflammatory drugs in the prevention and treatment of type 2 diabetes mellitus. *J. Pharm. Pract.* 30, 549–556. doi: 10.1177/0897190016649551
- Benoit, M., Desnues, B., and Mege, J.-L. (2008). Macrophage polarization in bacterial infections. *J. Immunol.* 181, 3733–3739. doi: 10.4049/jimmunol.181.6.3733
- Bernal, W. (2016). The liver in systemic disease: sepsis and critical illness. *Clin. Liver Dis.* 7, 88–91. doi: 10.1002/cld.543
- Biddinger, S. B., Hernandez-Ono, A., Rask-Madsen, C., Haas, J. T., Alemán, J. O., Suzuki, R., et al. (2008). Hepatic insulin resistance is sufficient to produce dyslipidemia and susceptibility to atherosclerosis. *Cell Metab.* 7, 125–134. doi: 10.1016/j.cmet.2007.11.013
- Bobryshev, Y. V., Ivanova, E. A., Chistiakov, D. A., Nikiforov, N. G., and Orekhov, A. N. (2016). Macrophages and their role in atherosclerosis: pathophysiology and transcriptome analysis. *Biomed Res. Int.* 2016, 1–13. doi: 10.1155/2016/9582430
- Boison, D., and Yegutkin, G. G. (2019). Adenosine metabolism: emerging concepts for cancer therapy. *Cancer Cell* 36, 582–596. doi: 10.1016/j.ccell.2019.10.007
- Bowser, J. L., Lee, J. W., Yuan, X., and Eltzschig, H. K. (2017). The hypoxia-adenosine link during inflammation. *J. Appl. Physiol.* 123, 1303–1320. doi: 10.1152/jappphysiol.00101.2017
- Browne, N., Heelan, M., and Kavanagh, K. (2013). An analysis of the structural and functional similarities of insect hemocytes and mammalian phagocytes. *Virulence* 4, 597–603. doi: 10.4161/viru.25906
- Bunker, B. D., Nellimootil, T. T., Boileau, R. M., Classen, A. K., and Bilder, D. (2015). The transcriptional response to tumorigenic polarity loss in *Drosophila*. *eLife* 4:e03189. doi: 10.7554/eLife.03189
- Burns, J., and Manda, G. (2017). Metabolic pathways of the warburg effect in health and disease: perspectives of choice, chain or chance. *Int. J. Mol. Sci.* 18:2755. doi: 10.3390/ijms18122755
- Castellano, J., Aledo, R., Sendra, J., Costales, P., Juan-Babot, O., Badimon, L., et al. (2011). Hypoxia stimulates low-density lipoprotein receptor-related protein-1 expression through hypoxia-inducible factor-1 α in human vascular smooth muscle cells. *Arterioscler. Thromb. Vasc. Biol.* 31, 1411–1420. doi: 10.1161/ATVBAHA.111.225490
- Castoldi, A., Naffah de Souza, C., Câmara, N. O. S., and Moraes-Vieira, P. M. (2016). The macrophage switch in obesity development. *Front. Immunol.* 6:637. doi: 10.3389/fimmu.2015.00637
- Cattenoz, P. B., Sakr, R., Pavlidaki, A., Delaporte, C., Riba, A., Molina, N., et al. (2020). Temporal specificity and heterogeneity of *Drosophila* immune cells. *EMBO J.* 39:e104486. doi: 10.15252/embj.2020104486

- Chakrabarti, S., Dudzic, J. P., Li, X., Collas, E. J., Boquete, J.-P., and Lemaître, B. (2016). Remote control of intestinal stem cell activity by haemocytes in *Drosophila*. *PLoS Genet.* 12:e1006089. doi: 10.1371/journal.pgen.1006089
- Chen, C., Pore, N., Behrooz, A., Ismail-Beigi, F., and Maity, A. (2001). Regulation of glut1 mRNA by Hypoxia-inducible Factor-1. *J. Biol. Chem.* 276, 9519–9525. doi: 10.1074/jbc.M010144200
- Cheng, L., Baonza, A., and Grifoni, D. (2018). *Drosophila* models of human disease. *Biomed. Res. Int.* 2018:7214974. doi: 10.1155/2018/7214974
- Cho, B., Sprattford, C. M., Yoon, S., Cha, N., Banerjee, U., and Shim, J. (2018). Systemic control of immune cell development by integrated carbon dioxide and hypoxia chemosensation in *Drosophila*. *Nat. Commun.* 9:2679. doi: 10.1038/s41467-018-04990-3
- Cho, Y.-R., Ann, S. H., Won, K.-B., Park, G.-M., Kim, Y.-G., Yang, D. H., et al. (2019). Association between insulin resistance, hyperglycemia, and coronary artery disease according to the presence of diabetes. *Sci. Rep.* 9:6129. doi: 10.1038/s41598-019-42700-1
- Corcoran, S. E., and O'Neill, L. A. J. (2016). HIF1a and metabolic reprogramming in inflammation. *J. Clin. Invest.* 126, 3699–3707. doi: 10.1172/JCI84431
- Cui, P., Shao, W., Huang, C., Wu, C.-J., Jiang, B., and Lin, D. (2019). Metabolic derangements of skeletal muscle from a murine model of glioma cachexia. *Skelet. Muscle* 9:3. doi: 10.1186/s13395-018-0188-4
- Davis, J. M., Zhao, Z., Stock, H. S., Mehl, K. A., Buggy, J., and Hand, G. A. (2003). Central nervous system effects of caffeine and adenosine on fatigue. *Am. J. Physiol. Integr. Comp. Physiol.* 284, R399–R404. doi: 10.1152/ajpregu.00386.2002
- de Deken, R. H. (1966). The Crabtree effect: a regulatory system in yeast. *J. Gen. Microbiol.* 44, 149–156. doi: 10.1099/00221287-44-2-149
- DeGregorio, E. (2002). The Toll and Imd pathways are the major regulators of the immune response in *Drosophila*. *EMBO J.* 21, 2568–2579. doi: 10.1093/emboj/21.11.2568
- de Luca, C., and Olefsky, J. M. (2008). Inflammation and insulin resistance. *FEBS Lett.* 582, 97–105. doi: 10.1016/j.febslet.2007.11.057
- Del Fabbro, E., Hui, D., Dalal, S., Dev, R., Nooruddin, Z. I., and Bruera, E. (2011). Clinical outcomes and contributors to weight loss in a cancer Cachexia clinic. *J. Palliat. Med.* 14, 1004–1008. doi: 10.1089/jpm.2011.0098
- Demas, G. E. (2004). The energetics of immunity: a neuroendocrine link between energy balance and immune function. *Horm. Behav.* 45, 173–180. doi: 10.1016/j.jyhbeh.2003.11.002
- Dengler, V. L., Galbraith, M. D., and Espinosa, J. M. (2014). Transcriptional regulation by hypoxia inducible factors. *Crit. Rev. Biochem. Mol. Biol.* 49, 1–15. doi: 10.3109/10409238.2013.838205
- Diaz-Ruiz, R., Rigoulet, M., and Devin, A. (2011). The Warburg and Crabtree effects: on the origin of cancer cell energy metabolism and of yeast glucose repression. *Biochim. Biophys. Acta – Bioenerg.* 1807, 568–576. doi: 10.1016/j.bbabi.2010.08.010
- D'Ignazio, L., and Rocha, S. (2016). Hypoxia induced NF- κ B. *Cells* 5:10. doi: 10.3390/cells5010010
- Dinarello, C. A. (2006). The paradox of pro-inflammatory cytokines in cancer. *Cancer Metast. Rev.* 25, 307–313. doi: 10.1007/s10555-006-9000-8
- Diskin, C., and Pålsson-McDermott, E. M. (2018). Metabolic modulation in macrophage effector function. *Front. Immunol.* 9:270. doi: 10.3389/fimmu.2018.00270
- Dodson, M., Castro-Portuguez, R., and Zhang, D. D. (2019). NRF2 plays a critical role in mitigating lipid peroxidation and ferroptosis. *Redox Biol.* 23, 101107. doi: 10.1016/j.redox.2019.101107
- Dolezal, T. (2015). Adenosine: a selfish-immunity signal? *Oncotarget* 6, 32307–32308. doi: 10.18632/oncotarget.4685
- Dolezal, T., Krejčová, G., Bajgar, A., Nedbalová, P., and Strasser, P. (2019). Molecular regulation of metabolism during immune response in insects. *Insect Biochem. Mol. Biol.* 109, 31–42. doi: 10.1016/j.ibmb.2019.04.005
- Duffy, J. B. (2002). GAL4 system in *Drosophila*: a fly geneticist's swiss army knife. *Genesis* 34, 1–15. doi: 10.1002/gene.10150
- Edholm, E.-S., Rhoo, K. H., and Robert, J. (2017). "Evolutionary aspects of macrophages polarization," in *Macrophages. Results and Problems in Cell Differentiation*, Vol. 62, ed. M. Kloc (Cham: Springer), 3–22. doi: 10.1007/978-3-319-54090-0_1
- Edwardson, D. W., Boudreau, J., Mapletoft, J., Lanner, C., Kovala, A. T., and Parissenti, A. M. (2017). Inflammatory cytokine production in tumor cells upon chemotherapy drug exposure or upon selection for drug resistance. *PLoS One* 12:e0183662. doi: 10.1371/journal.pone.0183662
- Eltzschig, H. K. (2013). Extracellular adenosine signaling in molecular medicine. *J. Mol. Med.* 91, 141–146. doi: 10.1007/s00109-013-0999-z
- Erridge, C. (2010). Endogenous ligands of TLR2 and TLR4: agonists or assistants? *J. Leukoc. Biol.* 87, 989–999. doi: 10.1189/jlb.1209775
- Escoll, P., and Buchrieser, C. (2018). Metabolic reprogramming of host cells upon bacterial infection: why shift to a Warburg-like metabolism? *FEBS J.* 285, 2146–2160. doi: 10.1111/febs.14446
- Felig, P., Marliss, E., and Cahill, G. F. (1969). Plasma amino acid levels and insulin secretion in obesity. *N. Engl. J. Med.* 281, 811–816. doi: 10.1056/NEJM196910092811503
- Ferrandon, D., Immler, J.-L., Hetru, C., and Hoffmann, J. A. (2007). The *Drosophila* systemic immune response: sensing and signalling during bacterial and fungal infections. *Nat. Rev. Immunol.* 7, 862–874. doi: 10.1038/nri2194
- Figueroa-Clarevega, A., and Bilder, D. (2015). Malignant *Drosophila* tumors interrupt insulin signaling to induce Cachexia-like wasting. *Dev. Cell* 33, 47–55. doi: 10.1016/j.devcel.2015.03.001
- Firth, J. D., Ebert, B. L., and Ratcliffe, P. J. (1995). Hypoxic regulation of lactate Dehydrogenase A. *J. Biol. Chem.* 270, 21021–21027. doi: 10.1074/jbc.270.36.21021
- Fonseca, G. W. P., da Farkas, J., Dora, E., von Haehling, S., and Lainscak, M. (2020). Cancer cachexia and related metabolic dysfunction. *Int. J. Mol. Sci.* 21:2321. doi: 10.3390/ijms21072321
- Forman, H. J., and Torres, M. (2002). Reactive oxygen species and cell signaling. *Am. J. Respir. Crit. Care Med.* 166, S4–S8. doi: 10.1164/rccm.2206007
- Franken, L., Schiwon, M., and Kurts, C. (2016). Macrophages: sentinels and regulators of the immune system. *Cell. Microbiol.* 18, 475–487. doi: 10.1111/cmi.12580
- Freire, P. P., Fernandez, G. J., Moraes, D., Cury, S. S., Dal Pai-Silva, M., Reis, P. P., et al. (2020). The expression landscape of cachexia-inducing factors in human cancers. *J. Cachexia. Sarcopen. Muscle* 11, 947–961. doi: 10.1002/jcsm.12565
- Galván-peña, S., and O'Neill, L. A. J. (2014). Metabolic reprogramming in macrophage polarization. *Front. Immunol.* 5:420. doi: 10.3389/fimmu.2014.00420
- Gandhi, C. R. (2020). Pro- and anti-fibrogenic functions of gram-negative bacterial Lipopolysaccharide in the liver. *Front. Med.* 7:130. doi: 10.3389/fmed.2020.00130
- Ganeshan, K., Nikkanen, J., Man, K., Leong, Y. A., Sogawa, Y., Maschek, J. A., et al. (2019). Energetic trade-offs and hypometabolic states promote disease tolerance. *Cell* 177, 399–413. doi: 10.1016/j.cell.2019.01.050
- Gao, L., Mejias, R., Echevarría, M., and López-Barneo, J. (2004). Induction of the glucose-6-phosphate dehydrogenase gene expression by chronic hypoxia in PC12 cells. *FEBS Lett.* 569, 256–260. doi: 10.1016/j.febslet.2004.06.004
- Garedew, A., and Moncada, S. (2008). Mitochondrial dysfunction and HIF1 stabilization in inflammation. *J. Cell Sci.* 121, 3468–3475. doi: 10.1242/jcs.034660
- Gibson, M. S., Domingues, N., and Vieira, O. V. (2018). Lipid and non-lipid factors affecting macrophage dysfunction and inflammation in atherosclerosis. *Front. Physiol.* 9:654. doi: 10.3389/fphys.2018.00654
- Gordon, S., and Martinez-Pomares, L. (2017). Physiological roles of macrophages. *Pflügers Arch. Eur. J. Physiol.* 469, 365–374. doi: 10.1007/s00424-017-1945-7
- Grenz, A., Homann, D., and Eltzschig, H. K. (2011). Extracellular adenosine: a safety signal that dampens hypoxia-induced inflammation during ischemia. *Antioxid. Redox Signal.* 15, 2221–2234. doi: 10.1089/ars.2010.3665
- Gunnerson, K. J., Shaw, A. D., Chawla, L. S., Bihorac, A., Al-Khafaji, A., Kashani, K., et al. (2016). TIMP2 \square IGFBP7 biomarker panel accurately predicts acute kidney injury in high-risk surgical patients. *J. Trauma Acute Care Surg.* 80, 243–249. doi: 10.1097/TA.0000000000000912
- Ham, J., and Evans, B. A. J. (2012). An emerging role for adenosine and its receptors in bone homeostasis. *Front. Endocrinol.* 3:113. doi: 10.3389/fendo.2012.00113
- Haskó, G., and Cronstein, B. (2013). Regulation of inflammation by adenosine. *Front. Immunol.* 4:85. doi: 10.3389/fimmu.2013.00085

- He, Q., Yang, Q., Zhou, Q., Zhu, H., Niu, W., Feng, J., et al. (2014). Effects of varying degrees of intermittent hypoxia on proinflammatory cytokines and adipokines in rats and 3T3-L1 adipocytes. *PLoS One* 9:e86326. doi: 10.1371/journal.pone.0086326
- Heikkilä, K., Ebrahim, S., and Lawlor, D. A. (2008). Systematic review of the association between circulating interleukin-6 (IL-6) and cancer. *Eur. J. Cancer* 44, 937–945. doi: 10.1016/j.ejca.2008.02.047
- Honegger, B., Galic, M., Köhler, K., Wittwer, F., Brogiolo, W., Hafen, E., et al. (2008). Imp-L2, a putative homolog of vertebrate IGF-binding protein 7, counteracts insulin signaling in *Drosophila* and is essential for starvation resistance. *J. Biol.* 7:10. doi: 10.1186/jbiol72
- Honors, M. A., and Kinzig, K. P. (2012). The role of insulin resistance in the development of muscle wasting during cancer cachexia. *J. Cachexia. Sarcopen. Muscle* 3, 5–11. doi: 10.1007/s13539-011-0051-5
- Hsu, C.-L., Lin, W., Seshasayee, D., Chen, Y.-H., Ding, X., Lin, Z., et al. (2012). Equilibrative nucleoside transporter 3 deficiency perturbs lysosome function and macrophage homeostasis. *Science* 335, 89–92. doi: 10.1126/science.1213682
- Hubler, M. J., and Kennedy, A. J. (2016). Role of lipids in the metabolism and activation of immune cells. *J. Nutr. Biochem.* 34, 1–7. doi: 10.1016/j.jnutbio.2015.11.002
- Imran, M., and Smith, H. L. (2007). The dynamics of bacterial infection, innate immune response, and antibiotic treatment. *Discret. Contin. Dyn. Syst. B* 8, 127–143. doi: 10.3934/dcdsb.2007.8.127
- Iommardini, L., Porcelli, A. M., Gasparre, G., and Kurelac, I. (2017). Non-canonical mechanisms regulating hypoxia-inducible factor 1 alpha in cancer. *Front. Oncol.* 7:286. doi: 10.3389/fonc.2017.00286
- Irving, P., Ubeda, J.-M., Doucet, D., Troxler, L., Lagueux, M., Zachary, D., et al. (2005). New insights into *Drosophila* larval haemocyte functions through genome-wide analysis. *Cell. Microbiol.* 7, 335–350. doi: 10.1111/j.1462-5822.2004.00462.x
- Jiang, H., Patel, P. H., Kohlmaier, A., Grenley, M. O., McEwen, D. G., and Edgar, B. A. (2009). Cytokine/Jak/Stat signaling mediates regeneration and homeostasis in the *Drosophila* Midgut. *Cell* 137, 1343–1355. doi: 10.1016/j.cell.2009.05.014
- Jin, N., Hatton, N., Swartz, D. R., Xia, X., Harrington, M. A., Larsen, S. H., et al. (2000). Hypoxia Activates jun-n-terminal kinase, extracellular signal-regulated protein kinase, and p38 kinase in pulmonary arteries. *Am. J. Respir. Cell Mol. Biol.* 23, 593–601. doi: 10.1165/ajrcmb.23.5.3921
- Johansson, K., Metzendorf, C., and Soderhall, K. (2005). Microarray analysis of immune challenged hemocytes. *Exp. Cell Res.* 305, 145–155. doi: 10.1016/j.yexcr.2004.12.018
- Jones, W., and Bianchi, K. (2015). Aerobic glycolysis: beyond proliferation. *Front. Immunol.* 6:227. doi: 10.3389/fimmu.2015.00227
- Kacsoh, B. Z., and Schlenke, T. A. (2012). High hemocyte load is associated with increased resistance against parasitoids in *Drosophila suzukii*, a relative of *D. melanogaster*. *PLoS One* 7:e34721. doi: 10.1371/journal.pone.0034721
- Kammerer, T., Faihs, V., Hulde, N., Stangl, M., Brettner, F., Rehm, M., et al. (2020). Hypoxic-inflammatory responses under acute hypoxia: in vitro experiments and prospective observational expedition trial. *Int. J. Mol. Sci.* 21:1034. doi: 10.3390/ijms21031034
- Karnovsky, M. L. (1962). Metabolic basis of phagocytic activity. *Physiol. Rev.* 42, 143–168. doi: 10.1152/physrev.1962.42.1.143
- Kazankov, K., Jørgensen, S. M. D., Thomsen, K. L., Møller, H. J., Vilstrup, H., George, J., et al. (2019). The role of macrophages in nonalcoholic fatty liver disease and nonalcoholic steatohepatitis. *Nat. Rev. Gastroenterol. Hepatol.* 16, 145–159. doi: 10.1038/s41575-018-0082-x
- Kedia-Mehta, N., and Finlay, D. K. (2019). Competition for nutrients and its role in controlling immuneresponses. *Nat. Commun.* 10:2123. doi: 10.1038/s41467-019-10015-4
- Khovidhunkit, W., Kim, M. S., Memon, R. A., Shigenaga, J. K., Moser, A. H., Feingold, K. R., et al. (2004). Effects of infection and inflammation on lipid and lipoprotein metabolism: mechanisms and consequences to the host. *J. Lipid Res.* 45, 1169–1196. doi: 10.1194/jlr.R300019-JLR200
- Kierdorf, K., Hersperger, F., Sharrock, J., Vincent, C. M., Ustaoglu, P., Dou, J., et al. (2020). Muscle function and homeostasis require cytokine inhibition of AKT activity in *Drosophila*. *eLife* 9:e051595. doi: 10.7554/eLife.51595
- Kim, J., Tchemyshov, I., Semenza, G. L., and Dang, C. V. (2006). HIF-1-mediated expression of pyruvate dehydrogenase kinase: a metabolic switch required for cellular adaptation to hypoxia. *Cell Metab.* 3, 177–185. doi: 10.1016/j.cmet.2006.02.002
- Koehler, F., Doehner, W., Hoernig, S., Witt, C., Anker, S. D., and John, M. (2007). Anorexia in chronic obstructive pulmonary disease—association to cachexia and hormonal derangement. *Int. J. Cardiol.* 119, 83–89. doi: 10.1016/j.ijcard.2006.07.088
- Koelwyn, G. J., Corr, E. M., Erbay, E., and Moore, K. J. (2018). Regulation of macrophage immunometabolism in atherosclerosis. *Nat. Immunol.* 19, 526–537. doi: 10.1038/s41590-018-0113-3
- Koivunen, P., Hirsilä, M., Remes, A. M., Hassinen, I. E., Kivirikko, K. I., and Myllyharju, J. (2007). Inhibition of Hypoxia-Inducible Factor (HIF) hydroxylases by citric acid cycle intermediates. *J. Biol. Chem.* 282, 4524–4532. doi: 10.1074/jbc.M610415200
- Koltai, T. (2020). Cancer cachexia has many symptoms but only one cause: anoxia. *F1000Res* 9:250. doi: 10.12688/f1000research.22624.1
- Korbecki, J., and Bajdak-Rusinek, K. (2019). The effect of palmitic acid on inflammatory response in macrophages: an overview of molecular mechanisms. *Inflamm. Res.* 68, 915–932. doi: 10.1007/s00011-019-01273-5
- Kraakman, M. J., Murphy, A. J., Jandeleit-Dahm, K., and Kammoun, H. L. (2014). Macrophage polarization in obesity and type 2 diabetes: weighing down our understanding of macrophage function? *Front. Immunol.* 5:470. doi: 10.3389/fimmu.2014.00470
- Krejčová, G., Bajgar, A., Nedbalová, P., Kovářová, J., Kamps-Hughes, N., Zemanová, H., et al. (2020). Macrophage-derived insulin/IGF antagonist ImpL2 regulates systemic metabolism for mounting an effective acute immuneresponse in *Drosophila*. *bioRxiv* [Preprint], doi: 10.1101/2020.09.24.311670
- Krejčová, G., Danielová, A., Nedbalová, P., Kazek, M., Strych, L., Chawla, G., et al. (2019). *Drosophila* macrophage switch to aerobic glycolysis to mount effective antibacterial defense. *eLife* 8:e050414. doi: 10.7554/eLife.50414
- Krishnan, J., Suter, M., Windak, R., Krebs, T., Felley, A., Montessuit, C., et al. (2009). Activation of aHIF1a-PPAR α axis underlies the integration of glycolytic and lipid anabolic pathways in pathological cardiac hypertrophy. *Cell Metab.* 9, 512–524. doi: 10.1016/j.cmet.2009.05.005
- Kühnlein, R. P. (2012). Lipid droplet-based storage fat metabolism in *Drosophila*. *J. Lipid Res.* 53, 1430–1436. doi: 10.1194/jlr.R024299
- Kullmann, S., Valenta, V., Wagner, R., Tschritter, O., Machann, J., Häring, H.-U., et al. (2020). Brain insulin sensitivity is linked to adiposity and body fat distribution. *Nat. Commun.* 11:1841. doi: 10.1038/s41467-020-15686-y
- Kwon, D., Cha, H.-J., Lee, H., Hong, S.-H., Park, C., Park, S.-H., et al. (2019). Protective effect of glutathione against oxidative stress-induced cytotoxicity in RAW 264.7 macrophages through activating the nuclear factor erythroid 2-Related Factor-2/Heme oxygenase-1 pathway. *Antioxidants* 8:82. doi: 10.3390/antiox8040082
- Kwon, Y., Song, W., Droujine, I. A., Hu, Y., Asara, J. M., and Perrimon, N. (2015). Systemic organ wasting induced by localized expression of the secreted insulin/igf antagonist ImpL2. *Dev. Cell* 33, 36–46. doi: 10.1016/j.devcel.2015.02.012
- Langin, D. (2013). Adipose tissue lipolysis and insulin sensitivity. *Endocr. Abstr.* 32:S32.3. doi: 10.1530/endoabs.32.S32.3
- Lee, G. J., Han, G., Yun, H. M., Lim, J. J., Noh, S., Lee, J., et al. (2018). Steroid signaling mediates nutritional regulation of juvenile body growth via IGF-binding protein in *Drosophila*. *Proc. Natl. Acad. Sci. U.S.A.* 115, 5992–5997. doi: 10.1073/pnas.1718834115
- Lee, S., and Dong, H. H. (2017). FoxO integration of insulin signaling with glucose and lipid metabolism. *J. Endocrinol.* 233, R67–R79. doi: 10.1530/JOE-17-0002
- Leonard, E. J., Skeel, A., Chiang, P. K., and Cantoni, G. L. (1978). The action of the adenosylhomocysteine hydrolase inhibitor, 3-deazaadenosine, on phagocytic function of mouse macrophages and human monocytes. *Biochem. Biophys. Res. Commun.* 84, 102–109. doi: 10.1016/0006-291X(78)90269-3
- Lewis, A., and Elks, P. M. (2019). Hypoxia induces macrophage tnf α expression via cyclooxygenase and prostaglandin E2 in vivo. *Front. Immunol.* 10:2321. doi: 10.3389/fimmu.2019.02321
- Lewis, G. F., Carpentier, A., Adeli, K., and Giacca, A. (2002). Disordered fat storage and mobilization in the pathogenesis of insulin resistance and Type 2 diabetes. *Endocr. Rev.* 23, 201–229. doi: 10.1210/edrv.23.2.0461
- Lim, Y.-M., Lim, H., Hur, K. Y., Quan, W., Lee, H.-Y., Cheon, H., et al. (2014). Systemic autophagy insufficiency compromises adaptation to metabolic stress

- and facilitates progression from obesity to diabetes. *Nat. Commun.* 5:4934. doi: 10.1038/ncomms5934
- Liou, G.-Y. (2017). Inflammatory cytokine signaling during development of pancreatic and prostate cancers. *J. Immunol. Res.* 2017, 1–10. doi: 10.1155/2017/7979637
- Liu, Y., Wu, M., Ling, J., Cai, L., Zhang, D., Gu, H. F., et al. (2015). Serum IGFBP7 levels associate with insulin resistance and the risk of metabolic syndrome in a Chinese population. *Sci. Rep.* 5:10227. doi: 10.1038/srep10227
- Loftus, R. M., and Finlay, D. K. (2016). Immunometabolism: cellular metabolism turns immunoregulator. *J. Biol. Chem.* 291, 1–10. doi: 10.1074/jbc.R115.693903
- Ma, J., Wei, K., Liu, J., Tang, K., Zhang, H., Zhu, L., et al. (2020). Glycogen metabolism regulates macrophage-mediated acute inflammatory responses. *Nat. Commun.* 11:1769. doi: 10.1038/s41467-020-15636-8
- Maier, A., Wu, H., Cordasic, N., Oefner, P., Dietel, B., Thiele, C., et al. (2017). Hypoxia-inducible protein 2 Hig2/Hilpda mediates neutral lipid accumulation in macrophages and contributes to atherosclerosis in apolipoprotein E-deficient mice. *FASEB J.* 31, 4971–4984. doi: 10.1096/fj.201700235R
- Mak, R. H., and Cheung, W. (2006). Energy homeostasis and cachexia in chronic kidney disease. *Pediatr. Nephrol.* 21, 1807–1814. doi: 10.1007/s00467-006-0194-3
- Makki, K., Froguel, P., and Wolowczuk, I. (2013). Adipose tissue in obesity-related inflammation and insulin resistance: cells, cytokines, and chemokines. *ISRN Inflamm.* 2013, 1–12. doi: 10.1155/2013/139239
- Marette, A. (2002). Mediators of cytokine-induced insulin resistance in obesity and other inflammatory settings. *Curr. Opin. Clin. Nutr. Metab. Care* 5, 377–383. doi: 10.1097/00075197-200207000-00005
- Marik, P. E., and Bellomo, R. (2013). Stress hyperglycemia: an essential survival response. *Crit. Care* 17:305. doi: 10.1186/cc12514
- Martínez-Castillo, M., Rosique-Oramas, D., Medina-Avila, Z., Pérez-Hernández, J. L., Higuera-De la Tijera, F., Santana-Vargas, D., et al. (2020). Differential production of insulin-like growth factor-binding proteins in liver fibrosis progression. *Mol. Cell. Biochem.* 469, 65–75. doi: 10.1007/s11010-020-03728-4
- Marxsen, J. H., Stengel, P., Doege, K., Heikkinen, P., Jokilehto, T., Wagner, T., et al. (2004). Hypoxia-inducible factor-1 (HIF-1) promotes its degradation by induction of HIF- α -prolyl-4-hydroxylases. *Biochem. J.* 381, 761–767. doi: 10.1042/BJ20040620
- Matrone, C., Pignataro, G., Molinaro, P., Irace, C., Scorziello, A., Di Renzo, G. F., et al. (2004). HIF-1 α reveals a binding activity to the promoter of iNOS gene after permanent middle cerebral artery occlusion. *J. Neurochem.* 90, 368–378. doi: 10.1111/j.1471-4159.2004.02483.x
- Melcarne, C., Lemaître, B., and Kurant, E. (2019). Phagocytosis in *Drosophila*: from molecules and cellular machinery to physiology. *Insect Biochem. Mol. Biol.* 109, 1–12. doi: 10.1016/j.ibmb.2019.04.002
- Mihajlovic, Z., Tanasic, D., Bajgar, A., Perez-Gomez, R., Steffal, P., and Krejci, A. (2019). Limeisa new protein linking immunity and metabolism in *Drosophila*. *Dev. Biol.* 452, 83–94. doi: 10.1016/j.ydbio.2019.05.005
- Mills, C. D., Lenz, L. L., and Ley, K. (2015). Macrophages at the fork in the road to health or disease. *Front. Immunol.* 6:59. doi: 10.3389/fimmu.2015.00059
- Mills, E. L., and O'Neill, L. A. (2016). Reprogramming mitochondrial metabolism in macrophages as an anti-inflammatory signal. *Eur. J. Immunol.* 46, 13–21. doi: 10.1002/eji.201445427
- Miska, J., Lee-Chang, C., Rashidi, A., Muroski, M. E., Chang, A. L., Lopez-Rosas, A., et al. (2019). HIF-1 α is a metabolic switch between glycolytic-driven migration and oxidative phosphorylation-driven immunosuppression of tregs in glioblastoma. *Cell Rep.* 27, 226–237. doi: 10.1016/j.celrep.2019.03.029
- Molaei, M., Vandehoef, C., and Karpac, J. (2019). NF- κ B shapes metabolic adaptation by attenuating foxo-mediated lipolysis in *Drosophila*. *Dev. Cell* 49, 802–810. doi: 10.1016/j.devcel.2019.04.009
- Morgantini, C., Jager, J., Li, X., Levi, L., Azzimato, V., Sulen, A., et al. (2019). Liver macrophages regulate systemic metabolism through non-inflammatory factors. *Nat. Metab.* 1, 445–459. doi: 10.1038/s42255-019-0044-9
- Mosser, D. M., and Edwards, J. P. (2008). Exploring the full spectrum of macrophage activation. *Nat. Rev. Immunol.* 8, 958–969. doi: 10.1038/nri2448
- Mylonis, I., Sembongi, H., Befani, C., Liakos, P., Sinicossoglou, S., and Simos, G. (2012). Hypoxia causes triglyceride accumulation by HIF-1-mediated stimulation of lipin 1 expression. *J. Cell Sci.* 125, 3485–3493. doi: 10.1242/jcs.106682
- Mylonis, I., Simos, G., and Paraskeva, E. (2019). Hypoxia-inducible factors and the regulation of lipid metabolism. *Cells* 8:214. doi: 10.3390/cells8030214
- Nagao, A., Kobayashi, M., Koyasu, S., Chow, C. C. T., and Harada, H. (2019). HIF-1-dependent reprogramming of glucose metabolic pathway of cancer cells and its therapeutic significance. *Int. J. Mol. Sci.* 20:238. doi: 10.3390/ijms20020238
- Nagy, C., and Haschemi, A. (2015). Time and demand are two critical dimensions of immunometabolism: the process of macrophage activation and the pentose phosphate pathway. *Front. Immunol.* 6:164. doi: 10.3389/fimmu.2015.00164
- Narsale, A. A., and Carson, J. A. (2014). Role of interleukin-6 in cachexia. *Curr. Opin. Support. Palliat. Care* 8, 321–327. doi: 10.1097/SPC.000000000000091
- Nässel, D. R., and Broeck, J. V. (2016). Insulin/IGF signaling in *Drosophila* and other insects: factors that regulate production, release and post-release action of the insulin-like peptides. *Cell. Mol. Life Sci.* 73, 271–290. doi: 10.1007/s00018-015-2063-3
- Nässel, D. R., Liu, Y., and Luo, J. (2015). Insulin/IGF signaling and its regulation in *Drosophila*. *Gen. Comp. Endocrinol.* 221, 255–266. doi: 10.1016/j.ygcen.2014.11.021
- Newsholme, P., Curi, R., Gordon, S., and Newsholme, E. A. (1986). Metabolism of glucose, glutamine, long-chain fatty acids and ketone bodies by murine macrophages. *Biochem. J.* 239, 121–125. doi: 10.1042/bj2390121
- Nonnenmacher, Y., and Hiller, K. (2018). Biochemistry of proinflammatory macrophage activation. *Cell. Mol. Life Sci.* 75, 2093–2109. doi: 10.1007/s00018-018-2784-1
- Obach, M., Navarro-Sabaté, À, Caro, J., Kong, X., Duran, J., and Gómez, M. (2004). 6-Phosphofructo-2-kinase (pfkfb3) gene promoter contains hypoxia-inducible Factor-1 binding sites necessary for transactivation in response to hypoxia. *J. Biol. Chem.* 279, 53562–53570. doi: 10.1074/jbc.M406096200
- Oldefest, M., Nowinski, J., Hung, C.-W., Neelsen, D., Trad, A., Tholey, A., et al. (2013). Upd3 - an ancestor of the four-helix bundle cytokines. *Biochem. Biophys. Res. Commun.* 436, 66–72. doi: 10.1016/j.bbrc.2013.04.107
- Olefsky, J. M., and Glass, C. K. (2010). Macrophages, inflammation, and insulin resistance. *Annu. Rev. Physiol.* 72, 219–246. doi: 10.1146/annurev-physiol-021909-135846
- Olson, J. M., Jinka, T. R., Larson, L. K., Danielson, J. J., Moore, J. T., Carpluck, J., et al. (2013). Circannual rhythm in body temperature, torpor, and sensitivity to A 1 adenosine receptor agonist in arctic ground squirrels. *J. Biol. Rhythms* 28, 201–207. doi: 10.1177/0748730413490667
- O'Neill, L. A. J. (2015). A broken krebs cycle in macrophages. *Immunity* 42, 393–394. doi: 10.1016/j.immuni.2015.02.017
- Owusu-Ansah, E., Song, W., and Perrimon, N. (2013). Muscle mitochondrial metabolism promotes longevity via systemic repression of insulin signaling. *Cell* 155, 699–712. doi: 10.1016/j.cell.2013.09.021
- Palazon, A., Goldrath, A. W., Nizet, V., and Johnson, R. S. (2014). HIF transcription factors, inflammation, and immunity. *Immunity* 41, 518–528. doi: 10.1016/j.immuni.2014.09.008
- Panday, A., Sahoo, M. K., Osorio, D., and Batra, S. (2015). NADPH oxidases: an overview from structure to innate immunity-associated pathologies. *Cell. Mol. Immunol.* 12, 5–23. doi: 10.1038/cmi.2014.89
- Patel, H. J., and Patel, B. M. (2017). TNF- α and cancer cachexia: molecular insights and clinical implications. *Life Sci.* 170, 56–63. doi: 10.1016/j.lfs.2016.11.033
- Pavlou, S., Wang, L., Xu, H., and Chen, M. (2017). Higher phagocytic activity of thioglycollate-elicited peritoneal macrophages related to metabolic status of the cells. *J. Inflamm.* 14:4. doi: 10.1186/s12950-017-0151-x
- Péan, C. B., Schieblier, M., Tan, S. W. S., Sharrock, J. A., Kierdorf, K., Brown, K. P., et al. (2017). Regulation of phagocyte triglyceride by a STAT-ATG2 pathway controls mycobacterial infection. *Nat. Commun.* 8:14642. doi: 10.1038/ncomms14642
- Perry, R. J., Samuel, V. T., Petersen, K. F., and Shulman, G. I. (2014). The role of hepatic lipids in hepatic insulin resistance and type 2 diabetes. *Nature* 510, 84–91. doi: 10.1038/nature13478
- Peyssonnaud, C., Cejudo-Martin, P., Doedens, A., Zinkernagel, A. S., Johnson, R. S., and Nizet, V. (2007). Cutting edge: essential role of hypoxia inducible Factor-1 α in development of lipopolysaccharide-induced sepsis. *J. Immunol.* 178, 7516–7519. doi: 10.4049/jimmunol.178.12.7516
- Pizarro, T. T., and Cominelli, F. (2007). Cloning IL-1 and the birth of a new era in cytokine biology. *J. Immunol.* 178, 5411–5412. doi: 10.4049/jimmunol.178.9.5411

- Popa, C., Netea, M. G., van Riel, P. L. C. M., van der Meer, J. W. M., and Stalenhoef, A. F. H. (2007). The role of TNF- α in chronic inflammatory conditions, intermediary metabolism, and cardiovascular risk. *J. Lipid Res.* 48, 751–762. doi: 10.1194/jlr.R600021-JLR200
- Porporato, P. E. (2016). Understanding cachexia as a cancer metabolism syndrome. *Oncogenesis* 5:e200. doi: 10.1038/oncis.2016.3
- Prabakaran, S. (2015). Mitochondria to nucleus: activate HIF1 α . *Sci. Signal.* 8:ec330. doi: 10.1126/scisignal.aad8189
- Puigserver, P., Rhee, J., Donovan, J., Walkey, C. J., Yoon, J. C., Oriente, F., et al. (2003). Insulin-regulated hepatic gluconeogenesis through FOXO1-PGC-1 α interaction. *Nature* 423, 550–555. doi: 10.1038/nature01667
- Rajan, A., and Perrimon, N. (2011). *Drosophila* as a model for interorgan communication: lessons from studies on energy homeostasis. *Dev. Cell* 21, 29–31. doi: 10.1016/j.devcel.2011.06.034
- Ramond, E., Dudzic, J. P., and Lemaitre, B. (2020). Comparative RNA-Seq analyses of *Drosophila* plasmacytes reveal genespecific signatures in response to clean injury and septic injury. *PLoS One* 15:e0235294. doi: 10.1371/journal.pone.0235294
- Ramond, E., Jamet, A., Coureuil, M., and Charbit, A. (2019). Pivotal role of mitochondria in macrophage response to bacterial pathogens. *Front. Immunol.* 10:2461. doi: 10.3389/fimmu.2019.02461
- Ratcliffe, N. A., and Rowley, A. F. (1975). Cellular defense reactions of insect hemocytes in vitro: phagocytosis in a new suspension culture system. *J. Invertebr. Pathol.* 26, 225–233. doi: 10.1016/0022-2011(75)90053-1
- Park, Y. M. (2014). CD36, a scavenger receptor implicated in atherosclerosis. *Exp. Mol. Med.* 46:e99. doi: 10.1038/emm.2014.38
- Remmerie, A., and Scott, C. L. (2018). Macrophages and lipid metabolism. *Cell. Immunol.* 330, 27–42. doi: 10.1016/j.cellimm.2018.01.020
- Riddle, S. R., Ahmad, A., Ahmad, S., Deeb, S. S., Malkki, M., Schneider, B. K., et al. (2000). Hypoxia induces hexokinase II gene expression in human lung cell line A549. *Am. J. Physiol. Cell. Mol. Physiol.* 278, L407–L416. doi: 10.1152/ajplung.2000.278.2.L407
- Riganti, C., Gazzano, E., Polimeni, M., Aldieri, E., and Ghigo, D. (2012). The pentose phosphate pathway: an antioxidant defense and a crossroad in tumor cell fate. *Free Radic. Biol. Med.* 53, 421–436. doi: 10.1016/j.freeradbiomed.2012.05.006
- Ristow, M., and Schmeisser, K. (2014). Mitohormesis: promoting health and lifespan by increased levels of reactive oxygen species (ROS). *Dose Response* 12, 288–341. doi: 10.2203/dose-response.13-035.Ristow
- Rossol, M., Heine, H., Meusch, U., Quandt, D., Klein, C., Sweet, M. J., et al. (2011). LPS-induced cytokine production in human monocytes and macrophages. *Crit. Rev. Immunol.* 31, 379–446. doi: 10.1615/CritRevImmunol.v31.i5.20
- Roth, K. J., and Coppel, B. L. (2015). Role of hypoxia-inducible factors in the development of liver fibrosis. *Cell. Mol. Gastroenterol. Hepatol.* 1, 589–597. doi: 10.1016/j.jcmgh.2015.09.005
- Rouzer, C. A., Scott, W. A., Griffith, O. W., Hamill, A. L., and Cohn, Z. A. (1982). Glutathione metabolism in resting and phagocytizing peritoneal macrophages. *J. Biol. Chem.* 257, 2002–2008. doi: 10.1016/s0021-9258(19)68139-1
- Ruan, W., Wu, M., Shi, L., Li, F., Dong, L., Qiu, Y., et al. (2017). Serum levels of IGFBP7 are elevated during acute exacerbation in COPD patients. *Int. J. Chron. Obstruct. Pulmon. Dis.* Volume 12, 1775–1780. doi: 10.2147/COPD.S132652
- Ryter, S. W., Koo, J. K., and Choi, A. M. K. (2014). Molecular regulation of autophagy and its implications for metabolic diseases. *Curr. Opin. Clin. Nutr. Metab. Care* 17, 329–337. doi: 10.1097/MCO.0000000000000068
- Sag, D., Carling, D., Stout, R. D., and Suttles, J. (2008). Adenosine 5'-monophosphate-activated protein Kinase promotes macrophage polarization to an anti-inflammatory functional phenotype. *J. Immunol.* 181, 8633–8641. doi: 10.4049/jimmunol.181.12.8633
- Salazar, J., Bermúdez, V., Olivares, L. C., Torres, W., Palmar, J., Añez, R., et al. (2018). Insulin resistance indices and coronary risk in adults from Maracaibo city, Venezuela: a cross-sectional study. *F1000Research* 7:44. doi: 10.12688/f1000research.13610.2
- Sancho, D., Enamorado, M., and Garaude, J. (2017). Innate immune function of mitochondrial metabolism. *Front. Immunol.* 8:527. doi: 10.3389/fimmu.2017.00527
- Santoleri, D., and Titchenell, P. M. (2019). Resolving the paradox of hepatic insulin resistance. *Cell. Mol. Gastroenterol. Hepatol.* 7, 447–456. doi: 10.1016/j.jcmgh.2018.10.016
- Sarkar, P., Stefi, R. V., Pasupuleti, M., Paray, B. A., Al-Sadoon, M. K., and Arockiaraj, J. (2020). Antioxidant molecular mechanism of adenosyl homocysteinase from cyanobacteria and its wound healing process in fibroblast cells. *Mol. Biol. Rep.* 47, 1821–1834. doi: 10.1007/s11033-020-05276-y
- Schrader, J., Haddy, F. J., and Gerlach, E. (1977). Release of adenosine, inosine and hypoxanthine from the isolated guinea pig heart during hypoxia, flow-autoregulation and reactive hyperemia. *Pflügers Arch. Eur. J. Physiol.* 369, 1–6. doi: 10.1007/BF00580802
- Schwartzburg, P. M. (2017). Catabolic and anabolic faces of insulin resistance and their disorders: a new insight into circadian control of metabolic disorders leading to diabetes. *Futur. Sci. OA* 3:FSO201. doi: 10.4155/fsoa-2017-0015
- Scialò, F., Fernández-Ayala, D. J., and Sanz, A. (2017). Role of mitochondrial reverse electron transport in ROS signaling: potential roles in health and disease. *Front. Physiol.* 8:428. doi: 10.3389/fphys.2017.00428
- Scott, B. N. V., Sarkar, T., Kratofil, R. M., Kubes, P., and Thanabalasuriar, A. (2019). Unraveling the host's immune response to infection: seeing is believing. *J. Leukoc. Biol.* 106, 323–335. doi: 10.1002/JLB.4R11218-503R
- Shen, G., and Li, X. (2017). "The multifaceted role of hypoxia-inducible Factor 1 (HIF1) in lipid metabolism," in *Hypoxia and Human Diseases*, eds J. Zheng and C. Zhou (London: InTechopen), doi: 10.5772/65340
- Shen, G.-M., Zhao, Y.-Z., Chen, M.-T., Zhang, F.-L., Liu, X.-L., Wang, Y., et al. (2012). Hypoxia-inducible factor-1 (HIF-1) promotes LDL and VLDL uptake through inducing VLDLR under hypoxia. *Biochem. J.* 441, 675–683. doi: 10.1042/BJ20111377
- Shi, J., Fan, J., Su, Q., and Yang, Z. (2019). Cytokines and abnormal glucose and lipid metabolism. *Front. Endocrinol.* 10:703. doi: 10.3389/fendo.2019.00703
- Shin, M., Cha, N., Koranteng, F., Cho, B., and Shim, J. (2020). Subpopulation of macrophage-like plasmacytes attenuates systemic growth via JAK/STAT in the *Drosophila* fat body. *Front. Immunol.* 11:63. doi: 10.3389/fimmu.2020.00063
- Shin, K. C., Hwang, I., Choe, S. S., Park, J., Ji, Y., Kim, J. I., et al. (2017). Macrophage VLDLR mediates obesity-induced insulin resistance with adipose tissue inflammation. *Nat. Commun.* 8:1087. doi: 10.1038/s41467-017-01232-w
- Siebert, I., Schödel, J., Nairz, M., Schatz, V., Dettmer, K., Dick, C., et al. (2015). Ferritin-mediated iron sequestration stabilizes hypoxia-inducible Factor-1 α upon LPS activation in the presence of ample oxygen. *Cell Rep.* 13, 2048–2055. doi: 10.1016/j.celrep.2015.11.005
- Silva, D., Moreira, D., Cordeiro-da-Silva, A., Quintas, C., Gonçalves, J., and Fresco, P. (2020). Intracellular adenosine released from THP-1 differentiated human macrophages is involved in an autocrine control of Leishmania parasitic burden, mediated by adenosine A2A and A2B receptors. *Eur. J. Pharmacol.* 885:173504. doi: 10.1016/j.ejphar.2020.173504
- Silva-Vilches, C., Ring, S., and Mahnke, K. (2018). ATP and its metabolite adenosine as regulators of dendritic cell activity. *Front. Immunol.* 9:2581. doi: 10.3389/fimmu.2018.02581
- Soeters, M. R., and Soeters, P. B. (2012). The evolutionary benefit of insulin resistance. *Clin. Nutr.* 31, 1002–1007. doi: 10.1016/j.cnu.2012.05.011
- Srikanthan, P., Hevener, A. L., and Karlamangla, A. S. (2010). Sarcopenia exacerbates obesity-associated insulin resistance and Dysglycemia: findings from the national health and nutrition examination survey III. *PLoS One* 5:e10805. doi: 10.1371/journal.pone.0010805
- Stenholm, S., Harris, T. B., Rantanen, T., Visser, M., Kritchevsky, S. B., and Ferrucci, L. (2008). Sarcopenic obesity: definition, cause and consequences. *Curr. Opin. Clin. Nutr. Metab. Care* 11, 693–700. doi: 10.1097/MCO.0b013e328312c37d
- Straub, R. H. (2014). Insulin resistance, selfish brain, and selfish immune system: an evolutionarily positively selected program used in chronic inflammatory diseases. *Arthritis Res. Ther.* 16:S4. doi: 10.1186/ar4688
- Stuart, L. M., and Ezekowitz, R. A. (2008). Phagocytosis and comparative innate immunity: learning on the fly. *Nat. Rev. Immunol.* 8, 131–141. doi: 10.1038/nri2240
- Stunault, M. I., Bories, G., Guinamard, R. R., and Ivanov, S. (2018). Metabolism plays a key role during macrophage activation. *Med. Inflamm.* 2018:2426138. doi: 10.1155/2018/2426138
- Tadaishi, M., Toriba, Y., Shimizu, M., and Kobayashi-Hattori, K. (2018). Adenosine stimulates hepatic glycogenolysis via adrenal glands-liver crosstalk in mice. *PLoS One* 13:e0209647. doi: 10.1371/journal.pone.0209647

- Tattikota, S. G., Cho, B., Liu, Y., Hu, Y., Barrera, V., Steinbaugh, M. J., et al. (2020). A single-cell survey of *Drosophila* blood. *eLife* 9:e54818. doi: 10.7554/eLife.54818
- Tehlivets, O., Malanovic, N., Visram, M., Pavkov-Keller, T., and Keller, W. (2013). S-adenosyl-L-homocysteine hydrolase and methylation disorders: yeast as a model system. *Biochim. Biophys. Acta Mol. Basis Dis.* 1832, 204–215. doi: 10.1016/j.bbdis.2012.09.007
- Teng, O., Ang, C. K. E., and Guan, X. L. (2017). Macrophage-bacteria interactions—alipid-centric relationship. *Front. Immunol.* 8:1836. doi: 10.3389/fimmu.2017.01836
- Texada, M. J., Jørgensen, A. F., Christensen, C. F., Koyama, T., Malita, A., Smith, D. K., et al. (2019). A fat-tissue sensor couples growth to oxygen availability by remotely controlling insulin secretion. *Nat. Commun.* 10:1955. doi: 10.1038/s41467-019-09943-y
- Theret, M., Mounier, R., and Rossi, F. (2019). The origins and non-canonical functions of macrophages in development and regeneration. *Development* 146:dev156000. doi: 10.1242/dev.156000
- Thomas, A. P., and Halestrap, A. P. (1981). The rôle of mitochondrial pyruvate transport in the stimulation by glucagon and phenylephrine of gluconeogenesis from lactate in isolated rat hepatocytes. *Biochem. J.* 198, 551–560. doi: 10.1042/bj1980551
- Tilg, H., and Hotamisligil, G. S. (2006). Nonalcoholic fatty liver disease: cytokine-adipokine interplay and regulation of insulin resistance. *Gastroenterol.* 131, 934–945. doi: 10.1053/j.gastro.2006.05.054
- Tonelli, C., Chio, I. I. C., and Tuveson, D. A. (2018). Transcriptional regulation by Nrf2. *Antioxid. Redox Signal.* 29, 1727–1745. doi: 10.1089/ars.2017.7342
- Van den Berghe, G. (2002). Beyond diabetes: saving lives with insulin in the ICU. *Int. J. Obes.* 26, S3–S8. doi: 10.1038/sj.ijo.0802171
- Van den Bossche, J., Baardman, J., and de Winther, M. P. J. (2015). Metabolic characterization of polarized M1 and M2 bone marrow-derived macrophages using real-time extracellular flux analysis. *J. Vis. Exp.* 2015:53424. doi: 10.3791/53424
- van Niekerk, G., Davis, T., and Engelbrecht, A.-M. (2017). Hyperglycaemia in critically ill patients: the immune system's sweet tooth. *Crit. Care* 21:202. doi: 10.1186/s13054-017-1775-1
- Vijayan, V., Pradhan, P., Braud, L., Fuchs, H. R., Gueler, F., Motterlini, R., et al. (2019). Human and murine macrophages exhibit differential metabolic responses to lipopolysaccharide - A divergent role for glycolysis. *Redox Biol.* 22:101147. doi: 10.1016/j.redox.2019.101147
- Wang, A., Luan, H. H., and Medzhitov, R. (2019). An evolutionary perspective on immunometabolism. *Science* 363:eaar3932. doi: 10.1126/science.aar3932
- Wang, C.-W., Purkayastha, A., Jones, K. T., Thaker, S. K., and Banerjee, U. (2016). In vivo genetic dissection of tumor growth and the Warburg effect. *eLife* 5:e018126. doi: 10.7554/eLife.18126
- Wang, L., Sexton, T. R., Venard, C., Giedt, M., Guo, Q., Chen, Q., et al. (2014). Pleiotropy of the *Drosophila* JAK pathway cytokine Unpaired 3 in development and aging. *Dev. Biol.* 395, 218–231. doi: 10.1016/j.ydbio.2014.09.015
- Wang, T., Liu, H., Lian, G., Zhang, S.-Y., Wang, X., and Jiang, C. (2017). HIF1 α -induced glycolysis metabolism is essential to the activation of inflammatory macrophages. *Med. Inflamm.* 2017, 1–10. doi: 10.1155/2017/9029327
- Warburg, O. (1956). On the origin of cancer cells. *Science* 123, 309–314. doi: 10.1126/science.123.3191.309
- Warburg, O., Wind, F., and Negelein, E. (1927). The metabolism of tumors in the body. *J. Gen. Physiol.* 8, 519–530. doi: 10.1085/jgp.8.6.519
- Watts, E. R., and Walmsley, S. R. (2019). Inflammation and hypoxia: HIF and PHD isoform selectivity. *Trends Mol. Med.* 25, 33–46.
- Werb, Z., and Cohn, Z. A. (1972). Plasma membrane synthesis in the macrophage following phagocytosis of polystyrene latex particles. *J. Biol. Chem.* 247, 2439–2446. doi: 10.1016/s0021-9258(19)45448-3
- Wolowczuk, I., Verwaerde, C., Viltart, O., Delanoye, A., Delacre, M., Pot, B., et al. (2008). Feeding our immune system: impact on metabolism. *Clin. Dev. Immunol.* 2008:639803. doi: 10.1155/2008/639803
- Woodcock, K. J., Kierdorf, K., Pouchelon, C. A., Vivancos, V., Dionne, M. S., and Geissmann, F. (2015). Macrophage-derived *upd3* cytokine causes impaired glucose homeostasis and reduced lifespan in *Drosophila* fed a lipid-rich diet. *Immunity* 42, 133–144. doi: 10.1016/j.immuni.2014.12.023
- Wynn, T. A., Chawla, A., and Pollard, J. W. (2013). Macrophage biology in development, homeostasis and disease. *Nature* 496, 445–455. doi: 10.1038/nature12034
- Xing, J., and Lu, J. (2016). HIF-1 α activation attenuates IL-6 and TNF- α pathways in hippocampus of rats following transient global ischemia. *Cell. Physiol. Biochem.* 39, 511–520. doi: 10.1159/000445643
- Xu, Q., Choksi, S., Qu, J., Jang, J., Choe, M., Banfi, B., et al. (2016). NADPH oxidases are essential for macrophage differentiation. *J. Biol. Chem.* 291, 20030–20041. doi: 10.1074/jbc.M116.731216
- Yamashita, A., Zhao, Y., Matsuura, Y., Yamasaki, K., Moriguchi-Goto, S., Sugita, C., et al. (2014). Increased metabolite levels of glycolysis and pentose phosphate pathway in rabbit atherosclerotic arteries and hypoxic macrophage. *PLoS One* 9:e86426. doi: 10.1371/journal.pone.0086426
- Yang, H., and Hultmark, D. (2017). *Drosophila* muscles regulate the immune response against wasp infection via carbohydrate metabolism. *Sci. Rep.* 7:15713. doi: 10.1038/s41598-017-15940-2
- Yang, H., Kronhamn, J., Ekström, J., Korkut, G. G., and Hultmark, D. (2015). JAK/STAT signaling in *Drosophila* muscles controls the cellular immune response against parasitoid infection. *EMBO Rep.* 16, 1664–1672. doi: 10.15252/embr.201540277
- Yang, W., Huang, J., Wu, H., Wang, Y., Du, Z., Ling, Y., et al. (2020). Molecular mechanisms of cancer cachexia-induced muscle atrophy (Review). *Mol. Med. Rep.* 22, 4967–4980. doi: 10.3892/mmr.2020.11608
- Zanin, R. F., Braganhol, E., Bergamin, L. S., Campesato, L. F. I., Filho, A. Z., Moreira, J. C. F., et al. (2012). Differential macrophage activation alters the expression profile of NTPDase and Ecto-5'-nucleotidase. *PLoS One* 7:e31205. doi: 10.1371/journal.pone.0031205
- Zeng, T., Zhang, C.-L., Xiao, M., Yang, R., and Xie, K.-Q. (2016). Critical roles of Kupffer cells in the pathogenesis of alcoholic liver disease: from basic science to clinical trials. *Front. Immunol.* 7:538. doi: 10.3389/fimmu.2016.00538
- Zhang, D., Zheng, H., Zhou, Y., Tang, X., Yu, B., and Li, J. (2007). Association of IL-1 β gene polymorphism with cachexia from locally advanced gastric cancer. *BMC Cancer* 7:45. doi: 10.1186/1471-2407-7-45

Conflict of Interest: The authors declare that the research was conducted in the absence of any commercial or financial relationships that could be construed as a potential conflict of interest.

Copyright © 2021 Bajgar, Krejčová and Doležal. This is an open-access article distributed under the terms of the Creative Commons Attribution License (CC BY). The use, distribution or reproduction in other forums is permitted, provided the original author(s) and the copyright owner(s) are credited and that the original publication in this journal is cited, in accordance with accepted academic practice. No use, distribution or reproduction is permitted which does not comply with these terms.

CHAPTER VI:

On the origin of the functional versatility of macrophages

Adam Bajgar, **Gabriela Krejčová**

Frontiers in Physiology, 2023, 14:10.3389/fphys.2023.1128984



OPEN ACCESS

EDITED BY

Geoffrey A. Head,
Baker Heart and Diabetes Institute,
Australia

REVIEWED BY

Tony De Tomaso,
University of California, Santa Barbara,
United States
Peter R. Corridon,
Khalifa University, United Arab Emirates
Volker Hartenstein,
University of California, Los Angeles,
United States

*CORRESPONDENCE

Adam Bajgar,
✉ bajgaradam@seznam.cz
Gabriela Krejčová,
✉ krejcovagabriela@seznam.cz

SPECIALTY SECTION

This article was submitted to Integrative
Physiology, a section of the journal
Frontiers in Physiology

RECEIVED 21 December 2022

ACCEPTED 07 February 2023

PUBLISHED 23 February 2023

CITATION

Bajgar A and Krejčová G (2023), On the
origin of the functional versatility
of macrophages.
Front. Physiol. 14:1128984.
doi: 10.3389/fphys.2023.1128984

COPYRIGHT

© 2023 Bajgar and Krejčová. This is an
open-access article distributed under the
terms of the [Creative Commons
Attribution License \(CC BY\)](https://creativecommons.org/licenses/by/4.0/). The use,
distribution or reproduction in other
forums is permitted, provided the original
author(s) and the copyright owner(s) are
credited and that the original publication
in this journal is cited, in accordance with
accepted academic practice. No use,
distribution or reproduction is permitted
which does not comply with these terms.

On the origin of the functional versatility of macrophages

Adam Bajgar^{1,2*} and Gabriela Krejčová^{1,2*}

¹Faculty of Science, Department of Molecular Biology and Genetics, University of South Bohemia, Ceske Budejovice, Czechia, ²Biology Centre, Institute of Entomology, Academy of Sciences, Ceske Budejovice, Czechia

Macrophages represent the most functionally versatile cells in the animal body. In addition to recognizing and destroying pathogens, macrophages remove senescent and exhausted cells, promote wound healing, and govern tissue and metabolic homeostasis. In addition, many specialized populations of tissue-resident macrophages exhibit highly specialized functions essential for the function of specific organs. Sometimes, however, macrophages cease to perform their protective function and their seemingly incomprehensible response to certain stimuli leads to pathology. In this study, we address the question of the origin of the functional versatility of macrophages. To this end, we have searched for the evolutionary origin of macrophages themselves and for the emergence of their characteristic properties. We hypothesize that many of the characteristic features of proinflammatory macrophages evolved in the unicellular ancestors of animals, and that the functional repertoire of macrophage-like amoebocytes further expanded with the evolution of multicellularity and the increasing complexity of tissues and organ systems. We suggest that the entire repertoire of macrophage functions evolved by repurposing and diversification of basic functions that evolved early in the evolution of metazoans under conditions barely comparable to that in tissues of multicellular organisms. We believe that by applying this perspective, we may find an explanation for the otherwise counterintuitive behavior of macrophages in many human pathologies.

KEYWORDS

Dictyostelium, acanthamoeba, Drosophila, plasmatocytes, archaeocytes, Porifera, macrophage polarization, origin of macrophages

Introduction

The human body is made up of more than two hundred types of cells (Castillo-Armengol et al., 2019). Unlike most cell types, macrophages display a striking level of functional versatility and an extraordinary degree of autonomy (Locati et al., 2020).

Macrophages represent the front line of the immune system, responsible for the recognition, phagocytosis, and elimination of pathogens and to control the inflammatory response by instructing other branches of the immune system via cytokine signaling (Cole et al., 2014). However, macrophage function is not limited to protection against foreign organisms. Macrophages are also involved in many homeostatic processes in the body (Biswas and Mantovani, 2012; Theret et al., 2019). Every day, millions of cells die in the human body and the constant substitution of cells and reconstitution of the extracellular matrix (ECM) governed by macrophages is fundamental for the health of any tissue in the body (Kwon et al., 2019; Batista-Gonzalez et al., 2020; Sender and Milo, 2021; Witherell et al., 2021).

Macrophages exhibit many specific characteristics predisposing them to be highly effective in the above functions. Macrophages are highly motile and crawl through the organism toward the site where they are needed (Xuan et al., 2015). Once in place, macrophages are sensitive to external signals and respond according to external conditions (Lavin and Merad, 2013). Their functional repertoire includes engulfing pathogens and removing damaged, senescent, or apoptotic cells. Internalized cellular material is processed and metabolically degraded in the phagolysosome. To this end, macrophages exhibit many specific metabolic pathways for processing and interconversion of phagocytosed organic material. In addition to sensing external signals, macrophages also excel in the production of a broad spectrum of signaling factors. Macrophages are central producers of cytokines in the body and are actively involved in interorgan signaling and regulation of homeostasis in healthy and pathological conditions (Arango Duque and Descoteaux, 2014).

The ability of macrophages to perform such a wide repertoire of functions is largely due to their metabolic plasticity. Sentinel macrophages typically reside in a quiescent state, referred to as M0, which serves as a baseline metabolic profile. From this state, macrophages can undergo metabolic polarization into various forms in response to different stimuli. Thus, various external factors trigger a specific macrophage expression program that leads to the modulation of major metabolic pathways to generate sufficient energy and specific metabolites required for an adequate functional response (Galvan-Pena and O'Neill, 2014). Therefore, metabolic polarization allows macrophages to adopt a specific functional polarization phenotype and perform unique functions efficiently (Liu et al., 2021). It was originally described that macrophages adopt two polarization phenotypes, defined as bactericidal (also known as pro-inflammatory; classically activated or M1) or healing (also known as anti-inflammatory; alternatively activated or M2) (Viola et al., 2019). However, more recent research has revealed many divergences from the polarized M1 and M2 types, such as metabolically activated macrophages (MMe) or macrophages activated by oxidized phospholipid (Mox) (Coats et al., 2017). Currently, the prevailing view is that M1 and M2 macrophages represent the two extremes of the entire continuum of all possible polarization phenotypes.

In addition to the general pro-inflammatory and homeostatic functions common to all macrophages, the population of tissue-resident macrophages found in virtually all tissues of the human body often perform highly specialized tasks (Nobs and Kopf, 2021). Among many others, some of the most well-studied tissue-resident macrophages include Kupffer cells in the liver, and microglia in the central nervous system, alveolar macrophages in the lungs, Langerhans cells in the skin, or peritoneal and adipose tissue macrophages (Wu and Hirschi, 2021). The progenitors of these tissue-resident macrophages migrate to destination tissue during embryonic development and their populations are sustained throughout the life of the individual by self-replication (Davies et al., 2013; Munro and Hughes, 2017). Tissue resident macrophages are functionally shaped by signaling factors characteristic for their particular tissue environment and exhibit distinct functional and morphological phenotypes. The role of tissue-resident macrophages ranges from fundamental functions,

such as antibacterial responses and removal of dead and senescent cells, to advanced functions, such as promoting stem cell proliferation, regulating local and systemic metabolism, promoting lipid metabolism and thermogenesis, controlling sinoatrial node action potential, governing hematopoiesis, regulating synaptic pruning, inducing vascularization, and removing amyloid plaques and other potentially harmful substances from the extracellular space (Gordon and Plüddemann, 2017).

From the preceding paragraphs, it is clear that the mononuclear phagocyte system represents a central system for maintaining homeostasis that controls many physiological processes. However, the role of macrophages in the organism is not beneficial in all circumstances, and macrophages also play a significant role in the induction of several pathological conditions (Sica et al., 2015).

Macrophages may become inadequately activated in response to external stimuli, resulting in behavior that may appear counterintuitive in certain situations (Parisi et al., 2018). Excessive production of pro-inflammatory factors or excessive deposition of ECM components often leads to tissue and organ dysfunction and progressive development of pathology.

Excessive pro-inflammatory macrophage polarization is typically observed in obesity, non-alcoholic fatty liver disease, atherosclerosis, and neurodegenerative diseases (Lauterbach and Wunderlich, 2017; Mammana et al., 2018; Barreby et al., 2022). Likewise, chronic adoption of M2 macrophage polarization is associated with liver fibrosis, chronic obstructive pulmonary disease, Alzheimer's disease, or cancer (Wang L. et al., 2019; Zhou et al., 2020). Pathologies in which macrophage activation plays a critical role are not limited to those listed here. In fact, lack of macrophage polarization plasticity in any tissue inevitably progresses to pathology. Nevertheless, the rationale behind the switch from the primarily protective role of macrophages to induction of pathology remains largely undetermined.

Fascinated by the functional versatility of macrophages, we seek to understand why macrophages have such an unusual degree of autonomy and responsibility. Understanding the evolutionary origins of macrophages may provide insight into how they have acquired critical properties necessary for their protective and homeostatic roles.

To reveal the origin of macrophages and their functional versatility, we decided to trace the characteristic features of mammalian macrophages back in the evolution of the animals. While investigating the origin of macrophage-like cells in the animal phyla, we realized that macrophage-like amoebocytes are present in virtually all multicellular animals.

We surmise that macrophage functional versatility reflects the ancient origin of these cells in free-living unicellular animals and that macrophage functional repertoire has further expanded with the emergence of multicellularity and the increasing complexity of the body plan of multicellular animals.

Information regarding unicellular animals and the emergence of multicellular animals is fragmented and can be inferred only from indirect evidence. Therefore, we decided to investigate the functional analogy between mammalian macrophages and free-living predatory amoeba (*Acanthamoeba*; Protists) (Tice et al.,

2016). We then combined this with knowledge from the clades represented by unicellular animals (Choanoflagellata, Filasterea, Ichtyosporidia; Holozoa) (Hehenberger et al., 2017) to formulate an idea of what functions may have already been present in the unicellular free-living ancestor of animals.

We next set out to compare the characteristic features of mammalian macrophages with those observed in a social facultative multicellular amoeba (*Dictyostelium discoideum*; Amoebozoa) (Romeralo et al., 2011) to explore the possibility that the emergence of multicellularity has gone along with the expansion of the functional repertoire of macrophage-like amoebocytes.

Following this idea, we compare the functions known in mammalian macrophages with those observed in macrophage-like amoebocytes in sponges (Porifera; Holozoa), which represent multicellular animals without yet fully differentiated tissues and organs (Nielsen, 2019) and can thus provide some indication of what functions might be present in macrophage ancestors at the emergence of multicellular organisms.

Subsequently, we analyzed the characteristics of primitive macrophage-like plasmatocytes in the fruit fly (*Drosophila melanogaster*; Metazoa, Insecta) as a representative of a simple animal with fully developed tissues and organs at a level of complexity comparable to that of mammals (Cheng et al., 2018). For a historical perspective on the early discoveries of macrophage functional variability, see Box 1. The phylogenetic relationship of the compared clades and lineages is shown in the Figure 1.

BOX1 Metchnikoff's predictions and the discovery of macrophages

More than a century has passed since Metchnikoff formulated his theory of phagocytosis as the central mechanism of the immune response, for which he was awarded the Nobel Prize (Kaufmann, 2008). The attention this hypothesis attracted in the scientific community has unfortunately overshadowed many of the other postulates Metchnikoff made regarding the function of macrophages in the body. These speculations become particularly interesting in light of current knowledge about the function of macrophages, which goes far beyond their bactericidal function in the organism (Tauber, 2003).

Metchnikoff discovered the immune role of macrophages when studying the function of mesodermal amoeboid cells moving freely in the body of primitive multicellular organisms. In doing so, he paid close attention to the role these cells play in nutrient acquisition in organisms that do not have a digestive cavity and identified how these cells shape multicellular organisms during evolution and ontogeny (Merien, 2016). Metchnikoff proposed that complex multicellular organisms are inherently disharmonious and that macrophages induce physiological inflammation to achieve a harmonious whole (Tauber, 2017).

Metchnikoff's exceptional observational skills and work ethic led him to recognize the importance of macrophages in maintaining nutritional, metabolic, and tissue homeostasis more than a century before the confirmation of this phenomenon by current molecular biological research.

Macrophage versatility is based on a few fundamental macrophage features

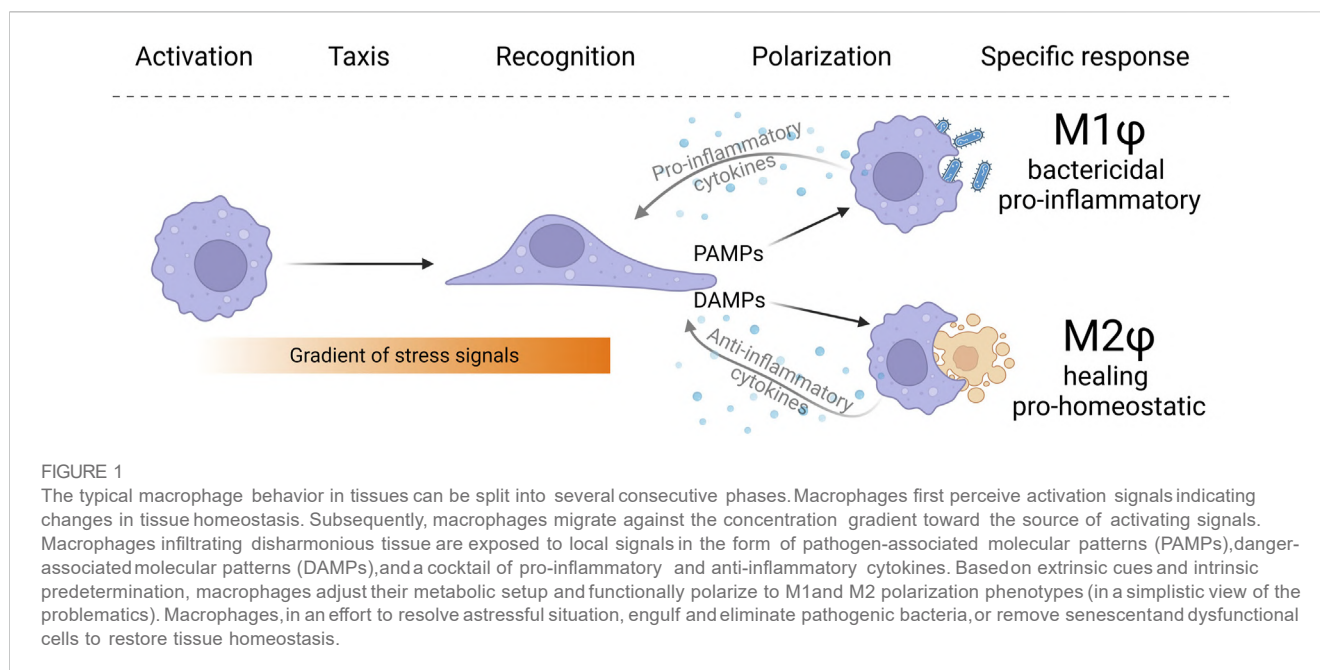
Although macrophages perform many functions in the body, their behavior can be divided into several basic features that make

them distinctly different from all other cells in the body. Generally, macrophages reside in the tissue in a quiescent state and calmly perceive signals from the environment (Holt and Grainger, 2012). Macrophages are equipped with a number of receptors for the recognition of chemoattractants and signaling substances that originate from indisposed cells and tissues, other immune cells, or produced by bacterial pathogens as their secondary metabolites. Most of the receptors recognizing the chemoattractant signals belong to the class of G-protein coupled receptors (GPCRs), such as formyl peptide receptor, folate receptor, adenosine receptor, purinergic receptors, and various chemokine receptors (Kim, 2018; O'Callaghan et al., 2021).

Upon chemokine recognition, the GPCR activates intracellular signaling that constitutes G-protein and arrestin as second messengers and leads to the activation of common stress response-related signaling cascades, such as PKC, PI3K-Akt, MAPK-ERK, AP, JAK-STAT, etc. The induced transcriptional program leads to increased cytoskeleton reorganization, cell shape changes, directed motility, secretion of lysosomal enzymes, phagocytosis, and activation of the respiratory burst (Wang X. et al., 2019).

Macrophages are chemotactically guided through the environment against the concentration gradient of extracellular chemical stimuli, such as chemokines, polyunsaturated fatty acid metabolites (leukotrienes and eicosanoids), components of the complement cascade (C3a, C5a), or formyl peptides (Sokol and Luster, 2015). Unlike most cell types in the mammalian organism, macrophages exhibit active migration, facilitated by rapid remodeling of the actin cytoskeleton. Macrophages primarily use two distinct types of migration, namely amoeboid and mesenchymal. Amoeboid migration is a rapid movement driven by an actin-rich pseudopod at the leading edge, hydrostatically generated blebs, and a highly contractile uropod at the trailing edge. This movement is characterized by weak or absent adhesion to the substrate and low-level proteolysis of the ECM. In contrast, mesenchymal movement is characterized by cell adhesion to the substrate via integrins, cadherins, or fibronectins and requires enzymatic disruption of binding to the ECM (Pizzagalli et al., 2022).

To effectively distinguish various pathogens from the body's own cells, macrophages must sense and recognize specific pathogen-associated antigens on the surface of the foreign cells. These molecules are recognized by immune-cell-specific receptors called pattern recognition receptors (PRRs) (Amarante-Mendes et al., 2018). Mammalian macrophages exhibit a wide spectrum of PRRs, categorized into several classes according to their structure. Many of these receptors, such as toll-like receptor family, scavenger receptors, c-type lectins, or NOD-like receptors, are evolutionarily ancient, and their ability to recognize pathogen-associated molecular patterns (PAMPs) has been shaped over the billions of years of coevolution between pathogen and host (Li and Wu, 2021). Antigen binding to PRR activates macrophage immune-related cascades, such as NFκB, ERK, JNK, and p38, which initiate complex signaling cascades that allow remodeling of the macrophage cytoskeleton and formation of membrane invaginations to engulf the particle and form a phagosome.



Subsequently, the primary phagosome fuses with acidic lysosomes, which contain a mixture of enzymes that cleave the phagocytosed material. During the respiratory burst, the NADPH oxidase NOX2 pumps massive amounts of reactive oxygen species (ROS) into the phagolysosome to destroy its contents. Elimination of pathogenic bacteria is enhanced by the activity of natural resistance-associated macrophage proteins (NRAMP) transporters, which pump divalent ions onto the phagolysosome lumen. Additionally, macrophages polarize toward a pro-inflammatory state, releasing a mixture of pro-inflammatory cytokines and opsonizing factors (Mogensen, 2009).

The underlying mechanism enabling these changes is the modification of cellular metabolism. Strikingly, pro-inflammatory macrophages adopt aerobic glycolysis as the predominant method of ATP production, driven by the stabilization of the transcription factor HIF1 α (Wang et al., 2017). While oxidative phosphorylation in mitochondria generates significantly more ATP per glucose molecule, M1 macrophages favor aerobic glycolysis, likely due to the rate of ATP production. In addition, aerobic glycolysis allows increased NADPH production in the pentose phosphate pathways, which is used as a building block for many biomolecules. Since pyruvate is converted to lactate by lactate dehydrogenase and excreted from the cell, the TCA cycle is supplemented with glutamine causing it to be “interrupted” or “rewired”. As a result, TCA cycle intermediates accumulate and contribute to further stabilization of HIF1 α . At the same time, mitochondria, which are liberated from generating ATP in oxidative phosphorylation, instead generate ROS by the reversed electron flux at the respiratory chain complex I (Viola et al., 2019). M1 polarization is also characterized by the specific utilization of arginine, which is converted by L-arginase to citrulline, and growth-inhibiting NO, which is transported to the phagolysosome (Palmieri et al., 2020).

M1 polarization is associated with the production of pro-inflammatory cytokines, such as IL-1, IL-6, or INF γ , which further inform other cells of danger (Nonnenmacher and Hiller, 2018). Once the pathogen is eliminated, the immune response is not yet complete, M2 macrophages need to be recruited to promote the resolution of inflammation and restore homeostasis.

In addition to pathogenic activation, macrophages are activated by signals produced by damaged, metabolically stressed cells and tissues, known as DAMPs (danger-associated molecular patterns), leading to M2 macrophage polarization (Ferrante and Leibovich, 2012). While the functions of M1 macrophages are relatively simple, the functions of M2 macrophages are more diverse. The main goals of M2 macrophages are to resolve inflammation, protect against viral and fungal infections, promote angiogenesis, facilitate ECM remodeling, support tissue healing, and regeneration, and remove senescent and damaged cells by efferocytosis (Wang L. et al., 2021). One of the important properties of M2 macrophages is the maintenance of immunological tolerance, i.e., the prevention of an immune reaction against host antigens. Thus, their function is particularly crucial in organs that must tolerate foreign antigens, such as those of the developing fetus or developing spermatids in the testis (Porta et al., 2009). This tolerogenic property also allows the presence of symbiotic bacteria. However, excessive adoption of M2 macrophage polarization may become detrimental as it induces tissue fibrosis, leading to chronic infections and promotion of tumor cell growth (Lin et al., 2019).

M2 macrophages differ significantly from their M1 counterparts in cellular metabolism, which determines their different function. While the amino acid arginine serves as a substrate for iNOS in M1 macrophages, as it is essential for the production of ROS (Rodríguez et al., 2017), M2 macrophages primarily use arginine

as a substrate for arginase, promoting its conversion to ornithine and urea. Ornithine is subsequently used as a substrate for forming ECM components, making M2 macrophages essential contributors to tissue regeneration and wound healing (Szondi et al., 2021). Hence, after the elimination of pathogenic invaders, pro-inflammatory macrophages are gradually replaced by M2 macrophages, which trigger the regeneration of the wounded tissue and promote vascularization, ECM synthesis, and inflammation resolution. In addition, M2 macrophages participate in ECM remodeling by producing matrix metalloproteases, cathepsins, and other enzymes that reorganize collagen fibers and by modulating fibroblast function (Witherell et al., 2021).

M2 macrophages are also responsible for maintaining tissue homeostasis under physiological conditions by detecting and removing apoptotic and damaged cells through efferocytosis. The term “efferocytosis” was introduced by deCathelineau and Henson, (2003) to describe the phagocytosis of apoptotic cells. Unlike phagocytosis of foreign objects, which triggers inflammation and antigen presentation, efferocytosis of apoptotic cells upregulates anti-inflammatory cytokines and compounds promoting tissue healing. During efferocytosis, macrophages are guided chemotactically to apoptotic and senescent cells through the detection of “find me” signals, such as nucleotides (ATP, ADP, or UDP), lysophosphatidylcholine, or sphingosine-1-phosphate (Ravichandran, 2010). The receptors responsible for recognizing apoptotic cells differ from those involved in phagocytosis. Subsequently, macrophages respond to “eat me” signal molecules, such as phosphatidylserine, oxidized phospholipids, DNA, or annexin A1, exposed on the surface of the cells destined for efferocytosis. While the engulfment process resembles macropinocytosis, the machinery fusing the efferosome with the lysosome is analogous to phagolysosome formation. Therefore, M2 macrophages exhibit a wide spectrum of enzymes that can metabolize phospholipids and DNA fragments and neutralize otherwise dangerous modified lipids and proteins (Martin et al., 2014).

M2 macrophages can be divided into different polarization subtypes, such as M2a, M2b, M2c, and M2d, based on the specific cocktail of chemokines, cytokines, and growth factors they polarize with and subsequently produce (Ross et al., 2021). In addition, plethoras of polarization phenotypes have also been described in the context of hypertrophic adipocytes or atherosclerotic plaques. For example, ingestion of heme by macrophages leads to the adoption of the Mhem polarization phenotype, internalization of hemoglobin to M (Hb), and the exposure of oxidized lipids to Mox (Lin et al., 2021). Since these macrophage subsets are often characterized only by mammalian-specific surface markers and do not exhibit a characteristic functional profile, tracking them during evolution is impossible (Natoli and Monticelli, 2014). For this reason, in this paper, we focus only on the functionally well-characterized macrophages M1 and M2 as representatives of the two phenotypic extremes.

Overall, macrophages are truly unique cells of the animal body that can play many roles in different tissues and body contexts by combining several specific properties. In particular, macrophages are exceptional at sensing chemotactic signals,

exhibiting controlled active motility, recognizing molecular patterns associated with pathogen or tissue damage, and adopting metabolic and functional polarization accordingly. These properties predispose them to deal with stressful situations in the body (Figure 2).

Macrophage functional repertoire has expanded with the increasing complexity of the animal body

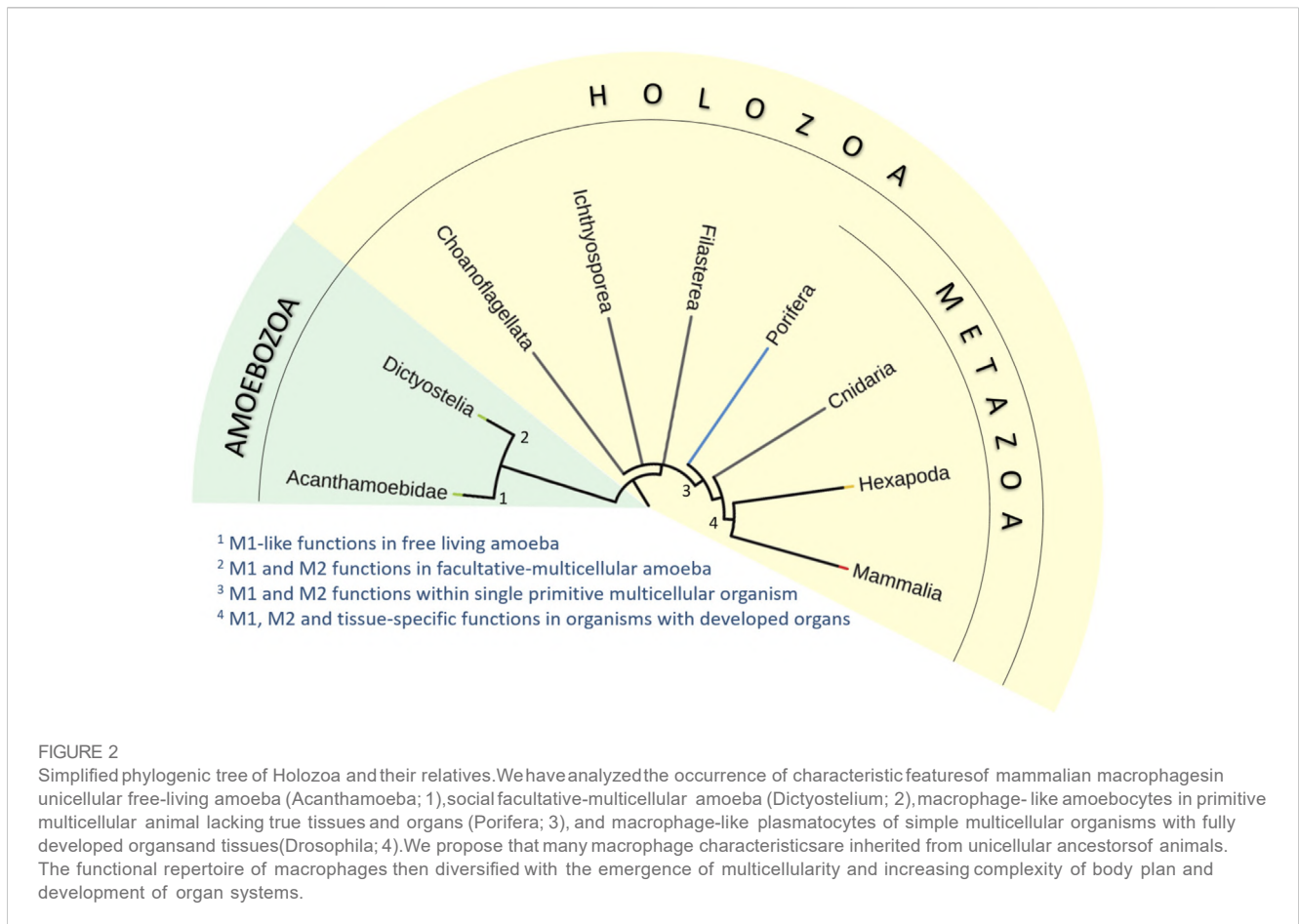
Free-living predatory amoebas share many similarities with M1 macrophages

By comparing the characteristics of mammalian macrophages with the prey-hunting strategies of free-living amoebae, we can find surprising similarities. *Acanthamoeba* and macrophages share the principal mechanisms used for chemotaxis towards bacteria, motility, interaction with bacteria, phagocytosis, the killing of bacteria in the phagolysosome, and production of antimicrobial peptides (Siddiqui and Khan, 2012a).

The underlying molecular mechanisms show a remarkable degree of similarity, documented by the fact that human intracellular pathogens use the same strategies to escape the bactericidal mechanism in the macrophage and *Acanthamoeba* (Molmeret et al., 2005). Therefore, *Acanthamoeba* is often viewed as a training ground for microbial organisms to become successful human and animal pathogens and a melting pot for horizontal gene transfer between different bacterial strains (Salah et al., 2009).

Acanthamoeba is a free-living heterotrophic Protist that specializes in hunting microbes for its nutritional needs. *Acanthamoeba* has two life stages; an active trophozooid or a dormant double-walled cyst, which can withstand adverse environmental conditions for long periods of time (Siddiqui and Khan, 2012b). In terms of life strategy, *Acanthamoeba* as professional phagocytic bactericidal omnivores do not differ significantly from the basal groups of Holozoa and are not expected to substantially differ from unicellular ancestors of animals (Lang et al., 2002).

Immediately, we can discern similarities between *Acanthamoeba* and mammalian macrophages with respect to size, behavior, cellular ultrastructure, and chemical composition (Rayamajhee et al., 2022). Like mammalian macrophages, *Acanthamoeba* can sense chemical signals from the environment and approach the signal source by chemotaxis through motility based on actin and myosin remodeling (Swart et al., 2018). In-depth studies of chemotactic factors have identified various bacterial metabolic products, such as formyl-methionyl-leucyl-phenylalanine, lipopolysaccharide, lipoteichoic acid, cAMP, lipid A, or N-acetylglucosamine. In analogy to mammalian macrophages, the perception of chemotactic signals in *Acanthamoeba* is mediated via GPCRs (Schuster and Levandowski, 1996). Most of these signals are products of bacterial metabolism or fragments of surface bacterial macromolecules and also serve as potent chemoattractants for mammalian macrophages and neutrophils (Nadesalingam et al., 2005).



A detailed study of crawling in free-living amoeba revealed that the migratory mechanisms used by macrophages and amoebae are identical (Campolo et al., 2021), indicating their ancient origin in the common ancestor of Amoebozoa and Opisthokonta.

Once macrophages approach the site of origin of chemotactic signals, they must recognize which cells are to be engulfed and eliminated in the phagolysosome. Many of the receptors used by macrophages to recognize pathogenic bacteria can also be found in some form in Acanthamoeba. For instance, the C-type lectin mannose receptor, which is abundantly expressed by mammalian macrophages, is used by Acanthamoeba to identify prey and engulf it (Allen and Dawidowicz, 1990).

Acanthamoeba recognizes and binds the bacteria, and the subsequent processes of phagocytosis and destruction of the pathogen show a high degree of similarity to mammalian macrophages. Pathogen recognition leads to massive reorganization of F-actin filaments in both macrophages and Acanthamoeba, resulting in dynamic probing, disruption of the cortical F-actin layer, nucleation and polymerization of F-actin filaments, phagosome closure, and particle internalization (Bowers, 1977; Alsam et al., 2005). Internalized bacteria are inactivated and enzymatically processed in the phagolysosome. Ultrastructural analysis of Acanthamoeba revealed that they contain many lysosomes containing a cocktail of degradative enzymes (Alsam et al., 2005; Salah et al., 2009). After fusing the

phagosome with the lysosome, V-ATPases embedded in the phagolysosomal membrane pump hydrogen ions inside the phagolysosome to acidify the phagolysosomal lumen (Akya et al., 2009). The bacteria are then exposed to superoxide ions and hydrogen peroxide, in a process called oxidative burst. The active form of oxygen is produced in the lumen of the phagolysosome by NADPH oxidase activity, supported by altered mitochondrial metabolism (Rayamajhee et al., 2022). To further inhibit the ability of bacteria to avoid the phagolysosome, additional transporters are housed in the phagolysosomal membrane. NRAMPs transport sequestered divalent ions (Mn^{2+} , Fe^{2+} , Zn^{2+} , and Cu^{2+}) outside the phagolysosomes, thereby limiting the ability of engulfed bacterial to use metalloenzymes required to escape the phagolysosome (Siddiqui et al., 2019).

Overall, mammalian macrophages and Acanthamoeba display striking similarities in the molecular mechanisms involved in directional motility, recognition, binding, engulfment, and phagolysosome processing of bacteria.

To get a better idea of the characteristics of the last unicellular common ancestor of animals, we can compare the genomic information of primitive multicellular animals with their unicellular relatives forming the basal clades in a phylogenetic tree of Holozoa, such as Filasterea, Ichthyosporea, and Choanoflagellata (Ros-Rocher et al., 2021). We can assume that the genes shared by these groups were already present in the

unicellular ancestors of modern multicellular animals. Therefore, we can expect that the last unicellular ancestor of animals already possessed a wide repertoire of genes required for multicellularity, such as molecules for intercellular adhesion, communication, and interaction with the ECM (King, 2004). We speculate that many of these genes are analogous to those characteristically used by macrophages to carry out similar functions.

Given that most of the characteristic features of macrophages observed in *Acanthamoeba* are associated with bacterial recognition, endocytosis, and elimination, we hypothesize that these abilities later evolved into a protective bactericidal function as part of the host immune response in multicellular animals (Hartenstein and Martinez, 2019). This suggests that the evolutionary origin of the bactericidal function of mammalian macrophages arose prior to the branching of Amoebozoa and Opisthokonta, most likely in the environment of a free-living unicellular amoeboid cell.

Moreover, this implies that the features underlying the function of M1 bactericidal macrophages represent an ancestral macrophage phenotype and that M2-like macrophage features arose later in evolution, potentially coinciding with the emergence of multicellularity, as discussed in the following paragraphs.

Macrophage homeostatic features arose along with multicellularity

Based on comparisons of macrophages with free-living predatory *Acanthamoeba* and basal unicellular relatives of metazoans, we hypothesize that many specific features of macrophages associated with their bactericidal function derive from unicellular animal ancestors. However, *Acanthamoeba* does not possess analogous homeostatic, regulatory, and metabolic functions as mammalian macrophages. We, therefore, explore the possibility that the functional repertoire of macrophages has expanded substantially with the evolution of multicellularity.

We explore the analogy between the features observed in mammalian macrophages and *D. discoideum*, a close relative of *Acanthamoeba*, used as a model organism to investigate facultative multicellularity (Bozzaro, 2013). *Dictyostelium* possesses a complex life cycle. Typically, *Dictyostelium* resides in the vegetative state of free-living haploid amoeba that divide periodically by mitosis and prey on microbes for nutrition. When food becomes scarce, starving vegetative amoebae enter a social life form, or a sexual cycle. During the social cycle, the amoebae aggregate to form a multicellular pseudoplasmodium (also known as a slug). The slug conforms to all the parameters of a multicellular organism. The originally amoeboid vegetative cells differentiate into four distinct cell types that coordinate their behavior and give rise to a fruiting body that produces resistant spores (Flowers et al., 2010).

In terms of their biology, the vegetative cells of *Dictyostelium* resemble the trophozooids of *Acanthamoeba*. Therefore, it is not surprising that, like *Acanthamoeba*, vegetative cells of *Dictyostelium* also share many features with mammalian pro-inflammatory macrophages (Bozzaro and Eichinger, 2011). Observations from *Dictyostelium* vegetative cells conveniently complement our previous statements, discussed in the following paragraph. Interestingly, despite the vegetative cells of *Dictyostelium* being

freely motile, we can observe a certain degree of sociality. The behavior of these vegetative amoebae is coordinated by mutual communication of soluble signaling factors, which could provide the basis for the later emergence of cytokine signaling in macrophages. In fact, similar communication has been observed in *Acanthamoeba* (Golé et al., 2011).

Vegetative cells of *Dictyostelium* perceive signals from their environment and localize bacteria as a nutrient source through a gradient of their secondary metabolites, such as folic acid, retinoic acid, lipopolysaccharides, and lysophosphatidic acid (Iglesias, 2012). The perception of these chemotactic signals is mediated by GPCRs (e.g., folic acid receptor, retinoic acid receptor) that trigger strong chemotaxis and foraging behavior (Iglesias, 2012). Recently, it was shown that vegetative *Dictyostelium* cells are also attracted to signaling factors of a non-biological nature. Exposure of vegetative cells to a gradient of Mg^{2+} , Zn^{2+} , or hydrogen peroxide induces high chemotactic motility (Consalvo et al., 2019). Most factors that activate vegetative amoebae of *Dictyostelium* also have a strong activating and chemotactic effect on mammalian macrophages (Cammer and Cox, 2014). This is consistent with the observation that the vast majority of receptors carried by vegetative cells of *Dictyostelium* are retained in mammalian macrophages. Indeed, exposure of macrophages to the chemoattractants mentioned above leads to increased macrophage motility (Xu et al., 2021).

Dictyostelium is equipped with a wide spectrum of receptors that recognize pathogens and other cells to be engulfed, which are classified as (PRRs). These surface receptors show substantial homology to many mammalian PRRs, such as scavenger receptors (LIMP-2), toll-like receptors (tirA, tirB), leucine-rich repeats receptors (LrrA), and C-type lectin receptors. Activation of these receptors triggers intracellular signaling cascades initiating phagocytosis, phagosome maturation and bacterial killing, and stress-related cascades and detoxification response (Dunn et al., 2018).

The process of F-actin remodeling and phagolysosome formation starts with the activation of one of the GPCRs. For example, activation of the folate receptor or the homolog of the toll-like receptor tirA leads to activation of conserved RAS-PI3K and ERK-MAPK signaling, resulting in induction of actin polymerization, increased motility and phagocytosis (Chen et al., 2007). Actin nucleation and branching are mediated by actin remodeling complexes consisting of WASp Arp2/3 and SCAR/WAVE proteins (Vogel et al., 1980). The mechanism described above in *Dictyostelium* resembles that observed in mammalian macrophages, in which activation of surface toll-like receptors (TLRs) or Fc receptors analogously initiates increased motility, phagocytosis, and production of pro-inflammatory factors (Schmitz et al., 2004). The detailed mechanism of phagolysosome maturation in *Dictyostelium* is now well described (Cosson and Lima, 2014). Interestingly, this mechanism is principally homologous to that of mammalian macrophages. Internalized bacteria are eliminated in the phagolysosome by the sequestration of divalent ions by the activity of NRAMT transporters and by ROS production by the mitochondrial NADH-dependent oxidase NOX2 (Lardy et al., 2005). Maturation of the phagolysosome containing indigestible bacterial remnants leads to their exocytosis and neutralization of

the phagolysosome. Alternatively, ingested bacterial remnants are processed by autophagy, which is particularly important during starvation and infection by intracellular pathogens (Mesquita et al., 2017). The remarkable analogy of these processes between Dictyostelium and the mammalian macrophage rule out the possibility of convergent evolution and further supports the adoption of features characteristic of bactericidal macrophages already in our unicellular ancestors. In general, many features of vegetative amoebas of Dictyostelium resemble those observed in M1 mammalian macrophages.

In certain situations, vegetative amoeboid cells can switch from unicellular to multicellular life. Amoeboid vegetative cells constantly coordinate cell growth and division through signals that inform each other about their density and nutrient availability (Loomis, 2014). Nutritionally supplied cells continuously produce prestarvation factor (PSF), which inhibits cell behavior leading to aggregation. When PSF production decreases due to nutrient deficiency, cells begin to produce conditioned medium factor (CMF), which triggers the release of a pulse of cAMP. The cAMP signal is further amplified by surrounding cells, creating a concentration gradient that allows aggregation (Clarke and Gomer, 1995).

The cellular cascade that transduces the extracellular cAMP signal is of particular interest. Extracellular cAMP binds to the G-protein-coupled chemoattractant receptor cAR1, which serves as a docking receptor for β -Arrestin. This interaction triggers signaling through second messengers well known from mammalian cells, such as GSK3, ERK, Ras/GTP, and PI3K, and leads to activation of the effectors PKB, PKA, STAT, and TORC2, which drive an expression program controlled by the GATA family transcription factors (Loomis, 2014; Singer et al., 2019).

The transition from the unicellular to the multicellular life stage is associated with significant transcriptomic changes. These changes are achieved primarily through the propagation of repressive epigenetic modifications that functionally shape amoeboid cells to become more cooperative. ATAC-seq analysis of vegetative cells undergoing transition revealed that the most significantly enhanced genes are classified as factors regulating ECM organization, cell adhesion, differentiation, and morphogenesis (Wang S. Y. et al., 2021). Recently, it has been shown that alternation of mitochondrial metabolism is a prerequisite for adopting tolerogenic cell behavior and multicellularity (Glöckner et al., 2016; Singer et al., 2019; Kelly et al., 2021). This process highly resembles cAMP tolerogenic behavior of mammalian myeloid cells required for macrophages to perform tissue homeostatic tasks. (Sciarra et al., 2014).

When transitioning to the social phase of the life cycle, Dictyostelium cells inevitably encounter many problems common to multicellular animals, indicating an increased need for self-recognition and regulation. Previously, it has been described that the social life stage of Dictyostelium is associated with various types of cellular relationships, such as cheating and allocheating, but also altruism and self-sacrifice (Strassmann and Queller, 2011).

The multicellular body of the pseudoplasmodium consists of thousands of cells. Most of the cells in the body are destined to form future morphological structures of the sorocarp, such as stem cells, cup cells, and spores (Jang and Gomer, 2011). However, when tracing the evolution of macrophage-like features, a fourth subpopulation of sentinel cells deserves particular attention.

Sentinel cells have protective, homeostatic, and regulatory functions and, therefore, resemble the primitive immune system of multicellular organisms. Sentinel cells are free-moving cells that phagocytose bacteria and toxins until they are eventually eliminated. Compared to other slug cells, sentinel cells show increased expression of the gene coding for Toll-interleukin receptor domain-containing protein (tirA), which is analogous to the mammalian toll-like receptors (Brock et al., 2016a).

Sentinel cells protect the slug from potentially pathogenic bacteria by releasing extracellular DNA traps and producing ROS to the external space (Zhang and Soldati, 2016). In case of infection by intracellular bacteria, sentinel cells cleanse the slug of infected cells, keeping the rest of the organism healthy and giving rise to uninfected spores (Farinholt et al., 2019). In addition to their protective role, sentinel cells exhibit a high degree of tolerogenic behavior and can discriminate between genetically related and unrelated cells in aggregation (Hirose et al., 2011). Thus, in the multicellular stage of life, only closely related cells are nourished by sentinel cells. Indeed, their tolerogenic internal predetermination is represented by the rather unexpected observation that the multicellular stage of Dictyostelium can maintain commensal bacteria, in a specific form of farming for nutritional symbiosis (Brock et al., 2013; Brock et al., 2016b). By these features, these sentinel cells of the slug resemble the functions of mammalian M2 macrophages.

Collectively, the features observed in Dictyostelium cells during the transition from the unicellular to the multicellular life stage may provide critical insight into how macrophage-like features emerged with multicellularity in animals.

To explore this idea, we took inspiration from a study that compared the genomes of multicellular animals and their unicellular relatives to identify the genes present in the last common multicellular ancestor of animals which expanded upon the emergence of multicellularity (Ros-Rocher et al., 2021). Such genes are mostly related to intercellular signaling, signal transduction, adhesion molecules, and regulators of the cytoskeleton. Furthermore, multicellular animals also show an increase in the repertoire of transcription factors and genes mediating epigenetic modifications, suggesting the need for temporal functional plasticity and restriction of specific traits to certain subpopulations of cells in the multicellular body (Hinman and Cary, 2017; Herron et al., 2018).

As mentioned, we may assume that the transition to multicellularity is conditioned by several adaptations on various levels of regulation, including epigenetic remodeling, transcriptional programming, metabolism, and cell behavior. The most significant changes are related to enhanced expression of adhesive molecules, signaling factors, enzymes involved in remodeling of ECM, and adoption of tolerogenic predetermination.

Comparison of macrophage-like properties in unicellular vegetative amoebae and sentinel cells in multicellular slugs reveals a functional shift of macrophage-like properties, from clearly pro-inflammatory and bactericidal, to protective but also tolerogenic and regulatory. Furthermore, we speculate that many of the functions that arose in unicellular amoebae to hunt microbes were functionally repurposed and served as a solid basis for the evolution of multicellularity. For an overview of the evolving hypotheses concerning the primary cell type in animals, see Box 2.

BOX 2 macrophages in perspective of emerging multicellularity

The emergence of multicellular animals is a fascinating event in the evolution of metazoans. Formulation of the theory of common descent in the nineteenth century led many famous evolutionary and developmental biologists to seek a thorough explanation of what the hypothetical last common ancestor of all animals (the mysterious “Urmetazoan”) may have looked like (King, 2004). Among the most famous is Earnest Haeckel, whose theories suggested that the most ancestral animal cell was the amoeboid cell, which, under certain conditions, could have progressed to the colonial stage of life (Brunet and King, 2022). However, this theory was challenged by Elie Metchnikoff, who was convinced that the most ancestral animal cell was equipped with a flagellum, as is observed in basal groups of Holozoa, such as Porifera and Choanoflagellata (Brunet and King, 2022). However, Metchnikoff's theory had major discrepancies, as it failed to explain the striking similarity between the amoeboid cells observed in animals and the unicellular Protista.

Recently, this obstacle has been resolved by the discovery that Choanoflagellata are able to switch to amoeboid cells under certain circumstances (Brunet et al., 2021). In addition, it has been found that amoeboid cells can give rise to all other cell types in Porifera (Müller, 2006). This suggests that amoeboid cells represent the most ancestral cell type in metazoans, and that the amoeboid cell type has been retained and is present throughout the metazoan phylogenetic tree, rather than being evolutionarily discontinued (Brunet and King, 2017). According to the current generally accepted theory, the ancestor of animals was a facultative multicellular organism that alternated cell types between free-moving social amoebae and a multicellular stage in which amoebocytes differentiate into collar containing flagellated cells (Brunet and King, 2017). As the complexity of multicellular organisms increased, as did the need for molecules responsible for cell colony cohesion, signaling, cell differentiation, and maintenance of homeostasis (Brooke and Holland, 2003; Grau-Bové et al., 2017).

Macrophage-like amoebocytes perform both M1 and M2 features within Porifera

In the previous section, we described that in the multicellular stage of the social amoeba *D. discoideum*, subpopulations of sentinel cells retain features of professional phagocytes, and play a protective, regulatory, and homeostatic role in the pseudoplasmodium. This raises the question of whether the presence of amoeboid cells fulfilling these tasks is essential for the functioning of multicellular organisms. Virtually every known multicellular animal has a highly motile professional phagocyte that performs protective, healing, regenerative, regulatory, and homeostatic functions in the organism (Brunet et al., 2021).

We can gain a comprehensive understanding of the range of functions that professional phagocytes can perform in a primitive multicellular organism by studying sponges (Porifera), which represent a phylum of basal multicellular organisms with incomplete tissues and organ systems (Feuda et al., 2017). Members of Porifera phylogenetically represent the most ancestral metazoans. They are primitive multicellular heterotrophic organisms and represent the sister group of multicellular animals. These aquatic creatures depend on filtering water from which they obtain nutrients. Although they lack distinct tissues and organs, such as nervous, digestive, or circulatory systems, they possess several cell types with specialized functions (Thacker et al., 2014).

The structure of the sponge body is relatively simple. The body is formed by a gel-like, amorphous matrix called the mesohyl, sandwiched between two layers of cells, the outer pinacoderm

and the inner choanoderm. The mesohyl is composed of ECM components commonly found in other animals, such as collagen, dermatopontin, galectin, and fibronectin-like glycoproteins (Dahihande and Thakur, 2021). Most sponges live a sedentary lifestyle and filter nutrients from the water using specialized cells called choanocytes. Choanocytes are equipped with flagella, whose movement creates water flow, and cilia, which form a filtering collar to trap food particles. The food particles are internalized by the choanocytes by nutritive phagocytosis and processed in food vacuoles (Laundon et al., 2019). Nutrients must then be distributed throughout the body, from choanocytes to other cell types. This function is performed by archaeocytes, which receive nutrients from choanocytes and transport them, by virtue of their high motility, throughout the mesohyl to the nutritionally demanding cells (Hartenstein and Martinez, 2019).

As already mentioned, the protective role of macrophages originates from the wild unicellular ancestors of animals, in which it evolved as a nutritional phagocytosis of bacteria. Choanocytes and archaeocytes are professional phagocytic cells in Porifera. The identity of these cells is not completely fixed and both cells can undergo a change to the opposite cell type under certain conditions. As such, it is difficult to distinguish which of these two cell types represents the ancestor of macrophages in bilaterians (Nakanishi et al., 2014). Since archaeocytes are freely motile and play a protective role in sponges, they show functional similarities to macrophages of bilaterians, therefore, it is feasible that archaeocytes represent the ancestors of these cells. The mechanism of nutrient uptake by choanocyte-like cells and nutrient distribution by freely motile amoebocytes is highly conserved in animals, with the exception of vertebrates and insects (Hartenstein and Martinez, 2019).

Archaeocytes, also called amoebocytes, are macrophage-like cells dispersed in the mesohyl of the sponge. Archaeocytes are unique from other sponge cells because they retain a significant degree of totipotency and can give rise to any other cell type. An isolated suspension of archaeocytes can regenerate the entire body of sponges, suggesting that they represent their ancestral cell type (Ereskovsky et al., 2021).

Archaeocytes were originally described by Elie Metchnikoff in 1892 and denoted as macrophages of the sponge by Van de Vyver more than a century later (Müller, 2003). Sponges are exposed to many potential pathogens and foreign particles from filtering the water and need an effective system for their elimination (Dzik, 2010). Archaeocytes play a central role in the protection of sponges from pathogens. Sequencing of the Porifera genome revealed that sponges exhibit a broad spectrum of pathogen recognition receptors that are homologous to the main PRR groups found in mammals, such as GPCRs, NOD-like receptors, cysteine-rich receptors, scavenger receptors, and receptors from the immunoglobulin superfamily (Wiens et al., 2005; Srivastava et al., 2010). A recent study also documented the presence of the TLR-mediated signaling cascade (Germer et al., 2017).

Upon recognition of PAMPs, archaeocytes activate the signal transduction pathway in which MyD88 acts as a second messenger and activates effector transcription factors known in mammalian immune response, such as IRAK, TRAFs, and NF- κ B (Müller et al., 2009). Activation of these immune-related pathways induces the

production of galectins, perforins, and ROS as molecules participating in the opsonization of the pathogen and its elimination (Wiens et al., 2005). Until now, 39 different lectins have been identified in the genomes of the Porifera phylum, including C-type lectins, tachylectin-like, F-type lectins, and galectins (Gardères et al., 2015). Thus, archaeocytes, after their activation by pathogens, exhibit features, and behavior with a high degree of homology to mammalian proinflammatory macrophages.

However, many situations require an advanced level of coordination and tolerant behavior of archaeocytes. In the following paragraphs, we will discuss the indispensable role of archaeocytes in immune tolerance, healing, regeneration, self-identification, and reproduction.

Archaeocytes display surprising tolerogenic potential, as commensal bacteria do not invoke bactericidal behavior. However, the tolerogenic mechanism has not yet been satisfactorily elucidated (Maldonado, 2016; Carrier et al., 2022). Archaeocytes are also indispensable for healing and tissue regeneration (Boury-Esnault, 1977). During healing, the wound is infiltrated by archaeocytes and damaged cells are cleared from the local environment. Archaeocytes then secrete components of ECM and differentiate into other cell types, giving rise to the regular structure of the body. At this point, the archaeocytes may also phagocytose the grey cells, which contain large amounts of glycogen and osmiophilic inclusions and thus serve as a nutrient reservoir (Fernández-Busquets et al., 2002).

Sponges possess the ability of whole body regeneration, either from a body fragment or by aggregation of dissociated cells. After the cells of the sponge body are dissociated to a cell suspension, the cells dedifferentiate to amoebocyte morphotypes, and the archaeocytes represent the most abundant cell type in the suspension. Subsequently, the cells aggregate, presumably due to pseudopodial activity, and differentiate into the appropriate cell types to form the body of the sponge (Buscema et al., 1980). Strikingly, if the bodies of two distinct sponges are dissociated into single-cell suspension, the cells sort in a species-specific manner and the two individuals are eventually reconstituted. Moreover, archaeocytes are sufficient to reconstitute functional sponges without any other cell type (Lavrov and Kosevich, 2014). Hence, they represent the totipotent stem cells of the organism. These observations undeniably demonstrate Porifera's ability to recognize its own genetically related cells from others.

Transplantation studies have further contributed to the understanding of this phenomenon. Whether a graft is accepted or rejected depends on the phylogenetic distance between the recipient and the donor. It has been shown that a graft comprised of cells from the same species and strain fuses with the recipient and is eventually accepted. Transplantation of an allograft causes the formation of a barrier between the transplanted tissues or a cytotoxic reaction at the graft interface, leading to the separation of the allograft cells (Smith and Hindeman, 1986). A small subset of cell types are involved in allograft rejection. Archaeocytes and lophocytes, which are recruited from the mesoglea and migrate along the border of both tissues, either phagocytose healthy donor cells to separate the tissues or exhibit cytotoxic activity to destroy cells in contact (Gaino et al., 1999; Fernández-Busquets et al., 2002).

Overall, the presented information indicates that archaeocytes perform characteristic functions of M1 bactericidal and M2 tolerogenic macrophages within signal organisms according to the situational context. Particularly, archaeocytes display an exceptional level of totipotency and autonomy (Zhang et al., 2003; Müller, 2006). We may speculate that archaeocytes execute important regulatory tasks in the sponge body and thus functionally precede the role of neural and endocrine system.

We observe that as the complexity of multicellular organisms increases, the repertoire of functions performed by macrophage-like amoebocytes increases. This can be attributed to the need for a higher degree of regulation and maintenance of homeostasis or to the fact that specialized cells (in this case choanocytes) have taken over the original nutritional function of amoebocytes, thus providing macrophages with the opportunity to acquire additional diverse functions.

Macrophage-like cells in animals with specialized tissues display rich repertoire of functions

Considering macrophage functions have diversified in animal evolution with the increasing complexity of the body, it is important to pay close attention to the macrophage-like plasmatocytes in *D. melanogaster*, a simple animal with clearly defined tissues and organs.

Drosophila is a simple, genetically tractable model organism, often used to model human diseases. Over a century of genetic and molecular biological research has led to many fundamental discoveries and a knowledge base that is unparalleled by any other invertebrate model used for biological research (Jennings, 2011). Research on the innate immune system of *Drosophila* has provided one of the major breakthroughs in immunology, the discovery of the Toll receptor and downstream immunity-related signaling cascade (Lemaitre et al., 1996). Since then, *Drosophila* has become a widely used model organism for research on host-microbe interactions, immune signaling pathways, wound healing, phagocytosis, clearance of apoptotic and damaged cells, tissue repair, immuno-metabolism, etc. (Razzell et al., 2011).

Most innate immune pathways known in mammals are highly conserved in *Drosophila*, including PRRs, second messengers, transcription factors, and effector molecules (Govind, 2008). Given that the conservation of immune pathways has been extensively described in many previous works, we mention them only briefly with emphasis on their evolutionary development and instead focus on immune-unrelated properties of plasmatocytes, such as their role in morphogenesis, regulation of metabolism, their tissue-specific roles, and their ability to phenotypically polarize.

Compared to basal clades of animals, the *Drosophila* immune system shows several significant advances. Firstly, the cellular branch of the immune system is represented by three distinct cell types with characteristic immunity-related functions. Crystal cells and lamellocytes are essential for the melanization reaction and the encapsulation of foreign objects that cannot be simply phagocytized, such as parasitoid eggs. Plasmatocytes are professional phagocytes that resemble macrophages in many of their properties (Gold and Brückner, 2015) with a high degree of molecular conservation of the underlying mechanisms (Melcamed et al., 2019).

The evolutionary novelty of the tunable immune response can be further documented by the variation of immune cascade activation following the recognition of different pathogens by PRRs on plasmatocytes. While fungi and Gram-positive bacteria elicit an immune response by activating the Toll receptor, Gram-negative bacteria predominantly activate the peptidoglycan receptor PGRP-LC and the downstream immune cascade IMD (DeGregorio, 2002). The components of the Toll and IMD immune cascades are highly conserved and show homology with downstream signaling from Toll-like receptors, NOD, GPCRs, and TNFR (Martinelli and Reichhart, 2005). Importantly, the diversity of immune-related signaling pathways enables the production of a cocktail of destructive effector molecules specifically tailored to the given pathogen, leading to an effective immune response while limiting immune-mediated damage to the host.

Moreover, the immune-related signaling pathways are accompanied by the production of various signaling factors that further influence other branches of the immune system and modify the function of other organs and tissues. Many of these factors can be denoted as true cytokines because their mammalian homologues are important regulators of the immune response, such as unpaired3 (IL-6) or eiger (TNF α) (Vanha-aho et al., 2016).

In addition to their protective functions, plasmatocytes also have many macrophage-like properties essential for tissue homeostasis. They are responsible for clearing apoptotic, senescent, and damaged cells through efferocytosis and express various genes required for the remodeling of the ECM (Preethi et al., 2020). These abilities predispose them to play important roles in fundamental processes of multicellular organisms, such as embryonic morphogenesis, tissue healing, and regeneration. Indeed, plasmatocytes are essential for the patterning and developmental morphogenesis of the ventral nerve cord, intestine, heart, and skeletal muscle (Yamitzky and Volk, 1995; Olofsson and Page, 2005).

However, the participation of plasmatocytes in embryonic morphogenesis can be disrupted by the production of danger signals. In an experimental model of laser-induced injury in the *Drosophila* embryo, plasmatocytes are attracted to the site of the wound by oxygen peroxide produced by the injured cells. Plasmatocytes infiltrating the wounded tissue clear the damaged cells and provide ECM components and growth factors necessary for tissue regeneration (Wood et al., 2002). Interestingly, the underlying mechanism of wound healing that includes transcription factors, actin organization, cell infiltration, and morphogenesis appears to be conserved between *Drosophila* and mammals at the molecular level (Belacortu and Paricio, 2011).

Although it has been well documented that *Drosophila* plasmatocytes can perform both bactericidal and healing functions, the question whether plasmatocytes adopt functional and metabolic polarization has not yet been satisfactorily answered. Upon bacterial infection in adult flies, plasmatocytes enter a state that closely resembles the pro-inflammatory polarization of mammalian macrophages. Plasmatocytes stimulated by streptococcal infection exhibit increased transcriptional activity of hypoxia-inducible factor 1 α (HIF1 α), a master regulator of metabolic reprogramming in mammalian M1 macrophages. The transcriptional program directed by HIF1 α is required for the infection-induced increase in glycolytic flux, glucose consumption, and accelerated conversion of pyruvate to

lactate in *Drosophila* plasmatocytes. This metabolic reprogramming, which closely resembles aerobic glycolysis in mammalian M1 macrophages, is essential for increased bactericidal activity of plasmatocytes and resistance of flies to bacterial infection (Krejčová et al., 2019). Transcriptomic data obtained in an independent experimental system indicate that metabolic rearrangement of plasmatocytes may be a general prerequisite for the bactericidal function of these cells (Ramond et al., 2020).

Plasmatocyte polarization that resembles mammalian M2 macrophages has been observed in an experimental model of retinal tissue injury. In this scenario, plasmatocytes infiltrate the wound and promote tissue healing, presumably by increasing the expression of arginase, an enzyme promoting the conversion of arginine to ornithine necessary for tissue regeneration (Neves et al., 2016), which is the hallmark of M2 macrophage polarization in mammalian macrophages (Rath et al., 2014). Whether plasmatocytes adopt an M2-like phenotype during other situations, such as during efferocytosis or wound healing, remains to be investigated.

The idea of functional diversification of plasmatocytes in *Drosophila* also finds support in single-cell transcriptomic analysis of *Drosophila* immune cells. The available data suggest that despite the morphological uniformity, plasmatocytes consist of more than ten distinct subpopulations that differ markedly in their expression pattern and expression of characteristic markers (Cho et al., 2020; Tattikota et al., 2020). Albeit, functional confirmation of these observations is currently lacking. In depth analysis of single-cell data revealed that a particular population of plasmatocytes express a substantial number of genes related to lipid metabolism, lipid catabolism, and sphingolipid processing, indicating certain adipocyte features are also present in plasmatocytes (Tattikota et al., 2020).

Of the many situations in the fly life cycle, the most important metabolic role of plasmatocytes, arguably, during metamorphosis. During the transition of the larva into the adult, the lymph gland is broken down, and plasmatocytes are released into the circulation (Kharat et al., 2022). The vast majority of larval tissues undergo extensive histolysis, and adult tissues form de novo from imaginal discs. However, the energy accumulated during the larval life stage must be transferred to the adult (Merkey et al., 2011). Thus, cells that are no longer needed are removed during metamorphosis by plasmatocytes infiltrating the histolysis-undergoing tissues. Within a short period of time, thousands of cells must be efferocytosed and the building material recycled into a suitable, reusable form (Storelli et al., 2019). In this situation, cells predisposed to efficient processing of lipids and sphingolipids may be highly desirable.

Plasmatocytes not only serve as metabolically active cells per se, but also significantly regulate the metabolism of other tissues. During bacterial infection, plasmatocytes produce the factor called Imaginal morphogenesis protein-Late2 (ImpL2), which reduces insulin signaling in the fat body. In turn, the fat body produces lipoproteins and carbohydrates that replenish activated immune cells (Krejčová et al., 2019). Thus, plasmatocytes orchestrate metabolic homeostasis and nutrient redistribution during the stress response. Their role in regulating systemic metabolism has been further documented in flies fed a high-fat diet. During excessive energy intake, plasmatocytes exposed to

excessive lipids secrete IMPL2, leading to increased circulating glucose levels. Therefore, suppression of Impl2 in plasmatocytes improves metabolism in obese flies (Morgantini et al., 2019). The pro-inflammatory effect of lipids on plasmatocytes was confirmed in an independent study. Plasmatocytes exposed to excessive amounts of lipids engulf the lipids through the activity of the scavenger receptor croquemort, which is homologous to mammalian CD36. Lipid accumulation in the plasmatocyte cytosol leads to increased production of the cytokine unpaired3 (upd3) and systemic attenuation of insulin signaling via JAK/STAT signaling (Woodcock et al., 2015). Interestingly, upd3 production by plasmatocytes may have an adaptive significance in addition to its pathological role analogically to Impl2. It has been shown experimentally that sustained production of UPD3 by plasmatocytes is required for the regular distribution of lipids between tissues in the body and that a missing UPD3 signal leads to lipid accumulation in muscles (Kierdorf et al., 2020).

It is unclear whether *Drosophila* has tissue macrophages as we know them in mammals. Functionally, the cells that most closely resemble the concept of tissue macrophages in *Drosophila* are cells that can be functionally considered as microglia. Microglia are the resident macrophages of the mammalian central nervous system (CNS) and are responsible for the immune protection of neurons and elimination of toxic and harmful substances, and for the maintenance, neuronal pruning, and proper functioning of synapses in CNS (Lee et al., 2021).

Glial cells in *Drosophila*, similar to their mammalian counterpart, form the brain-blood barrier and maintain homeostasis of the CNS of flies. Although no plasmatocytes reside in the *Drosophila* brain under physiological conditions, glial cells display molecular parallels regarding their phagocytic receptors six microns under (simu) and draper (dpr) (Kim et al., 2020). Glial cells expressing Simu and dpr are required for clearance of the impaired neurons and neuronal debris, and the lack of expression these receptors leads to neurodegeneration (Elliott and Ravichandran, 2008). Moreover, a microglia-like glial subtype called MANF (Mesencephalic Astrocyte Derived Neurotrophic Factor) immuno-reactive cells has been described in the *Drosophila* brain during metamorphosis under certain conditions. These cells are extremely rich in lysosomes and express dpr (Stratoulia and Heino, 2015). In addition, cortex glia and ensheathing cells are non-professional phagocytes engulfing apoptotic cells during the development of the nervous system and degenerating axons, respectively (Doherty et al., 2009; Kurant, 2011).

Since insects lack the adaptive immune system that evolved 500 million years ago in jawed fish, they must rely solely on innate immunity. Nonetheless, it has been described that the innate immune system can also be “trained”, and display certain memory traits. The phenomenon of “innate immune memory” was proposed by Netea et al. (2020), who conducted this research on mammalian models. This concept has also been addressed in *Drosophila*. It has been documented that fruit flies display enhanced survival of streptococcal infection if re-encountered by an otherwise lethal dose of the same bacteria and that this protective mechanism lies in the action of phagocytes and the Toll signaling pathway (Pham et al., 2007). However, such protection could not be invoked against all the bacteria examined.

As evidenced by advances made in recent years, plasmatocytes in *Drosophila* perform a strikingly wide range of roles that encompass the functional repertoire of M1 and M2 macrophages. In addition, experimental data demonstrate that plasmatocytes are capable of entering different polarization phenotypes over time. Moreover, several lines of evidence suggest that plasmatocytes are not a uniform population and consist of many distinct subpopulations of plasmatocyte phenotypes. Particularly, their ability to regulate the metabolism of other tissues via signaling factors might be of interest. In terms of the pathological role of mammalian macrophages, it is an interesting observation that exposure of plasmatocytes to excessive amounts of lipids may lead to macrophage polarization, reminiscent of Mox polarization in mammalian macrophages. Whether *Drosophila* possesses a functional analogy to mammalian tissue-resident macrophages remains to be determined.

Macrophage functional versatility as a legacy of animal origin

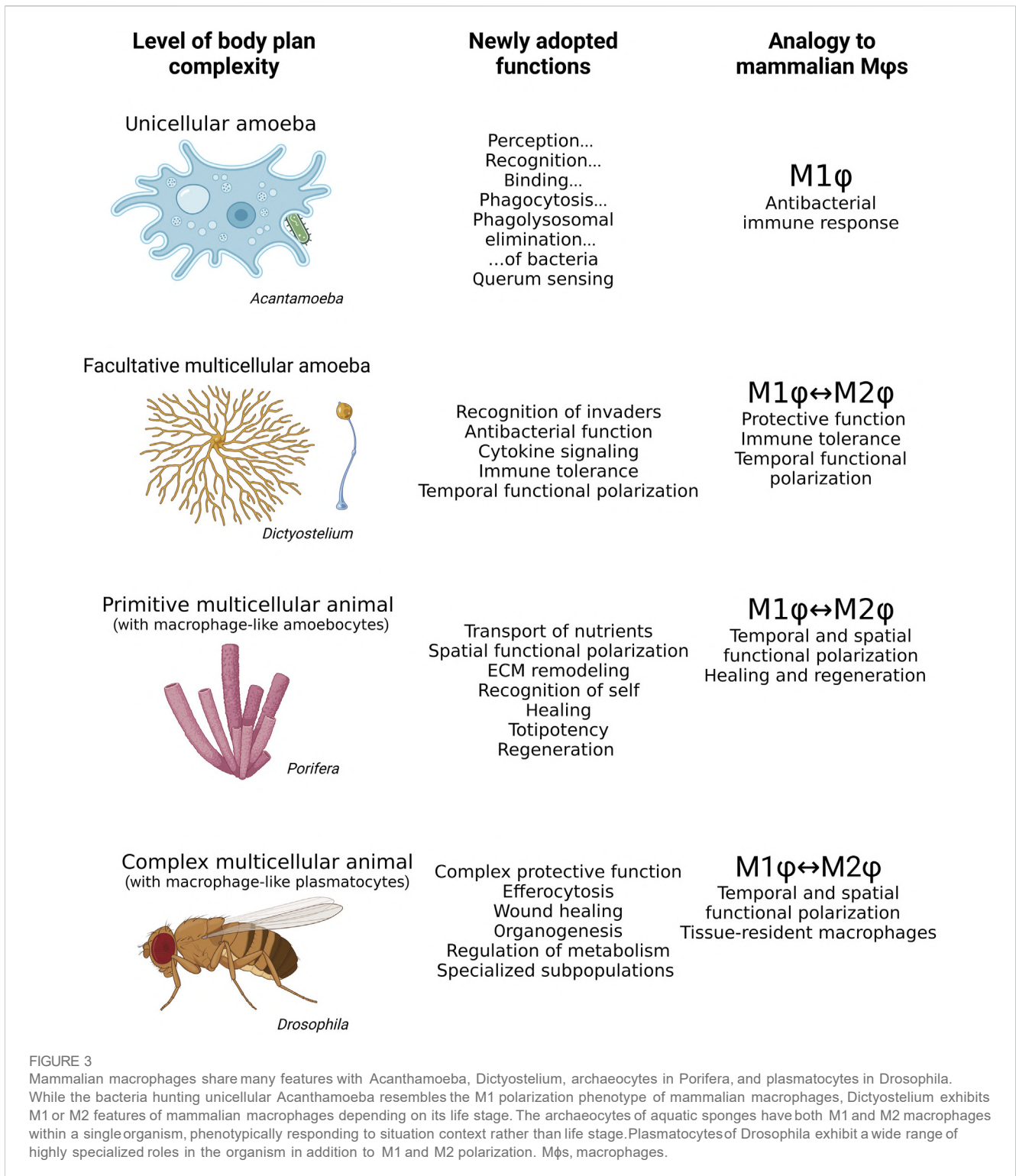
In the previous paragraphs, we have discussed how the rising complexity of body plans corresponds with the adoption of crucial macrophage features (Figure 3). Nevertheless, the question of why macrophages are predisposed to exceptional functional versatility remains to be addressed.

Recently, the theoretical concept of the origin of multicellular animals has been revisited. It is generally accepted that amoebocytes represent the most ancestral cell type of all Holozoa. Primitive facultative multicellular animals consisted of a cluster of a few cell types, temporally forming multicellular colonies (Ros-Rocher et al., 2021).

The observations from *Dictyostelium* and *Porifera* indicate that amoebocytes, the last common ancestor of multicellular animals, represent the ancestral super-ordinated cells that must have been widely distributed and capable of functionalities performed in more complex animals by specialized tissues and organs. They were most likely able to differentiate into all other cell types, control their number, and govern protective, nutritional, regulatory, and homeostatic functions. Therefore, we expect these cells to be already highly functionally versatile with a certain level of plasticity and autonomy.

Given that macrophage-like amoebocytes represent an archetypal cellular type in animals (Cavalier-Smith, 2017), the second cell type commonly diversified in early multicellular organisms are cells specialized for acquiring nutrients from the environment (Sogabe et al., 2019). We can hypothesize that as amoebocytes no longer needed to obtain nutrients for themselves, they evolved to perform other functions in the multicellular body. However, the differentiation of individual specialized cells imposed the requirement to evenly distribute resources, coordinate the function of individual cells, and maintain homeostasis in response to changing external biotic and abiotic factors (Bich et al., 2019). These requirements demand a certain level of regulation, and before the development of the circulatory, endocrine, and neuronal systems, the amoebocytes were predisposed to perform such functions (Dyakonova, 2022).

We believe that macrophage functional versatility may be a heritage of their origin in unicellular and early multicellular animals, where the universality of macrophage-like amoebocytes was essential for



resistance to different types of environmental and biological stress. Over millions of years of evolution from amoebocytes to macrophages, macrophage-like cells have taken advantage of their initial versatility and gradually achieved their full functional repertoire along with the increasing complexity of the animal body. Although we might assume that the functional variability of macrophages would decrease with the

emergence of organ systems, the opposite is true. Every tissue in the mammalian body contains a population of tissue-resident macrophages that often perform highly specialized functions (Mass et al., 2016). Collectively, maintaining functionally versatile amoeboid cells that can easily change their functional repertoire to suit emerging needs seem to be an adaptive strategy.

The origin of macrophage functions may explain their pathological effect in mammals

In general, it can be assumed that the acquisition of new functions of macrophages in evolution can be achieved by changing their original archetypal role and adapting it to the current context (Brosius, 2019). This can be documented, for instance, by a functional shift from mechanisms evolved to hunt bacteria to an antibacterial protective role of macrophages. The mechanism required by unicellular amoeboid cells to identify, approach, phagocytose, and digest bacteria in the phagolysosome for nutritional reasons was later shown to be advantageous for macrophages in multicellular organisms for protection against pathogenic bacteria (Hartenstein and Martinez, 2019). Another such example is the rich repertoire of genes originally used in the unicellular ancestor of animals for amoeboid crawling and attachment to surface structures, which evolved into a broad repertoire of surface receptors and adhesion molecules used by macrophages in multicellular organisms for sensing surrounding tissues and motility (Hynes and Zhao, 2000).

Thus, many signaling pathways in macrophages and other myeloid cells may carry remnants of their evolutionary origin without retaining their initial adaptive function in a complex multicellular organism. Such vestigial molecular relationships may underlie the pathological behavior of macrophages. For example, the folate receptor, formyl-peptide receptor, or cAMP signaling represent the shift of adaptive functions originally developed in macrophage-like amoebocytes to their pathological effect in macrophages. We believe that many analogous comparisons can be found when applying this perspective to human pathologies.

Folate, a secondary metabolite of bacteria, is a potent chemoattractant for amoeboid vegetative cells of *Dictyostelium* (Driel, 1981). The folate gradient is perceived via a G-protein coupled folate receptor at nanomolar concentrations and leads to the activation of chemotaxis and machinery required for phagocytosis and bacterial processing in the phagolysosome (Pan et al., 2016). Interestingly, increased expression of folate receptors are a hallmark of pro-inflammatory mammalian macrophages (Steinz et al., 2022). In particular, folate receptor β (FR- β) has been identified as a specific surface receptor for highly pro-inflammatory macrophages, such as those found in the synovial tissue of arthritic patients, in atherosclerotic plaques, or in pulmonary fibrosis (Chandrupatla et al., 2019). Activation of macrophage FR- β leads to their pro-inflammatory polarization and production of cytokines that further perpetuate the chronic inflammatory state. Inhibition of the folate receptor has thus been recognized as a possible avenue for treating arthritis and atherosclerosis, making FR- β agonist Methotrexate the first-choice treatment for these diseases (Xia et al., 2009).

Similar functional dualism can be observed for other GPCRs carried by mammalian myeloid cells, such as the formyl peptide receptor (FPR) abundantly expressed by macrophages and neutrophils (Chen et al., 2017). Activation of FPR serves as a potent signal leading to enhanced directional motility, the production of ROS, the release of pro-inflammatory cytokines, and acceleration of phagocytic and bactericidal machinery (Liang et al., 2020). Since formyl peptides are released by bacteria as their

secondary metabolite, the response mediated via the FPR receptor is important for resistance to bacterial pathogens (Dorward et al., 2015). However, under stress conditions, formyl peptides are released from the mitochondria of stressed and damaged tissues, leading to infiltration of the affected tissue by macrophages and neutrophils, which induce inflammation even under sterile conditions (Wenceslau et al., 2013). Therefore, excessive activation of FPR on macrophages and neutrophils underpins the progressive development of many human inflammatory diseases, such as neurodegeneration, cardiovascular diseases, and pulmonary fibrosis (Trojan et al., 2020; Caso et al., 2021).

In both cases, inadequate activation of receptors, initially designed to detect bacterial secondary metabolites and tracking bacteria in the environment, causes pathology in a complex multicellular organism, where their activation can occur even under sterile conditions (Lu et al., 2021).

Nonetheless, the repurposing of ancestral signaling is not limited to bacterial detection and localization mechanisms. As described previously, metabolically stressed vegetative amoebae of *Dictyostelium* produce cAMP as a potent aggregation chemoattractant (Singer et al., 2019). Sensing of extracellular cAMP leads to the activation of stress-related cellular pathways, remodeling of cellular metabolism, and epigenetic remodeling, resulting in a transition to multicellularity, increased production of ECM components, and tolerogenicity (Wang S. Y. et al., 2021). Interestingly, many lines of evidence suggest that extracellular cAMP (ex-cAMP) strongly effects the recruitment and reprogramming of monocytes and macrophages and induces efferocytosis of damaged or exhausted surrounding cells (Negreiros-Lima et al., 2020). Exposure of monocytes to ex-cAMP enhances the production of cytokines with known anti-inflammatory effects, such as IL-6 and IL-10, and ameliorates response to pro-inflammatory stimuli (Sciaraffa et al., 2014).

cAMP in the extracellular space is cleaved by ectonucleotidases to extracellular adenosine and sensed by the adenosine receptor abundantly expressed by macrophages and other myeloid cells (Haskó and Pacher, 2012). Adenosine and cAMP are released from damaged, hypoxic, and metabolically stressed tissues. Activation of adenosine receptors causes potent anti-inflammatory effects and plays an essential role in tissue regeneration and maintenance of tissue homeostasis (Pasquini et al., 2021). Interestingly, cAMP is an important secondary messenger in mammalian immune cells that activates identical downstream cascades in *Dictyostelium* amoebocytes, leading to the inhibition of NF κ B and activation of anti-inflammatory tolerogenic polarization (Tavares et al., 2020).

Thus, we can assume that cAMP signaling, which appeared in evolution at the origin of multicellular animals, may play an adaptive role in the immune system up to the present day. However, adopting a tolerogenic program through the activation of adenosine and cAMP signaling also has a role in pathology. Increased adenosine and cAMP production by metabolically demanding and often hypoxic neoplastic tumors leads to the induction of tolerogenic polarization in surrounding immune cells (Strakhova et al., 2020). Hence, tumor-associated macrophages often promote tumor growth, instead of elimination, by providing nutrients and growth factors and promoting vascularization (Moeini and Niedźwiedzka-Rystwej, 2021).

Thus, the repurposing of the features of the macrophage ancestors may be adaptive, as evidenced by protection against pathogenic bacteria, but may contribute to the development of many pathologies.

Discussion

The hypotheses we present here are speculative, convincing evidence that documents events that took place in the distant past in evolution is limited. However, this may change significantly with the growing list of organisms with fully sequenced genomes and well-annotated transcriptomes. Many of these newly sequenced species provide information allowing speculation regarding the nature of the last unicellular and first multicellular ancestors of animals. These data provide evidence of genes that were prerequisites for the emergence of multicellularity and the development of advanced multicellular body structures. An interesting example of such an approach can be found in the work of Ros-Rocher and colleagues, and it is feasible that analogous analyses can yield valuable information in the future (Ros-Rocher et al., 2021). Regarding the origin of macrophage functional versatility, the effort requires tracing macrophage characteristic features in evolution. Recent work conducted by Nagahata and colleagues, which, on the genetic level, supports the hypotheses that many functions typical of bactericidal macrophages evolved from a common ancestor of animals, and that many characteristic macrophage features are adaptations of free-living unicellular bacterivorous amoebae (Nagahata et al., 2022; Rayamajhee et al., 2022).

The majority of macrophage-like features that are observed in amoebae resemble those of bactericidal (M1) macrophages. This indicates that the bactericidal macrophage polarization represents an ancestral polarization type and the protective function of macrophages evolved from hunting microbes for nutritional reasons (Desjardins et al., 2005; Hartenstein and Martinez, 2019).

Inspired by the currently revised theory of the origin of animal multicellularity (Brunet and King, 2017), we believe that amoebocytes, as the ancestral type of animal cells, play a central role in the origin of multicellularity. Amoebocytes display several features that may be considered prerequisites for the emergence of multicellularity, such as the ability to deposit and remodel ECM, remove senescent and damaged cells, respond to various signals, regulate the function of other cells by signaling factors, and recognize genetically related cells in the colony (Misevic, 1999). These features are required by multicellular organisms and also resemble the characteristics of healing (M2) macrophages. Therefore, we suggest that along with the emergence of multicellular animals, the macrophage-like amoeboid cells acquired macrophage-like properties characteristic of M2 macrophages.

Given that the last common ancestor of animals likely switched between free-living and colonial life stages during its life cycle in response to extrinsic cues (Brunet et al., 2021), it is possible that the macrophage-like amoebocytes had the capacity for phenotypic polarization in a context-dependent manner, before the emergence of multicellularity. While the wild-type social amoeba shows features observed predominantly in M1 macrophages, amoebocytes participating in colonial life stages have changed their biology and acquired features characteristic predominantly of M2 macrophages.

We can hypothesize that the divergence of macrophage functions in emerging multicellular organisms was driven by the differentiation of specialized cell types for obtaining nutrition, the

growing need for harmonizing force, and the recognition of cellular identity. The diversification of the functional repertoire of macrophages in primitive multicellular organisms (Porifera) suggests that, together with the increasing complexity of body plans, there is a need for polarization of macrophage-like archaeocytes into both phenotypes within a single organism, with the polarization phenotype depending on context rather than life stage (Degnan et al., 2015). We may hypothesize that the regulatory role of macrophage-like amoebocytes precedes the function of the endocrine and nervous systems in primitive multicellular organisms, indicating a superior regulatory role of amoebocytes over other cells in the body.

Upon the evolution of complex multicellular organisms, macrophages expanded their functions, reaching their full potential, participating in development, organogenesis, immune protection, self-recognition, tissue and metabolic homeostasis maintenance, and many tissue- and context-specific tasks (Mase et al., 2021). It is likely that these functions will be revealed in future research in virtually all complex multicellular animals.

We present a perspective of evolutionary biology, combined with knowledge from modern biomedical research. Both approaches can be mutually inspiring in future research on the biology of macrophage-like cells. One critical feature which contributes to the functional versatility of macrophages is their ability to adopt distinct metabolic polarization phenotypes, which are determined by epigenetic modifications and activation of specific signaling cascades. Therefore, investigating polarization phenotypes of unicellular and facultative multicellular relatives of true animals would be of interest. A seminal study addressing this was performed on *Dictyostelium*, carried out in the laboratory of Erika Pearce, one of the leading scientists working on macrophage immuno-metabolism (Kelly et al., 2021). This work demonstrated a link between cell metabolism and the transition to the multicellular stage. In addition, the traits of early relatives of animals can be explored for their significance to mammalian macrophage biology. One such example is the potentially conserved nutritional role of macrophage-like amoebocytes in *Dictyostelium* and sponges in the macrophages of higher animals and humans.

In addition, we believe that understanding the role of ancestral macrophage-like cells may help to understand the biology of mammalian macrophages and possibly discover new functions. Given the ancestral origin of macrophage functions, some difficult-to-understand pathological behaviors of macrophages can be explained by the activation of ancient vestigial functions that may appear counterintuitive in a specific context in a complex multicellular body. We believe that this perspective may shed new light on the function and pathogenesis of macrophages in animals and humans.

Data availability statement

The original contributions presented in the study are included in the article/supplementary material, further inquiries can be directed to the corresponding authors.

Author contributions

AB and GK participated in the conceptualization of the manuscript, preparation of the figures, and writing of the text and its graphic design.

Funding

The authors acknowledge funding from the Grant Agency of the Czech Republic to AB (Project 20-14030Sand 23-06133S; www.gacr.cz). GK was supported by USB Grant Agency (Project 026/2021/P).

Acknowledgments

We thank to our technician Lucie Hrádková for her enthusiasm and support. We would like to thank the reviewers for their inspiring suggestions how to improve the manuscript and to members of our families for their patience. We would like to acknowledge BioRender, iTol, and PhyloT which were used for

generation of figures. Finally, we would like to thank the editorial team and service for their expertise and excellent work they made. We are very grateful to Becky Collier for proofreading and all her support.

Conflict of interest

The authors declare that the research was conducted in the absence of any commercial or financial relationships that could be construed as a potential conflict of interest.

Publisher's note

All claims expressed in this article are solely those of the authors and do not necessarily represent those of their affiliated organizations, or those of the publisher, the editors and the reviewers. Any product that may be evaluated in this article, or claim that may be made by its manufacturer, is not guaranteed or endorsed by the publisher.

References

- Akya, A., Pointon, A., and Thomas, C. (2009). Mechanism involved in phagocytosis and killing of *Listeria monocytogenes* by *Acanthamoeba polyphaga*. *Parasitol. Res.* 105, 1375–1383. doi:10.1007/s00436-009-1565-z
- Allen, P. G., and Dawidowicz, E. A. (1990). Phagocytosis in *Acanthamoeba*: I. A mannose receptor is responsible for the binding and phagocytosis of yeast. *J. Cell. Physiol.* 145, 508–513. doi:10.1002/jcp.1041450317
- Alsam, S., Sissons, J., Dudley, R., and Khan, N. A. (2005). Mechanisms associated with *Acanthamoeba castellanii* (T4) phagocytosis. *Parasitol. Res.* 96, 402–409. doi:10.1007/s00436-005-1401-z
- Amarante-Mendes, G. P., Adjemian, S., Branco, L. M., Zanetti, L. C., Weinlich, R., and Bortoluci, K. R. (2018). Pattern recognition receptors and the host cell death molecular machinery. *Front. Immunol.* 9, 2379. doi:10.3389/fimmu.2018.02379
- Arango Duque, G., and Descoiteaux, A. (2014). Macrophage cytokines: Involvement in immunity and infectious diseases. *Front. Immunol.* 5, 491. doi:10.3389/fimmu.2014.00491
- Bareby, E., Chen, P., and Aouadi, M. (2022). Macrophage functional diversity in NAFLD—More than inflammation. *Nat. Rev. Endocrinol.* 18, 461–472. doi:10.1038/s41574-022-00675-6
- Batista-Gonzalez, A., Vidal, R., Criollo, A., and Carreño, L. J. (2020). New insights on the role of lipid metabolism in the metabolic reprogramming of macrophages. *Front. Immunol.* 10. doi:10.3389/fimmu.2019.02993
- Belacortu, Y., and Paricio, N. (2011). *Drosophila* as a model of wound healing and tissue regeneration in vertebrates. *Dev. Dyn.* 240, 2379–2404. doi:10.1002/dvdy.22753
- Bich, L., Pradeu, T., and Moreau, J.-F. (2019). Understanding multicellularity: The functional organization of the intercellular space. *Front. Physiol.* 10, 1170. doi:10.3389/fphys.2019.01170
- Biswas, S. K., and Mantovani, A. (2012). Orchestration of metabolism by macrophages. *Cell Metab.* 15, 432–437. doi:10.1016/j.cmet.2011.11.013
- Boury-Esnault, N. (1977). A cell type in sponges involved in the metabolism of glycogen. The gray cells. *Cell Tissue Res.* 175, 523–539. doi:10.1007/BF00222416
- Bowers, B. (1977). Comparison of pinocytosis and phagocytosis in *Acanthamoeba castellanii*. *Exp. Cell Res.* 110, 409–417. doi:10.1016/0014-4827(77)90307-x
- Bozzaro, S., and Eichinger, L. (2011). The professional phagocyte *Dictyostelium discoideum* as a model host for bacterial pathogens. *Curr. Drug Targets* 12, 942–954. doi:10.2174/138945011795677782
- Bozzaro, S. (2013). The model organism *Dictyostelium discoideum*. *Methods Mol. Biol.* 983, 17–37. doi:10.1007/978-1-62703-302-2_2
- Brock, D. A., Callison, W. E., Strassmann, J. E., and Queller, D. C. (2016a). Sentinel cells, symbiotic bacteria and toxin resistance in the social amoeba *Dictyostelium discoideum*. *Proc. R. Soc. B Biol. Sci.* 283, 20152727. doi:10.1098/rspb.2015.2727
- Brock, D. A., Jones, K., Queller, D. C., and Strassmann, J. E. (2016b). Which phenotypic traits of *Dictyostelium discoideum* farmers are conferred by their bacterial symbionts? *Symbiosis* 68, 39–48. doi:10.1007/s13199-015-0352-0
- Brock, D. A., Read, S., Bozhchenko, A., Queller, D. C., and Strassmann, J. E. (2013). Social amoeba farmers carry defensive symbionts to protect and privatize their crops. *Nat. Commun.* 4, 2385. doi:10.1038/ncomms3385
- Brooke, N. M., and Holland, P. W. (2003). The evolution of multicellularity and early animal genomes. *Curr. Opin. Genet. Dev.* 13, 599–603. doi:10.1016/j.gde.2003.09.002
- Brosius, J. (2019). Exaptation at the molecular genetic level. *Sci. China Life Sci.* 62, 437–452. doi:10.1007/s11427-018-9447-8
- Brunet, T., Albert, M., Roman, W., Coyle, M. C., Spitzer, D. C., and King, N. (2021). A flagellate-to-amoeboid switch in the closest living relatives of animals. *Elife* 10, e61037. doi:10.7554/eLife.61037
- Brunet, T., and King, N. (2017). The origin of animal multicellularity and cell differentiation. *Dev. Cell* 43, 124–140. doi:10.1016/j.devcel.2017.09.016
- Brunet, T., and King, N. (2022). "The single-celled ancestors of animals," in *The evolution of multicellularity* (Boca Raton: CRC Press), 251–278.
- Buscema, M., Sutter, D., and Vyver, G. (1980). Ultrastructural study of differentiation processes during aggregation of purified sponge archaeocytes. *Wilhelm Roux's Arch. Dev. Biol.* 188, 45–53. doi:10.1007/BF00848609
- Cammer, M., and Cox, D. (2014). Chemotactic responses by macrophages to a directional source of a cytokine delivered by a micropipette. *Methods Mol. Biol.* 1172, 125–135. doi:10.1007/978-1-4939-0928-5_11
- Campolo, A., Harris, V., Walters, R., Miller, E., Patterson, B., and Crary, M. (2021). Continuous real-time motility analysis of *Acanthamoeba* reveals sustained movement in absence of nutrients. *Pathogens* 10, 995. doi:10.3390/pathogens10080995
- Carrier, T. J., Maldonado, M., Schmittmann, L., Pita, L., Bosch, T. C. G., and Hentschel, U. (2022). Symbiont transmission in marine sponges: Reproduction, development, and metamorphosis. *BMC Biol.* 20, 100. doi:10.1186/s12915-022-01291-6
- Caso, V. M., Manzo, V., Pecchillo Cimmino, T., Conti, V., Caso, P., Esposito, G., et al. (2021). Regulation of inflammation and oxidative stress by formyl peptide receptors in cardiovascular disease progression. *Life* 11, 243. doi:10.3390/life11030243
- Castillo-Armengol, J., Fajas, L., and Lopez-Mejia, I. C. (2019). Inter-organ communication: A gatekeeper for metabolic health. *EMBO Rep.* 20, e47903. doi:10.15252/embr.201947903
- Cavalier-Smith, T. (2017). Origin of animal multicellularity: Precursors, causes, consequences—the choanoflagellate/sponge transition, neurogenesis and the cambrian explosion. *Philos. Trans. R. Soc. B Biol. Sci.* 372, 20150476. doi:10.1098/rstb.2015.0476
- Chandrupatla, D. M. S. H., Molthoff, C. F. M., Lammertsma, A. A., van der Laken, C. J., and Jansen, G. (2019). The folate receptor β as a macrophage-mediated imaging and therapeutic target in rheumatoid arthritis. *Drug Deliv. Transl. Res.* 9, 366–378. doi:10.1007/s13346-018-0589-2

Chen, G., Zhuchenko, O., and Kuspa, A. (2007). Immune-like phagocyte activity in the social amoeba. *Science* 317, 678–681. doi:10.1126/science.1143991

Chen, K., Bao, Z., Gong, W., Tang, P., Yoshimura, T., and Wang, J. M. (2017). Regulation of inflammation by members of the formyl-peptide receptor family. *J. Autoimmun.* 85, 64–77. doi:10.1016/j.jaut.2017.06.012

Cheng, L., Baonza, A., and Grifoni, D. (2018). Drosophila models of human disease. *Biomed. Res. Int.* 1–2, 7214974. doi:10.1155/2018/7214974

Cho, B., Yoon, S.-H., Lee, D., Koranteng, F., Tattikota, S. G., Cha, N., et al. (2020). Single-cell transcriptome maps of myeloid blood cell lineages in *Drosophila*. *Nat. Commun.* 11, 4483. doi:10.1038/s41467-020-18135-y

Clarke, M., and Gomer, R. H. (1995). PSF and CMF, autocrine factors that regulate gene expression during growth and early development of *Dictyostelium*. *Experientia* 51, 1124–1134. doi:10.1007/BF01944730

Coats, B. R., Schoenfelt, K. Q., Barbosa-Lorenzi, V. C., Peris, E., Cui, C., Hoffman, A., et al. (2017). Metabolically activated adipose tissue macrophages perform detrimental and beneficial functions during diet-induced obesity. *Cell Rep.* 20, 3149–3161. doi:10.1016/j.celrep.2017.08.096

Cole, J., Aberdein, J., Jubrail, J., and Dockrell, D. H. (2014). The role of macrophages in the innate immune response to *Streptococcus pneumoniae* and *Staphylococcus aureus*. *Adv. Microb. Physiol.* 65, 125–202. doi:10.1016/bs.ampbs.2014.08.004

Consalvo, K. M., Rijal, R., Tang, Y., Kirolos, S. A., Smith, M. R., and Gomer, R. H. (2019). Extracellular signaling in *Dictyostelium*. *Int. J. Dev. Biol.* 63, 395–405. doi:10.1387/ijdb.190259rg

Cosson, P., and Lima, W. C. (2014). Intracellular killing of bacteria: Is *Dictyostelium* a model macrophage or an alien? *Cell. Microbiol.* 16, 816–823. doi:10.1111/cmi.12291

Dahihande, A. S., and Thakur, N. L. (2021). Differences in the structural components influence the pumping capacity of marine sponges. *Front. Mar. Sci.* 8. doi:10.3389/fmars.2021.671362

Davies, L. C., Jenkins, S. J., Allen, J. E., and Taylor, P. R. (2013). Tissue-resident macrophages. *Nat. Immunol.* 14, 986–995. doi:10.1038/ni.2705

DeGregorio, E., Spellman, P. T., Tzou, P., Rubin, G. M., and Lemaitre, B. (2002). The Toll and Imd pathways are the major regulators of the immune response in *Drosophila*. *EMBO J.* 21, 2568–2579. doi:10.1093/emboj/21.11.2568

deCathelineau, A. M., and Henson, P. M. (2003). The final step in programmed cell death: Phagocytes carry apoptotic cells to the grave. *Essays Biochem.* 39, 105–117. doi:10.1042/bse0390105

Degnan, B. M., Adamska, M., Richards, G. S., Larroux, C., Leininger, S., Bergum, B., et al. (2015). “Porifera,” in *Evolutionary developmental biology of invertebrates* (Vienna: Springer Vienna).

Desjardins, M., Houde, M., and Gagnon, E. (2005). Phagocytosis: The convoluted way from nutrition to adaptive immunity. *Immunol. Rev.* 207, 158–165. doi:10.1111/j.0105-2896.2005.00319.x

Doherty, J., Logan, M. A., Tasdemir, O. E., and Freeman, M. R. (2009). Ensheathing glia function as phagocytes in the adult *Drosophila* brain. *J. Neurosci.* 29, 4768–4781. doi:10.1523/JNEUROSCI.5951-08.2009

Dorward, D. A., Lucas, C. D., Chapman, G. B., Haslett, C., Dhaliwal, K., and Rossi, A. G. (2015). The role of formylated peptides and formyl peptide receptor 1 in governing neutrophil function during acute inflammation. *Am. J. Pathol.* 185, 1172–1184. doi:10.1016/j.ajpath.2015.01.020

Driel, R. (1981). Binding of the chemoattractant folic acid by *Dictyostelium discoideum* cells. *Eur. J. Biochem.* 115, 391–395. doi:10.1111/j.1432-1033.1981.tb05250.x

Dunn, J. D., Bosmani, C., Barisch, C., Raykov, L., Lefrançois, L. H., Cardenal-Muñoz, E., et al. (2018). Eat prey, live: *Dictyostelium discoideum* as a model for cell-autonomous defenses. *Front. Immunol.* 8, 1906. doi:10.3389/fimmu.2017.01906

Dyakonova, V. E. (2022). Origin and evolution of the nervous system: New data from comparative whole genome studies of multicellular animals. *Russ. J. Dev. Biol.* 53, 55–64. doi:10.1134/s1062360422010088

Dzik, J. M. (2010). The ancestry and cumulative evolution of immunoreactions. *Acta Biochim. Pol.* 57, 443–466. doi:10.18388/abp.2010_2431

Elliott, M. R., and Ravichandran, K. S. (2008). Death in the CNS: Six-Microns-Under. *Cell* 133, 393–395. doi:10.1016/j.cell.2008.04.014

Ereskovsky, A., Borisenko, I. E., Bolshakov, F. V., and Lavrov, A. I. (2021). Whole-body regeneration in sponges: Diversity, fine mechanisms, and future prospects. *Genes (Basel)*. 12, 506. doi:10.3390/genes12040506

Farinholt, T., Dinh, C., and Kuspa, A. (2019). Microbiome management in the social amoeba *Dictyostelium discoideum* compared to humans. *Int. J. Dev. Biol.* 63, 447–450. doi:10.1387/ijdb.190240ak

Fernández-Busquets, X., Kuhns, W. J., Simpson, T. L., Ho, M., Gerosa, D., Grob, M., et al. (2002). Cell adhesion-related proteins as specific markers of sponge cell types involved in allogeneic recognition. *Dev. Comp. Immunol.* 26, 313–323. doi:10.1016/s0145-305x(01)00079-9

Ferrante, C. J., and Leibovich, S. J. (2012). Regulation of macrophage polarization and wound healing. *Adv. Wound Care* 1, 10–16. doi:10.1089/wound.2011.0307

Feuda, R., Dohrmann, M., Pett, W., Philippe, H., Rota-Stabelli, O., Lartillot, N., et al. (2017). Improved modeling of compositional heterogeneity supports sponges as sister to all other animals. *Curr. Biol.* 27, 3864–3870.e4. doi:10.1016/j.cub.2017.11.008

Flowers, J. M., Li, S. I., Stathos, A., Saxer, G., Ostrowski, E. A., Queller, D. C., et al. (2010). Variation, sex, and social cooperation: Molecular population genetics of the social amoeba *Dictyostelium discoideum*. *PLoS Genet.* 6, e1001013. doi:10.1371/journal.pgen.1001013

Gaino, E., Bavestrello, G., and Magnino, G. (1999). Self/non-self recognition in sponges. *Ital. J. Zool.* 66, 299–315. doi:10.1080/11250009909356270

Galván-Peña, S., and O'Neill, L. A. J. (2014). Metabolic reprogramming in macrophage polarization. *Front. Immunol.* 5. doi:10.3389/fimmu.2014.00420

Gardères, J., Bourguet-Kondracki, M.-L., Hamer, B., Batel, R., Schröder, H., and Müller, W. (2015). Porifera lectins: Diversity, physiological roles and biotechnological potential. *Mar. Drugs* 13, 5059–5101. doi:10.3390/md13085059

Germer, J., Cerveau, N., and Jackson, D. J. (2017). The holo-transcriptome of a calcified early branching metazoan. *Front. Mar. Sci.* 4, 81. doi:10.3389/fmars.2017.00081

Glöckner, G., Lawal, H. M., Felder, M., Singh, R., Singer, G., Weijer, C. J., et al. (2016). The multicellularity genes of dictyostelid social amoebas. *Nat. Commun.* 7, 12085. doi:10.1038/ncomms12085

Gold, K. S., and Brückner, K. (2015). Macrophages and cellular immunity in *Drosophila melanogaster*. *Semin. Immunol.* 27, 357–368. doi:10.1016/j.smim.2016.03.010

Golé, L., Rivière, C., Hayakawa, Y., and Rieu, J.-P. (2011). A quorum-sensing factor in vegetative *Dictyostelium discoideum* cells revealed by quantitative migration analysis. *PLoS One* 6, e26901. doi:10.1371/journal.pone.0026901

Gordon, S., and Plüddemann, A. (2017). Tissue macrophages: Heterogeneity and functions. *BMC Biol.* 15, 53. doi:10.1186/s12915-017-0392-4

Govind, S. (2008). Innate immunity in *Drosophila*: Pathogens and pathways. *Insect Sci.* 15, 29–43. doi:10.1111/j.1744-7917.2008.00185.x

Grau-Bové, X., Torruella, G., Donachie, S., Suga, H., Leonard, G., Richards, T. A., et al. (2017). Dynamics of genomic innovation in the unicellular ancestry of animals. *Elife* 6, e26036. doi:10.7554/eLife.26036

Hartenstein, V., and Martinez, P. (2019). Phagocytosis in cellular defense and nutrition: A food-centered approach to the evolution of macrophages. *Cell Tissue Res.* 377, 527–547. doi:10.1007/s00441-019-03096-6

Haskó, G., and Pacher, P. (2012). Regulation of macrophage function by adenosine. *Arterioscler. Thromb. Vasc. Biol.* 32, 865–869. doi:10.1161/ATVBAHA.111.226852

Hehenberger, E., Tikhonov, D. V., Kolisko, M., del Campo, J., Esaulov, A. S., Mylnikov, A. P., et al. (2017). Novel predators reshape holozoan phylogeny and reveal the presence of a two-component signaling system in the ancestor of animals. *Curr. Biol.* 27, 2043–2050.e6. doi:10.1016/j.cub.2017.06.006

Herron, M. D., Ratcliff, W. C., Boswell, J., and Rosenzweig, F. (2018). Genetics of a de novo origin of undifferentiated multicellularity. *R. Soc. Open Sci.* 5, 180912. doi:10.1098/rsos.180912

Hinman, V., and Cary, G. (2017). The evolution of gene regulation. *Elife* 6, e27291. doi:10.7554/eLife.27291

Hirose, S., Benabentos, R., Ho, H.-I., Kuspa, A., and Shaulsky, G. (2011). Self-recognition in social amoebae is mediated by allelic pairs of tiger genes. *Science* 333, 467–470. doi:10.1126/science.1203903

Holt, D. J., and Grainger, D. W. (2012). Senescence and quiescence induced compromised function in cultured macrophages. *Biomaterials* 33, 7497–7507. doi:10.1016/j.biomaterials.2012.06.099

Hynes, R. O., and Zhao, Q. (2000). The evolution of cell adhesion. *J. Cell Biol.* 150, F89–F96. doi:10.1083/jcb.150.2.f89

Iglesias, P. A. (2012). Chemoattractant signaling in *Dictyostelium*: Adaptation and amplification. *Sci. Signal.* 5, pe8. doi:10.1126/scisignal.2002897

Jang, W., and Gomer, R. H. (2011). Initial cell type choice in *Dictyostelium*. *Eukaryot. Cell* 10, 150–155. doi:10.1128/EC.00219-10

Jennings, B. H. (2011). *Drosophila* – A versatile model in biology & medicine. *Mat. Today* 14, 190–195. doi:10.1016/s1369-7021(11)70113-4

Kaufmann, S. H. E. (2008). Immunology’s foundation: The 100-year anniversary of the Nobel prize to Paul Ehrlich and Elie Metchnikoff. *Nat. Immunol.* 9, 705–712. doi:10.1038/ni0708-705

Kelly, B., Carrizo, G. E., Edwards-Hicks, J., Sanin, D. E., Stanczak, M. A., Priesnitz, C., et al. (2021). Sulfur sequestration promotes multicellularity during nutrient limitation. *Nature* 591, 471–476. doi:10.1038/s41586-021-03270-3

Kharrat, B., Csordás, G., and Honti, V. (2022). Peeling back the layers of lymph gland structure and regulation. *Int. J. Mol. Sci.* 23, 7767. doi:10.3390/ijms23147767

Kierdorf, K., Hersperger, F., Sharrock, J., Vincent, C. M., Ustaoglu, P., Dou, J., et al. (2020). Muscle function and homeostasis require cytokine inhibition of AKT activity in *Drosophila*. *Elife* 9, e51595. doi:10.7554/eLife.51595

Kim, C. H. (2018). Immunoregulation by microbiome metabolites. *Immunology* 154, 220–229. doi:10.1111/imm.12930

- Kim, T., Song, B., and Lee, I.-S. (2020). *Drosophila* glia: Models for human neurodevelopmental and neurodegenerative disorders. *Int. J. Mol. Sci.* 21, 4859. doi:10.3390/ijms21144859
- King, N. (2004). The unicellular ancestry of animal development. *Dev. Cell* 7, 313–325. doi:10.1016/j.devcel.2004.08.010
- Krejčová, G., Danielová, A., Nedbalová, P., Kazek, M., Strych, L., Chawla, G., et al. (2019). *Drosophila* macrophages switch to aerobic glycolysis to mount effective antibacterial defense. *Elife* 8, e50414. doi:10.7554/eLife.50414
- Kurant, E. (2011). Keeping the CNS clear: Glial phagocytic functions in *Drosophila*. *Glia* 59, 1304–1311. doi:10.1002/glia.21098
- Kwon, D. H., Lee, H., Park, C., Hong, S.-H., Hong, S. H., Kim, G.-Y., et al. (2019). Glutathione-induced immune-stimulatory activity by promoting M1-like macrophages polarization via potential ROS scavenging capacity. *Antioxidants* 8, 413. doi:10.3390/antiox8090413
- Lang, B. F., O'Kelly, C., Nerad, T., Gray, M. W., and Burger, G. (2002). The closest unicellular relatives of animals. *Curr. Biol.* 12, 1773–1778. doi:10.1016/s0960-9822(02)01187-9
- Lardy, B., Bof, M., Aubry, L., Paclet, M. H., Morel, F., Satre, M., et al. (2005). NADPH oxidase homologs are required for normal cell differentiation and morphogenesis in *Dictyostelium discoideum*. *Biochim. Biophys. Acta - Mol. Cell Res.* 1744, 199–212. doi:10.1016/j.bbamcr.2005.02.004
- Laundon, D., Larson, B. T., McDonald, K., King, N., and Burkhardt, P. (2019). The architecture of cell differentiation in choanoflagellates and sponge choanocytes. *PLoS Biol.* 17, e3000226. doi:10.1371/journal.pbio.3000226
- Lauterbach, M. A. R., and Wunderlich, F. T. (2017). Macrophage function in obesity-induced inflammation and insulin resistance. *Pflügers Arch. - Eur. J. Physiol.* 469, 385–396. doi:10.1007/s00424-017-1955-5
- Lavin, Y., and Merad, M. (2013). Macrophages: Gatekeepers of tissue integrity. *Cancer Immunol. Res.* 1, 201–209. doi:10.1158/2326-6066.CIR-13-0117
- Lavrov, A. I., and Kosevich, I. A. (2014). Sponge cell reaggregation: Mechanisms and dynamics of the process. *Russ. J. Dev. Biol.* 45, 205–223. doi:10.1134/s1062360414040067
- Lee, E., Eo, J.-C., Lee, C., and Yu, J.-W. (2021). Distinct features of brain-resident macrophages: Microglia and non-parenchymal brain macrophages. *Mol. Cells* 44, 281–291. doi:10.14348/molcells.2021.0060
- Lemaitre, B., Nicolas, E., Michaut, L., Reichhart, J.-M., and Hoffmann, J. A. (1996). The dorsoventral regulatory gene cassette *spätzle/Toll/cactus* controls the potent antifungal response in *Drosophila* adults. *Cell* 86, 973–983. doi:10.1016/s0092-8674(00)80172-5
- Li, D., and Wu, M. (2021). Pattern recognition receptors in health and diseases. *Signal Transduct. Target. Ther.* 6, 291. doi:10.1038/s41392-021-00687-0
- Liang, W., Chen, K., Gong, W., Yoshimura, T., Le, Y., Wang, Y., et al. (2020). The contribution of chemoattractant GPCRs, formylpeptide receptors, to inflammation and cancer. *Front. Endocrinol. (Lausanne)* 11, 17. doi:10.3389/fendo.2020.00017
- Lin, P., Ji, H.-H., Li, Y.-J., and Guo, S.-D. (2021). Macrophage plasticity and atherosclerosis therapy. *Front. Mol. Biosci.* 8, 679797. doi:10.3389/fmolb.2021.679797
- Lin, Y., Xu, J., and Lan, H. (2019). Tumor-associated macrophages in tumor metastasis: Biological roles and clinical therapeutic applications. *J. Hematol. Oncol.* 12, 76. doi:10.1186/s13045-019-0760-3
- Liu, Y., Xu, R., Gu, H., Zhang, E., Qu, J., Cao, W., et al. (2021). Metabolic reprogramming in macrophage responses. *Biomark. Res.* 9, 1. doi:10.1186/s40364-020-00251-y
- Locati, M., Curtale, G., and Mantovani, A. (2020). Diversity, mechanisms, and significance of macrophage plasticity. *Annu. Rev. Pathol. Mech. Dis.* 15, 123–147. doi:10.1146/annurev-pathmechdis-012418-012718
- Loomis, W. F. (2014). Cell signaling during development of *Dictyostelium*. *Dev. Biol.* 391, 1–16. doi:10.1016/j.ydbio.2014.04.001
- Lu, Y. J., Wheeler, L. W., Chu, H., Kleindl, P. J., Pugh, M., You, F., et al. (2021). Targeting folate receptor beta on monocytes/macrophages renders rapid inflammation resolution independent of root causes. *Cell Rep. Med.* 2, 100422. doi:10.1016/j.xcrm.2021.100422
- Maldonado, M. (2016). Spongewast that fuels marine oligotrophic food webs: A reassessment of its origin and nature. *Mar. Ecol. Prog. Ser.* 37, 477–491. doi:10.1111/maec.12256
- Mammana, S., Fagone, P., Cavalli, E., Basile, M., Petralia, M., Nicoletti, F., et al. (2018). The role of macrophages in neuroinflammatory and neurodegenerative pathways of Alzheimer's disease, amyotrophic lateral sclerosis, and multiple sclerosis: Pathogenetic cellular effectors and potential therapeutic targets. *Int. J. Mol. Sci.* 19, 831. doi:10.3390/ijms19030831
- Martin, C. J., Peters, K. N., and Behar, S. M. (2014). Macrophages clean up: Efferocytosis and microbial control. *Curr. Opin. Microbiol.* 17, 17–23. doi:10.1016/j.mib.2013.10.007
- Martinelli, C., and Reichhart, J.-M. (2005). Evolution and integration of innate immune systems from fruit flies to man: Lessons and questions. *J. Endotoxin Res.* 11, 243–248. doi:10.1179/096805105X37411
- Mase, A., Augsburger, J., and Brückner, K. (2021). Macrophages and their organ location shape each other in development and homeostasis—a *Drosophila* perspective. *Front. Cell Dev. Biol.* 9, 630272. doi:10.3389/fcell.2021.630272
- Mass, E., Ballesteros, I., Farlik, M., Halbritter, F., Günther, P., Crozet, L., et al. (2016). Specification of tissue-resident macrophages during organogenesis. *Science* 351, aaf4238. doi:10.1126/science.aaf4238
- Melcarne, C., Lemaitre, B., and Kurant, E. (2019). Phagocytosis in *Drosophila*: From molecules and cellular machinery to physiology. *Insect Biochem. Mol. Biol.* 109, 1–12. doi:10.1016/j.ibmb.2019.04.002
- Merien, F. (2016). A journey with Elie Metchnikoff: From innate cell mechanisms in infectious disease to quantum biology. *Front. Public Heal.* 4, 125. doi:10.3389/fpubh.2016.00125
- Merkey, A. B., Wong, C. K., Hoshizaki, D. K., and Gibbs, A. G. (2011). Energetics of metamorphosis in *Drosophila melanogaster*. *J. Insect Physiol.* 57, 1437–1445. doi:10.1016/j.jinsphys.2011.07.013
- Mesquita, A., Cardenal-Muñoz, E., Dominguez, E., Muñoz-Braceras, S., Nuñez-Corcuera, B., Phillips, B. A., et al. (2017). Autophagy in *Dictyostelium*: Mechanisms, regulation and disease as a biomedical model. *Autophagy* 13, 24–40. doi:10.1080/15548627.2016.1226737
- Misevic, G. N. (1999). Molecular self-recognition and adhesion via proteoglycan to proteoglycan interactions as a pathway to multicellularity: Atomic force microscopy and color coded bead measurements in sponges. *Microsc. Res. Tech.* 44, 304–309. doi:10.1002/(SICI)1097-0029(19990215)44:4<304::AID-JEMT9>3.0.CO;2-X
- Moeini, P., and Niedźwiedzka-Rystwek, P. (2021). Tumor-associated macrophages: Combination of therapies, the approach to improve cancer treatment. *Int. J. Mol. Sci.* 22, 7239. doi:10.3390/ijms22137239
- Mogensen, T. H. (2009). Pathogen recognition and inflammatory signaling in innate immune defenses. *Clin. Microbiol. Rev.* 22, 240–273. doi:10.1128/CMR.00046-08
- Molmeret, M., Horn, M., Wagner, M., Santic, M., and Abu Kwaik, Y. (2005). Amoebae as training grounds for intracellular bacterial pathogens. *Appl. Environ. Microbiol.* 71, 20–28. doi:10.1128/AEM.71.1.20-28.2005
- Morgantini, C., Jager, J., Li, X., Levi, L., Azzimato, V., Sulen, A., et al. (2019). Liver macrophages regulate systemic metabolism through non-inflammatory factors. *Nat. Metab.* 1, 445–459. doi:10.1038/s42255-019-0044-9
- Müller, W. E. G., Custódio, M. R., Wiens, M., Zilberberg, C., Châtel, A., Müller, I. M., et al. (2009). "Effect of bacterial infection on stem cell pattern in Porifera," in *Stem cells in marine organisms* (Dordrecht: Springer Netherlands).
- Muller, W. E. G., and Müller, I. M. (2003). Origin of the metazoan immune system: Identification of the molecules and their functions in sponges. *Integr. Comp. Biol.* 43, 281–292. doi:10.1093/icb/43.2.281
- Müller, W. E. G. (2006). The stem cell concept in sponges (Porifera): Metazoan traits. *Semin. Cell Dev. Biol.* 17, 481–491. doi:10.1016/j.semcdb.2006.05.006
- Munro, D. A. D., and Hughes, J. (2017). The origins and functions of tissue-resident macrophages in kidney development. *Front. Physiol.* 8, 837. doi:10.3389/fphys.2017.00837
- Nadesalingam, J., Dodds, A. W., Reid, K. B. M., and Palaniyar, N. (2005). Mannose-binding lectin recognizes peptidoglycan via the N-acetyl glucosamine moiety, and inhibits ligand-induced proinflammatory effect and promotes chemokine production by macrophages. *J. Immunol.* 175, 1785–1794. doi:10.4049/jimmunol.175.3.1785
- Nagahata, Y., Masuda, K., Nishimura, Y., Ikawa, T., Kawaoka, S., Kitawaki, T., et al. (2022). Tracing the evolutionary history of blood cells to the unicellular ancestor of animals. *Blood* 140, 2611–2625. doi:10.1182/blood.2022016286
- Nakanishi, N., Sogabe, S., and Degnan, B. M. (2014). Evolutionary origin of gastrulation: Insights from sponge development. *BMC Biol.* 12, 26. doi:10.1186/1741-7007-12-26
- Natoli, G., and Monticelli, S. (2014). Macrophage activation: Glancing into diversity. *Immunity* 40, 175–177. doi:10.1016/j.immuni.2014.01.004
- Negreiros-Lima, G. L., Lima, K. M., Moreira, I. Z., Jardim, B. L. O., Vago, J. P., Galvão, I., et al. (2020). Cyclic AMP regulates key features of macrophages via PKA: Recruitment, reprogramming and efferocytosis. *Cells* 9, 128. doi:10.3390/cells9010128
- Netea, M. G., Dominguez-Andrés, J., Barreiro, L. B., Chavakis, T., Divangahi, M., Fuchs, E., et al. (2020). Defining trained immunity and its role in health and disease. *Nat. Rev. Immunol.* 20, 375–388. doi:10.1038/s41577-020-0285-6
- Neves, J., Zhu, J., Sousa-Victor, P., Korjikusic, M., Riley, R., Chew, S., et al. (2016). Immune modulation by MANF promotes tissue repair and regenerative success in the retina. *Science* 351, aaf3646. doi:10.1126/science.aaf3646
- Nielsen, C. (2019). Early animal evolution: A morphologist's view. *R. Soc. Open Sci.* 6, 190638. doi:10.1098/rsos.190638
- Nobs, S. P., and Kopf, M. (2021). Tissue-resident macrophages: Guardians of organ homeostasis. *Trends Immunol.* 42, 495–507. doi:10.1016/j.it.2021.04.007
- Nonnenmacher, Y., and Hiller, K. (2018). Biochemistry of proinflammatory macrophage activation. *Cell. Mol. Life Sci.* 75, 2093–2109. doi:10.1007/s00018-018-2784-1

- O'Callaghan, A. A., Dempsey, E., Iyer, N., Stiegeler, S., Mercurio, K., and Corr, S. C. (2021). Intestinal metabolites influence macrophage phagocytosis and clearance of bacterial infection. *Front. Cell. Infect. Microbiol.* 11, 622491. doi:10.3389/fcimb.2021.622491
- Olofsson, B., and Page, D. T. (2005). Condensation of the central nervous system in embryonic *Drosophila* is inhibited by blocking hemocytomigration or neural activity. *Dev. Biol.* 279, 233–243. doi:10.1016/j.ydbio.2004.12.020
- Palmieri, E. M., Gonzalez-Cotto, M., Baseler, W. A., Davies, L. C., Ghesquière, B., Maio, N., et al. (2020). Nitric oxide orchestrates metabolic rewiring in M1 macrophages by targeting aconitase 2 and pyruvate dehydrogenase. *Nat. Commun.* 11, 698. doi:10.1038/s41467-020-14433-7
- Pan, M., Xu, X., Chen, Y., and Jin, T. (2016). Identification of a chemoattractant G-protein-coupled receptor for folic acid that controls both chemotaxis and phagocytosis. *Dev. Cell* 36, 428–439. doi:10.1016/j.devcel.2016.01.012
- Parisi, L., Gini, E., Baci, D., Tremolati, M., Fanuli, M., Bassani, B., et al. (2018). Macrophage polarization in chronic inflammatory diseases: Killers or builders? *J. Immunol. Res.* 2018, 1–25. doi:10.1155/2018/8917804
- Pasquini, S., Contri, C., Borea, P. A., Vincenzi, F., and Varani, K. (2021). Adenosine and inflammation: Here, there and everywhere. *Int. J. Mol. Sci.* 22, 7685. doi:10.3390/ijms22147685
- Pham, L. N., Dionne, M. S., Shirasu-Hiza, M., and Schneider, D. S. (2007). A specific primed immune response in *Drosophila* is dependent on phagocytes. *PLoS Pathog.* 3, e26. doi:10.1371/journal.ppat.0030026
- Pizzagalli, D. U., Puffer, A., Thelen, M., Krause, R., and Gonzalez, S. F. (2022). In vivo motility patterns displayed by immune cells under inflammatory conditions. *Front. Immunol.* 12, 804159. doi:10.3389/fimmu.2021.804159
- Porta, C., Rimoldi, M., Raes, G., Brys, L., Ghezzi, P., Di Liberto, D., et al. (2009). Tolerance and M2 (alternative) macrophage polarization are related processes orchestrated by p50 nuclear factor κB. *Proc. Natl. Acad. Sci.* 106, 14978–14983. doi:10.1073/pnas.0809784106
- Preethi, P., Tomar, A., Madhwal, S., and Mukherjee, T. (2020). Immune control of animal growth in homeostasis and nutritional stress in *Drosophila*. *Front. Immunol.* 11, 1528. doi:10.3389/fimmu.2020.01528
- Ramond, E., Dudicz, J. P., and Lemaître, B. (2020). Comparative RNA-Seq analyses of *Drosophila* plasmacytes reveal genespecific signatures in response to clean injury and septic injury. *PLoS One* 15, e0235294. doi:10.1371/journal.pone.0235294
- Rath, M., Mäzler, I., Kropf, P., Closs, E. I., and Munder, M. (2014). Metabolism via arginase or nitric oxide synthase: Two competing arginine pathways in macrophages. *Front. Immunol.* 5, 532. doi:10.3389/fimmu.2014.00532
- Ravichandran, K. S. (2010). Find-me and eat-me signals in apoptotic cell clearance: Progress and conundrums. *J. Exp. Med.* 207, 1807–1817. doi:10.1084/jem.20101157
- Rayamajhee, B., Willcox, M. D. P., Henriquez, F. L., Petsoglou, C., Subedi, D., and Camt, N. (2022). *Acanthamoeba*, an environmental phagocyte enhancing survival and transmission of human pathogens. *Trends Parasitol.* 38, 975–990. doi:10.1016/j.pt.2022.08.007
- Razzell, W., Wood, W., and Martin, P. (2011). Swatting flies: Modelling wound healing and inflammation in *Drosophila*. *Dis. Model. Mech.* 4, 569–574. doi:10.1242/dmm.006825
- Rodriguez, P. C., Ochoa, A. C., and Al-Khami, A. A. (2017). Arginine metabolism in myeloid cell shapes innate and adaptive immunity. *Front. Immunol.* 8, 93. doi:10.3389/fimmu.2017.00093
- Romeralo, M., Cavender, J. C., Landolt, J. C., Stephenson, S. L., and Baldauf, S. L. (2011). An expanded phylogeny of social amoebas (*Dictyostelia*) shows increasing diversity and new morphological patterns. *BMC Evol. Biol.* 11, 84. doi:10.1186/1471-2148-11-84
- Ros-Rocher, N., Pérez-Posada, A., Leger, M. M., and Ruiz-Trillo, I. (2021). The origin of animals: An ancestral reconstruction of the unicellular-to-multicellular transition. *Open Biol.* 11, 200359. doi:10.1098/rsob.200359
- Ross, E. A., Devitt, A., and Johnson, J. R. (2021). Macrophages: The good, the bad, and the glutinous. *Front. Immunol.* 12, 708186. doi:10.3389/fimmu.2021.708186
- Salah, I. B., Ghigo, E., and Drancourt, M. (2009). Free-living amoebae: A training field for macrophage resistance of mycobacteria. *Clin. Microbiol. Infect.* 15, 894–905. doi:10.1111/j.1469-0691.2009.03011.x
- Schmitz, F., Mages, J., Heit, A., Lang, R., and Wagner, H. (2004). Transcriptional activation induced in macrophages by toll-like receptor (TLR) ligands: From expression profiling to a model of TLR signaling. *Eur. J. Immunol.* 34, 2863–2873. doi:10.1002/eji.200425228
- Schuster, F. L., and Levandowsky, M. (1996). Chemosensory responses of *Acanthamoeba castellanii*: Visual analysis of random movement and responses to chemical signals. *J. Eukaryot. Microbiol.* 43, 150–158. doi:10.1111/j.1550-7408.1996.tb04496.x
- Sciaraffia, E., Riccomi, A., Lindstedt, R., Gesa, V., Cirelli, E., Patrizio, M., et al. (2014). Human monocytes respond to extracellular cAMP through A2A and A2B adenosine receptors. *J. Leukoc. Biol.* 96, 113–122. doi:10.1189/jlb.3A0513-302RR
- Sender, R., and Milo, R. (2021). The distribution of cellular turnover in the human body. *Nat. Med.* 27, 45–48. doi:10.1038/s41591-020-01182-9
- Sica, A., Erreni, M., Allavena, P., and Porta, C. (2015). Macrophage polarization in pathology. *Cell. Mol. Life Sci.* 72, 4111–4126. doi:10.1007/s00018-015-1995-y
- Siddiqui, R., and Khan, N. A. (2012a). *Acanthamoeba* is an evolutionary ancestor of macrophages: A myth or reality? *Exp. Parasitol.* 130, 95–97. doi:10.1016/j.exppara.2011.11.005
- Siddiqui, R., and Khan, N. A. (2012b). Biology and pathogenesis of *Acanthamoeba*. *Parasit. Vectors* 5, 6. doi:10.1186/1756-3305-5-6
- Siddiqui, R., Roberts, S. K., Ong, T. Y. Y., Mungroo, M. R., Anwar, A., and Khan, N. A. (2019). Novel insights into the potential role of ion transport in sensory perception in *Acanthamoeba*. *Parasit. Vectors* 12, 538. doi:10.1186/s13071-019-3785-0
- Singer, G., Araki, T., and Weijer, C. J. (2019). Oscillatory cAMP cell-cell signaling persists during multicellular *Dictyostelium* development. *Commun. Biol.* 2, 139. doi:10.1038/s42003-019-0371-0
- Smith, L. C., and Hildemann, W. H. (1986). Allograft rejection, autograft fusion and inflammatory responses to injury in *Callyspongia diffusa* (Porifera; Demospongia). *Proc. R. Soc. Lond. Ser. B. Biol. Sci.* 226, 445–464. doi:10.1098/rspb.1986.0003
- Sogabe, S., Hatleberg, W. L., Kocot, K. M., Say, T. E., Stoupin, D., Roper, K. E., et al. (2019). Pluripotency and the origin of animal multicellularity. *Nature* 570, 519–522. doi:10.1038/s41586-019-1290-4
- Sokol, C. L., and Luster, A. D. (2015). The chemokine system in innate immunity. *Cold Spring Harb. Perspect. Biol.* 7, a016303. doi:10.1101/cshperspect.a016303
- Srivastava, M., Simakov, O., Chapman, J., Fahey, B., Gauthier, M. E. A., Mitros, T., et al. (2019). The *Amphimedon queenslandica* genome and the evolution of animal complexity. *Nature* 466, 720–726. doi:10.1038/nature09201
- Steinz, M. M., Ezzoglian, A., Khodadust, F., Molthoff, C. F. M., Srinivasarao, M., Low, P. S., et al. (2022). Folate receptor beta for macrophage imaging in rheumatoid arthritis. *Front. Immunol.* 13, 819163. doi:10.3389/fimmu.2022.819163
- Storelli, G., Nam, H.-J., Simcox, J., Villanueva, C. J., and Thummel, C. S. (2019). *Drosophila* HNF4 directs a switch in lipid metabolism that supports the transition to adulthood. *Dev. Cell* 48, 200–214. doi:10.1016/j.devcel.2018.11.030
- Strakhova, R., Cadassou, O., Cros-Perial, E., and Jordheim, L. P. (2020). Regulation of tumor infiltrated innate immune cells by adenosine. *Purinergic Signal* 16, 289–295. doi:10.1007/s11302-020-09701-6
- Strassmann, J. E., and Queller, D. C. (2011). Evolution of cooperation and control of cheating in a social microbe. *Proc. Natl. Acad. Sci.* 108, 10855–10862. doi:10.1073/pnas.1102451108
- Stratoulas, V., and Heino, T. I. (2015). MANF silencing, immunity induction or autophagy trigger an unusual cell type in metamorphosing *Drosophila* brain. *Cell. Mol. Life Sci.* 72, 1989–2004. doi:10.1007/s00018-014-1789-7
- Swart, A. L., Harrison, C. F., Eichinger, L., Steinert, M., and Hilbi, H. (2018). *Acanthamoeba* and *Dictyostelium* as cellular models for Legionella infection. *Front. Cell. Infect. Microbiol.* 8, 61. doi:10.3389/fcimb.2018.00061
- Szondi, D. C., Wong, J. K., Vardy, L. A., and Cruickshank, S. M. (2021). Arginase signalling as a key player in chronic wound pathophysiology and healing. *Front. Mol. Biosci.* 8, 773866. doi:10.3389/fmolb.2021.773866
- Tattikota, S. G., Cho, B., Liu, Y., Hu, Y., Barrera, V., Steinbaugh, M. J., et al. (2020). A single-cell survey of *Drosophila* blood. *Elife* 9, e54818. doi:10.7554/elife.54818
- Tauber, A. I. (2017). "A history of the immune self," in *Immunity* (United Kingdom: Oxford University Press), 23–56.
- Tauber, A. I. (2003). Metchnikoff and the phagocytosis theory. *Nat. Rev. Mol. Cell Biol.* 4, 897–901. doi:10.1038/nrm1244
- Tavares, L. P., Negreiros-Lima, G. L., Lima, K. M., E Silva, P. M. R., Pinho, V., Teixeira, M. M., et al. (2020). Blame the signaling: Role of cAMP for the resolution of inflammation. *Pharmacol. Res.* 159, 105030. doi:10.1016/j.phrs.2020.105030
- Thacker, R. W., Diaz, M. C., Kerner, A., Vignes-Lebbe, R., Segerdell, E., Haendel, M. A., et al. (2014). The Porifera ontology (PORO): Enhancing sponges systematics with an anatomy ontology. *J. Biomed. Semant.* 5, 39. doi:10.1186/2041-1480-5-39
- Theret, M., Mounier, R., and Rossi, F. (2019). The origins and non-canonical functions of macrophages in development and regeneration. *Development* 146, dev156000. doi:10.1242/dev.156000
- Tice, A. K., Shadwick, L. L., Fiore-Donno, A. M., Geisen, S., Kang, S., Schuler, G. A., et al. (2016). Expansion of the molecular and morphological diversity of *Acanthamoebidae* (Centramoebida, Amoebozoa) and identification of a novel life cycle type within the group. *Biol. Direct* 11, 69. doi:10.1186/s13062-016-0171-0
- Trojan, E., Bryniarska, N., Leśkiewicz, M., Regulska, M., Chamera, K., Szuster-Gluszczak, M., et al. (2020). The contribution of formyl peptide receptor dysfunction to the course of neuroinflammation: A potential role in the brain pathology. *Curr. Neuropharmacol.* 18, 229–249. doi:10.2174/1570159X17666191019170244
- Vanha-aho, L.-M., Valanne, S., and Rämetsä, M. (2016). Cytokines in *Drosophila* immunity. *Immunol. Lett.* 170, 42–51. doi:10.1016/j.imlet.2015.12.005
- Viola, A., Munari, F., Sánchez-Rodríguez, R., Scolari, T., and Castegna, A. (2019). The metabolic signature of macrophage responses. *Front. Immunol.* 10, 1462. doi:10.3389/fimmu.2019.01462

- Vogel, G., Thilo, L., Schwarz, H., and Steinhart, R. (1980). Mechanism of phagocytosis in dictyostelium discoideum: Phagocytosis mediated by different recognition sites as disclosed by mutants with altered phagocytotic properties. *J. Cell Biol.* 86, 456–465. doi:10.1083/jcb.86.2.456
- Wang, L., Li, H., Tang, Y., and Yao, P. (2021a). Potential mechanisms and effects of efferocytosis in atherosclerosis. *Front. Endocrinol. (Lausanne)* 11, 11. doi:10.3389/fendo.2020.585285
- Wang, L., Zhang, S., Wu, H., Rong, X., and Guo, J. (2019a). M2b macrophage polarization and its roles in diseases. *J. Leukoc. Biol.* 106, 345–358. doi:10.1002/JLB.3RU1018-378RR
- Wang, S. Y., Pollina, E. A., Wang, I.-H., Pino, L. K., Bushnell, H. L., Takashima, K., et al. (2021b). Role of epigenetics in unicellular to multicellular transition in *Dictyostelium*. *Genome Biol.* 22, 134. doi:10.1186/s13059-021-02360-9
- Wang, T., Liu, H., Lian, G., Zhang, S.-Y., Wang, X., and Jiang, C. (2017). HIF1 α -induced glycolysis metabolism is essential to the activation of inflammatory macrophages. *Mediat. Inflamm.* 2017, 1–10. doi:10.1155/2017/9029327
- Wang, X., Iyer, A., Lyons, A. B., Körner, H., and Wei, W. (2019b). Emerging roles for G-protein coupled receptors in development and activation of macrophages. *Front. Immunol.* 10. doi:10.3389/fimmu.2019.02031
- Wenceslau, C. F., McCarthy, C. G., Goulopoulou, S., Szasz, T., NeSmith, E. G., and Webb, R. C. (2013). Mitochondrial-derived N-formyl peptides: Novel links between trauma, vascular collapse and sepsis. *Med. Hypotheses* 81, 532–535. doi:10.1016/j.mehy.2013.06.026
- Wiens, M., Korzhev, M., Krasko, A., Thakur, N. L., Perović-Ottstadt, S., Breter, H. J., et al. (2005). Innate immune defense of the sponge *Suberites domuncula* against bacteria involves a MyD88-dependent signaling pathway. Induction of a perforin-like molecule. *J. Biol. Chem.* 280, 27949–27959. doi:10.1074/jbc.M504049200
- Witherell, C. E., Sao, K., Brisson, B. K., Han, B., Volk, S. W., Petrie, R. J., et al. (2021). Regulation of extracellular matrix assembly and structure by hybrid M1/M2 macrophages. *Biomaterials* 269, 120667. doi:10.1016/j.biomaterials.2021.120667
- Wood, W., Jacinto, A., Grose, R., Woolner, S., Gale, J., Wilson, C., et al. (2002). Wound healing recapitulates morphogenesis in *Drosophila* embryos. *Nat. Cell Biol.* 4, 907–912. doi:10.1038/ncb875
- Woodcock, K. J., Kierdorf, K., Pouchelon, C. A., Vivancos, V., Dionne, M. S., and Geissmann, F. (2015). Macrophage-Derived *upd3* cytokine causes impaired glucose homeostasis and reduced lifespan in *Drosophila* fed a lipid-rich diet. *Immunity* 42, 133–144. doi:10.1016/j.immuni.2014.12.023
- Wu, Y., and Hirschi, K. K. (2021). Tissue-resident macrophage development and function. *Front. Cell Dev. Biol.* 8. doi:10.3389/fcell.2020.617879
- Xia, W., Hilgenbrink, A. R., Matteson, E. L., Lockwood, M. B., Cheng, J.-X., and Low, P. S. (2009). A functional folate receptor is induced during macrophage activation and can be used to target drugs to activated macrophages. *Blood* 113, 438–446. doi:10.1182/blood-2008-04-150789
- Xu, X., Pan, M., and Jin, T. (2021). How phagocytes acquired the capability of hunting and removing pathogens from a human body: Lessons learned from chemotaxis and phagocytosis of *Dictyostelium discoideum* (review). *Front. Cell Dev. Biol.* 9, 724940. doi:10.3389/fcell.2021.724940
- Xuan, W., Qu, Q., Zheng, B., Xiong, S., and Fan, G.-H. (2015). The chemotaxis of M1 and M2 macrophages is regulated by different chemokines. *J. Leukoc. Biol.* 97, 61–69. doi:10.1189/jlb.1A0314-170R
- Yamitzky, T., and Volk, T. (1995). Laminin is required for heart, somatic muscles, and gut development in the *Drosophila* embryo. *Dev. Biol.* 169, 609–618. doi:10.1006/dbio.1995.1173
- Zhang, X., Cao, X., Zhang, W., Yu, X., and Jin, M. (2003). Primmorphs from archaeocytes-dominant cell population of the sponge *Hymeria acida* n. sp.: Improved cell proliferation and spiculogenesis. *Biotechnol. Bioeng.* 84, 583–590. doi:10.1002/bit.10811
- Zhang, X., and Soldati, T. (2016). Of amoebae and men: Extracellular DNA traps as an ancient cell-intrinsic defense mechanism. *Front. Immunol.* 7, 269. doi:10.3389/fimmu.2016.00269
- Zhou, J., Tang, Z., Gao, S., Li, C., Feng, Y., and Zhou, X. (2020). Tumor-associated macrophages: Recent insights and therapies. *Front. Oncol.* 10, 188. doi:10.3389/fonc.2020.00188

CHAPTER VII:

Yeast glucan particles enable intracellular protein delivery in *Drosophila* without compromising the immune system

Adam Bajgar, Ivan Saloň, **Gabriela Krejčová**, Tomáš Doležal, Marek Jindra, František Štěpánek

Biomaterials Science, 2019, 7:4708-4719

ARTICLE

Yeast glucan particles enable intracellular protein delivery in *Drosophila* without compromising the immune systemAdam Bajgar^{a,b+}, Ivan Saloň^{b+}, Gabriela Krejčová^a, Tomáš Doležal^a, Marek Jindra^c, František Štěpánek^{b,*}

Glucan particles derived from yeast have been recently proposed as potential drug delivery carriers. Here, we demonstrate the potential of glucan particles for protein delivery *in vivo*, using the insect *Drosophila melanogaster* as a model organism.

By employing genetic tools, we demonstrate the capacity of yeast glucan particles to spread efficiently through the *Drosophila* body, to enter macrophages and to deliver an active transcription factor protein successfully. Moreover, the glucan particles were nontoxic and induced only minimal immune response. The injection of glucan particles did not impair the ability of *Drosophila* to fight and survive infection by pathogenic bacteria. From this study, *Drosophila* emerges as an excellent model to test and develop drug delivery systems based on glucan particles, specifically aimed to regulate macrophages.

1 Introduction

The design and optimisation of drug delivery systems is an exceptionally parametrically rich problem that requires *in vivo* testing as an integral part of the design loop, since high fidelity prediction of *in vivo* behavior from *in vitro* data is not yet generally possible^{1,2,3}. The testing of all particular modifications of a drug delivery system in laboratory animals such as mice is not feasible not only for ethical reasons but also due to factors such as poor reproducibility of preclinical studies, time- and financial constraints^{4,5,6,7}. While the creation of organ-on-chip models for pre-clinical testing became highly investigated by the scientific community and these tools can prove the pharmacological effect of new drug candidates and confirm the absence of toxicity without harming or sacrificing animals, the cellular response in organ-on-chip models is still far from that in a real living organism^{8,9,10,11,12}.

On the other hand, human disease models investigating innate immunity, cancer, cardiovascular diseases, diabetes, infectious

diseases, neurodegeneration, Alzheimer's disease, Parkinson's disease, sleep, seizure disorders and cognitive disorders are well known in the fly *Drosophila melanogaster* because many basic biological, physiological, and neurological properties are conserved between mammals and the fruit fly^{13,14,15,16,17,18,19,20}. Nearly 75 % of human disease-causing genes are believed to have a functional homolog in *Drosophila*²¹ which makes it suitable for identifying new drug targets and drug candidates²². Therefore, we aim to demonstrate that *Drosophila* can serve as a model for the testing of drug delivery systems based on glucan particles (GPs) as a versatile carrier able to deliver bioactive substances *in vivo* and specifically to macrophages.

Macrophages as an essential part of the innate immune response are in the spotlight of the immunology research for their versatile role within living systems^{23,24}. Current research shows that macrophages are not only involved in phagocytosis of bacteria and apoptotic cells but also play essential functions in the formation of developing tissues or in the maintenance of metabolic homeostasis^{25,26}. With an increasing amount of knowledge, it is becoming clear that these immune cells react very plastically to signals from the extracellular space and represent a very heterogeneous population with different organ-specific roles²⁷. Under healthy conditions, macrophages can fluently modulate their polarisation program and actively react to changing situation, while chronic dysregulation of their activity frequently causes severe pathologies, such as immune deficiencies, chronic inflammatory diseases, neurodegeneration or metabolic syndrome²⁸. The mechanisms behind these diseases are very complex and require the ability to study molecular pathways at the level of cell-specific signaling, as well as of the systemic response of an organism. Owing to their unique ability to engulf foreign objects, macrophages can be exploited for targeted drug delivery more

^a University of South Bohemia, Faculty of Sciences, Department of Molecular Biology and Genetics, Branišovská 1160/31, 37005 České Budějovice, Czech Republic.

^b University of Chemistry and Technology Prague, Department of Chemical Engineering, Technická 3, 166 28 Prague, Czech Republic.

^c Biology Centre CAS, Institute of Entomology, Branišovská 1160/31, 37005 České Budějovice, Czech Republic.

† These authors contributed equally.

* Corresponding author. E-mail: Frantisek.Stepanek@vscht.cz; Phone: +420 220 443 231.

Electronic Supplementary Information (ESI) available

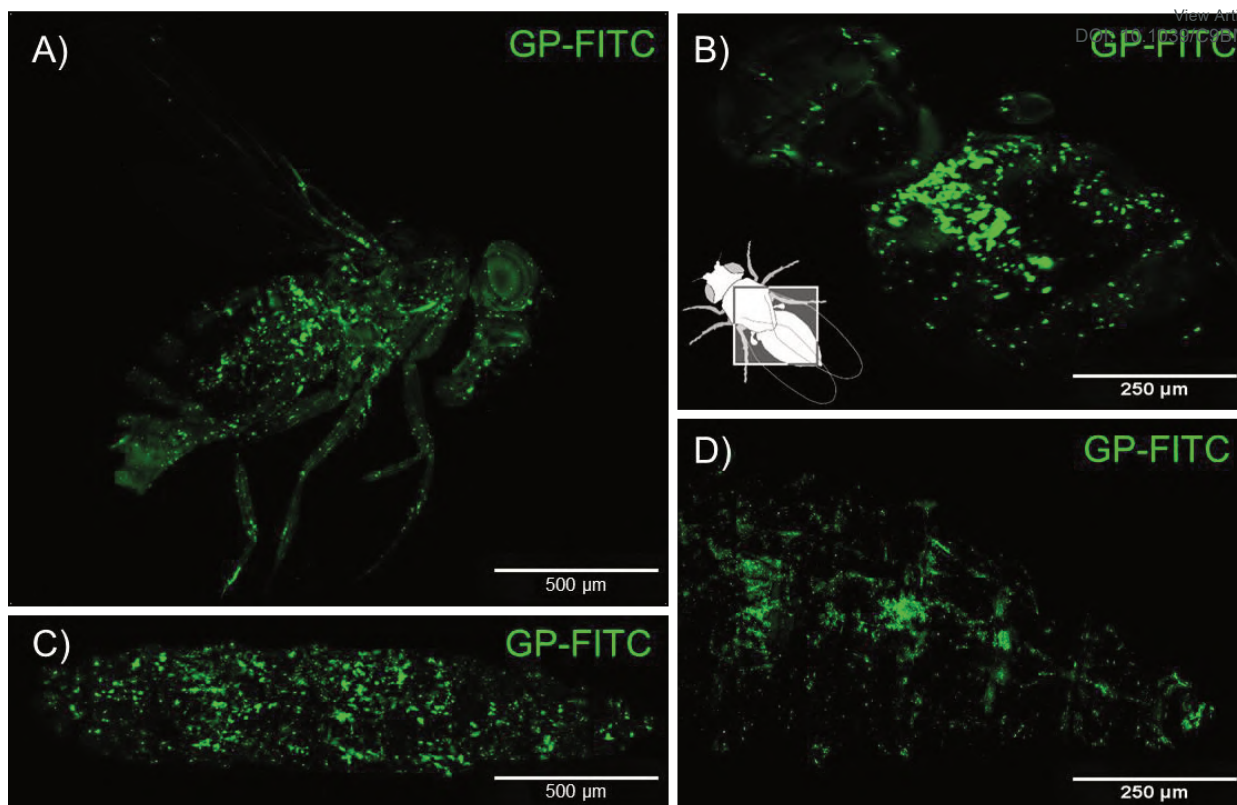


Fig. 1. GP-FITC can spread through the body of both adult flies and larvae after injection, reaching even distal parts of the body. (A) Confocal image of the whole adult fly – lateral view. Green spots represent sites of GP-FITC accumulation 30 minutes after injection. (B) Dorsal view of the adult fly abdomen – GP-FITC particles accumulate in the sites of dorsal hubs – sites around the aorta characteristic by a high occurrence of macrophages. (C) Confocal image of the whole 3rd instar larva – lateral view with head on the right-hand side of the image. (D) Dorsal view of the larval body in detail, GP-FITC particles accumulate in sites of expected sub-epithelial hemocyte patches.

easily than other cell types²⁹. This feature, together with their central role in the regulation of many biological processes, makes macrophages a promising target in the development of intelligent drug delivery strategies^{30, 31}. Given their motility, macrophages can also serve as Trojan horses for further transport of drug carriers^{32, 33, 34}.

Key factors that influence the phagocytosis of drug delivery systems by macrophages include particle size, shape, elasticity, and surface chemistry³⁵. Macrophage toll-like receptors and other pattern recognition receptors recognize pathogen-associated molecular patterns common to most microbes. Among the molecular motifs recognized by macrophages are beta-glucans, carbohydrate polymers found in the cell walls of fungi, yeast, plants, and bacteria. Several *in vitro* studies have demonstrated the intrinsic adjuvant capacity of β -1,3-glucans from yeast and fungi in enhancing the functional activity of macrophages, neutrophils, dendritic cells, and epithelial cells. Particulate β -glucans may serve as a suitable vaccine delivery platform³⁵ because they are generally recognized as safe since 2007 and established in large animals and humans³⁶. Encapsulation of antigens into GPs purified from *Saccharomyces cerevisiae* can serve in the vaccination against diseases such as tularemia and cryptococcosis caused by

intracellular pathogens infecting macrophages in the host organism but also in other oral vaccine formulations^{37, 38}. A down-regulation of gene expression in macrophages by using the delivery of siRNA in glucan particles was recently tested on mammals^{39, 40}. This approach represents a stepping stone for GP delivery systems carrying various compounds as a cargo. Here, we propose *Drosophila* as a model organism combining the features of a simple and inexpensive, yet relevant and well-defined system for the preclinical studies of macrophage-specific drug delivery systems. Specifically, we show that GPs spread through the whole *Drosophila* organism quickly and accumulate in sites of macrophage occurrence. We provide evidence that GPs colocalise with macrophages and are efficiently phagocytosed with only a negligible effect on immune response activation. Crucially, using the Gal4/UAS system, we demonstrate that GPs can deliver a functional molecular cargo into the macrophages *in vivo* to activate gene expression.

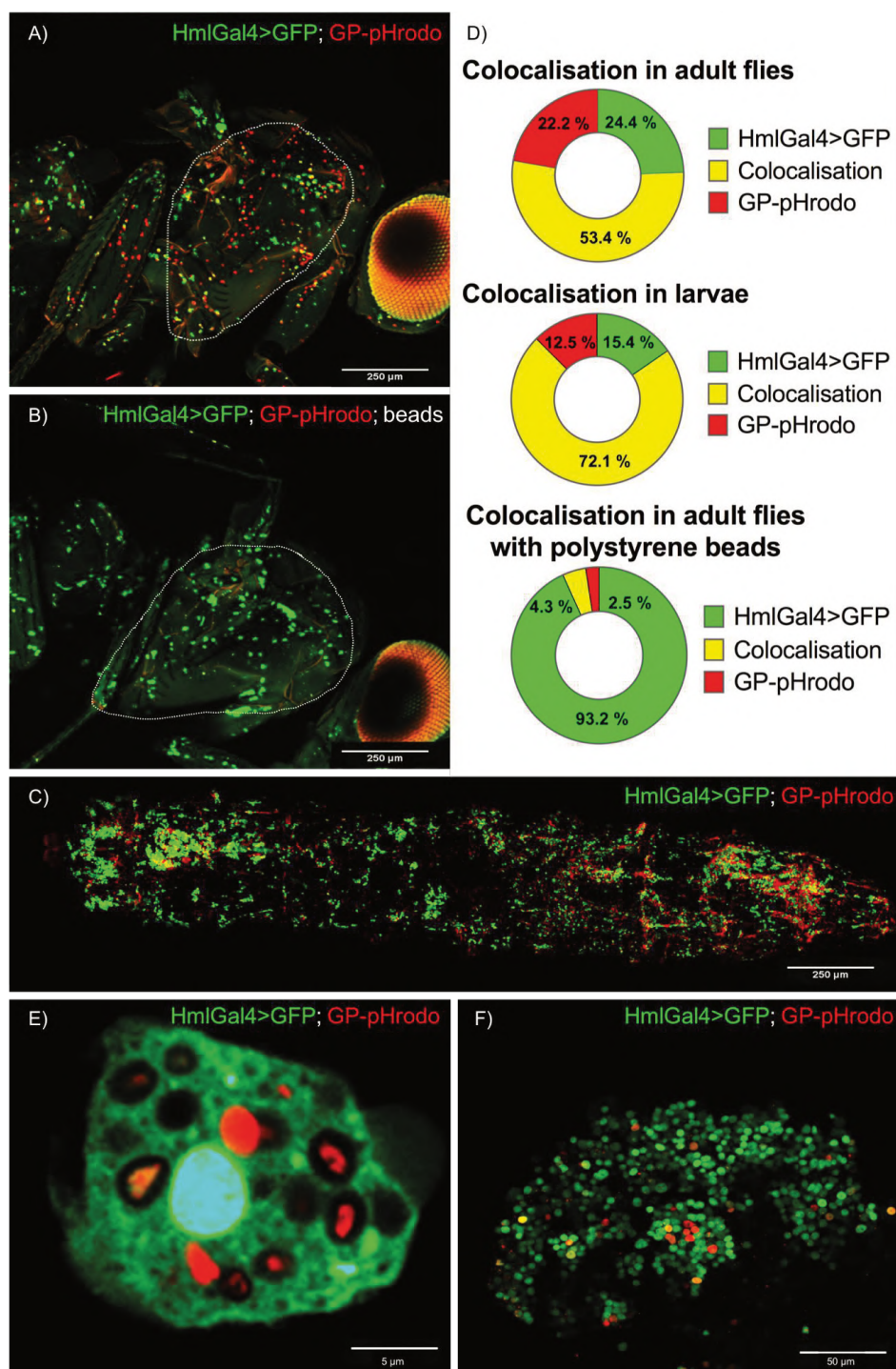


Fig.2. GP-pHrodo particles (red fluorescent signal) colocalization with HmlGal4>GFP macrophages (green fluorescent signal) in adult flies and in 3rd instar larvae. **(A)** Confocal image of an adult fly, **(B)** adult fly pre-treated by the injection of polystyrene beads to saturate the macrophages, **(C)** 3rd instar larva. **(D)** Quantitative analysis of colocalisation, represented by yellow fluorescence (GP internalized by macrophages), compared to regions showing only green fluorescence (empty macrophages) or red fluorescence (GP phagocytosed by other phagocytic cells), evaluated for adult flies, adult flies with abrogated phagocytosis and for larvae. The numbers represent data from 15 counted individuals, counts were made on the standardized confocal images in the defined morphological region of the individuals. **(E)** Detailed confocal image of a single macrophage internalizing GP-pHrodo (blue color for DAPI). **(F)** Dissected lymph gland (hematopoietic tissue) of a larva containing several phagocytosing cells.

2 Results

2.1 Glucan particles spread through the whole organism quickly and accumulate in sites of macrophage occurrence

A suspension of GPs modified with fluorescein isothiocyanate (GP-FITC) was introduced into the circulation of living fruit flies and larvae by injection. Feeding, as an alternative delivery method, proved not to be effective (Fig. S1). The amount of GPs injected into the fly can be scaled by dilutions, which helps to define a suitable dose. An appropriate volume injected into the abdomen of an adult fly without damaging its functions and not exceeding the physical limits of the body was found to be 50 nL of a 0.1% (w/w) suspension of GP-FITC particles, which corresponds to approximately 7500 particles. The bright green signal of individual particles observed with confocal fluorescence microscopy gave us information about the GP distribution within the *Drosophila* body at the adult and larval stages (Fig. 1). Immediately after injection, we have observed accumulation of GPs at the site of puncture, but the glucan particles retained their colloidal stability and were able to spread through the hemolymph within 15–20 min after injection spontaneously (Fig. S2). The particles accumulated mostly at the sites densely populated by macrophages. In adult flies, these regions are located in dorsal hubs and along the aorta, but the GPs were able to reach even distal parts of the fly's body such as legs and antennae (Fig. 1A, B). In the larval stadium, GPs accumulate at the sites of high macrophage occurrence – under the cuticle and in locations of hematopoietic pockets and lymph gland (Fig. 1C, D). The fact that GPs are responsible for observed dotted pattern typical for distribution of immune cells was further proven by injection of FITC alone while this treatment resulted in dispersed fluorescence in the whole fly body without occurrence of obvious localisation into the particular structures (Fig. S3).

2.2 Glucan particles colocalise with macrophages and are efficiently phagocytosed

To bring evidence that the macrophages truly internalise GPs, we modified GPs with a pH-sensitive fluorescent dye pHrodo (GP-pHrodo). The molecule shows bright red fluorescence in an acidic environment, which occurs explicitly in the phagolysosomes. Thus, the molecule can be used for the detection of phagocytic cells. To show the localisation of phagocytosed GP-pHrodo in macrophages, we have combined GP-pHrodo injection with genetically driven production of green fluorescent protein (GFP) under a hemocyte-specific driver hemolectin (Hml-Gal4>GFP). This combination was used to assess the efficiency of GP internalisation in both 3rd instar larvae and adult flies (Fig. 2A, C). Empty macrophages are visualised in bright green while macrophages containing GPs are yellow. The colocalisation of GPs and macrophages was quantified within defined anatomical regions, the thorax in adult flies and the dorsal side of the A5-abdominal segment in larvae. The high incidence of colocalisation is documented by the fact that 53.4% of Hml>GFP positive macrophages in adult

flies showed the yellow signal of internalised GPs (Fig. 2D). The rate of colocalisation in larvae was even higher (72.1%, Fig. 2E). Some of the cells only contained the red fluorescent signal, suggesting that cells other than Hml>GFP positive macrophages can also scavenge the GPs. As the HmlGal4 driver is known to mark only approximately 85% of the macrophage population⁴¹, the red signal most likely represents GP phagocytosis by the remaining Hml>GFP negative macrophages. The observation of a single macrophage gave us information about its ability to uptake a high number of GPs in multiple phagolysosomes (Fig. 2E). The dissection of immune tissue in the larval stage of *Drosophila* revealed a somewhat surprising presence of several positive cells also in the lymph gland (Fig. 2F). This observation suggests that some of the lymph gland cells are capable of active phagocytosis.

To further show that the GP-pHrodo positive signal is produced explicitly by phagocytosing cells we carried out a control experiment in which we abrogated the phagocytic activity of macrophages in advance by the injection of polystyrene particles. This pre-treatment resulted in an almost complete dampening of the previously observed signal in adult flies (Fig. 2A, B). To exclude the possibility that the pHrodo molecule plays a role in the phagocytic activation and that a high amount of particles stay in the extracellular space, we confirmed our observations in two additional control experiments. First, we co-injected GP-FITC together with *S. aureus*-pHrodo cell wall fragments commonly used in *Drosophila* to study phagocytosis⁴². Second, we injected GP-FITC into flies carrying a nuclearly localised hemocyte-specific red fluorescent signal (Hml-dsRed). Both of these controls yielded results consistent with the original experiment using GP-pHrodo particles (Fig. S4), *i.e.*, a high degree of colocalisation. Based on these results it can be claimed that macrophages actively internalise GPs and that a pH-sensitive fluorophore modification of the GP delivery system in combination with genetically encoded tools for marking the target tissues can visualise the uptake and localisation of GPs in *Drosophila* macrophages.

2.3 Glucan particles can deliver cargo into the macrophages *in vivo*

We next tested whether GPs can be used for the delivery of bioactive molecules into the macrophages. To exploit the ability of GPs to deliver cargo, we loaded the GPs with a 32-kDa Gal4 protein (GP-Gal4). Gal4 is a transcriptional activator of the upstream activating sequence (UAS), which is frequently used in *Drosophila*⁴³ to study targeted gene expression. We injected the GP-Gal4 particles into adult flies carrying a UASmCherry transgenic reporter wherein expression of the red fluorescent protein mCherry is controlled by the UAS. The UAS-dependent production of mCherry can only be triggered by the exogenous Gal4 protein which, moreover, cannot cross cell boundaries and spread into surrounding tissues. Thus, the flies show no

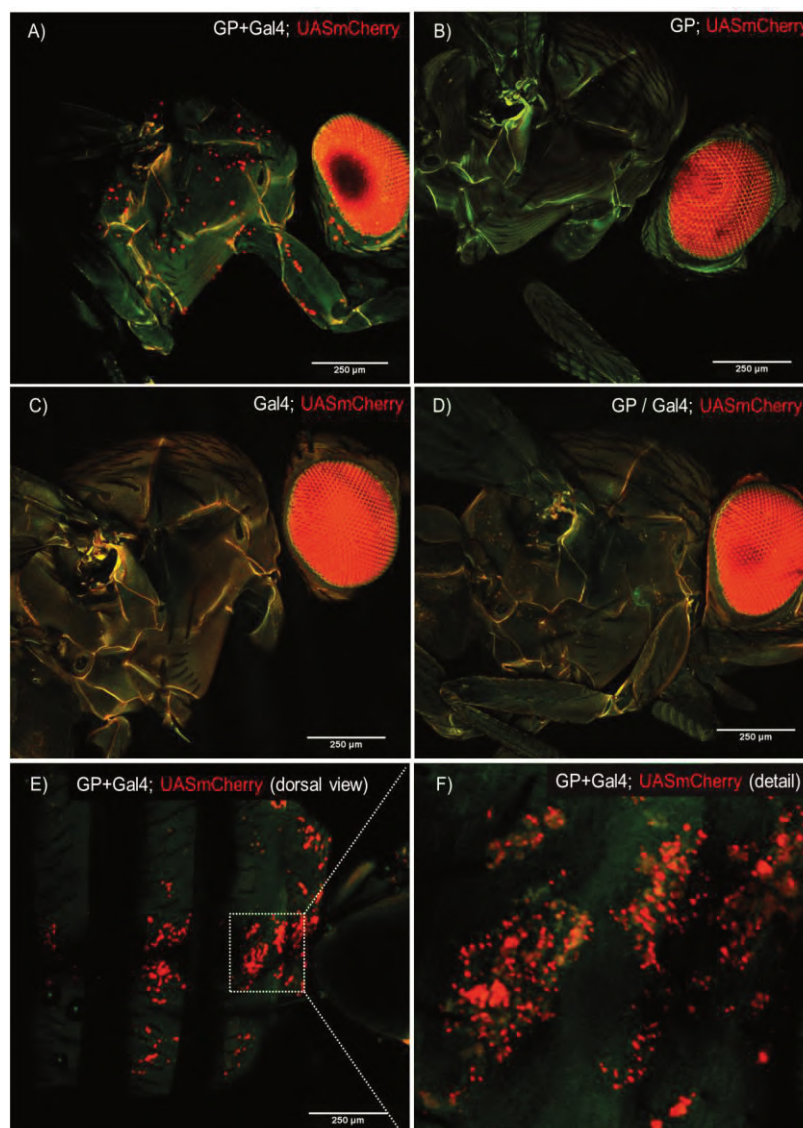


Fig. 3. GP can be used for the delivery of Gal4 protein to trigger the expression of a reporter gene. **(A)** Flies treated by the injection of GP loaded with Gal4 resulted in the activation of UAS mCherry reporter construct. Coinjection of empty GP together with Gal4 **(B)** as well as the injection of empty GP **(C)** or Gal4 **(D)** individually gave no positive signal. **(E)** Dorsal view of flies injected with Gal4 loaded GP shows a strong fluorescent signal in a pattern typical for macrophages surrounding the aorta **(F)**.

fluorescent signal under normal conditions; however, they produce red fluorescence in the presence of Gal4 in the macrophages. Approximately 60 min following injection of the GP-Gal4 particles into adult flies, the mCherry signal could be detected in the macrophages (Fig. 3A) and also proved by pull down assay (Fig. S5). As expected, no such signal appeared when UASmCherry flies were injected with either empty GPs or the Gal4 protein alone (Fig. 3B, C). Importantly, the coinjection of a mixture of empty GPs with free Gal4 also could not activate mCherry expression (Fig. 3D), demonstrating that the Gal4 protein could only be delivered to the macrophages via the GPs. Further evidence of the unique role of GPs in the delivery of Gal4 to macrophages was provided by employing GP-FITC as the Gal4 carrying particles, and observing their colocalisation with the mCherry signal. The red fluorescence of the mCherry reporter was found only in those macrophages that also

contained phagocytosed GP-FITC (Fig. S6). From the drug delivery point of view, this is a very significant result as it offers a new route by which protein-based therapeutic substances can be efficiently delivered to cells. Even though the result of this experiment is clear, it appears that the number of mCherry positive cells in Fig. 3A is lower relative to the number of macrophages targeted with GP-pHrodo particles (Fig. 2A). We hypothesise that in the case of GP-Gal4, the cells have to receive an amount of the Gal4 protein sufficient to trigger a robust detectable expression. In addition to the thorax, we observed many mCherry expressing cells on the dorsal side of the adult fly abdomen (Fig. 3E, F). Consistent with the normal macrophage localisation and function in scavenging foreign objects from the circulation, these cells surrounded the aorta and displayed a robust mCherry signal, perhaps caused by an increased influx of the blood-borne GP-Gal4 complex.

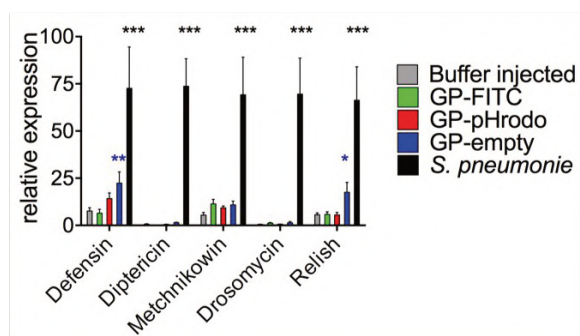
2.4 Empty glucan particles have a negligible effect on immune response activation

To identify the limits of GPs use in drug delivery and immunology research, we examined the potential impacts of GPs on the activation of the immune response, gene expression, longevity, and resistance to bacterial infection. We first assessed the expression of antimicrobial peptides and the Toll reporter gene *Relish* in response to the injection of GPs and their modifications. For comparison, we triggered the immune response by injecting 20 000 units of *Streptococcus pneumoniae* (*Sp*), a treatment commonly used to induce sepsis¹⁸. The data show that contrary to *Sp* injection, the treatment with GPs had only a mild or no effect on the expression of the immune response pathway genes (Fig. 4A). Next, we analysed the survival of individual flies for 30 days following the injections (Fig. 4B). Interestingly, there was a slight but statistically significant decrease in the survival rate of flies injected with empty GPs (Fig. 4B), which correlated with the increased expression of *Defensin* and *Relish* mRNAs (Fig. 4A). The effect of

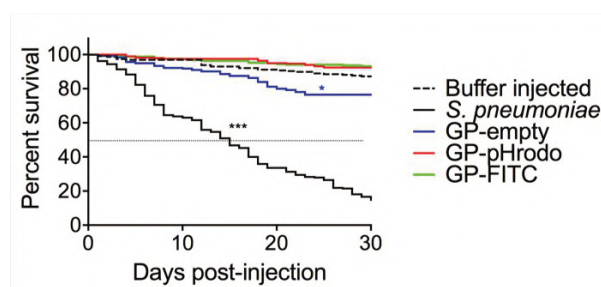
empty GPs on the activation of the immune response in comparison with other modified GPs might be explained by the covalently bound fluorescent dyes masking some surface bioactive glucan moieties.

To test whether GPs might interfere with a standard immune response to a pathogen, we deployed GPs 24 h before the injection with *Sp* and monitored individual survival after that. Resistance to *Sp* infection is known to mainly rely on phagocytic activity⁴⁴. Therefore, we compared the survival rate and bacterial growth following GP injection with a situation where phagocytosis was compromised by the injection of polystyrene beads. The results show that relative to the polystyrene beads treatment, the effect of GPs on the survival of *Sp* infected flies was minor, comparable to injection with buffer only (Fig. 4C). Consistently, blocking phagocytosis by polystyrene beads reduced the ability of the flies to suppress bacterial growth, whereas GP injection did not (Fig. 4D). The low immunogenicity and toxicity can be attributed to the complete removal of cellular components from the GPs during their preparation from yeast⁴⁵. Still, the epitopes on the GP surface, particularly β -1,3-

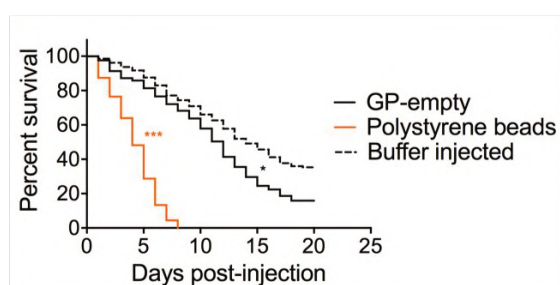
A) Expression of immune response genes



B) Survival rate after GP injection



C) Survival rate of *S. pneumoniae* infected flies



D) Effect of GPs on infection resistance

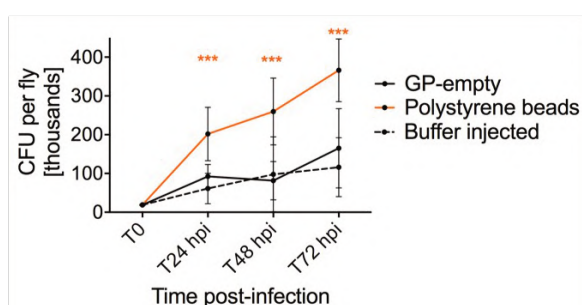


Fig. 4. Injection of GP has a negligible effect on the activation of the immune response, the vitality of individuals and their ability to fight and resist bacterial infection. (A) The expression levels of particular immune response readouts (*Defensin*, *Diptericin*, *Metchnikowin*, *Drosomycin*, and *Relish*) were measured by qPCR after the injection of plain glucan particles (blue), pHrodo labeled glucan particles (red) and FITC labeled glucan particles (green) in comparison to the injection of *Streptococcus pneumoniae* (black) as a positive control and buffer (grey) as a negative control. (B) The flies that underwent the same treatment were observed for the survival rate for 30 days (each treatment was carried out on more than 300 individuals). (C) The survival of bacterial infection was observed after the injection of 20 000 *Sp* units per fly. The flies were pre-treated 24 hours before the infection either by glucan particles, buffer as a negative control, and polystyrene beads abrogating phagocytosis as a positive control. (D) In parallel, the number of colony forming units (bacteria) per fly was assayed in this treatment.

and β -1,6-glucans, can be recognised by macrophages and phagocytosed⁴⁶. Similarly, low immunogenicity was also reported after the injection of heat-killed bacterial culture, which does not represent a real danger for the host and is efficiently phagocytosed without massive immune response⁴⁷.

3 Discussion

Current progress in macrophage biology identifies macrophage subpopulations residing in different tissues as very heterogeneous but possessing organ-specific functions⁴⁸. Therefore, macrophage-specific targeting can serve as a tool for research into many elusive diseases. Macrophage targeting is based on phagocytosis, using specific particles as a "bait" loaded with an active compound to affect the biology of the cells⁴⁹. Glucan polysaccharides were shown to be specifically recognised and to induce phagocytosis in both mammals and *Drosophila*^{46, 50, 51, 52}. Glucan particles prepared from *Saccharomyces cerevisiae*²⁹ could thus serve as a potent delivery system for direct macrophage-specific targeting. These particles can be modified to influence the release of encapsulated cargo⁵³, which makes them appealing for use in pharmaceutical applications²⁹. For example, glucan particles loaded with RNAi were efficiently applied for the regulation of viral infection in shrimps⁵⁴. In mammalian model organisms, glucan particles were used for the direct targeting of liver macrophages to treat a metabolic syndrome⁵⁵.

Due to increasing discovery rate of new drug candidates, there is a rising need to replace mammals by more simple, cheaper and ethically acceptable model organisms for *in vivo* preclinical testing^{56, 57}. Thanks to more than one-hundred years long history in experimental research and a high degree of similarity with mammals, *Drosophila* could emerge as such a model organism and enable the evaluation of basic features such as toxicity, immunogenicity, and immune recognition. However, the data considering the testing of drug delivery systems in the *Drosophila* model organism are scarce or completely missing^{58, 59}. We demonstrate that glucan particles can be used as a system for targeted drug delivery to macrophages in *Drosophila*, with the potential not only in preclinical testing but also for use in insect immunological research. Thanks to the high versatility of genetic tools, the fruit fly is widely used as a model organism for dissecting molecular mechanisms behind macrophage behavior^{60, 61}. The unique set of reporters together with the possibility of tissue-specific drivers provide an opportunity to decipher regulatory pathways in processes such as embryonal development, regulation of hematopoietic niche maintenance, activation of central immune pathways, immune response to cancer, and control of resistance and tolerance to infection^{62, 63, 64, 65}.

Glucan particles injected into the hemolymph were found to be very effectively distributed throughout the *Drosophila* body and phagocytosed with high coverage of all macrophages. The

colocalisation of glucan particles was observed in all organs and tissues where the macrophages reside, but there was always a subpopulation of empty macrophages in the injected flies, suggesting some functional plurality in *Drosophila* immune cells. Further analysis of this phenomenon could form the basis of research into "stealth" particles that avoid detection by the immune system⁶⁶. We observed an unusually high accumulation of glucan particles in the dorsal part of the abdomen. In this region there is a high accumulation of macrophages surrounding the aorta and a high flow of the hemolymph; this is also the proposed site of adult hematopoiesis⁶⁷, which makes it an attractive target for the *in vivo* testing of hematopoietic agents^{68, 69}. The ability of glucan particles to deliver cargo to macrophages *in vivo* was demonstrated by the delivery of Gal4 protein into the target cells using flies encoding the genomic UASmCherry construct and observing the production of a fluorescent reporter. Only Gal4 delivered via glucan particles produced a positive signal; neither the injection of GPs or Gal4 alone nor the coinjection of Gal4 and GPs resulted in phenocopy production.

These results show that the *Drosophila* immune system can efficiently recognise and remove glucan particles from the circulation. Glucans have been documented to have a stimulatory effect on the immune system and trigger a specific anti-fungal immune response in mammals⁷⁰. We, therefore, measured known markers of immune system activation and observed only a mild activation of antimicrobial peptides with almost no impact on the vitality of individuals. Additionally, the immune capacity was analysed by injecting GPs into the flies 24 hours before the reinjection of pathogenic bacteria. Data from this immunological assay clearly show that neither bacterial resistance nor bacterial killing is influenced by GP treatment, suggesting that the injection of GPs does not limit the ability of *Drosophila* to fight bacteria by phagocytosis. We, therefore, believe that the combination of glucan particles as a tool for drug delivery and *Drosophila* as a model organism makes a unique opportunity for *in vivo* testing in the context of cancer, immunity, and metabolism research.

4 Conclusions

We have demonstrated that *Drosophila* is a suitable model organism for testing glucan particles as a macrophage-specific drug delivery system *in vivo*. We proved that GPs can be delivered by injection directly into the circulatory system and that this treatment results in a fast distribution of GPs into the macrophages over the whole body of both adult flies and larvae. We documented that GPs can be used *in vivo* for the delivery of a transcription protein to macrophages. We analysed the impact of GP treatment on the vitality of individuals and elicitation of their immune response in the normal state and response to bacterial infection. All these experiments represent important steps in establishing the use of GPs as a tool in the field of insect immunology research together with the establishment of *Drosophila* as a suitable model organism for *in vivo* testing of drug delivery systems and their modifications.

5 Experimental section

5.1 Glucan particles preparation and modifications

Glucan particles were prepared from baker's yeast⁴⁵. Wet yeast was added into 1M NaOH, the material was heated for 1 hour at 90 °C and then centrifuged at 14,500 G for 5 minutes. The supernatant was discarded, and this step was repeated three times. The alkali-insoluble solids were then mixed with HCl solution added to the dispersion with the resulting pH = 4.5, heated to 75 °C for 2 hours and then centrifuged at 14,500 G for 5 minutes. Insoluble solids were washed 3 times in deionized water, 4 times in isopropanol and finally 2 times in acetone. Every step was followed by centrifugation at 14,500 G for 10 minutes. The final product was lyophilized to form a dry powder. The lyophilized glucan particles were stored in a refrigerator for further use. The size distribution and morphology of the GPs were characterised by static light scattering and scanning electron microscopy, respectively (Fig. S7).

5.2 Synthesis of GP-FITC

To prepare FITC labeled glucan particles, 100 mg GPs, 5 mL of DMSO (PENTA) and 2 mg of FITC (Sigma-Aldrich) were mixed in a round-bottom flask. Then 1 mg of tin-ethyl hexanoate (Sigma-Aldrich) and subsequently 2 drops of pyridine (Lach-Ner) were added into the suspension containing all reactants. The synthesis was carried out for 1 h at 95 °C and mixed by a magnetic stirrer at 500 RPM. After cooling down, the content of the reaction mixture was centrifuged for 3 min at 12,000 G. The supernatant containing unreacted material was discarded. The pellet was washed by water three times, and then by 99.9 % ethanol (PENTA) three times. Finally, the pellet was redispersed in approx. 50 mL of deionised water and dialysed against deionised water for 5 days under dark with an exchange of water every day. After this step, the suspension was lyophilized to obtain a dry powder and stored in a refrigerator for further use. The successful attachment of FITC was verified by fluorescence spectroscopy and laser scanning confocal microscopy (Fig. S7). It has also been verified that the modification of GPs was not detrimental to their colloidal stability (Fig. S7).

5.3 Synthesis of GP-pHrodo

Glucan particles labeled with pHrodo™ we prepared by first dispersing 10 mg of GPs in 100 µL of sodium bicarbonate buffer (pH=9.3, 0.1 M) in an Eppendorf tube, diluted with 900 µL of deionized water and sonicated for 5 min on the sonication bath. This step was followed by the addition of 2 µL of pHrodo™ succinimidyl ester ($M_w \sim 650$ g/mol) 10 mM of dimethylsulfoxide (DMSO) solution (pHrodo® Red Microscale Labeling Kit, Thermo Fisher Scientific) to the suspension and left to react for 15 min at room temperature protected from light. The resulting reaction mixture was centrifuged for 3 min at 12,000 G, and the supernatant was discarded. The pellet was then washed once with deionised water, once with 99.9% ethanol (PENTA), three times with acetone and finally dried on the air in the dark and

stored in a freezer. The successful attachment of pHrodo was verified by fluorescence spectroscopy at neutral and acidic pH and laser scanning confocal microscopy (Fig. S7). It has also been verified that the modification of GPs was not detrimental to their colloidal stability (Fig. S7).

5.4 Gal4 protein loading

To prepare glucan particles loaded with Gal4 protein, 100 µL of 49.5 µg/mL aqueous solution of the Gal4 protein (Sigma-Aldrich) was pipetted to 10 mg of dry GP or GP-FITC powder placed in an Eppendorf tube. The protein solution was absorbed by the volume of GPs by capillary forces. Then the whole content of the Eppendorf tube was then lyophilized and stored in a freezer. This loading method has been previously proved to be efficient for the encapsulation of substances including vitamin B12, caffeine and bovine serum albumin (BSA)⁴⁵. The release kinetics of BSA from GPs was shown to occur over a typical time of 24 h at 20 °C, with only approx. 10 % released after 2 hours⁴⁵. Therefore, it can be expected that the spontaneous leakage of Gal4 from the GPs over a time period of 30 min will be negligible and the majority of Gal4 will be injected into the fruit flies in the GP-encapsulated form.

5.5 Fly culture and manipulation

All fly strains used in this work were held in standard conditions of 25 °C, 60% humidity and food supply *ad libitum*. We used two different fly strains for the visualization of macrophages: I. combination of macrophage-specific driver Hml Gal4 and reporter gene (enhanced green fluorescent protein eGFP), under control of artificial UAS promoter (final genotype - Hml Gal4; UAS eGFP); II. Hml recombinant protein fused with a dsRed fluorescent label, containing nuclear localisation signal (final genotype Hml dsRed). Both these lines gave us a bright fluorescent signal enabling us to detect macrophages without the need for dissection, using an inverted fluorescent microscope (Olympus IX71) or a confocal microscope (Olympus Fluoview 1000). As a control, we used a white fly strain based on the CantonS genotype, commonly used as a control in our laboratory and representing a genetic background for all the lines that were used. The flies were grown on corn-meal medium (8 % cornmeal, 5 % glucose, 4 % yeast, 1 % agar) at 25 °C. For dietary treatment individuals were held on a high-fat diet consisting of 1 % cornmeal, 5 % glucose, 2.5 % yeasts, 1 % agar, and 10 % lard.

5.6 Injections

In all experiments 0.1% (w/w) suspension of GPs or modified GPs in PBS (pH 7.4, 1X, tablets from Sigma-Aldrich) was used. The suspension was prepared by sonication on an ice bath for 5 min at 25 W, and vortexed just before injection to ensure well-dispersed particles. Flies were anesthetized with carbon dioxide. The Eppendorf Femtojet microinjector and a drawn glass needle were used to inject precisely 50 nL of GP suspension, bacteria or buffer into the fly at the cuticle on the ventrolateral side of the abdomen. For FITC injection experiment 50 nL of 6M FITC in PBS was injected into the flies carrying the genotype UAS mCherry. Flies were analyzed 45

minutes after injection by confocal microscopy. For injections of larvae, the third instar larvae were collected, rinsed in PBS and mounted on a double side tape. The sharpened needle in combination with Femtojet microinjector was used for injections. Larvae showing high melanisation were excluded from further analyses.

5.7 Glucan particle observation and detection of colocalization with hemocytes

The flies were fixed by 4% paraformaldehyde in PBS and imaged using confocal microscopy with maximal projection from five different layers; the same settings of the Z-stack range and the same intensity of lasers were used for all animals. The cells were observed in whole flies to detect possible significant changes in distal parts. The exact number of macrophages was determined by counting Hml>GFP-positive cells within a selected thorax region as depicted in Fig. 2C, D using the Fiji software and compared by Student t-tests using the GraphPad Prism software. The number of GP phagocytosing cells was determined by the injection of GP-pHrodo 40 min prior to fixing flies. To control the spontaneous fluorescence of pHrodo labeled glucan particles, a few flies were fixed immediately after injection and showed no red fluorescent signal. Another control of phagocytosis specific pHrodo signal was made by the pretreatment of flies with the injection of 50 nL of polystyrene beads one hour before the GP injection. The injection of polystyrene beads (1 μm in diameter, Sigma L5530) is known to dampen phagocytosis and resulted in no red fluorescent signal. We used two other strategies to show phagocytosis of glucan particles by the immune cells: I. we coinjected FITC labeled glucan particles together with phagocytosis marker pHrodo Red *S.aureus* Bioparticles (ThermoFisher Scientific); II. we injected FITC labeled glucan particles into the flies carrying HMLdsRed genotype – in all the cases the flies were assayed as described above. For the detection of glucan particle phagocytosis in the larva, we bled the larvae and quantified the colocalisation on a hemocyte sample in a defined region of Bürker chamber.

5.8 Bacterial strains and culturing conditions

Streptococcus pneumoniae strain EJ1 (D39 streptomycin-resistant derivative) was stored at $-80\text{ }^{\circ}\text{C}$ in Tryptic Soy Broth (TSB) media containing 25% glycerol. For experiments, bacteria were streaked onto TSB agar plates containing 100 $\mu\text{g}/\text{mL}$ streptomycin and incubated at $37\text{ }^{\circ}\text{C}$ overnight; a fresh plate was prepared for each experiment. Single colonies were used to inoculate 3 mL of TSB with 100 000 units of catalase (Sigma C40) and incubated overnight at $37\text{ }^{\circ}\text{C}$ + 5% CO_2 without shaking. The morning cultures were 2x diluted in TSB with a fresh catalase and grown for an additional 4 hours, reaching an approximate 0.4 OD_{600} . Final cultures were concentrated by centrifugation and resuspended in phosphate buffered saline (PBS) so that the concentration corresponded to OD_{600} 2.4 and stored on ice prior to injection.

5.9 Pathogen load measurement

Single flies were homogenised in PBS using a motorized plastic pestle in 1.5 ml tubes. The lysate containing *S.pneumoniae* was

plated in spots onto TSB agar plates containing streptomycin in serial dilutions and incubated overnight at $37\text{ }^{\circ}\text{C}$ before manual counting. The pathogen loads of 16 flies were determined for each treatment in each experiment, and at least three independent infection experiments were conducted. The results were combined into one graph (in all presented cases, individual experiments showed comparable results). Values were compared using unpaired t-tests corrected for multiple comparisons using the Holm-Sidak method in the GraphPad Prism software.

5.10 Survival analysis

Two hundred flies were injected for each treatment in one experiment; at least three independent infection experiments were repeated and combined into one survival curve (in all presented cases, individual experiments showed comparable results). Injected flies were placed into vials with 20 flies per vial, transferred to a fresh vial every other day and checked daily to determine mortality. Flies were kept at $29\text{ }^{\circ}\text{C}$. The survival curves were generated by GraphPad Prism software and analyzed by Log-rank and Gehan-Breslow-Wilcoxon (more weight to deaths at early time points) tests.

5.11 Gene Expression

Gene expression was analysed by quantitative real-time PCR. Whole flies were, and the total RNA was isolated by Trizol reagent (Ambion) according to the manufacturer's protocol. DNA contamination was removed by using Turbo DNase free kit (Ambion) according to the protocol ($37\text{ }^{\circ}\text{C}$ 30 min) with subsequent inactivation of DNase by DNase inactivation reagent (5 min spin at 12,000 G at room temperature). Reverse transcription was done by the Superscript III reverse transcriptase (Invitrogen), and the amounts of mRNA of particular genes were quantified using the IQ Sybr Green Supermix Mastermix (BioRad) on a CFX 1000 Touch Real-time cyclor (BioRad). In all cases, the expression was normalized to the expression of Ribosomal protein 49 (Rp49) and values relative to Rp49 amounts were compared and shown in the graphs. The primer sequences can be found in Table 1. Samples were collected from three independent infection experiments with three technical replicates for each trial and compared by unpaired t-tests using the GraphPad Prism software.

5.12 mCherry pull down assay

For this experiment we injected 50 nL of 0.25%, 1%, and 4% (w/w) solution of Gal4-loaded GP-FITC in PBS into the flies carrying the genotype UAS mCherry. Five hours after injection, 15 flies were collected and frozen at $-80\text{ }^{\circ}\text{C}$. The flies were homogenised and proteins were extracted according to RFP-Trap protocol (Chromotec). Extracted mCherry proteins were analysed by SDS PAGE (10%) and the size of gained protein was compared with a protein ladder (Precision Plus Protein™ Dual Color Standards, BioRad), as well as with positive control represented by flies carrying mCherry expression.

Conflicts of interest

There are no conflicts to declare.

Acknowledgements

Financial support by the Czech Science Foundation (GACR project no. 18-14466S) and the Agency for Healthcare research (AZV project no. 16-27522A) is gratefully acknowledged.

Notes and references

- Kakkar A, Traverso G, Farokhzad OC, Weissleder R, Langer R. Evolution of macromolecular complexity in drug delivery systems. *Nature Reviews Chemistry* **1**, 0063 (2017).
- Lounkine E, Keiser MJ, Whitebread S, Mikhailov D, Hamon J, Jenkins JL, Lavan P, Weber E, Doak AK, Cote S, Shoichet BK, Urban L. Large-scale prediction and testing of drug activity on side-effect targets. *Nature* **486**, 361-368 (2012).
- Nicolaou KC. Advancing the Drug Discovery and Development Process. *Angewandte Chemie-International Edition* **53**, 9128-9140 (2014).
- Rosenblum D, Joshi N, Tao W, Karp JM, Peer D. Progress and challenges towards targeted delivery of cancer therapeutics. *Nature Communications* **9**, 1410 (2018).
- Ioannidis JPA, Kim BYS, Trounson A. How to design preclinical studies in nanomedicine and cell therapy to maximize the prospects of clinical translation. *Nature Biomedical Engineering* **2**, 797-809 (2018).
- Begley CG, Ellis LM. Raise standards for preclinical cancer research. *Nature* **483**, 531-533 (2012).
- Avorn J. The \$2.6 Billion Pill - Methodologic and Policy Considerations. *The New England Journal of Medicine* **372**, 1877-1879 (2015).
- Zhang BY, Korolj A, Lai BFL, Radisic M. Advances in organ-on-a-chip engineering. *Nature Reviews Materials* **3**, 257-278 (2018).
- Bhatia SN, Ingber DE. Microfluidic organs-on-chips. *Nature Biotechnology* **32**, 760-772 (2014).
- Ingber DE. Reverse Engineering Human Pathophysiology with Organs-on-Chips. *Cell* **164**, 1105-1109 (2016).
- Bhise NS, Ribas J, Manoharan V, Zhang YS, Polini A, Massa S, Dokmeci MR, Khademhosseini A. Organ-on-a-chip platforms for studying drug delivery systems. *Journal of Controlled Release* **190**, 82-93 (2014).
- Esch EW, Bahinski A, Huh D. Organs-on-chips at the frontiers of drug discovery. *Nature Reviews Drug Discovery* **14**, 248-260 (2015).
- Wang LH, Kounatidis I, Ligoxygakis P. Drosophila as a model to study the role of blood cells in inflammation, innate immunity and cancer. *Frontiers in Cellular and Infection Microbiology* **3**, 113 (2014).
- Ugur B, Chen KC, Bellen HJ. Drosophila tools and assays for the study of human diseases. *Disease Models & Mechanisms* **9**, 235-244 (2016).
- Pendleton RG, Parvez F, Sayed M, Hillman R. Effects of pharmacological agents upon a transgenic model of Parkinson's disease in *Drosophila melanogaster*. *Journal of Pharmacology and Experimental Therapeutics* **300**, 91-96 (2002).
- Perrimon N, Bonini NM, Dhillon P. Fruit flies on the front line: the translational impact of *Drosophila*. *Disease Models & Mechanisms* **9**, 229-231 (2016).
- Li HJ, Jasper H. Gastrointestinal stem cells in health and disease: from flies to humans. *Disease Models & Mechanisms* **9**, 487-499 (2016).
- Dionne MS, Schneider DS. Models of infectious diseases in the fruit fly *Drosophila melanogaster*. *Disease Models & Mechanisms* **1**, 43-49 (2008).
- Wong ACN, Vanhove AS, Watnick PI. The interplay between intestinal bacteria and host metabolism in health and disease: lessons from *Drosophila melanogaster*. *Disease Models & Mechanisms* **9**, 271-281 (2016).
- Alfa RW, Kim SK. Using *Drosophila* to discover mechanisms underlying type 2 diabetes. *Disease Models & Mechanisms* **9**, 365-376 (2016).
- Pandey UB, Nichols CD. Human disease models in *Drosophila melanogaster* and the role of the fly in therapeutic drug discovery. *Pharmacological Reviews* **63**, 411-436 (2011).
- Gonzalez C. *Drosophila melanogaster*: a model and a tool to investigate malignancy and identify new therapeutics. *Nature Reviews Cancer* **13**, 172-183 (2013).
- Ginhoux F, Jung S. Monocytes and macrophages: developmental pathways and tissue homeostasis. *Nature Reviews Immunology* **14**, 392-404 (2014).
- Wynn TA, Chawla A, Pollard JW. Macrophage biology in development, homeostasis and disease. *Nature* **496**, 445-455 (2013).
- Chen Y, Zhang X. Pivotal regulators of tissue homeostasis and cancer: macrophages. *Experimental Hematology & Oncology* **6**, 23 (2017).
- A-Gonzalez N, Quintana JA, García-Silva S, Mazariegos M, González de la Aleja A, Nicolás-Ávila JA, Walter W, Adrover JM, Crainiciuc G, Kuchroo VK, Rothlin CV, Peinado H, Castrillo A, Ricote M, Hidalgo A. Phagocytosis imprints heterogeneity in tissue-resident macrophages. *The Journal of Experimental Medicine* **214**, 1281-1296 (2017).
- Shapouri-Moghaddam A, Mohammadian S, Vazini H, Taghadosi M, Esmaeili SA, Mardani F, Seifi B, Mohammadi A, Afshari JT, Sahebkar A. Macrophage plasticity, polarization, and function in health and disease. *Journal of Cellular Physiology* **233**, 6425-6440 (2018).
- Parisi L, Gini E, Baci D, Tremolati M, Fanuli M, Bassani B, Farronato G, Bruno A, Mortara L. Macrophage polarization in chronic inflammatory diseases: killers or builders? *Journal of Immunology Research* **2018**, 8917804 (2018).
- Soto ER, Caras AC, Kut LC, Castle MK, Ostroff GR. Glucan particles for macrophage targeted delivery of nanoparticles. *Journal of Drug Delivery* **2012**, 143524 (2012).
- Cassetta L, Pollard JW. Targeting macrophages: therapeutic approaches in cancer. *Nature Reviews Drug Discovery* **17**, 887-904 (2018).
- Lavin Y, Mortha A, Rahman A, Merad M. Regulation of macrophage development and function in peripheral tissues. *Nature Reviews Immunology* **15**, 731-744 (2015).
- Klyachko NL, Polak R, Haney MJ, Zhao Y, Gomes Neto RJ, Hill MC, Kabanov AV, Cohen RE, Rubner MF, Batrakova EV. Macrophages with cellular backpacks for targeted drug delivery to the brain. *Biomaterials* **140**, 79-87 (2017).
- Dou H, Destache CJ, Morehead JR, Mosley RL, Boska MD, Kingsley J, Gorantla S, Poluektova L, Nelson JA, Chaubal M, Werling J, Kipp J, Rabinow BE, Gendelman HE. Development of a macrophage-based nanoparticle platform for antiretroviral drug delivery. *Blood* **108**, 2827-2835 (2006).
- Miller MA, Zheng Y-R, Gadde S, Pfirschke C, Zope H, Engblom C, Kohler RH, Iwamoto Y, Yang KS, Askevold B, Kolishetti N, Pittet M, Lippard SJ, Farokhzad OC, Weissleder R. Tumour-associated macrophages act as a slow-release reservoir of nano-therapeutic Pt(IV) pro-drug. *Nature Communications* **6**, 8692 (2015).
- Blanco E, Shen H, Ferrari M. Principles of nanoparticle design for overcoming biological barriers to drug delivery. *Nature Biotechnology* **33**, 941-951 (2015).

- 36 De Smet R, Allais L, Cuvelier CA. Recent advances in oral vaccine development: yeast-derived beta-glucan particles. *Hum Vaccin Immunother* **10**, 1309-1318 (2014).
- 37 Whelan AO, Flick-Smith HC, Homan J, Shen ZT, Carpenter Z, Khoshkenar P, Abraham A, Walker NJ, Levitz SM, Ostroff GR, Oyston PCF. Protection induced by a Francisella tularensis subunit vaccine delivered by glucan particles. *PLoS ONE* **13**, e0200213 (2018).
- 38 Specht CA, Lee CK, Huang H, Hester MM, Liu J, Luckie BA, Torres Santana MA, Mirza Z, Khoshkenar P, Abraham A, Shen ZT, Lodge JK, Akalin A, Homan J, Ostroff GR, Levitz SM. Vaccination with recombinant Cryptococcus proteins in glucan particles protects mice against cryptococcosis in a manner dependent upon mouse strain and cryptococcal species. *Mbio* **8**, e01872-17 (2017).
- 39 Tesz GJ, Aouadi M, Prot M, Nicoloso SM, Boutet E, Amano SU, Goller A, Wang M, Guo CA, Salomon WE, Virbasius JV, Baum RA, O'Connor MJ, Jr., Soto E, Ostroff GR, Czech MP. Glucan particles for selective delivery of siRNA to phagocytic cells in mice. *Biochemical Journal* **436**, 351-362 (2011).
- 40 Aouadi M, Tesz GJ, Nicoloso SM, Wang M, Chouinard M, Soto E, Ostroff GR, Czech MP. Orally delivered siRNA targeting macrophage Map4k4 suppresses systemic inflammation. *Nature* **458**, 1180-1184 (2009).
- 41 Woodcock K. The homeostasis and function of plasmacytes in adult Drosophila. *Doctoral Thesis*, King's College London, (2013).
- 42 Horn L, Leips J, Starz-Gaiano M. Phagocytic ability declines with age in adult Drosophila hemocytes. *Aging Cell* **13**, 719-728 (2014).
- 43 Brand AH, Perrimon N. Targeted gene-expression as a means of altering cell fates and generating dominant phenotypes. *Development* **118**, 401-415 (1993).
- 44 Pham LN, Dionne MS, Shirasu-Hiza M, Schneider DS. A specific primed immune response in Drosophila is dependent on phagocytes. *PLoS Pathogens* **3**, e26 (2007).
- 45 Salon I, Hanus J, Ulbrich P, Stepanek F. Suspension stability and diffusion properties of yeast glucan microparticles. *Food and Bioprocess Technology* **99**, 128-135 (2016).
- 46 Whitten MM, Tew IF, Lee BL, Ratcliffe NA. A novel role for an insect apolipoprotein (apolipoprotein III) in beta-1,3-glucan pattern recognition and cellular encapsulation reactions. *Journal of Immunology* **172**, 2177-2185 (2004).
- 47 Akbar MA, Tracy C, Kahr WHA, Kramer H. The full-of-bacteria gene is required for phagosome maturation during immune defense in Drosophila. *Journal of Cell Biology* **192**, 383-390 (2011).
- 48 Davies LC, Taylor PR. Tissue-resident macrophages: then and now. *Immunology* **144**, 541-548 (2015).
- 49 Lee WH, Loo CY, Traini D, Young PM. Nano- and micro-based inhaled drug delivery systems for targeting alveolar macrophages. *Expert Opinion on Drug Delivery* **12**, 1009-1026 (2015).
- 50 Brown GD, Herre J, Williams DL, Willment JA, Marshall ASJ, Gordon S. Dectin-1 mediates the biological effects of β -glucans. *The Journal of Experimental Medicine* **197**, 1119-1124 (2003).
- 51 Ma J, Underhill DM. beta-Glucan signaling connects phagocytosis to autophagy. *Glycobiology* **23**, 1047-1051 (2013).
- 52 Rubin-Bejerano I, Abeijon C, Magnelli P, Grisafi P, Fink GR. Phagocytosis by human neutrophils is stimulated by a unique fungal cell wall component. *Cell Host & Microbe* **2**, 55-67 (2007).
- 53 Cohen JL, Shen Y, Aouadi M, Vangala P, Tencerova M, Amano SU, Nicoloso SM, Yawe JC, Czech MP. Peptide- and amine-modified glucan particles for the delivery of therapeutic siRNA. *Molecular Pharmaceutics* **13**, 964-978 (2016). View Article Online
DOI: 10.1039/C9BM00539K
- 54 Zhu F, Zhang X. Protection of shrimp against white spot syndrome virus (WSSV) with beta-1,3-D-glucan-encapsulated vp28-siRNA particles. *Marine Biotechnology* **14**, 63-68 (2012).
- 55 Tencerova M, Aouadi M, Vangala P, Nicoloso SM, Yawe JC, Cohen JL, Shen Y, Garcia-Menendez L, Pedersen DJ, Gallagher-Dorval K, Perugini RA, Gupta OT, Czech MP. Activated Kupffer cells inhibit insulin sensitivity in obese mice. *The FASEB Journal* **29**, 2959-2969 (2015).
- 56 Chakraborty C, Sharma AR, Sharma G, Lee SS. Zebrafish: A complete animal model to enumerate the nanoparticle toxicity. *Journal of Nanobiotechnology* **14**, 65 (2016).
- 57 Lee KY, Jang GH, Byun CH, Jeun M, Searson PC, Lee KH. Zebrafish models for functional and toxicological screening of nanoscale drug delivery systems: promoting preclinical applications. *Bioscience Reports* **37**, 3 (2017).
- 58 Schulman VK, Folker ES, Baylies MK. A method for reversible drug delivery to internal tissues of Drosophila embryos. *Fly* **7**, 193-203 (2013).
- 59 Jiang S, Teng CP, Puah WC, Wasser M, Win KY, Han MY. Oral administration and selective uptake of polymeric nanoparticles in Drosophila larvae as an in vivo model. *ACS Biomaterials Science & Engineering* **1**, 1077-1084 (2015).
- 60 Gold KS, Bruckner K. Macrophages and cellular immunity in Drosophila melanogaster. *Seminars in Immunology* **27**, 357-368 (2015).
- 61 Wood W, Martin P. Macrophage functions in tissue patterning and disease: New insights from the fly. *Developmental Cell* **40**, 221-233 (2017).
- 62 Ratheesh A, Belyaeva V, Siekhaus DE. Drosophila immune cell migration and adhesion during embryonic development and larval immune responses. *Current Opinion in Cell Biology* **36**, 71-79 (2015).
- 63 Bangi E. Drosophila at the intersection of infection, inflammation, and cancer. *Frontiers in Cellular and Infection Microbiology* **3**, 103 (2013).
- 64 Govind S. Innate immunity in Drosophila: Pathogens and pathways. *Insect Science* **15**, 29-43 (2008).
- 65 Wang L, Kounatidis I, Ligoxygakis P. Drosophila as a model to study the role of blood cells in inflammation, innate immunity and cancer. *Frontiers in Cellular and Infection Microbiology* **3**, 113 (2014).
- 66 Butcher NJ, Mortimer GM, Minchin RF. Drug delivery: Unravelling the stealth effect. *Nature Nanotechnology* **11**, 310-311 (2016).
- 67 Ghosh S, Singh A, Mandal S, Mandal L. Active hematopoietic hubs in Drosophila adults generate hemocytes and contribute to immune response. *Developmental Cell* **33**, 478-488 (2015).
- 68 Unger EF, Thompson AM, Blank MJ, Temple R. Erythropoiesis-stimulating agents--time for a reevaluation. *The New England Journal of Medicine* **362**, 189-192 (2010).
- 69 Kaushansky K. Hunting for hematopoietic transcriptional networks. *Proceedings of the National Academy of Sciences* **115**, 9818-9820 (2018).
- 70 Hunter KW, Gault RA, Berner MD. Preparation of microparticulate β -glucan from Saccharomyces cerevisiae for use in immune potentiation. *Letters in Applied Microbiology* **35**, 267-271 (2002).

Supplementary material

Yeast glucan particles enable intracellular protein delivery in *Drosophila* without compromising the immune system

Adam Bajgar, Ivan Saloň, Gabriela Krejčová, Tomáš Doležal, Marek Jindra, František Štěpánek

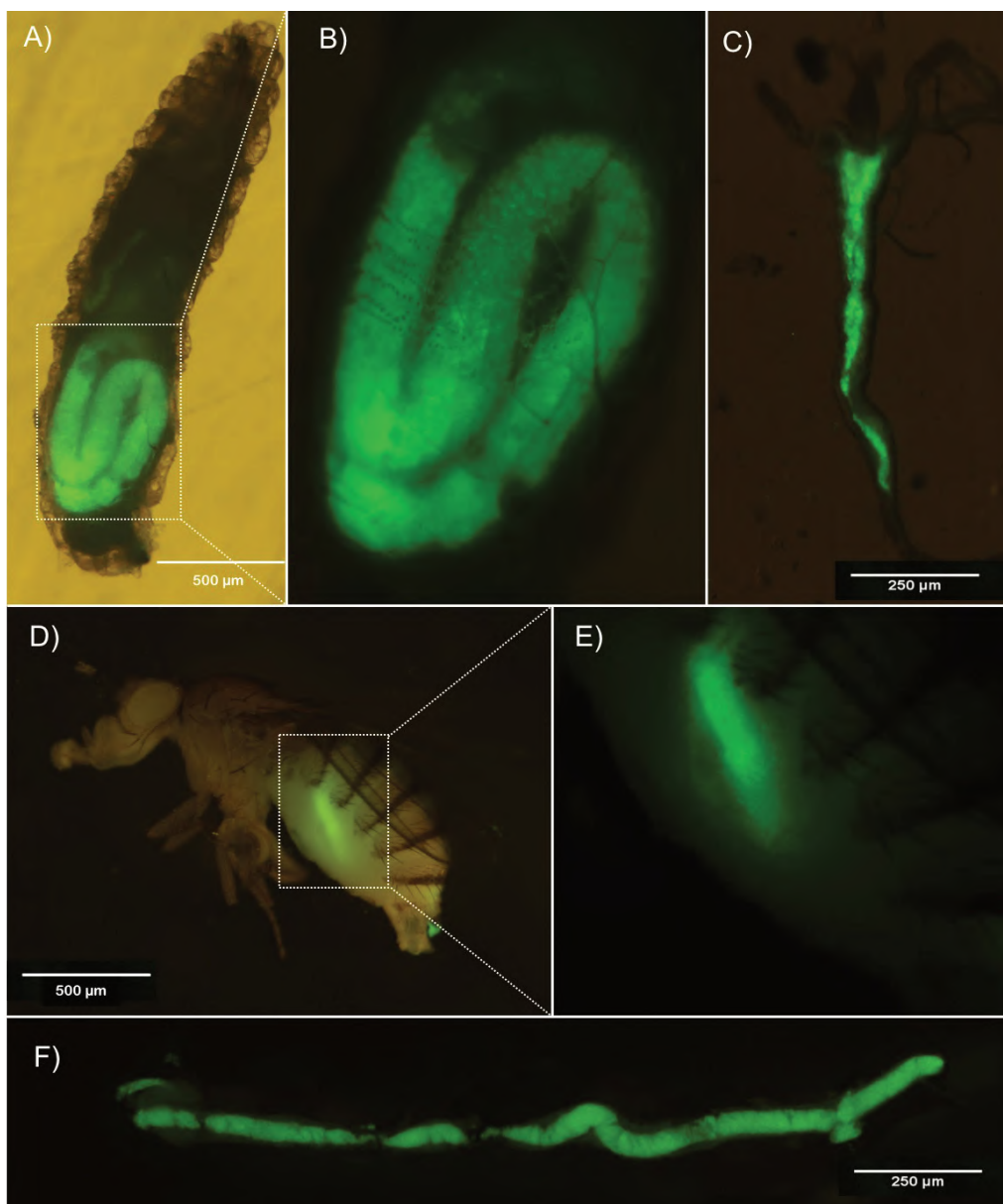


Fig. S1. Since flies possess a functionally developed gastro-intestinal tract, it was tried to deliver glucan particles into the *Drosophila* circulation by feeding (100 uL of 1% GP-FITC particle suspension mixed with a cornmeal diet in ratio 1:9). However, this simple way of delivery system was not effective. Even in individuals held on a high fat diet, resulting in higher permeabilisation of the gut wall, the glucan particles remained in the gut and were excreted after a few hours. **(A, B)** Binocular microscope image of GP-FITC fed larvae. **(C)** The same is documented also on dissected gut. **(D, E)** The same pattern has been observed also in adult flies where GP-FITC particles cannot get through the gut wall barrier similarly as in larvae. **(F)** The same is documented also on the dissected gut. The confocal images are representative of more than 15 analysed individuals.

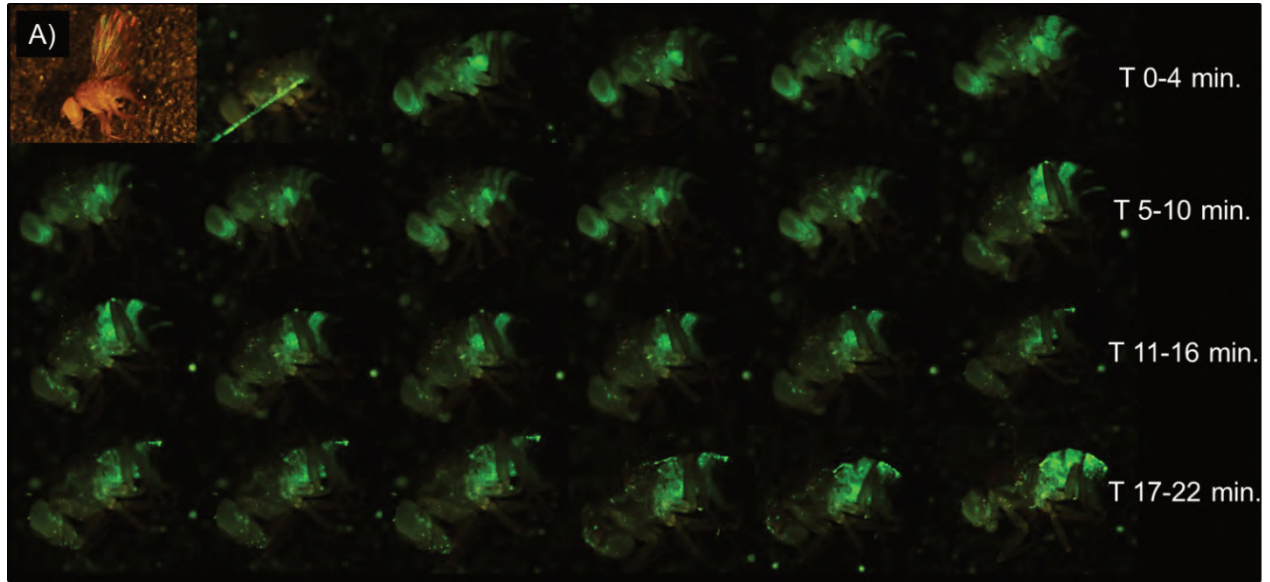


Fig. S2. Time progress of a typical injection event. FITC labeled glucan particles spread through the body and within twenty minutes they are distributed in all the body compartments including distal parts. Binocular microscope images were collated into a time series. The image sequence is representative images of more than 15 analysed individuals.

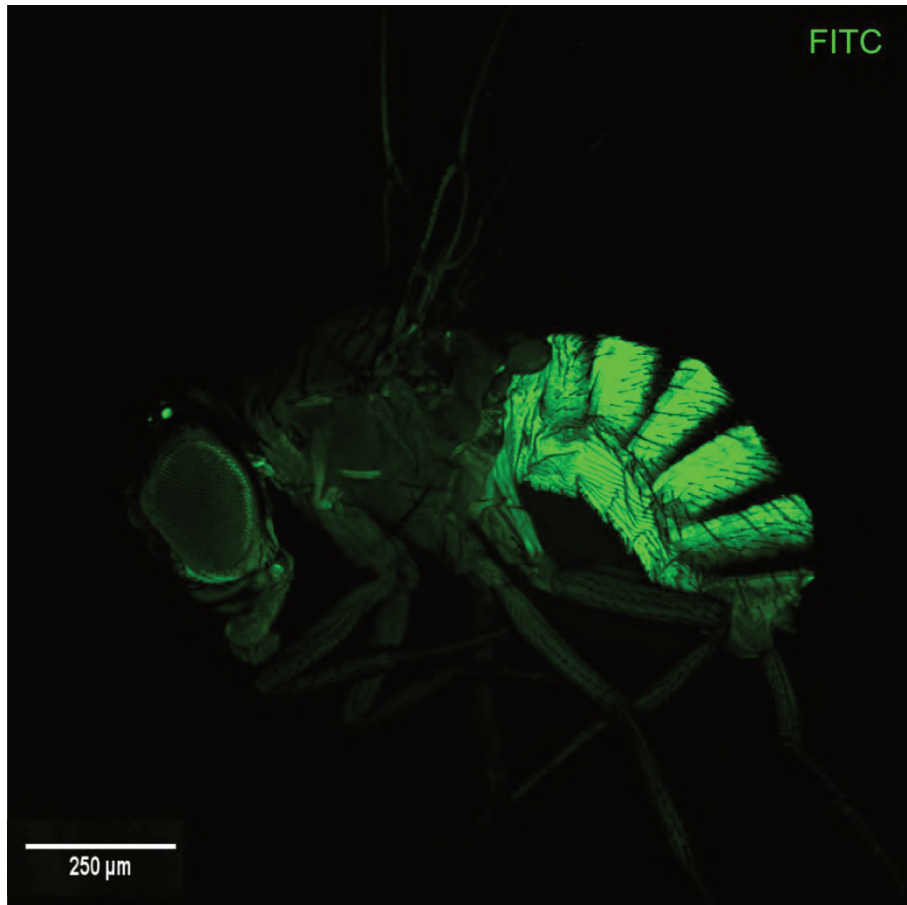


Fig. S3. Fly injected with a 6M FITC solution in PBS. Colocalisation is not seen in this case and the body of the fruit fly is uniformly fluorescent.

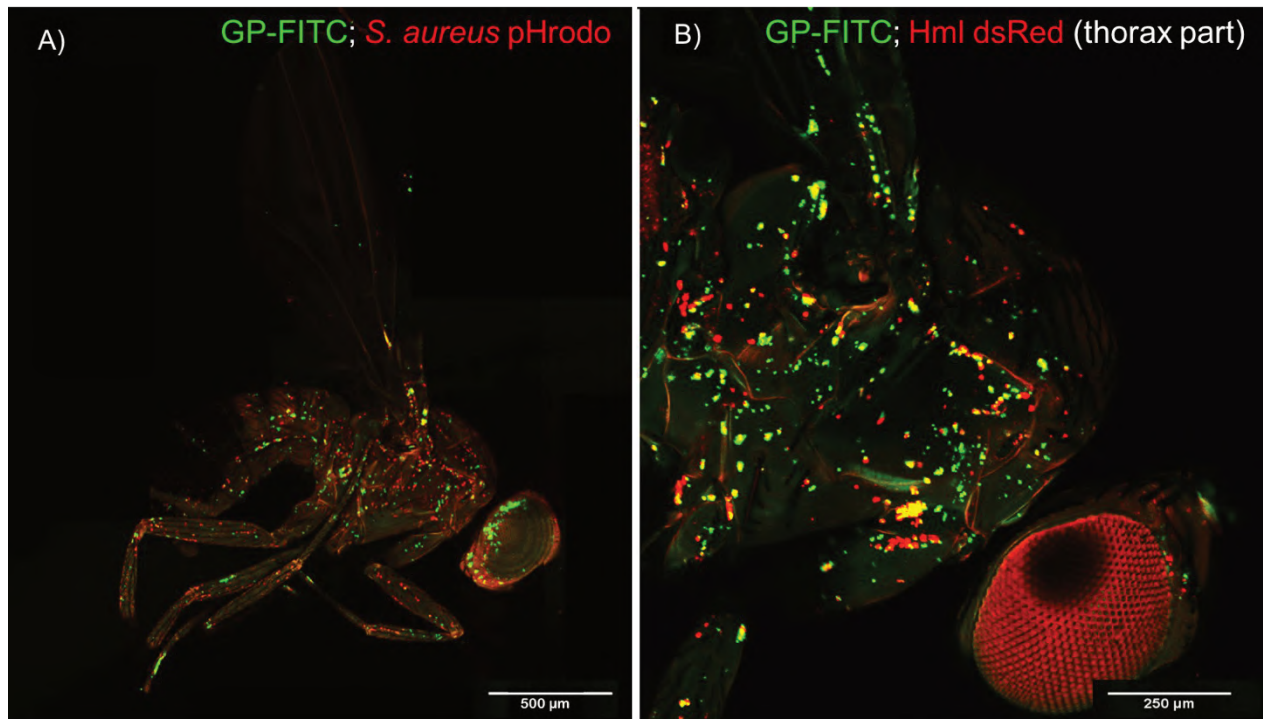


Fig. S4. Colocalisation of labeled glucan particles with macrophages and phagocytic spots was verified by two approaches. **(A)** Fly coinjected with GP-FITC particles and pHrodo labeled *S. aureus* cell wall lysates. High level of colocalisation can be seen in this case. **(B)** GP-FITC particles were injected into the fly with a genomic construct Hml dsRed marking the nuclei of macrophages by a red fluorescent protein. Both confocal images are representative of more than 15 analysed individuals.

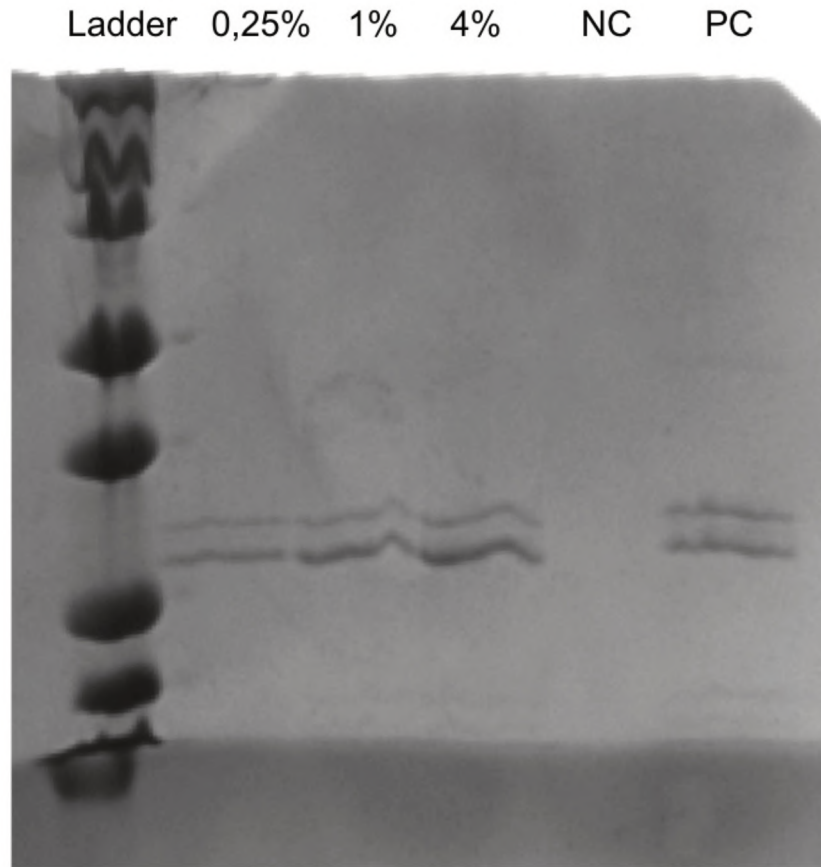


Fig. S5. The amount of mCherry protein produced in response to GP-FITC Gal4 loaded particles was determined by pull down assay and analysis of extracted proteins on SDS PAGE using RFP Trap (Chromotec) as described in Section 5.12. The observed size of the trapped protein corresponds to the expected size (34 kDa) of the protein and the data show that the amount of the protein is increasing with the number of injected particles into the living flies. The GP-FITC Gal4 loaded particles were injected to the flies in concentrations of 0.25 %, 1 % and 4 % (w/w) as indicated. The negative control (NC) were flies without mCherry expression, the positive control (PC) were flies naturally expressing mCherry.

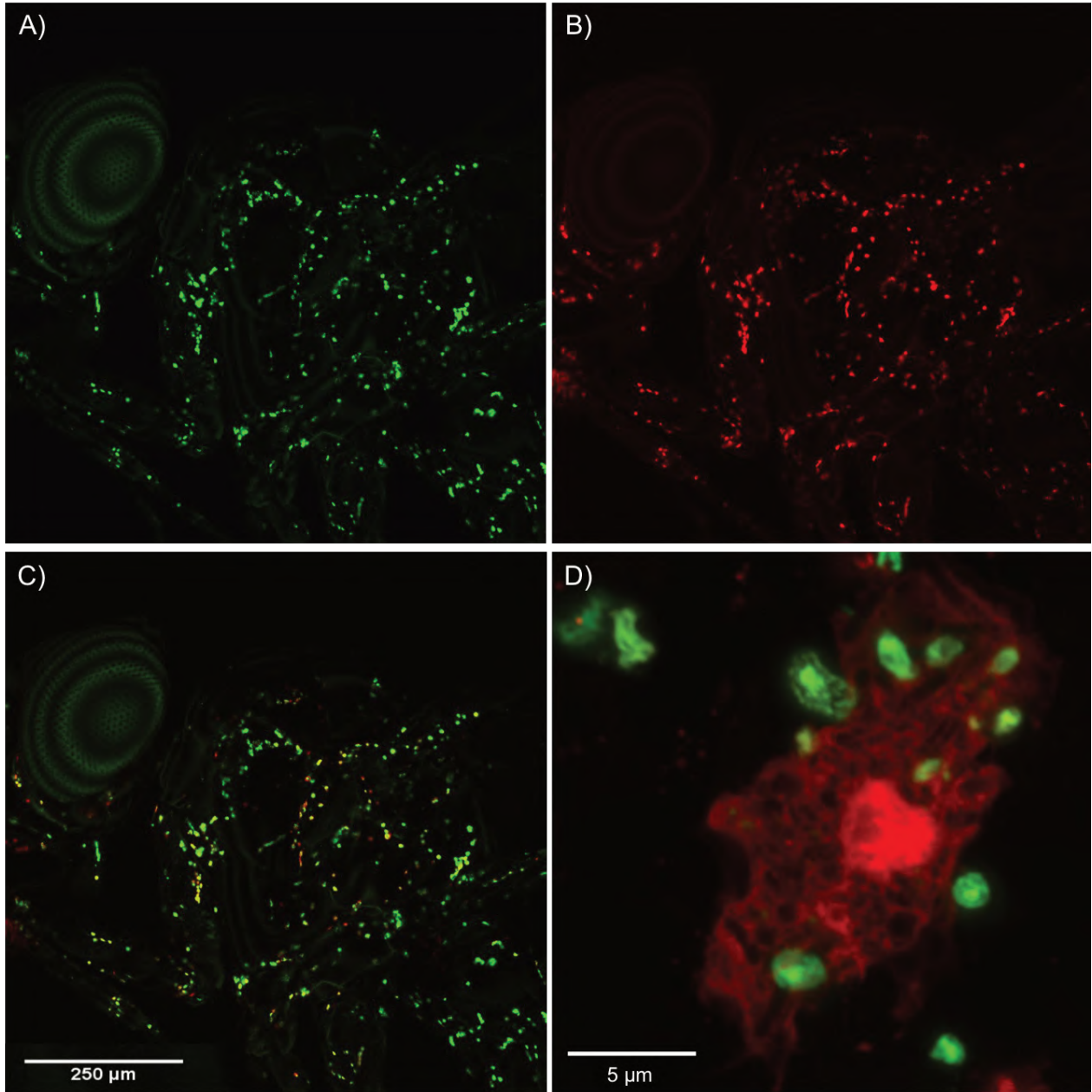


Fig. S6. Delivery of Gal4 by GP-FITC into macrophages with mCherry expression. A) Green signal of GP-FITC. B) Red signal of mCherry expressing cells. C) Merge of green and red signal. D) Detail of one macrophage targeted with GP-FITC and expressing mCherry.

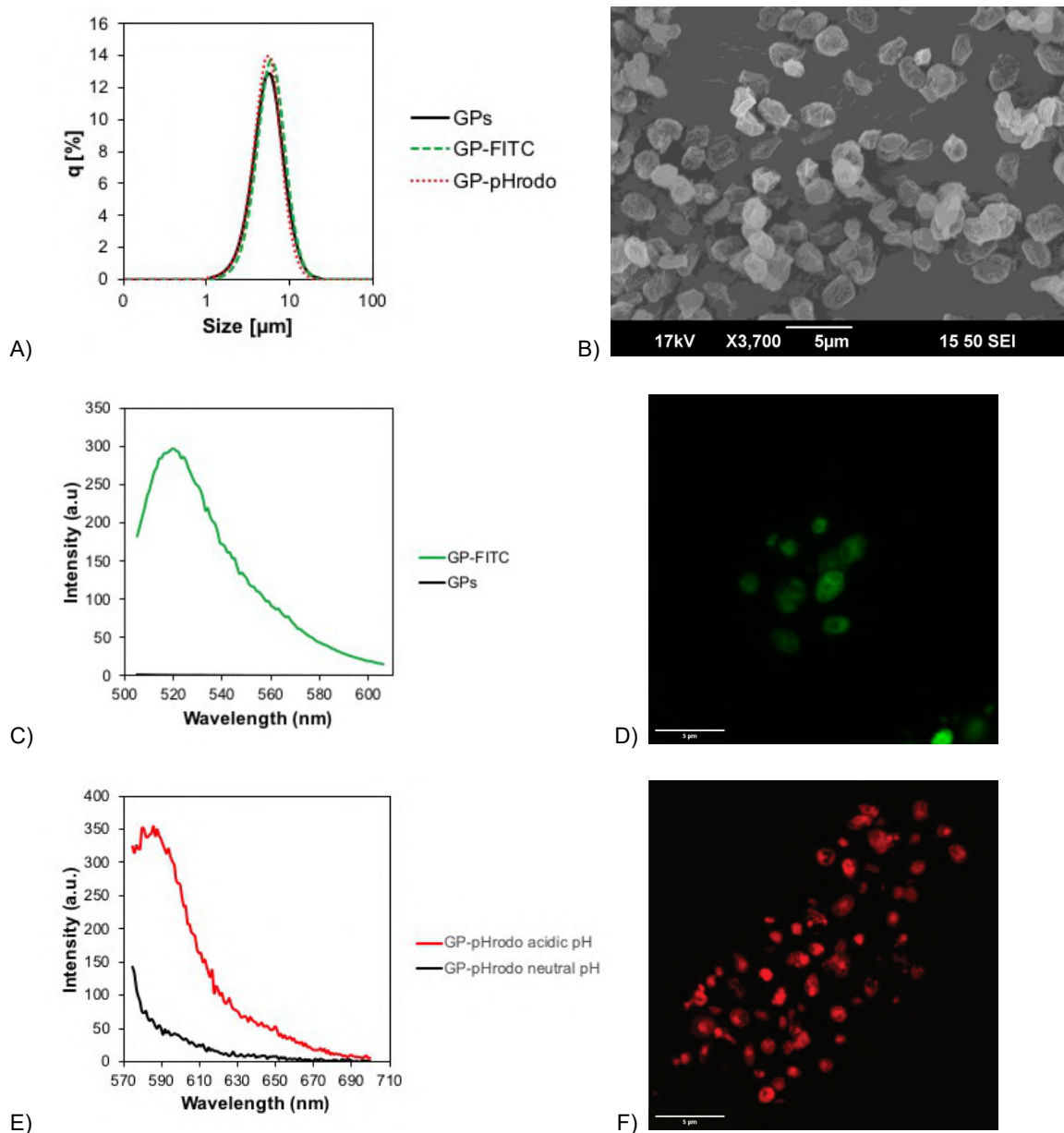


Fig. S7. A) Comparison of particle size distribution of plain and fluorescently labeled GPs, demonstrating that the attachment of fluorescent probes did not influence the colloidal stability of glucan particles. The size distributions were obtained by static light scattering (Horiba Partica LA 950/S2) in the wet state after dispersion in PBS by sonication. B) SEM micrograph of plain GPs for reference. C), E) Emission spectra of plain and fluorescently labeled GPs, demonstrating the successful attachment of fluorescent probes. GPs were suspended in PBS and fluorescence spectra were acquired by a Carry Eclipse (Agilent Technologies) fluorescence spectrophotometer with excitation wavelengths 488 nm for GP-FITC and 560 nm for GP-pHrodo. D), F) LSCM micrographs of fluorescently labeled GPs, demonstrating the successful attachment of fluorescent probes without affecting the particle size or morphology.

CHAPTER VIII:

Macrophages play a nutritive role in post-metamorphic maturation in *Drosophila*

Gabriela Krejčová, Adéla Danielová, Hana Sehadová, Filip Dyčka, Jíří Kubásek, Martin Moos, Adam Bajgar

Under review in *Development*

1 Macrophages play a nutritive role in post-metamorphic maturation in *Drosophila*

2 Gabriela Krejčová^{1*}, Adéla Danielová¹, Hana Sehadová², Filip Dyčka³, Jiří Kubásek⁴, Martin Moos², Adam
3 Bajgar^{1,2*}

4 **Affiliations**

5 ¹*Department of Molecular Biology and Genetics; Faculty of Science; University of South Bohemia; Ceske
6 Budejovice, 37005, Czech Republic.*

7 ²*Institute of Entomology; Biology Centre CAS; Ceske Budejovice, 37005, Czech Republic.*

8 ³*Department of Chemistry, Faculty of Science, University of South Bohemia, Ceske Budejovice, 37005,
9 Czech Republic.*

10 ⁴*Department of Experimental Plant Biology; Faculty of Science; University of South Bohemia; Ceske
11 Budejovice, 37005, Czech Republic.*

12

13 *Correspondence: bajgaradam@seznam.cz, krejcovagabriela@seznam.cz

14

15 **Abstract**

16 In the body of multicellular organisms, macrophages play an indispensable role in maintaining tissue
17 homeostasis by removing old, apoptotic and damaged cells. In addition, macrophages allow significant
18 remodeling of body plans during embryonic morphogenesis, regeneration and metamorphosis. Although
19 the huge amount of organic matter that must be removed during these processes represents a potential
20 source of nutrients, their further utilization by the organism has not yet been addressed.

21 Here, we document that during metamorphosis, *Drosophila* larval adipose tissue is infiltrated by
22 macrophages, which remove dying adipocytes by efferocytosis and engulf leaking RNA-protein granules
23 and lipids. Consequently, the infiltrating macrophages transiently adopt the adipocyte-like metabolic
24 profile to convert remnants of dying adipocytes to lipoproteins and storage peptides that nutritionally
25 support post-metamorphic development. This process is fundamental for the full maturation of ovaries
26 and the achievement of early fecundity of individuals. Whether macrophages play an analogous role in
27 other situations of apoptotic cell removal remains to be elucidated.

28

29 **Summary statement:** Macrophages adopt a unique metabolic profile to convert engulfed cell mass into
30 lipoproteins and storage peptides that metabolically supplement other tissues during post-metamorphic
31 maturation in *Drosophila*.

32 **Running title:** Macrophages recycle nutrients

33 **Keywords:** *Drosophila* macrophages, efferocytosis, metamorphosis, macrophage metabolic polarization,
34 post-metamorphic maturation, lipoproteins.

35 Introduction

36 A continuous cycle of removing senescent, damaged, and apoptotic cells and replacing them with new
37 ones is essential for the health of all multicellular organisms (Doran, Yurdagul and Tabas, 2020). The
38 number of dying cells in a healthy organism reaches tens of billions every day, and their removal is
39 therefore essential to maintain tissue homeostasis (Elliott and Ravichandran, 2016). Macrophages play a
40 key role in this process. Senescent, damaged, and apoptotic cells produce characteristic signals that allow
41 their recognition and removal by a process called efferocytosis (Elliott and Ravichandran, 2016). While the
42 mechanism by which macrophages recognize and engulf these cells is well understood (Hochreiter-
43 Hufford and Ravichandran, 2013), it is unclear whether and how the remnants of the disposed cells are
44 handled in the organism. It can be assumed that the structural components of the engulfed apoptotic cells
45 are further recycled and reused by the organism to avoid wasting the nutrients and building blocks. To
46 this end, the matter of the dying cellular debris must be converted into a form of nutrients suitable for
47 transport, storage, or direct utilization. This phenomenon can be expected to be particularly important in
48 situations where certain tissues undergo massive remodeling, such as embryonic morphogenesis,
49 regeneration, or metamorphosis (Ghosh, Ghosh and Mandal, 2020; Mezu-Ndubuisi and Maheshwari,
50 2021).

51 Holometabolous insects have ecologically separated periods of growth and nutrient accumulation
52 from periods of reproductive activity. Because these two stages are connected with different ecological
53 requirements, individuals must undergo a major transformation of their body plan during complete
54 metamorphosis. In this process, the majority of larval tissues undergo histolysis and most adult structures
55 emerge from the imaginal discs (ten Brink, de Roos and Dieckmann, 2019). This poses a fundamental
56 problem to the individual of how to transfer nutrient and energy reserves from the larval to the adult life
57 stage.

58 In growing larvae, energy-rich carbohydrates, lipids and storage peptides are stored primarily in the
59 central metabolic organ, the fat body, and in the circulating hemolymph (Poças, Crosbie and Mirth, 2022).
60 At the onset of metamorphosis, the peak of the steroid hormone ecdysone triggers preparation for the
61 upcoming period of nutrient scarcity (Juarez-Carreño *et al.*, 2021). The storage peptides and
62 carbohydrates from the hemolymph are resorbed into the polytene adipocytes of the fat body, where
63 they, together with abundant mRNA transcripts, and organelles such as endoplasmic reticulum and
64 mitochondria, give rise to ribonucleoprotein granules (RNP granules) (Locke and Collins, 1965; Tysell and
65 Butterworth, 1978). Thus, the adipocytes become hypertrophic and the fat body is massively infiltrated
66 by larval macrophage-like cells called plasmatocytes (Ghosh, Ghosh and Mandal, 2020). However,

67 publications investigating the role of macrophages in the whole process are relatively scarce and the
68 macrophage role in adipose tissue remodeling is considered of negligible importance (Nelliot, Bond and
69 Hoshizaki, 2006).

70 Nutrients stored in adipocytes are not significantly utilized during metamorphosis and serve
71 predominantly for the emergence and post-metamorphic maturation of the reproductive organs, the
72 formation of adult fat reserves, and cuticle tanning (Aguila *et al.*, 2007; Storelli *et al.*, 2019). Therefore, all
73 stores from adipocytes are fully utilized during the first 72 hours of adult *Drosophila* life, and larval
74 adipocytes are completely depleted during this short period (Rehman and Varghese, 2021). Although
75 larval fat body reserves are essential for these processes, the mechanism of nutrient mobilization from
76 histolysis-undergoing adipocytes has not yet been revealed. This is of particular interest because the
77 formation of RNP granules together with ribosome sequestration indicates limited translation in the
78 histolyzing adipocytes, while the adult fat body is not yet fully established (Rode *et al.*, 2018; Tsuyama *et*
79 *al.*, 2023). Thus, the individual must overcome this metabolically sensitive period without any apparent
80 functional central metabolic organ.

81 The mutual interactions between macrophages and adipocytes have been most studied in the
82 pathogenesis of obesity and metabolic syndrome (Li, Yun and Mu, 2020). Hypertrophic adipose tissue in
83 obese individuals is heavily infiltrated by macrophages, which form characteristic crown-like structures
84 around adipocytes and, in response to excessive lipid intake, become foamy and significantly increase
85 their ability to process engulfed lipids (Aouadi *et al.*, 2014; Dahik, Frisdal and Le Goff, 2020). However, this
86 phenomenon is not exclusively connected with obesity and the adipose tissue also appears to be
87 infiltrated by macrophages in other stressful situations such as starvation, infection, or congenital
88 dyslipidemia, however, their role under these circumstances remains enigmatic (Kosteli *et al.*, 2010; Silva
89 *et al.*, 2019).

90 We have shown that the larval fat body of *Drosophila* is massively infiltrated during metamorphosis by
91 macrophages that take up lipids and RNP granules from dying adipocytes. Infiltrating macrophages display
92 many of the characteristics of adipocytes at the transcriptomic, proteomic, and morphological levels and
93 significantly participate in the processing and redistribution of nutrients from the histolyzing adipocytes
94 that nutritionally support post-metamorphic maturation and female fecundity.

95
96
97
98

99 Results

100 Macrophages participate in adipose tissue remodeling during insect metamorphosis

101 To understand the mechanism of nutrient mobilization for post-metamorphic maturation, we first
102 characterized the progress of fat body remodeling at the level of its ultrastructure over the course of
103 metamorphosis.

104 Initially, the fat body of third instar larvae consist of polygonal sheet-like cells with cytosol filled
105 predominantly with lipid droplets. At the onset of metamorphosis, however, the individual adipocytes
106 become more spherical and resorb storage peptides and carbohydrates from the circulation into the cell's
107 cytosol, thereby becoming hypertrophic. Confocal microscopy analysis of flies bearing the *croquemort-*
108 *GFP* construct, which is specifically expressed in macrophages, revealed that as the metamorphosis
109 proceeds and larval fat body disintegrates, macrophages infiltrate this tissue and closely interact with
110 hypertrophic adipocytes (Fig. 1A).

111 Resorbed storage peptides accumulate in the cytosol, where, together with autophagy of the rough
112 endoplasmic reticulum and other cytosolic organelles, they give rise to a matter which later condenses
113 into electron-dense RNP granules (Fig. 1B and Fig. S1A), which are strongly autofluorescent (Fig. 1A). While
114 at the onset of metamorphosis, the organelles still can be distinguished within the RNP granules (Fig. 1C),
115 later, the RNP granules become denser, contain a urate crystalline core (Locke and Collins, 1965) (Fig. 1D),
116 and fuse into the granules of larger diameter (Fig. 2A).

117 While changes in the ultrastructure of adipocytes are rather gradual over the course of
118 metamorphosis, the remodeling of the fat body accelerates dramatically about the individual's
119 emergence. Utilization of nutrients from the larval adipocytes is essential for successful metamorphosis
120 as flies carrying the adipocyte-specific overexpression of the dominant-negative form of the ecdysone
121 receptor are unable to form RNP granules and exhibit a significant mortality rate at the emergence (Fig.
122 S1B, C, D).

123 During the first 48 hours post-eclosion, the number of RNP granules in the cytosol of adipocytes
124 decreases significantly (Fig. 2B). This decrease can be attributed to the disintegration of granules in
125 adipocyte cytosol as dilated endoplasmic reticulum with dilated cisternae and other organelles
126 suddenly appear in close vicinity of the plasma membrane (Fig. 2C) and in extracellular space (Fig. 2D).
127 RNP granules also disintegrate to some extent via budding, as described earlier (Locke and Collins, 1965)
128 (Fig. 2E). Additionally, the whole RNP granules and lipid droplets can be observed to be expelled by
129 exhausted adipocytes to their surroundings (Fig. 2F, G).

130 As the number of RNP granules within adipocytes decreases (Fig. 2B), it eventually leads to the
131 occurrence of adipocytes filled only with lipid droplets and (Fig. S2A). Along with the release of nutrients,
132 adipocytes gradually decrease in diameter and eventually disappear entirely during the first 72 hours of
133 post-metamorphic development (Fig. 2H, I). Notably, the matter from adipocytes can be observed in the
134 cytosol of the infiltrating macrophages (Fig.S2B, C). Although previous work has suggested that
135 macrophages play a negligible role in adipose tissue remodeling in *Drosophila* (Nelliot, Bond and
136 Hoshizaki, 2006), our data show that previously used genetic tools for their depletion are not fully
137 functional and do not lead to a significant limitation of macrophage function (for details see
138 [Supplementary information](#)). The same conclusion was drawn by Stephenson and colleagues (Stephenson
139 *et al.*, 2022). In addition, using a newly established line of macrophage-specific Gal4 driver (*Hm^{le9-P2a} Gal4*),
140 they demonstrated that macrophages play an indispensable role during metamorphosis (Stephenson *et al.*,
141 2022). Their data are in congruence with our observations that flies with macrophage-specific
142 overexpression of the pro-apoptotic protein *grim* using the *Hm^{le9-P2a} Gal4* driver line (Stephenson *et al.*,
143 2022) die shortly after the pre-pupa to pupa transition and display certain morphological abnormalities.
144 In particular, these pupae lack visible anterior spiracles, and do not undergo head eversion otherwise
145 observed in pupal stage P4 (Fig. 3A). Moreover, the body cavity of these individuals contains the debris of
146 non-phagocytosed larval muscles (Fig. 3B) and less disintegrated larval fat body compared to controls (Fig.
147 3C).

148 To overcome lethality at this stage of metamorphosis, the construct used for ablation of macrophages
149 was activated after pupal stage P8 by combining a macrophage-specific driver with temperature-sensitive
150 inhibitor protein (*Hm^{le9-P2a} Gal4, Tub Gal80^{TS}*). Delayed ablation of macrophages allows the individuals to
151 finish metamorphosis even without these cells at the time of emergence. However, the emerged
152 individuals display abnormal post-metamorphic maturation, as they have significantly delayed ovarian
153 development (Fig. 3D, E) and are unable to expand their wings (Fig. 3F), as suggested in a previous study
154 (Kiger, Natzle and Green, 2001).

155 Given that the entire fat body mass of larvae, which constitutes about 23% of the body of newly
156 emerged virgins, completely disappears during the first three days after emergence (Fig. 2I, Fig. S1E, Fig.
157 S2D and [Movie 1](#), [Movie 2](#), [Movie 3](#)), we assume an extremely rapid redistribution of nutrients. We
158 decided to inspect the macrophage role in this process, as the data presented above document their
159 infiltration into adipose tissue and their importance for post-metamorphic maturation (Fig. 1A, Fig. 3D, E,
160 F).

161

162 Macrophages transiently acquire adipocyte-like metabolic features

163 Further examination of macrophages infiltrating adipose tissue revealed a surprisingly close interaction
164 between macrophages and adipocytes. Confocal imaging of the larval adipose tissue dissected from
165 freshly emerged flies bearing the *Crq>GFP* construct revealed that the macrophages form crown-like
166 structures around the hypertrophic adipocytes (Fig. 4A and Fig. S3A) and cover a significant portion of
167 their surface (Fig. 4B, C and Fig. S3B).

168 Infiltrating macrophages intercalate their lamellipodia into the adipocytes with disrupted plasma
169 membrane and clear either fragments or the whole depleted cells via efferocytosis (Fig. 4D).

170 Transmission electron microscopy revealed that macrophages show signs of increased processing of lipids,
171 RNP granules, and other cellular debris. The RNP complexes may be abundantly found in the cytosol of
172 infiltrating macrophages as leaking RNP granules are endocytosed and subsequently untangled by these
173 cells (Fig. 4E, F and Fig. S2C). Excessive lipid uptake and efferocytosis leads to a frequent occurrence of
174 multilamellar bodies (Fig. 4F and Fig. S3C), structures attributed to lysosomal processing and storage of
175 polar lipids (Schmitz and Müller, 1991). Eventually, the infiltrating macrophages are reminiscent of foamy
176 macrophages known from obese mammals and closely resemble adipocytes themselves in their
177 ultrastructure (Fig. 4G and Fig. S3D, E). Lipidomics analysis showed that the macrophages isolated from
178 freshly emerged virgins have significantly increased levels of total lipids when compared to macrophages
179 from larval stage L3W (Fig. 5A). This observation is further supported by elevated cholesterol and
180 cholesteryl-ester levels during metamorphosis and early post-metamorphic development (Fig. S3F). As
181 the post-metamorphic development proceeds and the adipocytes slowly disappear, the percentage of the
182 macrophage cytosol occupied by lipid droplets increases substantially (Fig. 5B, C). The lipidomic profile of
183 macrophages isolated from freshly emerged flies is shifted toward an increased abundance of polar lipids
184 and ceramides when compared to adipocytes in terms of composition and prevalence of lipid species (Fig.
185 5D).

186 Transcriptomic profiling of macrophages isolated from newly emerged virgin flies revealed that these
187 cells primarily increase the expression of genes involved in the synthesis of energy-rich metabolites and
188 their precursors. In particular, the genes involved in lipid metabolism and lipoprotein biosynthetic process
189 are significantly upregulated in these cells compared to macrophages isolated from L3W (Fig. 5E).
190 Targeted analysis showed that macrophages in freshly emerged flies display enhanced expression of
191 genes involved in lipoprotein assembly, production of storage peptides, and processing of sphingolipids
192 (Fig. S4A).

193 This observation was rather unexpected as these metabolic processes are thought to be almost
194 exclusive to adipocytes. Moreover, many genes strongly elevated in macrophages during post-
195 metamorphic maturation are recognized as characteristic fat body markers (Leader *et al.*, 2018), such as
196 the storage peptides (*Fat body protein 2*, *Larval serum proteins 1* and *2*, *Odorant-binding proteins*) and
197 lipoproteins (*apolipoporphin*, *Apolipoprotein lipid transfer particle*, or *Neuropeptide-like precursor 2*) (Fig.
198 S4B). Nonetheless, in addition to these genes, the macrophages also highly express genes considered to
199 be plasmatocyte markers, such as *croquemort*, *peroxidasin*, *serpent*, *Hemolectin*, *Nimrod C1*, and *eater*
200 (Fig. S4B). Notably, the co-expression of adipocyte- and macrophage-specific markers can be detected
201 only in macrophages isolated from freshly emerged flies since the adipocyte-like markers are not
202 upregulated in the macrophages isolated from 10-day adult flies (Fig. S4B). These data indicate that during
203 early post-metamorphic development, macrophages temporarily adopt a unique phenotypic polarization,
204 which comprises the phagocytic capability of macrophages and the metabolic features of adipocytes.
205 Interestingly, their phenotype is reminiscent of adipohemocytes and secreting plasmatocytes identified
206 in recent single-cell RNAseqs of larval immune cells (Cattenoz *et al.*, 2020; Cho *et al.*, 2020). Indeed, all
207 the identified markers of adipohemocytes and secreting plasmatocytes are expressed at elevated levels
208 in macrophages of newly emerged flies (Fig. S4B).

209 To confirm this unexpected polarization phenotype, we generated a fly line in which the proteins
210 secreted by macrophages were labeled by ectopic expression of engineered promiscuous biotin ligase
211 (BirA-G3) (Droujinine *et al.*, 2021) in these cells. Proteomic analysis of biotinylated proteins isolated from
212 hemolymph confirms our previous notion that macrophages translate and secrete storage peptides and
213 lipoproteins into circulation. We identified 18 macrophage-secreted proteins (predominantly
214 lipoproteins, storage peptides, and enzymes involved in lipid metabolism) that are secreted by both
215 macrophages and adipocytes during post-metamorphic maturation, whilst none of these proteins have
216 been found to be produced by macrophages in fully mature flies (10 days after emergence) (Fig. 5F). This
217 indicates that macrophages transiently adopt this unique adipocyte-like polarization to facilitate the
218 mobilization of nutritionally rich substances from the adipocytes.

219

220 Production of lipoproteins by macrophages promotes post-metamorphic maturation of ovaries

221 The presented data document that macrophages facilitate the mobilization of nutrients from larval
222 adipocytes in the form of storage peptides and lipoproteins. We hypothesize that the mobilized nutrients
223 are used for post-metamorphic maturation, which is necessary for rapid adaptation to adult life and
224 reproduction. To investigate the importance of macrophage-mediated nutrient mobilization for this

225 process, we silenced the expression of *apolipoprotein* (*apolpp*) exclusively in these cells using the
226 macrophage-specific promoter *croquemort* (*Crq>apolpp^{RNAi}*, see Fig. S5A for RNAi efficiency). *Apolpp*
227 represents a major component of lipoproteins in *Drosophila* and is essential for the transport of lipids
228 between tissues (Palm *et al.*, 2012). The expression of *apolpp* in macrophages increases continuously
229 during metamorphosis and peaks in these cells 24 hours after emergence (Fig. 6A). The production of
230 *apolpp* by macrophages in freshly emerged flies is further documented by the occurrence of a strong GFP
231 signal in these cells in flies bearing the APOLPP-GFP reporter. To a lesser extent, the GFP signal can also
232 be observed on the surface of the RNP granules in larval adipocytes, (Fig. 6B), consistent with the
233 proteomic analysis (Fig. 5F).

234 The macrophage-specific knockdown of *apolpp* expression leads to an accumulation of neutral lipids
235 in macrophages (Fig. 6C, D). Simultaneously, the macrophage-specific *apolpp* knockdown results in a
236 reduction of lipid deposits in maturing ovaries as manifested by a decrease in free fatty acid levels (FFAs)
237 (Fig. 7A and Fig. S5B). Moreover, the amount of ¹³C-labeled FFAs incorporated into this tissue over the
238 course of metamorphosis is also significantly decreased (Fig. 7B and Fig. S5C). In consequence, the
239 maturation of the ovaries is delayed significantly in these flies. Ovaries of flies with the macrophage-
240 specific *apolpp* knockdown exhibit reduced fluorescence signal of the lipophilic dye (Fig. 7C) and their
241 maturation is significantly delayed (Fig. 7D, Fig. 7E and Fig. S5D). Accordingly, these females lay fewer eggs
242 during the first 72 hours of adult life and exhibit significantly lower fecundity compared to controls (Fig.
243 7F, G).

244 Delay in ovary maturation can be accounted for apoptotic regression of maturing egg chambers as it
245 is observed in adult flies exposed to nutrition scarcity (Barth *et al.*, 2011). Increase level of apoptosis in
246 ovaries has been also previously associated with disruption of sphingolipid metabolism in this tissue (Phan
247 *et al.*, 2007). Nonetheless, the ovaries of flies with macrophage-specific knockdown of *apolpp* do not
248 exhibit any signs of apoptosis (Fig. S5E) and their size is comparable to the controls in one-week-old flies
249 (Fig. 7H, I), suggesting that silencing of *apolpp* in macrophages can be explained by delayed initiation of
250 ovary maturation at the onset of adult life stage. In parallel to lipid transport to ovaries, lipids from larval
251 adipocytes are transported to adult fat body tissue formed from independent cellular lineage. Therefore,
252 we inspected the number of larval adipocytes and morphology of the adult fat body in flies with the
253 macrophage-specific *apolpp* knockdown. Nonetheless, we found no difference neither in the number of
254 larval adipocytes during the first three days after emergence nor in the amount of lipid stores in adult fat
255 body between control flies and flies lacking *apolpp* expression in macrophages (Fig. S5F, G, H).

256 Overall, our data demonstrate that the production of APOLPP by macrophages is required for the
257 redistribution of stores during post-metamorphic development and for achieving early ovarian maturation
258 and fecundity (Fig. 8A).

259

260 Discussion

261 Macrophages are functionally versatile cells that perform many diverse roles in the organism (Murray
262 and Wynn, 2011). We found that during *Drosophila* metamorphosis, macrophages infiltrate the larval
263 adipose tissue and actively participate in the clearance of dying adipocytes and their cellular remnants.
264 The infiltrating macrophages are exposed to an excessive load of leaking lipids, organelles, membranes,
265 and RNP granules and undergo a characteristic phenotypic polarization by temporally adopting adipocyte-
266 like features. As the endocytosed cellular matter is digested in the phagolysosome, the macrophages
267 enhance the expression of genes involved in the assembly and release of lipoproteins and the production
268 of storage peptides. Macrophages thus convert the raw cellular matter into an easily transportable and
269 exploitable form of lipoproteins and storage peptides, to be subsequently used for post-metamorphic
270 maturation. The intervention of macrophage production of lipoproteins by silencing *apolpp* expression in
271 these cells leads to delayed ovary development and reduced fecundity. Thus, the macrophages promote
272 the transfer of energy between the larval and adult life stage.

273 Our data indicate that under certain conditions, *Drosophila* macrophages can acquire metabolically
274 nutritive roles and generate suitable nutrients from digested cellular remnants to support other tissues in
275 the body. Although this metabolic role might be rather unexpected for macrophages, this function may
276 originate from the nutritive phagocytosis that is currently hypothesized to precede macrophage
277 protective role in immune response (Hartenstein and Martinez, 2019). The process of phagocytosis and
278 processing of engulfed material is highly conserved within the animal clade. Even the free-living unicellular
279 ancestors of all animals performed phagocytosis to obtain nutrients from engulfed bacteria and foreign
280 eukaryotic cells (Desjardins, Houde and Gagnon, 2005). A similar form of nutritive phagocytosis is common
281 also in multicellular animals, in which professional nutritive phagocytes process endocytosed material and
282 provide it in a suitable form to other cells in the body (Mills, 2020). Macrophages as professional
283 phagocytes play a central role in maintaining tissue homeostasis by clearing damaged, apoptotic and
284 senescent cells (Lavin *et al.*, 2015). In this process, which is essential for the health of tissues and organs,
285 tens of billions of cells are removed and replaced by new ones every day in the human body (Doran,
286 Yurdagul and Tabas, 2020). Based on our data, it is reasonable to assume that the nutritive value of these

287 cells and the building blocks they contain are not merely wasted. However, whether macrophages play
288 analogous role during metamorphosis of amphibians, embryonal morphogenesis, as well as daily cellular
289 turnover, remains to be elucidated.

290 The mechanism of macrophage metabolic polarization during metamorphosis may be complex and has
291 not yet been fully elucidated. One trigger that induces the adoption of a transient adipocyte-like
292 polarization of *Drosophila* macrophages may be their mere exposure to the histolyzing cells along with
293 the excessive amount of leaking lipids, ribosomes, and other cellular fragments (Elliott, Koster and
294 Murphy, 2017). In parallel, the macrophage function may also be affected by hormonal signaling.
295 Ecdysone, the most important regulator of metamorphosis in arthropods, has been shown to be a potent
296 regulator of macrophages during *Drosophila* metamorphosis. It enhances macrophage motility and
297 triggers the expression of genes involved in the enzymatic remodeling of the extracellular matrix,
298 neutralization of toxic compounds, and efferocytosis (Regan et al., 2013).

299 The adoption of macrophage adipocyte-like metabolic polarization may have also an alternative
300 explanation. At the onset of metamorphosis, the adipocytes retain storage peptides from the circulation
301 and sequester the endoplasmic reticulum- and RNA into RNP granules (Tysell and Butterworth, 1978).
302 These transient organelles resemble the stress granules, which formation in response to stress conditions
303 has been extensively studied in many mammalian and insect cell lines. The formation of RNP granules
304 protects the presynthesized mRNA molecules from their degradation resulting in stalled translation under
305 adverse conditions (Ivanov et al., 2019; Kipper et al., 2022). After overcoming the stress period the mRNA
306 translation can be promptly restored (Riggs *et al.*, 2020; Campos-Melo *et al.*, 2021). As the RNP granules
307 are expelled from larval adipocytes in *Drosophila* and may be frequently found disentangled in the
308 macrophage's cytosol, we hypothesize that the mRNA bound in RNP granules may serve as a template for
309 translation in macrophages, which may thus acquire the adipocyte-like features. This strategy may be
310 particularly efficient in the case of larval adipocytes, which produce mRNA in multiple copies from
311 polythene chromosomes. Although there is no clear evidence supporting this hypothesis, this
312 phenomenon deserves more attention in future research.

313 Over the past decade, the role of macrophages in insect metamorphosis has been considered negligible
314 (Nelliott, Bond and Hoshizaki, 2006). Recently, however, it has been demonstrated that macrophages show
315 striking level of resistance to the tools used in these initial attempts of their depletion and that
316 macrophage function is essential for successful progress of metamorphosis (Stephenson et al., 2022). It is
317 evident that macrophages interact closely with the larval adipocytes and engulf them via efferocytosis
318 (Ghosh, Ghosh and Mandal, 2020). The phenotypic profile of macrophages during post-metamorphic

319 development is of particular interest when compared to two independent single-cell RNAseqs of
320 *Drosophila* larval hemocytes. In these publications, the authors identified subpopulations of
321 plasmatocytes, which upregulate the expression of lipophorins and storage peptides, denoted as
322 adipohemocytes or secretory plasmatocytes (Tattikota et al., 2020; Cattenoz et al., 2020).

323 Infiltration of adipose tissue by macrophages is a hallmark of obesity, diabetes, and metabolic
324 syndrome (Boutens and Stienstra, 2016). Nevertheless, recent observations have revealed that adipose
325 tissue is also infiltrated in other situations of metabolic stress such as starvation, dyslipidemia, and
326 bacterial or viral infection (Surmi and Hasty, 2008; Kosteli *et al.*, 2010; Silva *et al.*, 2019). These
327 observations indicate that the adipose tissue-associated macrophages may play a hitherto undiscovered
328 role in the regulation of metabolism and the clearance of exhausted and moribund adipocytes. Although
329 *D. melanogaster* represents a frequently used model organism for the study of human diseases including
330 diabetes, metabolic syndrome, or cachexia, the model has suffered from the under-investigated
331 interaction between macrophages and adipocytes (Graham and Pick, 2017; Álvarez-Rendón, Salceda and
332 Riesgo-Escovar, 2018; Chatterjee and Perrimon, 2021). Here, we describe an adaptive physiological
333 process, during which macrophages display features observed otherwise in mammalian macrophages
334 under pathophysiological conditions such as metabolic syndrome, obesity and atherosclerosis (Hariri *et*
335 *al.*, 2000). We believe that our discoveries may open novel avenues for the study of obesity and obesity-
336 related diseases in the *Drosophila* model.

337

338 **Acknowledgments**

339 The authors gratefully acknowledge financial support from the Czech Republic Grant Agency for AB
340 (project 20-14030S and 23-06133S; www.gacr.cz). GK was supported by the USB Grant Agency (project
341 050/2019/P). We thank Lucie Hrádková for laboratory services and support. We thank the Laboratory of
342 Microscopy and Histology and the Electron Microscopy Laboratory of the Biological Centre of the CAS, v.
343 v. i., for assistance in the preparation of histological samples. We thank Mark C. Dionne, Gabor Juhasz, Alf
344 Herzig and John Nambu for providing the fly lines. Other fly populations were obtained from the
345 Bloomington Center (Bloomington, IN) and the VDRC (Vienna, Austria). We also thank Petra Berkova and
346 Petr Simek for lipidomics services, and the Department of Medical Biology (USB) for allowing the use of
347 the S3eBioRad sorter. We also thank the developers of Fiji: an open-source platform for bioimaging
348 analysis (doi:10.1038/nmeth.2019), LipidSuite: a suitable platform for lipidomic analysis, TCC: an online
349 platform for transcriptomic data processing, and iDep94: an alternative online platform for transcriptomic

350 data analysis. Graphical summaries used in project conceptualization and data presentation were
351 performed using BioRender as an online graphical platform for creating biological schematics.

References

- 352 Aguila, J. R., Suszko, J., Gibbs, A. G. and Hoshizaki, D. K. (2007) 'The role of larval fat cells in adult
353 *Drosophila melanogaster*', *Journal of Experimental Biology*, 210(6), pp. 956–963. doi:
354 10.1242/jeb.001586.
- 355 Álvarez-Rendón, J. P., Salceda, R. and Riesgo-Escovar, J. R. (2018) 'Drosophila melanogaster as a Model
356 for Diabetes Type 2 Progression', *BioMed Research International*, 2018, pp. 1–16. doi:
357 10.1155/2018/1417528.
- 358 Aouadi, M., Vangala, P., Yawe, J. C., Tencerova, M., Nicoloso, S. M., Cohen, J. L., Shen, Y. and Czech, M. P.
359 (2014) 'Lipid storage by adipose tissue macrophages regulates systemic glucose tolerance', *American*
360 *Journal of Physiology-Endocrinology and Metabolism*, 307(4), pp. E374–E383. doi:
361 10.1152/ajpendo.00187.2014.
- 362 Barth, J. M. I., Szabad, J., Hafen, E. and Köhler, K. (2011) 'Autophagy in Drosophila ovaries is induced by
363 starvation and is required for oogenesis', *Cell Death & Differentiation*, 18(6), pp. 915–924. doi:
364 10.1038/cdd.2010.157.
- 365 Boutens, L. and Stienstra, R. (2016) 'Adipose tissue macrophages: going off track during obesity',
366 *Diabetologia*, 59(5), pp. 879–894. doi: 10.1007/s00125-016-3904-9.
- 367 ten Brink, H., de Roos, A. M. and Dieckmann, U. (2019) 'The Evolutionary Ecology of Metamorphosis',
368 *The American Naturalist*, 193(5), pp. E116–E131. doi: 10.1086/701779.
- 369 Campos-Melo, D., Hawley, Z. C. E., Droppelmann, C. A. and Strong, M. J. (2021) 'The Integral Role of RNA
370 in Stress Granule Formation and Function', *Frontiers in Cell and Developmental Biology*, 9. doi:
371 10.3389/fcell.2021.621779.
- 372 Cattenoz, P. B., Sakr, R., Pavlidaki, A., Delaporte, C., Riba, A., Molina, N., Hariharan, N., Mukherjee, T.
373 and Giangrande, A. (2020) 'Temporal specificity and heterogeneity of Drosophila immune cells', *The*
374 *EMBO Journal*, 39(12). doi: 10.15252/embj.2020104486.
- 375 Dahik, V. D., Frisdal, E. and Le Goff, W. (2020) 'Rewiring of Lipid Metabolism in Adipose Tissue
376 Macrophages in Obesity: Impact on Insulin Resistance and Type 2 Diabetes', *International Journal of*
377 *Molecular Sciences*, 21(15), p. 5505. doi: 10.3390/ijms21155505.
- 378 Desjardins, M., Houde, M. and Gagnon, E. (2005) 'Phagocytosis: the convoluted way from nutrition to

379 adaptive immunity', *Immunological Reviews*, 207(1), pp. 158–165. doi: 10.1111/j.0105-
380 2896.2005.00319.x.

381 Doran, A. C., Yurdagul, A. and Tabas, I. (2020) 'Efferocytosis in health and disease', *Nature Reviews*
382 *Immunology*, 20(4), pp. 254–267. doi: 10.1038/s41577-019-0240-6.

383 Droujinine, I. A., Meyer, A. S., Wang, D., Udeshi, N. D., Hu, Y., Rocco, D., McMahon, J. A., Yang, R., Guo,
384 J., Mu, L., Carey, D. K., Svinkina, T., Zeng, R., Branon, T., Tabatabai, A., Bosch, J. A., Asara, J. M., Ting, A.
385 Y., Carr, S. A., McMahon, A. P. and Perrimon, N. (2021) 'Proteomics of protein trafficking by in vivo
386 tissue-specific labeling', *Nature Communications*, 12(1), p. 2382. doi: 10.1038/s41467-021-22599-x.

387 Elliott, M. R., Koster, K. M. and Murphy, P. S. (2017) 'Efferocytosis Signaling in the Regulation of
388 Macrophage Inflammatory Responses', *The Journal of Immunology*, 198(4), pp. 1387–1394. doi:
389 10.4049/jimmunol.1601520.

390 Elliott, M. R. and Ravichandran, K. S. (2016) 'The Dynamics of Apoptotic Cell Clearance', *Developmental*
391 *Cell*, 38(2), pp. 147–160. doi: 10.1016/j.devcel.2016.06.029.

392 Ghosh, S., Ghosh, S. and Mandal, L. (2020) 'Drosophila metamorphosis involves hemocyte mediated
393 macroendocytosis and efferocytosis', *The International Journal of Developmental Biology*, 64(4-5-6), pp.
394 319–329. doi: 10.1387/ijdb.190215lm.

395 Graham, P. and Pick, L. (2017) 'Drosophila as a Model for Diabetes and Diseases of Insulin Resistance',
396 in, pp. 397–419. doi: 10.1016/bs.ctdb.2016.07.011.

397 Hariri, M., Millane, G., Guimond, M.-P., Guay, G., Dennis, J. W. and Nabi, I. R. (2000) 'Biogenesis of
398 Multilamellar Bodies via Autophagy', *Molecular Biology of the Cell*. Edited by D. Botstein, 11(1), pp. 255–
399 268. doi: 10.1091/mbc.11.1.255.

400 Hartenstein, V. and Martinez, P. (2019) 'Phagocytosis in cellular defense and nutrition: a food-centered
401 approach to the evolution of macrophages', *Cell and Tissue Research*, 377(3), pp. 527–547. doi:
402 10.1007/s00441-019-03096-6.

403 Hochreiter-Hufford, A. and Ravichandran, K. S. (2013) 'Clearing the Dead: Apoptotic Cell Sensing,
404 Recognition, Engulfment, and Digestion', *Cold Spring Harbor Perspectives in Biology*, 5(1), pp. a008748–
405 a008748. doi: 10.1101/cshperspect.a008748.

406 Chatterjee, N. and Perrimon, N. (2021) 'What fuels the fly: Energy metabolism in Drosophila and its
407 application to the study of obesity and diabetes', *Science Advances*, 7(24). doi: 10.1126/sciadv.abg4336.

408 Cho, B., Yoon, S.-H., Lee, D., Koranteng, F., Tattikota, S. G., Cha, N., Shin, M., Do, H., Hu, Y., Oh, S. Y., Lee,

409 D., Vipin Menon, A., Moon, S. J., Perrimon, N., Nam, J.-W. and Shim, J. (2020) 'Single-cell transcriptome
410 maps of myeloid blood cell lineages in *Drosophila*', *Nature Communications*, 11(1), p. 4483. doi:
411 10.1038/s41467-020-18135-y.

412 Ivanov, P., Kedersha, N. and Anderson, P. (2019) 'Stress Granules and Processing Bodies in Translational
413 Control', *Cold Spring Harbor Perspectives in Biology*, 11(5), p. a032813. doi:
414 10.1101/cshperspect.a032813.

415 Juarez-Carreño, S., Vallejo, D. M., Carranza-Valencia, J., Palomino-Schätzlein, M., Ramon-Cañellas, P.,
416 Santoro, R., de Hartog, E., Ferres-Marco, D., Romero, A., Peterson, H. P., Ballesta-Illan, E., Pineda-
417 Lucena, A., Dominguez, M. and Morante, J. (2021) 'Body-fat sensor triggers ribosome maturation in the
418 steroidogenic gland to initiate sexual maturation in *Drosophila*', *Cell Reports*, 37(2), p. 109830. doi:
419 10.1016/j.celrep.2021.109830.

420 Kiger, J. A., Natzle, J. E. and Green, M. M. (2001) 'Hemocytes are essential for wing maturation in
421 *Drosophila melanogaster*', *Proceedings of the National Academy of Sciences*, 98(18), pp. 10190–10195.
422 doi: 10.1073/pnas.181338998.

423 Kosteli, A., Sugaru, E., Haemmerle, G., Martin, J. F., Lei, J., Zechner, R. and Ferrante, A. W. (2010) 'Weight
424 loss and lipolysis promote a dynamic immune response in murine adipose tissue', *Journal of Clinical*
425 *Investigation*, 120(10), pp. 3466–3479. doi: 10.1172/JCI42845.

426 Lavin, Y., Mortha, A., Rahman, A. and Merad, M. (2015) 'Regulation of macrophage development and
427 function in peripheral tissues', *Nature Reviews Immunology*, 15(12), pp. 731–744. doi: 10.1038/nri3920.

428 Leader, D. P., Krause, S. A., Pandit, A., Davies, S. A. and Dow, J. A. T. (2018) 'FlyAtlas 2: a new version of
429 the *Drosophila melanogaster* expression atlas with RNA-Seq, miRNA-Seq and sex-specific data', *Nucleic*
430 *Acids Research*, 46(D1), pp. D809–D815. doi: 10.1093/nar/gkx976.

431 Li, Y., Yun, K. and Mu, R. (2020) 'A review on the biology and properties of adipose tissue macrophages
432 involved in adipose tissue physiological and pathophysiological processes', *Lipids in Health and Disease*,
433 19(1), p. 164. doi: 10.1186/s12944-020-01342-3.

434 Locke, M. and Collins, J. V. (1965) 'The structure and formation of protein granules in the fat body of an
435 insect', *Journal of Cell Biology*, 26(3), pp. 857–884. doi: 10.1083/jcb.26.3.857.

436 Mezu-Ndubuisi, O. J. and Maheshwari, A. (2021) 'Role of macrophages in fetal development and
437 perinatal disorders', *Pediatric Research*, 90(3), pp. 513–523. doi: 10.1038/s41390-020-01209-4.

438 Mills, D. B. (2020) 'The origin of phagocytosis in Earth history', *Interface Focus*, 10(4), p. 20200019. doi:
439 10.1098/rsfs.2020.0019.

440 Murray, P. J. and Wynn, T. A. (2011) 'Protective and pathogenic functions of macrophage subsets',
441 *Nature Reviews Immunology*, 11(11), pp. 723–737. doi: 10.1038/nri3073.

442 Nelliott, A., Bond, N. and Hoshizaki, D. K. (2006) 'Fat-body remodeling in *Drosophila melanogaster*',
443 *genesis*, 44(8), pp. 396–400. doi: 10.1002/dvg.20229.

444 Palm, W., Sampaio, J. L., Brankatschk, M., Carvalho, M., Mahmoud, A., Shevchenko, A. and Eaton, S.
445 (2012) 'Lipoproteins in *Drosophila melanogaster*—Assembly, Function, and Influence on Tissue Lipid
446 Composition', *PLoS Genetics*. Edited by R. P. Kühnlein, 8(7), p. e1002828. doi:
447 10.1371/journal.pgen.1002828.

448 Phan, V. H., Herr, D. R., Panton, D., Fyrst, H., Saba, J. D. and Harris, G. L. (2007) 'Disruption of
449 sphingolipid metabolism elicits apoptosis-associated reproductive defects in *Drosophila*', *Developmental*
450 *Biology*, 309(2), pp. 329–341. doi: 10.1016/j.ydbio.2007.07.021.

451 Poças, G. M., Crosbie, A. E. and Mirth, C. K. (2022) 'When does diet matter? The roles of larval and adult
452 nutrition in regulating adult size traits in *Drosophila melanogaster*', *Journal of Insect Physiology*, 139, p.
453 104051. doi: 10.1016/j.jinsphys.2020.104051.

454 Regan, J. C., Brandão, A. S., Leitão, A. B., Mantas Dias, Â. R., Sucena, É., Jacinto, A. and Zaidman-Rémy, A.
455 (2013) 'Steroid Hormone Signaling Is Essential to Regulate Innate Immune Cells and Fight Bacterial
456 Infection in *Drosophila*', *PLoS Pathogens*. Edited by D. S. Schneider, 9(10), p. e1003720. doi:
457 10.1371/journal.ppat.1003720.

458 Rehman, N. and Varghese, J. (2021) 'Larval nutrition influences adult fat stores and starvation resistance
459 in *Drosophila*', *PLOS ONE*. Edited by K.-J. Min, 16(2), p. e0247175. doi: 10.1371/journal.pone.0247175.

460 Riggs, C. L., Kedersha, N., Ivanov, P. and Anderson, P. (2020) 'Mammalian stress granules and P bodies at
461 a glance', *Journal of Cell Science*, 133(16). doi: 10.1242/jcs.242487.

462 Rode, S., Ohm, H., Anhäuser, L., Wagner, M., Rosing, M., Deng, X., Sin, O., Leidel, S. A., Storkebaum, E.,
463 Rentmeister, A., Zhu, S. and Rumpf, S. (2018) 'Differential Requirement for Translation Initiation Factor
464 Pathways during Ecdysone-Dependent Neuronal Remodeling in *Drosophila*', *Cell Reports*, 24(9), p. 2287–
465 2299.e4. doi: 10.1016/j.celrep.2018.07.074.

466 Schmitz, G. and Müller, G. (1991) 'Structure and function of lamellar bodies, lipid-protein complexes
467 involved in storage and secretion of cellular lipids.', *Journal of Lipid Research*, 32(10), pp. 1539–1570.
468 doi: 10.1016/S0022-2275(20)41642-6.

469 Silva, H. M., Báfica, A., Rodrigues-Luiz, G. F., Chi, J., Santos, P. d'Emery A., Reis, B. S., Hoytema van
470 Konijnenburg, D. P., Crane, A., Arifa, R. D. N., Martin, P., Mendes, D. A. G. B., Mansur, D. S., Torres, V. J.,

471 Cadwell, K., Cohen, P., Mucida, D. and Lafaille, J. J. (2019) 'Vasculature-associated fat macrophages
472 readily adapt to inflammatory and metabolic challenges', *Journal of Experimental Medicine*, 216(4), pp.
473 786–806. doi: 10.1084/jem.20181049.

474 Stephenson, H. N., Streeck, R., Grüblinger, F., Goosmann, C. and Herzig, A. (2022) 'Hemocytes are
475 essential for *Drosophila melanogaster* post-embryonic development, independent of control of the
476 microbiota', *Development*, 149(18). doi: 10.1242/dev.200286.

477 Storelli, G., Nam, H.-J., Simcox, J., Villanueva, C. J. and Thummel, C. S. (2019) 'Drosophila HNF4 Directs a
478 Switch in Lipid Metabolism that Supports the Transition to Adulthood', *Developmental Cell*, 48(2), p.
479 200–214.e6. doi: 10.1016/j.devcel.2018.11.030.

480 Surmi, B. and Hasty, A. (2008) 'Macrophage infiltration into adipose tissue: initiation, propagation and
481 remodeling', *Future Lipidology*, 3(5), pp. 545–556. doi: 10.2217/17460875.3.5.545.

482 Tattikota, S. G., Cho, B., Liu, Y., Hu, Y., Barrera, V., Steinbaugh, M. J., Yoon, S.-H., Comjean, A., Li, F.,
483 Dervis, F., Hung, R.-J., Nam, J.-W., Ho Sui, S., Shim, J. and Perrimon, N. (2020) 'A single-cell survey of
484 *Drosophila* blood', *eLife*, 9. doi: 10.7554/eLife.54818.

485 Tsuyama, T., Hayashi, Y., Komai, H., Shimono, K. and Uemura, T. (2023) 'Dynamic de novo adipose tissue
486 development during metamorphosis in *Drosophila melanogaster*', *Development*. doi:
487 10.1242/dev.200815.

488 Tysell, B. and Butterworth, F. M. (1978) 'Different rate of protein granule formation in the larval fat body
489 of *Drosophila melanogaster*', *Journal of Insect Physiology*, 24(3), pp. 201–206. doi: 10.1016/0022-
490 1910(78)90035-5.

491 **Methods**

492 ***Drosophila melanogaster* strains and culture**

493 The flies were raised on a diet containing cornmeal (80 g/l), sucrose (50 g/l), yeast (40 g/l), agar (10 g/l),
494 and 10%-methylparaben (16.7 mL/l) and maintained in a humidity-controlled environment with a natural
495 12 h/12 h light/dark cycle at 25°C. The larvae were developed in vials with plenty of food and particular
496 care was taken not to have too many individuals in one vial to avoid possible adverse effects that could
497 be attributed to metabolic or other stress. Flies were categorized according to their morphological
498 features, and no obvious differences in developmental time or pupal mortality were observed unless

499 explicitly stated in the manuscript. The flies of the following genotypes were used in the crosses resulting
 500 in the genotypes analyzed.
 501

<i>apolpp^{RNAi}</i>	Bloomington Drosophila Stock Center	BDSC: 28946
CrqGal4>2xeGFP	Provided by Marc C. Dionne	
Lpp-GFP	Vienna Drosophila Resource Center	v318255
Lsp2Gal4	Bloomington Drosophila Stock Center	BDSC: 6357
TRiP ^{control}	Bloomington Drosophila Stock Center	BDSC: 35786
EcR ^{DN}	Bloomington Drosophila Stock Center	BDSC: 6872
BirA	Bloomington Drosophila Stock Center	BDSC: 93424
UAS-Grim	Provided by John Nambu	
UAS-Rpr; UAS-Hid	Provided by John Nambu	
Hml_e9-P2a Gal4	Provided by Alf Herzig	
Atg8a-mCherry	Provided by Gabor Juhasz	

502

503 **Phenotypic analyses**

504 Pupariation rate analyses – sixty larvae of a given genotype were placed in individual vials. Their
 505 developmental status was checked at regular daily intervals and the number of pupated individuals was
 506 counted. The experiments were carried out in an incubator with controlled light and dark regime and
 507 controlled temperature and humidity. These data were recorded by a data logger and checked regularly.

508 Egg laying analysis – twenty-five freshly emerged virgins of a given genotype were placed in a vial
 509 containing ten males of the control genotype. Each day, flies were transferred to a fresh vial and the
 510 number of eggs laid was counted for the subsequent three days.

511 Eclosion rate analysis – the eclosion rate was assessed by counting the number of flies that emerged from
512 75 larvae placed in a vial containing standard fly food. Experiments were conducted in a light and dark
513 controlled incubator with controlled temperature and humidity.

514 Counting of adipocytes

515 To determine the number of larval adipocytes on the fly abdomen, flies were anesthetized and adipocytes
516 were washed from the ruptured abdomen in a drop of PBS on a microscope slide. Analysis was performed
517 on an inverted microscope. Larval adipocytes were identified by characteristic morphological features in
518 the bright field.

519 Tissue dissections and isolations

520 Isolation of macrophages – macrophages were isolated from flies based on the expression of endogenous
521 GFP protein in these cells. *Crq>Gal4 UAS-eGFP* male flies were used for isolation of macrophages by using
522 fluorescence-activated cell sorting (FACS) The flies were anesthetized with CO₂, washed in PBS, and
523 homogenized in 600 mL of ice-cold PBS using a pestle. The homogenate was sieved through a nylon cell
524 strainer (40 μm). This strainer was then additionally washed with 200 μL of ice-cold PBS, which was added
525 to the homogenate subsequently. The samples were centrifuged (3 min, 4°C, 3,500 RPM) and the
526 supernatant was washed with ice-cold PBS after each centrifugation (three times). Before sorting, samples
527 were transferred to FACS polystyrene tubes using a disposable bacterial filter (50 μm, Sysmex) and
528 macrophages were sorted into 100 μL of PBS using an S3™ Cell Sorter (BioRad). Isolated cells were verified
529 by fluorescence microscopy and differential interference contrast for their morphology and viability.
530 Different numbers of isolated macrophages were used in different subsequent analyses. To this end,
531 different numbers of flies were used for their isolation, specifically 90 flies were used to isolate 20,000
532 macrophages for qPCR analysis; approximately 160 flies were used to isolate 50,000 macrophages for
533 metabolic analysis; approximately 300 flies were used to isolate 100,000 and 200,000 macrophages for
534 lipidomic and transcriptomic analyses.

535 Isolation of hemolymph – for hemolymph isolation, 25 flies for each sample were anesthetized on ice and
536 punctured in the abdomen and thorax. Flies were then transferred to Eppendorf tubes with a silica
537 membrane, covered with glass beads, and spun in a centrifuge (10 min, 4°C, 8,500 rpm). The hemolymph
538 was collected at the bottom of a collection tube containing 50 μl of ice-cold PBS to prevent hemolymph
539 clotting and melanization. The supernatant was transferred into a fresh Eppendorf tube to avoid possible
540 contaminants from circulating plasmatocytes.

541 Isolation of the fat body and ovaries – to isolate the larval fat body residues and ovaries from the
542 abdomen, subjects were dissected in ice-cold PBS. Individuals destined for dissection were attached with
543 tiny entomological pins to a Sylgard polymer-coated dish. The abdomen was opened with spring scissors
544 in five sections and the abdomen was spread and secured at the corners with additional pins. For
545 subsequent metabolic and confocal analyses, ovaries were carefully dissected with tweezers by pulling
546 them out of the body by the oviduct. The individual free-floating adipocytes were collected by pipette
547 with a wide bore 1ml pipette tip.

548

549 **Gene expression analysis**

550 The macrophages were isolated by using a cell sorter as described above. Macrophages were
551 subsequently transferred to TRIzol Reagent (Invitrogen) and homogenized using a DEPC-treated pestle.
552 RNA was extracted by TRIzol Reagent (Invitrogen) according to the manufacturer's protocol. Superscript
553 III Reverse Transcriptase (Invitrogen) primed by oligo(dT)20 primer was used for reverse transcription.
554 Relative expression rates for particular genes were quantified on a 384CFX 1000 Touch Real-Time Cycler
555 (BioRad) using the TP 2x SYBR Master Mix (Top-Bio) in three technical replicates according to the following
556 protocol: initial denaturation - 3 min at 95°C, amplification – 15 s at 94°C, 20 s at 56°C, 25 s at 72°C for 40
557 cycles. Melting curve analysis was performed at 65–85°C/step 0.5°C. The qPCR data were analyzed using
558 double delta Ct analysis, and the expression of *apolpp* was normalized to the expression of Ribosomal
559 protein 49 (Rp49, Ribosomal protein L32; FBgn0002626) in the corresponding sample. The relative values
560 (fold change) to control are shown in the graphs.

561 **Measurement of cholesterol and cholesteryl-ester in macrophages**

562 To measure metabolite concentration in macrophages, the samples were split for the isolation of
563 metabolites and proteins that were used for sample normalization if not stated otherwise. Samples were
564 homogenized in 200 µL of PBS and centrifuged (3 min, 4°C, 8,000 RPM) to discard insoluble debris. For the
565 analysis of metabolites in macrophages, the sample was obtained from 90 individuals. Samples for analysis
566 of lipids were processed by an adapted protocol originally developed by Bligh and Dyer for the isolation
567 of lipid fraction from biological samples. A Bicinchoninic Acid Assay (BCA) Kit (Sigma) was used for protein
568 quantification according to the supplier's protocol and the absorbance was measured at 595 nm.
569 Cholesterol and cholesteryl esters were measured on isolated lipid fraction by using the
570 Cholesterol/Cholesteryl Ester Quantitation Kit (Sigma) according to the supplier's protocol. Samples for
571 metabolite concentration were collected from four independent experiments.

572 **Preparation of paraffin sagittal sections and Mallory trichrome staining**

573 Paraffin sections were prepared for P1, P4, P8, and P15 pupal stages, for freshly emerged adult females
574 and fly one, two, and five days old. First flies were fixed in 4%PFA in PBS for two hours. For pupal stages,
575 the layers of the puparium were removed prior to the fixation. All the analyzed individuals were punctured
576 by a tungsten needle before fixation. After prefixation in PFA, specimens were postfixed in Bouin-Hollande
577 solution (constituting from picric acid (0,9%), formaldehyde (9%), acetic acid (5%), 10%HgCl₂ and distilled
578 water. Samples were fixed in BHS for 24 hours. Dehydrated samples were subsequently embedded in
579 paraffin, sectioned with a thickness of 10µm on rotation microtome Leica RM2165 and stained by Mallory
580 trichrome staining. Sagittal sections were analyzed by using an inverted fluorescent microscope Olympus
581 Axioplan BX63.

582 **HPF freezing and TEM**

583 For the transmission electron microscopy analysis, flies were fixed by the HPF-FS method. The fly
584 abdomens were frozen in the presence of 20% bovine serum albumin using a Leica EM PACT2 high-
585 pressure freezer. FS (FSLeica EM ASF2) was carried in 2% OsO₄ diluted in 100% acetone at – 90 °C for 96
586 h. Then specimens were warmed up at a rate of 5 °C h⁻¹, left at – 20°for 24 h, and at 4 °C for another 24
587 h. At room temperature, specimens were rinsed three times in 100% acetone and incubated in a graded
588 series of SPI-pon resin (SPI) solutions (25%, 50% 75%) diluted in acetone, for 1 h at each step. Tissues were
589 incubated in pure resin overnight, embedded in fresh resin, and polymerized at 60 °C for 48 h. Ultrathin
590 sections (70 nm) were cut using an ultramicrotome Leica UCT (Leica Microsystems), counterstained with
591 uranyl acetate for 30 min, and lead citrate for 20 min. Samples were examined by a JEOL TEM 1010
592 operated at 80kV. The TEM images were false-colored in Adobe Photoshop software.

593 **X-ray computed tomography**

594 For the uCT analysis, the flies were anesthetized using CO₂, dipped in 70% ethanol to remove the
595 hydrophobic layer, and submerged into the Bouin-Holland Sublimate for at least three days. Subsequently,
596 the samples were thoroughly washed in 1x PBS and transferred to the Lugol solution (Sigma, L6146-1L)
597 for at least four days for tissue contrast. The flies were then washed in mineral oil (Sigma, 330779-1L) and
598 scanned in a 10um pipette tip using the SkyScan 1272 (Bruker) at source voltage 40kV, source current
599 200uA, image pixel size 1,4 um, and rotation step 0.100 deg. The reconstruction was done in NRecon and
600 3D visualization was achieved in CTvox Micro-CT Volume Rendering Software (Bruker). The segmentation,
601 computation of the volume of ovaries, and computation of the relative percentage of ovary volume to the

602 volume of the fly's body were conducted in the Avizo software (Thermo Scientific) using the Volume
603 Fraction module.

604 **Staining of lipids**

605 Flies were dissected in ice-cold PBS and fixed with 4% PFA in PBS (Polysciences). After 20 min, the tissues
606 were washed and stained for neutral lipids by using NileRed or Bodipy. Lipid staining was accompanied by
607 the staining of nuclei and cytoskeleton, which allowed us to infer the morphology of the tissue and to
608 quantify adequately the amount of lipids in the cells. The tissues were then washed and mounted in an
609 Aqua Polymount (Polysciences). Tissues were imaged using an Olympus FluoView 3000 confocal
610 microscope (Olympus). The content of lipids in macrophages, ovaries, and larval adipose tissue was
611 analyzed using Fiji software. Samples were collected in four independent experiments and representative
612 images are shown.

613 **Lipidomic analysis**

614 Fat bodies from six flies and one hundred thousand isolated macrophages were obtained for each
615 analyzed group. Tissue lipid fraction was extracted by 500 μ l of cold chloroform: methanol solution (v/v;
616 2:1). The samples were then homogenized by a Tissue Lyser II (Qiagen, Prague, Czech Republic) at 50 Hz,
617 -18°C for 5 min and kept further in an ultrasonic bath (0°C , 5 min). Further, the mixture was centrifuged
618 at 10,000 RPM at 4°C for 10 min followed by the removal of the supernatant. The extraction step was
619 repeated under the same conditions. The lower layer of pooled supernatant was evaporated to dryness
620 under a gentle stream of Argon. The dry total lipid extract was re-dissolved in 50 μ l of chloroform:
621 methanol solution (v/v; 2:1) and directly measured using a standard method. Briefly, high-performance
622 liquid chromatography (Accela 600 pump, Accela AS autosampler) combined with mass spectrometry LTQ-
623 XL (all Thermo Fisher Scientific, San Jose, CA, USA) were used. The chromatographic conditions were as
624 follows: Injection volume 5 μ l; column
625 Gemini 3 μ M C18 HPLC column (150 \times 2 mm ID, Phenomenex, Torrance, CA, USA) at 35°C ; the mobile
626 phase (A) 5 mM ammonium acetate in methanol with ammonia (0.025%), (B) water and (C) isopropanol:
627 MeOH (8:2); gradient change of A:B:C as follows: 0 min: 92:8:0, 7 min: 97:3:0, 12 min: 100:0:0, 19 min:
628 93:0:7, 20-29 min: 90:0:10, 40-45 min: 40:0:60, 48 min: 100:0:0, and 50-65 min: 92:8:0 with flow rate 200
629 μ l/min. The mass spectrometry condition: positive (3kV) and negative ($-2,5\text{kV}$) ion detection mode;
630 capillary temperature 200°C . Eluted ions were detected with full scan mode from 200 to 1000 Da with the
631 collisionally induced MS2 fragmentation (NCE 35). Data were acquired and processed by means of
632 XCalibur 4.0 software (Thermo Fisher). The corrected areas under individual analytical peaks were

633 expressed in percentages assuming that the total area of all detected is 100%. Lipidomics data were
634 subsequently analyzed in the online platform LipidSuite (<https://suite.lipidr.org/>). Data were inputted by
635 the K-Nearest Neighbours method (KNN), and normalization was performed by the PQN algorithm.
636 Subsequently, data were explored by PCA and OPLS-DA methods. Differential analysis of lipidomic data
637 was done by univariate analysis and visualized in Volcano plots.

638 **Proteomic analysis**

639

640 The hemolymph samples were subjected to in-solution digestion before MS analysis. Proteins were
641 reduced with 10 mM 1,4-dithiothreitol (DTT) at 56 °C for 45 minutes and alkylated with 55 mM
642 iodoacetamide at room temperature in the dark for 20 minutes. The alkylation was quenched with 50 mM
643 DTT. Trypsin (Sigma Aldrich) was used for proteolytic fragmentation at a ratio 50:1 (protein: trypsin)
644 overnight at 37 °C. The digestion was terminated by the addition of formic acid to a final concentration of
645 2.5% and peptides were purified using Stage tip solid-phase C18 discs.

646 The obtained peptides were dissolved in 30 µl of 3 % acetonitrile/0.1 % formic acid. The peptide
647 analysis was carried out on an UltiMate 3000 RSLCnano system (Thermo Fisher Scientific, MA USA) on line
648 coupled to mass spectrometer timsTOF Pro (Bruker Daltonics, Bremen, Germany). The peptide solution of
649 2 µl was injected onto an Acclaim™ PepMap™ 100 C18 trapping column (300 µm i.d., 5 mm length, particle
650 size 5 µm, pore size 100 Å; Thermo Fisher Scientific) at a 2.5 µl/min flow rate of 2 % acetonitrile/0.1 %
651 formic acid for 2 min. The peptides were eluted from the trapping column onto an Acclaim™ PepMap™
652 100 C18 analytical column (75 µm i.d., 150 mm length, particle size 2 µm, pore size 100 Å; Thermo Fisher
653 Scientific) and separated by a 48 min long linear gradient of 5–35 % acetonitrile/0.1 % formic acid at a
654 constant flow rate of 0.3 µl/min. The column oven temperature was set at 35 °C. Data were acquired in
655 PASEF scan mode with positive polarity. Electrospray ionization was performed using a CaptiveSpray
656 (Bruker Daltonics) with capillary voltage at 1500 V, dry gas at 3 l/min and dry temperature at 180 °C. Ions
657 were accumulated for 100 ms and 10 PASEF MS/MS scans were acquired per topN acquisition cycle. An
658 ion mobility range (1/K0) was set at 0.6–1.6 Vs/cm². Mass spectra were collected over a m/z range of 100
659 to 1700. A polygon filtering was applied to exclude the low m/z of singly charged ions. The target intensity
660 was set at 20,000 to repeatedly select precursors for PASEF MS/MS repetitions. The precursors that
661 reached the target intensity were then excluded for 0.4 min. Collision energies were changed from 20 to
662 59 eV in 5 steps of equal width between 0.6 and 1.6 Vs/cm² of 1/K0 values.

663 Raw MS data were processed in MaxQuant software (version 1.6.14) with an integrated Andromeda
664 search engine. Database of *Drosophila melanogaster* available in Uniprot (08. 11. 2022) supplemented
665 with the contaminant database included in the MaxQuant software was used to identify proteins. The
666 default parameters for the TIMS-DDA search type and Bruker TIMS instrument were applied. Trypsin/P
667 was set as an enzyme allowing up to two missed cleavages in specific digestion mode; the
668 carbamidomethylation of cysteine was used as fixed modification; N-terminal protein acetylation and
669 methionine oxidation were applied as variable modifications; the minimum and maximum peptide length
670 was set to 8 and 25 amino acids, respectively. Precursor ion tolerance was set at 20 and 10 ppm in the first
671 and the main peptide search, respectively; the mass tolerance for MS/MS fragment ions was set at 40
672 ppm. Peptide Spectrum Match (PSM) and protein identifications were filtered using a target-decoy
673 approach at a false discovery rate (FDR) of 1%. Label-free quantification of proteins was done using the
674 algorithm integrated into MaxQuant.

675 Protein tables obtained from MaxQuant were analyzed using Perseus software (version 1.6.14.0). The
676 data were filtered to eliminate hits to the reverse database, contaminants and proteins were only
677 identified with modified peptides. Proteins identified by only one peptide along with a score lower than
678 40 were excluded from further analysis.

679

680 **Incorporation of ¹³C free fatty acids**

681 For assaying ¹³C-FFA distribution during post-metamorphic development, the larvae were reared on fly
682 food containing 50µL ¹³C Fatty Acid Mix (Cambridge Isotope Laboratories), 5mg/mL in chloroform per each
683 vial for 5 hours. Analysis of ¹³C content in the fat body and the rest of the body indicates that this approach
684 leads to approximately 80% of labeled carbons accumulating in the larval fat body. Freshly emerged
685 individuals have been transferred to unlabeled food and remnants of larval fat body, hemolymph, and
686 ovaries were analyzed for ¹³C content 48 hours after eclosion. Lipid fraction from the samples was isolated
687 through an adapted Bligh and Dyer procedure and free fatty acids were liberated from complexes by a
688 lipase from *Aspergillus niger*. Homogenized and filtered chloroform extracts (100 µL) were put in glass
689 inserts in 2 mL chromatographic vials and their ¹³C enrichment was analyzed compound-specific. 1 µL
690 was injected in a split/splitless injector of a gas chromatograph, GC (Trace 1310, Thermo, Bremen,
691 Germany), injector at 250 °C. The injection was splitless for 1.5 min, then split with flow 100 mL/min for
692 the next one min, and 5 mL/min (gas saver) for the rest of the analysis. Semipolar capillary column Zebron,
693 ZB-FFAP (Phenomenex, Torrance CA, USA, 30m x 0.25 mm x 0.25 µm film thickness) with a flow rate of 1.5

694 mL/min of helium was used as a carrier. The temperature program was: 50 °C during injection and for the
695 next two min, then 50 to 200 °C with a slope of 30 °C/min, 200 to 235 °C with a slope of 3 °C/min, and hold
696 at 235 °C for the rest 32 min (total run time ca 51 min). Eluting compounds were oxidized to CO₂ via IsoLink
697 II interphase (Thermo, Bremen, Germany) at 1000 °C and introduced to continuous-flow isotope ratio MS
698 (Delta V Advantage, Thermo, Bremen, Germany). Compounds were identified using retention times of
699 fatty acid standards. ¹³C sample abundance was expressed in At-% ¹³C and “¹³C excess” calculated as
700 follow:

701 $^{13}\text{C excess} = A^{13}\text{Cs} - A^{13}\text{Cn}$

702 Where A¹³Cs is the absolute ¹³C abundance of labeled samples and A¹³Cn absolute ¹³C abundance of
703 natural lipids.

704 **Transcriptomic analysis**

705 For transcriptomic analysis, macrophages isolated from wandering larvae, freshly emerged individuals,
706 and 10-day-old flies were used. The details of the isolation procedure may be found above. Two hundred
707 thousand macrophages were used for the isolation of RNA by TriZol (Ambion). Sequenation libraries were
708 prepared by using siTOOLS riboPOOL *D. melanogaster* RNA kit (EastPort) followed by subtraction of
709 ribosomal fraction by NEBNext Ultra II Directional RNA kit (Illumina). The quality of prepared RNA libraries
710 was assayed by Bioanalyzer and all samples reached an RIN score over the threshold of 7. Sequencing
711 analysis was performed by using the NovaSeq instrument (Illumina). Raw sequencing data were processed
712 by standard bioinformatics workflow for trimming barcodes and adapters. Trimmed reads were aligned
713 to reference *D. melanogaster* genome BDGP6.95 (Ensembl release). Trimming, mapping, and analysis of
714 quality were performed in CLC Genomic Workbench 21.0.5 software via standard workflow for RNA-seq
715 and Differential gene expression analysis. Subsequent search of transcriptomic data for enhanced and
716 silenced pathways and biological processes was done by using TCC, and iDep94 platforms combined with
717 String and FlyMine databases.

718 **Phagocytic activity**

719 Flies with induced tools for macrophage depletion were injected with 50 nl of pHrodo™ Red *S. aureus*
720 (Thermo Fischer Scientific) to assay their phagocytic capability. After 45 minutes the abdomens of
721 analyzed flies were dissected in PBS and then fixed for 20 min with 4% PFA. Aqua Polymount (Polysciences)
722 was used to mount the sample. Macrophages were imaged using an Olympus FluoView 3000 confocal
723 microscope and red dots depicting phagocytic events were counted manually per cell.

724

725 **Tissue-specific tracing of proteins (BirA)**

726 Circulating proteins were analyzed for their site of origin in freshly emerged flies and flies ten days after
727 emergence. For this purpose, flies carrying promiscuous biotin ligase either under macrophage-specific or
728 fat body-specific promotor have been generated (*CrqGal4>UAS Bir-A*; *FB-Gal4>UAS Bir-A*). These flies
729 were held over their development on diet with an enhanced content of biotin prepared according to
730 Droujinine et al. 2021, Nature Communications). Briefly, biotin diluted in ethanol has been added to the
731 standard drosophila diet before it completely cooling to a final concentration of 50 μ M. Hemolymph from
732 an analyzed individual was isolated as stated above. The hemolymph samples were spun by centrifugation
733 to avoid any cellular contaminants. The biotinylated protein fraction was subtracted by magnetic
734 separation by using streptavidin-coated magnetic particles (Sigma) according to the provider's
735 instructions. Along with subtraction, samples of hemolymph from control genotypes and samples
736 processed without magnetic isolation were processed and analyzed for the identification of naturally
737 highly biotinylated circulating proteins.

738 **Statistics**

739 Box plots, heat maps, and donut graphs were generated in GraphPad Prism9 software. 2way ANOVA was
740 used for multiple comparison testing, followed by Tukey's or Šídák's multiple comparisons tests. Ordinary
741 one-way ANOVA followed by Dunnett's multiple comparisons test was used to compare the results with
742 the corresponding control group. An unpaired t-test was used for pair reciprocal comparison of datasets.
743 Bar plots display mean and standard deviation. The statistical significance of the test is depicted in plots
744 by using the following GP code ($p < 0.05 = *$; $p < 0.001 = **$; $p < 0.0001 = ***$). Normality and homogeneity of
745 variations were tested by the Anderson-Darling test, D'Agostino Pearsons' test, and Shapiro-Wilk test.
746 Data showing significant deviances from normal distribution was normalized by Log2-transformation. For
747 complex differential analysis of omics data, we processed the data through an online platform for
748 transcriptomic data analysis (TCC - based on the following R-packages (*edgeR*, *DESeq*, *baySeq*, and
749 *NBPSeq*), iDep95 - based on the following R-packages (*limma*, *DESeq2*, *GSEA*, *PAGE*, *GACE*, *RactomePA*,
750 *Kallisto*, *Galaxy*) followed by subsequent analysis of assigned biological processes in Kegg pathways
751 (www.genome.jp/kegg/pathway) and Flymine databases (<https://www.flymine.org/flymine>). An online
752 platform for lipidomic data analysis (LipidSuite – based on the R-package *lipidr*) was employed for
753 differential comparison of obtained lipidomic datasets.

754

755 **List of primers used in this work**

756

apolpp Forward: TTGGAATCCTAGCTTCTGTGCT	CG11064	FBgn0087002
apolpp Reverse: AGTCATAGTAGTTGCCGGGTAT	CG11064	FBgn0087002
Rp49 Forward: AAGCTGTCGCACAAATGGCG	CG7939	FBgn0002626
Rp49 Reverse: GCACGTTGTGCACCAGGAAC	CG7939	FBgn0002626

757

758

759

760

761 Figure 1:

762 **The progress of fat body remodeling during metamorphosis and post-metamorphic maturation**

763 (A) Representative confocal images documenting the onset of fat body disintegration (WP), infiltration of
764 macrophages (*Crq>GFP*; green), and formation of RNA-protein granules (autofluorescence; cyan). Lipids
765 were stained by NileRed (magenta), DAPI marks nuclei (cyan). (B) Representative transmission electron
766 micrograph documenting the formation of RNA-protein granules around the adipocyte nucleus. (C)
767 Representative transmission electron micrograph showing RNA-protein granules in which
768 autophagocytosed mitochondria and ribosomes can be distinguished. (D) Representative transmission
769 electron micrograph documenting fusion of the RNA-protein granules, which contain a crystalline core. *In*
770 *B-D*, cyan pseudocoloring depicts RNA-protein granules, blue nuclei, magenta lipid droplets, green
771 macrophage, yellow mitochondria, red ribosomes. L3, late 3rd instar larvae; L3W, wandering 3rd instar
772 larvae; WP, white prepupa; P8, pupal stage 8; V0, freshly emerged fly; V24, 1 day old virgin; V48, two days
773 old virgin.

774

775 Figure 2:

776 **The changes in the fat body morphology and ultrastructure during metamorphosis**

777 (A) The diameter of RNA-protein granules in adipocytes in the course of metamorphosis. (B) Number of
778 RNA-protein granules per adipocyte in the course of metamorphosis. (C-D) Representative transmission
779 electron micrograph showing the deliberated endoplasmic reticulum and mitochondria in the cytosol of
780 the adipocyte (C) and in extracellular space (D). (E) Representative transmission electron micrograph
781 documenting disintegration of the RNA-protein granules at 24 hours post eclosion via budding (cyan

782 pseudocoloring) of the granules or dissolving (blue pseudocoloring). **(F-G)** Lipids (F) and RNA-protein
783 granules (G) leaking from the histolysing adipocytes. **(H)** Diameter of larval adipocytes in the course of
784 metamorphosis. **(I)** Number of larval adipocytes per abdomen of flies at respective time points after
785 emergence.

786 *Data in A, B, and H were quantified from histological sections of 5 flies stained by Mallory trichrome*
787 *staining and the results were compared by One-way ANOVA. The dots represent individual values with a*
788 *line/bar showing mean \pm SD. Asterisks mark statistically significant differences (* $p < 0.05$; ** $p < 0.01$;*
789 **** $p < 0.001$). In pseudocolored TEM images - lipid droplets in magenta, macrophages in green, ribosomes*
790 *in red, mitochondria in yellow, RNA-protein granules in cyan, and disintegrating RNA-protein granules in*
791 *blue. Wp, white prepupa; P8, pupal stage 8; P15, pupal stage 16; V0, freshly emerged fly; V24, 1 day old*
792 *virgin; V48, two days old virgin.*

793

794 Figure 3:

795 **Macrophages are indispensable for successful metamorphosis.** **(A)** Representative images of control
796 pupae (*Crq>GFP*; lower row) and pupae bearing the *Hml^{e9-P2A}-GAL4>UAS Grim* genetic construct (upper
797 row). Arrow marks missing anterior spiracles, arrowhead shows a lacking head eversion. **(B)**
798 Representative confocal images depicting the presence of non-phagocytosed debris of larval muscles
799 (visualized by phalloidin, magenta) dissected from pupae bearing the *Hml^{e9-P2A}-GAL4>UAS Grim* genetic
800 construct. Autofluorescence is shown in a cyan channel. **(C)** Reconstructed micro-computed tomography
801 images of control (*Crq>GFP*; left) pupae and pupae bearing the *Hml^{e9-P2A}-GAL4>UAS Grim* genetic construct
802 (right). The arrow shows debris of non-phagocytosed larval muscles. **(D)** Representative images of flies
803 bearing the *Hml^{e9-P2A}-GAL4>TubGal80^{TS}; UAS Grim* genetic construct (right), depicting their inability of
804 wing expansion compared to controls (left) at 24 hours post eclosion. **(E)** Representative confocal images
805 of ovaries dissected from flies bearing the *Hml^{e9-P2A}-GAL4>TubGal80^{TS}; UAS Grim* genetic construct (right),
806 depicting their delayed development compared to controls (left) at 8 hours post eclosion. *P1, pupal stage*
807 *P1; P3, pupal stage P3; P5, pupal stage P5, P9, pupal stage P9; V24, 1 day old virgin.*

808

809 Figure 4:

810 **Macrophages heavily infiltrate the larval fat body during metamorphosis.** **(A)** Representative confocal
811 image showing the crown-like structures formed by infiltrating macrophages (*Crq>GFP*). Lipids were
812 stained by NileRed (magenta). Lighter magenta spheres are the RNA-protein granules. **(B)** Representative
813 confocal image of dissected individual larval adipocyte with attached macrophages (*Crq>GFP*; green).
814 Lipids were stained by NileRed (magenta), DAPI marks nuclei (cyan). Autofluorescence of the RNA-protein
815 granules in cyan. From a Z-stack of 7 layers. **(C)** Representative confocal image of the dissected adipocytes
816 (*C7 mCD8>GFP*; green). The infiltrating macrophages were stained by anti-NimC1 (magenta); nuclei by
817 DAPI (cyan). From a Z-stack of 7 layers. **(D)** Representative transmission electron micrograph showing
818 efferocytosis of an adipocyte with damaged plasma membrane by a macrophage. Macrophage nucleus in
819 blue. **(E)** Representative transmission electron micrograph depicting the transport of dilated cisternae of
820 endoplasmic reticulum from the adipocyte to the macrophage (arrow). **(F)** Representative transmission
821 electron micrograph documenting the presence of the disintegrating RNA-protein granule in a

822 macrophage. (G) Representative transmission electron micrograph of the adipocyte with attached foamy
823 macrophages.

824 *In pseudocolored TEM images - macrophages in green, ribosomes in red, RNAi-protein granules in cyan,*
825 *multilamellar bodies in orange, lipid droplets in magenta, and nuclei in blue. V0, freshly emerged fly; V24,*
826 *1 day old virgin.*

827

828 Figure 5:

829 **Macrophages acquire the adipocyte-like metabolic profile during post-metamorphic development. (A)**

830 Fold change of relative content of total lipids in macrophages isolated from L3W and V0 as determined by
831 lipidomics analysis. *The data were obtained from 90 flies per replicate. Individual dots represent biological*
832 *replicates with a line/bar showing mean \pm SD. (B) Percentage of cytosol occupied by lipid droplets in*
833 *macrophages isolated at respective time points after emergence. Data were quantified from 10 flies per*
834 *replicate. The data were obtained from three independent experiments. The dots represent values of*
835 *individual macrophages with a line/bar showing mean \pm SD. (C) Representative confocal image of a*
836 *macrophage (*Crq*>*GFP*; green) showing accumulation of lipids (NileRed; magenta) in the cytosol. (D)*
837 *Proportional prevalence of lipid species in the fat body (FB) and macrophages (M ϕ) isolated from V0 as*
838 *determined by lipidomics analysis. (E) GAGE analysis of transcriptomics data documenting upregulated*
839 *(red) and downregulated (green) biological processes in macrophages isolated from V0 compared to L3W.*
840 *(F) Venn diagrams displaying a number of proteins secreted by the adipocytes from L3, macrophages*
841 *isolated from V0 (V0M ϕ), and adult flies (M ϕ) as determined by proteomics analysis of biotinylated*
842 *hemolymph fraction (by using tissue-specific overexpression of *BirA(G3)*).*

843 *In A and B, the results were compared by Student's t-test. Asterisks mark statistically significant differences*
844 *(** p <0.01; *** p <0.001). L3W, wandering 3rd instar larvae; V0, freshly emerged fly; V24, 1 day old virgin;*
845 *V48, two days old virgin.*

846

847 Figure 6:

848

849 **Macrophages express *apolpp* during the post-metamorphic development.**

850 (A) The expression of *apolpp* in macrophages isolated from individuals at respective developmental
851 stages (L3W, P8, P15, V0, V24, and V48hpe). Expression levels normalized against *rp49* are reported as
852 fold change relative to *apolpp* levels in L3W arbitrarily set to 1. Results compared by One-way ANOVA.
853 *Individual dots represent biological replicates with a line/bar showing mean \pm SD. (B) Representative*
854 *confocal images of the larval fat body and infiltrating macrophages stained by the macrophage-specific*
855 *anti-NimC1 antibody (magenta) dissected from flies bearing the *apolpp-GFP* construct. Nuclei were*
856 *stained by DAPI (cyan). The image on the right consists of a Z-stack of 8 layers. (C) Percentage of cytosol*
857 *occupied by lipid droplets in macrophages isolated from control flies (*Crq*>*GFP*) and flies with a*
858 *macrophage-specific *apolpp* knockdown (*Crq*>*GFP*; *apolpp*^{RNAi}) at V24. Data were quantified from 10 flies*
859 *per replicate. The data were obtained from three independent experiments. The dots represent values of*
860 *individual macrophages with a line/bar showing mean \pm SD. The results were compared by Student's t-*
861 *test. (D) Representative confocal images of macrophages isolated from control flies (*Crq*>*GFP*) and flies*
862 *with a macrophage-specific *apolpp* knockdown (*Crq*>*GFP*; *apolpp*^{RNAi}). The lipids were stained by NileRed*
863 *(magenta).*

864 *V0, freshly emerged fly.*

865

866 Figure 7:

867 **Macrophages express *apolpp* to ensure the maturation of ovaries.** (A) A sum of peak area of free fatty
868 acids measured in ovaries of control individuals (*Crq>GFP*) and flies with macrophage-specific knockdown
869 of *apolpp* (*Crq>GFP; apolpp^{RNAi}*) at 8hpe. (B) The amount of ¹³C-labeled free fatty acids (AT%) measured in
870 ovaries of control individuals (*Crq>GFP*) and flies with macrophage-specific knockdown of *apolpp*
871 (*Crq>GFP; apolpp^{RNAi}*) at 8hpe. (C) Representative confocal images of varioles (left) and ovaries (right)
872 dissected from control individuals (*Crq>GFP*) and flies with macrophage-specific knockdown of *apolpp*
873 (*Crq>GFP; apolpp^{RNAi}*) at 8hpe. Lipids were stained by BODIPY (green) actin was labeled by phalloidin
874 (magenta), and DAPI marks nuclei (cyan). (D) Number of egg chambers reaching the developmental stage
875 10 and older in control individuals (*Crq>GFP*) and flies with macrophage-specific knockdown of *apolpp*
876 (*Crq>GFP; apolpp^{RNAi}*) at 8hpe. (E) X-ray computed tomography images of control individuals (*Crq>GFP*)
877 and flies with macrophage-specific knockdown of *apolpp* (*Crq>GFP; apolpp^{RNAi}*) at 8hpe with highlighted
878 contour of ovaries (dashed line). (F) An average number of eggs laid by control females (*Crq>GFP*) and
879 flies with macrophage-specific knockdown of *apolpp* (*Crq>GFP; apolpp^{RNAi}*) in the first three days after
880 emergence. Individual dots display biological replicates (25 females per replicate). The data were
881 compared by One-way ANOVA. (G) An average number of pupae developed from the sum of eggs laid by
882 one female in the first three days after emergence by control females (*Crq>GFP*) and flies with
883 macrophage-specific knockdown of *apolpp* (*Crq>GFP; apolpp^{RNAi}*). Individual dots display biological
884 replicates (25 females per replicate). The data were compared by Student's *t*-test. (H) Representative
885 confocal images of ovaries dissected from control individuals (*Hml^{ie9-P2A}-GAL4*) and flies with macrophage-
886 specific knockdown of *apolpp* (*Hml^{ie9-P2A}-GAL4; apolpp^{RNAi}*) at 7 days post-eclosion. Lipids were stained by
887 BODIPY (green) actin was labeled by phalloidin (magenta), and DAPI marks nuclei (cyan). (I) Size of ovaries
888 dissected from control individuals (*Hml^{ie9-P2A}-GAL4*) and flies with macrophage-specific knockdown of
889 *apolpp* (*Hml^{ie9-P2A}-GAL4; apolpp^{RNAi}*) at 7 days post-eclosion.
890 In A, B, D, and I, data were compared by Student's *t*-test. Individual dots display biological replicates. hpe,
891 hours post-eclosion.

892

893 Figure 8:

894 **Schematic representation of the proposed role of macrophages during post-metamorphic maturation**
895 **in *Drosophila*.**

896

897 Figure S1:

898 (A) Representative confocal image of the fat body dissected from white prepupae (WP) bearing Atg8a-
899 mCherry reporter construct under the natural promoter of this gene, which marks the autophagic events
900 (magenta). Lipids were stained by BODIPY (green), DAPI marks nuclei (cyan). (B) Representative confocal
901 images depicting the abrogated formation of RNA-protein granules (autofluorescence, cyan) in adipocytes
902 of flies overexpressing the dominant negative form of ecdysone receptor specifically in these cells

903 (*Lsp2>Gal4; EcR^{DN}*) compared to controls (*Lsp2>Gal4; TRiP^{control}*). Lipids were stained by BODIPY (green).
904 (C) Representative transmission electron micrographs depicting the lack of RNA-protein granules
905 (pseudocolored in cyan) in adipocytes of flies overexpressing the dominant negative form of ecdysone
906 receptor specifically in these cells (*Lsp2>Gal4; EcR^{DN}*) compared to controls (*Lsp2>Gal4; TRiP^{control}*). The
907 right panel shows mitochondria (pseudocolored in yellow) and fragments of endoplasmic reticulum
908 (pseudocolored in red) sequestered into RNA-protein granules in the larval fat body of flies overexpressing
909 dominant negative form of ecdysone receptor specifically in adipocytes (*Lsp2>Gal4; EcR^{DN}*) and intact
910 mitochondria and endoplasmic reticulum in cytosol of controls (*Lsp2>Gal4; TRiP^{control}*). Lipid droplets in
911 magenta, nuclei in blue. (D) Percentage of eclosed individuals overexpressing dominant negative form of
912 ecdysone receptor specifically in adipocytes (*Lsp2>Gal4; EcR^{DN}*) compared to controls (*Lsp2>Gal4;*
913 *TRiP^{control}*). The data were obtained from three independent experiments, individual dots represent
914 biological replicates with line/bar showing mean \pm SD. Asterisks mark statistically significant differences (
915 *** $p < 0.001$). (E) Representative images of sagittal histological cross-sections of *Drosophila melanogaster*
916 in respective time-points during the metamorphosis and post-metamorphic development contrasted by
917 Mallory's trichrome staining. The arrows depict the distribution of the larval fat body.
918 *WP/P1, white prepupa; P4, pupal stage 4; P8, pupal stage 8; P15, pupal stage 15; V0, freshly emerged fly;*
919 *V24, 1 day old virgin; V48, two days old virgin; V150, five days old female.*

920

921 Figure S2:

922 (A) Representative transmission electron micrograph documenting the rare occurrence of RNA-protein
923 granules in adipocytes at V48. (B, C) Representative transmission electron micrographs documenting the
924 presence of RNA-protein granules of the adipocyte origin in macrophages. (D) Representative tomographs
925 depicting the size of ovaries and volume of the abdominal larval fat body in V0, V24, and V48.
926 *In A-C, RNA-protein granules are pseudocolored in cyan, lipid droplets in magenta, macrophages in green,*
927 *and nuclei in blue. V0, freshly emerged virgin; V24, 1 day old virgin; V48, two days old virgin.*

928

929 Figure S3:

930 (A, B) Representative pseudocoloured scanning electron microscopy images showing macrophages
931 (green) forming the crown-like structures around the histolysing adipocytes in V0. (C) Representative
932 transmission electron micrograph displaying the presence of multilamellar bodies in macrophages. (D)
933 Representative transmission electron micrograph showing that the macrophages resemble the adipocytes
934 in their ultrastructure in V48. (E) Representative transmission electron micrograph documenting the
935 disrupted plasma membrane of adipocytes and the presence of huge amounts of lipids in the macrophage
936 cytosol, which gives them a foam cell appearance in V48. (F) The amount of cholesterol and cholesteryl-
937 ester in macrophages during the course of metamorphosis. Data was compared by One-way ANOVA. The
938 individual dots represent biological replicates, and asterisks mark statistically significant differences
939 (* $p < 0.05$; *** $p < 0.001$). 90 flies were used per replicate.

940 *In C-E, macrophages are pseudocolored in green, lipid droplets in magenta, and multilamellar bodies in*
941 *orange. L3W, wandering 3rd instar larvae; P8, pupal stage 8; P15, pupal stage 15; V0, freshly emerged fly;*
942 *V24, 1 day old virgin; V48, two days old virgin.*

943

944 Figure S4:

945 (A) Heat maps depicting the expression of genes involved in lipid and lipoprotein metabolism, production
946 of storage peptides, and sphingolipid metabolism in macrophages isolated from L3W and V0 as
947 determined by the transcriptomic analysis. Data are displayed as Log2 fold change in V0 compared to
948 L3W. (B) Expression of adipohemocyte, plasmatocyte, fat body, and secretory hemocyte markers in
949 macrophages isolated from L3W, V0, and 10 days old adult flies as determined by the transcriptomics
950 analysis.

951 *L3W, wandering 3rd instar larvae; V0, freshly emerged fly.*

952

953 Figure S5:

954 (A) Gene expression of *apolpp* in macrophages isolated from control flies (*Crq>GFP*) and flies with
955 macrophage-specific knockdown of *apolpp* (*Crq>GFP; apolpp^{RNAi}*) documenting the efficiency of the gene
956 knockdown. Expression levels normalized against *rp49* are reported as fold change relative to *apolpp*
957 levels in controls arbitrarily set to 1. The results were compared by Student's t-test. (B) A sum of peak
958 area of free fatty acids measured in whole flies, hemolymph, and ovaries of control individuals (*Crq>GFP*)
959 and flies with macrophage-specific knockdown of *apolpp* (*Crq>GFP; apolpp^{RNAi}*) at 8 hours post eclosion.
960 (C) The amount of ¹³C-labeled free fatty acids (atom percent - AT%) measured in whole flies, hemolymph,
961 and ovaries of control individuals (*Crq>GFP*) and flies with macrophage-specific knockdown of *apolpp*
962 (*Crq>GFP; apolpp^{RNAi}*) at 8 hours post-eclosion. (D) Position, size, and volume of ovaries in control
963 (*Crq>GFP*) females and females with macrophage-specific knockdown of *apolpp* (*Crq>GFP; apolpp^{RNAi}*) as
964 determined from the reconstructed X-ray computed tomography 3D model. (E) Representative confocal
965 microscopy images of ovaries dissected from control (*Hml^{ε9-P2A}-GAL4*) individuals and flies with
966 macrophage-specific knockdown of *apolpp* (*Hml^{ε9-P2A}-GAL4; apolpp^{RNAi}*) showing the absence of magenta
967 signal in their nuclei, which indicates no apoptosis (TUNEL staining; magenta). DAPI marks nuclei (cyan);
968 phalloidin visualizes membranes (green). (F) Representative confocal microscopy images of adult fat body
969 dissected from control individuals (*Crq>GFP*) and flies with macrophage-specific knockdown of *apolpp*
970 (*Crq>GFP; apolpp^{RNAi}*). Lipids stained by NileRed (magenta), nuclei by DAPI (cyan). (G) Percentage of
971 cytosol occupied by lipid droplets in the adult fat body dissected from 1 day old control individuals
972 (*Crq>GFP*) and flies with macrophage-specific knockdown of *apolpp* (*Crq>GFP; apolpp^{RNAi}*). The data were
973 obtained by analysis of confocal images depicted in F. (H) Number of larval adipocytes dissected from the
974 abdomen of control flies and flies with macrophage-specific knockdown of *apolpp* (*Hml^{ε9-P2A}-GAL4 >*
975 *TubGal80^{TS}; apolpp^{RNAi}*). *In A-C, G, and H, the results were compared by Student's t-test. The individual*
976 *dots represent biological replicates with a line/bar showing mean ± SD, asterisks mark statistically*
977 *significant differences (*p<0.05; **p<0.01; ***p<0.001).*

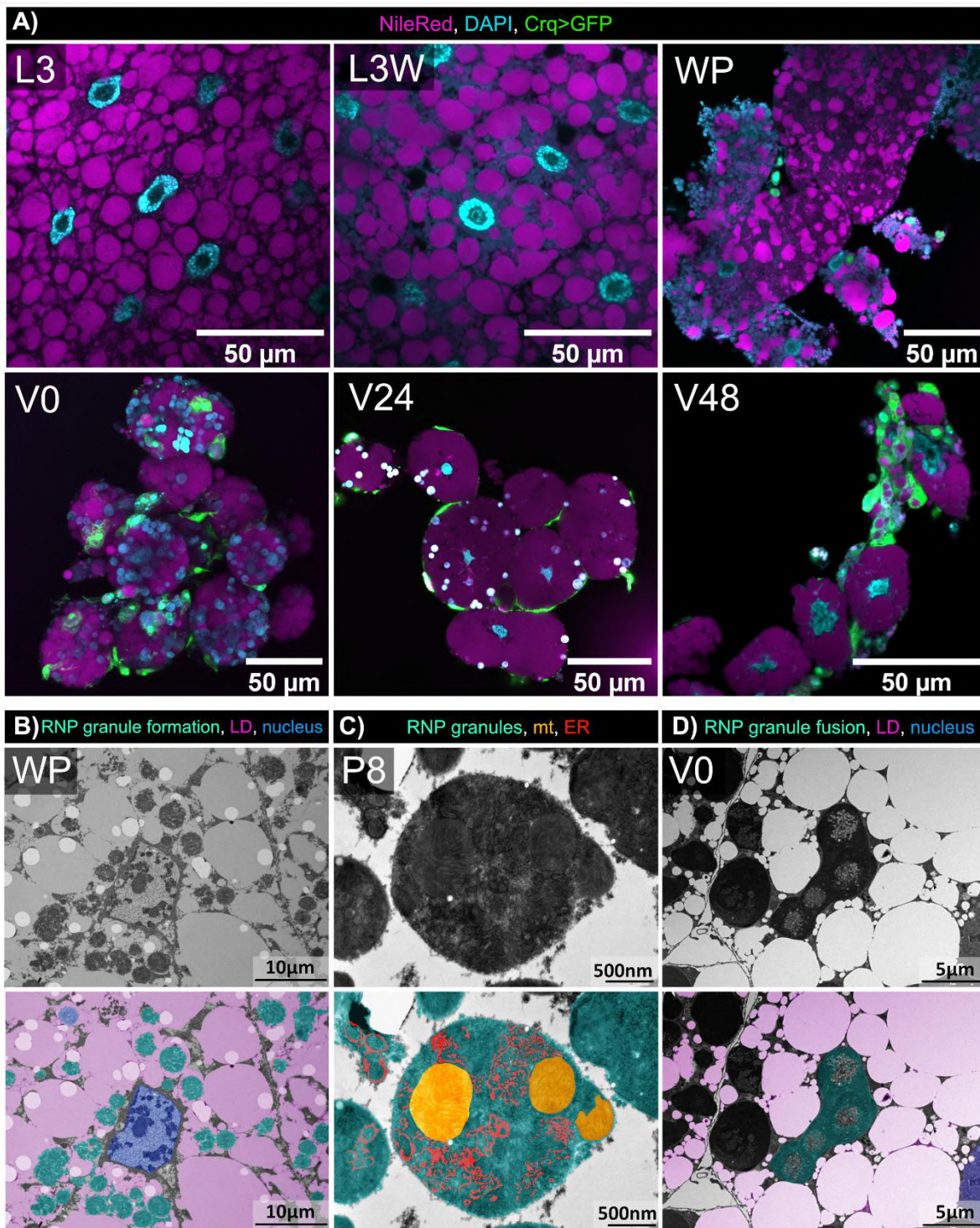
978

979

980

981

982

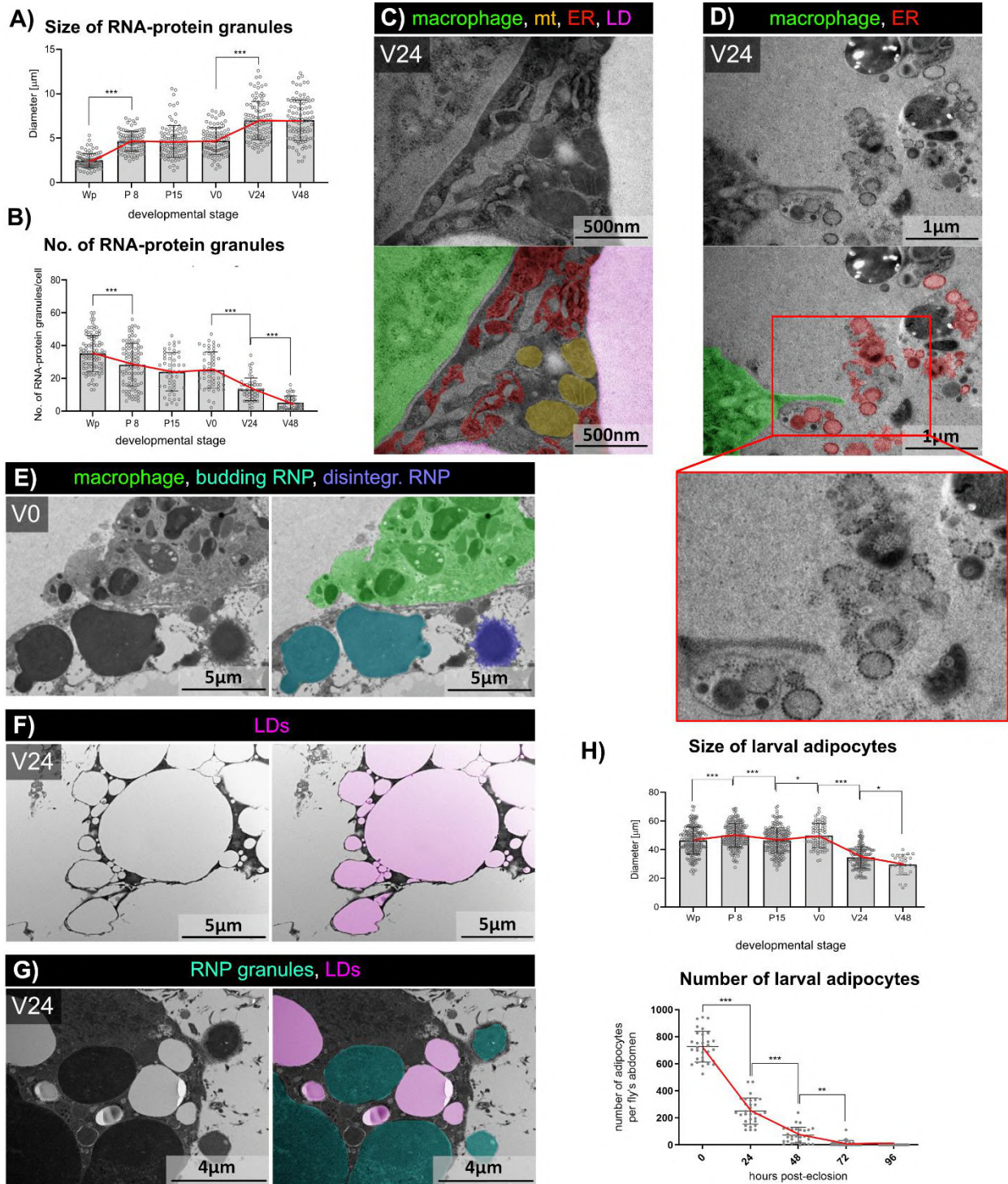


984

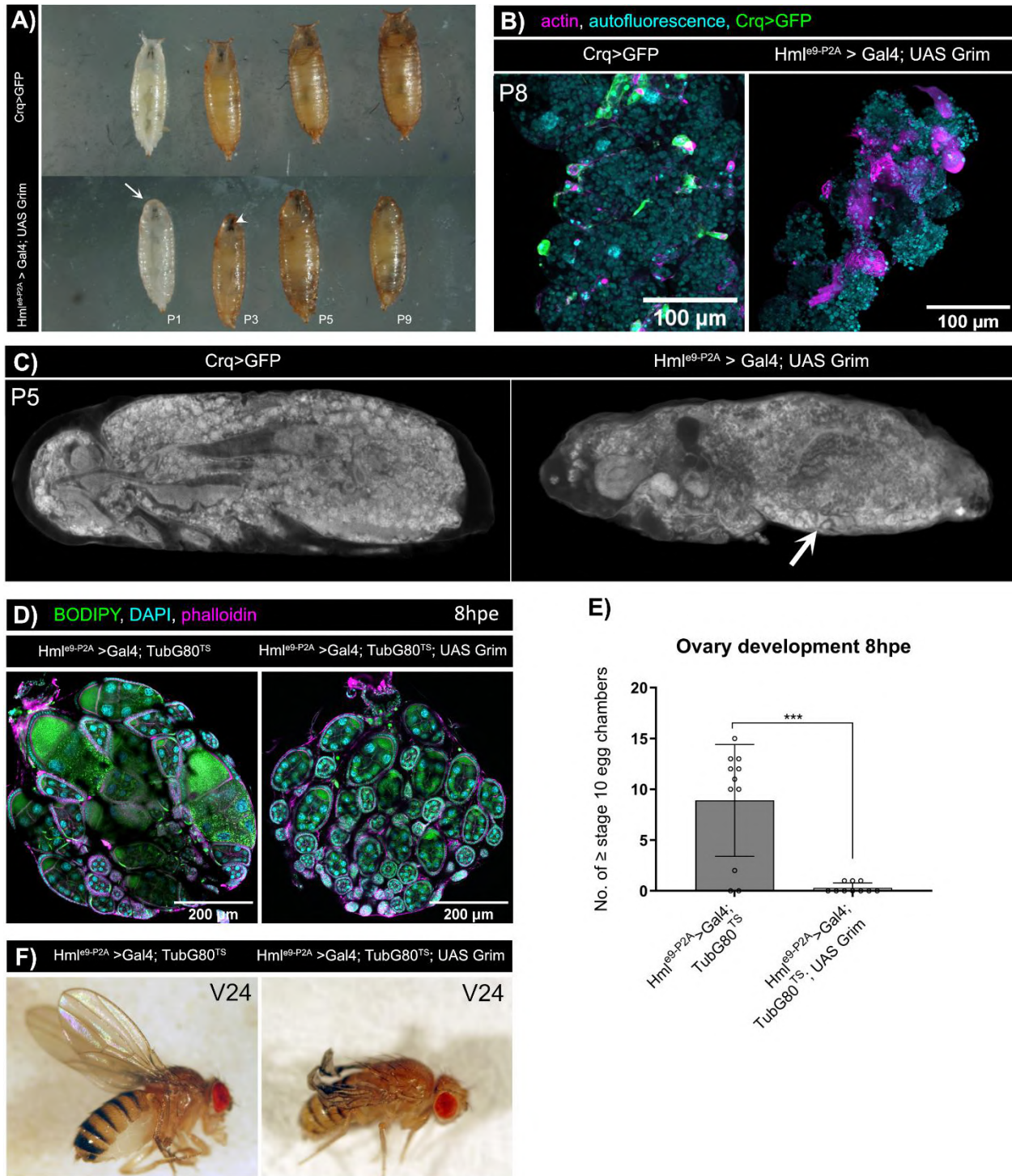
985

986

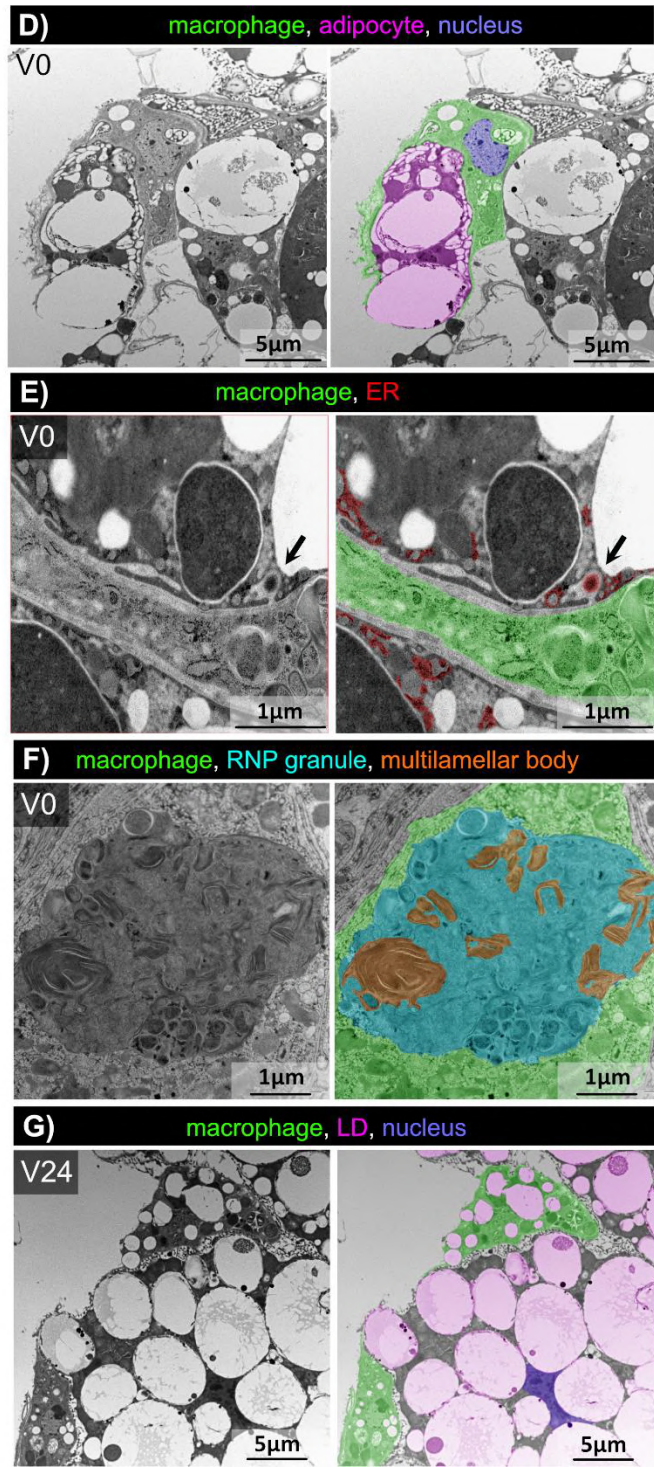
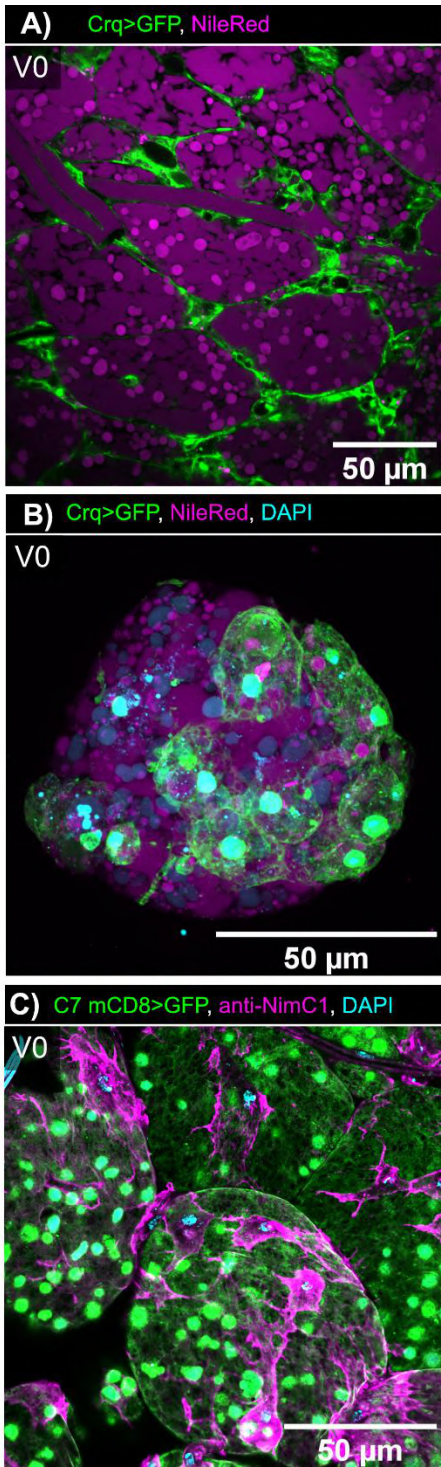
987



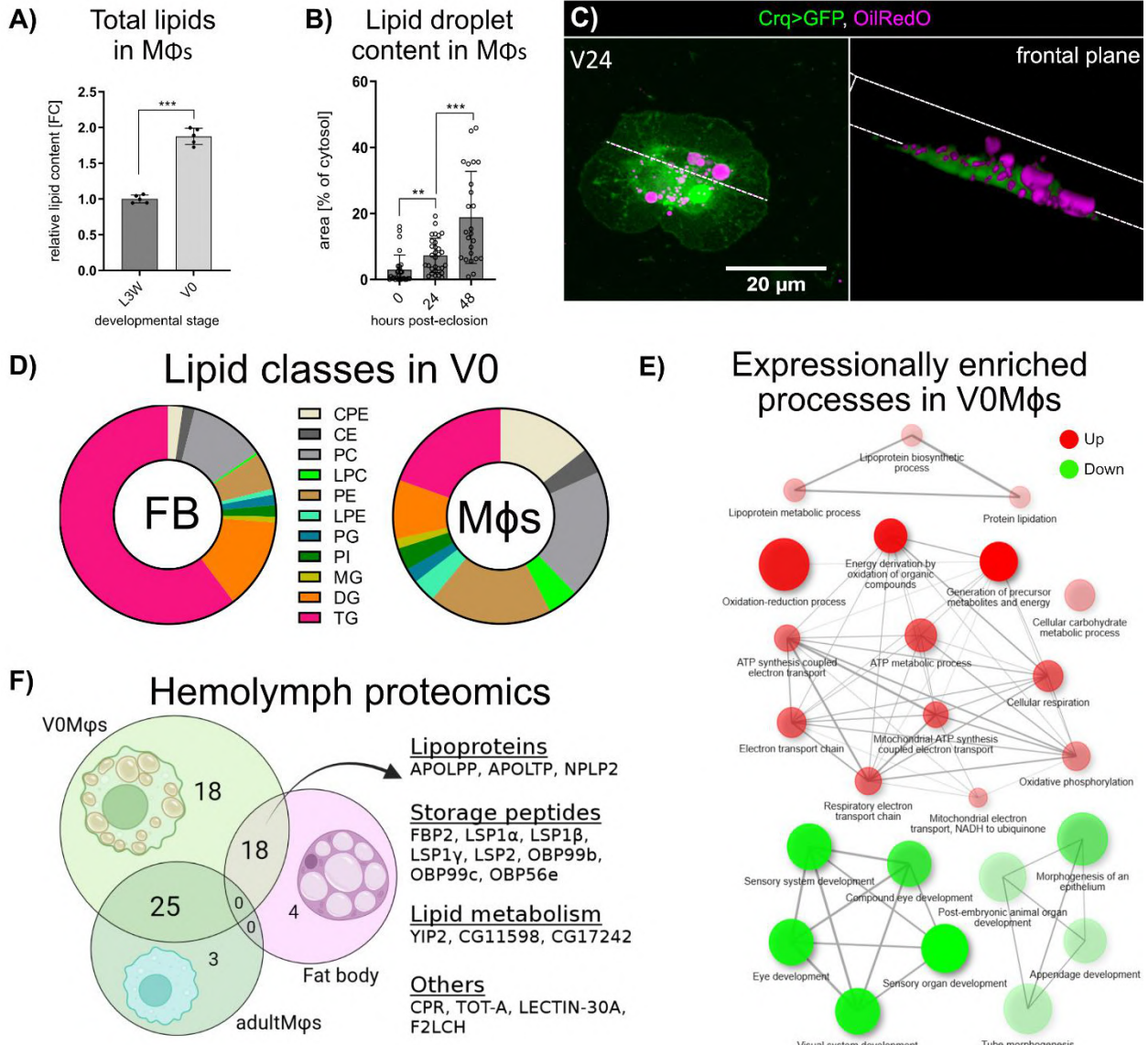
989
990
991
992



994
995
996
997

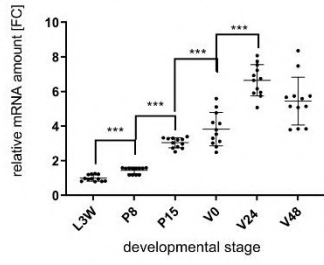


999
1000
1001
1002

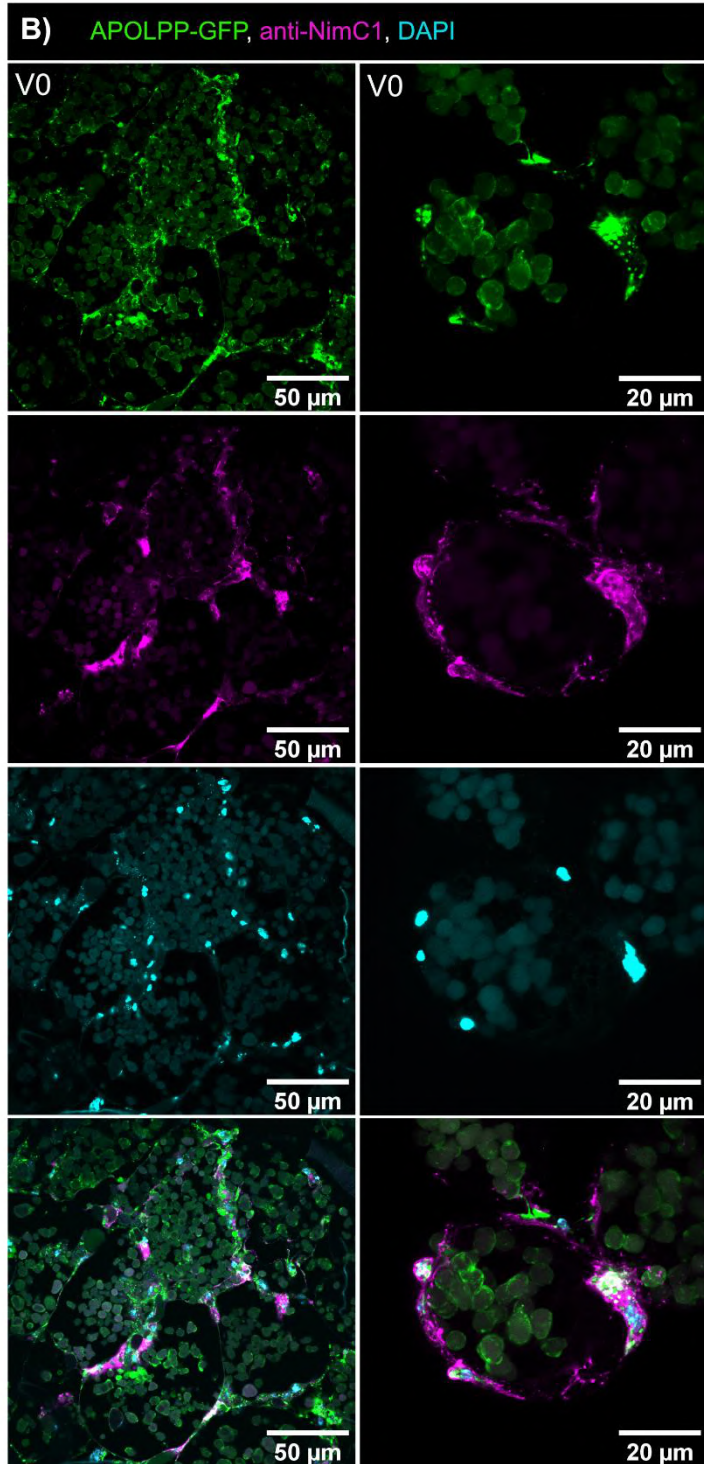
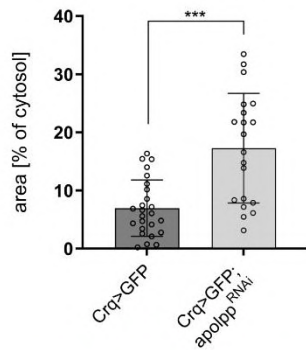


1004
1005
1006
1007
1008
1009
1010
1011
1012

A) Expression of *apolpp* in MΦs



C) Lipid content in V24MΦs

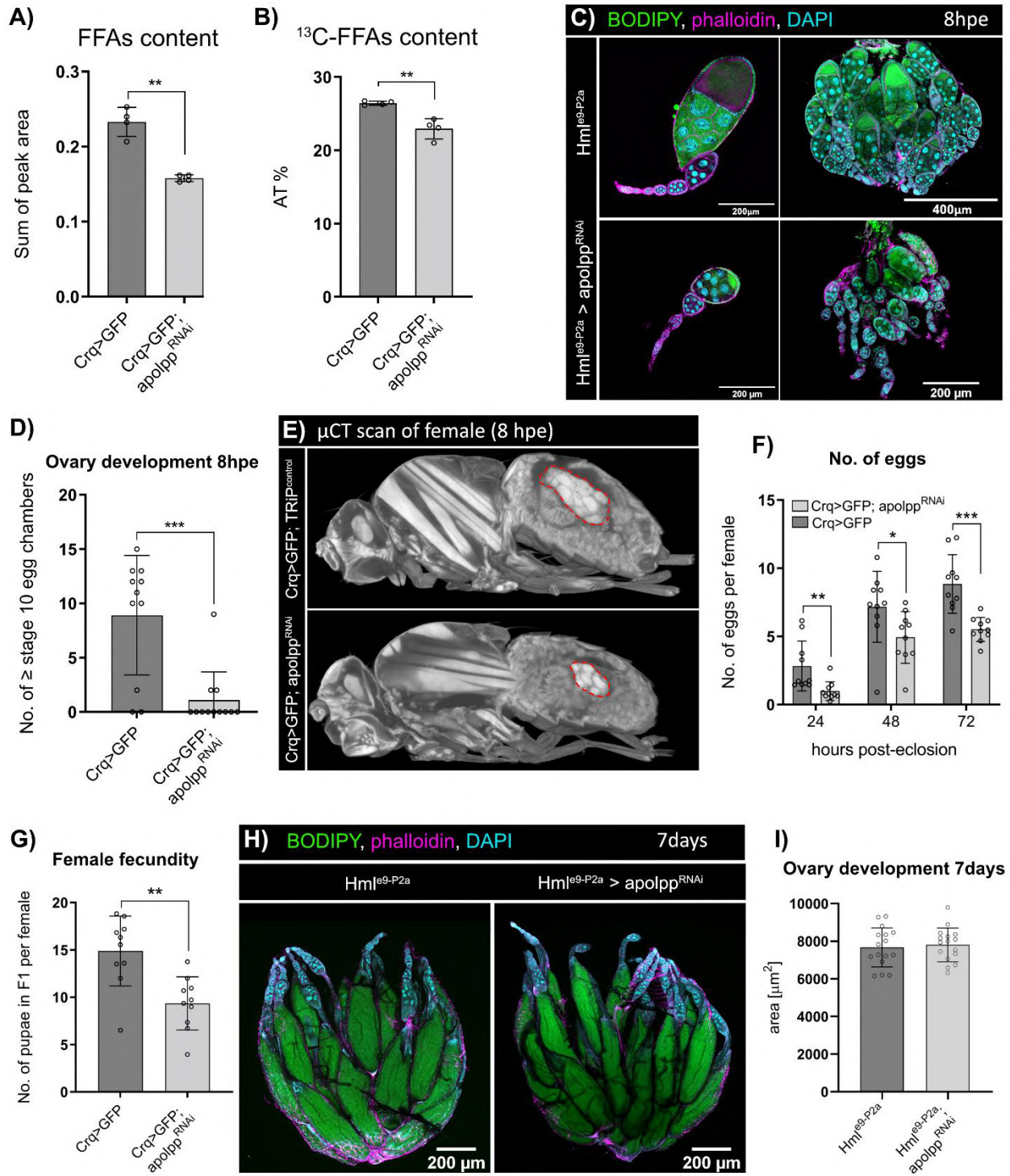


1014

1015

1016

1017



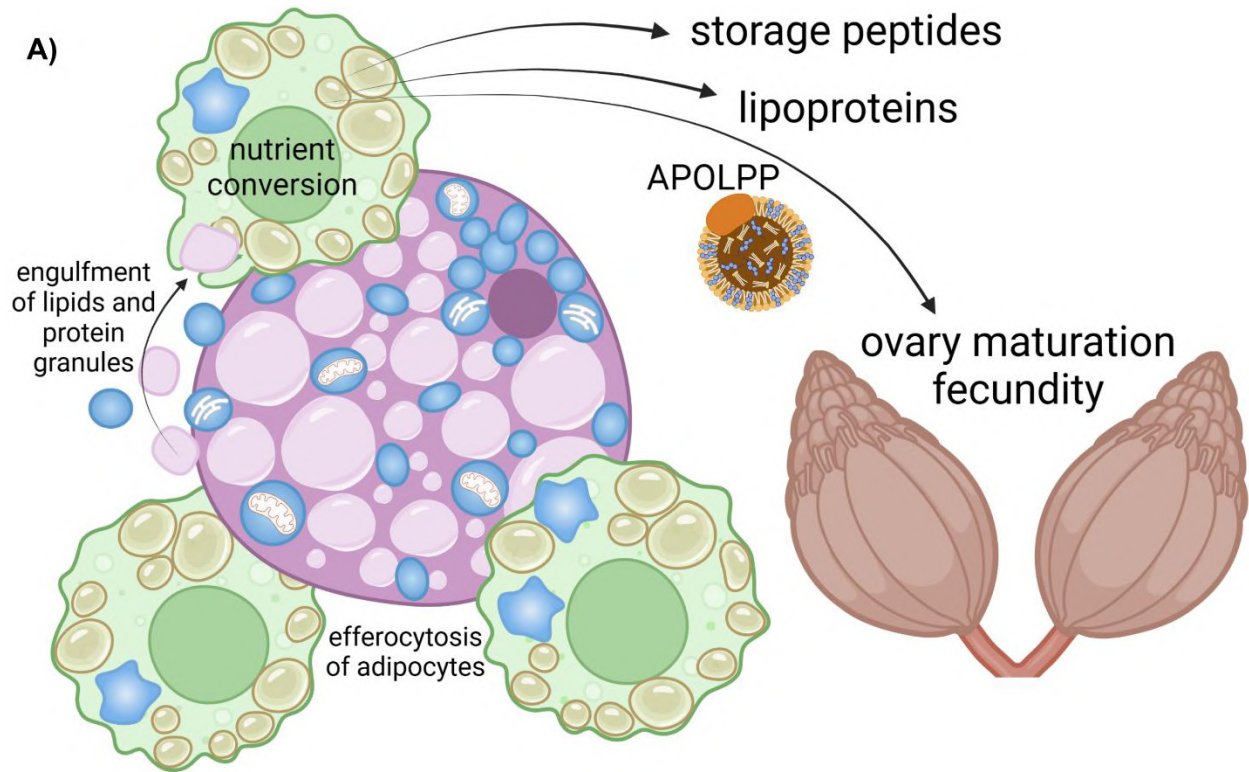
1019

1020

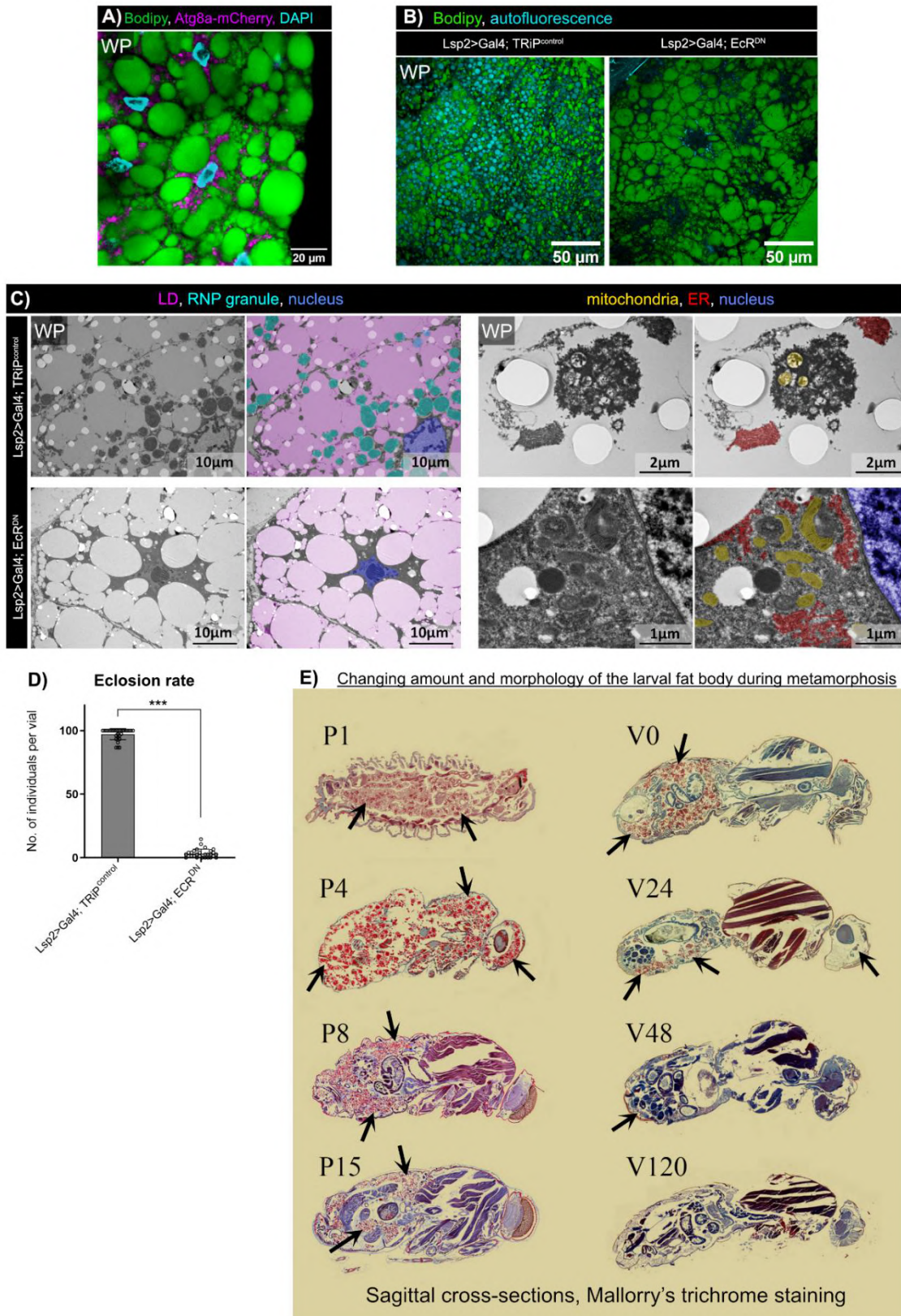
1021

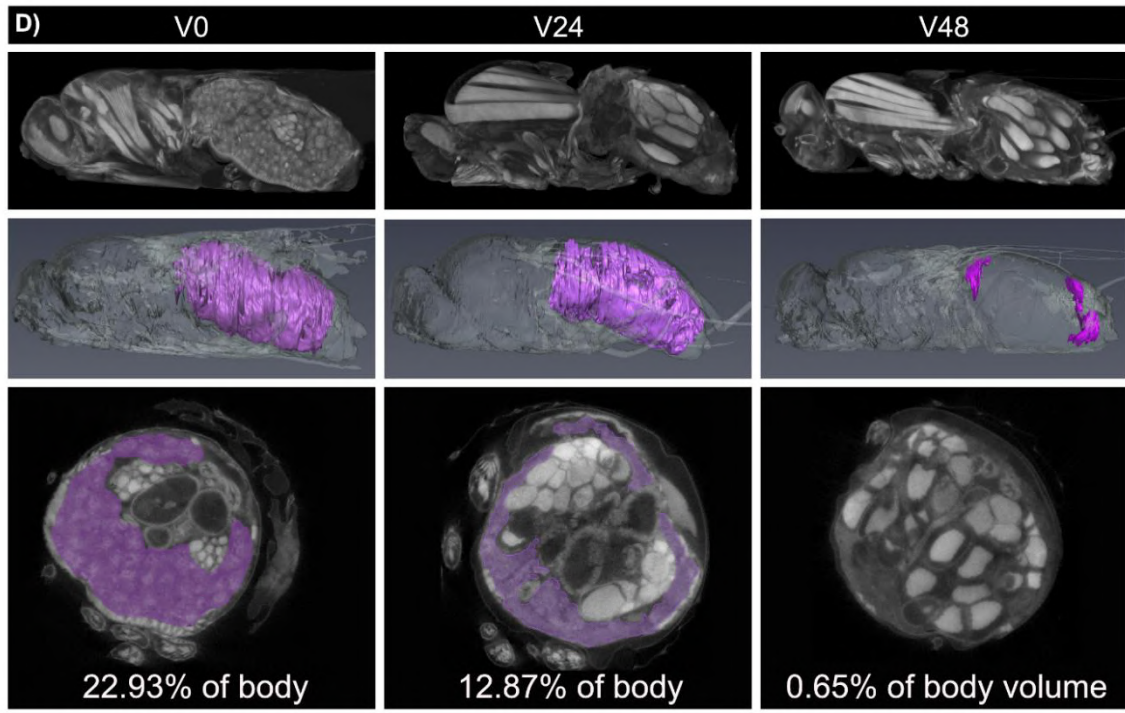
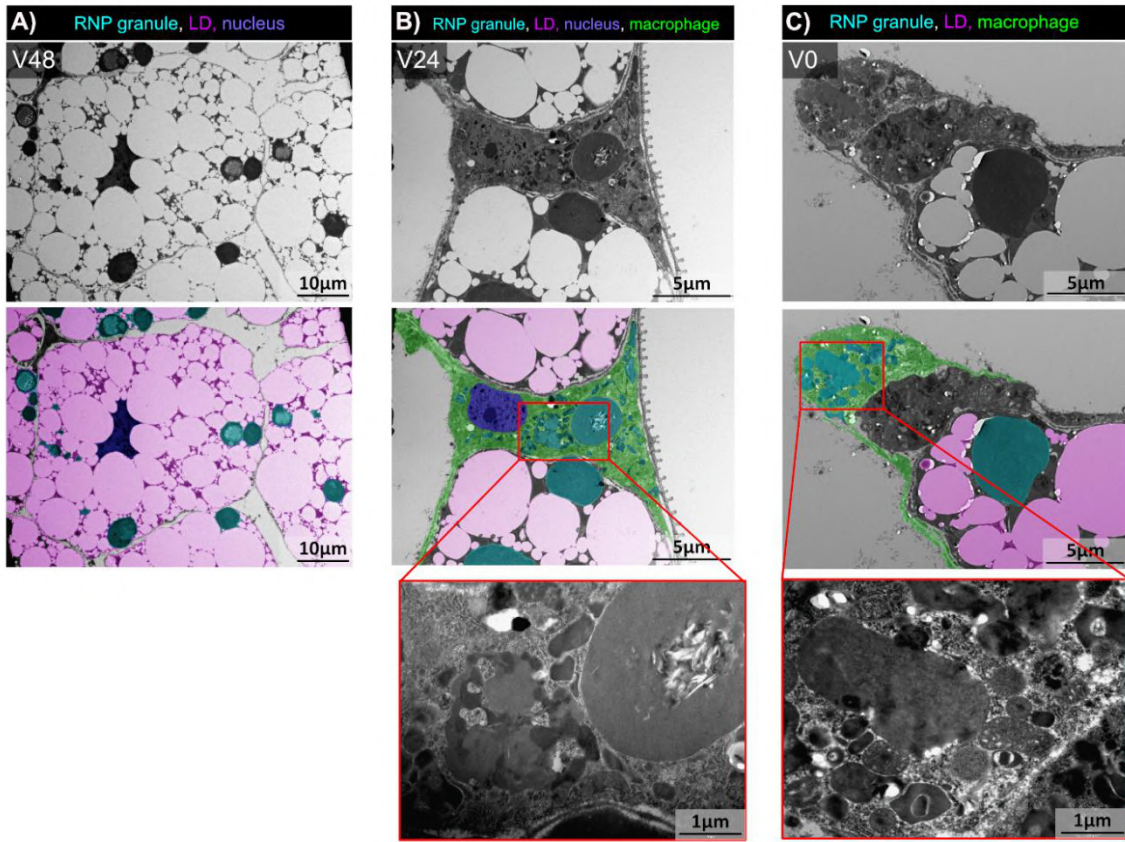
1022

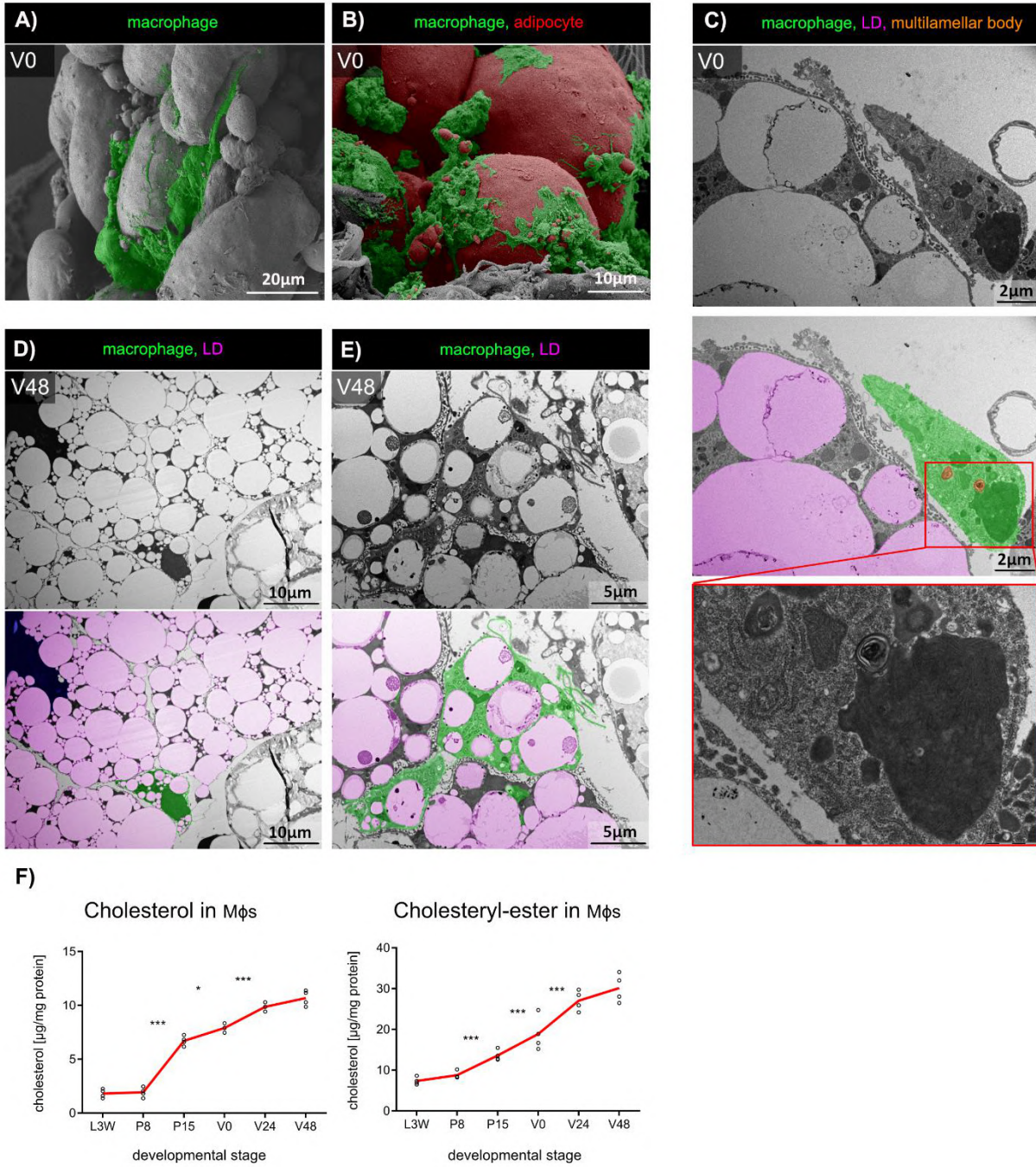
1023 Fig.8



1024
1025
1026
1027
1028
1029
1030
1031
1032
1033
1034
1035
1036
1037
1038







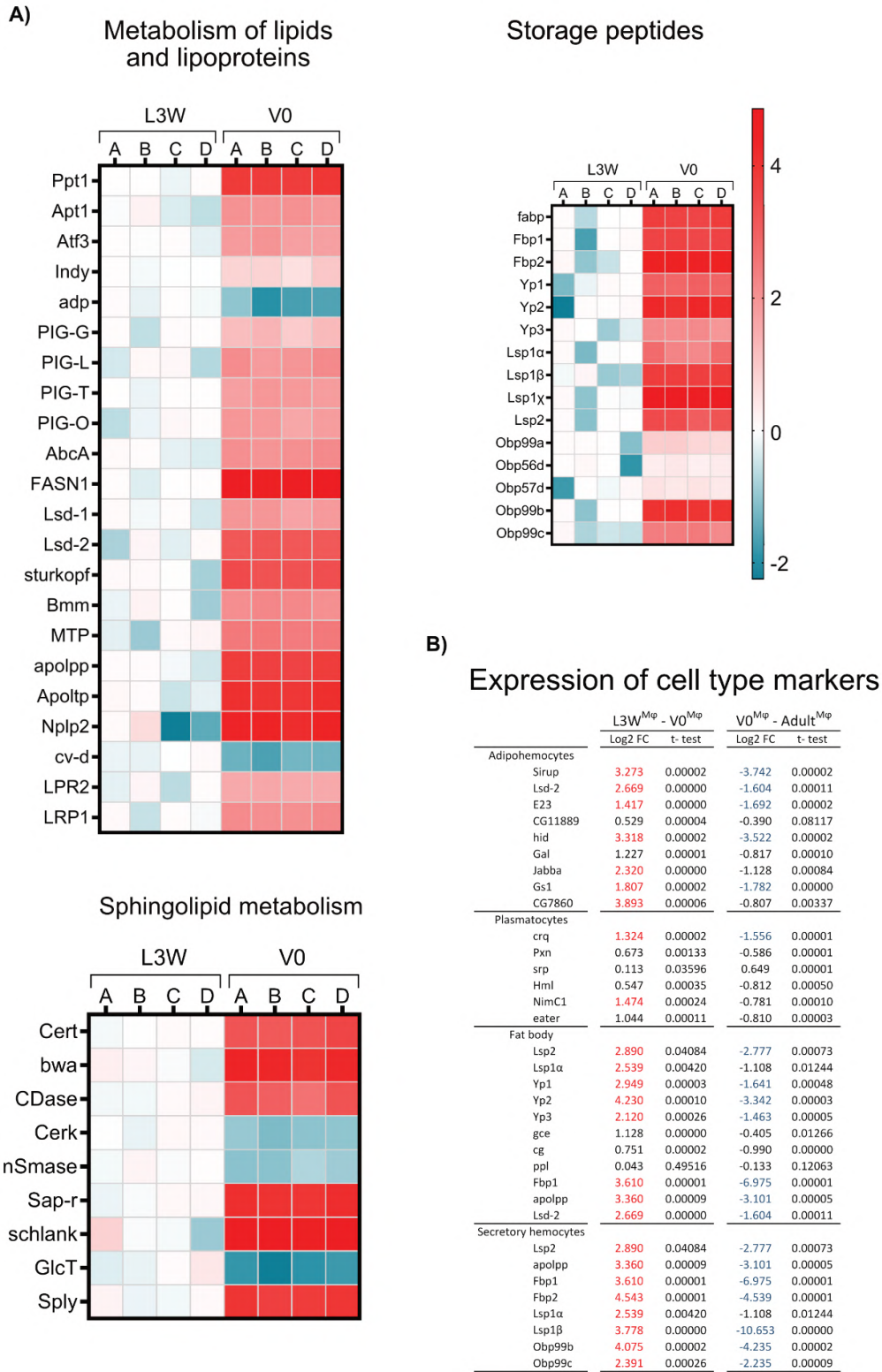
1044

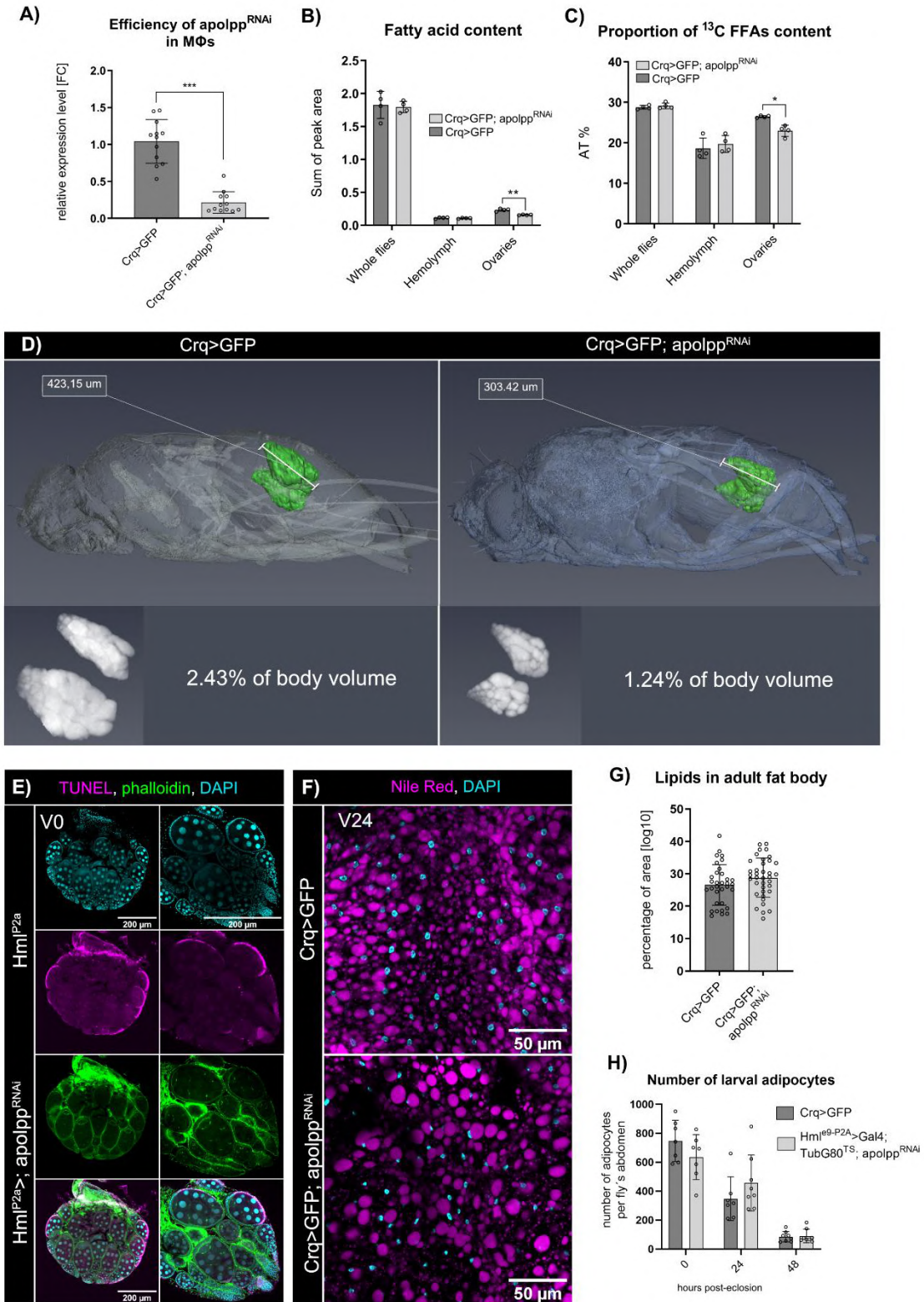
1045

1046

1047

1048





CHAPTER IX:

Macrophage-specific delivery of atorvastatin by yeast glucan particles intervenes bactericidal function in *Drosophila*

Gabriela Krejčová, Gabriela Ruphuy, Petra Šalamúnová, Erik Sonntag, František Štěpánek, Adam Bajgar

Under review in *Insect Molecular Biology*

1 Macrophage-specific delivery of atorvastatin by yeast glucan 2 particles intervenes bactericidal function in *Drosophila*

3 Gabriela Krejčová^{1,2}, Gabriela Ruphuy³, Petra Šalamúnová³, Erik Sonntag³, František Štěpánek³ and
4 Adam Bajgar^{1,2,4*}

5 1 University of South Bohemia, Faculty of Science, Dep. of Molecular Biology and Genetics, České Budějovice, Czech
6 Republic.

7 2 Biology Centre CAS, Institute of Entomology, České Budějovice, Czech Republic.

8 3 University of Chemistry and Technology Prague, Department of Chemical Engineering, Prague, Czech Republic.

9 4 Lead contact

10 * Correspondence: bajgaradam@seznam.cz, bajgaa00@prf.jcu.cz

11 12 **Abstract**

13 Adjustment of the metabolic program of macrophages is essential for fighting pathogens. However,
14 its dysregulation underlies the development of chronic inflammatory diseases. Regulation of
15 macrophage metabolism is therefore considered a suitable strategy for the treatment of these states.
16 Although many small-molecule inhibitors affecting macrophage metabolism have been identified *in*
17 *vitro*, their administration requires tools for macrophage-specific delivery to avoid potential side
18 effects. Here we used *Drosophila melanogaster* as a simple *in vivo* experimental model for testing of
19 such delivery tools. We found that yeast-derived glucan particles (GPs) are suitable for macrophage-
20 specific delivery of the inhibitor of mevalonate pathway, atorvastatin. Systemic administration of GPs
21 loaded with atorvastatin inhibits the enzymatic activity of Hydroxy-methyl-glutaryl-CoA reductase
22 (HMGCR), a rate-limiting enzyme in the mevalonate pathway specifically in macrophages without
23 compromising other tissues. Moreover, we show that decreased HMGCR activity prevents
24 macrophage pro-inflammatory polarization leading to compromised bactericidal activity and
25 decreased individual's survival of infection.

37 Introduction

38 Macrophages are functionally versatile cells governing many physiological processes in the body,
39 ranging from the protection against pathogenic invaders to the maintenance of tissue and metabolic
40 homeostasis^{1,2}. Adoption of particular polarization phenotype is determined by macrophage cellular
41 metabolism that can be finely tuned to generate the right amount of energy and precursors required
42 for desired task. Functional plasticity of macrophages is, therefore, fundamental for individual's health
43^{3,4}. While temporary pro-inflammatory polarization of macrophages is necessary to combat invading
44 bacterial pathogens^{5,6}, chronic production of macrophage pro-inflammatory factors leads to the
45 progressive development of metabolic, cardiovascular and neurodegenerative diseases^{7,8}. Regulation
46 of macrophage metabolism is thus considered as a suitable therapeutic approach for reverting
47 macrophage pro-inflammatory polarization and treat these frequently occurring syndromes⁹⁻¹¹.

48 Therefore, it is necessary to develop tools that allow experimental and clinical manipulation of
49 macrophage cellular metabolism without affecting the functionality of other tissues. As professional
50 phagocytes, macrophages tend to internalize foreign objects into their phagosome and clear them
51 from the circulation. Thus, offering an attractive bait loaded with metabolism-regulating drugs
52 represents an attractive approach for targeting macrophage cellular metabolism and function¹²⁻¹⁵.
53 Recently, three hundred FDA-approved drugs with the potential to induce or reverse macrophage pro-
54 inflammatory polarization have been identified in *in vitro* high throughput screens^{9,16}. However, many
55 of these promising compounds belongs to the family of small molecule metabolic inhibitors and their
56 systemic administration may be accompanied by adverse side effects due to their impact on non-
57 immune tissues¹⁷.

58 Therefore, there is a need for simple experimental model that allows for rapid and cheap *in vivo*
59 testing of various drugs and engineered delivery systems for effective macrophage-specific regulation
60 of cellular metabolism without affecting other organs and tissues.

61 Fruit fly, *Drosophila melanogaster*, represents a simple and frequently used organism for the
62 modelling of human diseases¹⁸. The possibility to perform cell type-specific genetic manipulations *in*
63 *vivo* allows for investigation of complex physiological processes with tissue-specific resolution^{19,20}.
64 Innate immune system shows striking level of analogy between *Drosophila* and mammals including
65 the main immune and metabolic pathways²¹. Indeed, professional phagocytes display a remarkable
66 level of homology in their function at the level of perception of danger signals, activation of
67 phagocytosis, and production of bactericidal compounds and destruction of pathogens in the
68 phagolysosome^{22,23,24}. Similar to their mammalian counterparts, *Drosophila* macrophages adjust their
69 metabolic setup along with their functional polarization²⁵. In particular, acute streptococcal infection
70 leads to the adoption of a pro-inflammatory macrophage polarization characterized by a metabolic
71 shift toward aerobic glycolysis driven by the transcription factor *Hypoxia inducible factor 1 alpha*
72 (*Hif1α*)²⁵. Therefore, *Drosophila* macrophages can be used for primary testing of macrophage-specific
73 administration of small metabolic inhibitors with potential anti-inflammatory effects *in vivo*. However,
74 it should be clearly stated that innate immune system of insects has also certain limitations such as a
75 lack of signalling towards the adaptive branch of immune system^{26,27}.

76 Fungal glucan cytoskeleton is recognized by various immune-related receptors in both mammals
77 and insects and administration of glucan-containing compounds in various forms has been found to
78 have immuno-stimulating effects under certain conditions^{28,29,30}. Glucan particles have thus long been
79 considered as a potential immuno-modulators, vaccine adjuvants, and even macrophage-specific
80 delivery tools. GPs loaded with various anti-inflammatory compounds, such as curcumin, resveratrol,

81 or rapamycin, were efficiently used previously for the treatment of chronic inflammatory states in
82 mice ^{31–34}. Moreover, the administration of GPs has been shown to be a suitable approach for
83 macrophage-specific delivery of short interfering RNAs *in vivo* resulting in macrophage-specific
84 knockdown of a target gene ^{35,36}. Thus, intravenous or periventricular administration of GPs loaded
85 with short interfering RNA induces macrophage-specific gene knockdown in mice without the need to
86 introduce complex genetic constructs ^{37,38}.

87 We have previously shown that the injection of yeast-derived glucan particles (GPs) into the
88 abdomen of adult *Drosophila* flies leads to their rapid distribution throughout the body and exclusive
89 internalization by macrophages ³⁹. GPs, produced by the removal of soluble organic compounds from
90 yeast cells except for the β -1,3-glucan polysaccharide shells, are recognized by an evolutionary
91 conserved receptor *Gram-negative bacteria binding protein 1* expressed predominantly by
92 professional phagocytes ⁴⁰. Administration of GPs is connected with negligible immunogenicity in flies
93 and does not compromise macrophage bactericidal function ³⁹. GPs can be loaded with various
94 compounds and easily modified with covalently bound fluorescent dyes, allowing their distribution
95 and quantification to be monitored ¹⁴.

96 Here, we show that systemic administration of yeast-derived GPs loaded with atorvastatin
97 attenuates the HMGCR enzymatic activity exclusively in *Drosophila* macrophages without
98 compromising other tissues. Reduced HMGCR function subsequently impairs bactericidal polarization
99 of macrophages, leading to increased pathogen burden and reduced survival of individuals during
100 infection. Moreover, our data document that the mevalonate pathway is fundamental for the function
101 of *Drosophila* macrophages during streptococcal infection. GPs may thus potentially serve as a suitable
102 tool for the delivery of metabolism-regulating drugs to control macrophage polarization *in vivo*.

103
104

105 Results

106 *Hmgcr* activity is increased in *Drosophila* macrophages upon infection

107 To elicit the pro-inflammatory polarization of macrophages, we employed a standardized *in vivo*
108 model of infection based on the injection of 20,000 streptococci into the abdomen of adult flies. This
109 treatment leads to a strong activation of the immune system within the first 24 hours, when
110 phagocytosis and bactericidal function of macrophages are crucial for limiting the bacterial burden ⁴¹.
111 During the acute phase of the infection, *Drosophila* macrophages undergo a substantial remodelling
112 of their cellular metabolism directed by the transcription factor HIF1 α ²⁵.

113 We found that in addition to the previously described metabolic shift towards aerobic glycolysis ²⁵,
114 the macrophages also display enhanced expression of genes involved in the mevalonate pathway and
115 subsequent synthesis of terpenoids (Figure 1A, Figure S1A, for the list of the most up- and down-
116 regulated genes see Supplementary Table S1). Transcriptomic analysis of the macrophages revealed
117 that the rate-limiting enzyme of the mevalonate pathway, *Hmgcr*, is abundantly expressed in
118 macrophages and its expression is strongly increased upon infection (Figure 1B, C). These
119 observations are in agreement with the results obtained from macrophage-specific RT-qPCR analysis,
120 which shows that *Hmgcr* expression increases early upon infection and reaches maximum expression
121 levels at 72 hours post-infection (Figure 1D). Macrophages represent the dominant cells expressing
122 *Hmgcr* in the body of infected *Drosophila*. While the fat body and muscles also show a relatively high
123 level of *Hmgcr* expression, its level does not increase after infection in these tissues (Figure 1E).

124 Investigating the link between macrophage activation and *Hmgcr* expression, we found that
125 macrophage-specific knockdown of *Hif1α* prevents the infection-induced increase in *Hmgcr*
126 expression in these cells, suggesting that HIF1α-driven metabolic remodelling also involves increased
127 activity of the mevalonate pathway (Figure 1F, see Figure S1B for RNAi efficiency). The expression data
128 are in congruence with the enzymatic activity of HMGCR, which is strongly enhanced in macrophages
129 isolated from infected flies (Figure 1G).

130 Collectively, these data document that infection-activated *Drosophila* macrophages increase the
131 expression and activity of HMGCR, the rate-limiting enzyme of the mevalonate pathway, presumably
132 to produce sufficient amounts of isoprenoids for their bactericidal function.

133 **Atorvastatin encapsulated in yeast glucan particles inhibits *Hmgcr* macrophage-specifically**

134 The enhanced activity of HMGCR in *Drosophila* infection-activated macrophages represent an ideal
135 opportunity to test the potential of GPs as a tool for macrophage-specific delivery of metabolic
136 inhibitors. For inhibition of HMGCR, we used atorvastatin (Ato) as the most commonly prescribed
137 statin with known inhibitory effect. To rule out potential cytotoxic effects of GPs and GPs loaded with
138 atorvastatin (Ato-GPs), we performed an *in vitro* cytotoxicity test using cell lines of murine
139 macrophages (Raw 264.7) and porcine liver primary cell cultures (PLP). No cytotoxic effects of either
140 plain GPs or Ato-GPs composites were observed (Supplementary Table S2 and S3). Prior to drug
141 encapsulation, the integrity, dispersibility, size and ultrastructure of freshly prepared glucan particles
142 were evaluated by electron microscopy (Figure 2A, B).

143 At 45 minutes after the intra-abdominal injection of GPs, they were found exclusively attached on
144 the surface or internalized by macrophages (Figure 2C, D). Further analysis of GPs distribution in the
145 fly's body revealed that they all are endocytosed by macrophages within the first 24 hours post-
146 infection (Figure 2E, F). Based on these observations, we established an experimental setup in which
147 Ato-GPs are administered 48 hours prior to infection, which makes a satisfactory time-frame for the
148 induction of the inhibitory effects of atorvastatin. The impact of the treatment was analysed 48 hours
149 post-infection since HMGCR reaches the maximum of its enzymatic activity at this time-point (Figure
150 3A).

151 To determine the minimum effective dose of atorvastatin on HMGCR enzymatic activity, we tested
152 the effect of glucan particles loaded with 1, 5, 10 and 15 wt.% of atorvastatin in isolated macrophages.
153 For the HMGCR enzymatic activity assays, we used two controls to verify that the reaction proceeded
154 as expected. The first control is based on the addition of 5μgP of recombinant HMGCR, thus
155 representing the kinetics of maximal HMGCR activity that can be achieved in the reaction
156 (+HMGCR^{control}). The kinetics of reaction with inhibited HMGCR enzymatic activity was represented by
157 control based on addition of excessive amount of pravastatin a potent HMGCR inhibitor to the slurry
158 of homogenized cells (Pravastatin^{control}). All tested doses of atorvastatin strongly reduce the HMGCR
159 enzymatic activity in macrophages to a level comparable to Pravastatin^{control}. Contrary to that,
160 macrophages isolated from infected flies, which were injected only by the injection buffer (Buff), or
161 empty GPs, display HMGCR enzymatic activity comparable to +HMGCR^{control}. Since the composite
162 carrying 5 wt.% of atorvastatin in GPs represents the lowest dose with the maximum inhibitory
163 activity, this concentration has been used for all subsequent experiments (Figure 3B). To confirm that
164 the observed effects may be accounted to the delivery of atorvastatin loaded in GPs (Ato-GPs), we
165 conducted an experiment determining the effects of all individual components of the injected
166 composites (empty glucan particles, GPs; unbound atorvastatin, Ato; and empty glucan particles co-
167 injected along with unbound atorvastatin, Ato x GPs) (Figure 3C). In parallel, we induced macrophage-

168 specific knockdown of *Hmgcr* ($M\phi_Hmgcr^{RNAi}$), by expression of dsRNA under the control of
169 macrophage-specific promoter (fly strain of genotype *Crq>Gal4, UAS-Hmgcr^{RNAi}*). This approach
170 effectively silences the expression of *Hmgcr* gene and was therefore used as a positive control in the
171 subsequent experiments (see [Figure S1C](#) for RNAi efficiency). Potential effect of all injected
172 composites on the expression of *Hmgcr* in macrophages has been excluded ([Figure S1D](#)).

173 While the administration of Ato-GPs inhibits the HMGCR activity in macrophages upon infection,
174 this effect cannot be induced by the administration of either GPs or Ato alone, nor by their co-injection
175 (Ato x GPs) ([Figure 3D](#)). That can be attributed by accumulation of Ato delivered encapsulated in GPs
176 in cytosol of macrophages, while comparable dose of atorvastatin administered systemically alone or
177 co-injected with empty GPs is taken up also by other tissues. This is consistent with our observation
178 that the inhibitory effect of Ato-GPs on HMGCR enzymatic activity is exclusive to macrophages without
179 affecting the HMGCR activity in non-phagocytic tissues, as documented here by the fat body and
180 muscles. Interestingly, the injection of Ato or Ato x GPs significantly decreases the HMGCR enzymatic
181 activity in the fat body, but not in muscles and macrophages ([Figure 3E, F](#)). This can be explained by
182 the high enzymatic activity of HMGCR in adipose tissue and its high ability to take up free Ato from
183 the circulation compared to other tissues in the body.

184

185 **Atorvastatin encapsulated in yeast glucan particles abrogates macrophage function**

186 Next, we investigated whether the inhibition of HMGCR affects the activation of macrophages and
187 individual's resistance to infection. Abdominal administration of Ato-GPs was found to impair the
188 ability of macrophages to adequately react to the presence of bacterial invaders in comparison to
189 control flies. This is documented by decreased expression of the characteristic readouts of activated
190 humoral immune response (antimicrobial peptides *DiptericinA*, *Drosocin*, *Metchnikowin*; and Jun-
191 kinase activity reporter *basket*) in macrophages and decreased expression level of markers of
192 macrophage metabolic polarization towards aerobic glycolysis (*Lactate dehydrogenase*, *Enolase*)
193 ([Figure 4A](#)). This is consistent with decreased bactericidal capability of macrophages manifested by
194 elevated bacterial burden and reduced individual's survival of infection ([Figure 4B, C](#)). Impaired
195 macrophage activation and decreased resistance to infection of flies treated by Ato-GPs can be
196 phenocopied by induction of macrophage-specific *Hmgcr* knockdown as discussed previously ([Figure](#)
197 [3C, D, E](#)). While the reduced ability of macrophages to fight bacterial infection after atorvastatin
198 administration might be regarded as a "negative" outcome, the suppression of proinflammatory
199 polarization can also be considered a "positive" outcome if the intended purpose is to modulate
200 macrophage activity, as might be the case, e.g., in chronic inflammatory or autoimmune diseases.

201

202

203 **Discussion**

204 The regulation of macrophage metabolism has been recognized as a possible strategy for the
205 treatment of chronic inflammatory diseases ^{5,6}. Although many potent small-molecule metabolic
206 inhibitors have been identified recently, their application requires tools for macrophage-specific
207 delivery ⁴².

208 In this study, we used acute streptococcal infection in *Drosophila* as a well-established *in vivo*
209 experimental system to test GPs as a macrophage-specific delivery tool of small-molecule metabolic

210 inhibitors with anti-inflammatory effects. GPs, based on beta-glucan shells of common bakers' yeast,
211 represent an attractive bait for macrophages and are rapidly internalized^{13,14}. The degradable
212 polysaccharide structure of GPs allows for the encapsulation of various compounds by spray-drying⁴³.
213 We used this technique to prepare composites carrying different concentrations of atorvastatin, a
214 commonly used inhibitor of HMGCR and mevalonate pathway.

215 We found that infection-activated *Drosophila* macrophages upregulate the activity of the
216 mevalonate pathway. The acceleration of the mevalonate pathway in pro-inflammatory macrophages
217 can be explained by the need for synthesis of molecules that allow macrophages to enhance their
218 motility and generate sufficient capacity for bacterial killing and inter-organ signalization⁴⁴⁻⁴⁷. Farnesyl
219 pyrophosphate produced in the mevalonate cascade serves as a substrate for the synthesis of
220 cholesterol, isoprenoids, and posttranslational modifications of proteins by prenylation^{48,49}. The
221 multiple products of the mevalonate pathway complicate the explanation of which molecules are
222 essential for macrophage function. Given that arthropods (including insects and our model organism
223 *Drosophila*) have lost the ability to synthesize cholesterol and are thus cholesterol auxotrophs⁵⁰, we
224 suggest that the mevalonate pathway in *Drosophila* macrophages is essential for the synthesis of the
225 terpenoid backbone used for the synthesis of steroid compounds⁵¹. Interestingly, the mevalonate
226 pathway is essential for the formation of innate immune memory in mammalian macrophages.
227 Although the mechanism of "trained immunity" has not yet been fully elucidated, it is thought to
228 involve epigenetic stabilization of macrophage metabolic settings that may be affected by a lack of
229 necessary substrates^{52,53}.

230 Glucan particles were used as a delivery tool for administration of several anti-inflammatory
231 compounds for experimental treatment of chronic inflammatory stated in mice^{30,32,31,33,54}. Here we
232 show that GPs represent a suitable tool for macrophage-specific delivery of small metabolic inhibitors
233 with potential to affect macrophage metabolic polarization. Macrophage-specific inhibition of HMGCR
234 enzymatic activity, either by Ato-GPs or genetic tools, prevents complete macrophage activation,
235 leading to their compromised ability to fight pathogenic bacteria and reduced resistance to infection.
236 Although administration of free atorvastatin reduces HMGCR enzymatic activity in the fat body,
237 loading the exact concentration of atorvastatin into GPs eliminates this side effect and limits its
238 inhibitory effects to be exclusively macrophage-specific.

239

240 **Experimental Procedures**

241

242 **EXPERIMENTAL MODEL**

243

244 *Drosophila melanogaster* strains and culture

245 The flies were raised on a diet containing cornmeal (80 g/l), sucrose (50 g/l), yeast (40 g/l), agar (10
246 g/l), and 10%-methylparaben (16.7 mL/l) and maintained in a humidity-controlled environment with
247 a natural 12 h/12 h light/dark cycle at 25°C. Prior to the experiments, flies were kept in plastic vials on
248 a sucrose-free cornmeal diet (cornmeal 53.5 g/l, yeast 28.2 g/l, agar 6.2 g/l and 10%-methylparaben
249 16.7 mL/l) for 7 days. Flies infected with *S. pneumoniae* were kept on a sucrose-free cornmeal diet in
250 incubators at 29°C due to the temperature sensitivity of *S. pneumoniae*. Infected individuals were
251 transferred to fresh vials every other day without the use of CO₂ to ensure good food condition. Flies

252 infected with *L. monocytogenes* were kept on a sucrose-free cornmeal diet at 25°C. Strains used for
 253 particular experiments are listed in Table 1.

254

255 Table 1. Genotypes of fly strains used in particular experiments

Figure	Abbreviated genotype	Full genotype description
Fig. 1F	CrqGFP>KK ^{control}	+/+; Crq-Gal4, UAS-2xeGFP/KKcontrol; +/+
Fig. 1F	CrqGFP>Hif1α ^{RNAi}	w1118/+; Crq-Gal4, UAS-2xeGFP/+; UAS-Hif1αRNAi/+
Fig. 3C,D,E	Hmgcr ^{RNAi}	w1118/+; UAS-HmgcrRNAi/Crq-Gal4, UAS-2xeGFP; +/+
Fig. S1B	CrqGFP>KK ^{control}	+/+; Crq-Gal4, UAS-2xeGFP/KKcontrol; +/+
Fig. S1B	CrqGFP>KK ^{control}	+/+; Crq-Gal4, UAS-2xeGFP/KKcontrol; +/+
Fig. S1C	CrqGFP>TRiP ^{control}	+/+; Crq-Gal4, UAS-2xeGFP/TRiPcontrol; +/+
Fig. S1C	CrqGFP>Hmgcr ^{RNAi}	w1118/+; UAS-HmgcrRNAi/Crq-Gal4, UAS-2xeGFP; +/+
General	CqrGFP	w1118/ w1118; Crq-Gal4, UAS-2xeGFP/Crq-Gal4, UAS-2xeGFP

256

257 Bacterial strain and fly injection

258 The *Streptococcus pneumoniae* strain EJ1 was stored at -80°C in Tryptic Soy Broth (TSB) media
 259 containing 10% glycerol. For the experiments, bacteria were streaked onto agar plates containing 3%
 260 TSB and 100 mg/mL streptomycin and subsequently incubated at 37°C in 5% CO₂ overnight. Single
 261 colonies were inoculated into 3 mL of TSB liquid media with 100 mg/mL of streptomycin and 100,000
 262 units of catalase and incubated at 37°C + 5% CO₂ overnight. Bacterial density was measured after an
 263 additional 4 h so that it reached an approximate 0.4 OD₆₀₀. Final bacterial cultures were centrifuged
 264 and dissolved in PBS so the final OD reached 2.4. The *S. pneumoniae* culture was kept on ice prior to
 265 injection and during the injection itself. Seven-day-old males were anaesthetized with CO₂ and
 266 injected with 50 nL culture containing 20,000 *S. pneumoniae* bacteria or 50 nL of mock buffer (PBS)
 267 into the ventrolateral side of the abdomen using an Eppendorf Femtojet microinjector.

268 Survival analysis

269 *Streptococcus*-injected flies were kept at 29°C in vials with approximately 30 individuals per vial and
 270 were transferred to fresh food every other day. Dead flies were counted daily. At least three
 271 independent experiments were performed and combined into a single survival curve generated in
 272 Graphpad Prism software; individual experiments showed comparable results. The average number
 273 of individuals was more than 500 for each genotype and replicate.

274 Pathogen load measurement

275 Single flies were homogenized in PBS using a motorized plastic pestle in 1.5 mL tubes. Bacteria were
 276 plated in spots onto TSB (*S. pneumoniae*) agar plates containing streptomycin in serial dilutions and
 277 incubated overnight at 37°C before manual counting. Pathogen loads of 16 flies were determined for
 278 each genotype and treatment in each experiment; at least three independent infection experiments
 279 were conducted and the results were combined into one graph (in all presented cases, individual
 280 experiments showed comparable results).

281

282 Isolation of macrophages

283 GFP-labeled macrophages were isolated from *Crq-Gal4, UAS-eGFP* male flies using fluorescence-
 284 activated cell sorting (FACS). Approximately 200 flies were anaesthetized with CO₂, washed in PBS and
 285 homogenized in 600 mL of PBS using a pestle. The homogenate was sieved through a nylon cell strainer

286 (40 µm). This strainer was then additionally washed with 200 µL of PBS, which was added to the
287 homogenate subsequently. The samples were centrifuged (3 min, 4°C, 3,500 RPM) and the
288 supernatant was washed with ice-cold PBS after each centrifugation (three times). Prior to sorting,
289 samples were transferred to FACS polystyrene tubes using a disposable bacterial filter (50 µm, Sysmex)
290 and macrophages were sorted into 100 µL of PBS using a S3™ Cell Sorter (BioRad). Isolated cells were
291 verified by fluorescence microscopy and differential interference contrast.

292

293 **METHOD DETAILS**

294

295 Scanning electron microscopy

296 For the scanning electron microscopy analysis, flies were injected with *S. pneumoniae* 24 hours before
297 their dissection and fixation. Thy fly abdomens were opened in PBS and fixed in 2,5% glutaraldehyde
298 in 0.1 M phosphate buffer (pH = 7.2) for one week at 4°C. Subsequently, the opened abdomens were
299 dehydrated through an acetone series and dried to critical point by point dryer CPD 2 (Pelco TM) and
300 attached to an aluminium target. For contrasting, the samples were coated with gold by using a
301 sputter coated E5100 (Polar Equipment Ltd.). Macrophages were examined with JEOL SEM JSM 7401F.
302 Electron images were false colorized in Adobe Photoshop software.

303 Transmission electron microscopy

304 For the transmission electron microscopy analysis, flies were infected with *S. pneumoniae* and injected
305 atorvastatin loaded glucan particles 24 hours prior their dissection. Dissected abdomens were fixed
306 by 2,5% glutaraldehyde in PBS. Specimens were rinsed three times in 100% acetone and infiltrated in
307 graded series of SP-1000 resin (SPI) solutions (25%, 50% 75%) diluted in acetone, 1 h at each step.
308 Tissues were immersed in pure resin overnight, embedded in fresh resin and polymerized at 60 °C for
309 48 h. Ultrathin sections (70 nm) were cut using an ultramicrotome Leica UCT (Leica Microsystems),
310 counterstained with uranyl acetate for 30 min and lead citrate for 20 min. Samples were examined by
311 a JEOL TEM 1010 operated at 80kV. The TEM images were false colorized in Adobe Photoshop
312 software.

313 Transcriptomics

314 For transcriptomic analysis, macrophages from flies infected by *S. pneumoniae* or injected with PBS
315 were isolated by cell sorter as described in the section “Isolation of macrophages”. Two hundred
316 thousand macrophages were used for isolation of RNA by TriZol (Ambion). Sequenation libraries were
317 prepared by using siTOOLS riboPOOL *D. melanogaster* RNA kit (EastPort) followed by subtraction of
318 ribosomal fraction by NEBNext Ultra II Directional RNA kit (Illumina). Quality of prepared RNA libraries
319 were assayed by Bioanalyzer and for all samples reached RIN score over the threshold of 7. Sequencing
320 analysis was performed by using NovaSeq instrument (Illumina). Raw sequencing data were processed
321 by standard bioinformatics workflow for trimming of barcodes and adapters. Trimmed reads were
322 aligned to reference *D. melanogaster* genome BDGP6.95 (Ensembl release). Trimming, mapping and
323 analysis of quality was performed in CLC Genomic Workbench 21.0.5 software via standard workflow
324 for RNA-seq and Differential gene expression analysis. Subsequent search of transcriptomic data for
325 enhanced and silenced pathways and biological processes was done by using TCC, iDep94 platforms
326 combined with String and FlyMine databases.

327 Gene expression analysis

328 Gene expression analyses were performed on several types of samples: six whole flies, six thoraxes,
 329 six fat bodies, or 20,000 isolated macrophages. Macrophages were isolated by a cell sorter (S3e Cell
 330 Sorter, BioRad) as described in the section Isolation of macrophages, while dissections were made in
 331 PBS, transferred to TRIzol Reagent (Invitrogen) and homogenized using a DEPC-treated pestle.
 332 Subsequently, RNA was extracted by TRIzol Reagent (Invitrogen) according to the manufacturer's
 333 protocol. Superscript III Reverse Transcriptase (Invitrogen) primed by oligo-dT primer was used for
 334 reverse transcription. Relative expression rates for particular genes were quantified on a 96CFX 1000
 335 Touch Real-Time Cycler (BioRad) using the TP 2x SYBR Master Mix (Top-Bio) in three technical
 336 replicates with the following protocol: initial denaturation - 3 min at 95°C, amplification – 15 s at 94°C,
 337 20 s at 56°C, 25 s at 72°C for 40 cycles. Melting curve analysis was performed at 65–85°C/step 0.5°C.
 338 Primers used for the quantification of particular genes are listed below (Table 2). The qPCR data were
 339 analyzed using double delta Ct analysis, and the expressions of specific genes were normalized to the
 340 expression of *Ribosomal protein 49 (Rp49)* in the corresponding sample. The relative values (fold
 341 change) to control are shown in the graphs. Samples for gene expression analysis were collected from
 342 three independent experiments.

343 Table 2. Table of primers used for quantitative expression analysis

Gene specific primers used in the study				
Sequence-based	Ldh forward: 5'CAGAGAAGTGGAAACGAGCTG3'	KRD	CG1016	FBgn0001
Sequence-based	Ldh reverse: 5'CATGTTCCGCCAAAACGGAG3'	KRD	CG1016	FBgn0001
Sequence-based	Pfk forward: 5'AGCTCACATTTCCAACATCG3'	KRD	CG4001	FBgn0003
Sequence-based	Pfk reverse: 5'TTTGATCACCAGAATCACTGC3'	KRD	CG4001	FBgn0003
Sequence-based	Pgi forward: 5'ACTGTCAATCTGTCTGTCCA3'	KRD	CG8251	FBgn0003
Sequence-based	Pgi reverse: 5'GATAACAGGAGCATTCTTCTCG3'	KRD	CG8251	FBgn0003
Sequence-based	Rp49 forward: 5'AAGCTGTCGCACAAATGGCG3'	KRD	CG7939	FBgn0002
Sequence-based	Rp49 reverse: 5'GCACGTTGTGCACCAGGAAC3'	KRD	CG7939	FBgn0002
Sequence-based	Hif1α forward: 5'CCAAAGGAGAAAAGAAGGAAC3'	KRD	CG4505	FBgn0266
Sequence-based	Hif1α reverse: 5'GAATCTTGAGGAAAGCGATG3'	KRD	CG4505	FBgn0266
Sequence-based	Bsk forward: 5'TACGGCCCATAGGATCAGGT3'	KRD	CG5680	FBgn0000
Sequence-based	Bsk reverse: 5'CCCTATATGCTCGCTTGCA3'	KRD	CG5680	FBgn0000
Sequence-based	Metch forward: 5'AACTTAATCTTGGAGCGA3'	KRD	CG8175	FBgn0014
Sequence-based	Metch reverse: 5'CGGTCTTGGTTGGTTAG3'	KRD	CG8175	FBgn0014
Sequence-based	DptA forward: 5'GCTGCGAATCGCTTCTACT3'	KRD	CG1276	FBgn0004
Sequence-based	DptA reverse: 5'TGGTGGAGTGGGCTTCATG3'	KRD	CG1276	FBgn0004
Sequence-based	Dro forward: 5'CCATCGTTTTCTGCT3'	KRD	CG1081	FBgn0010
Sequence-based	Dro reverse: 5'CCATCGTTTTCTGCT3'	KRD	CG1081	FBgn0010
Sequence-based	Hmgcr forward: 5'CCGCAATATGGTGACTGC3'	KRD	CG1036	FBgn0263
Sequence-based	Hmgcr reverse: 5'CGATTGTCCATGGAGAT3'	KRD	CG1036	FBgn0263

344

345 Preparation of glucan particles

346 Glucan particles were obtained from dry baker's yeast (Pakmaya, Ankara, Turkey). Isopropanol,
 347 hydrochloric acid and sodium hydroxide were purchased from Penta, Czech Republic. Fluorescein
 348 isothiocyanate (FITC) and acetonitrile were purchase from Merck Life Science s.r.o., Czech Republic.
 349 Acetone and ethanol were purchased from Lach-Ner, Czech Republic. Atorvastatin was kindly provided
 350 by Zentiva, k.s. Deionized water (conductivity 1.1 μS cm⁻¹) was produced by ionex device Aqual 25
 351 from Aqual (Czech Republic). Glucan particles were prepared based on the methodology described
 352 previously (Saloň et al. 2016). Briefly, dry yeast was suspended in NaOH 1M solution at a concentration

353 of 250 g/L and heated to 90 °C for 1 hour under continuous stirring. The suspension was then
354 separated by centrifugation and the supernatant was discarded. This alkaline extraction step was
355 repeated 2 more times. Afterwards, the slurry was resuspended in water and the pH of the suspension
356 was adjusted to 4.5 by addition of HCl solution. The acidic suspension was heated to 75 °C for 2 hours
357 under continuous stirring, after which the slurry was recuperated by centrifugation, washed with
358 deionized water (3 times), isopropanol (4 times) and acetone (2 times), and dried by lyophilization for
359 2 days.

360

361 Glucan particle labelling

362 Glucan particles for fluorescence microscopy visualisation were labelled with fluorescein
363 isothiocyanate (FITC) or rhodamine B isothiocyanate using slightly modified procedure (Hong et al.
364 2015). First, 500 mg of glucan particles and 5 mg of FITC or rhodamine (dissolved at 2.5 mg/mL in
365 acetonitrile) were added to 50 mL of sodium carbonate buffer (0.1 M, pH 9.2), and kept for 24 h in a
366 dark place. Afterwards, 10 mL of tris buffer (10 mL, 1M, pH 8.3) were added and the suspension was
367 incubated for 30 minutes. The labelled glucan particles were recovered by centrifugation and washed
368 with deionized water (5 times), ethanol (5 times), and acetone (3 times), and dried under vacuum.

369 Glucan particle loading with atorvastatin

370 Encapsulation of atorvastatin into GPs was done by spray drying (Ruphuy et al. 2020) at ATO/GP mass
371 ratios of 1, 5, 10 and 15 wt.%. First, solutions of atorvastatin in ethanol were prepared at
372 concentrations 0.2, 1.0, 2.0 and 3.0 mg/mL. Next, glucan particles were added to each solution to form
373 suspensions with a GP concentration of 20 mg/mL. Each suspension was spray dried using the Mini
374 Spray Dryer B-290 (Büchi, Switzerland) equipped with the ultrasonic package and operated in inert
375 loop under N₂ atmosphere. The operating conditions were: 120 °C inlet temperature, 5.0 mL/min feed
376 rate, 246 L/h (20%) N₂ flow rate and 2.4 W power outlet at the nozzle. This approach leads to
377 encapsulation of atorvastatin in the cavity inside the GPs.

378 For the determination of the drug loading content and efficiency, atorvastatin was extracted from the
379 ATO/GP composites by adding 10.0 mg of the microparticles to a 10.0 mL of methanol. The dispersions
380 were placed in an ultrasonication bath for 10 min to guarantee the complete extraction of the
381 atorvastatin from the glucan particles. The final concentration of atorvastatin in the produced
382 composites was measured by high-performance liquid chromatography (HPLC) with DAD UV detection
383 (G1315D), coupled with Waters Symmetry column (75 mm x 4.6 mm; 3.5 µm) and mobile phase
384 consisting of ammonium acetate buffer (10 mM; pH 3.0; pH adjusted by trifluoroacetic acid) and

Table 3. Solvent gradient for HPLC method

Time [min]	Acetonitrile [%]	Ammonium Acetate buffer [%]	Flow [ml/min]
0	40	60	1
1.3	40	60	1
5	70	30	1
7	70	30	1
8	40	60	1

385 acetonitrile (gradient grade, ≥99.9%), with the solvent gradient according to Table 3. The obtained
386 concentrations are summarized in Table 4.

Table 4. Concentration of produced composites

Sample	Final Ato-GP concentration [wt %]	Loading efficiency [wt %]
Ato-GP 1%	1.31 ± 0.02	121,7%
Ato-GP 5%	6.06 ± 0.10	113%
Ato-GP 10%	11.39 ± 0.22	108,0%
Ato-GP 15%	15.87 ± 0.34	100,6%

387
388
389
390

391 Cytotoxicity test

392 The cytotoxicity testing of glucan particle composites was conducted using Porcine liver primary cells
393 (PLP) and the RAW 264.7 cell line. The samples for testing included crude atorvastatin in two forms:
394 one in PBS and the other in Dimethyl Sulfoxide (DMSO). Additionally, composites containing
395 atorvastatin in concentration range from 0.08 to 10% (w/w) and pure glucan particles (GPs) were
396 tested. To prepare the suspensions, 0.50 mg of crude atorvastatin, composites, or GPs were dispersed
397 in 1 mL of PBS, followed by vortex mixing. In the case of crude atorvastatin in DMSO, 25 mg of the
398 substance was dissolved in 1 mL of DMSO, and then 4 mL of PBS were added. The resulting suspension
399 was subjected to ultrasonic bath treatment for 5 minutes to ensure proper dispersion. Cytotoxic effect
400 of administered solutions was analyzed after 24 hours by MTT assay or cell counting.

401

402 **STATISTICAL ANALYSIS**

403

404 Statistics

405 Box plots and heat maps were generated in GraphPad Prism9 software. 2way ANOVA was used for
406 multiple comparison testing, followed by Sidak's multiple-comparison test. Bar plots display mean and
407 standard deviation. Statistical significance of test is depicted in plots by using following GP code
408 ($p < 0.0332 = *$; $p < 0.0021 = **$; $p < 0.0002 = ***$). Normality and homogeneity of variations was tested by
409 Anderson-Darling test, D'Agostino Pearsons test, and Shapiro-Wilk test. For survival analyses, the data
410 sets were compared by Log-rank and Grehan-Breslow Wilcoxon test and for comparison of colony
411 forming units Mann-Whitney test was employed. For complex differential analysis of omics data, we
412 processed the data through online platform for transcriptomic data analysis (TCC(Sun et al. 2013)-
413 based on the following R-packages (*edgeR*, *DESeq*, *baySeq*, and *NBPSeg*), iDep95(Ge, Son, and Yao
414 2018)- based on the following R-packages (*limma*, *DESeq2*, *GSEA*, *PAGE*, *GACE*, *RactomePA*, *Kallisto*,
415 *Galaxy*) followed by subsequent analysis of assigned biological processes in Kegg pathways* and
416 Flymine databases**.

417 *<https://www.genome.jp/kegg/pathway>

418 **<https://www.flymine.org/flymine>

419

420 **Data and Code Availability**

421 RNA-seq data have been deposited at GEO and are publicly available as of the
422 date of publication. Accession numbers are listed in the key resources table. Microscopy data reported
423 in this paper will be shared by the lead contact upon request.

424 **Acknowledgements**

425 The authors acknowledge funding from the Grant Agency of the Czech Republic to AB (Projects 20-
426 14030S; 23-06133S www.gacr.cz) and FS (19-26127X). GK was supported by USB Grant Agency (Project
427 026/2021/P). We thank to Lucie Hrádková for laboratory services, enthusiasm and support. We thank
428 to Marc Dionne for Crq>GFP fly line. Other fly stocks were obtained from the Bloomington Center
429 (Bloomington, IN) and the VDRC (Vienna, Austria). The *S. pneumoniae* bacterial strain was obtained
430 from Dr. David Schneider. We also thank to Jarka Lieskovska from the Department of Medical Biology
431 (USB) for allowing us to use the S3eBioRad sorter, Hana Sehadova and Lucie Pauchova from Biology
432 Centre CAS for allowing us to use a confocal and electron microscopes and help with sample
433 preparations. We are also grateful to developers of Fiji: an open-source platform for biological-image
434 analysis ([doi:10.1038/nmeth.2019](https://doi.org/10.1038/nmeth.2019)), TCC: online platform for transcriptomic data analysis, iDep94: an
435 alternative online platform for transcriptomic data analysis. We are grateful to Ivan Saloň for useful
436 discussions.

437

438 **Author Contributions**

439 AB, GK, and FS conceptualized the project, designed the experiments and wrote the manuscript. AB
440 and GK performed most of the experiment concerning the *Drosophila* model. GRC, PS, ES and FS
441 designed and prepared the composites used in this work.

442

443 **Declaration of Interests**

444 The authors declare no competing interests.

445

446

447 **Inclusion and diversity**

448 We support inclusive, diverse, and equitable conduct of research.

449

450 **References**

- 451 1. Mantovani, A., Biswas, S. K., Galdiero, M. R., Sica, A. & Locati, M. Macrophage plasticity and
452 polarization in tissue repair and remodelling. *J. Pathol.* **229**, 176–185 (2013).
- 453 2. Sreejit, G., Fleetwood, A. J., Murphy, A. J. & Nagareddy, P. R. Origins and diversity of

- 454 macrophages in health and disease. *Clin. Transl. Immunol.* **9**, (2020).
- 455 3. Lee, M.-S. & Bensinger, S. J. Reprogramming cholesterol metabolism in macrophages and its
456 role in host defense against cholesterol-dependent cytolysins. *Cell. Mol. Immunol.* **19**, 327–
457 336 (2022).
- 458 4. Das, A. *et al.* Monocyte and Macrophage Plasticity in Tissue Repair and Regeneration. *Am. J.*
459 *Pathol.* **185**, 2596–2606 (2015).
- 460 5. Valledor, A. F., Comalada, M., Santamaría-Babi, L. F., Lloberas, J. & Celada, A. in 1–20 (2010).
461 doi:10.1016/B978-0-12-380995-7.00001-X
- 462 6. Kolliniati, O., Ieronymaki, E., Vergadi, E. & Tsatsanis, C. Metabolic Regulation of Macrophage
463 Activation. *J. Innate Immun.* **14**, 51–68 (2022).
- 464 7. Yan, J. & Horng, T. Lipid Metabolism in Regulation of Macrophage Functions. *Trends Cell Biol.*
465 **30**, 979–989 (2020).
- 466 8. Ardura, J. A. *et al.* Targeting Macrophages: Friends or Foes in Disease? *Front. Pharmacol.* **10**,
467 (2019).
- 468 9. Covarrubias, A. J., Aksoylar, H. I. & Horng, T. Control of macrophage metabolism and
469 activation by mTOR and Akt signaling. *Semin. Immunol.* **27**, 286–296 (2015).
- 470 10. Fleming, B. D. & Mosser, D. M. Regulatory macrophages: Setting the Threshold for Therapy.
471 *Eur. J. Immunol.* **41**, 2498–2502 (2011).
- 472 11. Hu, K. *et al.* Macrophage Functions and Regulation: Roles in Diseases and Implications in
473 Therapeutics. *J. Immunol. Res.* **2018**, 1–2 (2018).
- 474 12. Jain, N. K., Mishra, V. & Mehra, N. K. Targeted drug delivery to macrophages. *Expert Opin.*
475 *Drug Deliv.* **10**, 353–367 (2013).
- 476 13. Hu, G. *et al.* Nanoparticles Targeting Macrophages as Potential Clinical Therapeutic Agents
477 Against Cancer and Inflammation. *Front. Immunol.* **10**, (2019).
- 478 14. Boltnarova, B. *et al.* PLGA Based Nanospheres as a Potent Macrophage-Specific Drug Delivery
479 System. *Nanomaterials* **11**, 749 (2021).
- 480 15. Liang, T. *et al.* Recent Advances in Macrophage-Mediated Drug Delivery Systems. *Int. J.*
481 *Nanomedicine* **Volume 16**, 2703–2714 (2021).
- 482 16. Hu, G. *et al.* High-throughput phenotypic screen and transcriptional analysis identify new
483 compounds and targets for macrophage reprogramming. *Nat. Commun.* **12**, 773 (2021).
- 484 17. Zhong, L. *et al.* Small molecules in targeted cancer therapy: advances, challenges, and future
485 perspectives. *Signal Transduct. Target. Ther.* **6**, 201 (2021).
- 486 18. Cheng, L., Baonza, A. & Grifoni, D. Drosophila Models of Human Disease. *Biomed Res. Int.*
487 **2018**, 1–2 (2018).
- 488 19. Moraes, K. C. M. & Montagne, J. Drosophila melanogaster: A Powerful Tiny Animal Model for
489 the Study of Metabolic Hepatic Diseases. *Front. Physiol.* **12**, (2021).

- 490 20. Harnish, J. M., Link, N. & Yamamoto, S. *Drosophila* as a Model for Infectious Diseases. *Int. J.*
491 *Mol. Sci.* **22**, 2724 (2021).
- 492 21. Dushay, M. S. & Eldon, E. D. *Drosophila* Immune Responses as Models for Human Immunity.
493 *Am. J. Hum. Genet.* **62**, 10–14 (1998).
- 494 22. Ulvila, J., Vanha-aho, L.-M. & Rämetsä, M. *Drosophila* phagocytosis - still many unknowns under
495 the surface. *APMIS* **119**, 651–662 (2011).
- 496 23. Gold, K. S. & Brückner, K. Macrophages and cellular immunity in *Drosophila melanogaster*.
497 *Semin. Immunol.* **27**, 357–368 (2015).
- 498 24. Evans, C. J., Hartenstein, V. & Banerjee, U. Thicker Than Blood. *Dev. Cell* **5**, 673–690 (2003).
- 499 25. Krejčová, G. *et al.* *Drosophila* macrophages switch to aerobic glycolysis to mount effective
500 antibacterial defense. *Elife* **8**, (2019).
- 501 26. Medzhitov, R. & Janeway, C. Fly immunity: great expectations. *Genome Biol.* **1**, reviews106.1
502 (2000).
- 503 27. Martinelli, C. & Reichhart, J.-M. Evolution and integration of innate immune systems from
504 fruit flies to man: lessons and questions. *J. Endotoxin Res.* **11**, 243–248 (2005).
- 505 28. Soto, E. R., Caras, A. C., Kut, L. C., Castle, M. K. & Ostroff, G. R. Glucan Particles for
506 Macrophage Targeted Delivery of Nanoparticles. *J. Drug Deliv.* **2012**, 1–13 (2012).
- 507 29. Vetvicka, V., Vannucci, L. & Sima, P. β -glucan as a new tool in vaccine development. *Scand. J.*
508 *Immunol.* **91**, (2020).
- 509 30. Wu, Y. *et al.* Bioinspired yeast-based β -glucan system for oral drug delivery. *Carbohydr.*
510 *Polym.* **319**, 121163 (2023).
- 511 31. Plavcová, Z. *et al.* Curcumin encapsulation in yeast glucan particles promotes its anti-
512 inflammatory potential in vitro. *Int. J. Pharm.* **568**, 118532 (2019).
- 513 32. Abraham, A., Ostroff, G., Levitz, S. M. & Oyston, P. C. F. A novel vaccine platform using glucan
514 particles for induction of protective responses against *Francisella tularensis* and other
515 pathogens. *Clin. Exp. Immunol.* **198**, 143–152 (2019).
- 516 33. Vetvicka, V. & Vetvickova, J. Glucan–Resveratrol–Vitamin C Combination Offers Protection
517 against Toxic Agents. *Toxins (Basel)*. **4**, 1301–1308 (2012).
- 518 34. Šalamúnová, P. *et al.* Serum and lymph pharmacokinetics of nilotinib delivered by yeast
519 glucan particles per os. *Int. J. Pharm.* **634**, 122627 (2023).
- 520 35. Aouadi, M. *et al.* Lipid storage by adipose tissue macrophages regulates systemic glucose
521 tolerance. *Am. J. Physiol. Metab.* **307**, E374–E383 (2014).
- 522 36. Barreby, E., Sulen, A. & Aouadi, M. in 49–57 (2019). doi:10.1007/978-1-4939-9130-3_4
- 523 37. Tesz, G. J. *et al.* Glucan particles for selective delivery of siRNA to phagocytic cells in mice.
524 *Biochem. J.* **436**, 351–362 (2011).

- 525 38. Tencerova, M. in 65–73 (2020). doi:10.1007/978-1-0716-0704-6_8
- 526 39. Bajgar, A. *et al.* Yeast glucan particles enable intracellular protein delivery in *Drosophila*
527 without compromising the immune system. *Biomater. Sci.* **7**, 4708–4719 (2019).
- 528 40. Kim, Y.-S. *et al.* Gram-negative Bacteria-binding Protein, a Pattern Recognition Receptor for
529 Lipopolysaccharide and β -1,3-Glucan That Mediates the Signaling for the Induction of Innate
530 Immune Genes in *Drosophila melanogaster* Cells. *J. Biol. Chem.* **275**, 32721–32727 (2000).
- 531 41. Bajgar, A. & Dolezal, T. Extracellular adenosine modulates host-pathogen interactions
532 through regulation of systemic metabolism during immune response in *Drosophila*. *PLoS*
533 *Pathog.* **14**, e1007022 (2018).
- 534 42. Mukhtar, M. *et al.* Drug delivery to macrophages: a review of nano-therapeutics targeted
535 approach for inflammatory disorders and cancer. *Expert Opin. Drug Deliv.* **17**, 1239–1257
536 (2020).
- 537 43. Ruphuy, G. *et al.* Encapsulation of poorly soluble drugs in yeast glucan particles by spray
538 drying improves dispersion and dissolution properties. *Int. J. Pharm.* **576**, 118990 (2020).
- 539 44. Sakai, M. *et al.* HMG-CoA reductase inhibitors suppress macrophage growth induced by
540 oxidized low density lipoprotein. *Atherosclerosis* **133**, 51–59 (1997).
- 541 45. Zhu, X. *et al.* Increased Cellular Free Cholesterol in Macrophage-specific Abca1 Knock-out
542 Mice Enhances Pro-inflammatory Response of Macrophages. *J. Biol. Chem.* **283**, 22930–22941
543 (2008).
- 544 46. Wang, M. & Hajishengallis, G. Lipid raft-dependent uptake, signalling and intracellular fate of
545 *Porphyromonas gingivalis* in mouse macrophages. *Cell. Microbiol.* **10**, 2029–2042 (2008).
- 546 47. Takei, A. *et al.* Myeloid HMG-CoA Reductase Determines Adipose Tissue Inflammation, Insulin
547 Resistance, and Hepatic Steatosis in Diet-Induced Obese Mice. *Diabetes* **69**, 158–164 (2020).
- 548 48. Kim, J. *et al.* Sufficient production of geranylgeraniol is required to maintain endotoxin
549 tolerance in macrophages. *J. Lipid Res.* **54**, 3430–3437 (2013).
- 550 49. Nathan, J. A. Squalene and cholesterol in the balance at the ER membrane. *Proc. Natl. Acad.*
551 *Sci.* **117**, 8228–8230 (2020).
- 552 50. Jing, X. & Behmer, S. T. Insect Sterol Nutrition: Physiological Mechanisms, Ecology, and
553 Applications. *Annu. Rev. Entomol.* **65**, 251–271 (2020).
- 554 51. Norris, P. C. & Dennis, E. A. A lipidomic perspective on inflammatory macrophage eicosanoid
555 signaling. *Adv. Biol. Regul.* **54**, 99–110 (2014).
- 556 52. Netea, M. G. *et al.* Defining trained immunity and its role in health and disease. *Nat. Rev.*
557 *Immunol.* **20**, 375–388 (2020).
- 558 53. Bekkering, S. *et al.* Metabolic Induction of Trained Immunity through the Mevalonate
559 Pathway. *Cell* **172**, 135–146.e9 (2018).
- 560 54. Bajgar, A. *et al.* Yeast glucan particles enable intracellular protein delivery in *Drosophila*
561 without compromising the immune system. *Biomater. Sci.* (2019). doi:10.1039/c9bm00539k

562 **Figure 1: HMGR activity is increased in *Drosophila* macrophages upon infection**

563 (A) Heat map documenting differential expression of genes involved in the mevalonate pathway in macrophages isolated
564 from infected individuals (INF) compared to controls (CON); expressed as Log₂ fold change in infected flies compared to
565 controls. (B) MA plot showing differentially expressed genes in control vs. infection-activated macrophages with highlighted
566 coordinates of *Hmgcr*. (C) Expression level of *Hmgcr* in macrophages isolated from infected individuals (INF) compared to
567 controls (CON); data are presented as raw count level (counts per million). (D) Gene expression of *Hmgcr* in macrophages
568 isolated from control (CON) and infected (INF) flies at 0, 24, 72, and 120 hours post infection (hpi). Expression levels
569 normalized against *rp49* are reported as fold change relative to levels of *Hmgcr* in macrophages isolated from non-infected
570 flies at 0hpi, which was arbitrarily set to 1. (E) Gene expression of *Hmgcr* in macrophages, fat body and muscles dissected
571 from control (CON) and infected (INF) flies at 24hpi. Expression levels normalized against *rp49* are reported as fold change
572 relative to level of *Hmgcr* in macrophages isolated from non-infected flies, which was arbitrarily set to 1. (F) Gene expression
573 of *Hmgcr* in macrophages isolated from non-infected (CON) and infected (INF) control flies (CrqGFP>KK^{control}) and flies with
574 macrophage-specific *Hif1α* knockdown (CrqGFP>Hif1α^{RNAi}). Expression levels normalized against *rp49* are reported as fold
575 change relative to level of *Hif1α* in non-infected CrqGFP>KK^{control} flies, which was arbitrarily set to 1. (G) The enzymatic activity
576 of HMGR in macrophages isolated from control (CON) and infected flies (INF) at 0, 6, 72, and 120hpi. The activity is depicted
577 as a fold change of the initial NADPH level in non-infected controls at 0hpi at 20 minutes from the beginning of the reaction.
578 Data collected from four independent experiments. In D-E, the data were compared by 2way ANOVA followed by Šídák's
579 multiple comparisons test. In F, the data were compared by 2way ANOVA Tukey's multiple comparisons test. Data were
580 obtained from four independent experiments. The individual dots represent biological replicates with line/bar showing mean
581 ± SD, asterisks mark statistically significant differences (*p<0.05; **p<0.01; ***p<0.001).

582

583 **Figure 2: Systemic administration of glucan particles leads to their internalization by *Drosophila* macrophages**

584 (A) Representative scanning electron micrograph depicting derivatized glucan particles with no cargo. (B) Representative
585 transmission electron micrograph showing internal structure of an empty glucan particle. (C) Representative pseudocoloured
586 scanning electron micrograph of a macrophage (green) engulfing glucan particles (magenta) and binding *Streptococcus*
587 *pneumoniae* (beige). (D) Representative confocal microscopy image of macrophages (Crq>GFP, green) containing
588 rhodamine-labeled glucan particles (red). The cytoskeleton was stained by phalloidin (cyan). (E) Representative
589 pseudocoloured transmission electron micrograph of a macrophage (green), containing lipid inclusions (yellow) and
590 scavenged glucan particles (magenta), documenting that the internalization of glucan particles does not affect macrophage
591 ability to engulf bacteria (*S. pneumoniae*, dark blue). The darker colour in the GPs core is related to the equatorial cross
592 section of the particle. (F) Detailed representative pseudocoloured transmission electron micrograph of a macrophage
593 (green) documenting the ultrastructure of internalized glucan particle (magenta). The darker colour in the GPs core is related
594 to the equatorial cross section of the particle.

595

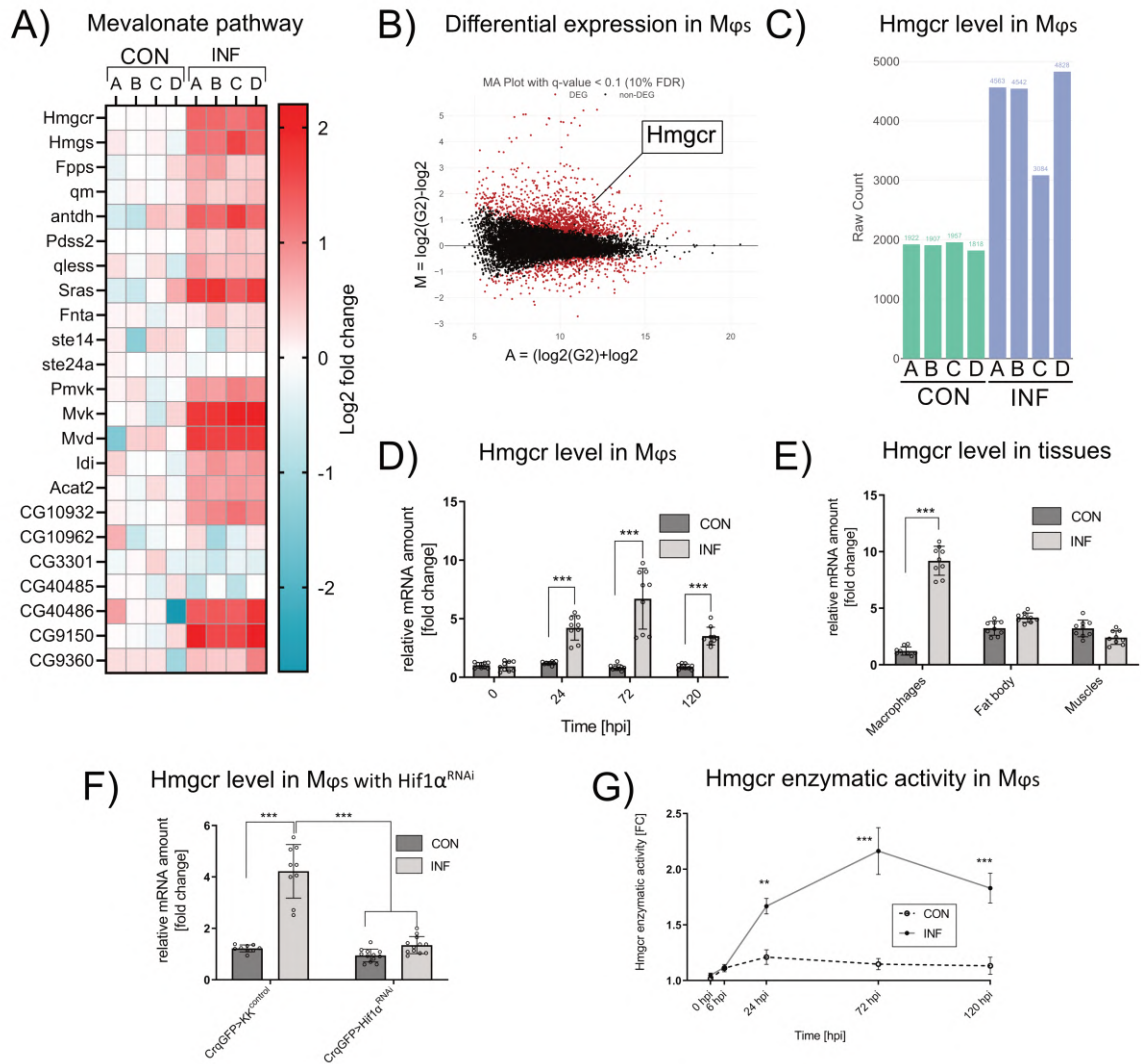
596 **Figure 3: Atorvastatin encapsulated in yeast glucan particles inhibits HMGR macrophage-specifically**

597 (A) Schematic representation of the experimental design. (B) The enzymatic activity of HMGR at 20 minutes from the
598 beginning of the reaction in macrophages isolated from flies injected with buffer (Buff) or GPs loaded with 1, 5, 10 or 15%
599 (w/v) of atorvastatin. Addition of pravastatin or HMGR enzyme to the reaction was used as a positive and negative control,
600 respectively. Red circle marks the concentration used for the subsequent experiments. (C) Schematic representation of the
601 injected substances. (D) The enzymatic activity of HMGR at 20 minutes from the beginning of the reaction in macrophages
602 isolated from infected flies, which were injected with GPs loaded with 5% atorvastatin (Ato-GPs), empty glucan particles
603 (GPs), atorvastatin (Ato), or co-injected with atorvastatin and GPs (Ato x GPs) 48 hours before the infection. (E) The enzymatic
604 activity of HMGR at 20 minutes from the beginning of the reaction in the fat body dissected from flies injected with 5%
605 atorvastatin (Ato-GPs), empty glucan particles (GPs), atorvastatin (Ato), or co-injected with atorvastatin and GPs (Ato x GPs)
606 48 hours before buffer injection or infection. Addition of pravastatin or HMGR enzyme to the reaction was used as a positive
607 and negative control, respectively. (F) The enzymatic activity of *Hmgcr* at 20 minutes from the beginning of the reaction in
608 muscles dissected from flies injected with 5% atorvastatin (Ato-GPs), empty glucan particles (GPs), atorvastatin (Ato), or co-
609 injected with atorvastatin and GPs (Ato x GPs) 48 hours before buffer injection or infection. Addition of pravastatin or HMGR
610 enzyme to the reaction was used as a positive and negative control, respectively. Data were obtained from four independent
611 experiments. The results were compared by 2way ANOVA Tukey's multiple comparisons test. The individual dots represent
612 biological replicates with line/bar showing mean ± SD, asterisks mark statistically significant differences (*p<0.05; **p<0.01;
613 ***p<0.001).

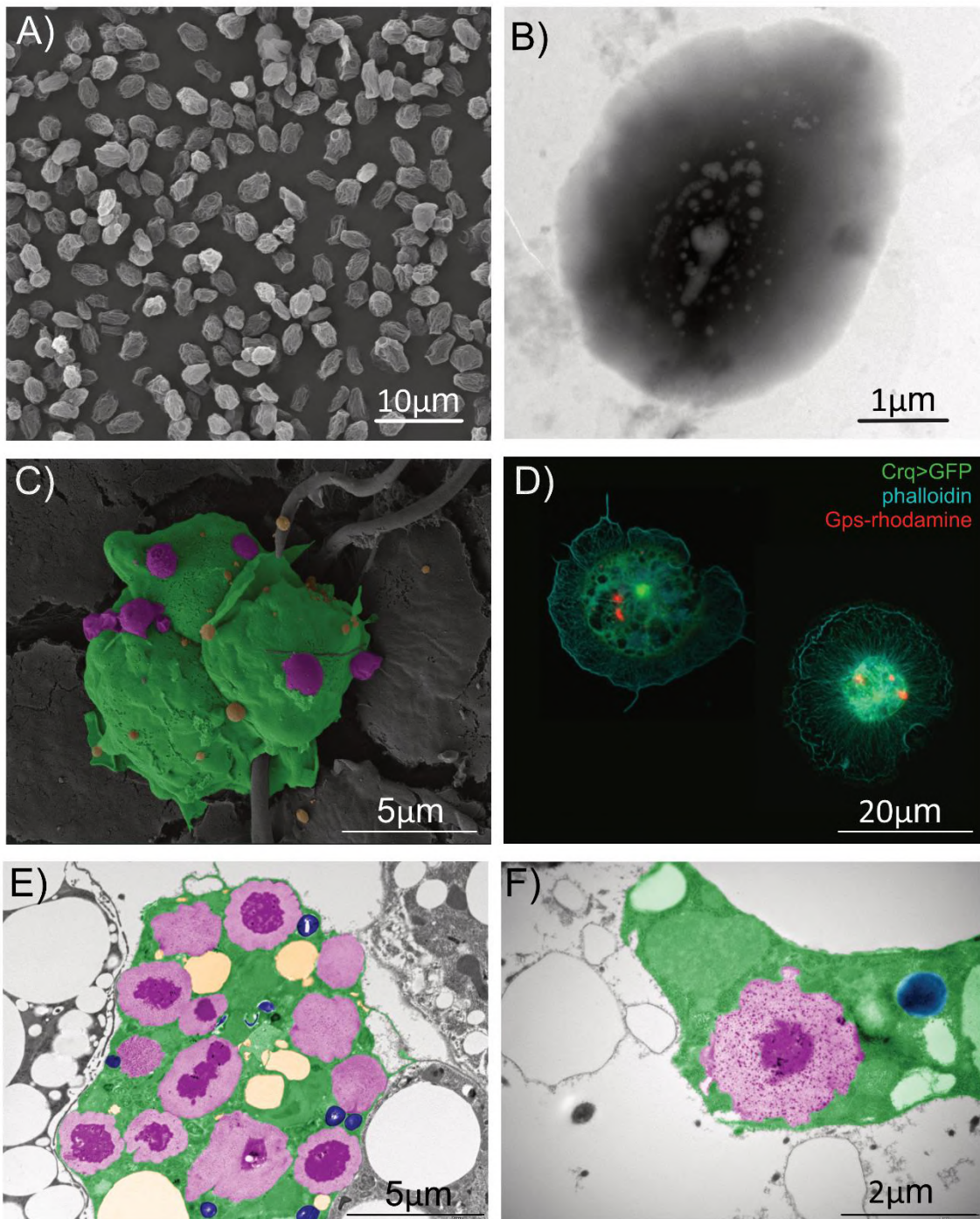
614

615 **Figure 4: HMGR activity in macrophages is fundamental for resistance to streptococcal infection in *Drosophila***
616 (A) Gene expression of characteristic readouts of humoral immune response (*Diptericin A*, *Drosocin*, *Metchnikowin*), stress
617 response (*basket*) and macrophage metabolic polarization (*Lactate dehydrogenase*, *Enolase*) in macrophages isolated from
618 infected flies injected with GPs loaded with 5% atorvastatin (Ato-GPs) and compared to those injected with empty glucan
619 particles (GPs), atorvastatin (Ato), or co-injected with atorvastatin and GPs (Ato x GPs). Macrophages from flies with
620 macrophage-specific knockdown of *Hmgcr* (*Hmgcr^{RNAi}*) were used as a positive control. Expression levels normalized against
621 *rp49* are reported as fold change relative to levels of *Diptericin A*, *Drosocin*, *Metchnikowin*, *basket*, *Lactate dehydrogenase*
622 and *Enolase*, respectively, in flies injected with Ato, which were arbitrarily set to 1. The results were compared by 2way
623 ANOVA Tukey's multiple comparisons test. Data were obtained from four independent experiments. (B) The number of
624 colony-forming units (CFUs) in infected flies, which were injected with GPs loaded with 5% atorvastatin (Ato-GPs) compared
625 to flies injected with empty glucan particles (GPs), atorvastatin (Ato), or co-injected with atorvastatin and GPs (Ato x GPs).
626 Flies with macrophage-specific knockdown of *Hmgcr* (*Hmgcr^{RNAi}*) were used as a positive control. The individual dots in the
627 plot represent the number of bacteria (colony forming units - CFUs) in thousands per one fly. Data were obtained from three
628 independent experiments. The results were compared by 2way ANOVA Tukey's multiple comparisons test. (C) Survival of
629 infected flies, which were injected with GPs loaded with 5% atorvastatin (Ato-GPs) is decreased compared to flies injected
630 with empty glucan particles (GPs), atorvastatin (Ato), or co-injected with atorvastatin and glucan particles (Ato x GPs). Flies
631 with macrophage-specific knockdown of *Hmgcr* (*Hmgcr^{RNAi}*) were used as a positive control. Three independent experiments
632 were performed and combined into each survival curve; the number of individuals per replicate was at least 600 for each
633 group. The data sets were compared by Log-rank and Grehan-Breslow Wilcoxon test. The individual dots represent biological
634 replicates with line/bar showing mean \pm SD, asterisks mark statistically significant differences (* $p < 0.05$; ** $p < 0.01$;
635 *** $p < 0.001$).

636
637
638
639
640
641
642
643
644
645
646
647
648
649
650
651
652
653
654
655
656
657
658
659
660
661
662
663
664
665



667
 668
 669
 670
 671
 672
 673
 674
 675
 676
 677

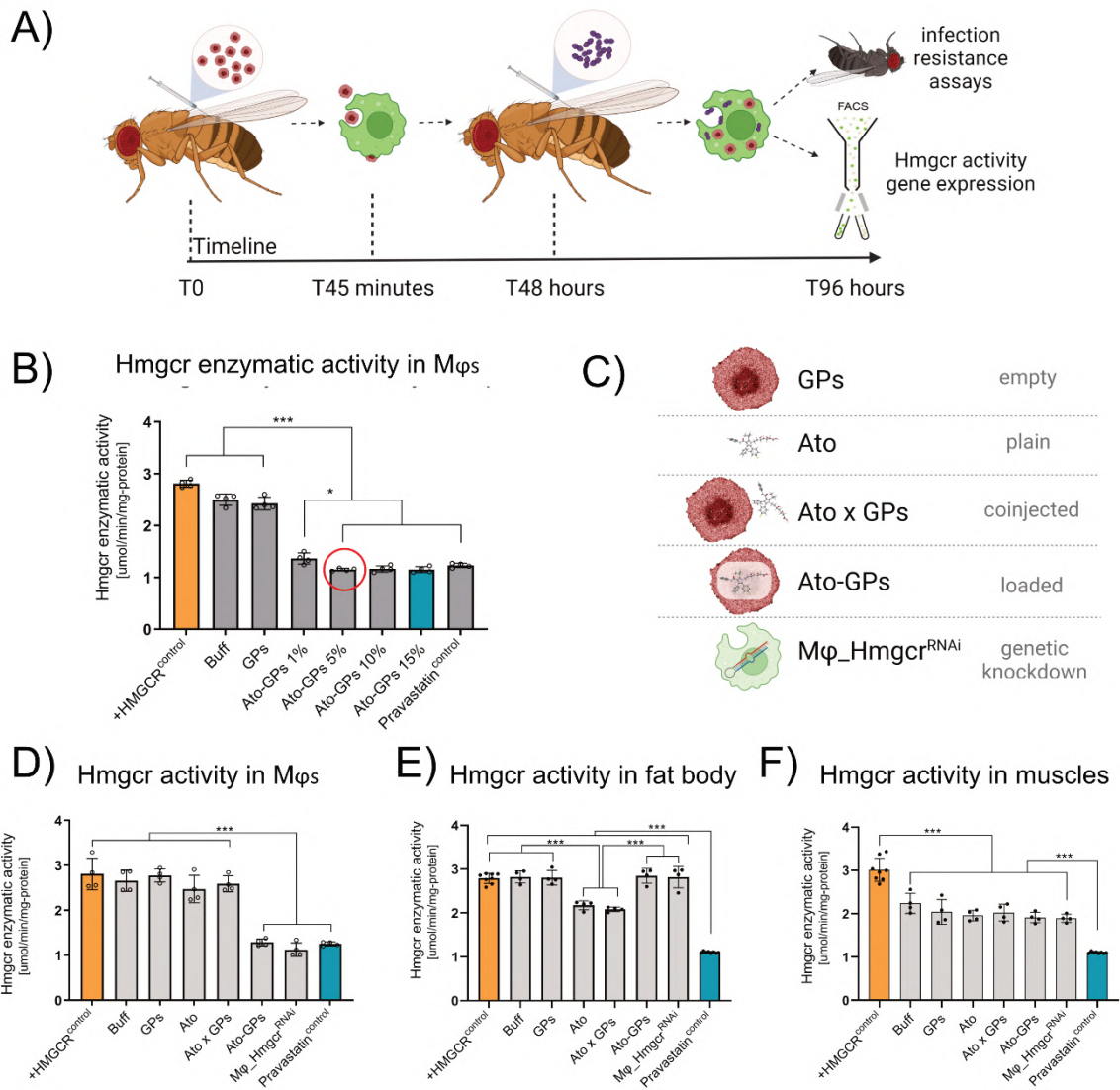


679

680

681

682



684

685

686

687

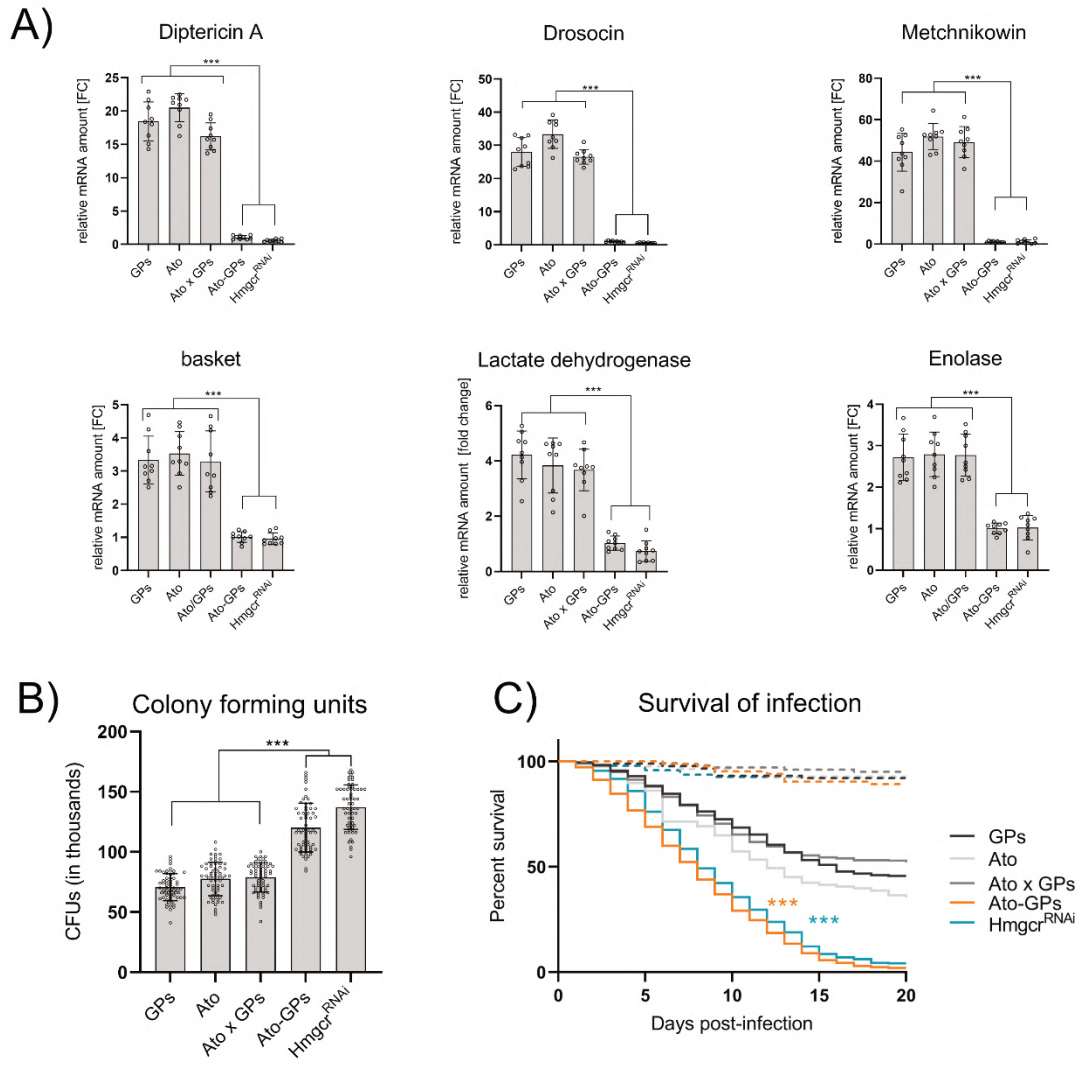
688

689

690

691

692



694
 695
 696
 697
 698
 699
 700
 701
 702
 703
 704

705 **SUPPLEMENTAL INFORMATION**

706 **Table S1:** Top 50 up- and downregulated genes in *Drosophila* macrophages in response to
 707 streptococcal infection.

Generated from raw data in TCC-GUI: Graphical User Interface for TCC package

Gene Name	Q Value (FDR)	A Value	M Value	P Value	Rank
AttC	0	12.171	5.231	0	1
AttB	0	10.202	4.751	0	2
AttA	0	10.667	4.72	0	3
TotB	0	10.059	4.768	0	4
Fst	0	10.09	3.785	0	5
Fbp2	0	7.859	5.049	0	6
imd	0	10.027	3.159	0	7
DptB	0	11.165	4.621	0	8
BomS1	0	11.085	2.969	0	9
Ldh	0	10.598	3.058	0	10
CecA1	0	9.382	4.887	0	11
TotX	0	9.346	4.904	0	12
edin	0	7.999	5.053	0	13
Spn88Eb	0	10.249	3.062	0	14
TotF	0	9.223	4.662	0	15
IM18	0	10.464	4.254	0	16
Aplip1	0	11.377	2.556	0	17
Imd	0	8.296	4.25	0	18
GNBP-like3	0	10.329	2.606	0	19
G6P	0	9.251	2.864	0	20
Rab18	0	10.225	2.65	0	21
SPH93	0	10.746	2.905	0	22
Rel	0	12.672	2.139	0	23
Mec2	0	11.434	2.555	0	24
Tep2	0	14.091	2.682	0	25
DptA	0	10.863	4.914	0	26
Dro	0	11.375	5.202	0	27
Mtk	0	11.892	2.564	0	28
Hayan	0	10.392	3.121	0	29
PGRP-SC2	0	10.654	2.615	0	30
Toll-7	0	11.913	1.959	0	31
BaraA1	0	13.471	2.096	0	32
bsk	0	10.624	2.054	0	33
PGRP-SB1	0	9.958	2.39	0	34
NimC3	0	7.161	3.998	0	35
PGRP-SD	0	9.91	2.446	0	36
BaraA2	0	13.469	2.035	0	37
Socs36E	0	11.06	2.046	0	38
Diedel	0	7.331	4.95	0	39
CG30392	0	10	2.171	0	40
CG12116	0	11.393	2.015	0	41
BomBc1	0	10.875	2.602	0	42
Ets21C	0	9.7	2.47	0	43
Def	0	7.456	4.146	0	44
CG42662	0	8.721	2.818	0	45
fkh	0	10.954	1.802	0	46
Mtch	0	11.941	1.691	0	47
Irc	0	12.998	2.218	0	48
ImpL2	0	11.551	1.791	0	49
Jon99Cii	0	13.199	-1.682	0	50

708

Generated from raw data in TCC-GUI: Graphical User Interface for TCC package

Gene Name	Q Value (FDR)	A Value	M Value	P Value	Rank
Abd-B	1	8.973	-0.001	0.998	11452
Agpat2	1	9.806	0.002	0.996	11437
asf1	1	7.453	0.003	0.996	11435
CG10038	1	7.591	0	1	11477
CG11666	1	6.186	0.003	1	11477
CG13012	1	7.205	0.002	1	11463
CG13018	1	6.104	-0.006	1	11477
CG14160	1	7.71	-0.003	0.997	11449
CG14223	1	6.802	-0.001	1	11465
CG14346	1	7.598	-0.001	1	11462
CG14841	1	6.321	-0.006	1	11477
CG1492	1	8.298	-0.003	0.997	11444
CG15035	1	9.521	-0.002	0.997	11442
CG17233	1	10.717	0	0.999	11458
CG18231	1	8.883	0	1	11477
CG1835	1	9.444	-0.001	0.998	11453
CG31404	1	9.342	0	1	11477
CG32201	1	7.596	-0.004	0.997	11443
CG34204	1	8.26	-0.001	1	11477
CG34231	1	5.883	-0.001	1	11477
CG34461	1	6.207	-0.004	1	11477
CG42445	1	7.08	0.002	1	11477
CG43338	1	5.997	-0.002	1	11467
CG4891	1	7.522	0	1	11477
CG6044	1	9.895	-0.001	0.999	11459
CG6610	1	6.068	0.008	1	11477
CG6867	1	9.059	0.002	0.996	11436
CG7691	1	6.28	0.002	1	11477
CG9967	1	6.864	-0.001	1	11477
ck	1	10.872	0	0.999	11460
cu	1	11.115	-0.001	0.996	11438
cv-c	1	12.605	-0.001	0.996	11440
CycC	1	7.667	-0.001	1	11477
da	1	11.32	0.001	0.998	11451
dati	1	10.262	-0.001	0.999	11455
Fs	1	8.554	-0.001	0.999	11456
gdrd	1	9.607	0.001	0.996	11441
GlcAT-I	1	8.307	0	1	11477
Gpdh2	1	9.136	0.002	0.996	11439
Gyc76C	1	10.813	0.001	0.998	11454
HP4	1	7.651	-0.004	0.997	11445
miple2	1	7.806	0.002	1	11466
mthl3	1	6.953	-0.001	1	11477
mus312	1	8.418	0	1	11477
Ppcdc	1	8.378	-0.002	0.997	11446
Ras64B	1	9.369	0.001	0.998	11450
Reck	1	8.63	-0.001	1	11461
SecCl	1	9.595	-0.001	0.999	11457
TpnC73F	1	7.777	0.003	0.997	11447
Trf4	1	7.8	-0.001	1	11463

709

710

711

712 **Table S2:** Ato-GPs display low cytotoxic effects in murine macrophages. The cytotoxic effects of the
 713 drug and the composite are represented as a growth inhibitory concentration (GI50).

714

Murine macrophages Raw 264.7

	Ato (PBS)	Ato (DMSO)	Ato-GP 10%
GI50 [µg/ml] Rep. 1	4.89	2.87	>250
GI50 [µg/ml] Rep. 2	5.21	3.12	>250
Average	5.05	3	N/A
SD	0.23	0.18	N/A

715

716

717 **Table S3:** Ato-GPs display low cytotoxic effects in porcine liver primary cells. The cytotoxic effects of
 718 the drug and the composites are represented as a growth inhibitory concentration (GI50).

Porcine liver primary cells

	Ato (PBS)	Ato (DMSO)	GPS	Ato-GP 0,08%	Ato-GP 0,17%	Ato-GP 0,8%
GI50 [µg/ml] Rep. 1	18.52	12.82	>250	>250	>250	>250
GI50 [µg/ml] Rep. 2	17.82	13.54	>250	>250	>250	>250
Average	18.17	13.18	N/A	N/A	N/A	N/A
SD	0.49	0.51	N/A	N/A	N/A	N/A

719

720

721

722

723

724

725

726

727

728

729

730

731

732

733

734

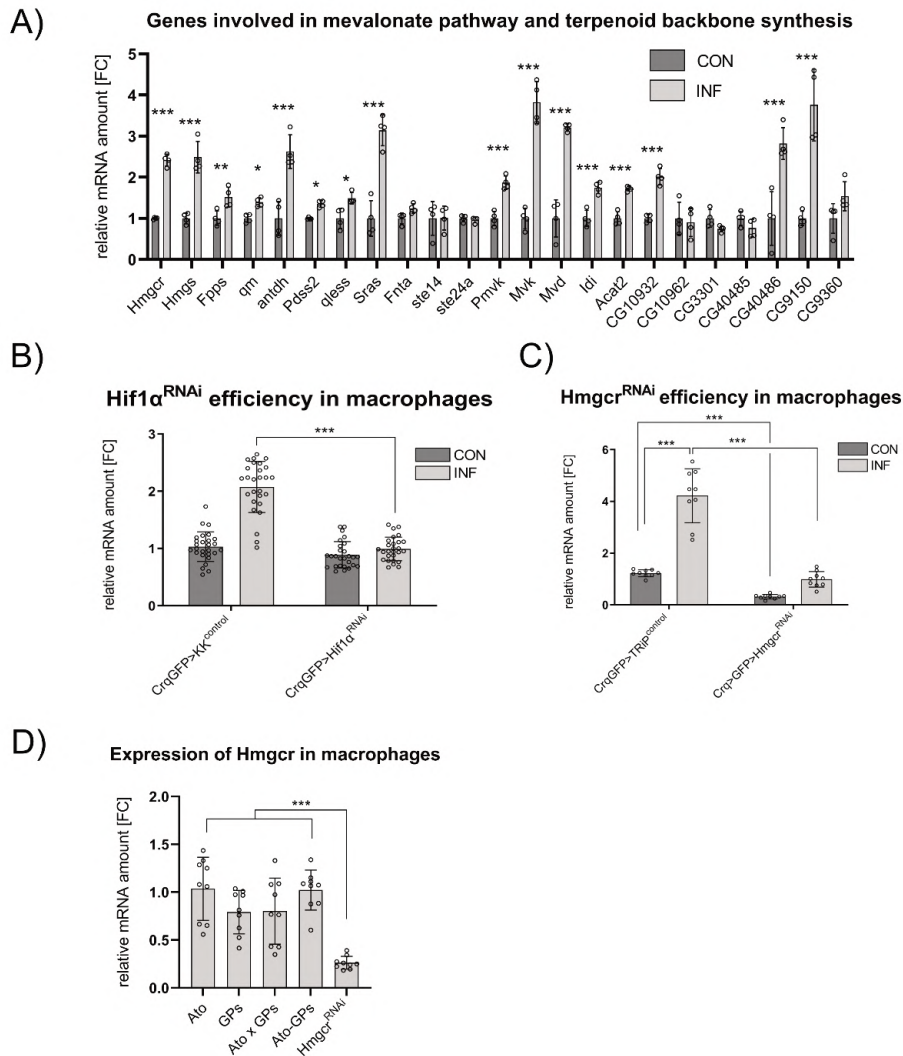
735

736

737

738

739



741

742 **Figure S1:** (A) Relative mRNA amount of genes involved in mevalonate pathway and terpenoid backbone biosynthesis in
 743 macrophages isolated from control (CON) and infected (INF) flies at 24 hours post infection. Expression levels are presented
 744 as a fold-change relative to the levels of Hmgcr in macrophages isolated from control flies, which was arbitrarily set to 1.
 745 Data were obtained from four independent experiments. The data sets were compared by 2way ANOVA followed by Šídák's
 746 multiple comparisons test. (B) Gene expression of Hif1 α in control (KKcontrol) macrophages and macrophages with
 747 macrophage-specific Hif1 α knockdown (Hif1 α RNAi) isolated from non-infected (CON) or infected (INF) flies. Expression levels
 748 normalized against rp49 are reported as fold change relative to levels of Hif1 α in non-infected (CON) KKcontrol flies, which
 749 was arbitrarily set to 1. (C) Gene expression of Hmgcr in control (KKcontrol) macrophages and macrophages with
 750 macrophage-specific Hmgcr knockdown (HmgcrRNAi) isolated from non-infected (CON) or infected (INF) flies. Expression
 751 levels normalized against rp49 are reported as fold change relative to levels of Hmgcr in non-infected (CON) TRIpcontrol flies,
 752 which was arbitrarily set to 1. (D) Gene expression of Hmgcr in macrophages isolated from infected flies, which were injected
 753 with GPs loaded with 5% atorvastatin (Ato-GPs), empty glucan particles (GPs), atorvastatin (Ato), or co-injected with
 754 atorvastatin and glucan particles (Ato x GPs) 48 hours before the infection. Flies with macrophage-specific knockdown of
 755 Hmgcr (HmgcrRNAi) were used as a positive control. Expression levels normalized against rp49 are reported as fold change
 756 relative to levels of Hmgcr in flies injected with Ato, which was arbitrarily set to 1. In B-D, the data were compared by 2way
 757 ANOVA Tukey's multiple comparisons test. The individual dots represent biological replicates with line/bar showing mean \pm
 758 SD, asterisks mark statistically significant differences (* p <0.05; ** p <0.01; *** p <0.001).

CHAPTER X:

Magnetic yeast glucan particles for antibody-free separation of viable macrophages from *Drosophila melanogaster*

Gabriela Krejčová, Ivan Saloň, Vojtěch Klimša, Pavel Ulbrich, Ayse Beyza Aysan, Adam Bajgar, František Štěpánek

Under review in *ACS Biomaterials Science & Engineering*

Magnetic yeast glucan particles for antibody-free separation of viable macrophages from *Drosophila melanogaster*

Gabriela Krejčová ^{a#}, Ivan Saloň ^{b#}, Vojtěch Klimša ^b, Pavel Ulbrich ^c, Ayse Beyza Aysan ^b, Adam Bajgar ^{ab*}, František Štěpánek ^{b*}

^a Department of Molecular Biology and Genetics, Faculty of Sciences, University of South Bohemia, Branišovská 1160/31, 37005 České Budějovice, Czech Republic

^b Department of Chemical Engineering, University of Chemistry and Technology Prague, Technická 5, 166 28 Prague 6, Czech Republic

^c Department of Biochemistry and Microbiology, University of Chemistry and Technology, Prague, Technická 5, 166 28 Prague 6, Czech Republic

These authors contributed equally

* Corresponding authors: bajgaa00@prf.jcu.cz (A. Bajgar), stepanef@vscht.cz (F. Štěpánek)

Abstract

Currently available methods for cell separation are generally based on fluorescent labelling using either endogenously expressed fluorescent markers or the binding of antibodies or antibody mimetics to surface antigenic epitopes. However, such modification of the target cells represents potential contamination by non-native proteins, which may affect further cell response and be outright undesirable in applications such as cell expansion for diagnostic or therapeutic applications including immunotherapy. We present a label- and antibody-free method for separating macrophages from living *Drosophila*, based on their ability to preferentially phagocytose whole yeast glucan particles (GPs). Using a novel de-swelling entrapment approach based on spray drying, we have successfully fabricated yeast glucan particles with previously unachievable content of magnetic iron oxide nanoparticles, while retaining their surface features responsible for phagocytosis. We demonstrate that magnetic yeast glucan particles enable macrophage separation at comparable yields to fluorescence-activated cell sorting, without compromising their viability or affecting their normal function and gene expression. The use of magnetic yeast glucan particles is broadly applicable to situations where viable macrophages separated from living organisms are subsequently used for analyses such as gene expression, metabolomics, proteomics, single-cell transcriptomics, or enzymatic activity analysis.

Keywords: β -glucan particles; iron oxide nanoparticles; spray drying; cell separation; phagocytosis.

Introduction

Cell manipulation and processing are crucial operations in biomedical research when working with living animals, tissues, and cells. Doing it in a lean and effective manner without compromising cellular functions is key for the further use of separated cells. Currently used techniques include micro pipetting¹, microfluidics², high-gradient magnetic cell sorting³ and predominantly fluorescence-activated cell sorting (FACS)⁴. Existing methods are generally based on fluorescent labelling of the target cells using either endogenously expressed fluorescent markers or the binding of antibodies or antibody mimetics to surface antigenic epitopes. In the case of magnetic cell sorting, currently used methods use antigen coupled magnetic nanoparticles that bind to the cell surface. While these approaches are perfectly acceptable in many applications such as *ex post* metabolomic analysis, there are also situations where the addition of non-native proteins to the separated cells is undesirable^{5,6}, particularly if the cells are to be used for immuno-analysis, diagnostic or therapeutic purposes⁷. The cell viability can be compromised, and normal cellular functions including immune response can be affected by phenomena such as antigen shedding⁸. From the regulatory perspective in cell therapy, the contamination of the therapeutic product by non-autologous or adventitious proteins can be problematic.

Whole yeast glucan particles (GPs) are porous polysaccharide shells predominantly formed by β -glucans, obtained from common baker's yeast by a series of washing and extraction steps⁹. Although most cellular components of the original yeast are removed, GPs retain surface structural features that make them readily recognised by dectin-1 receptors of immune cells and actively phagocytosed. This property of GPs has been well documented both *ex vivo*^{10, 11} and *in vivo*^{12, 13}. Owing to their immunogenicity and porous nature, GPs lend themselves as vehicles for the encapsulation and targeted delivery of various bioactive substances¹⁴⁻¹⁷. Proposed diagnostic and therapeutic applications of GPs include their use as vaccine adjuvants¹⁸, as immuno-active drug delivery systems for the treatment of inflammatory bowel disease, as a means of improving the bioavailability of poorly soluble drugs via lymphatic transport¹³, or as contrast agents for imaging^{19,20}. It has been recently shown that GPs injected into living *Drosophila* are rapidly distributed through the haemolymph and selectively taken up by macrophages without compromising their normal function⁹.

This feature of GPs could be used for label-free macrophage separation by a magnetic field but achieving sufficiently high magnetic response of GPs without compromising their morphology and surface molecular motifs has so far eluded the scientific community. In the present work, we introduce a novel method that yields composite GPs with an unprecedentedly strong response to magnetic field while retaining their structural and functional properties. The method is based on encapsulating independently prepared magnetic iron oxide nanoparticles into GPs by spray drying. A solvent temporarily swells the

1
2
3 polysaccharide GP shell, enabling colloiddally stable magnetic iron oxide nanoparticles to diffuse into its
4 inner structure. By rapid solvent evaporation during spray drying, the polysaccharide shell de-swells
5 and magnetic nanoparticles are irreversibly trapped within the GPs at a high concentration while a native
6 GP surface is preserved. We report a comprehensive physico-chemical characterisation of magnetic
7 GPs, demonstrate their *in vivo* biodistribution, cell uptake, and successful application for magnetic
8 separation. Furthermore, we show that the normal function and gene expression profile of the separated
9 macrophages are preserved.
10
11
12
13
14
15

16 **Materials and methods**

17 **Preparation of yeast glucan particles**

18
19
20 Glucan particles (GPs) were obtained from baker's yeast (*Saccharomyces cerevisiae*) using a series of
21 washing and extraction steps as reported previously¹⁴. 25 g of baker's yeast was added into 100 mL of
22 1M NaOH, mixed to form a suspension and the material was heated for 1 h at 90 °C and then centrifuged
23 at 14 500 g for 5 min (Dynamica Velocity 14, Austria). The supernatant was discarded, and this step
24 was repeated twice. The processed alkali-insoluble solids were then mixed with 10 mL of HCl solution
25 (pH 4.5), heated to 75 °C for 2 h and then centrifuged at 14 500 g for 5 min. The insoluble solids were
26 washed 3 times in deionised water, 4 times in isopropanol and finally 2 times in acetone. Each washing
27 step was followed by centrifugation at 14 500 g for 5 min. The final product was freeze dried to form
28 a white dry powder and stored in a refrigerator for further use.
29
30
31
32
33
34
35
36

37 **Preparation of yeast glucan particles modified with Rhodamine B**

38 As a reference for visualisation experiments, Rhodamine B modified yeast glucan particles (GP-RhodB)
39 were prepared by dispersing of 50 mg of glucan particles in 10 mL of 0.1M carbonate-bicarbonate buffer
40 with pH 9.2 containing 1 mg of Rhodamine B isothiocyanate dissolved in 500 µL of ethanol in a round-
41 bottom flask. The suspension was sonicated in sonication bath for 15 min. The suspension was then kept
42 at 37 °C for 12 h under constant magnetic stirring at 500 rpm. The content of the reaction mixture was
43 then washed 16 times and centrifuged for 3 min at 6000 g. Supernatant containing unreacted material
44 was discarded and the obtained pellet was freeze-dried and stored in refrigerator for further use.
45
46
47
48
49
50

51 **Synthesis of dextran coated iron oxide nanoparticles**

52 Dextran coated iron oxide nanoparticles (IONs) were synthesised as follows: 0.75 g iron (III) chloride
53 hexahydrate (Sigma Aldrich) and 0.375 g of iron (II) chloride tetrahydrate (Sigma Aldrich) were
54 dissolved in 15 mL of deionised water and kept in a 100mL three-neck flask equipped with a reverse
55 cooler and nitrogen atmosphere under vigorous stirring. 500 mg of 70 kDa dextran (Sigma Aldrich)
56 dissolved in 25 mL of deionised water was added, the mixture was then heated to 85 °C and 2.5 mL of
57
58
59
60

25% NH_4OH (Penta) was added dropwise into the reaction vessel. The reaction mixture was kept at 85 °C for 1 h and then cooled to room temperature. The nanoparticles were separated by magnetic decantation and washed 3 times with deionised water. The nanoparticle suspension was subsequently dialysed for 24 h against deionised water. The dialysate was sonicated for 10 min in a sonication bath and centrifuged at 1500 g for 5 min to remove any larger agglomerates. After centrifugation, the supernatant was filtered by a 0.2 μm PVDF (polyvinylidene difluoride) filter to obtain a nanoparticle suspension^{21, 22}.

Preparation of magnetic yeast glucan particles

Composite magnetic yeast glucan particles (mGPs) containing dextran-coated iron oxide nanoparticles were prepared by spray drying as shown schematically in Fig. 1. 100 mg of yeast glucan particles (either plain GPs or GP-RhodB) were dispersed and homogenised by ULTRA-TURRAX in a prepared mixture containing 500 μL of IONs (0.215 mg/mL), 25 mL of deionised water and 75 mL of 96% ethanol. After dispersing, the suspension was immediately spray-dried using a Mini Spray Dryer B-290 (Büchi, Switzerland) operated in inert loop under N_2 atmosphere. Spray drying was conducted using a 1.4 mm diameter, 2-fluid nozzle and operating conditions consisting of 120 °C inlet temperature, 5 mL/min suspension feed rate, and 800 L/h (50%) N_2 flow rate¹⁵. The outlet temperature was 70–75 °C.

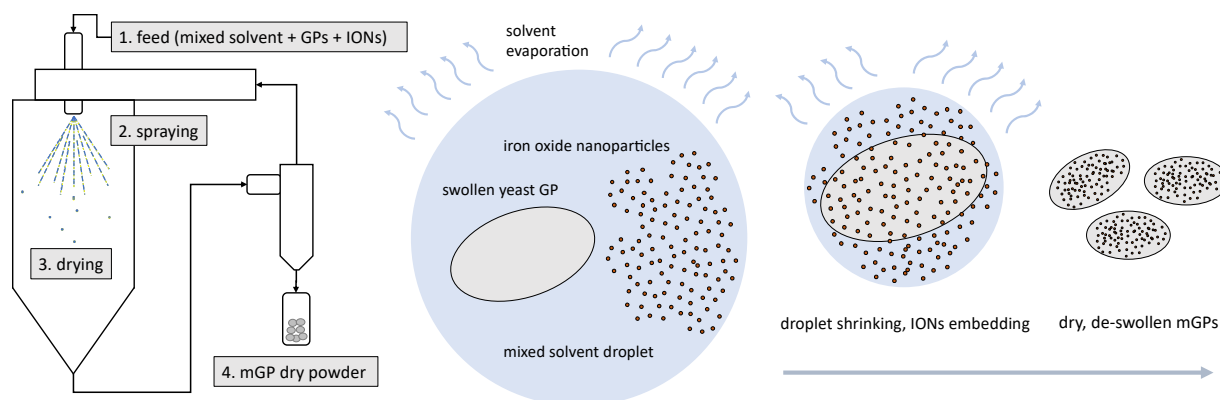


Fig. 1: Scheme of the mGP preparation process by spray drying. Left – overall process scheme. Right – mechanism of IONs embedding into GPs during droplet evaporation in the spray drying chamber.

Particle size analysis

The size distribution of the prepared magnetic nanoparticles (IONs) was evaluated by Dynamic Light Scattering (DLS), using the Zetasizer Nano-ZS (Malvern Instruments, UK). Before the measurement, 10 μL of the sample was added to 2 mL of deionised water, filtered by a 0.2 μm PVD filter and placed into a disposable cuvette. The size distribution of GPs, mGPs and mGPs-RhodB were evaluated by the static light scattering method using the Horiba Partica LA 950/S2 instrument. Prior to the measurement the particle suspension was sonicated by Sonopuls HD 3100 (Bandelin Electronic) for 5 min at 25 W without pulses.

Electron microscopy

The surface morphology and shape of GPs and mGPs were examined by a Scanning Electron Microscope (SEM) Jeol JCM- 5700. Samples were sputter-coated (Emitech K550X) by a 5 nm layer of gold prior to SEM analysis. Transmission Electron Microscope (TEM) Jeol JEM-1010 was used for the examination of the size and surface morphology of IONs and mGPs, without any staining procedure prior to the analyses. The elemental analysis of mGPs was determined by energy-dispersive X-ray spectroscopy (EDX) using the Thermo Scientific Phenom ProX desktop SEM with Phenom EDS software and semi-automated scanning option.

Atomic Absorption Spectroscopy

The iron content in mGP samples and in solution was evaluated by Atomic Absorption Spectroscopy (AAS) using Agilent 280FS AA with flame atomization technique. Fe (Flame) method at 248.3 nm was used with a flame type: acetylene – air.

X-ray powder diffraction

Crystallinity and the presence of iron oxide in composite mGPs was evaluated by recording the diffraction intensities of the samples from 6° to 110° 2θ angle using a PANalytical X'Pert PRO with a High Score Plus diffractometer. Data evaluation was performed in the software package HighScore Plus 4.0.

***Drosophila melanogaster* strains and culture**

The flies were raised on a standard diet containing cornmeal (80 g/L), sucrose (50 g/L), yeast (40 g/L), agar (10.433 g/L), and 10%-methylparaben (16.7 mL/L) and were maintained in a humidity-controlled environment with a natural 12 h/12 h light/dark cycle at 25 °C. We used CrqGal4>GFP fly line for the visualization of macrophages. This strain carries a macrophage-specific driver Crq Gal4 and reporter gene (enhanced green fluorescent protein eGFP), under control of artificial UAS promoter (genotype $w^{1118}/w^{1118}; Crq-Gal4, UAS-2xeGFP/Crq-Gal4, UAS-2xeGFP$).

Injection of flies

The suspension of IONs, mGPs or mGPs-RhodB was prepared by sonication on an ice bath for 5 min at 25 W, and vortexed just before injection to ensure well-dispersed particles. CrqGal4>GFP male flies were anaesthetised using CO₂ and injected with 50 nL of 0.1% (w/w) suspension, in case of mGPs or mGPs-RhodB, into the ventrolateral side of the abdomen using an Eppendorf Femtojet microinjector.

Visualization of magnetic yeast glucan particles distribution *in vivo*

To analyze magnetic particle distribution in *Drosophila*, CrqGal4>GFP flies were injected with 50 nL of 0.1% (w/w) mGPs or mGPs-RhodB. After 45 min, the fly abdomens were opened in 4% PFA (Polysciences) in PBS and fixed for 20 min. Subsequently, the tissues were washed in PBS. Aqua Polymount (Polysciences) was used to mount the sample. The samples were imaged using inverted fluorescent microscope (Olympus IX71) or confocal microscope (Olympus FluoView 1000).

Visualization of mGPs uptake by *Drosophila* phagocytes

To visualize mGPs uptake by *Drosophila* phagocytosing cells, we prepared samples for confocal and both scanning and transmission electron microscopy. For the analysis using a confocal microscope, CrqGal4>GFP flies were injected with 50 nL of 0.1% (w/w) mGPs-RhodB. After 45 min, the fly abdomens were opened in a drop of PBS on an imaging slide in order to wash up the macrophages, which were let to attach to the imaging slide for 25 min. Subsequently, the macrophages were fixed with 4% PFA (Polysciences) in PBS. After 20 mi, the samples were stained with Alexa Fluor™ Plus 405 Phalloidin (Invitrogen) for 40 min. Aqua Polymount (Polysciences) was used to mount the sample. Macrophages were imaged using an Olympus FluoView 3000 confocal microscope.

For the scanning electron microscopy analysis, CrqGal4>GFP flies were injected with 50 nL of 0.1% (w/w) mGPs. After 45 min, the fly abdomens were opened in PBS and fixed in 2.5% glutaraldehyde in 0.1 M phosphate buffer (pH = 7.2) for one week at 4°C. Subsequently, the opened abdomens were dehydrated through an acetone series and dried to critical point by point dryer CPD 2 (Pelco TM) and attached to an aluminium target. For contrasting, the samples were coated with gold by using a sputter coated E5100 (Polar Equipment Ltd.). Macrophages were examined with JEOL SEM JSM 7401F. Electron images were false coloured in Adobe Photoshop software.

For the transmission electron microscopy analysis, CrqGal4>GFP flies were injected with 50 nL of 0.1% (w/w) mGPs. After 45 min, the fly abdomens were cut off and placed in 2,5% glutaraldehyde in 0.1 M phosphate buffer (pH = 7.2) for one week at 4°C. Subsequently, the samples for TEM were post-fixed in osmium tetroxide for 2 h at 4 °C, washed at 4 °C, dehydrated through an acetone series and embedded in EPON resin. A series of ultrathin sections were prepared by using a Leica UCT ultramicrotome (Leica Microsystems), counterstained with uranyl acetate and lead citrate and subsequently examined in a JEOL TEM 1010 operated at 80 kV. The TEM images were false coloured in Adobe Photoshop software.

Magnetic yeast glucan particles separation of macrophages

At 60 min after injection of mGPs, the flies were washed in PBS and homogenised in 600 mL of PBS using a pestle. The homogenate was sieved through a nylon cell strainer (40 µm). This strainer was then

1
2
3 additionally washed with 200 μ L of PBS, which was added to the homogenate subsequently. The
4 samples were centrifuged (3 min, 4 °C, 3,500 RPM) and the supernatant was washed with ice-cold PBS
5 after each centrifugation (3 times). Prior to mGPs separation, samples were transferred to FACS
6 polystyrene tubes using a disposable bacterial filter (50 μ m, Sysmex).
7
8

9
10
11 The macrophages were separated from the sample using the QuadroMACS™ Separator (Miltenyi
12 Biotec) according to the manufacturer's protocol. In brief, the magnetic LS column (Miltenyi Biotec)
13 was placed in the QuadroMACS™ Separator and rinse before isolation with equilibrative buffer (PBS,
14 0.5 % BSA, 2 mM EDTA, pH 7.2). Subsequently, the sample with the cell suspension was loaded into
15 the LS column and the flow through was discarded. To wash off the remaining cells, the LS column was
16 washed 3 times with 1 mL of equilibrative buffer (Miltenyi Biotec). To obtain the phagocytosing cells,
17 the LS column was removed from the QuadroMACS™ Separator, washed with 2 mL of rinsing buffer
18 (PBS, 0.5 % BSA, 2 mM EDTA, pH 7.2) and the flow though was collected into a nuclease free
19 Eppendorf tube.
20
21
22
23
24
25

26 27 **Analysis of macrophage viability after magnetic separation**

28 Macrophages obtained by mGPs separation were let to attach to the imaging slide for 25 min.
29 Subsequently, the macrophages were fixed with 4% paraformaldehyde (PFA) in PBS (Polysciences).
30 After 20 min, the samples were stained with Alexa Fluor™ Plus 405 Phalloidin (Invitrogen) for 40 min.
31 Aqua polymount (Polysciences) was used to mount the sample. Macrophages were imaged using an
32 Olympus FluoView 3000 confocal microscope. Apart from visual assessment of cytoskeleton
33 remodelling, cell viability was also determined quantitatively by letting the isolated macrophages to
34 spread on the surface of the Neubauer counting chamber, staining by trypan blue in a ratio of 1:1 to
35 a final concentration of 0.02 %, and counting.
36
37
38
39
40
41

42 **FACS isolation of macrophages**

43 As a reference experiment, GFP-expressing macrophages were isolated from CrqGal4>GFP male flies
44 using fluorescence-activated cell sorting (FACS). Three hundred flies were anaesthetised with CO₂,
45 washed in PBS and homogenised in 600 mL of PBS using a pestle. The homogenate was sieved through
46 a nylon cell strainer (40 μ m). This strainer was then additionally washed with 200 μ L of PBS, which
47 was added to the homogenate subsequently. The samples were centrifuged (3 min, 4 °C, 800 g) and the
48 supernatant was washed with ice-cold PBS after each centrifugation (3 times). Prior to sorting, samples
49 were transferred to FACS polystyrene tubes using a disposable bacterial filter (50 μ m, Sysmex) and
50 macrophages were sorted into 100 μ L of PBS using a S3™ Cell Sorter (BioRad). Isolated cells were
51 verified by fluorescence microscopy and differential interference contrast.
52
53
54
55
56
57
58
59
60

Gene expression analysis

Gene expression analysis was performed on 100 000 of isolated macrophages. Macrophages were isolated by a cell sorter (S3e Cell Sorter, BioRad) as described in the section Isolation of macrophages, transferred to TRIzol Reagent (Invitrogen) and homogenised using a DEPC-treated pestle. Subsequently, RNA was extracted by TRIzol Reagent (Invitrogen) according to the manufacturer's protocol. Superscript III Reverse Transcriptase (Invitrogen) primed by oligo(dT)20 primer was used for reverse transcription. Relative expression rates for particular genes were quantified on a CFX 1000 Touch Real-Time Cycler (BioRad) using the TP 2x SYBR Master Mix (Top-Bio) in three technical replicates with the following protocol: initial denaturation - 3 min at 95 °C, amplification – 15 s at 94 °C, 20 s at 56 °C, 25 s at 72 °C for 40 cycles. Melting curve analysis was performed at 65–85 °C/step 0.5 °C. The qPCR data were analysed using double delta Ct analysis, and the expressions of specific genes were normalised to the expression of Ribosomal protein 49 (Rp49) in the corresponding sample. The relative values (fold change) to control are shown in the graphs. Samples for gene expression analysis were collected from three independent experiments.

Primer sequences^{30,31}

Rp49 Forward: AAGCTGTCGCACAAATGGCG

Rp49 Reverse: GCACGTTGTGCACCAGGAAC

Hemolectin Forward: GCGTACGAAGGAGATTCTC

Hemolectin Reverse: CACCTCGTGCTTCTGTGT

Croquemort Forward: CTTCTGGCCGGGTATTGCAG

Croquemort Reverse: GCTTTCATAGGCATCAGT

Lactate dehydrogenase Forward: CAGAGAAGTGGAACGAGCTG

Lactate dehydrogenase Reverse: CATGTTCGCCCAAACGGAG

Basket Forward: TACGGCCCATAGGATCAGGT

Basket Reverse: CCCTATATGCTCGCTTGGCA

Relish Forward: ACAGGACCGCATATCG

Relish Reverse: GTGGGGTATTTCCGGC

Diptericin A Forward: GCTGCGCAATCGCTTCTACT

Diptericin A Reverse: TGGTGGAGTGGGCTTCATG

Defensin Forward: GTTCTTCGTTCTCGTGG

Defensin Reverse: CTTTGAACCCCTTGGC

Metchnikowin Forward: AACTTAATCTTGGAGCGA

Metchnikowin Reverse: CGGTCTTGTTGGTTAG

Drosocin Forward: CCATCGTTTTCTGCT

Drosocin Reverse: CCATCGTTTTCTGCT

Enolase Forward: CAACATCCAGTCCAACAAGG

1
2
3 Enolase Reverse: GTTCTTGAAGTCCAGATCGT
4 Phosphofructokinase Forward: AGCTCACATTTCCAAACATCG
5
6 Phosphofructokinase Reverse: TTTGATCACCAGAATCACTGC
7
8 Phosphoglucose isomerase Forward: ACTGTCAATCTGTCTGTCCA
9
10 Phosphoglucose isomerase Reverse: GATAACAGGAGCATTCTTCTCG
11
12 Unpaired3 Forward: AGAACACCTGCAATCTGAAGC
13
14 Unpaired3 Reverse: TCTTGGTGCTCACTGTGGCC
15
16 Imaginal morphogenesis protein late 2 Forward: TTCGCGGTTTCTGGGCACCC
17
18 Imaginal morphogenesis protein late 2 Reverse: GCGCGTCCGATCGTCGCATA
19
20 Eiger Forward: AGCTGATCCCCCTGGTTTTG
21
22 Eiger Reverse: GCCAGATCGTTAGTGCGAGA
23
24 Stat92E forward: CTGGGCATTCACAACAATCCAC
25
26 Stat92E reverse: GTATTGCGCGTAACGAACCG.
27

28 **Results and discussion**

29 **Physico-chemical properties of mGPs**

30
31
32 After the incorporation of iron oxide nanoparticles (IONs) by spray drying, magnetic yeast glucan
33 particles (mGPs) retained the characteristic wrinkled ellipsoid shape known from plain glucan particles
34 (Fig. 2a,b). The volume-mean particle size of mGPs determined by laser diffraction was $5.1 \pm 1.9 \mu\text{m}$
35 (Fig. 2c), which is consistent both with the size of original yeast and with values previously reported for
36 unmodified GPs¹⁴. The fact that the incorporation of magnetic particles did not cause aggregation or
37 changes in the surface morphology of mGPs is crucial for subsequent uptake by phagocytosing cells.
38 Energy-dispersive X-ray spectroscopy (EDX) of plain and magnetic glucan particles (Fig. 2d,e) proved
39 the presence of IONs in mGPs. The Fe content of mGPs determined by EDX was 1.4 % (Table 1). Iron
40 content determined independently by AAS was 1.2 ± 0.1 %. Transmission Electron Microscopy (TEM)
41 analysis revealed that IONs were uniformly distributed within the polysaccharide shell of mGPs
42 (Fig. 2f). Prior to their incorporation into mGPs, dextran-coated IONs had a volume-mean diameter of
43 124.1 nm (measured by dynamic light scattering in water) with a polydispersity index 0.144 (Fig. 2g
44 inset). After incorporation into mGPs, IONs remained well dispersed within the glucan shell (Fig. 2g).
45 Note that the individual iron oxide cores visible as darker spots in the TEM image are smaller than the
46 equivalent hydrodynamic diameter of fully hydrated dextran-coated IONs measured by DLS. This is
47 because the dextran coating is not distinguishable from the beta-glucan background, and also because
48 magnetic nanoparticles are known to form temporary clusters in aqueous media.
49
50
51
52
53
54
55
56
57
58
59
60

The presence of iron oxide in the composite mGPs was additionally proven by measuring XRPD spectra (Fig. 2h). The characteristic crystalline peaks of iron oxide at 21.5°, 35.1°, 67.3°, and 74.4° 2θ were clearly visible in mGPs, while no such peaks were present in plain GPs. A crucial feature with respect to further application is the stability of mGPs in aqueous media in terms of IONs retention. To detect potential loss of IONs during magnetic manipulation in an aqueous medium, mGPs were repeatedly separated by a magnet and redispersed. No free IONs could be detected in the supernatant, indicating that the embedding of IONs in the polysaccharide shell of mGPs was sufficiently strong to prevent the loss of magnetic properties over time. The full characterisation of the magnetic properties of IONs including magnetization curves at 5K and 300K, field cooled and zero field cooled susceptibility have been reported in our recent work²⁹. The macroscopic manifestation of their magnetic properties is the ability to attract mGPs to a permanent magnet and separate them from solution as shown in Fig. 2.

Tab. 1: EDX analysis of mGPs.

Sample	Element symbol	Atomic number	Atomic concentration %
plain GPs	C	6	81.7
	O	8	18.3
	Fe	26	0.0
mGPs	C	6	76.9
	O	8	21.7
	Fe	26	1.4

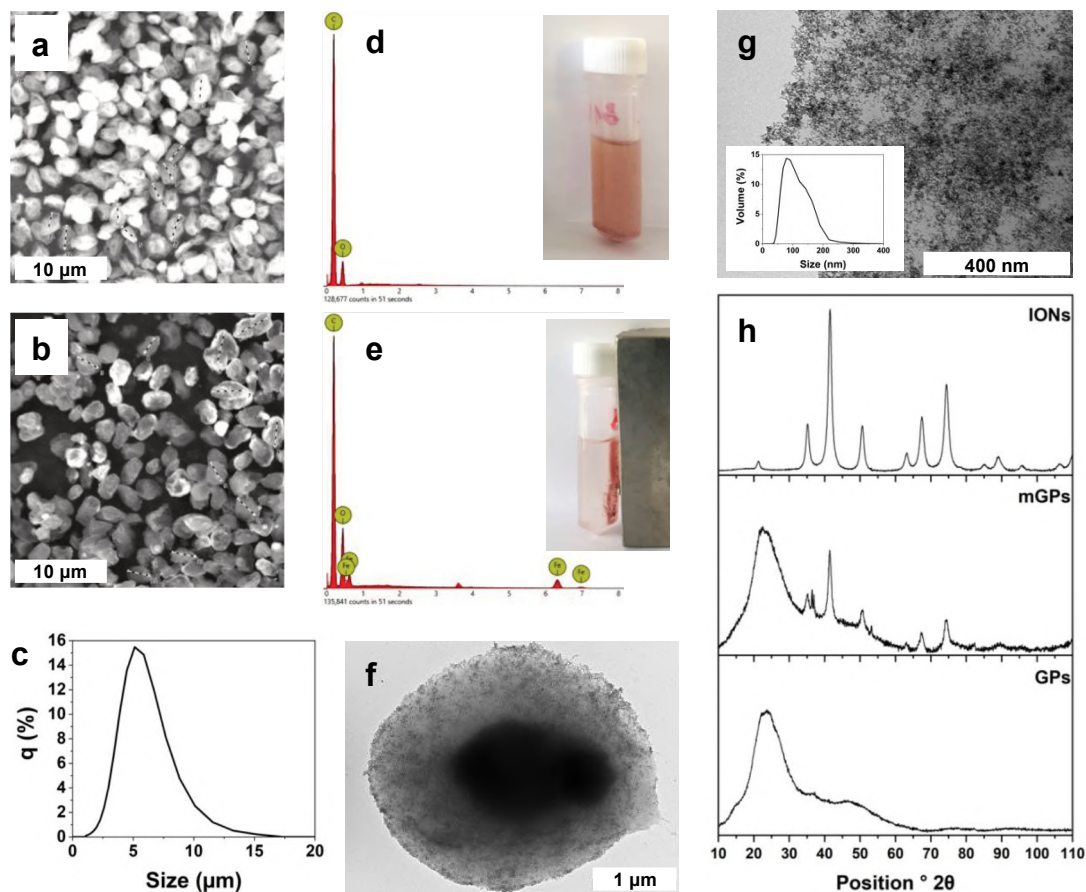
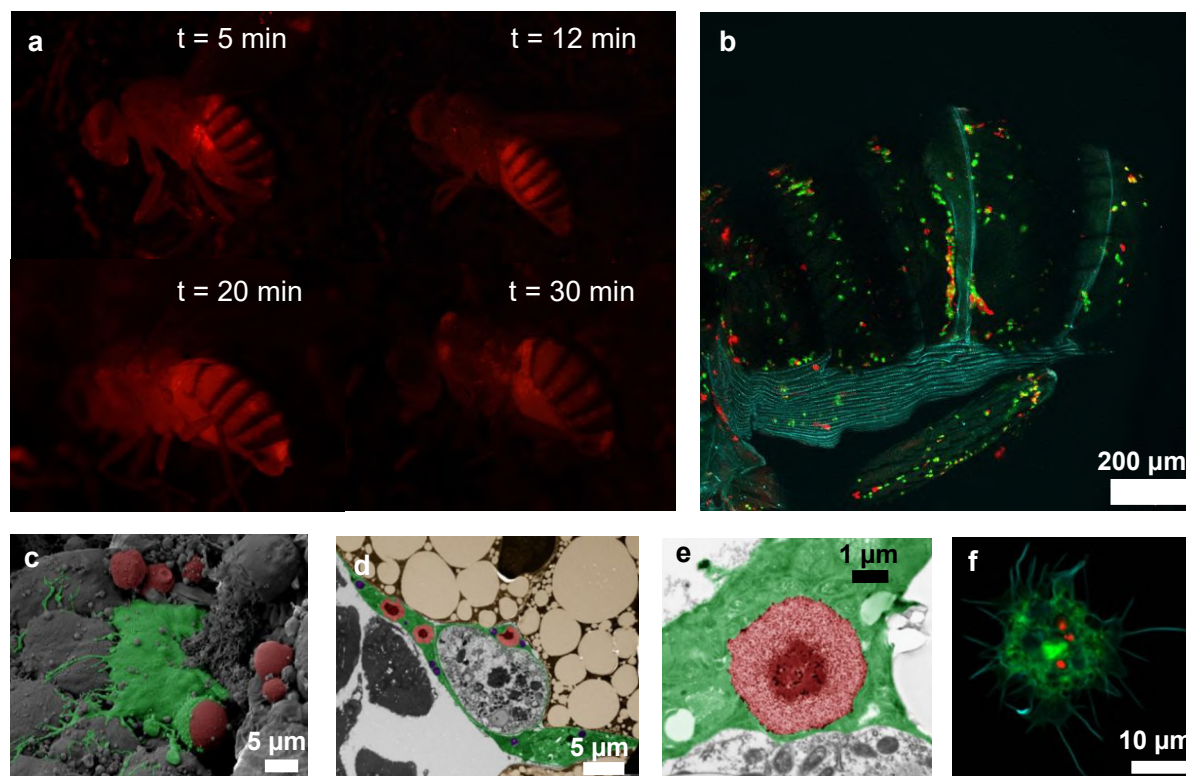


Fig. 2: **a** Scanning electron micrograph (SEM) of plain glukan particles. **b** SEM of mGPs. The scale bar in both SEMs is 8 μm . **c** Particle size distribution of mGPs in water, measured by static light scattering; the volume-mean particle size is $5.1 \pm 1.9 \mu\text{m}$. **d** Energy-dispersive X-ray (EDX) spectrum of plain glukan particles. **e** EDX spectrum of mGPs, proving the presence of iron. The macroscopic manifestation of iron oxide presence in mGPs is their attraction to a magnet as shown in the inset. **f** Transmission electron micrograph (TEM) of a single mGP. The scale bar represents 1000 nm. **g** Detailed TEM showing how iron oxide nanoparticles (IONs) are entrapped and uniformly dispersed within the mGP shell. The scale bar represents 200 nm. The volume-weighted particle size distribution of dextran-coated IONs in water before incorporation into mGPs, measured by DLS, is shown as inset. **h** X-ray powder diffraction (XRPD) spectra of iron oxide nanoparticles (IONs), plain glukan particles (GPs), and magnetic glukan particles (mGPs), proving the presence of iron oxide in mGPs.

Biodistribution and macrophage uptake of mGPs

For investigating the biodistribution of mGPs and subsequent magnetic separation of viable macrophages, a *Drosophila melanogaster* strain bearing an endogenous construct for GFP protein expression in macrophages (Crq>Gal4; UAS2xGFP) was employed. Such macrophages are easily recognised for assaying their morphology and counting. The injection of 0.1 % w/w mGPs led to a fast

1
2
3 systemic distribution through the opened circulatory system of the fly (Fig. 3a). Within 20-30 min after
4 injection, mGPs could be found throughout the body of adult *Drosophila* including distal parts. Within
5 1 hour after injection, clear co-localisation in areas occupied by macrophages was observable (Fig. 3b),
6 which is consistent with the *in vivo* behaviour of plain GPs reported earlier. The internalization of mGPs
7 by macrophages has been proven by the analysis of whole-body cross-sections by SEM and TEM
8 (Fig. 3c-e). Analysis of dissected immune cells revealed that macrophages internalised multiple mGPs
9 (Fig. 3f). In a control experiment, free IONs (not encapsulated in mGPs) injected into adult flies were
10 found not to specifically accumulate in macrophages (Fig. S1, Supporting information).



11
12
13
14
15
16
17
18
19
20
21
22
23
24
25
26
27
28
29
30
31
32
33
34
35
36
37
38
39
40
41 **Fig. 3: a** Time progress of mGP biodistribution in *Drosophila* after injection. Within 20 min, mGPs
42 reach even distal parts of the body of adult flies. **b** Distribution of mGPs (red) in adult *Drosophila* at
43 1 hour after injection, showing co-localisation with macrophages (green). **c** Pseudo-coloured SEM
44 micrograph showing the process of engulfment of mGPs (red) by a macrophage (green) at 20 min after
45 injection. **d** Pseudo-coloured TEM micrograph showing the localization of endocytosed mGPs (red) in
46 the macrophages (green) at 1 hour after injection. **e** TEM micrograph showing the detail of an
47 endocytosed mGP (red) in the cytosol of *Drosophila* macrophage (green). **f** Representative confocal
48 image of a phagocytosing cell (green) from a CrqGal4>GFP adult *Drosophila* injected by mGPs (red)
49 at 1 hour after injection. Actin stained by phalloidin (cyan).

56 Magnetic cell separation and gene expression

Flies injected with mGPs were homogenised 45 min after particle administration and the homogenates were used for magnetic column separation (QuadroMACS™ Separator, LS Columns, Miltenyi Biotec). In parallel, tissue homogenates from flies injected only with a buffer were processed by FACS separation of GFP-expressing macrophages as a control (Fig. 4a). The statistical data accompanying Fig. 4a based on four independent biological replicas are summarised in Table 2. Before magnetic separation, the homogenate contained $0.458\% \pm 0.049\%$ of GFP-positive cells (macrophages). The residue after magnetic separation contained $0.042\% \pm 0.006\%$ of GFP-positive cells, which represents approx. 9.3 % of the original. Thus, magnetic separation was able to extract approx. 90.7 % of all GFP-positive cells originally present in the homogenate, which is comparable to the yield obtained from FACS. The sensitivity of the method, defined as the fraction of macrophages targeted by mGP administration, was $97.9\% \pm 2.5\%$ (N=90; 4 replicates), while its selectivity, defined as the fraction macrophages within the population of cells that have engulfed mGPs, was $100\% \pm 0\%$ (N=100; 5 replicates). Details of the sensitivity and selectivity measurement are provided in Supporting Information. The subsequent isolation of RNA from samples obtained by both approaches provided comparable amount of RNA (Fig. 4d). This was confirmed by quantifying purified RNA on a nanodrop instrument and quantifying the expression level of Rp49, commonly used as a housekeeping gene in *Drosophila*. The concentration of Rp49 in the case of macrophages separated by mGPs and by FACS was 630.6 ± 117.3 ng/ μ L and 586.9 ± 115.4 ng/ μ L, respectively.

Tab. 2: Sort data accompanying Fig. 4a.

Before mag. separation	Rep.1	Rep.2	Rep.3	Rep.4	Average	St.Dev.
Sorted cells	10123021	10185447	10066524	10121254	10124062	48606
GFP possitive	43528	52561	48211	41231	46383	5040
Percent	0.430	0.516	0.479	0.407	0.458	0.049
After mag. separation	Rep.1	Rep.2	Rep.3	Rep.4	Average	St.Dev.
Sorted cells	10185894	10024653	10144874	10132241	10121916	68768
GFP possitive	4086	5112	3844	4117	4290	562
Percent	0.040	0.051	0.038	0.041	0.042	0.006

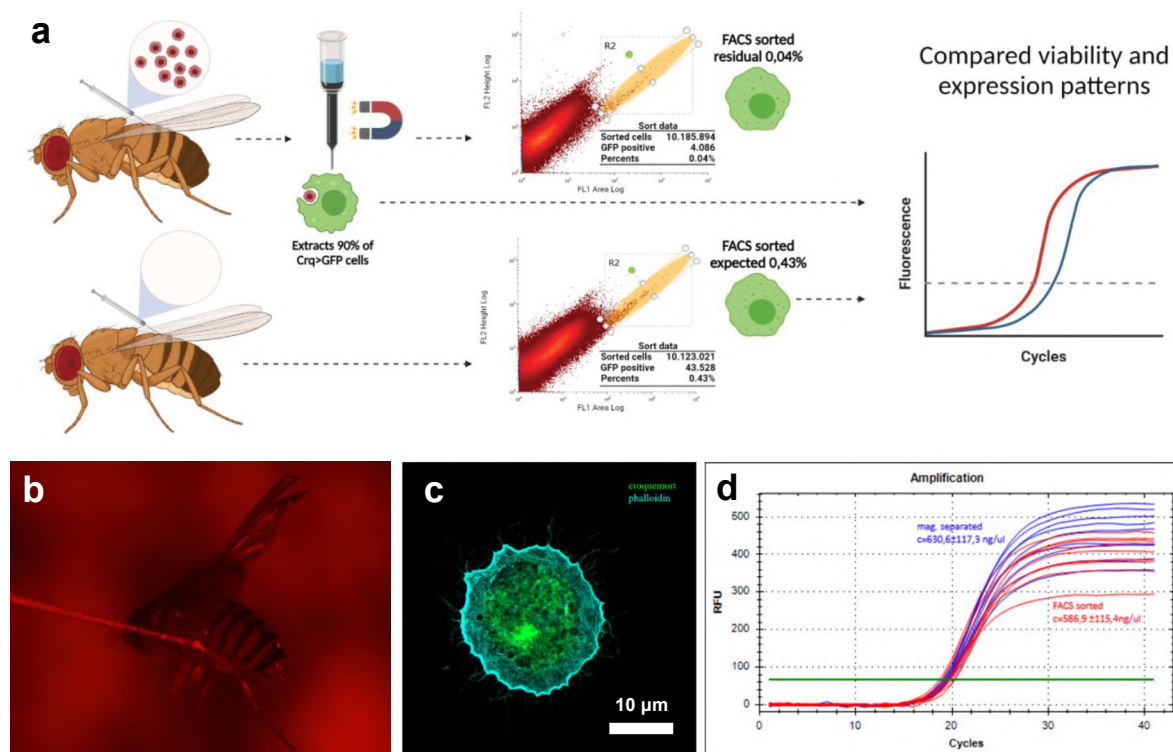


Fig. 4: **a** Schematic representation of the cell separation process. Upper panel: *CrqGal4>GFP* adult flies were injected with 50 nL of 0.1% (w/w) mGPs. The flies were homogenised, and the homogenate was magnetically sieved, resulting in the retention of approx. 90 % of phagocytosing cells. The permeate was collected and FACS sorted based on the endogenously expressed GFP signal (G2 gate). The sorter detected the residual 10 % of unseparated macrophages, constituting 0.04 % out of the overall cell count. Lower panel: In a reference macrophage isolation experiment without mGP injection, the macrophages were sorted from the homogenate only by FACS, giving a yield of 0.46 % out of the overall cell count (Table 2). The phagocytosing cells obtained by mGPs-based magnetic separation and FACS sorter show comparable viability and were subsequently used for RT-qPCR. **b** Visualisation of the injection of adult fly with mGPs. **c** Confocal microscopy visualization of croquemort and phalloidin present in living macrophage after magnetic separation. **d** Quantification of the expression level of Rp49 (commonly used as a housekeeping gene in *Drosophila*) for magnetically and FACS-sorted macrophages.

The viability of the magnetically separated macrophages determined by tryptophan blue assay was 95.5 %. The good condition of the isolated cells manifested itself also by their characteristic spreading phenotype on the surface of a microscopic slide and cytoskeleton remodelling (Fig. 4c). Finally, the expression level of macrophage-specific markers (Hemolectin, croquemort), and immune-related genes (Defensine, Drosocin, Metchnikowin, Dipteracin A), and characteristic readout of cellular stress pathways (Relish, basket) were analysed for both techniques, revealing that macrophages separated by means of magnetic glucan particles possess natural physiological features (Fig. 5). This indicates that the mGP were not cytotoxic and their uptake did not cause any anomalous physiological response in the

macrophages. The expression level of inflammatory cytokines was not found to be significantly different between magnetically separated and FACS-sorted macrophages (Fig. 5), indicating that neither the engulfment of mGPs nor the magnetic separation process itself resulted in the activation of inflammatory response. The macrophages separated by means of mGPs can in principle be subsequently used for various analyses such as gene expression analysis, metabolomics, proteomics, single-cell transcriptomics, and enzymatic activity analysis^{7, 23-25}.

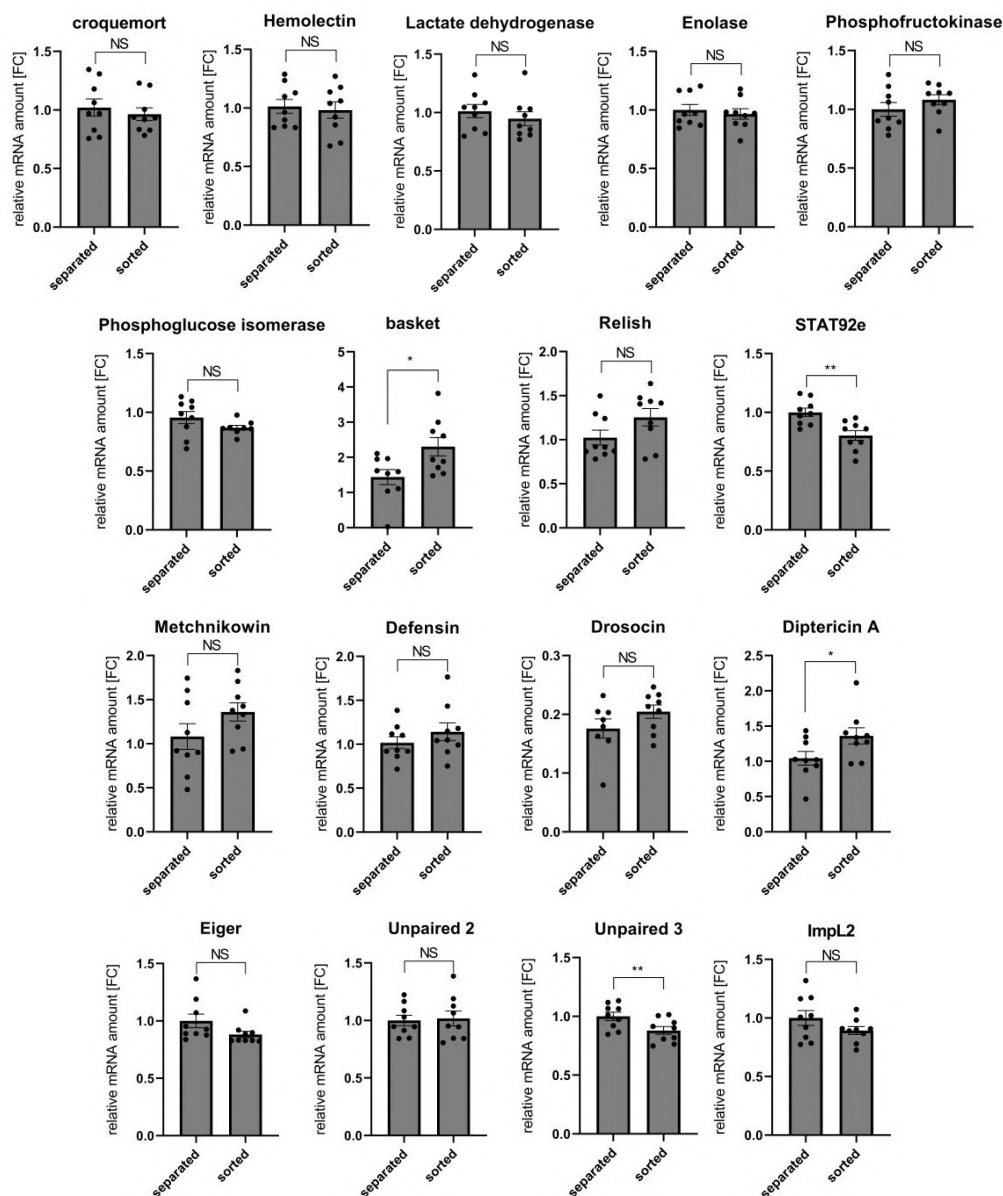


Fig. 5: Comparison of gene expression of macrophage markers (croquemort, Hemolectin), glycolytic gene (Lactate dehydrogenase, Enolase, Phosphofruktokinase, Phosphoglucose isomerase), stress and immune response genes (basket, Relish, STAT92e), antimicrobial peptides (Metchnikowin, Diptericin A, Drosocin, Defensin), and cytokines (Eiger, Upd2, Upd3, ImpL2) in phagocytosing cells

1
2
3 obtained by mGPs based magnetic separation and FACS sorter. The results were compared by 2way
4 ANOVA followed by Tukey's multiple comparisons test. Expression levels normalised against Rp49
5 are reported as fold change relative to levels of analysed gene expression in mGPs separated phagocytes,
6 which were arbitrarily set to 1. The individual dots represent biological replicates with line/bar showing
7 mean \pm SD, asterisks mark statistically significant differences (* p <0.05; ** p <0.01), NS marks
8 statistically insignificant differences.
9
10
11
12
13

14 **Conclusion**

15
16
17 We have prepared magnetic yeast glucan particles (mGPs) using a new approach based on the de-
18 swelling of porous polysaccharide shell during rapid solvent evaporation during spray drying. This
19 enables the irreversible entrapment of a large quantity of independently prepared iron oxide nanoparticle
20 into the mGP structure, in which they remain homogeneously dispersed without undesired
21 agglomeration or clustering. When injected into living *Drosophila*, mGP quickly spread across the body
22 and were readily and selectively taken up by macrophages. This enabled subsequent macrophage
23 isolation from tissue homogenates by a magnetic separation column²⁶⁻²⁸. The key to the successful
24 application of mGPs for magnetic cell separation were three properties: (i) preservation of the size,
25 surface morphology and structural motifs characteristic of original GPs, which are a pre-requisite for
26 immune recognition and efficient phagocytosis; (ii) high concentration of embedded IONs, which is
27 a pre-requisite for generating a sufficiently strong response of the particles to an external magnetic field;
28 and (iii) biocompatibility, which is pre-requisite for good viability and further application of the isolated
29 cells without compromising normal cellular functions and gene expression.
30
31
32
33
34
35
36
37
38
39

40 Unlike magnetic separation based on attaching magnetic beads to the external cell surface *via* specific
41 antibodies, the method based on mGPs has several advantages: (i) it enables antibody- and label-free
42 isolation of immune cells; (ii) it covers all cells in the host organism that may participate in the
43 engulfment of pathogens, with no need for knowing these cells *a priori*; (iii) due to a highly
44 evolutionarily conserved feature (phagocytosis), the method can be used basically in all animals, not
45 just insects; (iv) the method allows short processing time, it is gentle, and the cells are exposed only to
46 physiological buffers and no additional chemicals. Overall, it can be concluded that the fabrication of
47 magnetic yeast glucan particles (mGPs) represents a suitable strategy for isolating macrophages,
48 sufficient in amount and in quality to perform gene expression analyses. Since this approach is
49 independent of having endogenously expressed fluorescent markers or binding of cells via specific
50 antibodies against surface antigenic epitope, it may also be adapted for other situations where it is
51 desirable to separate a population of live phagocytic cells from insect and non-insect species. Of course,
52 it should also be noted that the presence of mGPs in the macrophages may not be universally desirable
53
54
55
56
57
58
59
60

1
2
3 (e.g. when studying iron metabolism), but based on the data presented in this work (viability,
4 functionality and gene expression), the magnetically separated macrophages were not negatively
5 affected by the engulfment of mGPs.
6
7
8

9 **Supporting Information**

10 SI-1 contains the results of a reference experiment in which free iron oxide nanoparticles (i.e., not
11 embedded within mGPs) were injected into *Drosophila*. The experiments demonstrated that: (i) unlike
12 mGPs, free magnetic nanoparticles are not specifically taken up by macrophages; and (ii) macrophages
13 from *Drosophila* treated with free nanoparticle are not sufficiently magneto-responsive and cannot be
14 separated by a magnetic field. SI-2 contains information on the evaluation of Selectivity, Sensitivity and
15 Purity of the magnetic separation method. SI-3 contains information about the gating strategy used for
16 cell sorting.
17
18
19
20
21
22

23 **Acknowledgement**

24 We would like to acknowledge financial support by the Czech Science Foundation, projects no. 19-
25 26127X (F.S) and 20-14030S (A.B.).
26
27
28
29

30 **Author contributions**

31 G. K. and I. S. have contributed equally to this work. I. S., G. K., A. B., and F. Š. conceived the project.
32 I. S., G. K. and V. K. conducted the experiments. A. B. A. developed method for the preparation of
33 nanoparticles and synthesised IONs. P. U. analysed nanoparticles and composite particles on TEM. I.
34 S., G. K., A. B. and F. Š. designed the experiments and analysed the results. A. B. and F. Š. supervised
35 the study, provided guidance, and funding. I. S., G. K., A. B. and F. Š. wrote the initial draft of the
36 manuscript. I. S. and F. Š. wrote the final manuscript with input from all authors.
37
38
39
40
41
42

43 **Competing financial interests**

44 The authors declare no competing financial interests.
45
46
47

48 **References**

- 49 (1) Hochmuth, R. M. Micropipette aspiration of living cells. *Journal of biomechanics* 2000, 33 (1), 15-
50 22.
51 (2) Robert, D.; Pamme, N.; Conjeaud, H.; Gazeau, F.; Iles, A.; Wilhelm, C. Cell sorting by endocytotic
52 capacity in a microfluidic magnetophoresis device. *Lab on a Chip* 2011, 11 (11), 1902-1910.
53 (3) Miltenyi, S.; Müller, W.; Weichel, W.; Radbruch, A. High gradient magnetic cell separation with
54 MACS. *Cytometry: The Journal of the International Society for Analytical Cytology* 1990, 11 (2), 231-
55 238.
56 (4) Fu, A. Y.; Spence, C.; Scherer, A.; Arnold, F. H.; Quake, S. R. A microfabricated fluorescence-activated
57 cell sorter. *Nature Biotechnology* 1999, 17 (11), 1109-1111.
58 (5) Levine, B. L.; Miskin, J.; Wonnacott, K.; Keir, C. Global manufacturing of CAR T cell therapy.
59 *Molecular Therapy-Methods & Clinical Development* 2017, 4, 92-101.
60

- 1
2
3 (6) Bieback, K.; Fernandez-Munoz, B.; Pati, S.; Schäfer, R. Gaps in the knowledge of human platelet
4 lysate as a cell culture supplement for cell therapy: a joint publication from the AABB and the
5 International Society for Cell & Gene Therapy. *Cytotherapy* 2019, 21 (9), 911-924.
- 6 (7) Warkiani, M. E.; Khoo, B. L.; Wu, L.; Tay, A. K. P.; Bhagat, A. A. S.; Han, J.; Lim, C. T. Ultra-fast, label-
7 free isolation of circulating tumor cells from blood using spiral microfluidics. *Nature protocols* 2016, 11
8 (1), 134-148.
- 9 (8) Law, S. Antigen shedding and metastasis of tumour cells. *Clinical and experimental immunology*
10 1991, 85 (1), 1.
- 11 (9) Bajgar, A.; Saloň, I.; Krejčová, G.; Doležal, T.; Jindra, M.; Štěpánek, F. Yeast glucan particles enable
12 intracellular protein delivery in *Drosophila* without compromising the immune system. *Biomaterials*
13 *Science* 2019, 7 (11), 4708-4719.
- 14 (10) Soto, E. R.; Caras, A. C.; Kut, L. C.; Castle, M. K.; Ostroff, G. R. Glucan particles for macrophage
15 targeted delivery of nanoparticles. *Journal of Drug Delivery* 2012, 2012, 143524.
- 16 (11) Rotrekl, D.; Devriendt, B.; Cox, E.; Kavanová, L.; Faldyna, M.; Šalamúnová, P.; Baďo, Z.; Prokopec,
17 V.; Štěpánek, F.; Hanuš, J. Glucan particles as suitable carriers for the natural anti-inflammatory
18 compounds curcumin and diplacone—Evaluation in an ex vivo model. *International Journal of*
19 *Pharmaceutics* 2020, 582, 119318.
- 20 (12) Aouadi, M.; Tesz, G. J.; Nicoloso, S. M.; Wang, M.; Chouinard, M.; Soto, E.; Ostroff, G. R.; Czech, M.
21 P. Orally delivered siRNA targeting macrophage Map4k4 suppresses systemic inflammation. *Nature*
22 2009, 458 (7242), 1180-1184.
- 23 (13) Šalamúnová, P.; Krejčí, T.; Ryšánek, P.; Saloň, I.; Kroupová, J.; Hubatová-Vacková, A.; Petřík, J.;
24 Grus, T.; Lukáč, P.; Kozlík, P. Serum and lymph pharmacokinetics of nilotinib delivered by yeast glucan
25 particles per os. *International Journal of Pharmaceutics* 2023, 122627.
- 26 (14) Saloň, I.; Hanuš, J.; Ulbrich, P.; Štěpánek, F. Suspension stability and diffusion properties of yeast
27 glucan microparticles. *Food and Bioprocess Processing* 2016, 99, 128-135.
- 28 (15) Ruphuy, G.; Saloň, I.; Tomas, J.; Šalamúnová, P.; Hanuš, J.; Štěpánek, F. Encapsulation of poorly
29 soluble drugs in yeast glucan particles by spray drying improves dispersion and dissolution properties.
30 *International Journal of Pharmaceutics* 2020, 576, 118990.
- 31 (16) Šalamúnová, P.; Saloň, I.; Ruphuy, G.; Kroupová, J.; Balouch, M.; Hanuš, J.; Štěpánek, F. Evaluation
32 of β -glucan particles as dual-function carriers for poorly soluble drugs. *European Journal of*
33 *Pharmaceutics and Biopharmaceutics* 2021, 168, 15-25.
- 34 (17) Mirza, Z.; Soto, E. R.; Hu, Y.; Nguyen, T.-T.; Koch, D.; Aroian, R. V.; Ostroff, G. R. Anthelmintic
35 activity of yeast particle-encapsulated terpenes. *Molecules* 2020, 25 (13), 2958.
- 36 (18) Baert, K.; De Geest, B. G.; De Rycke, R.; Da Fonseca Antunes, A. B.; De Greve, H.; Cox, E.; Devriendt,
37 B. β -glucan microparticles targeted to epithelial APN as oral antigen delivery system. *Journal of*
38 *Controlled Release* 2015, 220, 149-159.
- 39 (19) Patel, A.; Asik, D.; Snyder, E. M.; Dilillo, A. E.; Cullen, P. J.; Morrow, J. R. Binding and release of FeIII
40 complexes from glucan particles for the delivery of T1 MRI contrast agents. *ChemMedChem* 2020, 15
41 (12), 1050-1057.
- 42 (20) Figueiredo, S.; Moreira, J. N.; Geraldés, C. F. G. C.; Rizzitelli, S.; Aime, S.; Terreno, E. Yeast cell wall
43 particles: a promising class of nature-inspired microcarriers for multimodal imaging. *Chemical*
44 *Communications* 2011, 47 (38), 10635-10637.
- 45 (21) Hauser, A. K.; Mathias, R.; Anderson, K. W.; Hilt, J. Z. The effects of synthesis method on the
46 physical and chemical properties of dextran coated iron oxide nanoparticles. *Materials chemistry and*
47 *physics* 2015, 160, 177-186.
- 48 (22) Aysan, A. B.; Knejzlík, Z.; Ulbrich, P.; Šoltys, M.; Zdražil, A.; Štěpánek, F. Effect of surface
49 functionalisation on the interaction of iron oxide nanoparticles with polymerase chain reaction.
50 *Colloids and Surfaces B: Biointerfaces* 2017, 153, 69-76.
- 51 (23) Vollmers, A. C.; Mekonen, H. E.; Campos, S.; Carpenter, S.; Vollmers, C. Generation of an isoform-
52 level transcriptome atlas of macrophage activation. *Journal of Biological Chemistry* 2021, 296.
- 53
54
55
56
57
58
59
60

- 1
2
3 (24) Rattigan, K. M.; Pountain, A. W.; Regnault, C.; Achcar, F.; Vincent, I. M.; Goodyear, C. S.; Barrett,
4 M. P. Metabolomic profiling of macrophages determines the discrete metabolomic signature and
5 metabolomic interactome triggered by polarising immune stimuli. *PLoS ONE* 2018, 13 (3), e0194126.
6 (25) Specht, H.; Emmott, E.; Petelski, A. A.; Huffman, R. G.; Perlman, D. H.; Serra, M.; Kharchenko, P.;
7 Koller, A.; Slavov, N. Single-cell proteomic and transcriptomic analysis of macrophage heterogeneity
8 using SCoPE2. *Genome biology* 2021, 22 (1), 1-27.
9 (26) Grützkau, A.; Radbruch, A. Small but mighty: How the MACS[®]-technology based on nanosized
10 superparamagnetic particles has helped to analyze the immune system within the last 20 years.
11 *Cytometry Part A* 2010, 77 (7), 643-647.
12 (27) Radbruch, A.; Mechtold, B.; Thiel, A.; Miltenyi, S.; Pflüger, E. High-gradient magnetic cell sorting.
13 *Methods in cell biology* 1994, 42, 387-403.
14 (28) Zborowski, M. Physics of magnetic cell sorting. In *Scientific and clinical applications of magnetic*
15 *carriers*, Springer, 1997; pp 205-231.
16 (29) Navrátil, O.; Lizoňová, D.; Slonková, K.; Mašková, L.; Zdražil, A.; Sedmidubský, D.; Štěpánek, F.
17 Antibiotic depot system with radiofrequency controlled drug release. *Colloids and Surfaces B:*
18 *Biointerfaces* 2022, 217, 112618.
19 (30) Neyen, C.; Bretscher, A.J.; Binggeli, O; Lemaitre, B. Methods to study *Drosophila* immunity.
20 *Methods* 2014, 68, 116-128.
21 (31) DRSC FlyPrimerBank (flyrnai.org)
22
23
24
25
26
27
28
29
30
31
32
33
34
35
36
37
38
39
40
41
42
43
44
45
46
47
48
49
50
51
52
53
54
55
56
57
58
59
60

Supporting Information

Magnetic yeast glucan particles for antibody-free separation of viable macrophages from *Drosophila melanogaster*

Gabriela Krejčová, Ivan Saloň, Vojtěch Klimša, Pavel Ulbrich, Ayse Beyza Aysan, Adam Bajgar, František Štěpánek

SI-1: *In vivo* localisation of free IONs

After injecting adult *Drosophila* with the dextran coated iron oxide nanoparticles (IONs) of approximate 10 nm size their distribution was analysed throughout the body. Most of these particles were found in the colocalisation with *Drosophila* macrophages, however there was a significant accumulation of clustering magnetic particles in circulation, aortic region, and oenocytes (Fig. S1). Moreover, despite the substantial accumulation of these particles in macrophages, they did not produce enough magnetic force necessary for the magnetic separation of the cells.

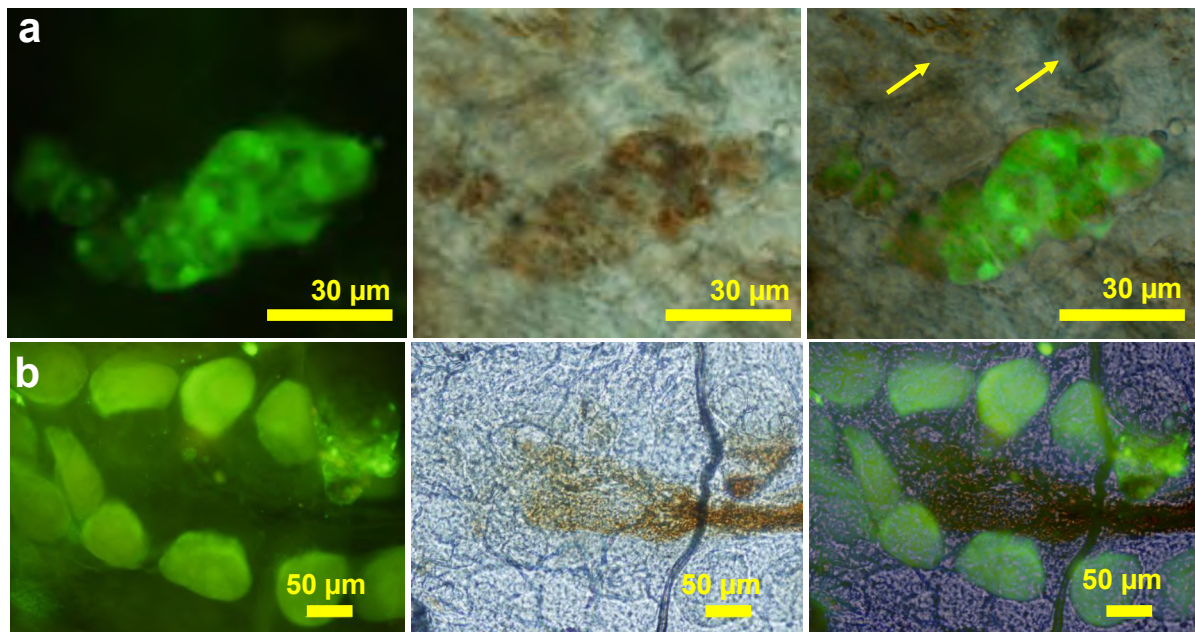


Fig. S1: **a** Injection of CrqGal4>GFP adult *Drosophila* by unbound Dex-SPIONs (brown) results in their ectopic localisation. Arrows show the localization of the nanoparticles outside the macrophages (green). **b** Ectopic deposition of magnetic nanoparticles (brown) in the aorta. Autofluorescence in the green channel was used to visualize the pericardial cells.

SI-2: Evaluation of Selectivity, Sensitivity and Purity

Sensitivity – what proportion of macrophages was targeted by mGP administration?

Experimental approach: flies bearing GFP positive macrophages (GREEN) were injected by Rhodamine-labeled GPs (RED). Cell-sorted macrophages based on GFP signal were subsequently inspected for the presence of Rhodamine-GPs by confocal microscopy. The experiment was done in four replicates, the percentage of cells containing GPs was as follows.

Sensitivity	GFP positive cells	containing RHOD.-GPs	Percent	Stdev.
	20	20	100.0	
	23	23	100.0	
	22	21	95.5	
	25	24	96.0	
Sum/sum/average/stdev.	90	88	97.9	2.5

Selectivity – to what extent could mGPs be engulfed by other cells than macrophages?

Experimental approach based on image analysis: TEM images of the mGP-injected flies were inspected on the distribution of mGPs throughout the body. Result: from 100 inspected TEM images, mGPs were found only in macrophages-like cells. mGPs were found in 142 macrophage-like cells in all inspected TEM images (N=150), that means in 94.7%.

Experimental approach based on fluorescence: flies carrying GFP-positive macrophages (GREEN) were injected by both mGPs (no color) and phagocytic marker Sa-pHrodo (RED). Cells containing mGPs were isolated and inspected for the presence of phagocytic marker by confocal microscopy. Nuclei of all isolated cells were labeled by DAPI (BLUE).

Selectivity	mGPs-separated cells	pHrodo content	Percent	Stdev.
	25	25	100	
	25	25	100	
	25	25	100	
	25	25	100	
Sum/sum/average/stdev.	100	100	100	0

Purity – how many of mGP separated cells are GFP positive and how many of them are macrophages?

Experimental approach: Flies were co-injected with mGPs and independent phagocytic marker (S.a. pHrodo, giving the red fluorescent signal). After magnetic cell separation, the fraction of cells displaying the signal of phagocytic marker was calculated. Result: 100% of mGP separated cells display phagocytosis of S.a. pHrodo marker, from which 98.0%±2.3% were GFP positive (N=100; 4 replicates).

Purity	mGPs-separated cells	GFP signal	Percent	Stdev.
	25	24	96	
	25	25	100	
	25	24	96	
	25	25	100	
Sum/sum/average/stdev.	100	98	98.0	2.3

SI-3: Gating strategy

The gating strategy was based on the comparison of fly strain bearing GFP-positive macrophages and controls. In the first window shown below, the duplets and bigger cell clusters were excluded in side- and forward-scatter scanners. GFP-positive macrophages were detected as a cloud of cells missing in the negative controls (genetically related flies missing the GFP-reporter). The identity of cells was confirmed by microscopy observation of GFP signal and the ability of these cells to spread on microscopy glass and phagocyte S.a. pHrodo labelled particles. Negative is shown on the left, positive on the right in Fig. S2 bellow.

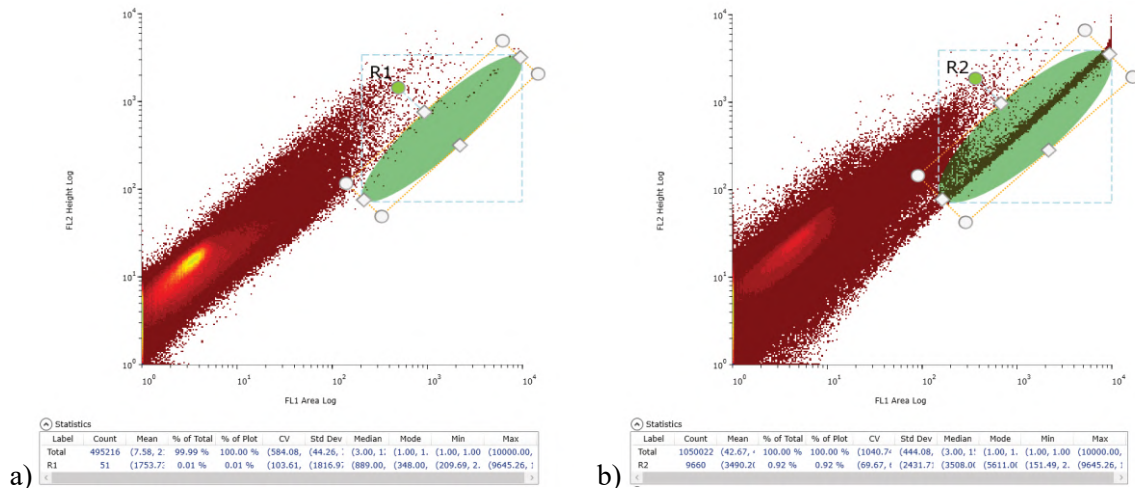


Fig. S2: Sort gating for GFP-expressing macrophages. a) negative, b) positive.

Macrophages represent immensely versatile cells whose functions range from protection of the organism against invading pathogens, wound healing and regeneration to clearance of senescent and apoptotic cells, destruction of tumors and foreign materials, morphogenesis, and maintenance of homeostasis. Regarding their involvement in bacterial infection, they have been studied mainly for their “canonical” roles, such as the ability to recognize, engulf and destroy pathogens and to activate the adaptive immune response. Their “non-canonical” role in regulating systemic metabolic setup during the acute immune response has not been fully explored up to now.

Significant deviations in systemic metabolic setup, loss of stores, and aberrations in levels of circulating carbohydrates and lipids are well-known phenomena accompanying severe infectious states in humans and even in insects (Gallin, Kaye and O’Leary, 1969; Sammalkorpi *et al.*, 1988; Grunfeld *et al.*, 1992; Hardardóttir, Grunfeld and Feingold, 1995; Chambers, Song and Schneider, 2012). Yet, the mechanism underlying these systemic metabolic changes is not completely understood.

Activated macrophages are highly energy demanding cells due to their pro-inflammatory metabolic polarization. Mammalian macrophages challenged by bacterial pathogens undergo a cellular metabolic switch characterized by aerobic glycolysis and thus increased demands for glucose and other metabolites. We hypothesize that to satisfy these needs, systemic energy handling must be adjusted accordingly to suppress nutrient consumption by non-immune tissues and induce mobilization of energy stores that will be available to activated immune cells. In this regard, we assume that activated macrophages become superior to other tissues during infection and that macrophage metabolic activation is the driving force behind the induction of systemic metabolic changes commonly observed in septic patients. This theory is supported by a number of publications documenting the trade-offs between immune system activation vs. reproduction or growth (Gray and Bradley, 2005; McKean *et al.*, 2008; Bashir-Tanoli and Tinsley, 2014; Howick and Lazzaro, 2014; Bajgar *et al.*, 2015). Nonetheless, experimental evidence for this phenomenon is lacking.

Drosophila melanogaster represents an excellent model organism for such immunometabolic studies. Yet, the metabolic setup of immune cells has not been properly addressed in insects so far, and the M1/M2 polarization paradigm has not been investigated in fruit flies up to now. The evidence of metabolic rearrangement toward aerobic glycolysis is only indirect, as elevated expression of glycolytic enzymes including *Ldh* can be found in transcriptomic analyses of larval immune cells in response to wasp infestation and *Escherichia coli* infection (Irving *et al.*, 2005; Johansson, Metzendorf and Söderhäll, 2005). Thus, the immunometabolic studies in flies suffer significantly from a lack of knowledge about whether insect immune cells undergo metabolic polarization after stimulation analogous to what has been described in vertebrates (Mills, 2012).

Therefore, the first objective was to investigate the metabolic setup of activated macrophages in *Drosophila*. To induce severe infection, the fruit flies were injected with a precisely balanced dose of *S.*

pneumoniae, an extracellular Gram positive pathogenic bacterium. Whether an individual survives such an infection depends heavily of the ability of macrophages to engulf and eliminate this bacterium. Subsequent analyses of activated macrophages revealed that they exhibit increased uptake of glucose and higher expression and activity of glycolytic enzymes, including LDH, which converts pyruvate to lactate. In agreement with these data, the titer of lactate was found to be elevated in the circulation of infected flies. Notably, these changes were induced by the transcription factor HIF1 α , as flies with macrophage-specific HIF1 α knockdown do not display the aforementioned infection-induced metabolic rearrangement in immune cells. Moreover, we have demonstrated that such a cellular metabolic switch is essential for resistance to infection since flies with macrophage-specific silencing of LDH or HIF1 α display elevated pathogen burden and reduced survival of the infection. The results of this work thus document that insect immune cells undergo a pro-inflammatory metabolic polarization to aerobic glycolysis upon infection similar to their mammalian counterparts and that the mechanism of its induction is conserved between fruit flies and mammals. Taken together, we addressed an apparent gap in insect immunometabolic research and experimentally documented that insect immune cells polarize to an M1-like phenotype when challenged by bacterial infection. Further evidence for metabolic polarization of *Drosophila* immune cells was provided a year later by Madhwal and colleagues. In this work, the authors revealed that the expression of *Hif1 α* and *Ldh* is upregulated in lamellocytes after wasp infestation and their knockdown results in perturbed lamellocyte formation (Madhwal *et al.*, 2020).

Additionally, we revealed that infection induces metabolic rearrangement not only in the insect immune cells themselves, but also significantly affects systemic energy handling. Indeed, we detected elevated titers of circulating glucose, trehalose, triglycerides, cholesterol, and cholesteryl-ester during the acute phase of infection, while glycogen and lipid stores become depleted in the fat body. Interestingly, we revealed that these systemic changes are induced by activated immune cells, as we previously hypothesized. In particular, they are caused by the adoption of pro-inflammatory metabolic polarization of the immune cells, as macrophage-specific knockdown of either LDH or HIF1 α prevents these systemic changes.

Based on these data, we further focused on unraveling the molecular mechanism of induction of the systemic metabolic rearrangement. We speculated that immune cells release certain signaling molecules whose production must be linked to pro-inflammatory cell polarization, and which may thus translate the metabolic demands of the activated macrophages to non-immune organs. To reveal such signaling factors, we performed RNA-seq analysis of macrophages isolated from flies challenged with streptococcal infection. Among others, we noticed that activated macrophages dramatically increase the expression of *Impl2*. This factor has been previously described to be secreted by neoplastic tumor cells and acts as a potent inducer of systemic organ wasting since it evokes degeneration of ovaries, fat body and muscles (Figuroa-Clarevega and Bilder, 2015; Kwon *et al.*, 2015). In addition, it is known to affect insulin signaling (Honegger *et al.*, 2008). For these reasons, we further tested its potential involvement in infection-induced adjustment of systemic metabolism. We revealed that the production of IMPL2 by

activated macrophages is linked to their pro-inflammatory metabolic polarization, since its expression is directly regulated by HIF1 α , a master-regulator of the M1 metabolic switch. Moreover, the macrophage-derived IMPL2 indeed induces increased levels of carbohydrates and lipids in the circulation of infected flies. The underlying mechanism behind these systemic metabolic changes is the attenuation of insulin signaling in adipose tissue *via* the previously described affinity of IMPL2 for DILPs (Honegger *et al.*, 2008). As a result, adipose tissue adopts a FOXO-dependent transcription program, leading to increased expression of lipolytic enzymes and genes involved in lipoprotein assembly. Increased levels of circulating nutrients are subsequently utilized by activated macrophages to efficiently eliminate the pathogen, as flies with macrophage-specific *Impl2* knockdown or fat body-specific silencing of lipases and genes involved in lipoprotein assembly display decreased phagocytic capability, increased pathogen load, and impaired survival of infection. Nonetheless, what the macrophages need the lipids for remains a matter of debate. We speculate that they may be utilized for remodeling of the membrane, synthesis of catecholamines, and epigenetic reprogramming (Remmerie and Scott, 2018; Yan and Horng, 2020). Interestingly, research conducted by Lee and colleagues has shown that that Yki-induced tumors overcome the action of IMPL2 by locally increasing Wnt/Wingless (Lee *et al.*, 2021). Despite we did not investigate the level of insulin sensitivity in macrophages, this study may suggest a mechanism by which the immune system can potentially evade IMPL2-induced insulin resistance. Importantly, our data document that both macrophage metabolic polarization and IMPL2-induced systemic metabolic changes are essential for survival of infection. Hence, our data suggest that silencing of insulin signaling may be perceived as an adaptive process in the context of infection, although it is mostly described as an adverse state in conjunction with obesity and diabetes.

In this project, we also generated data indicating that the mammalian IMPL2 homolog IGBBP7 secreted by Kupffer cells exerts an analogous effect on hepatocytes in the mammalian liver during experimental simulation of infectious states. We showed that THP-1 cell lines of human macrophages produce the mammalian *Impl2* homolog *IGFBP7* in response to LPS treatment. In line with our observations in fruit flies, the expression of *IGFBP7* is transcriptionally regulated by HIF1 α . Elevated *IGFBP7* levels were also detected in samples of human liver macrophages after LPS treatment. In addition, administration of recombinant IGBBP7 to 3D liver spheroids resulted in elevated titers of LDL and VLDL in the culture medium, and its silencing resulted in decreased expression of apolipoproteins in murine hepatocytes. These data thus suggest that macrophage-induced mobilization of lipoproteins represents an evolutionarily conserved mechanism by which phagocytes secure nutrients for their function upon bacterial infection. Although the molecular mechanism underlying IGBBP7-induced mobilization of lipoproteins in hepatocytes was not addressed in this study, we have documented the mechanism of its action under different conditions in another paper.

In collaboration with Dr. Aouadi's research team (Aouadi Lab, Karolinska Institutet, Stockholm, Sweden), we showed that Kupffer cells produce IGBBP7 in obese individuals fed a high fat diet. Analogous to what we observed in infection, IGBBP7 regulates liver metabolism and induces

hyperglycemia. In particular, it binds to the insulin receptor and evokes lipogenesis and gluconeogenesis in hepatocytes *via* activation of ERK signaling due to increased recruitment of an upstream regulator of the ERK pathway, Shc, to the insulin receptor. *IGFBP7* mRNA has previously been described as a target of adenosine deaminase acting on RNA (ADAR) enzymes (Levanon, 2005; Godfried Sie *et al.*, 2012). In our conditions, *IGFBP7* RNA was edited at a higher frequency in obese insulin resistant individuals than in insulin sensitive patients. Moreover, Kupffer cell-specific silencing of *Igfbp7* expression significantly improved blood glucose levels and alleviated hepatic steatosis in mice.

In agreement with the mammalian data, the expression of *ImpL2* is significantly elevated in macrophages in response to high fat feeding. Moreover, macrophage-specific knockdown of *ImpL2* leads to a decrease in circulating glucose levels and prevents lipid accumulation in these individuals at the whole-body level. Given that silencing of *Igfbp7/ImpL2* specifically in Kupffer cells/insect macrophages improves systemic metabolism in mice and flies, respectively, we propose that IGFBP7 could serve as a potential therapeutic target in insulin resistant individuals. In conclusion, despite the production of IGFBP7/IMPL2 by macrophages is beneficial upon infection by extracellular bacteria, it becomes maladaptive when induced chronically in obese individuals.

Improper macrophage activation and the subsequent secretion of cytokines and other signaling factors have been repeatedly documented to play an adverse role during many chronic pathological conditions such as metabolic syndrome, atherosclerosis or autoimmune diseases (Van Lent *et al.*, 1998; Lumeng *et al.*, 2008; McNelis and Olefsky, 2014; von Ehr, Bode and Hilgendorf, 2022). Thus, there is an inquiry for macrophage-specific delivery systems of various metabolic inhibitors or other drugs to reverse their polarization phenotype without affecting other tissues. In an attempt to develop such, we tested the feasibility of yeast-derived GPs. β -glucans are carbohydrate polymers present in the cell walls of yeast, fungi, bacteria, and plants and are readily recognized by macrophages. It has been suggested that GPs can be exploited as a vaccine delivery vehicle since they have been widely recognized as safe since 2007 and established well in large animals and humans (De Smet, Allais and Cuvelier, 2014; Blanco, Shen and Ferrari, 2015). However, their preclinical testing requires a suitable model organism that is simple and inexpensive, yet relevant and well defined. We propose that *Drosophila melanogaster* represents such a system.

In our research, the GPs were prepared in collaboration with the research group of Prof. František Štěpánek (Chobotix, VSCHT, Prague, Czech Republic) by purification of *S. cerevisiae*. We have shown that these particles composed of β -1,3-glucans spread through the fruit fly body within 20 minutes and accumulate in sites of macrophage occurrence subsequently. Indeed, they become efficiently engulfed by these cells and have a negligible effect on expression of AMPs in macrophages. Moreover, they do not compromise the capability of these cells to fight pathogen. These data thus provided a stepping stone for GP-based delivery tools carrying various compounds as cargo.

First, we first tested the suitability of GPs for macrophage-specific delivery of transcription factors. To this end, GPs were loaded with Gal4, as it is commonly used in *Drosophila* to study targeted

gene expression and hence it allows for easy monitoring. Indeed, injection of the Gal4 protein encapsulated in GPs into adult flies bearing the UAS-mCherry transgenic reporter leads to the production of a red fluorescent signal exclusively in macrophages. We thus believe that *D. melanogaster* represents a suitable model for *in vivo* testing of phagocyte-specific delivery systems and that GPs are an effective tool for an intracellular protein delivery to phagocytes.

Recently, 300 FDA-approved drugs have been identified *in vitro* that affect macrophage metabolic settings (Hu *et al.*, 2021). However, their administration should be limited to macrophages, as systemic administration of many of these drugs may be accompanied by various adverse effects. Hence, in a follow-up project, we aimed to exploit GPs to deliver a small-molecule metabolic inhibitor atorvastatin, a widely described drug for lowering cholesterol levels *via* inhibition of HMGCR, a rate-limiting enzyme in the mevalonate pathway. Atorvastatin encapsulated in GPs results in decreased enzymatic activity of HMGCR specifically in macrophages without affecting any other tissue tested, and we therefore propose that GPs are also suitable for macrophage-specific delivery of small-metabolite inhibitors.

In addition, while conducting this research, we revealed that macrophages require the mevalonate pathway to effectively fight the pathogen. Notably, both the macrophage-specific delivery of atorvastatin by GPs and the macrophage-specific silencing of HMGCR results in decreased expression of AMPs and glycolytic enzymes in these cells. In agreement with this data, macrophages display decreased bactericidal capability, resulting in reduced individual's survival of infection. Since insects must rely on dietary supplementation of cholesterol as they have lost the ability to synthesize this molecule, explaining the necessity of the mevalonate pathway for survival of the infection may be more complex. We suggest that it is crucial for terpenoid backbone synthesis used for the production of steroid compounds (Norris and Dennis, 2014). Interestingly, it has been documented that the mevalonate pathway is indispensable for the formation of trained immunity in mammalian macrophages, and hence this explanation should be addressed by subsequent research (Bekkering *et al.*, 2018). Our results thus indicate that while suppression of pro-inflammatory macrophage polarization may be perceived as beneficial if the intended purpose is to affect macrophage activity, the potential negative impact of atorvastatin on macrophage bactericidal function should be addressed in mammals, and a similar study should be conducted in vertebrates, as this drug was the most prescribed medicine in the US in 2020 (Statista, 2023).

Finally, this thesis shows that GPs can be used also for label-free isolation of macrophages when loaded with magnetic nanoparticles. While intra-abdominal injection of mere paramagnetic nanoparticle leads to their uptake also by tissues other than immune cells, their administration as cargo encapsulated in GPs results in macrophage-specific uptake. Subsequently, using a magnetic column, the phagocytes can be isolated from the whole-fly homogenate in sufficient quality and quantity for gene expression analyses. This method thus allows the separation of all cells that may be involved in pathogen uptake without the need for prior knowledge of these cells, and without the use of antibodies and markers. In

addition, this method allows a short processing time and is gentle, as macrophages are exposed only to physiological buffers and no additional chemicals. Since this approach of macrophage separation is based on the ability common to all phagocytes, it opens avenues of isolation of macrophages and their subsequent study in non-model insect species such as the agriculturally relevant *Apis mellifera* or vectors of diseases, e.g. *Aedes aegypti*. Nonetheless, the presence of magnetic particles in macrophages may not be desirable in some subsequent analyses. Similarly, their fate after they reach the phagolysosome was not addressed in our study, and we are not certain whether macrophages are able to eventually degrade or expel them.

Macrophages display a striking array of functions. This work contributes to revealing not only their “non-canonical” function in regulating systemic metabolism during immune challenge and in obese individuals, but also during insect metamorphosis. Although the presence of macrophages in larval adipose tissue during metamorphosis has been reported already in 2006, their action in this tissue was considered of a negligible importance (Nelliot, Bond and Hoshizaki, 2006). The authors used overexpression of the proapoptotic protein head involution defective (*hid*) under the control of a macrophage-specific construct *srphemo-Gal4>GFP*, resulting in the absence of GFP-positive macrophages and unaffected dissociation of larval adipocytes. Therefore, they concluded that macrophages play a dispensable role in fat body remodeling during *Drosophila* metamorphosis (Nelliot, Bond and Hoshizaki, 2006). Although some studies have reported a reduction in eclosion rates after macrophage ablation, they have been rescued by germ-free conditions or antibiotics (Charroux and Royet, 2009; Defaye *et al.*, 2009; Shia *et al.*, 2009; Arefin *et al.*, 2015). However, here we document that activators of apoptosis do not induce complete macrophage death when overexpressed in these cells using traditional macrophage-specific Gal4 drivers. Indeed, these cells are still present in the crown-like structures around larval adipocytes, are capable of phagocytosis, and also exhibit the ability to spread when placed on a microscopic slide. Recently, a novel macrophage-specific driver line, *Hml^{e9-P2A}>GAL4*, was generated (Stephenson *et al.*, 2022). Using this potent driver, the authors have shown that macrophages are critical for post-embryonic development even in germ-free conditions since ablation of macrophages by this driver is pupal lethal (Stephenson *et al.*, 2022). These results are consistent with our data showing that individuals bearing the *Hml^{e9-P2A}>GAL4; UAS Grim* construct die shortly after the prepupa-pupa transition. In addition, we revealed that when the ablation construct is activated after this critical period thanks to its combination with the temperature-sensitive Gal80 protein, the individuals are capable of emergence, but nevertheless display certain morphological aberrations, including delayed ovarian development. In 2020, the infiltrating macrophages were shown to perform efferocytosis and macroendocytosis of larval adipocytes during fruit fly metamorphosis (Ghosh, Ghosh and Mandal, 2020). The association of pupal macrophages with adipocytes has also been suggested in the flesh fly *Sarcophaga peregrina*, and the macrophages were thought to stimulate degradation of the fat body ECM by releasing Cathepsin B, which is triggered *via* interaction with adipocytes by a 200 kDa

specific membrane protein (Kurata, Komano and Natori, 1989; Kurata, Kobayashi and Natori, 1991; Takahashi, Kurata and Natori, 1993). Later, however, it was reported that this protein is myosin heavy chain derived from degraded larval muscles and not directly from pupal macrophages (Takahashi, Kurata and Natori, 1993; Natori *et al.*, 1999). The exact role of macrophages in the post-metamorphic maturation has therefore not yet been elucidated.

We have revealed that as *Drosophila* macrophages infiltrate the histolyzing larval fat body and perform efferocytosis of the adipocytes, they adopt a unique adipocyte-like polarization phenotype that is reminiscent of secretory plasmacytes or adipohemocytes found in recent single cell RNA-seqs of larval hemocytes (Cattenoz *et al.*, 2020; Tattikota *et al.*, 2020). In addition, we show that the macrophages form crown-like structures around adipocytes and that they engulf leaking lipids and RNA-protein granules from these cells. In turn, they acquire a foamy phenotype and display enhanced lipid and lipoprotein metabolic processes and increased cellular respiration and energy derivation as revealed by transcriptomic analysis. Nonetheless, whether they display this phenotype because the larval fat body is no longer functional and the adult adipose tissue is not yet fully mature at this stage awaits investigation. We hypothesize that the phenotype may be adopted in response to the efferocytosis itself or that macrophages may be instructed by the mRNA bound in the RNA-protein granules engulfed from adipocytes. Interestingly, the macrophages infiltrating larval fat body also resemble adipose tissue macrophages found in obese mammalian adipose tissue in their ultrastructure (Shapiro *et al.*, 2013). Hence, the relevance of macrophages infiltrating the larval fat body during metamorphosis and post-metamorphic development in *D. melanogaster* as a model for mammalian adipose tissue macrophages in obese individuals should be tested in subsequent research.

Moreover, this thesis shows that the adipocyte-like macrophages contribute to post-metamorphic maturation of ovaries *via* the production of apolipoprotein *apolpp*. Therefore, in this context, macrophages play a nutritive function, and recycle the matter from the larval stage and convert it into energy and nutrients that are used for achieving early fecundity in adult flies. This study may also shed light on macrophage contribution to rebuilding of body plan such as during tadpole tail resorption or shaping of the limb in mice. In addition, it may also provide hints on the role of macrophages in the potential recycling of components from apoptotic cells engulfed during daily cell turnover.

Interestingly, metamorphosis is not the only situation where we have observed infiltration of insect adipose tissue by macrophages. Indeed, this is a phenomenon that we have noted also in other situations, especially under conditions of metabolic stress, such as bacterial infection, starvation, and heat- and experimentally induced lipolysis. While there are no publications describing infiltration of the fat body during these conditions in *Drosophila* to the best of our knowledge, there is a scarce number of publications mentioning this cellular interaction during caloric restriction and infection in mammalian systems (Kosteli *et al.*, 2010; Silva *et al.*, 2019). Therefore, our goal in future research is to dissect the role of adipose tissue-infiltrating macrophages during these conditions.

7 REFERENCES

- Acharya, D. *et al.* (2020) ‘Complement Receptor-Mediated Phagocytosis Induces Proinflammatory Cytokine Production in Murine Macrophages’, *Frontiers in Immunology*, 10. doi: 10.3389/fimmu.2019.03049.
- Agier, J., Efenberger, M. and Brzezińska-Błaszczuk, E. (2015) ‘Review paper Cathelicidin impact on inflammatory cells’, *Central European Journal of Immunology*, 2, pp. 225–235. doi: 10.5114/ceji.2015.51359.
- Agrawal, N. *et al.* (2016) ‘The *Drosophila* TNF Eiger Is an Adipokine that Acts on Insulin-Producing Cells to Mediate Nutrient Response’, *Cell Metabolism*, 23(4), pp. 675–684. doi: 10.1016/j.cmet.2016.03.003.
- Ajuwon, K. M. and Spurlock, M. E. (2005) ‘Palmitate Activates the NF- κ B Transcription Factor and Induces IL-6 and TNF α Expression in 3T3-L1 Adipocytes’, *The Journal of Nutrition*, 135(8), pp. 1841–1846. doi: 10.1093/jn/135.8.1841.
- Alaarg, A. *et al.* (2017) ‘A systematic comparison of clinically viable nanomedicines targeting HMG-CoA reductase in inflammatory atherosclerosis’, *Journal of Controlled Release*, 262, pp. 47–57. doi: 10.1016/j.jconrel.2017.07.013.
- Allaman, I., Bélanger, M. and Magistretti, P. J. (2011) ‘Astrocyte–neuron metabolic relationships: for better and for worse’, *Trends in Neurosciences*, 34(2), pp. 76–87. doi: 10.1016/j.tins.2010.12.001.
- Amarante-Mendes, G. P. *et al.* (2018) ‘Pattern Recognition Receptors and the Host Cell Death Molecular Machinery’, *Frontiers in Immunology*, 9. doi: 10.3389/fimmu.2018.02379.
- Arch, M. *et al.* (2022) ‘*Drosophila melanogaster* as a model to study innate immune memory’, *Frontiers in Microbiology*, 13. doi: 10.3389/fmicb.2022.991678.
- Arefin, B. *et al.* (2015) ‘Apoptosis in Hemocytes Induces a Shift in Effector Mechanisms in the *Drosophila* Immune System and Leads to a Pro-Inflammatory State’, *PLOS ONE*. Edited by K. Michel, 10(8), p. e0136593. doi: 10.1371/journal.pone.0136593.
- Armitage, E. L., Roddie, H. G. and Evans, I. R. (2020) ‘Overexposure to apoptosis via disrupted glial specification perturbs *Drosophila* macrophage function and reveals roles of the CNS during injury’, *Cell Death & Disease*, 11(8), p. 627. doi: 10.1038/s41419-020-02875-2.
- Awasaki, T. *et al.* (2006) ‘Essential Role of the Apoptotic Cell Engulfment Genes *draper* and *ced-6* in Programmed Axon Pruning during *Drosophila* Metamorphosis’, *Neuron*, 50(6), pp. 855–867. doi:

10.1016/j.neuron.2006.04.027.

Ayyaz, A., Li, H. and Jasper, H. (2015) 'Haemocytes control stem cell activity in the *Drosophila* intestine', *Nature Cell Biology*, 17(6), pp. 736–748. doi: 10.1038/ncb3174.

Baardman, J. *et al.* (2015) 'Metabolic–epigenetic crosstalk in macrophage activation', *Epigenomics*, 7(7), pp. 1155–1164. doi: 10.2217/epi.15.71.

de Back, D. Z. *et al.* (2014) 'Of macrophages and red blood cells; a complex love story', *Frontiers in Physiology*, 5. doi: 10.3389/fphys.2014.00009.

Bäck, M. *et al.* (2019) 'Inflammation and its resolution in atherosclerosis: mediators and therapeutic opportunities', *Nature Reviews Cardiology*. doi: 10.1038/s41569-019-0169-2.

Bain, C. C. *et al.* (2014) 'Constant replenishment from circulating monocytes maintains the macrophage pool in the intestine of adult mice', *Nature Immunology*, 15(10), pp. 929–937. doi: 10.1038/ni.2967.

Bajgar, A. *et al.* (2015) 'Extracellular Adenosine Mediates a Systemic Metabolic Switch during Immune Response', *PLOS Biology*. Edited by M. S. Dionne, 13(4), p. e1002135. doi: 10.1371/journal.pbio.1002135.

Bajgar, A. and Dolezal, T. (2018) 'Extracellular adenosine modulates host-pathogen interactions through regulation of systemic metabolism during immune response in *Drosophila*', *PLOS Pathogens*. Edited by B. P. Lazzaro, 14(4), p. e1007022. doi: 10.1371/journal.ppat.1007022.

Bajgar, A. and Krejčová, G. (2023) 'On the origin of the functional versatility of macrophages', *Frontiers in Physiology*, 14. doi: 10.3389/fphys.2023.1128984.

Bartholomay, L. C. *et al.* (2004) 'Description of the Transcriptomes of Immune Response-Activated Hemocytes from the Mosquito Vectors *Aedes aegypti* and *Armigeres subalbatus*', *Infection and Immunity*, 72(7), pp. 4114–4126. doi: 10.1128/IAI.72.7.4114-4126.2004.

Bashir-Tanoli, S. and Tinsley, M. C. (2014) 'Immune response costs are associated with changes in resource acquisition and not resource reallocation', *Functional Ecology*. Edited by I. Moore, 28(4), pp. 1011–1019. doi: 10.1111/1365-2435.12236.

Bekkering, S. *et al.* (2018) 'Metabolic Induction of Trained Immunity through the Mevalonate Pathway', *Cell*, 172(1–2), pp. 135–146.e9. doi: 10.1016/j.cell.2017.11.025.

Blanco, E., Shen, H. and Ferrari, M. (2015) 'Principles of nanoparticle design for overcoming biological barriers to drug delivery', *Nature Biotechnology*, 33(9), pp. 941–951. doi: 10.1038/nbt.3330.

- Van De Bor, V. *et al.* (2015) ‘Companion Blood Cells Control Ovarian Stem Cell Niche Microenvironment and Homeostasis’, *Cell Reports*, 13(3), pp. 546–560. doi: 10.1016/j.celrep.2015.09.008.
- Borisenko, G. G. *et al.* (2003) ‘Macrophage recognition of externalized phosphatidylserine and phagocytosis of apoptotic Jurkat cells—existence of a threshold’, *Archives of Biochemistry and Biophysics*, 413(1), pp. 41–52. doi: 10.1016/S0003-9861(03)00083-3.
- Van den Bossche, J. *et al.* (2016) ‘Mitochondrial Dysfunction Prevents Repolarization of Inflammatory Macrophages’, *Cell Reports*, 17(3), pp. 684–696. doi: 10.1016/j.celrep.2016.09.008.
- Van den Bossche, J., O’Neill, L. A. and Menon, D. (2017) ‘Macrophage Immunometabolism: Where Are We (Going)?’, *Trends in Immunology*, 38(6), pp. 395–406. doi: 10.1016/j.it.2017.03.001.
- Bou Aoun, R. *et al.* (2011) ‘Analysis of Thioester-Containing Proteins during the Innate Immune Response of *Drosophila melanogaster*’, *Journal of Innate Immunity*, 3(1), pp. 52–64. doi: 10.1159/000321554.
- Boulet, M. *et al.* (2021) ‘Characterization of the *Drosophila* Adult Hematopoietic System Reveals a Rare Cell Population With Differentiation and Proliferation Potential’, *Frontiers in Cell and Developmental Biology*, 9. doi: 10.3389/fcell.2021.739357.
- Boyle, J. J. *et al.* (2009) ‘Coronary Intraplaque Hemorrhage Evokes a Novel Atheroprotective Macrophage Phenotype’, *The American Journal of Pathology*, 174(3), pp. 1097–1108. doi: 10.2353/ajpath.2009.080431.
- Brandt, S. M. *et al.* (2004) ‘Secreted Bacterial Effectors and Host-Produced Eiger/TNF Drive Death in a *Salmonella*-Infected Fruit Fly’, *PLoS Biology*. Edited by Shizuo Akira, 2(12), p. e418. doi: 10.1371/journal.pbio.0020418.
- Brännström, M. and Norman, R. J. (1993) ‘Involvement of leukocytes and cytokines in the ovulatory process and corpus luteum function’, *Human Reproduction*, 8(10), pp. 1762–1775. doi: 10.1093/oxfordjournals.humrep.a137929.
- Brock, D. A. *et al.* (2013) ‘Social amoeba farmers carry defensive symbionts to protect and privatize their crops’, *Nature Communications*, 4(1), p. 2385. doi: 10.1038/ncomms3385.
- Brock, D. A., Callison, W. É., *et al.* (2016) ‘Sentinel cells, symbiotic bacteria and toxin resistance in the social amoeba *Dictyostelium discoideum*’, *Proceedings of the Royal Society B: Biological Sciences*, 283(1829), p. 20152727. doi: 10.1098/rspb.2015.2727.
- Brock, D. A., Jones, K., *et al.* (2016) ‘Which phenotypic traits of *Dictyostelium discoideum* farmers are conferred by their bacterial symbionts?’, *Symbiosis*, 68(1–3), pp. 39–48. doi: 10.1007/s13199-015-

0352-0.

Bunt, S. *et al.* (2010) 'Hemocyte-Secreted Type IV Collagen Enhances BMP Signaling to Guide Renal Tubule Morphogenesis in *Drosophila*', *Developmental Cell*, 19(2), pp. 296–306. doi: 10.1016/j.devcel.2010.07.019.

Carp, H. (1982) 'Mitochondrial N-formylmethionyl proteins as chemoattractants for neutrophils.', *The Journal of experimental medicine*, 155(1), pp. 264–275. doi: 10.1084/jem.155.1.264.

Carrau, T. *et al.* (2021) 'The Cellular Innate Immune Response of the Invasive Pest Insect *Drosophila suzukii* against *Pseudomonas entomophila* Involves the Release of Extracellular Traps', *Cells*, 10(12), p. 3320. doi: 10.3390/cells10123320.

Carrier, T. J. *et al.* (2022) 'Symbiont transmission in marine sponges: reproduction, development, and metamorphosis', *BMC Biology*, 20(1), p. 100. doi: 10.1186/s12915-022-01291-6.

Carson, M. J. *et al.* (2006) 'CNS immune privilege: hiding in plain sight.', *Immunological reviews*, 213, pp. 48–65. doi: 10.1111/j.1600-065X.2006.00441.x.

Caso, V. M. *et al.* (2021) 'Regulation of Inflammation and Oxidative Stress by Formyl Peptide Receptors in Cardiovascular Disease Progression', *Life*, 11(3), p. 243. doi: 10.3390/life11030243.

Cassetta, L. and Pollard, J. W. (2018) 'Targeting macrophages: therapeutic approaches in cancer', *Nature Reviews Drug Discovery*, 17(12), pp. 887–904. doi: 10.1038/nrd.2018.169.

Cattenoz, P. B. *et al.* (2020) 'Temporal specificity and heterogeneity of *Drosophila* immune cells', *The EMBO Journal*, 39(12). doi: 10.15252/embj.2020104486.

Chakrabarti, S. *et al.* (2016) 'Remote Control of Intestinal Stem Cell Activity by Haemocytes in *Drosophila*', *PLoS Genetics*. Edited by U. Banerjee, 12(5), p. e1006089. doi: 10.1371/journal.pgen.1006089.

Chakrabarti, S. and Visweswariah, S. S. (2020) 'Intramacrophage ROS Primes the Innate Immune System via JAK/STAT and Toll Activation', *Cell Reports*, 33(6), p. 108368. doi: 10.1016/j.celrep.2020.108368.

Chambers, M. C., Song, K. H. and Schneider, D. S. (2012) '*Listeria monocytogenes* Infection Causes Metabolic Shifts in *Drosophila melanogaster*', *PLoS ONE*. Edited by N. E. Freitag, 7(12), p. e50679. doi: 10.1371/journal.pone.0050679.

Champagne, C. M. *et al.* (2002) 'Macrophage cell lines produce osteoinductive signals that include bone morphogenetic protein-2', *Bone*, 30(1), pp. 26–31. doi: 10.1016/S8756-3282(01)00638-X.

Chandrupatla, D. M. S. H. *et al.* (2019) 'The folate receptor β as a macrophage-mediated imaging and

therapeutic target in rheumatoid arthritis', *Drug Delivery and Translational Research*, 9(1), pp. 366–378. doi: 10.1007/s13346-018-0589-2.

Chang, M. K. *et al.* (2008) 'Osteal Tissue Macrophages Are Intercalated throughout Human and Mouse Bone Lining Tissues and Regulate Osteoblast Function In Vitro and In Vivo', *The Journal of Immunology*, 181(2), pp. 1232–1244. doi: 10.4049/jimmunol.181.2.1232.

Charroux, B. and Royet, J. (2009) 'Elimination of plasmacytes by targeted apoptosis reveals their role in multiple aspects of the *Drosophila* immune response', *Proceedings of the National Academy of Sciences*, 106(24), pp. 9797–9802. doi: 10.1073/pnas.0903971106.

Chen, K. *et al.* (2020) 'Communications Between Bone Marrow Macrophages and Bone Cells in Bone Remodeling', *Frontiers in Cell and Developmental Biology*, 8. doi: 10.3389/fcell.2020.598263.

Cheng, S.-C. *et al.* (2014) 'mTOR- and HIF-1 α -mediated aerobic glycolysis as metabolic basis for trained immunity', *Science*, 345(6204). doi: 10.1126/science.1250684.

Cho, B. *et al.* (2020) 'Single-cell transcriptome maps of myeloid blood cell lineages in *Drosophila*', *Nature Communications*, 11(1), p. 4483. doi: 10.1038/s41467-020-18135-y.

Cho, N. K. *et al.* (2002) 'Developmental Control of Blood Cell Migration by the *Drosophila* VEGF Pathway', *Cell*, 108(6), pp. 865–876. doi: 10.1016/S0092-8674(02)00676-1.

Cho, S. W. *et al.* (2014) 'Osteal macrophages support physiologic skeletal remodeling and anabolic actions of parathyroid hormone in bone', *Proceedings of the National Academy of Sciences*, 111(4), pp. 1545–1550. doi: 10.1073/pnas.1315153111.

Cinti, S. *et al.* (2005) 'Adipocyte death defines macrophage localization and function in adipose tissue of obese mice and humans', *Journal of Lipid Research*, 46(11), pp. 2347–2355. doi: 10.1194/jlr.M500294-JLR200.

Coats, B. R. *et al.* (2017) 'Metabolically Activated Adipose Tissue Macrophages Perform Detrimental and Beneficial Functions during Diet-Induced Obesity', *Cell Reports*, 20(13), pp. 3149–3161. doi: 10.1016/j.celrep.2017.08.096.

Cohen, P. E., Zhu, L. and Pollard, J. W. (1997) 'Absence of Colony Stimulating Factor-1 in Osteopetrotic (csfmp/csfp) Mice Disrupts Estrous Cycles and Ovulation¹', *Biology of Reproduction*, 56(1), pp. 110–118. doi: 10.1095/biolreprod56.1.110.

Condello, C. *et al.* (2015) 'Microglia constitute a barrier that prevents neurotoxic protofibrillar A β 42 hotspots around plaques', *Nature Communications*, 6(1), p. 6176. doi: 10.1038/ncomms7176.

Cordero, J. B. *et al.* (2010) 'Oncogenic Ras Diverts a Host TNF Tumor Suppressor Activity into Tumor Promoter', *Developmental Cell*, 18(6), pp. 999–1011. doi: 10.1016/j.devcel.2010.05.014.

- Corliss, B. A. *et al.* (2016) 'Macrophages: An Inflammatory Link Between Angiogenesis and Lymphangiogenesis', *Microcirculation*, 23(2), pp. 95–121. doi: 10.1111/micc.12259.
- Crabtree, H. G. (1929) 'Observations on the carbohydrate metabolism of tumours.', *The Biochemical journal*, 23(3), pp. 536–45. doi: 10.1042/bj0230536.
- Crosby, W. H. and Benjamin, N. R. (1957) 'Siderocytes and the Spleen', *Blood*, 12(2), pp. 165–170. doi: 10.1182/blood.V12.2.165.165.
- Crozatier, M. and Meister, M. (2007) 'Drosophila haematopoiesis', *Cellular Microbiology*, 9(5), pp. 1117–1126. doi: 10.1111/j.1462-5822.2007.00930.x.
- Cuchel, M. and Rader, D. J. (2006) 'Macrophage Reverse Cholesterol Transport', *Circulation*, 113(21), pp. 2548–2555. doi: 10.1161/CIRCULATIONAHA.104.475715.
- Cypess, A. M. *et al.* (2009) 'Identification and Importance of Brown Adipose Tissue in Adult Humans', *New England Journal of Medicine*, 360(15), pp. 1509–1517. doi: 10.1056/NEJMoa0810780.
- Davidson, A. J. and Wood, W. (2020) 'Macrophages Use Distinct Actin Regulators to Switch Engulfment Strategies and Ensure Phagocytic Plasticity In Vivo', *Cell Reports*, 31(8), p. 107692. doi: 10.1016/j.celrep.2020.107692.
- DeFalco, T. *et al.* (2014) 'Yolk-sac-derived macrophages regulate fetal testis vascularization and morphogenesis', *Proceedings of the National Academy of Sciences*, 111(23). doi: 10.1073/pnas.1400057111.
- Defaye, A. *et al.* (2009) 'Genetic Ablation of Drosophila Phagocytes Reveals Their Contribution to Both Development and Resistance to Bacterial Infection', *Journal of Innate Immunity*, 1(4), pp. 322–334. doi: 10.1159/000210264.
- Dolezal, T. *et al.* (2019) 'Molecular regulations of metabolism during immune response in insects', *Insect Biochemistry and Molecular Biology*, 109, pp. 31–42. doi: 10.1016/j.ibmb.2019.04.005.
- Doulias, P.-T. *et al.* (2013) 'Nitric Oxide Regulates Mitochondrial Fatty Acid Metabolism Through Reversible Protein S -Nitrosylation', *Science Signaling*, 6(256). doi: 10.1126/scisignal.2003252.
- Driel, R. (1981) 'Binding of the Chemoattractant Folic Acid by Dictyostelium discoideum Cells', *European Journal of Biochemistry*, 115(2), pp. 391–395. doi: 10.1111/j.1432-1033.1981.tb05250.x.
- Du, Y. *et al.* (2021) 'Macrophage polarization: an effective approach to targeted therapy of inflammatory bowel disease', *Expert Opinion on Therapeutic Targets*, 25(3), pp. 191–209. doi: 10.1080/14728222.2021.1901079.

- Efeyan, A., Comb, W. C. and Sabatini, D. M. (2015) 'Nutrient-sensing mechanisms and pathways', *Nature*, 517(7534), pp. 302–310. doi: 10.1038/nature14190.
- von Ehr, A., Bode, C. and Hilgendorf, I. (2022) 'Macrophages in Atheromatous Plaque Developmental Stages', *Frontiers in Cardiovascular Medicine*, 9. doi: 10.3389/fcvm.2022.865367.
- Ereskovsky, A. *et al.* (2021) 'Whole-Body Regeneration in Sponges: Diversity, Fine Mechanisms, and Future Prospects', *Genes*, 12(4), p. 506. doi: 10.3390/genes12040506.
- Evans, I. R. and Wood, W. (2014) 'Drosophila blood cell chemotaxis', *Current Opinion in Cell Biology*, 30, pp. 1–8. doi: 10.1016/j.ceb.2014.04.002.
- Everts, B. *et al.* (2012) 'Commitment to glycolysis sustains survival of NO-producing inflammatory dendritic cells', *Blood*, 120(7), pp. 1422–1431. doi: 10.1182/blood-2012-03-419747.
- Fan, F. *et al.* (2021) 'Glycolytic Metabolism Is Critical for the Innate Antibacterial Defense in Acute Streptococcus pneumoniae Otitis Media', *Frontiers in Immunology*, 12. doi: 10.3389/fimmu.2021.624775.
- Fantin, A. *et al.* (2010) 'Tissue macrophages act as cellular chaperones for vascular anastomosis downstream of VEGF-mediated endothelial tip cell induction', *Blood*, 116(5), pp. 829–840. doi: 10.1182/blood-2009-12-257832.
- Faulhaber, L. M. and Karp, R. D. (1992) 'A diphasic immune response against bacteria in the American cockroach.', *Immunology*, 75(2), pp. 378–81. Available at: <http://www.ncbi.nlm.nih.gov/pubmed/1384723>.
- Feingold, K. R. *et al.* (2012) 'Mechanisms of triglyceride accumulation in activated macrophages', *Journal of Leukocyte Biology*, 92(4), pp. 829–839. doi: 10.1189/jlb.1111537.
- Figueroa-Clavevega, A. and Bilder, D. (2015) 'Malignant Drosophila Tumors Interrupt Insulin Signaling to Induce Cachexia-like Wasting', *Developmental Cell*, 33(1), pp. 47–55. doi: 10.1016/j.devcel.2015.03.001.
- Finicelli, M. *et al.* (2022) 'The Emerging Role of Macrophages in Chronic Obstructive Pulmonary Disease: The Potential Impact of Oxidative Stress and Extracellular Vesicle on Macrophage Polarization and Function', *Antioxidants*, 11(3), p. 464. doi: 10.3390/antiox11030464.
- Franc, N. C. *et al.* (1996) 'Croquemort, A Novel Drosophila Hemocyte/Macrophage Receptor that Recognizes Apoptotic Cells', *Immunity*, 4(5), pp. 431–443. doi: 10.1016/S1074-7613(00)80410-0.
- Franc, N. C. *et al.* (1999) 'Requirement for Croquemort in Phagocytosis of Apoptotic Cells in Drosophila', *Science*, 284(5422), pp. 1991–1994. doi: 10.1126/science.284.5422.1991.

- Francis, R. *et al.* (2020) ‘Glycolytic inhibitor 2-deoxyglucose suppresses inflammatory response in innate immune cells and experimental staphylococcal endophthalmitis’, *Experimental Eye Research*, 197, p. 108079. doi: 10.1016/j.exer.2020.108079.
- Frangie, C. and Daher, J. (2022) ‘Role of myeloperoxidase in inflammation and atherosclerosis (Review)’, *Biomedical Reports*, 16(6), p. 53. doi: 10.3892/br.2022.1536.
- Franz, A., Wood, W. and Martin, P. (2018) ‘Fat Body Cells Are Motile and Actively Migrate to Wounds to Drive Repair and Prevent Infection’, *Developmental Cell*, 44(4), pp. 460-470.e3. doi: 10.1016/j.devcel.2018.01.026.
- Freemerman, A. J. *et al.* (2014) ‘Metabolic Reprogramming of Macrophages’, *Journal of Biological Chemistry*, 289(11), pp. 7884–7896. doi: 10.1074/jbc.M113.522037.
- Fu, L., Wen, L. and Shi, Y.-B. (2018) ‘Role of Thyroid Hormone Receptor in Amphibian Development’, in, pp. 247–263. doi: 10.1007/978-1-4939-7902-8_20.
- Fu, Y. *et al.* (2020) ‘Single-cell RNA sequencing identifies novel cell types in Drosophila blood’, *Journal of Genetics and Genomics*, 47(4), pp. 175–186. doi: 10.1016/j.jgg.2020.02.004.
- Gadd, V. L. *et al.* (2014) ‘The portal inflammatory infiltrate and ductular reaction in human nonalcoholic fatty liver disease’, *Hepatology*, 59(4), pp. 1393–1405. doi: 10.1002/hep.26937.
- Gallin, J. I., Kaye, D. and O’Leary, W. M. (1969) ‘Serum Lipids in Infection’, *New England Journal of Medicine*, 281(20), pp. 1081–1086. doi: 10.1056/NEJM196911132812001.
- Galván-Peña, S. and O’Neill, L. A. J. (2014) ‘Metabolic Reprogramming in Macrophage Polarization’, *Frontiers in Immunology*, 5. doi: 10.3389/fimmu.2014.00420.
- Ganz, T. (2012) ‘Macrophages and Systemic Iron Homeostasis’, *Journal of Innate Immunity*, 4(5–6), pp. 446–453. doi: 10.1159/000336423.
- Garbán, H. J. and Bonavida, B. (1999) ‘Nitric Oxide Sensitizes Ovarian Tumor Cells to Fas-Induced Apoptosis’, *Gynecologic Oncology*, 73(2), pp. 257–264. doi: 10.1006/gyno.1999.5374.
- Gautier, E. L. *et al.* (2012) ‘Gene-expression profiles and transcriptional regulatory pathways that underlie the identity and diversity of mouse tissue macrophages’, *Nature Immunology*, 13(11), pp. 1118–1128. doi: 10.1038/ni.2419.
- Germer, J., Cerveau, N. and Jackson, D. J. (2017) ‘The Holo-Transcriptome of a Calcified Early Branching Metazoan’, *Frontiers in Marine Science*, 4. doi: 10.3389/fmars.2017.00081.
- Ghosh, S. *et al.* (2015) ‘Active Hematopoietic Hubs in Drosophila Adults Generate Hemocytes and Contribute to Immune Response’, *Developmental Cell*, 33(4), pp. 478–488. doi:

10.1016/j.devcel.2015.03.014.

Ghosh, Saikat, Ghosh, Sushmit and Mandal, L. (2020) 'Drosophila metamorphosis involves hemocyte mediated macroendocytosis and efferocytosis', *The International Journal of Developmental Biology*, 64(4-5-6), pp. 319-329. doi: 10.1387/ijdb.190215lm.

Gleissner, C. A. *et al.* (2010) 'CXC Chemokine Ligand 4 Induces a Unique Transcriptome in Monocyte-Derived Macrophages', *The Journal of Immunology*, 184(9), pp. 4810-4818. doi: 10.4049/jimmunol.0901368.

Glomset, J. A. (1968) 'The plasma lecithins:cholesterol acyltransferase reaction.', *Journal of lipid research*, 9(2), pp. 155-67. Available at: <http://www.ncbi.nlm.nih.gov/pubmed/4868699>.

Godfried Sie, C. *et al.* (2012) 'IGFBP7's susceptibility to proteolysis is altered by A-to-I RNA editing of its transcript', *FEBS Letters*, 586(16), pp. 2313-2317. doi: 10.1016/j.febslet.2012.06.037.

Godwin, J. W., Pinto, A. R. and Rosenthal, N. A. (2013) 'Macrophages are required for adult salamander limb regeneration', *Proceedings of the National Academy of Sciences*, 110(23), pp. 9415-9420. doi: 10.1073/pnas.1300290110.

Gomes, F. M. *et al.* (2022) 'Molecular mechanisms of insect immune memory and pathogen transmission', *PLOS Pathogens*. Edited by A. R. Odom John, 18(12), p. e1010939. doi: 10.1371/journal.ppat.1010939.

Gordon, S. and Taylor, P. R. (2005) 'Monocyte and macrophage heterogeneity', *Nature Reviews Immunology*, 5(12), pp. 953-964. doi: 10.1038/nri1733.

Goren, I. *et al.* (2009) 'A Transgenic Mouse Model of Inducible Macrophage Depletion', *The American Journal of Pathology*, 175(1), pp. 132-147. doi: 10.2353/ajpath.2009.081002.

Goto, A. *et al.* (2001) 'A Drosophila haemocyte-specific protein, hemolectin, similar to human von Willebrand factor', *Biochemical Journal*, 359(1), p. 99. doi: 10.1042/0264-6021:3590099.

Goto, A., Kadowaki, T. and Kitagawa, Y. (2003) 'Drosophila hemolectin gene is expressed in embryonic and larval hemocytes and its knock down causes bleeding defects', *Developmental Biology*, 264(2), pp. 582-591. doi: 10.1016/j.ydbio.2003.06.001.

Gouon-Evans, V., Rothenberg, M. E. and Pollard, J. W. (2000) 'Postnatal mammary gland development requires macrophages and eosinophils', *Development*, 127(11), pp. 2269-2282. doi: 10.1242/dev.127.11.2269.

Gray, E. M. and Bradley, T. J. (2005) 'Malarial infection in *Aedes aegypti* : effects on feeding, fecundity and metabolic rate', *Parasitology*, 132(02), p. 169. doi: 10.1017/S0031182005008966.

- De Gregorio, E. (2002) 'The Toll and Imd pathways are the major regulators of the immune response in *Drosophila*', *The EMBO Journal*, 21(11), pp. 2568–2579. doi: 10.1093/emboj/21.11.2568.
- Grunfeld, C. *et al.* (1992) 'Lipids, lipoproteins, triglyceride clearance, and cytokines in human immunodeficiency virus infection and the acquired immunodeficiency syndrome.', *The Journal of Clinical Endocrinology & Metabolism*, 74(5), pp. 1045–1052. doi: 10.1210/jcem.74.5.1373735.
- Hanson, M. A., Lemaitre, B. and Unckless, R. L. (2019) 'Dynamic Evolution of Antimicrobial Peptides Underscores Trade-Offs Between Immunity and Ecological Fitness', *Frontiers in Immunology*, 10. doi: 10.3389/fimmu.2019.02620.
- Hard, G. C. (1970) 'Some biochemical aspects of the immune macrophage.', *British journal of experimental pathology*, 51(1), pp. 97–105. Available at: <http://www.ncbi.nlm.nih.gov/pubmed/5434449>.
- Hardardóttir, I., Grunfeld, C. and Feingold, K. R. (1995) 'Effects of endotoxin on lipid metabolism', *Biochemical Society Transactions*, 23(4), pp. 1013–1018. doi: 10.1042/bst0231013.
- Harris, H. (1954) 'Role of Chemotaxis in Inflammation', *Physiological Reviews*, 34(3), pp. 529–562. doi: 10.1152/physrev.1954.34.3.529.
- Hartenstein, V. and Martinez, P. (2019) 'Phagocytosis in cellular defense and nutrition: a food-centered approach to the evolution of macrophages', *Cell and Tissue Research*, 377(3), pp. 527–547. doi: 10.1007/s00441-019-03096-6.
- He, W. *et al.* (2020) 'Drug delivery to macrophages: A review of targeting drugs and drug carriers to macrophages for inflammatory diseases', *Advanced Drug Delivery Reviews*, 165–166, pp. 15–40. doi: 10.1016/j.addr.2019.12.001.
- Hendriks, H. R. and Eestermans, I. L. (1986) 'Phagocytosis and lipofuscin accumulation in lymph node macrophages', *Mechanisms of Ageing and Development*, 35(2), pp. 161–167. doi: 10.1016/0047-6374(86)90006-0.
- Henrich, S. E. *et al.* (2019) 'Supramolecular Assembly of High-Density Lipoprotein Mimetic Nanoparticles Using Lipid-Conjugated Core Scaffolds', *Journal of the American Chemical Society*, 141(25), pp. 9753–9757. doi: 10.1021/jacs.9b00651.
- Hibbs, J. B., Taintor, R. R. and Vavrin, Z. (1987) 'Macrophage Cytotoxicity: Role for L-Arginine Deiminase and Imino Nitrogen Oxidation to Nitrite', *Science*, 235(4787), pp. 473–476. doi: 10.1126/science.2432665.
- Hirose, S. *et al.* (2011) 'Self-Recognition in Social Amoebae Is Mediated by Allelic Pairs of Tiger Genes', *Science*, 333(6041), pp. 467–470. doi: 10.1126/science.1203903.

- Hirschhäuser, A. *et al.* (2023) ‘Single-cell transcriptomics identifies new blood cell populations in *Drosophila* released at the onset of metamorphosis’, *Development*, 150(18). doi: 10.1242/dev.201767.
- Hoeffel, G. *et al.* (2015) ‘C-Myb⁺ Erythro-Myeloid Progenitor-Derived Fetal Monocytes Give Rise to Adult Tissue-Resident Macrophages’, *Immunity*, 42(4), pp. 665–678. doi: 10.1016/j.immuni.2015.03.011.
- Hoeffel, G. and Ginhoux, F. (2015) ‘Ontogeny of Tissue-Resident Macrophages’, *Frontiers in Immunology*, 6. doi: 10.3389/fimmu.2015.00486.
- Holz, A. *et al.* (2003) ‘The two origins of hemocytes in *Drosophila*’, *Development*, 130(20), pp. 4955–4962. doi: 10.1242/dev.00702.
- Honegger, B. *et al.* (2008) ‘Imp-L2, a putative homolog of vertebrate IGF-binding protein 7, counteracts insulin signaling in *Drosophila* and is essential for starvation resistance’, *Journal of Biology*, 7(3), p. 10. doi: 10.1186/jbiol72.
- Hong, H. and Tian, X. Y. (2020) ‘The Role of Macrophages in Vascular Repair and Regeneration after Ischemic Injury’, *International Journal of Molecular Sciences*, 21(17), p. 6328. doi: 10.3390/ijms21176328.
- Hopkinson-Woolley, J. *et al.* (1994) ‘Macrophage recruitment during limb development and wound healing in the embryonic and foetal mouse’, *Journal of Cell Science*, 107(5), pp. 1159–1167. doi: 10.1242/jcs.107.5.1159.
- Hotamisligil, G. S. and Erbay, E. (2008) ‘Nutrient sensing and inflammation in metabolic diseases’, *Nature Reviews Immunology*, 8(12), pp. 923–934. doi: 10.1038/nri2449.
- Howick, V. M. and Lazzaro, B. P. (2014) ‘Genotype and diet shape resistance and tolerance across distinct phases of bacterial infection’, *BMC Evolutionary Biology*, 14(1), p. 56. doi: 10.1186/1471-2148-14-56.
- Hu, G. *et al.* (2021) ‘High-throughput phenotypic screen and transcriptional analysis identify new compounds and targets for macrophage reprogramming’, *Nature Communications*, 12(1), p. 773. doi: 10.1038/s41467-021-21066-x.
- Huang, S. C.-C. *et al.* (2014) ‘Cell-intrinsic lysosomal lipolysis is essential for alternative activation of macrophages’, *Nature Immunology*, 15(9), pp. 846–855. doi: 10.1038/ni.2956.
- Hull-Thompson, J. *et al.* (2009) ‘Control of Metabolic Homeostasis by Stress Signaling Is Mediated by the Lipocalin NLaz’, *PLoS Genetics*. Edited by E. Rulifson, 5(4), p. e1000460. doi: 10.1371/journal.pgen.1000460.
- Hume, D. A. *et al.* (1983) ‘The mononuclear phagocyte system of the mouse defined by

- immunohistochemical localization of antigen F4/80. Relationship between macrophages, Langerhans cells, reticular cells, and dendritic cells in lymphoid and hematopoietic organs.', *The Journal of experimental medicine*, 158(5), pp. 1522–1536. doi: 10.1084/jem.158.5.1522.
- Igaki, T. (2002) 'Eiger, a TNF superfamily ligand that triggers the Drosophila JNK pathway', *The EMBO Journal*, 21(12), pp. 3009–3018. doi: 10.1093/emboj/cdf306.
- Ignarro, L. J. (1990) 'Biosynthesis and Metabolism of Endothelium-Derived Nitric Oxide', *Annual Review of Pharmacology and Toxicology*, 30(1), pp. 535–560. doi: 10.1146/annurev.pa.30.040190.002535.
- Imler, J.-L. and Bulet, P. (2005) 'Antimicrobial Peptides in Drosophila: Structures, Activities and Gene Regulation', in *Mechanisms of Epithelial Defense*. Basel: KARGER, pp. 1–21. doi: 10.1159/000086648.
- Imtiyaz, H. Z. and Simon, M. C. (2010) 'Hypoxia-Inducible Factors as Essential Regulators of Inflammation', in, pp. 105–120. doi: 10.1007/82_2010_74.
- Ingman, W. V. *et al.* (2006) 'Macrophages promote collagen fibrillogenesis around terminal end buds of the developing mammary gland', *Developmental Dynamics*, 235(12), pp. 3222–3229. doi: 10.1002/dvdy.20972.
- Irving, P. *et al.* (2005) 'New insights into Drosophila larval haemocyte functions through genome-wide analysis', *Cellular Microbiology*, 7(3), pp. 335–350. doi: 10.1111/j.1462-5822.2004.00462.x.
- Jenkins, S. J. *et al.* (2011) 'Local Macrophage Proliferation, Rather than Recruitment from the Blood, Is a Signature of T H 2 Inflammation', *Science*, 332(6035), pp. 1284–1288. doi: 10.1126/science.1204351.
- Jeong, S.-J., Lee, M.-N. and Oh, G. T. (2017) 'The Role of Macrophage Lipophagy in Reverse Cholesterol Transport', *Endocrinology and Metabolism*, 32(1), p. 41. doi: 10.3803/EnM.2017.32.1.41.
- Jha, A. K. *et al.* (2015) 'Network Integration of Parallel Metabolic and Transcriptional Data Reveals Metabolic Modules that Regulate Macrophage Polarization', *Immunity*, 42(3), pp. 419–430. doi: 10.1016/j.immuni.2015.02.005.
- Jilka, R. L. *et al.* (2007) 'Perspective: Quantifying Osteoblast and Osteocyte Apoptosis: Challenges and Rewards', *Journal of Bone and Mineral Research*, 22(10), pp. 1492–1501. doi: 10.1359/jbmr.070518.
- Jing, X. and Behmer, S. T. (2020) 'Insect Sterol Nutrition: Physiological Mechanisms, Ecology, and Applications', *Annual Review of Entomology*, 65(1), pp. 251–271. doi: 10.1146/annurev-ento-011019-025017.

- Johansson, K. C., Metzendorf, C. and Soderhall, K. (2005) 'Microarray analysis of immune challenged hemocytes', *Experimental Cell Research*, 305(1), pp. 145–155. doi: 10.1016/j.yexcr.2004.12.018.
- Jun, J. C. *et al.* (2017) 'Hypoxia-Inducible Factors and Cancer', *Current Sleep Medicine Reports*, 3(1), pp. 1–10. doi: 10.1007/s40675-017-0062-7.
- Kajihara, H., Totović, V. and Gedigk, P. (1975) '[Ultrastructure and morphogenesis of ceroid pigment. I. Phagocytosis and formation of lipid-containing lysosomes in Kupffer Cells after intravenous injection of unsaturated lipids (author's transl)].', *Virchows Archiv. B, Cell pathology*, 19(3), pp. 221–37. Available at: <http://www.ncbi.nlm.nih.gov/pubmed/813375>.
- Kajimura, S., Spiegelman, B. M. and Seale, P. (2015) 'Brown and Beige Fat: Physiological Roles beyond Heat Generation', *Cell Metabolism*, 22(4), pp. 546–559. doi: 10.1016/j.cmet.2015.09.007.
- Kalafatakis, I. and Karagogeos, D. (2021) 'Oligodendrocytes and Microglia: Key Players in Myelin Development, Damage and Repair', *Biomolecules*, 11(7), p. 1058. doi: 10.3390/biom11071058.
- Kalish, S. *et al.* (2017) 'M3 Macrophages Stop Division of Tumor Cells In Vitro and Extend Survival of Mice with Ehrlich Ascites Carcinoma', *Medical Science Monitor Basic Research*, 23, pp. 8–19. doi: 10.12659/MSMBR.902285.
- Kamaly, N. *et al.* (2016) 'Targeted Interleukin-10 Nanotherapeutics Developed with a Microfluidic Chip Enhance Resolution of Inflammation in Advanced Atherosclerosis', *ACS Nano*, 10(5), pp. 5280–5292. doi: 10.1021/acsnano.6b01114.
- Katsuyama, T. *et al.* (2015) 'During Drosophila disc regeneration, JAK/STAT coordinates cell proliferation with Dilp8-mediated developmental delay', *Proceedings of the National Academy of Sciences*, 112(18). doi: 10.1073/pnas.1423074112.
- Kaufman, R. (2017) 'Red Blood Cell Life Span, Senescence, and Destruction', in Benz, E., Berliner, N & Schiffman, F. (ed.) *Anemia: Pathophysiology, Diagnosis, and Management*. Cambridge: Cambridge University Press, pp. 19–22. doi: 10.1017/9781108586900.004.
- Kawai, T. and Akira, S. (2007) 'Signaling to NF- κ B by Toll-like receptors', *Trends in Molecular Medicine*, 13(11), pp. 460–469. doi: 10.1016/j.molmed.2007.09.002.
- Kawane, K. *et al.* (2001) 'Requirement of DNase II for Definitive Erythropoiesis in the Mouse Fetal Liver', *Science*, 292(5521), pp. 1546–1549. doi: 10.1126/science.292.5521.1546.
- Kelly, B. and O'Neill, L. A. (2015) 'Metabolic reprogramming in macrophages and dendritic cells in innate immunity', *Cell Research*, 25(7), pp. 771–784. doi: 10.1038/cr.2015.68.
- Kelsey, E. M. *et al.* (2012) 'Schnurri regulates hemocyte function to promote tissue recovery after

- DNA damage', *Journal of Cell Science*. doi: 10.1242/jcs.095323.
- Kendall, R. T. and Feghali-Bostwick, C. A. (2014) 'Fibroblasts in fibrosis: novel roles and mediators', *Frontiers in Pharmacology*, 5. doi: 10.3389/fphar.2014.00123.
- Kiger, J. A., Natzle, J. E. and Green, M. M. (2001) 'Hemocytes are essential for wing maturation in *Drosophila melanogaster*', *Proceedings of the National Academy of Sciences*, 98(18), pp. 10190–10195. doi: 10.1073/pnas.181338998.
- Kim, J. J. *et al.* (2010) 'TNF- α -induced ROS production triggering apoptosis is directly linked to Romo1 and Bcl-XL', *Cell Death & Differentiation*, 17(9), pp. 1420–1434. doi: 10.1038/cdd.2010.19.
- Kim, T., Song, B. and Lee, I.-S. (2020) 'Drosophila Glia: Models for Human Neurodevelopmental and Neurodegenerative Disorders', *International Journal of Molecular Sciences*, 21(14), p. 4859. doi: 10.3390/ijms21144859.
- King, P. T. *et al.* (2015) 'Nontypeable *Haemophilus influenzae* Induces Sustained Lung Oxidative Stress and Protease Expression', *PLOS ONE*. Edited by N. Palaniyar, 10(3), p. e0120371. doi: 10.1371/journal.pone.0120371.
- King, P. T. *et al.* (2017) 'Deoxyribonuclease 1 reduces pathogenic effects of cigarette smoke exposure in the lung', *Scientific Reports*, 7(1), p. 12128. doi: 10.1038/s41598-017-12474-5.
- Klebs, E. (1872) 'Beiträge zur Pathologischen Anatomie der Schusswunden', *Leipzig, von F. C. W. Vogel*.
- Klein, T. and Bischoff, R. (2011) 'Physiology and pathophysiology of matrix metalloproteases', *Amino Acids*, 41(2), pp. 271–290. doi: 10.1007/s00726-010-0689-x.
- Klimp, A. H. *et al.* (2002) 'A potential role of macrophage activation in the treatment of cancer', *Critical Reviews in Oncology/Hematology*, 44(2), pp. 143–161. doi: 10.1016/S1040-8428(01)00203-7.
- Knights, A. J. *et al.* (2021) 'Acetylcholine-synthesizing macrophages in subcutaneous fat are regulated by β 2 -adrenergic signaling', *The EMBO Journal*, 40(24). doi: 10.15252/embj.2020106061.
- Koch, R. (1878) 'Untersuchungen Über Die Aetiologie der Wundinfektionskrankheiten', *Leipzig: von F.C.W. Vogel*, p. 80.
- Kondo, H. *et al.* (1988) 'Iron metabolism in the erythrophagocytosing Kupffer cell', *Hepatology*, 8(1), pp. 32–38. doi: 10.1002/hep.1840080108.
- Korns, D. *et al.* (2011) 'Modulation of Macrophage Efferocytosis in Inflammation', *Frontiers in Immunology*, 2. doi: 10.3389/fimmu.2011.00057.
- Kosteli, A. *et al.* (2010) 'Kosteli 2010, JCI. Baja peso e inflamación..pdf', 120(10). doi:

10.1172/JCI42845.3466.

Krenkel, O. *et al.* (2018) ‘Therapeutic inhibition of inflammatory monocyte recruitment reduces steatohepatitis and liver fibrosis’, *Hepatology*, 67(4), pp. 1270–1283. doi: 10.1002/hep.29544.

Krieg, A. M. (2002) ‘CpG Motifs in Bacterial DNA and Their Immune Effects’, *Annual Review of Immunology*, 20(1), pp. 709–760. doi: 10.1146/annurev.immunol.20.100301.064842.

Kulkarni, A. *et al.* (2018) ‘A designer self-assembled supramolecule amplifies macrophage immune responses against aggressive cancer’, *Nature Biomedical Engineering*, 2(8), pp. 589–599. doi: 10.1038/s41551-018-0254-6.

Kurant, E. *et al.* (2008) ‘Six-Microns-Under Acts Upstream of Draper in the Glial Phagocytosis of Apoptotic Neurons’, *Cell*, 133(3), pp. 498–509. doi: 10.1016/j.cell.2008.02.052.

Kurata, S., Kobayashi, H. and Natori, S. (1991) ‘Participation of a 200-kDa hemocyte membrane protein in the dissociation of the fat body at the metamorphosis of *Sarcophaga*’, *Developmental Biology*, 146(1), pp. 179–185. doi: 10.1016/0012-1606(91)90458-F.

Kurata, S., Komano, H. and Natori, S. (1989) ‘Dissociation of *Sarcophaga peregrina* (flesh fly) fat body by pupal haemocytes in vitro’, *Journal of Insect Physiology*, 35(7), pp. 559–565. doi: 10.1016/0022-1910(89)90144-3.

Kurucz, É. *et al.* (2007) ‘Definition of *Drosophila* hemocyte subsets by cell-type specific antigens’, *Acta Biologica Hungarica*, 58(Supplement 1), pp. 95–111. doi: 10.1556/ABiol.58.2007.Suppl.8.

Kwon, Y. *et al.* (2015) ‘Systemic Organ Wasting Induced by Localized Expression of the Secreted Insulin/IGF Antagonist ImpL2’, *Developmental Cell*, 33(1), pp. 36–46. doi: 10.1016/j.devcel.2015.02.012.

Laundon, D. *et al.* (2019) ‘The architecture of cell differentiation in choanoflagellates and sponge choanocytes’, *PLOS Biology*. Edited by U. Technau, 17(4), p. e3000226. doi: 10.1371/journal.pbio.3000226.

Lavin, Y. *et al.* (2014) ‘Tissue-Resident Macrophage Enhancer Landscapes Are Shaped by the Local Microenvironment’, *Cell*, 159(6), pp. 1312–1326. doi: 10.1016/j.cell.2014.11.018.

Lebestky, T., Jung, S.-H. and Banerjee, U. (2003) ‘A Serrate-expressing signaling center controls *Drosophila* hematopoiesis’, *Genes & Development*, 17(3), pp. 348–353. doi: 10.1101/gad.1052803.

Lee, J. *et al.* (2021) ‘Tumors overcome the action of the wasting factor ImpL2 by locally elevating Wnt/Wingless’, *Proceedings of the National Academy of Sciences*, 118(23). doi: 10.1073/pnas.2020120118.

- Lee, S.-K. and Lorenzo, J. (2006) ‘Cytokines regulating osteoclast formation and function’, *Current Opinion in Rheumatology*, 18(4), pp. 411–418. doi: 10.1097/01.bor.0000231911.42666.78.
- Lefere, S. and Tacke, F. (2019) ‘Macrophages in obesity and non-alcoholic fatty liver disease: Crosstalk with metabolism’, *JHEP Reports*, 1(1), pp. 30–43. doi: 10.1016/j.jhepr.2019.02.004.
- Lemaitre, B. *et al.* (1996) ‘The Dorsoventral Regulatory Gene Cassette *spätzle*/Toll/cactus Controls the Potent Antifungal Response in *Drosophila* Adults’, *Cell*, 86(6), pp. 973–983. doi: 10.1016/S0092-8674(00)80172-5.
- Lemaitre, B. and Hoffmann, J. (2007) ‘The Host Defense of *Drosophila melanogaster*’, *Annual Review of Immunology*, 25(1), pp. 697–743. doi: 10.1146/annurev.immunol.25.022106.141615.
- Lemaitre, B. and Miguel-Aliaga, I. (2013) ‘The Digestive Tract of *Drosophila melanogaster*’, *Annual Review of Genetics*, 47(1), pp. 377–404. doi: 10.1146/annurev-genet-111212-133343.
- Van Lent, P. L. E. M. *et al.* (1998) ‘Local removal of phagocytic synovial lining cells by clodronate-liposomes decreases cartilage destruction during collagen type II arthritis’, *Annals of the Rheumatic Diseases*, 57(7), pp. 408–413. doi: 10.1136/ard.57.7.408.
- Levanon, E. Y. (2005) ‘Evolutionarily conserved human targets of adenosine to inosine RNA editing’, *Nucleic Acids Research*, 33(4), pp. 1162–1168. doi: 10.1093/nar/gki239.
- Lévesque, M. *et al.* (2007) ‘Transforming Growth Factor: β Signaling Is Essential for Limb Regeneration in Axolotls’, *PLoS ONE*. Edited by M. Blagosklonny, 2(11), p. e1227. doi: 10.1371/journal.pone.0001227.
- Li, W. (2012) ‘Eat-me signals: Keys to molecular phagocyte biology and “Appetite” control’, *Journal of Cellular Physiology*, 227(4), pp. 1291–1297. doi: 10.1002/jcp.22815.
- Li, X. *et al.* (2023) ‘Adipose tissue macrophages as potential targets for obesity and metabolic diseases’, *Frontiers in Immunology*, 14. doi: 10.3389/fimmu.2023.1153915.
- Liang, W. *et al.* (2020) ‘The Contribution of Chemoattractant GPCRs, Formylpeptide Receptors, to Inflammation and Cancer’, *Frontiers in Endocrinology*, 11. doi: 10.3389/fendo.2020.00017.
- Lichtenstein, A. (1991) ‘Mechanism of mammalian cell lysis mediated by peptide defensins. Evidence for an initial alteration of the plasma membrane.’, *Journal of Clinical Investigation*, 88(1), pp. 93–100. doi: 10.1172/JCI115310.
- Limmer, S. *et al.* (2014) ‘The *Drosophila* blood-brain barrier: development and function of a glial endothelium’, *Frontiers in Neuroscience*, 8. doi: 10.3389/fnins.2014.00365.
- Lindsay, S. A., Lin, S. J. H. and Wasserman, S. A. (2018) ‘Short-Form Bomanins Mediate Humoral

- Immunity in *Drosophila*', *Journal of Innate Immunity*, 10(4), pp. 306–314. doi: 10.1159/000489831.
- Liu, P.-S. *et al.* (2017) ' α -ketoglutarate orchestrates macrophage activation through metabolic and epigenetic reprogramming', *Nature Immunology*, 18(9), pp. 985–994. doi: 10.1038/ni.3796.
- Liu, P. *et al.* (2014) '*Escherichia coli* and *Candida albicans* Induced Macrophage Extracellular Trap-Like Structures with Limited Microbicidal Activity', *PLoS ONE*. Edited by N. Palaniyar, 9(2), p. e90042. doi: 10.1371/journal.pone.0090042.
- Lloyd, S. A. *et al.* (2009) 'Administration of high-dose macrophage colony-stimulating factor increases bone turnover and trabecular volume fraction', *Journal of Bone and Mineral Metabolism*, 27(5), pp. 546–554. doi: 10.1007/s00774-009-0071-9.
- Loberg, R. D. *et al.* (2007) 'CCL2 as an Important Mediator of Prostate Cancer Growth In Vivo through the Regulation of Macrophage Infiltration', *Neoplasia*, 9(7), pp. 556–562. doi: 10.1593/neo.07307.
- Locasale, J. W. and Cantley, L. C. (2011) 'Metabolic Flux and the Regulation of Mammalian Cell Growth', *Cell Metabolism*, 14(4), pp. 443–451. doi: 10.1016/j.cmet.2011.07.014.
- Lu, Y. *et al.* (2020) 'Pattern recognition receptors in *Drosophila* immune responses', *Developmental & Comparative Immunology*, 102, p. 103468. doi: 10.1016/j.dci.2019.103468.
- Lumeng, C. N. *et al.* (2007) 'Increased Inflammatory Properties of Adipose Tissue Macrophages Recruited During Diet-Induced Obesity', *Diabetes*, 56(1), pp. 16–23. doi: 10.2337/db06-1076.
- Lumeng, C. N. *et al.* (2008) 'Phenotypic switching of adipose tissue macrophages with obesity is generated by spatiotemporal differences in macrophage subtypes', *Diabetes*, 57(12), pp. 3239–3246. doi: 10.2337/db08-0872.
- MacDonald, J. M. *et al.* (2006) 'The *Drosophila* Cell Corpse Engulfment Receptor Draper Mediates Glial Clearance of Severed Axons', *Neuron*, 50(6), pp. 869–881. doi: 10.1016/j.neuron.2006.04.028.
- MacMicking, J., Xie, Q. and Nathan, C. (1997) 'Nitric oxide and macrophage function', *Annual Review of Immunology*, 15(1), pp. 323–350. doi: 10.1146/annurev.immunol.15.1.323.
- Madhwal, S. *et al.* (2020) 'Metabolic control of cellular immune-competency by odors in *Drosophila*', *eLife*, 9. doi: 10.7554/eLife.60376.
- Manaka, J. *et al.* (2004) 'Draper-mediated and Phosphatidylserine-independent Phagocytosis of Apoptotic Cells by *Drosophila* Hemocytes/Macrophages', *Journal of Biological Chemistry*, 279(46), pp. 48466–48476. doi: 10.1074/jbc.M408597200.
- Mantegazza, A. R. *et al.* (2013) 'Presentation of Phagocytosed Antigens by MHC Class I and II',

Traffic, 14(2), pp. 135–152. doi: 10.1111/tra.12026.

van Marken Lichtenbelt, W. D. *et al.* (2009) ‘Cold-Activated Brown Adipose Tissue in Healthy Men’, *New England Journal of Medicine*, 360(15), pp. 1500–1508. doi: 10.1056/NEJMoa0808718.

Martinez, F. O. and Gordon, S. (2014) ‘The M1 and M2 paradigm of macrophage activation: time for reassessment’, *F1000Prime Reports*, 6. doi: 10.12703/P6-13.

McKean, K. A. *et al.* (2008) ‘The evolutionary costs of immunological maintenance and deployment’, *BMC Evolutionary Biology*, 8(1), p. 76. doi: 10.1186/1471-2148-8-76.

McMullen, E. *et al.* (2023) ‘Glycolytically impaired *Drosophila* glial cells fuel neural metabolism via β -oxidation’, *Nature Communications*, 14(1), p. 2996. doi: 10.1038/s41467-023-38813-x.

McNelis, J. C. and Olefsky, J. M. (2014) ‘Macrophages, Immunity, and Metabolic Disease’, *Immunity*, 41(1), pp. 36–48. doi: 10.1016/j.immuni.2014.05.010.

Meister, M. and Lagueux, M. (2003) ‘*Drosophila* blood cells’, *Cellular Microbiology*, 5(9), pp. 573–580. doi: 10.1046/j.1462-5822.2003.00302.x.

Melcarne, C., Lemaitre, B. and Kurant, E. (2019) ‘Phagocytosis in *Drosophila*: From molecules and cellular machinery to physiology’, *Insect Biochemistry and Molecular Biology*, 109, pp. 1–12. doi: 10.1016/j.ibmb.2019.04.002.

Michl, J., Ohlbaum, D. J. and Silverstein, S. C. (1976) ‘2-Deoxyglucose selectively inhibits Fc and complement receptor-mediated phagocytosis in mouse peritoneal macrophages II. Dissociation of the inhibitory effects of 2-deoxyglucose on phagocytosis and ATP generation.’, *The Journal of experimental medicine*, 144(6), pp. 1484–1493. doi: 10.1084/jem.144.6.1484.

Mills, C. D. (2001) ‘Macrophage arginine metabolism to ornithine/urea or nitric oxide/citrulline: a life or death issue.’, *Critical reviews in immunology*, 21(5), pp. 399–425. Available at: <http://www.ncbi.nlm.nih.gov/pubmed/11942557>.

Mills, C. D. (2012) ‘M1 and M2 Macrophages: Oracles of Health and Disease.’, *Critical reviews in immunology*, 32(6), pp. 463–88. Available at: <http://www.ncbi.nlm.nih.gov/pubmed/23428224>.

Mills, E. L. and O’Neill, L. A. (2016) ‘Reprogramming mitochondrial metabolism in macrophages as an anti-inflammatory signal’, *European Journal of Immunology*, 46(1), pp. 13–21. doi: 10.1002/eji.201445427.

Mirza, R., DiPietro, L. A. and Koh, T. J. (2009) ‘Selective and Specific Macrophage Ablation Is Detrimental to Wound Healing in Mice’, *The American Journal of Pathology*, 175(6), pp. 2454–2462. doi: 10.2353/ajpath.2009.090248.

- Mogensen, T. H. (2009) 'Pathogen Recognition and Inflammatory Signaling in Innate Immune Defenses', *Clinical Microbiology Reviews*, 22(2), pp. 240–273. doi: 10.1128/CMR.00046-08.
- Mohlin, S. *et al.* (2017) 'Hypoxia, pseudohypoxia and cellular differentiation', *Experimental Cell Research*, 356(2), pp. 192–196. doi: 10.1016/j.yexcr.2017.03.007.
- Molawi, K. *et al.* (2014) 'Progressive replacement of embryo-derived cardiac macrophages with age', *Journal of Experimental Medicine*, 211(11), pp. 2151–2158. doi: 10.1084/jem.20140639.
- Mondotte, J. A. *et al.* (2018) 'Immune priming and clearance of orally acquired RNA viruses in *Drosophila*', *Nature Microbiology*, 3(12), pp. 1394–1403. doi: 10.1038/s41564-018-0265-9.
- Mondotte, J. A. *et al.* (2020) 'Evidence For Long-Lasting Transgenerational Antiviral Immunity in Insects', *Cell Reports*, 33(11), p. 108506. doi: 10.1016/j.celrep.2020.108506.
- Moore, K. J. and Tabas, I. (2011) 'Macrophages in the Pathogenesis of Atherosclerosis', *Cell*, 145(3), pp. 341–355. doi: 10.1016/j.cell.2011.04.005.
- Morioka, S. *et al.* (2018) 'Efferocytosis induces a novel SLC program to promote glucose uptake and lactate release', *Nature*, 563(7733), pp. 714–718. doi: 10.1038/s41586-018-0735-5.
- Mosser, D. M. and Edwards, J. P. (2008) 'Exploring the full spectrum of macrophage activation', *Nature Reviews Immunology*, 8(12), pp. 958–969. doi: 10.1038/nri2448.
- Müller, W. E. G. (2006) 'The stem cell concept in sponges (Porifera): Metazoan traits', *Seminars in Cell & Developmental Biology*, 17(4), pp. 481–491. doi: 10.1016/j.semcdb.2006.05.006.
- Muller, W., Steinman, R. and Cohn, Z. (1983) 'Membrane proteins of the vacuolar system. III. Further studies on the composition and recycling of endocytic vacuole membrane in cultured macrophages', *The Journal of Cell Biology*, 96(1), pp. 29–36. doi: 10.1083/jcb.96.1.29.
- Munn, D. H. *et al.* (1999) 'Inhibition of T Cell Proliferation by Macrophage Tryptophan Catabolism', *The Journal of Experimental Medicine*, 189(9), pp. 1363–1372. doi: 10.1084/jem.189.9.1363.
- Murano, I. *et al.* (2008) 'Dead adipocytes, detected as crown-like structures, are prevalent in visceral fat depots of genetically obese mice', *Journal of Lipid Research*, 49(7), pp. 1562–1568. doi: 10.1194/jlr.M800019-JLR200.
- Mushenkova, N. V. *et al.* (2021) 'Recognition of Oxidized Lipids by Macrophages and Its Role in Atherosclerosis Development', *Biomedicines*, 9(8), p. 915. doi: 10.3390/biomedicines9080915.
- Nakai, Y., Nakajima, K. and Yaoita, Y. (2017) 'Mechanisms of tail resorption during anuran metamorphosis', *Biomolecular Concepts*, 8(3–4), pp. 179–183. doi: 10.1515/bmc-2017-0022.
- Nakanishi, N., Sogabe, S. and Degnan, B. M. (2014) 'Evolutionary origin of gastrulation: insights

- from sponge development', *BMC Biology*, 12(1), p. 26. doi: 10.1186/1741-7007-12-26.
- Natori, S. *et al.* (1999) 'The roles of Sarcophaga defense molecules in immunity and metamorphosis', *Developmental & Comparative Immunology*, 23(4–5), pp. 317–328. doi: 10.1016/S0145-305X(99)00014-2.
- Nelliot, A., Bond, N. and Hoshizaki, D. K. (2006) 'Fat-body remodeling in *Drosophila melanogaster*', *genesis*, 44(8), pp. 396–400. doi: 10.1002/dvg.20229.
- Nemeth, E. *et al.* (2004) 'IL-6 mediates hypoferremia of inflammation by inducing the synthesis of the iron regulatory hormone hepcidin', *Journal of Clinical Investigation*, 113(9), pp. 1271–1276. doi: 10.1172/JCI20945.
- Netea, M. G., Quintin, J. and van der Meer, J. W. M. (2011) 'Trained Immunity: A Memory for Innate Host Defense', *Cell Host & Microbe*, 9(5), pp. 355–361. doi: 10.1016/j.chom.2011.04.006.
- Neves, J. *et al.* (2016) 'Immune modulation by MANF promotes tissue repair and regenerative success in the retina', *Science*, 353(6294). doi: 10.1126/science.aaf3646.
- Newsholme, P. *et al.* (1986) 'Metabolism of glucose, glutamine, long-chain fatty acids and ketone bodies by murine macrophages', *Biochemical Journal*, 239(1), pp. 121–125. doi: 10.1042/bj2390121.
- Nguyen, M.-A. *et al.* (2019) 'Delivery of MicroRNAs by Chitosan Nanoparticles to Functionally Alter Macrophage Cholesterol Efflux in Vitro and in Vivo', *ACS Nano*, 13(6), pp. 6491–6505. doi: 10.1021/acsnano.8b09679.
- Nie, S. *et al.* (2015) 'Detection of atherosclerotic lesions and intimal macrophages using CD36-targeted nanovesicles', *Journal of Controlled Release*, 220, pp. 61–70. doi: 10.1016/j.jconrel.2015.10.004.
- Nomura, M. *et al.* (2016) 'Fatty acid oxidation in macrophage polarization', *Nature Immunology*, 17(3), pp. 216–217. doi: 10.1038/ni.3366.
- Norris, P. C. and Dennis, E. A. (2014) 'A lipidomic perspective on inflammatory macrophage eicosanoid signaling', *Advances in Biological Regulation*, 54, pp. 99–110. doi: 10.1016/j.jbior.2013.09.009.
- Nucera, S., Biziato, D. and De Palma, M. (2011) 'The interplay between macrophages and angiogenesis in development, tissue injury and regeneration', *The International Journal of Developmental Biology*, 55(4–5), pp. 495–503. doi: 10.1387/ijdb.103227sn.
- O'Callaghan, A. A. *et al.* (2021) 'Intestinal Metabolites Influence Macrophage Phagocytosis and Clearance of Bacterial Infection', *Frontiers in Cellular and Infection Microbiology*, 11. doi: 10.3389/fcimb.2021.622491.

O'Neill, L. A. J. (2015) 'A Broken Krebs Cycle in Macrophages', *Immunity*, 42(3), pp. 393–394. doi: 10.1016/j.immuni.2015.02.017.

Ogle, M. E. *et al.* (2016) 'Monocytes and macrophages in tissue repair: Implications for immunoregenerative biomaterial design', *Experimental Biology and Medicine*, 241(10), pp. 1084–1097. doi: 10.1177/1535370216650293.

Oldefest, M. *et al.* (2013) 'Upd3 – An ancestor of the four-helix bundle cytokines', *Biochemical and Biophysical Research Communications*, 436(1), pp. 66–72. doi: 10.1016/j.bbrc.2013.04.107.

Olofsson, B. and Page, D. T. (2005) 'Condensation of the central nervous system in embryonic *Drosophila* is inhibited by blocking hemocyte migration or neural activity', *Developmental Biology*, 279(1), pp. 233–243. doi: 10.1016/j.ydbio.2004.12.020.

Ostuni, R. *et al.* (2015) 'Macrophages and cancer: from mechanisms to therapeutic implications', *Trends in Immunology*, 36(4), pp. 229–239. doi: 10.1016/j.it.2015.02.004.

Palmieri, E. M. *et al.* (2017) 'Pharmacologic or Genetic Targeting of Glutamine Synthetase Skews Macrophages toward an M1-like Phenotype and Inhibits Tumor Metastasis', *Cell Reports*, 20(7), pp. 1654–1666. doi: 10.1016/j.celrep.2017.07.054.

Pandey, S. *et al.* (2023) 'Dietary administration of the glycolytic inhibitor 2-deoxy-D-glucose reduces endotoxemia-induced inflammation and oxidative stress: Implications in PAMP-associated acute and chronic pathology', *Frontiers in Pharmacology*, 14. doi: 10.3389/fphar.2023.940129.

Paolicelli, R. C. *et al.* (2011) 'Synaptic Pruning by Microglia Is Necessary for Normal Brain Development', *Science*, 333(6048), pp. 1456–1458. doi: 10.1126/science.1202529.

Parisi, F. *et al.* (2014) 'Transformed Epithelia Trigger Non-Tissue-Autonomous Tumor Suppressor Response by Adipocytes via Activation of Toll and Eiger/TNF Signaling', *Cell Reports*, 6(5), pp. 855–867. doi: 10.1016/j.celrep.2014.01.039.

Pasco, M. Y. and Léopold, P. (2012) 'High Sugar-Induced Insulin Resistance in *Drosophila* Relies on the Lipocalin Neural Lazarillo', *PLoS ONE*. Edited by A. W. Shingleton, 7(5), p. e36583. doi: 10.1371/journal.pone.0036583.

Pastor-Pareja, J. C., Wu, M. and Xu, T. (2008) 'An innate immune response of blood cells to tumors and tissue damage in *Drosophila*', *Disease Models & Mechanisms*, 1(2–3), pp. 144–154. doi: 10.1242/dmm.000950.

Pavlou, S. *et al.* (2017) 'Higher phagocytic activity of thioglycollate-elicited peritoneal macrophages is related to metabolic status of the cells', *Journal of Inflammation*, 14(1), p. 4. doi: 10.1186/s12950-017-0151-x.

- Péan, C. B. *et al.* (2017) 'Regulation of phagocyte triglyceride by a STAT-ATG2 pathway controls mycobacterial infection', *Nature Communications*, 8(1), p. 14642. doi: 10.1038/ncomms14642.
- Pearce, E. L. and Pearce, E. J. (2013) 'Metabolic Pathways in Immune Cell Activation and Quiescence', *Immunity*, 38(4), pp. 633–643. doi: 10.1016/j.immuni.2013.04.005.
- Pellerin, L. and Magistretti, P. J. (1994) 'Glutamate uptake into astrocytes stimulates aerobic glycolysis: a mechanism coupling neuronal activity to glucose utilization.', *Proceedings of the National Academy of Sciences*, 91(22), pp. 10625–10629. doi: 10.1073/pnas.91.22.10625.
- Petrignani, B. *et al.* (2021) 'A secreted factor NimrodB4 promotes the elimination of apoptotic corpses by phagocytes in *Drosophila*', *EMBO reports*, 22(9). doi: 10.15252/embr.202052262.
- Peyssonnaud, C. *et al.* (2005) 'HIF-1 α expression regulates the bactericidal capacity of phagocytes', *Journal of Clinical Investigation*, 115(7), pp. 1806–1815. doi: 10.1172/JCI23865.
- Pham, L. N. *et al.* (2007) 'A Specific Primed Immune Response in *Drosophila* Is Dependent on Phagocytes', *PLoS Pathogens*. Edited by K. Vernick, 3(3), p. e26. doi: 10.1371/journal.ppat.0030026.
- Pinto, S. *et al.* (2022) 'Reimagining antibody-dependent cellular cytotoxicity in cancer: the potential of natural killer cell engagers', *Trends in Immunology*, 43(11), pp. 932–946. doi: 10.1016/j.it.2022.09.007.
- Pinto, S. B. *et al.* (2009) 'Discovery of Plasmodium modulators by genome-wide analysis of circulating hemocytes in *Anopheles gambiae*', *Proceedings of the National Academy of Sciences*, 106(50), pp. 21270–21275. doi: 10.1073/pnas.0909463106.
- Pizzagalli, D. U. *et al.* (2022) 'In Vivo Motility Patterns Displayed by Immune Cells Under Inflammatory Conditions', *Frontiers in Immunology*, 12. doi: 10.3389/fimmu.2021.804159.
- Pollard, J. W. and Hennighausen, L. (1994) 'Colony stimulating factor 1 is required for mammary gland development during pregnancy.', *Proceedings of the National Academy of Sciences*, 91(20), pp. 9312–9316. doi: 10.1073/pnas.91.20.9312.
- Pontejo, S. M. and Murphy, P. M. (2022) 'Chemokines and phosphatidylserine: New binding partners for apoptotic cell clearance', *Frontiers in Cell and Developmental Biology*, 10. doi: 10.3389/fcell.2022.943590.
- Purice, M. D. *et al.* (2017) 'A novel *Drosophila* injury model reveals severed axons are cleared through a Draper/MMP-1 signaling cascade', *eLife*, 6. doi: 10.7554/eLife.23611.
- Purice, M. D., Speese, S. D. and Logan, M. A. (2016) 'Delayed glial clearance of degenerating axons in aged *Drosophila* is due to reduced PI3K/Draper activity', *Nature Communications*, 7(1), p. 12871. doi: 10.1038/ncomms12871.

- Qatanani, M. and Lazar, M. A. (2007) 'Mechanisms of obesity-associated insulin resistance: many choices on the menu', *Genes & Development*, 21(12), pp. 1443–1455. doi: 10.1101/gad.1550907.
- Rada, B. (2019) 'Neutrophil Extracellular Traps', in, pp. 517–528. doi: 10.1007/978-1-4939-9424-3_31.
- Rae, F. *et al.* (2007) 'Characterisation and trophic functions of murine embryonic macrophages based upon the use of a Csf1r–EGFP transgene reporter', *Developmental Biology*, 308(1), pp. 232–246. doi: 10.1016/j.ydbio.2007.05.027.
- Ragland, S. A. and Criss, A. K. (2017) 'From bacterial killing to immune modulation: Recent insights into the functions of lysozyme', *PLOS Pathogens*. Edited by J. B. Bliska, 13(9), p. e1006512. doi: 10.1371/journal.ppat.1006512.
- Rayamajhee, B. *et al.* (2022) 'Acanthamoeba, an environmental phagocyte enhancing survival and transmission of human pathogens', *Trends in Parasitology*, 38(11), pp. 975–990. doi: 10.1016/j.pt.2022.08.007.
- Razzell, W., Wood, W. and Martin, P. (2011) 'Swatting flies: modelling wound healing and inflammation in *Drosophila*', *Disease Models & Mechanisms*, 4(5), pp. 569–574. doi: 10.1242/dmm.006825.
- Regan, J. C. *et al.* (2013) 'Steroid Hormone Signaling Is Essential to Regulate Innate Immune Cells and Fight Bacterial Infection in *Drosophila*', *PLoS Pathogens*. Edited by D. S. Schneider, 9(10), p. e1003720. doi: 10.1371/journal.ppat.1003720.
- Remmerie, A. and Scott, C. L. (2018) 'Macrophages and lipid metabolism', *Cellular Immunology*, 330, pp. 27–42. doi: 10.1016/j.cellimm.2018.01.020.
- Roddie, H. G. *et al.* (2019) 'Simu-dependent clearance of dying cells regulates macrophage function and inflammation resolution', *PLOS Biology*. Edited by A. Bhandoola, 17(5), p. e2006741. doi: 10.1371/journal.pbio.2006741.
- Röhrig, F. and Schulze, A. (2016) 'The multifaceted roles of fatty acid synthesis in cancer', *Nature Reviews Cancer*, 16(11), pp. 732–749. doi: 10.1038/nrc.2016.89.
- Rosales, C. and Uribe-Querol, E. (2017) 'Phagocytosis: A Fundamental Process in Immunity', *BioMed Research International*, 2017, pp. 1–18. doi: 10.1155/2017/9042851.
- Rosina, M. *et al.* (2022) 'Ejection of damaged mitochondria and their removal by macrophages ensure efficient thermogenesis in brown adipose tissue', *Cell Metabolism*, 34(4), pp. 533–548.e12. doi: 10.1016/j.cmet.2022.02.016.
- Ross, E. A., Devitt, A. and Johnson, J. R. (2021) 'Macrophages: The Good, the Bad, and the

- Gluttony', *Frontiers in Immunology*, 12. doi: 10.3389/fimmu.2021.708186.
- Ross, R. and Glomset, J. A. (1973) 'Atherosclerosis and the Arterial Smooth Muscle Cell', *Science*, 180(4093), pp. 1332–1339. doi: 10.1126/science.180.4093.1332.
- Sammalkorpi, K. *et al.* (1988) 'Changes in serum lipoprotein pattern induced by acute infections', *Metabolism*, 37(9), pp. 859–865. doi: 10.1016/0026-0495(88)90120-5.
- Sanchez Bosch, P. *et al.* (2019) 'Adult *Drosophila* Lack Hematopoiesis but Rely on a Blood Cell Reservoir at the Respiratory Epithelia to Relay Infection Signals to Surrounding Tissues', *Developmental Cell*, 51(6), pp. 787-803.e5. doi: 10.1016/j.devcel.2019.10.017.
- Saradna, A. *et al.* (2018) 'Macrophage polarization and allergic asthma', *Translational Research*, 191, pp. 1–14. doi: 10.1016/j.trsl.2017.09.002.
- Scheule, R. (2000) 'The role of CpG motifs in immunostimulation and gene therapy', *Advanced Drug Delivery Reviews*, 44(2–3), pp. 119–134. doi: 10.1016/S0169-409X(00)00090-9.
- Schiffmann, E., Corcoran, B. A. and Wahl, S. M. (1975) 'N-formylmethionyl peptides as chemoattractants for leucocytes.', *Proceedings of the National Academy of Sciences*, 72(3), pp. 1059–1062. doi: 10.1073/pnas.72.3.1059.
- Schneider, D. S. *et al.* (2007) 'Drosophila eiger Mutants Are Sensitive to Extracellular Pathogens', *PLoS Pathogens*. Edited by F. M. Ausubel, 3(3), p. e41. doi: 10.1371/journal.ppat.0030041.
- Schnitzer, B. *et al.* (1972) 'Pitting Function of the Spleen in Malaria: Ultrastructural Observations', *Science*, 177(4044), pp. 175–177. doi: 10.1126/science.177.4044.175.
- Schröder, N. W. J. *et al.* (2003) 'Lipoteichoic Acid (LTA) of *Streptococcus pneumoniae* and *Staphylococcus aureus* Activates Immune Cells via Toll-like Receptor (TLR)-2, Lipopolysaccharide-binding Protein (LBP), and CD14, whereas TLR-4 and MD-2 Are Not Involved', *Journal of Biological Chemistry*, 278(18), pp. 15587–15594. doi: 10.1074/jbc.M212829200.
- Schuster, F. L. and Levandowski, M. (1996) 'Chemosensory Responses of *Acanthamoeba castellanii*: Visual Analysis of Random Movement and Responses to Chemical Signals', *Journal of Eukaryotic Microbiology*, 43(2), pp. 150–158. doi: 10.1111/j.1550-7408.1996.tb04496.x.
- Sears, H. C. (2003) 'Macrophage-mediated corpse engulfment is required for normal *Drosophila* CNS morphogenesis', *Development*, 130(15), pp. 3557–3565. doi: 10.1242/dev.00586.
- Sears, H. C., Kennedy, C. J. and Garrity, P. A. (2003) 'Macrophage-mediated corpse engulfment is required for normal *Drosophila* CNS morphogenesis', *Development*, 130(15), pp. 3557–3565. doi: 10.1242/dev.00586.

- Sell, H., Deshaies, Y. and Richard, D. (2004) 'The brown adipocyte: update on its metabolic role', *The International Journal of Biochemistry & Cell Biology*, 36(11), pp. 2098–2104. doi: 10.1016/j.biocel.2004.04.003.
- Sengoopta, C. (1993) 'Rejuvenation and the Prolongation of Life: Science or Quackery?', *Perspectives in Biology and Medicine*, 37(1), pp. 55–66. doi: 10.1353/pbm.1994.0024.
- Shapiro, H. *et al.* (2013) 'Adipose Tissue Foam Cells Are Present in Human Obesity', *The Journal of Clinical Endocrinology & Metabolism*, 98(3), pp. 1173–1181. doi: 10.1210/jc.2012-2745.
- Shelby, K. S. and Popham, H. J. R. (2012) 'RNA-Seq Study of Microbially Induced Hemocyte Transcripts from Larval *Heliothis virescens* (Lepidoptera: Noctuidae)', *Insects*, 3(3), pp. 743–762. doi: 10.3390/insects3030743.
- Shi, H. *et al.* (2006) 'TLR4 links innate immunity and fatty acid-induced insulin resistance', *Journal of Clinical Investigation*, 116(11), pp. 3015–3025. doi: 10.1172/JCI28898.
- Shia, A. K. H. *et al.* (2009) 'Toll-dependent antimicrobial responses in *Drosophila* larval fat body require Spätzle secreted by haemocytes', *Journal of Cell Science*, 122(24), pp. 4505–4515. doi: 10.1242/jcs.049155.
- Shields, C. W. *et al.* (2020) 'Materials for Immunotherapy', *Advanced Materials*, 32(13). doi: 10.1002/adma.201901633.
- Siebert, I. *et al.* (2015) 'Ferritin-Mediated Iron Sequestration Stabilizes Hypoxia-Inducible Factor-1 α upon LPS Activation in the Presence of Ample Oxygen', *Cell Reports*, 13(10), pp. 2048–2055. doi: 10.1016/j.celrep.2015.11.005.
- Silva, H. M. *et al.* (2019) 'Vasculature-associated fat macrophages readily adapt to inflammatory and metabolic challenges', *Journal of Experimental Medicine*, 216(4), pp. 786–806. doi: 10.1084/jem.20181049.
- Simkin, J. *et al.* (2017) 'Macrophages are required to coordinate mouse digit tip regeneration', *Development*. doi: 10.1242/dev.150086.
- Sinder, B. P., Pettit, A. R. and McCauley, L. K. (2015) 'Macrophages: Their Emerging Roles in Bone', *Journal of Bone and Mineral Research*, 30(12), pp. 2140–2149. doi: 10.1002/jbmr.2735.
- Sitia, G. *et al.* (2011) 'Kupffer Cells Hasten Resolution of Liver Immunopathology in Mouse Models of Viral Hepatitis', *PLoS Pathogens*. Edited by J. J. Ou, 7(6), p. e1002061. doi: 10.1371/journal.ppat.1002061.
- Slauch, J. M. (2011) 'How does the oxidative burst of macrophages kill bacteria? Still an open question', *Molecular Microbiology*, 80(3), pp. 580–583. doi: 10.1111/j.1365-2958.2011.07612.x.

- De Smet, R., Allais, L. and Cuvelier, C. A. (2014) 'Recent advances in oral vaccine development', *Human Vaccines & Immunotherapeutics*, 10(5), pp. 1309–1318. doi: 10.4161/hv.28166.
- Sokol, C. L. and Luster, A. D. (2015) 'The Chemokine System in Innate Immunity', *Cold Spring Harbor Perspectives in Biology*, 7(5), p. a016303. doi: 10.1101/cshperspect.a016303.
- Sonnenfeld, M. J. and Jacobs, J. R. (1995) 'Macrophages and glia participate in the removal of apoptotic neurons from the Drosophila embryonic nervous system', *Journal of Comparative Neurology*, 359(4), pp. 644–652. doi: 10.1002/cne.903590410.
- Srivastava, M. *et al.* (2010) 'The Amphimedon queenslandica genome and the evolution of animal complexity', *Nature*, 466(7307), pp. 720–726. doi: 10.1038/nature09201.
- Statista (2023) 'Leading 20 U.S. pharma products by total prescriptions in 2020', (Aug 29). Available at: <https://www.statista.com/statistics/233986/top-us-pharma-products-by-prescriptions/>.
- Stephenson, H. N. *et al.* (2022) 'Hemocytes are essential for Drosophila melanogaster post-embryonic development, independent of control of the microbiota', *Development*, 149(18). doi: 10.1242/dev.200286.
- Stern, N. *et al.* (1986) 'The catabolism of lung surfactant by alveolar macrophages', *Biochimica et Biophysica Acta (BBA) - Lipids and Lipid Metabolism*, 877(3), pp. 323–333. doi: 10.1016/0005-2760(86)90196-7.
- Stramer, B. *et al.* (2005) 'Live imaging of wound inflammation in Drosophila embryos reveals key roles for small GTPases during in vivo cell migration', *The Journal of Cell Biology*, 168(4), pp. 567–573. doi: 10.1083/jcb.200405120.
- Straub, R. H. (2014) 'Insulin resistance, selfish brain, and selfish immune system: an evolutionarily positively selected program used in chronic inflammatory diseases', *Arthritis Research & Therapy*, 16(Suppl 2), p. S4. doi: 10.1186/ar4688.
- Tabas, I. and Bornfeldt, K. E. (2016) 'Macrophage Phenotype and Function in Different Stages of Atherosclerosis', *Circulation Research*, 118(4), pp. 653–667. doi: 10.1161/CIRCRESAHA.115.306256.
- Takahashi, N., Kurata, S. and Natori, S. (1993) 'Molecular cloning of cDNA for the 29 kDa proteinase participating in decomposition of the larval fat body during metamorphosis of Sarcophaga peregrina (flesh fly)', *FEBS Letters*, 334(2), pp. 153–157. doi: 10.1016/0014-5793(93)81702-2.
- Takeda, N. *et al.* (2010) 'Differential activation and antagonistic function of HIF- α isoforms in macrophages are essential for NO homeostasis', *Genes & Development*, 24(5), pp. 491–501. doi: 10.1101/gad.1881410.

- Tan, Z. *et al.* (2015) 'Pyruvate Dehydrogenase Kinase 1 Participates in Macrophage Polarization via Regulating Glucose Metabolism', *The Journal of Immunology*, 194(12), pp. 6082–6089. doi: 10.4049/jimmunol.1402469.
- Tanaka, E. M. and Reddien, P. W. (2011) 'The Cellular Basis for Animal Regeneration', *Developmental Cell*, 21(1), pp. 172–185. doi: 10.1016/j.devcel.2011.06.016.
- Tang, J. *et al.* (2015) 'Inhibiting macrophage proliferation suppresses atherosclerotic plaque inflammation', *Science Advances*, 1(3). doi: 10.1126/sciadv.1400223.
- Tattikota, S. G. *et al.* (2020) 'A single-cell survey of Drosophila blood', *eLife*, 9. doi: 10.7554/eLife.54818.
- Tauber, A. I. (2003) 'Metchnikoff and the phagocytosis theory', *Nature Reviews Molecular Cell Biology*, 4(11), pp. 897–901. doi: 10.1038/nrm1244.
- Tepass, U. *et al.* (1994) 'Embryonic origin of hemocytes and their relationship to cell death in Drosophila', *Development*, 120(7), pp. 1829–1837. doi: 10.1242/dev.120.7.1829.
- Teti, G., Biondo, C. and Beninati, C. (2016) 'The Phagocyte, Metchnikoff, and the Foundation of Immunology', *Microbiology Spectrum*. Edited by S. Gordon, 4(2). doi: 10.1128/microbiolspec.MCHD-0009-2015.
- Trojan, E. *et al.* (2020) 'The Contribution of Formyl Peptide Receptor Dysfunction to the Course of Neuroinflammation: A Potential Role in the Brain Pathology', *Current Neuropharmacology*, 18(3), pp. 229–249. doi: 10.2174/1570159X17666191019170244.
- Trzeciak, A., Wang, Y.-T. and Perry, J. S. A. (2021) 'First we eat, then we do everything else: The dynamic metabolic regulation of efferocytosis', *Cell Metabolism*, 33(11), pp. 2126–2141. doi: 10.1016/j.cmet.2021.08.001.
- Tsigkas, N. *et al.* (2016) 'Drug-loaded particles: "Trojan horses" in the therapy of atherosclerosis', *Atherosclerosis*, 251, pp. 528–530. doi: 10.1016/j.atherosclerosis.2016.06.050.
- Tu, J. *et al.* (2020) 'Synovial Macrophages in Rheumatoid Arthritis: The Past, Present, and Future', *Mediators of Inflammation*, 2020, pp. 1–8. doi: 10.1155/2020/1583647.
- Tucker, P. K., Evans, I. R. and Wood, W. (2011) 'Ena drives invasive macrophage migration in Drosophila embryos', *Disease Models & Mechanisms*, 4(1), pp. 126–134. doi: 10.1242/dmm.005694.
- Ueshima, E. *et al.* (2019) 'Macrophage-secreted TGF- β 1 contributes to fibroblast activation and ureteral stricture after ablation injury', *American Journal of Physiology-Renal Physiology*, 317(1), pp. F52–F64. doi: 10.1152/ajprenal.00260.2018.

- Ugur, B., Chen, K. and Bellen, H. J. (2016) 'Drosophila tools and assays for the study of human diseases', *Disease Models & Mechanisms*, 9(3), pp. 235–244. doi: 10.1242/dmm.023762.
- Vats, D. *et al.* (2006) 'Oxidative metabolism and PGC-1 β attenuate macrophage-mediated inflammation', *Cell Metabolism*, 4(3), p. 255. doi: 10.1016/j.cmet.2006.08.006.
- Veremeyko, T. *et al.* (2018) 'Cyclic AMP Pathway Suppress Autoimmune Neuroinflammation by Inhibiting Functions of Encephalitogenic CD4 T Cells and Enhancing M2 Macrophage Polarization at the Site of Inflammation', *Frontiers in Immunology*, 9. doi: 10.3389/fimmu.2018.00050.
- Viola, A. *et al.* (2019) 'The Metabolic Signature of Macrophage Responses', *Frontiers in Immunology*, 10. doi: 10.3389/fimmu.2019.01462.
- Wang, S. *et al.* (2021) 'Autophagy and Mitochondrial Homeostasis During Infection: A Double-Edged Sword', *Frontiers in Cell and Developmental Biology*, 9. doi: 10.3389/fcell.2021.738932.
- Wang, T. *et al.* (2017) 'HIF1 α -Induced Glycolysis Metabolism Is Essential to the Activation of Inflammatory Macrophages', *Mediators of Inflammation*, 2017, pp. 1–10. doi: 10.1155/2017/9029327.
- Wang, X. *et al.* (2019) 'Emerging Roles for G-protein Coupled Receptors in Development and Activation of Macrophages', *Frontiers in Immunology*, 10. doi: 10.3389/fimmu.2019.02031.
- Wang, X. and Lin, Y. (2008) 'Tumor necrosis factor and cancer, buddies or foes?', *Acta Pharmacologica Sinica*, 29(11), pp. 1275–1288. doi: 10.1111/j.1745-7254.2008.00889.x.
- Wang, Y.-N. *et al.* (2021) 'Slit3 secreted from M2-like macrophages increases sympathetic activity and thermogenesis in adipose tissue', *Nature Metabolism*, 3(11), pp. 1536–1551. doi: 10.1038/s42255-021-00482-9.
- Wang, Y. *et al.* (2018) 'Targeted Therapy of Atherosclerosis by a Broad-Spectrum Reactive Oxygen Species Scavenging Nanoparticle with Intrinsic Anti-inflammatory Activity', *ACS Nano*, 12(9), pp. 8943–8960. doi: 10.1021/acsnano.8b02037.
- Wang, Z. *et al.* (2010) 'Pathogen Entrapment by Transglutaminase—A Conserved Early Innate Immune Mechanism', *PLoS Pathogens*. Edited by D. S. Schneider, 6(2), p. e1000763. doi: 10.1371/journal.ppat.1000763.
- Warburg, O., Wind, F. and Negelein, E. (1927) 'The metabolism of tumors in the body', *Journal of General Physiology*, 8(6), pp. 519–530. doi: 10.1085/jgp.8.6.519.
- Watson, F. L. *et al.* (2005) 'Extensive Diversity of Ig-Superfamily Proteins in the Immune System of Insects', *Science*, 309(5742), pp. 1874–1878. doi: 10.1126/science.1116887.
- Weavers, H. *et al.* (2016) 'Corpse Engulfment Generates a Molecular Memory that Primes the

- Macrophage Inflammatory Response', *Cell*, 165(7), pp. 1658–1671. doi: 10.1016/j.cell.2016.04.049.
- Weber, R. (1964) 'Ultrastructural changes in regressing tail muscles of xenopus larvae at metamorphosis', *The Journal of Cell Biology*, 22(2), pp. 481–487. doi: 10.1083/jcb.22.2.481.
- Weinhouse, S. (1951) 'Studies on the fate of isotopically labeled metabolites in the oxidative metabolism of tumors.', *Cancer research*, 11(8), pp. 585–91. Available at: <http://www.ncbi.nlm.nih.gov/pubmed/14859221>.
- Weisberg, S. P. *et al.* (2003) 'Obesity is associated with macrophage accumulation in adipose tissue', *Journal of Clinical Investigation*, 112(12), pp. 1796–1808. doi: 10.1172/JCI19246.
- Wenceslau, C. F. *et al.* (2013) 'Mitochondrial-derived N-formyl peptides: Novel links between trauma, vascular collapse and sepsis', *Medical Hypotheses*, 81(4), pp. 532–535. doi: 10.1016/j.mehy.2013.06.026.
- Wernly, B. *et al.* (2016) 'Hyperglycemia in septic patients: an essential stress survival response in all, a robust marker for risk stratification in some, to be messed with in none', *Journal of Thoracic Disease*, 8(7), pp. E621–E624. doi: 10.21037/jtd.2016.05.24.
- Wiens, M. *et al.* (2005) 'Innate Immune Defense of the Sponge *Suberites domuncula* against Bacteria Involves a MyD88-dependent Signaling Pathway', *Journal of Biological Chemistry*, 280(30), pp. 27949–27959. doi: 10.1074/jbc.M504049200.
- Wilkins, B. S. and Wright, D. H. (2000) *Illustrated Pathology of the Spleen*. Cambridge: Cambridge University Press. doi: 10.1017/CBO9780511545979.
- Williams, N. C. and O'Neill, L. A. J. (2018) 'A Role for the Krebs Cycle Intermediate Citrate in Metabolic Reprogramming in Innate Immunity and Inflammation', *Frontiers in Immunology*, 9. doi: 10.3389/fimmu.2018.00141.
- Winkler, B. S., DeSantis, N. and Solomon, F. (1986) 'Multiple NADPH-producing pathways control glutathione (GSH) content in retina', *Experimental Eye Research*, 43(5), pp. 829–847. doi: 10.1016/S0014-4835(86)80013-6.
- Wood, W. and Martin, P. (2017) 'Macrophage Functions in Tissue Patterning and Disease: New Insights from the Fly', *Developmental Cell*, 40(3), pp. 221–233. doi: 10.1016/j.devcel.2017.01.001.
- Woodcock, K. J. *et al.* (2015) 'Macrophage-Derived upd3 Cytokine Causes Impaired Glucose Homeostasis and Reduced Lifespan in *Drosophila* Fed a Lipid-Rich Diet', *Immunity*, 42(1), pp. 133–144. doi: 10.1016/j.immuni.2014.12.023.
- Wu, J. *et al.* (2012) 'Beige Adipocytes Are a Distinct Type of Thermogenic Fat Cell in Mouse and Human', *Cell*, 150(2), pp. 366–376. doi: 10.1016/j.cell.2012.05.016.

- Wu, R. (2004) 'Macrophage contributions to ovarian function', *Human Reproduction Update*, 10(2), pp. 119–133. doi: 10.1093/humupd/dmh011.
- Wynn, T. and Barron, L. (2010) 'Macrophages: Master Regulators of Inflammation and Fibrosis', *Seminars in Liver Disease*, 30(03), pp. 245–257. doi: 10.1055/s-0030-1255354.
- Xia, W. *et al.* (2009) 'A functional folate receptor is induced during macrophage activation and can be used to target drugs to activated macrophages', *Blood*, 113(2), pp. 438–446. doi: 10.1182/blood-2008-04-150789.
- Xiao, X., Yeoh, B. S. and Vijay-Kumar, M. (2017) 'Lipocalin 2: An Emerging Player in Iron Homeostasis and Inflammation', *Annual Review of Nutrition*, 37(1), pp. 103–130. doi: 10.1146/annurev-nutr-071816-064559.
- Yan, J. and Horng, T. (2020) 'Lipid Metabolism in Regulation of Macrophage Functions', *Trends in Cell Biology*, 30(12), pp. 979–989. doi: 10.1016/j.tcb.2020.09.006.
- Yang, H. *et al.* (2015) 'JAK/STAT signaling in *Drosophila* muscles controls the cellular immune response against parasitoid infection', *EMBO reports*, 16(12), pp. 1664–1672. doi: 10.15252/embr.201540277.
- Yang, H. and Hultmark, D. (2017) '*Drosophila* muscles regulate the immune response against wasp infection via carbohydrate metabolism', *Scientific Reports*, 7(1), p. 15713. doi: 10.1038/s41598-017-15940-2.
- Yang, X. *et al.* (2007) 'Callus mineralization and maturation are delayed during fracture healing in interleukin-6 knockout mice', *Bone*, 41(6), pp. 928–936. doi: 10.1016/j.bone.2007.07.022.
- Yarnitzky, T. and Volk, T. (1995) 'Laminin Is Required for Heart, Somatic Muscles, and Gut Development in the *Drosophila* Embryo', *Developmental Biology*, 169(2), pp. 609–618. doi: 10.1006/dbio.1995.1173.
- Ye, M. *et al.* (2019) 'SR-A-Targeted Phase-Transition Nanoparticles for the Detection and Treatment of Atherosclerotic Vulnerable Plaques', *ACS Applied Materials & Interfaces*, 11(10), pp. 9702–9715. doi: 10.1021/acsami.8b18190.
- Yin, J. *et al.* (2017) 'The Role of Microglia and Macrophages in CNS Homeostasis, Autoimmunity, and Cancer', *Journal of Immunology Research*, 2017, pp. 1–12. doi: 10.1155/2017/5150678.
- Yona, S. and Gordon, S. (2015) 'From the Reticuloendothelial to Mononuclear Phagocyte System – The Unaccounted Years', *Frontiers in Immunology*, 6. doi: 10.3389/fimmu.2015.00328.
- Yu, S. *et al.* (2022) '*Drosophila* Innate Immunity Involves Multiple Signaling Pathways and Coordinated Communication Between Different Tissues', *Frontiers in Immunology*, 13. doi:

10.3389/fimmu.2022.905370.

Yue, Y. *et al.* (2015) 'IL4I1 Is a Novel Regulator of M2 Macrophage Polarization That Can Inhibit T Cell Activation via L-Tryptophan and Arginine Depletion and IL-10 Production', *PLOS ONE*. Edited by M. A. Olszewski, 10(11), p. e0142979. doi: 10.1371/journal.pone.0142979.

Yung, S. C., Parenti, D. and Murphy, P. M. (2011) 'Host Chemokines Bind to *Staphylococcus aureus* and Stimulate Protein A Release', *Journal of Biological Chemistry*, 286(7), pp. 5069–5077. doi: 10.1074/jbc.M110.195180.

Zaidman-Rémy, A. *et al.* (2012) 'The *Drosophila* larva as a tool to study gut-associated macrophages: PI3K regulates a discrete hemocyte population at the proventriculus', *Developmental & Comparative Immunology*, 36(4), pp. 638–647. doi: 10.1016/j.dci.2011.10.013.

Zanet, J. *et al.* (2012) 'Fascin promotes filopodia formation independent of its role in actin bundling', *Journal of Cell Biology*, 197(4), pp. 477–486. doi: 10.1083/jcb.201110135.

Zimmer, S. *et al.* (2016) 'Cyclodextrin promotes atherosclerosis regression via macrophage reprogramming', *Science Translational Medicine*, 8(333). doi: 10.1126/scitranslmed.aad6100.

8 CURRICULUM VITAE

Gabriela Krejčová

ORCID: 0000-0003-4648-973X

krejcg00@prf.jcu.cz

ResearcherID: JHF-8824-2023

krejcovagabriela@seznam.cz

Faculty of Science, University of South Bohemia in České Budějovice, Branišovská 1760/31a, 370 05 České Budějovice, Czech Republic

Date of birth: November 11 1993

Place of birth: Plzeň, Czech Republic

Nationality: Czech

EDUCATION

- | | |
|----------------|--|
| 2018 – present | Ph.D. student in Molecular and Cell Biology and Genetics, Faculty of Science, University of South Bohemia in České Budějovice, Czech Republic |
| 2016 – 2018 | Master's degree in Experimental Biology – Molecular and Cell Biology and Genetics, Faculty of Science, University of South Bohemia in České Budějovice, Czech Republic |
| 2013 – 2016 | Bachelor's degree in Biology, Faculty of Science, University of South Bohemia in České Budějovice, Czech Republic |

THESES

- | | |
|---------------------|---|
| Dissertation thesis | The role of macrophages in the regulation of systemic metabolism in <i>Drosophila</i> |
| Master thesis | Characterization of metabolic changes in hemocytes during the immune response in <i>D. melanogaster</i> |
| Bachelor thesis | Cancer immunotherapy based on combination of TLR signalling with phagocytosis activation |

RESEARCH POSITIONS

- | | |
|----------------|---|
| 2018 – present | Research Associate at the Faculty of Science, University of South Bohemia in České Budějovice, Czech Republic |
|----------------|---|

PUBLICATIONS

Krejčová, G., Saloň, I., Klimša, V., Ulbrich, P., Ayse, A., Bajgar, A., Štěpánek, F. (2023). Magnetic yeast glucan particles for antibody-free separation of viable macrophages from *Drosophila melanogaster*. Accepted in ACS Biomater. Sci. Eng. 10.1021/acsbomaterials.3c01199

Krejčová, G., Morgantini, C., Zemanová, H., Lauschke, V.M., Kovářová, J., Kubásek, J., Nedbalová, P., Kamps-Hughes, N., Moos, M., Aouadi, M., et al. (2023). Macrophage-derived insulin antagonist ImpL2 induces lipoprotein mobilization upon bacterial infection. EMBO J. 10.15252/embj.2023114086.

Bajgar, A., and **Krejčová, G.** (2023). On the origin of the functional versatility of macrophages. Front. Physiol. 14. 10.3389/fphys.2023.1128984.

Bajgar, A., **Krejčová, G.**, and Doležal, T. (2021). Polarization of Macrophages in Insects: Opening Gates for Immuno-Metabolic Research. Front. Cell Dev. Biol. 9. 10.3389/fcell.2021.629238.

Krejčová, G., Danielová, A., Nedbalová, P., Kazek, M., Strych, L., Chawla, G., Tennessen, J.M., Lieskovská, J., Jindra, M., Doležal, T., et al. (2019). *Drosophila* macrophages switch to aerobic glycolysis to mount effective antibacterial defense. Elife 8. 10.7554/eLife.50414.

Bajgar, A., Saloň, I., **Krejčová, G.**, Doležal, T., Jindra, M., and Štěpánek, F. (2019). Yeast glucan particles enable intracellular protein delivery in *Drosophila* without compromising the immune system. Biomater. Sci. 7, 4708–4719. 10.1039/C9BM00539K.

Doležal, T., **Krejčová, G.**, Bajgar, A., Nedbalová, P., and Strasser, P. (2019). Molecular regulations of metabolism during immune response in insects. Insect Biochem. Mol. Biol. 109, 31–42. 10.1016/j.ibmb.2019.04.005.

Morgantini, C., Jager, J., Li, X., Levi, L., Azzimato, V., Sulen, A., Barreby, E., Xu, C., Tencerova, M., Näslund, E.,.....**Krejčová, G.**, Bajgar, A., and Aouadi, M. (2019). Liver macrophages regulate systemic metabolism through non-inflammatory factors. Nat. Metab. 1, 445–459. 10.1038/s42255-019-0044-9.

Caisová, V., Uher, O., Nedbalová, P., Jochmanová, I., Kvardová, K., Masáková, K., **Krejčová, G.**, Paďouková, L., Chmelař, J., Kopecký, J., et al. (2018). Effective cancer immunotherapy based on combination of TLR agonists with stimulation of phagocytosis. *Int. Immunopharmacol.* 59, 86–96. 10.1016/j.intimp.2018.03.038.

Caisová, V., Vieru, A., Kumžáková, Z., Glaserová, S., Husníková, H., Vácová, N., **Krejčová, G.**, Paďouková, L., Jochmanová, I., Wolf, K.I., et al. (2016). Innate immunity based cancer immunotherapy: B16-F10 murine melanoma model. *BMC Cancer* 16, 940. 10.1186/s12885-016-2982-x.

MANUSCRIPTS IN PREPARATION

Krejčová, G., Danielová, A., Sehadová, H., Dyčka, F., Kubásek, J., Moos, M., Bajgar, A. (2023). Macrophages play a nutritive role in post-metamorphic maturation in *Drosophila*. Under review in *Development*.

Bajgar, A., **Krejčová, G.**, Ruphuy, G., Sonntag, E., Štěpánek, F. (2023). Macrophage-specific delivery of atorvastatin by yeast glucan particles intervenes bactericidal function in *Drosophila*. Under review in *Insect Molecular Biology*.

AWARDS AND FELLOWSHIPS

- | | |
|------|--|
| 2022 | First prize in the PhD Presentation Competition at the retreat of the Department of Molecular Biology and Genetics.
Second and third prize in Scientific Image Competition 2022 in the category Scientific merit at the Faculty of Science. |
| 2021 | 1-year Individual Research Project from the Grant Agency of the University of South Bohemia.
First prize in the PhD Presentation Competition at the retreat of the Department of Molecular Biology and Genetics.
First prize in Scientific Image Competition 2021 in the category Aesthetic merit and second prize in the category Scientific merit at the Department of Molecular Biology and Genetics. |
| 2019 | 2-year Individual Research Project from the Grant Agency of the University of South Bohemia.
Third prize in Scientific Image Competition 2019 in the category Scientific merit at the Department of Molecular Biology and Genetics. |
| 2018 | Dean's award for excellent master thesis and Rector's award for excellent study results.
First prize in Scientific Image Competition 2019 in the category Aesthetic merit at the Department of Molecular Biology and Genetics. |

- 2017 First prize in the PhD Presentation Competition at the retreat of the Department of Molecular Biology and Genetics.
- First and third prize in Scientific Image Competition 2019 in the category Aesthetic merit at the Department of Molecular Biology and Genetics.

CONFERENCES

- 2023 XII European Congress of Entomology in Heraklion, Crete. Poster presentation.
- 2022 Cell Symposia: Translational Immunometabolism, Basel, Switzerland. Poster presentation.
- Immunology Meets Philosophy, Prague, Czech Republic.
- Frontiers In Physiology and Disease, České Budějovice, Czech Republic. Oral presentation.
- 2019 European Drosophila Research Conference, Lausanne, Switzerland. Poster presentation.
- Frontiers In Insect Physiology, České Budějovice, Czech Republic. Oral presentation.

PEDAGOGICAL & OTHER ACTIVITIES

- 2023 – present Lecturer and tutorial lecturer for Techniques of microscopy for biologists (KMB/223 and KMB/223E)
- Micro-computed tomography demonstration during the Open days at the Faculty of Science, University of South Bohemia.
- 2022 – present Tutorial lecturer for Advanced methods of molecular biology (KMB/603 and KMB/603E)
- 2022 – present Consultant of master thesis “The role of macrophages in ketogenesis during stress response in *Drosophila*.”
- 2022 Reviewer of bachelor thesis “Analysis of variance in size of mite *Varroa destructor* in different habitats of honey bee breeding.”
- Confocal microscopy demonstration at the Night of Scientists, Biology Centre CAS.
- 2018 – present Tutorial lecturer for Basic methods in molecular biology (KMB/608) at the Faculty of Science, University of South Bohemia

© for non-published parts Gabriela Krejčová
krejcg00@prf.jcu.cz

The role of macrophages in the regulation of systemic metabolism in *Drosophila*

Ph.D. Thesis, 2023

All rights reserved

For non-commercial use only

University of South Bohemia in České Budějovice
Faculty of Science
Branišovská 1760
CZ-37005 České Budějovice, Czech Republic

Phone: +420 387 776 201

www.prf.jcu.cz, e-mail: sekret-fpr@prf.jcu.cz